The bone microenvironment as a master regulator of disseminated tumour cells responsible for breast cancer recurrence

A thesis submitted in partial fulfilment of the requirements for the degree of Doctor of Philosophy by

Thomas Ogola

Supervised by

Prof. Ingunn Holen and Dr. Penelope Ottewell

The University of Sheffield

Faculty of Medicine, Dentistry and Health

Department of Oncology and Metabolism

May 2022

My studentship and research was funded by Second Hope (now part of Breast Cancer Now)

Acknowledgements

First and foremost, I wish to express my gratitude for and thank my supervisor, Professor Ingunn Holen. I am very grateful for the opportunity to conduct this PhD in the first place, but also for her continued help and support over the duration of my PhD. I thank her for her help, support and knowledge, especially during the difficult times experienced during covid and lockdowns. Her guidance during the writing up of this thesis was especially valuable and has immensely benefited by academic writing. I would also like to expressly thank my co-supervisor Dr Penelope Ottewell for being more than a co-supervisor, as she was extremely helpful in practical tasks related to *in vivo* experiments that are the basis of most of my work. A big thank you to Professor Nicola J Brown too, whose Home Office Project licence facilitated the majority of my work.

A special mention must be given to all the members of the Holen and Ottewell labs. In particular, I would like to thank Alyson Evans, for being the best technician, a real resource and help in time of need, especially in cutting blocks for histology. Victoria Cookson really helped me in many experiments and provided me with cells integral to my experiments. Lewis Quayle was second to none in help with problems relating to dormancy and bioinformatics. Russell Hughes always had an interesting story and even more interesting information in regards to bone biology and really helped with PCR. Lubaid Saleh brought sunshine into the office and lab, helping me with many of my experiments. Diane Lefley was instrumental in my *in vivo* experiments, from setting up to finishing, as were Christopher George, Victor Canuas, Veli Kaan Aydin, Claudia Tulotta and Margheritta Puppo who was also a vital source of information for RNA extraction. All in all, without these people I would not have been able to perform all the experiments that I was able to.

I would also like to thank all the other members of staff in the University of Sheffield's department of Oncology and Metabolism who keep the various instruments running and reagents topped up, who are too many to mention. Special thanks to Orla Gallagher for her help with all things histology and Dr Timothy Wright for his help with RNA sequencing.

I would like to say that I would not even be at this stage if it wasn't for my loving, supporting family. My parents, Benson and Phyllis, I am eternally grateful for their presence in my life. My siblings, Daniel, Naomi and Deborah were also the best I could have chosen to help me get to this stage, and to continue to do life with. To my fiancée, Daisy, who has helped me through some of the hardest times of my life, especially during the time through which I completed this PhD, I cannot thank you enough.

Finally, I would like to thank the Almighty God, for life, for health and for all He has provided.

Declaration

I hereby declare that this thesis is an original report of my research work under the guidance of my supervisors Prof Ingunn Holen and Dr Penelope Ottewell. The experimental work was performed by myself and any contribution by others is explicitly indicated in the corresponding methodologies section. References have been provided on all supporting literatures and resources.

Abbreviations

Abbreviation	Meaning
BALB	Bagg and Albino (mouse strain)
BC	Breast Cancer
BHLHE41	Basic helix-loop-helix family member e41
BMC	Bone marrow cells
BMD	Bone mineral density
BMP	Bone morphogenetic protein
BMSC	Bone Marrow Stromal Cells
BSU	Biological Services Unit
CAPG	Macrophage-capping protein
CDK	Cyclin Dependent Kinase
CLP	Common Lymphoid Progenitor
CMP	Common Myeloid Progenitor
CPT	Cryoprotection
CXCL12	CXC motif chemokine-12
CXCL4	CXC motif chemokine ligand 4
CXCR4	CXC motif chemokine receptor-4
CaSR	Calcium Sensing Receptor
DC	Dendritic Cell
DFS	Disease Free Survival
DMFS	Disease Metastasis Free Survival
DMSO	Dimethylsulphoxide
DNA	Deoxyribonucleic acid
DPX	Proprietary brand name
DTC	Disseminated tumour cell
Dox	Doxorubicin
EBM	Embedding Media
ECM	Extracellular matrix
EDTA	EthyleneDiamineTetraacetic Acid
EDTA	Ethylenediaminetetraacetic acid
ELISA	Enzyme Linked Immuno-Sorbent Assay
EMT	Epithelial-to-mesenchymal transition
ER	Estrogen Receptor
ER	Oestrogen receptor
ERK	Extracellular signal-Regulated Kinase
FCS	Foetal Bovine Serum / Foetal Calf Serum
FCS	Foetal calf serum
FDG	FluoroDeoxy Glucose
FPPS	Farnesyl pyrophosphate synthase
GAS6	Growth arrest-specific 6

GCSF	Granulocyte Colony-Stimulating Factor
GIPC1	GIPC PDZ Domain Containing Family Member 1
GJIC	Gap-Junction Inter-cellular Signalling
GMCSF	Granulocyte Macrophage Colony-Stimulating Factor
HER2	Human epidermal growth factor receptor type-2
HLA	Human Leukocyte Antigen
HCMBD	Human Cancer Metastasis Database
HRP	Horseradish Peroxidase
HSC	Haematopoietic stem cell
i.c	Intracardiac
i.p	Intraperitoneal
i.v	Intravenous
IDO1	Indoleamine 2,3-dioxygenase 1
IGF	Insulin-Like Growth Factor
IL-6	Interleukin-6
IPP	Isopentenyl pyrophosphate
MAPK	Mitogen-activated protein kinase
MCP1	Monocyte Chemoattractant Protein 1
MEP	Megakaryocyte/Erythrocyte Progenitor
MET	Mesenchymal-to-epithelial transition
mg	Milligram
miRNA	micro RNA
ml	Millilitre
mm	Millimetre
MMP	Matrix Metalloproteinase
MMP2	Matrix metalloproteinase 2
MSC	Mesenchymal Stem Cell
N-BP	Nitrogen-containing bisphosphonates
NED	No Evidence of Disease
NR2F1	Nuclear receptor subfamily 2 group F member 1
OB	Osteoblast
OC	Osteoclast
OPG	Osteoprotegerin
OPN	Osteopontin
PARP	Poly (ADP-ribose) polymerase
p21	Cyclin-dependent kinase inhibitor-1
p27	Cyclin-dependent kinase inhibitor-1B
p38	p38 mitogen-activated protein kinase
PBS	Phosphate Buffered Saline
PCR	Polymerase Chain Reaction
PD	Programmed Death Ligand 1

PET	Positron Emission Tomography
PF4	Platelet Factor 4
PFA	Paraformaldehyde
PI3K	Phosphoinositide 3-kinase
PINP	N-terminal propeptide of type I procollagen
POSTN	Periostin
PPi	Inorganic phosphate
PR	Progesterone Receptor
PRM	Permeabilisation
PTH	Parathyroid Hormone
PTH1R	Type 1 Receptor for Parathyroid Hormone
PTHrP	Parathyroid Hormone Related Protein
PVP	PolyVinyl Pyrrolidone
RISC	RNA-Induced Silencing Complex
ROI	Region of Interest
ROS	Reactive Oxygen Species
SEM	Standard error of the mean
SNP	Single Nucleotide Polymorphism
SOX9	SRY-Box Transcription Factor 9
TGF	Transforming growth factor
THBSP1	Thrombospondin-1
TMB	3,3',5,5'-Tetramethylbenzidine
TNBC	Triple Negative Breast Cancer
TNBC	Triple-negative breast cancer
TRAP	Tartrate-Resistant Acid Phosphatase
VEGF	Vascular Endothelial Growth Factor
Zol	Zoledronic Acid
Zol	Acid
°C	Degrees Celsius
µCT	Computed MicroTomography
µg	Microgram
µl	Microlitre
µm	Micrometre

1 TABLE OF CONTENTS

Table of Figures

Summary

Advanced breast cancer is frequently associated with skeletal metastases characterised by dormancy and subsequent incurable metastatic outgrowth accompanied by skeletal related events. Disseminated tumour cells putatively assume residence in metastatic niches within the bone microenvironment, in locations that may be regularly occupied by resident cells and regulated by neighbouring cells in response to local and systemic signals.

My studies explored how modification of the bone microenvironment using a dietary approach (low calcium), a surgical intervention (ovariectomy) and pharmacological inhibition of bone resorption (Zol) impacted breast cancer cell development and progression within the bone *in vivo*.

The effect of a low calcium diet (0.1%) on the bone microenvironment of mature (12-week old) and dormant disseminated tumour cells was investigated in the absence and presence of bone-colonising tumour cells. In the absence of tumour cells, minor reductions of percent bone volume was detected after 28 days, with a reduction in PINP and increase in TRAP, without significant change to gene expression. Without existing literature on the effect of a low calcium diet on the outgrowth of *dormant* disseminated breast cancer cells, my research showed a low calcium diet in isolation did not sufficiently alter the bone microenvironment to trigger the outgrowth of *dormant* tumour cells.

To investigate the effect of repeated doses of Zol on outgrowing tumour cells in bone with rapid turnover, young (6-week old) mice were treated with four once-weekly clinically-relevant doses. Zol significantly increased trabecular percent bone volume, trabecular number and reduced trabecular separation. In agreement with existing literature Zol did not prevent or significantly delay the outgrowth of tumours in the bone with rapid turnover.

Profiling transcriptional changes to the mature (12-week old) bone microenvironment 14 days after ovariectomy, which has been shown to induce the outgrowth of dormant disseminated tumour cells, by RNA-seq revealed POSTN, MMP2, THBS2 and OPN as genes influencing the altered bone microenvironment. Comparison with publicly available RNA-seq data on the bone microenvironment of young (~30 years old), old (~73 years old) and old women treated with oestrogen for 3 weeks (~ 70 years old) found overlap between genes expressed by both young women and old women, suggesting caution in comparison. Comparing genes altered in the bone microenvironment of ovariectomised mice did not show overlap with genes found from *in vitro* dormant tumour cells. Deconvolution of bulk RNA-seq data to infer cell types did not show any significant differences. Further studies on dormancy gene signatures within the bone microenvironment are required.

1 INTRODUCTION

1.1. BREAST CANCER OVERVIEW

In the UK, cancer is the largest contributor to annual mortality, accounting for almost a third of all deaths. In the year 2014, this figure was approximately 167,000 persons. According to Cancer Research UK, 15% of new cancer cases in 2015 were breast cancer (BC), making it the highest-incidence cancer in the UK, with an increased rate of diagnosis of 20% from 1993 (UK, 2018), accounting for 11,563 deaths in 2016.

Despite an elevated incidence in diagnosis as compared to other cancer types among women, with 55,122 newly diagnosed in 2015, BC survival has been increasing (Coleman *et al*., 2011, UK, 2016, UK, 2018). The age-standardised 10-year breast cancer survival rate in women aged 15-99 shows a significant increase of 38% in survival statistics, from 40% in 1971, to 78% in 2011 (UK 2012). This is in part due to increased awareness, combined with early screening and a significant improvement in treatment options that are available for women with BC.

Breast cancer's represents multiple diseases, with 22 currently recognised morphological variants, that present a diverse mutational landscape (Sinn and Kreipe, 2013). However, stratification of BC remains in two broad groups; hormonal – also known as luminal and positive for either oestrogen receptor (ER+) or progesterone receptor (PR+) expression - and non-hormonal – also referred to as non-luminal and either positive or negative for human epidermal growth factor receptor - 2 (HER2) expression (see Figure 1-1) (Tong *et al*., 2018).

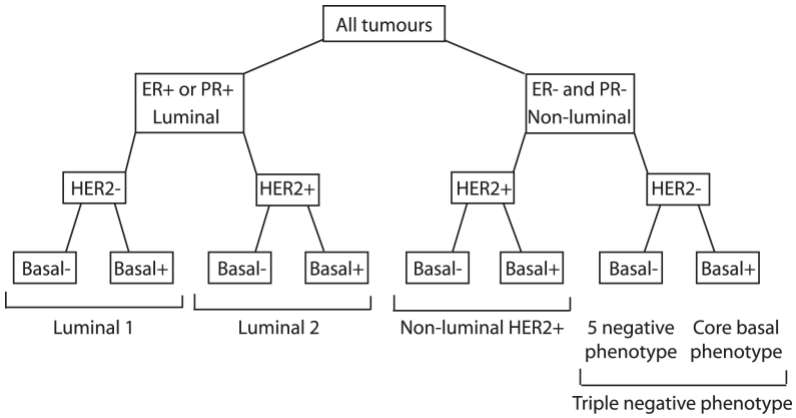

Figure 1-1: Breast cancer main sub-classes. Reprinted by permission from PLOS ONE: Medicine (Blows, Driver *et al*. 2010)

The sub-types of BC identified as hormonally-driven are more frequent in occurrence and have a more favourable outcome in comparison to the non-hormonal sub-type lacking HER2 expression, commonly called triple-negative BC (TNBC) (18.9% of BC patients), due to the advent of targeted therapies, such as Tamoxifen and Herceptin (Burt *et al*., 2017, Chen *et al*., 2008, Hudis and Gianni, 2011). Despite these improvements, breast cancer contributes to 7% of all deaths in the UK (2016 figures), and as such, warrants further investigation into improved therapies to maintain a trend of increasing survival (Cancer Research, 2016).

1.1.1 Current Therapies

For primary breast cancer, surgical excision of the bulk tumour tissue is the most common form of intervention in conjunction with adjuvant systemic therapy and/or radiotherapy. Systemic therapies used vary with molecular subtype and include Tamoxifen for ER+ and Herceptin for HER2+, which are therapies targeted at the particular molecular subtype. There is a further repertoire of drugs, such as Poly (ADP-ribose) polymerase (PARP) inhibitors olaparib and talazoparib used in situations where BRCA DNA repair protein mutations are clinically present, and alpelisib, a Phosphoinositide 3-kinase (PI3K) inhibitor and everolimus, an mTOR inhibitor, for postmenopausal women presenting with advanced HER2+ cancers. These targeted treatments have shown marked success for hormone-receptor positive and HER2+ cancers, but cytotoxic therapy remains the standard treatment for triple negative breast cancers (Lima *et al*., 2019).

1.1.2 Secondary Breast Cancer

Treatment of BC often results in no detectable re-occurrence in the primary breast tissue, yet it is estimated that 35% of patients with BC will develop secondary metastases at distant sites within 10 years of first diagnosis (Burt *et al*., 2017). Pan *et al.* performed a meta-analysis of 88 trials involving 62,923 ER-positive BC patients treated with endocrine therapy, and disease-free after 5 years; finding a steady recurrence from 5 to 20 years and showing significant recurrence in distant sites (Pan *et al*., 2017). This risk of recurrence persists and continues to increase beyond 20 years even for patients with the most favourable prognosis. Adjuvant chemotherapy in such cases achieves success, reducing 10-year recurrence by 30%, yet leaving an unmet clinical need (Demicheli *et al*., 2005). Better treatments targeting treatment-resistant cells may prevent or further delay onset of incurable metastatic disease, further improving patient outcomes.

1.2 Bone metastasis

Bone is a unique tissue rich in cells, yet possessing mineral characteristics that provide rigid structure. Bone has several compartments where cells of diverse origin and function reside (see Figure 1-2). It is the site of hematopoiesis and a major store for critical minerals, such as calcium and phosphate, as well as a store for growth-promoting cytokines and growth factors, such as insulin-like growth factor 1 (IGF-1) and transforming growth factor beta (TGFβ). As such, it provides a rich, complex, microenvironment that makes it favourable for the colonisation and growth of disseminated tumour cells.

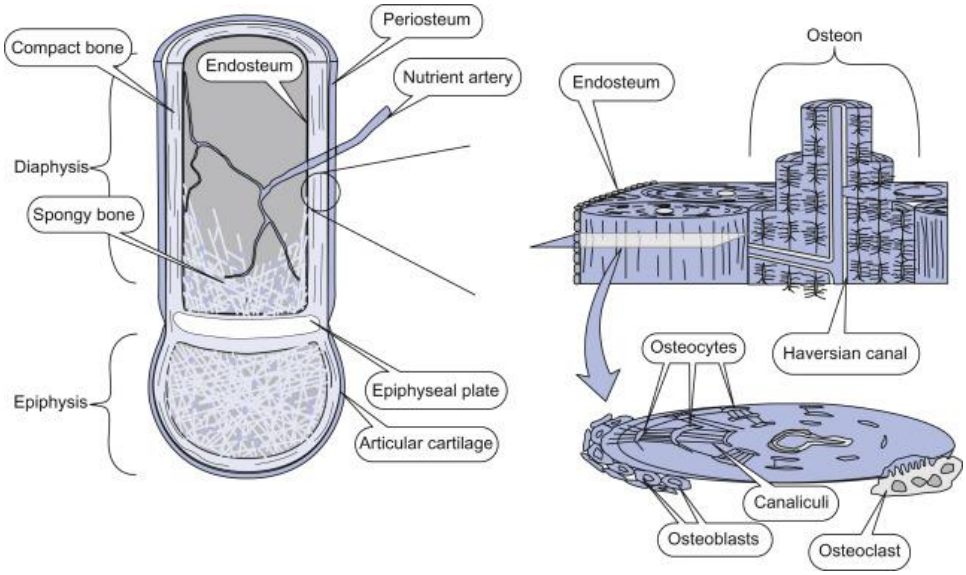

Figure 1-2: The various compartments of long bones. Reprinted by permission from Academic Press (Feher, 2017, Kennecke *et al*., 2010).

1.2.1 ORGANOTROPISM

Organotropism refers to a distinct affinity for tumour cells to metastasise to specific organs that is regulated by subtypes of the primary tumour, host organ microenvironment and cross-talk interactions between the cancer cells and the organ (Chen *et al*., 2018b).

Bone is a common organotrophic site for BC cell migration, and alongside the liver and lungs, represents a significant site of metastasis for BC cells. Disseminated tumour cells within the bone are found in up to 60-80% of BC patients, including those with multiple sites of metastasis. A further 17-37% of these patients harbor disseminated tumour cells that are solely in bone (Ahn *et al*., 2013, Coleman, 1997b, Yousefi *et al*., 2018). Disseminated tumour cells pose a significant challenge due to the ability to spread and colonise early; at diagnosis, 25-40% of patients are estimated to already possess bone disseminated tumour cells (DTC) (Ahn *et al*., 2013). One factor responsible for the prevalence of bone metastasis is the presence of chemotactic ligands secreted by bone resident cells, in particular stromal-derived-factor-1 (SDF-1 – also called CXCL12), as well as the expression of the ligands' associated receptor, such as CXCR4 receptor for SDF-1 ligand, making this site particularly favourable to disseminated BC homing (see Figure 1-3) (Wang *et al*., 2006).

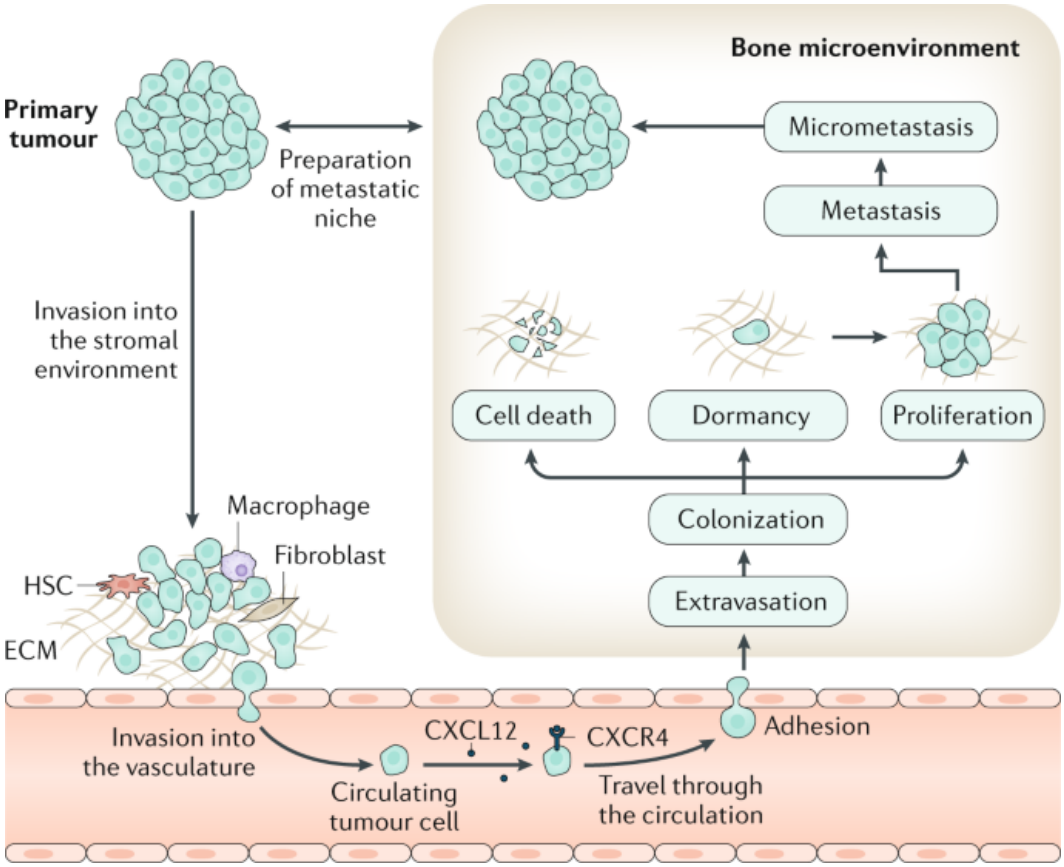

Figure 1-3: The steps of breast cancer bone metastasis. Cross-talk between the primary tumour and bone microenvironment prepare the metastatic niche, followed by invasion into stromal environment supported by tumour associated cells. Intravasation, circulation and subsequent homing to the bone through chemotaxis ensues. Extravasation and colonisation into the bone microenvironment whereby a proportion of BC cells successfully engraft and often undergo a period of dormancy prior to escape into overt metastasis. Reprinted by permission from Springer Nature (Coleman *et al.*, 2020b)

Upon recurrence of metastases in the bone, the disease is seldom curable. Current treatment for BC bone metastases is therefore mainly aimed at symptom palliation and preventing disease progression (Kennecke *et al*., 2010). In addition, to mortality associated with bone metastases, skeletal-related events increase morbidity of those living with significant tumour burden in the bone(Coleman and Rubens, 1987) (Clemons *et al*., 2012).

Skeletal-related events (SREs) in BC, primarily a result of osteolytic activity, include fractures, bone pain, hypercalcaemia, spinal cord compression and osteoporosis are problematic complications of bone metastases that have a negative impact on quality of life of BC patients (Clemons *et al*., 2012). The current volume and proportion of women experiencing BC bone metastases compels further research to unravel mechanistic understanding and possible interventions to extend life and improve its quality.

1.3 THE BONE MICROENVIRONMENT – MULTIPLE ROLES IN TUMOUR DEVELOPMENT AND PROGRESSION

The bone microenvironment is rich in cellular heterogeneity, being the site of hematopoiesis, as well as development of various constituents of bone. As such, it harbours many resident cells that have been shown to interact with metastatic tumour cells. The most important cells will be discussed in the following sections.

1.3.1 OSTEOCLASTS

Osteoclasts are cells from a hematopoietic lineage whose differentiation and activation heavily relies on macrophage colony-stimulating factor (M-CSF) and Receptor Activator of NFκB (RANK) ligand (RANKL) (Dougall, 2012). Indirect activation of osteoclast-induced bone resorption occurs through induction of osteoblast RANKL expression, such as through PTHrP and PGE_2.

Increased osteoclast-mediated bone resorption results in the release of tumour-promoting growth factors stored in the bone matrix, thereby activating proliferation signalling cascades in local cancer cells (Guise, 2002). Treatment with osteoclastic activity-inhibiting agents prevented outgrowth of tumours from DTCs, providing mechanistic evidence for a role for osteoclasts in this process (Ottewell *et al*., 2015). Activation of osteoclast activity may therefore be a mechanism by which quiescent DTCs escape dormancy and are triggered to proliferate by initiating the vicious cycle.

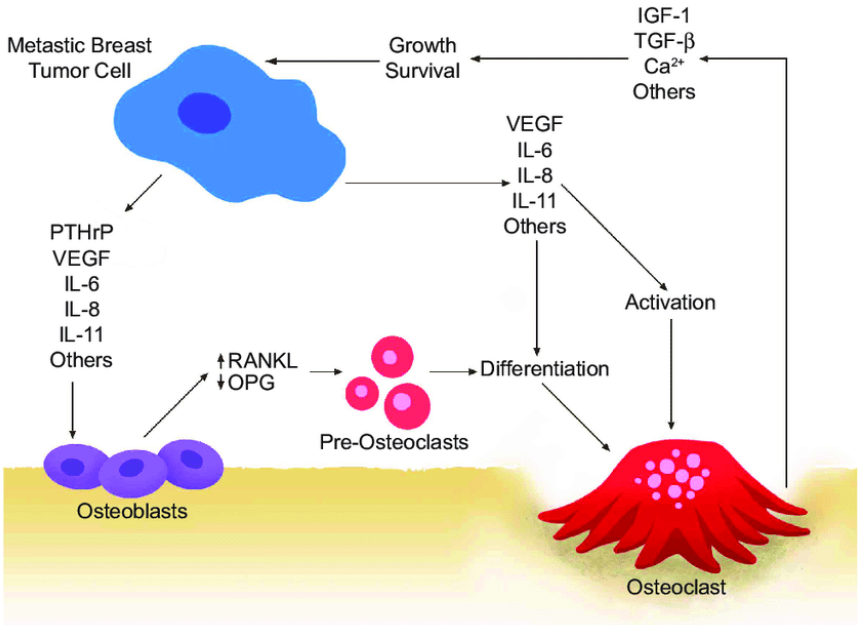

Figure 1-4: Multinucleation and differentiation of osteoclasts stimulated by various factors secreted by osteoblasts and tumour cells. Awakening of tumour cells by release of TFG-B and IGF-1 release following bone degradation may be sufficient to reverse dormancy into overt outgrowth. Reprinted by permission from International Journal of Molecular Science (Shemanko *et al*., 2016)

Soluble mediators of inflammatory activity, such as IL-1, IL-6 and TNFα, also drive osteoclast formation (Liu *et al*., 2005). The immune system is also involved in balancing excess bone resorption through inhibition of osteoclast formation by molecules such as IFN- γ, IL-4 and IL-10 (Dar *et al*., 2018). A number of cytokines (IL-4, IL-5, IL-10, IL-12, IL-13, IL-18), granulocyte-macrophage colony stimulating factor (GM-CSF) and interferons IFNα/β/γ produced by the immune component of the bone

microenvironment are further potent inhibitors of osteoclastogenesis, acting via inhibition of RANKL signalling (Del Fattore and Teti, 2012, Zhao and Ivashkiv, 2011).

1.3.2 Osteoblasts

Osteoblasts are cells of a mesenchymal origin, constituting approximately 4-6% of all bone cells, and are responsible for the formation of bone through the production of an organic collagenous matrix which is subsequently hardened by the deposition of inorganic mineral components such as calcium and phosphate (Mansour *et al*., 2017). Osteoblasts are also important in the maintenance of the hematopoietic stem cell (HSC) niche. Although the liver is the primary site of hematopoiesis during fetal development, HSCs subsequently home to the bone after birth, mediated by the secretion of SDF-1 (CXCL12) by osteoblasts, providing a chemotactic response by SDF-1 receptor CXCR4 expressed by HSCs, whereby they are maintained in close proximity to osteoblasts through this continual chemotactic call and response (Sugiyama *et al*., 2006).

The mechanisms whereby osteoblasts create and maintain the HSC niche also play a key role in the establishment of bone metastases due to their role in the homing of metastatic breast cancer cells. The key ligand/receptor axis responsible for breast cancer metastases to the bone is the interaction between the CXRC4 receptor expressed by the breast cancer cells, responding to chemotactic signals by the SDF-1(CXCL12) ligand secreted by osteoblasts, similar to HSC homing (Devignes *et al*., 2018). Furthermore, osteoblasts also regulate osteoclast function, through the secretion of M-CSF, RANKL and OPG, leading to an increase (M-CSF & RANKL) or reduction (OPG) of osteoclastogenesis which may encourage the growth of disseminated tumour cells within the bone (Boyce and Xing, 2007, Yamashita *et al*., 2012).

1.3.3 Osteocytes

Osteocytes are the most abundant cell type in the bone, differentiated from mature osteoblasts that are subsequently encased in the bone matrix. They are a major source of RANKL, regulating bone turnover. However, their role in altering tumour growth within the bone is not well characterised. Early research has suggested roles for osteocyte-secreted adenosine in the promotion of breast cancer cells (Zhou *et al*., 2015), while other groups have suggested that pressure exerted by prostate cancer bone metastases on the bone stimulates an increase of CCL5 and matrix metalloproteinases that alter the bone microenvironment and aid in secondary prostate cancer progression within the bone (Sottnik *et al*., 2015).

1.3.4 Mesenchymal Stem Cells

Mesenchymal stem cells (MSC) are pluripotent stem cells within the bone marrow with the ability to differentiate into a variety of cells including fibroblasts, chondrocytes, osteoblasts and adipocytes. These cells have been shown to associate proximally with various tumour types, promoting proliferation and migration, inducing a transcriptional shift in tumour cells that promotes disease

progression (Gasparetto, 2004, Karnoub *et al*., 2007, Zhang *et al*., 2013). However, the presence of MSCs is not entirely associated with poor prognosis, and in the case of multiple myeloma, are used in cell-based therapies such as autologous stem cell transplants to recover immune function, as well as agents for therapeutic agent delivery due to their tendency to locate close to tumour cells (Atsuta *et al*., 2013, Bi *et al*., 2014).

1.3.5 Cancer Associated Fibroblasts

Fibroblasts are stromal cells found in various tissues within the body that have become increasingly important in cancer biology (Augsten, 2014). Fibroblasts closely associated with tumours are referred to as cancer-associated fibroblasts (CAFs) and can act either as promoters or suppressors of cancer. CAFs have been extensively studied in primary tissue, and have been shown to promote tumour invasion, angiogenesis, matrix stiffening and chemoresistance (Calvo *et al*., 2013, Logsdon *et al*., 2017). Furthermore, they participate in lactate shuttling, a phenomenon key to the altered metabolism characteristic of tumour cells. CAFs can travel with metastatic cells from the primary site to the metastatic site and modulate tumour supportive immune cells, whose immunomodulatory function is enhanced through cross-talk with cancer cells(Duda *et al*., 2010, Harper and Sainson, 2014). Importantly, unlike transient and short lived tumour resident and infiltrating immune cells, CAFs persist under normal circumstances, meaning secreted molecules including cytokines and growth factors, as well as immune-modulatory functions can be sustained for a significant duration and therefore significantly impact the microenvironment within which they reside (Kraman *et al*., 2010). Fibroblasts are found within the bone microenvironment, differentiating from mesenchymal stem cells, both of which expand prior to tumour colonisation to the bone in the pre-metastatic niche and have been shown to have a significant role in establishing bone-tropic tumours (Mukaida *et al*., 2020, Quante *et al*., 2011).

1.3.6 Adipocytes

The bone marrow is a tissue highly enriched in adipocytes, whose role in mediating breast cancer colonisation and disease progress is being uncovered. Adipocytes are cells from the mesenchymal lineage, closely related to osteoblasts in differentiation steps, which results in an inverse reciprocal relationship between osteoblastogenesis and adopogenesis (Liu *et al*., 2020). Adipocytes act as storage of adipose tissue, but have been shown to serve as an endocrine organ through their secretion of signalling molecules, such as adipokines, cytokines, chemokines and growth factors that result in facilitating recruitment, invasion, survival, colonisation and proliferation of breast cancer cells, in addition to inducing angiogenesis and immune modulation (Liu *et al*., 2020). Further to producing various classical signalling molecules, adipocytes also secrete glycerol and free fatty acids (FFA) derived from stored lipids in the form of triglycerides and lipid droplets (Granneman and Moore, 2008, Martin and Parton, 2006). Released FFAs can be taken up by tumour cells in the microenvironment facilitated by lipid transporters such as translocase (CD36; FAT) and fatty acid-binding protein 4 (FABP4), which results in increased breast tumour cell proliferation (Zhao *et al*., 2017). The presence of tumour cells can further increase the lipolysis of stored lipids into glycerol and FFAs through

deactivation of adipose triglyceride lipase (ATGL) and phosphorylation of hormone-sensitive lipase (HSL) (Granneman *et al*., 2007, Haemmerle *et al*., 2006). The interaction between bone marrow adipocytes and metastatic tumour cells is under continued investigation which may provide potential therapeutic targets.

1.3.7 MACROPHAGES

Macrophages are mononuclear myeloid cells that originate from monocytes within the bone microenvironment whose differentiation, growth and chemotaxis are controlled by chemokines that include CCL2 (MCP-1 (monocyte chemoattractant protein 1)) and colony stimulating factor (CSF) 1 (Sierra-Filardi *et al*., 2014).

Macrophages form complex interactions with B cells and T cells modulating the adaptive response, which results in a modulated response to tumours. Activation within the microenvironment can induce polarization and activation into two broad phenotypes, whose effect on tumour development is divergent (Yunna *et al*., 2020). A pro-inflammatory and anti-tumour phenotype characterised by the secretion of IL-1, IL-6, IL-12 and IFN-γ which recruit and activate effector T cells responsible for eradication of tumours. In contrast, tumour-associated macrophages (TAMs) secrete factors such as IL-10 and TGF-β, suppressing $CD4^+$ helper T cells and $CD8^+$ effector activity, MMP-9 that remodels the extra-cellular matrix and VEFG-A; inducing angiogenesis that subsequently supports tumour growth and secreting reactive oxygen species (ROS) that maintain an inflammatory environment which is linked to poor prognosis (Biswas *et al*., 2006, Qian and Pollard, 2010). Within the bone microenvironment, osteal macrophages (osteomacs) exhibit similar phenotypes to the M1 and M2 polarised subtypes. However, through the combination of RANKL and M-CSF, osteomacs can differentiate into osteoclasts, altering bone metabolism balance to favour increased breakdown which supports tumour growth (Jeganathan *et al*., 2014). Further research is ongoing into defining the role of osteomacs in bone metastatic tumour growth.

1.3.8 MYELOID DERIVED SUPPRESSOR CELLS (MDSCS)

Myeloid derived suppressor cells (MDSCs) are a heterogenous group of cells consisting of immature macrophages, granulocytes, dendritic cells and myeloid progenitor cells, characterised by $CD11b^+Ly6G^{low}Ly6C^+$, a majority of which are interleukin-4Rα (IL-4Rα$^+$) and $F4/80^+$ (Buenrostro *et al*., 2014, Highfill *et al*., 2010). MDSCs have two broad cellular populations; one derived from monocyte populations (M-MDSC), and another derived from immature polymorphonuclear cells (PMN-MDSC), which are phenotypically and morphologically similar to monocytes and neutrophils respectively (Marvel and Gabrilovich, 2015). Within the tumour microenvironment, MDSCs have been characterised by immune suppression, by the expression of IL-10, TGF-β, arginase (ARG1), inducible nitric oxide synthase (iNOS) and sequestration of cysteine. This results in increased T-reg induction and reduces the expression of L-selectin by T-cells, creating an immunosuppressive environment that is less restrictive to tumour growth (Lindau *et al*., 2013, Youn *et al*., 2008). MDSCs have also been implicated in the remodelling of the tumour environment, EMT promotion and preparation of a pre-

metastatic niche (Ya *et al*., 2022). MDSCs are predominantly derived from the bone marrow where they are generated through granulocyte-macrophage colony stimulating factor (GM-CSF) and may affect tumour growth (Highfill *et al*., 2010). Targeting MDSCs therapeutically is an area of increasing research in the hope of deriving immunotherapeutic benefit.

1.3.9 T CELLS

T cells comprise a part of the adaptive immune system and are vital cells to antitumour response that mature in the thymus. T cells are frequently characterised into two broad categories dependent on the presence of a cell surface antigen; $CD4^+$ (helper cells) and $CD8^+$ (effector cells) (Seder and Ahmed, 2003). Research has demonstrated a clear role for $CD8^+$ cytotoxicity being vital to an antitumour response characterised by the secretion of IFN-γ. In breast cancer, IFN-γ secreting $CD8^+$ T cells have been shown to improve tumour burden by facilitating apoptosis and inducing growth arrest in a FVBN202 mouse mammary carcinoma (MMC) model (Kmieciak *et al*., 2011, Kmieciak *et al*., 2013). This is supported in work by Koebel *et al.* (2007) and Romero *et al.*(2014) whose data showed CD8+ ablative treatment induced overt regrowth of previously undetectable tumours in mice (Koebel *et al*., 2007, Romero *et al*., 2014). Vitetta *et al.* further showed BCL_1-Id* immunisation, that subsequently activates CD8+ T cells, conferred reduced growth compared to nude mice lacking FOXN1 gene; a regulator of thymus epithelial development and thus lacking adaptive T cell development (Vitetta *et al*., 1997). However, resistance to $CD8^+$ by cancer cells occurs through the downregulation of MHC I, and may further evade CTL targeting by overexpression of B7-H1 and B7.1, IL-3 and inactivation of SOCS1, a JAK/STAT negative regulator.

A downregulation or mutation of major histocompatibility complex I (MHC I) molecules may be a mechanism in the immune-evasion of tumour cells, as well acting as a cell-cycle regulator further associating it with the dormant phenotype (Garrido *et al*., 2012). The MHC I cell surface receptor, critical for $CD8^+$ T cell recognition, has been found to be downregulated in bone marrow (BM) DTCs isolated from patients, as well as the presence of MHC I^{low} Lgr5-GFP stem populations in patient hair follicles treated with adoptive transfer of T cell receptor (TCR) engineered cells (Agudo *et al*., 2018). This is further purported in mice where fibrosarcoma GR9-B11 dormant DTCs exhibited low/negative expression of MHC I compared to high expression in the primary site in murine models, suggesting downregulation of MHC I as an accessory avoidance of immune destruction (Romero *et al*., 2014). Downregulation of antigen presenting molecules MHC I and TAP proteins via transactivator NLRC5 reportedly assist quiescent muscle and hair follicle stem cells avoid T cell mediated elimination, and is reversed in cell cycle entry, linking antigen presentation, dormancy and immune evasion (Agudo *et al*., 2018). Induction of epigenetic alterations producing antigen loss via MHC I and upregulation of PD-L1 have also been shown to be effects of IFN-γ secreted by $CD8^+$ cells on tumour cells (Kmieciak *et al*., 2013, Payne *et al*., 2016). In addition to this evasion, $CD8^+$ T cells are in low abundance within the bone microenvironment and may not be very effective against tumour cells within the bone microenvironment (Mendoza-Reinoso *et al*., 2020).

A specific subset of $CD4^+$ T helper (Th) cells found within the bone microenvironment, Th17, is considered an inducer of osteoclastogenesis due to secretion of TNFα and RANKL, but lower IFN- γ expression than other Th cells. Furthermore, the Th17 subset is responsible for the production of IL-17, which drives osteoblast-mediated RANKL secretion (Sato *et al*., 2006). Roy *et al.* (2011) studied the correlation between type II collagen-induced inflammation on production of IL-17 and secondary metastases in a MMT-PyVMT mouse model, finding significant increases in secreted pro-inflammatory cytokines IL-17, IL-6, pro-MMP9, IGFII and M-CSF. Subsequent treatment with anti-IL-17 antibodies showed a reduction in the development of secondary metastases (Roy *et al*., 2011). This effect was accompanied with decreased numbers of osteoclasts and bone resorption, implicating osteoclasts in the development of secondary metastases. A conflicting role for IL-17 in osteoclast development has been proposed in the stimulation of GM-CSF, thereby inhibiting osteoclastogenesis , but evidence from mouse models have shown reduced osteoclast formation and activity with IL-17 inhibition, suggesting any downstream GM-CSF stimulation is outweighed by its pro-osteoclastogenic potency (Noster *et al*., 2014). Inhibition of Th17 cells within the bone microenvironment may reduce the potential for tumour growth by reducing the rate of osteoclast formation and activity.

1.3.10 T REGULATORY CELLS

T regulatory cells (Tregs) are regulators of the immune system that are critical to stifling the immune response and preventing excessive inflammation. The most well characterised subset of Tregs is the $CD4^+$ $Foxp3^+$ population, which either mature in the thymus, and thus classified as natural Tregs (nTreg) or can be induced from naïve $CD4^+$ cells in the periphery through TGF-β and IL-2, subsequently classed as induced Tregs (iTreg) (Adeegbe and Nishikawa, 2013). Tregs have various immunosuppressive functions, including the expression PD-1 and PD-L1 (Francisco *et al*., 2009). Due to this immunosuppressive phenotype, a high infiltration of Tregs within the tumour microenvironment is associated with poor outcome, as they repress the activity of immunoactivating $CD4^+$ helper cells and tumouricidal $CD8^+$ effector T cells (Jacobs *et al*., 2009). Tregs reside in the bone microenvironment where they play a role in maintaining hematopoietic stem cell homeostasis and contribute to the pro-hematopoietic immune privilege (Hirata *et al*., 2018, Nishikawa and Sakaguchi, 2010, Wang, 2006). Reducing the amount of Tregs and/or their influence on immune suppression within the bone microenvironment may improve the outcome of tumour therapies due to a reduction in immunosuppression, similar to immunotherapies targeting checkpoint blockades (Darvin *et al*., 2018).

1.3.11 NATURAL KILLER CELLS

Natural killer (NK) cells form a part of the innate immune system and play an important part in anti-tumour immunity by targeting tumour cells having stress induced markers, such as NKG2D or cells with downregulated MHC I antigen presenting receptors (Diefenbach *et al*., 2001). NK cells act by Fas-Fas ligand interactions as well as granule mediated exocytosis. This tumour-cytotoxic role is observed in the bone, where depletion of NK cells in bone metastasis mouse models have resulted in uncontrollable proliferation (Bidwell *et al*., 2012). NK cells can express PD-1, which can be activated

by PD-L1 expressed by bone resident Tregs and stromal cells, reducing their activity within the bone microenvironment (Quatrini *et al*., 2020). Increasing the activity of NK cells within the bone may result in increased eradication of secondary tumour cells.

Various cells play an important role in supporting or eliminating tumour cells within the bone microenvironment, which may provide promising therapeutic targets in addition to direct targeting of tumour cells within the bone microenvironment in order to achieve complete eradication of disseminated cancer cells.

1.4 Therapeutic Strategies for Bone Metastases

Current therapeutic strategies for BC bone metastases focus on reducing or slowing down the rate of tumour growth and alleviating SREs. These are often combination therapies targeting both the tumour and bone-resident cells responsible for osteolysis. Therapies used follow similar modalities to those used on the primary tumour, although due to the mineralised nature of bone, surgery is not often performed to remove the secondary tumour in the bone. Treatments include chemotherapy, radiotherapy, targeted agents (such as EGFR inhibitors and ooestrogen receptor inhibitors) and CDK4/6 inhibitors (such as Palbociclib). However, these treatments are not curative in a secondary setting, also often having resistance built up from treatments to the primary tumour. Increasing research shows promise in targeting the microenvironment in conjunction to targeting the cancer cells themselves in order to enhance current clinical endpoints. The following section will focus on strategies targeting the bone microenvironment.

1.4.1 RANK/RANKL inhibitors

RANKL, along with osteoprotegerin (OPG), act as key regulators of osteoclast development, affecting osteoclast-mediated bone resorption. RANKL is expressed on the surface of osteoblasts as a transmembrane protein which can be cleaved by proteases to release a soluble form. Both membrane-bound and soluble RANKL bind to osteoclast precursors expressing RANK, the target receptor for RANKL, leading to the formation of mature, multinucleated osteoclasts. Activated osteoclasts contributed to cancer-induced bone disease by degrading the bone matrix. A growing body of evidence suggests RANKL/RANK also plays an important role in the expansion of tumour cells in bone (Clezardin and Teti, 2007, Kearns *et al*., 2008).

Denosumab, a fully human monoclonal antibody against RANKL, is approved for use in secondary bone cancer of solid tumour origin, such as breast, kidney and lung. It is also used in men with prostate cancer suffering weakened bones due to hormonal therapy, as well as menopause-related bone fragility. Denosumab has shown superiority to other bone-targeted agents in delaying time to first, as well as reducing time to subsequent SREs in patients with secondary breast cancer within the bone. However, despite success in palliating cancer-induced bone disease, it does not show significant benefit in overall survival compared to bisphosphonates (Stopeck *et al*., 2010, Thomas *et al*., 2010).

1.4.2 SRC INHIBITORS

c-Src is part of a family of non-receptor tyrosine kinases which is involved in signal transduction downstream of various cell surface receptors such as integrins, E-cadherin and tyrosine kinase receptors. In addition it plays an important role in osteoclast function due to its activation in response to RANK/RANKL binding in conjunction with TRAF6 recruitment (Boyce *et al*., 2006) . In experimental models, mice that lacked src expression were protected from tumour-associated bone destruction, demonstrating that src-defective osteoclasts do not resorb bone (Bakewell *et al*., 2003). Src is also secreted by metastasized tumour cells into the microenvironment which may exacerbate tumour-induced bone destruction by increased osteoclast activation.

Several Src inhibitors, such as saracatinib, have been developed and have shown early efficacy in decreasing the levels of bone resorption markers in solid tumours and reduction of bone resorption similar to bisphosphonates (Baselga *et al*., 2010, M. Aklilu, 2011) . Preliminary data in randomised trials have shown dasatinib, another src inhibitor, was well tolerated and improved progression free survival in breast cancer patients with symptomatic bone metastases (Mayer *et al*., 2011). However, conflicting findings have suggested no improvement in reported pain or bone turnover markers in breast cancer patients with bone metastases, where the authors suggested further evaluation should rely on molecularly-defined patient cohorts (Schott *et al*., 2016).

1.4.3 TGF-B BLOCKADE

Transforming growth factor beta (TGF-β) is a multifunctional cytokine involved in various processes, inducing proliferation. Within the skeletal tissue it is found within the bone matrix and is released upon bone resorption. TGF-β acts as a major growth factor, which drives metastasis and the growth of disseminated tumour cells. It acts by binding transmembrane receptors ALK5, TβRI and TβRII, leading to the phosphorylation of intracellular signalling molecules Smad2 and Smad3 that form a complex, binding Smad 4 before translocating to the nucleus. Here, the Smad complex regulates the transcription of many factors, such as integrin αvβ3, IL-6, IL-8, IL-11, MMP-1 and CXCR-4 that are involved in the proliferation and formation of bone metastases of solid tumours, such as breast cancer. Within the bone microenvironment, TGF-β further stimulates breast cancer cells to secrete molecules such as parathyroid hormone related protein (PTHrP), IL-11 and connective tissue growth factor (CTGF(CCN2)) which induce osteoblasts into reducing OPG secretion and increasing RANKL secretion, further driving osteolysis.

Several treatment modalities have been developed in an attempt to inhibit TGF-β signalling in experimental breast cancer bone metastases, such as neutralising antibodies that sequester the protein itself, antisense oligonucleotides and small molecule inhibitors of TβRI. *In vivo* experiments have found that inhibition of TGF-β signalling reduces severity and incidence of osteolytic lesions, reversing bone loss (anti- TGF-β antibody 1D11) (Biswas *et al*., 2011), decreased tumour growth and progression (SD-208, a small molecule dual inhibitor of HIF1-α and TβRI) , and significantly reduced occurrence osteolytic bone metastases (YR-290, small molecule inhibitor of TβRI) (Fang *et al*., 2013).

Despite success *in vivo*, TGF-β treatments have not found corresponding success in clinical trials(Teixeira *et al*., 2020). It is thought that a poor understanding regarding the dual role of TGF-β signalling in cancer, dynamic signalling, functional differences of TGF-β freely solution compared to exosomes and the regulatory effects of the tumour microenvironment, such as by cancer-associated fibroblasts impact targeting this protein in a clinical setting (Teixeira *et al*., 2020).

1.4.4 CATHEPSIN K INHIBITORS

Cathepsin K is a potent member of the lysosomal cysteine protease family, playing an integral role in bone resorption which is regarded as a multi-step process. The role of cathepsin K secreted by osteoclasts into the resorptive pit is to mediate the proteolysis of type I collagen in the demineralisation of the bone matrix by osteoclast-secreted protons. A loss-of-function mutation in the human cathepsin K gene is found in patients with pycnodystosis, a rare genetic disorder characterised by impaired osteoclastic bone resorption, which phenotype is recapitulated in mice that have this gene ablated. In contrast, overexpression of cathepsin K in mice results in increased osteoclast-mediated bone resorption (Kim *et al*., 2009). These findings demonstrate the critical role cathepsin K plays in bone resorption, and has been the subject of preclinical investigation as a therapeutic agent in the setting of breast cancer bone metastasis.

In animal models of breast cancer bone metastasis, cathepsin K inhibitor AFG-495 showed a reduction of skeletal tumour burden and bone destruction (Le Gall *et al*., 2007). Although breast cancer cells also secrete cathepsin K, reduction of tumour burden was limited to skeletal sites, whereas sub-cutaneous tumours did not (Clezardin and Teti, 2007). Despite moderate success in preclinical studies, clinical trials of cathepsin K inhibitors have been characterised by shortcomings due to off-target toxicities, such as that exhibited by nitrogen-containing balicatib, whose lysosomotropic properties leads to accumulation in lysosomes and results in the inhibition of other cysteine cathepsins. This drug was withdrawn from a 12-month phase III trial in human osteoporosis patients due to adverse skin effects (Le Gall *et al*., 2008). Odacatinib, which does not exhibit the lysosomotropic effects of balicatib, was also withdrawn from clinical trials despite reducing resorption markers in women with breast cancer bone metastases following 4 weeks of treatment (Jensen *et al*., 2010).

1.4.5 CXCR4 INHIBITORS

C-X-C motif chemokine receptor type 4 (CXCR4) is a chemotactic receptor expressed by most cells including hematopoietic and endothelial cells (Shiozawa *et al*., 2011). The ligand for CXCR4, CXCL12 (stromal cell derived factor 1 (SDF-1)), is highly expressed by osteoblasts and acts as a mediator of chemotaxis of several cells towards the osteoblastic niche, such as hematopoietic stem cells (Sharma *et al*., 2011). Breast cancer cells overexpress CXCR4, which plays a significant role of bone homing by disseminated tumour cells, but also plays a role in their survival (Xu *et al*., 2015).

In experimental models, CXCR4 blockade by neutralising antibodies or synthetic antagonist led to a reduction in metastasis to bone and lung by CXCR4 expressing breast cancer cells. A phase I/II trial of

CTCE-9908, a synthetic peptide antagonist demonstrated safety, tolerability and modest response, with 6 patients out of 20 (30%) with advanced metastatic disease and no response to standard treatments having overall stable disease (Wong and Korz, 2008). However, concerns relating to the blockade of the CXCR4-CXCL12 axis leading to increased bone resorption, as indicated by preclinical data, have been raised as this may make the bone a more favourable site for tumour growth, slowing down development of anti-CXCR4 therapies (Hirbe *et al*., 2007).

1.4.6 INTEGRIN INHIBITORS

During bone resorption, osteoclasts form an actin ring surrounding the ruffled border vital to bone resorption. Furthermore, a sealing zone surrounding the resorption pit is formed by binding of vitronectin to osteoclast cell surface proteins. These functions are mediated by integrins, which play a significant role in osteoclast-mediated bone resorption. In particular, αvβ3 is key in osteoclast activity. Knockout of αvβ3 in mice, whose intracellular signal transduction involves c-Src and Syk, led to poor bone resorption and the development of osteopetrosis (Zou *et al*., 2007). Interestingly, treatment with αvβ3 antagonist PSK1404, showed reduced bone loss and tumour *in vivo* as well as some antiangiogenic effects *in vitro* (Zhao *et al*., 2007). Another antagonist, GLPG0187, reduced metastatic lesions and bone-metastatic ability *in vivo*, with reduced osteolytic tumour burden when combined with zoledronic acid or paclitaxel (Li *et al*., 2015).

1.4.7 DKK INHIBITORS

Dkk-1 is an inhibitor of osteoblastogenesis. Wnt-1 promotes osteoblastogenesis by binding to frizzled, which, in association with low-density lipoprotein (LRP) 5/6, leads to downstream β-catenin signalling and subsequent activation of genes involved in osteoblast differentiation and maturation. DKK-1 inhibits this process by binding to LRP5/6, preventing interaction with Wnt-1 and the prevention of the downstream signalling cascade. Blockade of DKK-1 through neutralising antibodies led to increase of osteoblast number, osteocalcin and trabecular bone in animal models of multiple myeloma (Yaccoby *et al*., 2007) (Fulciniti *et al*., 2009). This was also accompanied by a corresponding decrease of osteolysis and skeletal tumour growth, making DKK-1 an attractive target for cancer-induced bone disease. There are currently no trials of DKK-1 in breast cancer, but there have been studies into a Dkk-1 neutralising antibodies in relapse/refractory multiple myeloma in combination with zoledronic acid (Iyer *et al*., 2014). Further research is warranted to fully characterise the potential of Dkk-1 in breast cancer bone metastatic setting.

1.4.8 ACTIVIN A INHIBITORS

Activins are dimeric glycoproteins consisting of two alpha or beta subunits and belong to the TGF-β superfamily. Since the discovery of activins in 1986, they have been characterised as hormones, growth factors and cytokines. In particular, the activin A isoform was the most important in human physiology, being expressed in reproductive organs, brain, liver, lung, bone and the gut (Bloise *et al*.,

2019). Activin A regulates bone formation and regeneration, enhancing processes such as joint inflammation and rheumatoid arthritis.

Activin A acts by binding transmembrane serine/threonine kinase receptors; Act RII type-II receptor (Act RIIA) leading to recruitment and phosphorylation of ActRIB or activin-like kinase (ALK)4 type I receptors. Downstream signals are mediated by Smad2 and Smad3 entering the nucleus in conjunction with Smad4. This leads to inhibition of osteoblast differentiation and increasing osteoclast differentiation (Leto, 2010). Importantly, activin A has been found significantly increased in the serum of breast and prostate cancer patients with bone metastases (Leto *et al*., 2006).

In murine models of myeloma and breast cancer, blockade of activin A has shown stimulation of bone formation and reduction in osteolytic lesions (Leto, 2010) (Leto *et al*., 2006).

1.4.9 BISPHOSPHONATES

Bisphosphonates (BPs) are anti-resorptive agents that reduce bone loss by targeting osteoclast activity and are established therapeutics for osteolytic inflammatory and tumour-associated bone disease (Drake *et al*., 2008). In addition to BPs' success in inhibiting bone loss due to inflammation and cancer through selective induction of osteoclast apoptosis, they have been increasingly studied for their direct effects on tumours and immune modulation.

BPs are analogues of inorganic pyrophosphate (PPi). The structure of BPs allows the chelation of divalent metal ions and thus have high affinity for the bone, the body's main reservoir of calcium (Drake *et al*., 2008). This results in rapid systemic clearance and concentration in the bone due to BPs' affinity for hydroxyapatite crystals on the bone mineral surface. BPs are generally classified into two groups; non-nitrogen-containing (etidronate, clodronate and tiludronate) and nitrogen containing (alendronate, risedronate, ibandronate, pamidronate, and zoledronic acid), distinguished by the presence of nitrogen-containing R^2 side chains bound to the central carbon (Drake *et al*., 2008). Non-nitrogen-containing BPs possess structural similarity to PPi and are incorporated into newly formed adenosine triphosphate (ATP) by class II aminoacyl-transfer RNA synthases (Russell, 2006). These ATP analogues are non-hydrolysable and inhibit ATP-dependent cellular processes resulting in apoptosis after intracellular accumulation. Farnesyl pyrophosphate synthase (FPPS) is the primary target of nitrogen-containing bisphosphonates (N-BP) and subsequently results in the inhibition of protein prenylation leading to apoptosis (Dunford *et al*., 2001). Osteoclasts are considered to be the only cells capable of acidifying bone. They form a sealing zone by binding vitronectin on the bone surface, followed by acidification by the release of protons and tartrate-resistant acid phosphatase, which demineralise the tissue, exposing collagen proteins to the action of secreted proteases, such as cathepsin K (Feher, 2017). During bone resorption, mineral-bound BPs are released in resorption pits and subsequently taken up by osteoclasts in endocytic vesicles (Nakamura *et al*., 2012). Despite N-BPs' relatively indiscriminate mechanism of action (inhibiting a pathway essential for cholesterol synthesis), their increased uptake by osteoclasts during the resorption process means this cell type is their main target.

1.4.9.1 ZOLEDRONIC ACID

Zoledronic acid (Zol) is a nitrogenated bisphosphonate on the WHO's list of essential medicines, first approved in 2001 and subsequently approved for the use in various bone diseases, including osteoporosis, cancer-induced hypercalcemia and osteolysis and Paget's disease (Saad, 2005). Zol is the most potent BP and therefore the most commonly used to treat cancer induced bone disease, and has subsequently drawn attention in this setting in pre-clinical research. Despite mainly targeting osteoclasts, preclinical research has suggested Zol can have a direct effect on cancer cells and on other cells in the hematopoietic lineage, although the evidence is limited (Mahmood *et al*., 2020). The use of Zol alone has shown limited results in preventing cancer progression, but delays and limits SREs. It is therefore used primarily to reduce SREs in the metastatic setting, however it has also been investigated as an adjuvant treatment in post-menopausal women with early breast cancer.

Zol has been shown to decrease breast tumour cell proliferation and invasion *in vitro* (Mahmood *et al*., 2020). However, due to its strong affinity for bone and rapid clearance from circulation, direct effects *in vitro* are often not reflected *in vivo.* Despite having the potential to directly affect tumour cells following repeated high dosing *in vitro*, any observed anti-tumour effects *in vivo* are likely to be indirect following inhibition of osteoclast activity and release of bone-associated growth factors. Research into Zol in the cancer setting has therefore focused on its effect on the bone microenvironment which would indirectly influence tumour growth.

A major analysis into the adjuvant use of Zol was performed in the AZURE trial, a randomised open-label phase 3 trial of 3360 women in seven countries, investigated the adjuvant use of Zol in high-risk patients with early breast cancer (Coleman *et al*., 2014). In the overall study population Zol did not improve overall survival or distant recurrences, but reduced development of bone metastases. Significantly, in women who were at least 5 years post menopause, Zol improved invasive disease free survival (DFS), but did not affect all other menopausal groups. Significantly, this effect was observed widely among bisphosphonates, regardless of tumour oestrogen receptor status, suggesting a role for oestrogen in the microenvironment altering the actions of bisphosphonates (Early Breast Cancer Trialists' Collaborative, 2015).

Another clinical trial into the investigation of BPs in early stage cancer using, clodronate, NSABP B-34, found that, although no overall improvement in DFS was achieved in women with micrometastatic disease in the bone, subgroup analysis found that there were significantly fewer recurrences of metastatic disease in women aged ≥ 50 years old when treated with clodronate compared with placebo (Paterson *et al*., 2012). Similarly, in the ZO-FAST trial, postmenopausal women with oestrogen or progesterone receptor-positive early breast cancer (stage I, II or IIA) receiving adjuvant letrozole were assigned to one of three groups; i.) to immediately receive Zol treatment every 6 month, ii.) delayed Zol treatment initiated by fracture or on-study decrease in bone-mineral density (BMD) or iii.) no Zol treatment. The study found that at 60 months (final analysis), immediate Zol use reduced the risk of DFS events by 34% with fewer local and distant recurrences as compared to delayed Zol, but yet delayed Zol substantially improved DFS compared to those who received no Zol (Coleman *et al*.,

2013). These findings show correlations between oestrogen status and Zol, which lead to preclinical studies into the actions of Zol in various conditions, taking into account oestrogen and bone turnover.

One such preclinical investigation was carried out by Ottewell, *et al.* who used 12-week-old female BALB/C-nude mice with disseminated MDA-MB-231 breast cancer cells characterised by a dormant phenotype, before performing ovariectomy or sham surgery and treating with Zol or control. Their results showed that ovariectomised mice had increased bone turnover and 83% of animals had detectable tumours, compared with 17% of those which underwent a sham operation (Ottewell *et al*., 2015). Importantly, the ovariectomy-induced growth of DTCs was completely prevented by the use of Zol, whereas growth of DTCs in the sham-operated animals were unaffected. These results demonstrated that OVX-induced tumour growth was driven by osteoclast activity. The same results were achieved by using OPG-Fc to prevent osteoclast expansion and activation, supporting that DTC growth in this model is driven by OC activity. Combining these observations with results from clinical trial data reflect the beneficial impact of using Zol for early bone metastatic disease in post menopausal women, and suggests the link between Zol and oestrogen being in part due to bone turnover induced by osteoclasts.

The interaction between the tumour and the bone microenvironment at different stages of tumour growth is incompletely understood. Work by Ottewell *et al.* (2015) used a single dose of Zol, prior to subsequent injection of cells which prevented the outgrowth of disseminated tumour cells by increased bone turnover in an ovariectomised model. Despite this success, there are unanswered questions as to the tumour-bone interactions at different stages of tumour growth, and how Zol may affect later stages of tumour growth, as Zol alone has shown limited effects on tumour progression despite protecting bone (Ottewell *et al*., 2008). Current NICE guidelines indicate monthly dosing for patients who are at risk of SREs and in advanced malignancies involving bone (BNF, 2020).

A diagramatic illustration of the aforementioned therapeutic strategies can be seen in Figure 1-5. Therapeutics currently in clinical trials can be seen in Table 1-1.

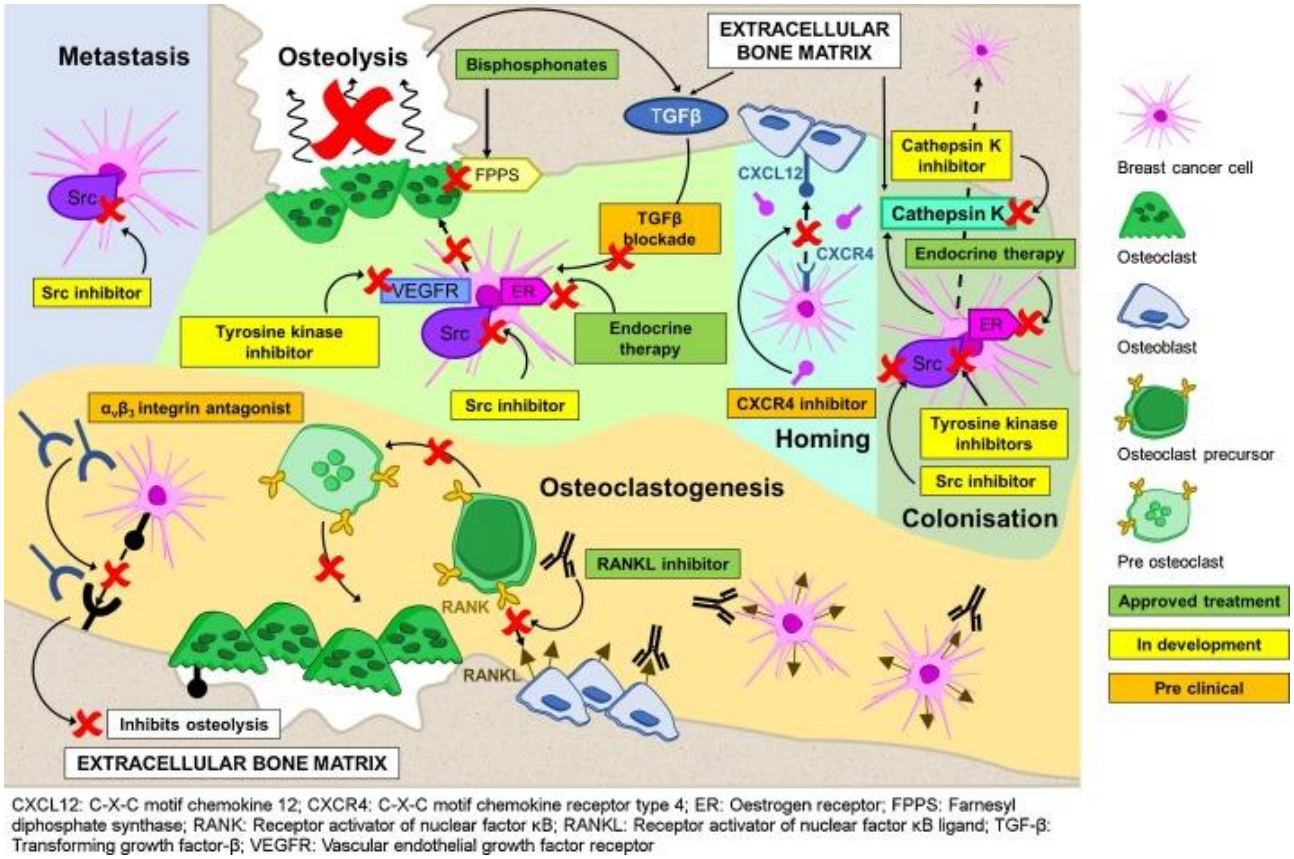

CXCL12: C-X-C motif chemokine 12; CXCR4: C-X-C motif chemokine receptor type 4; ER: Oestrogen receptor; FPPS: Farnesyl diphosphate synthase; RANK: Receptor activator of nuclear factor κB; RANKL: Receptor activator of nuclear factor κB ligand; TGF-β: Transforming growth factor-β; VEGFR: Vascular endothelial growth factor receptor

Figure 1-5: Targets within the bone microenvironment and their inhibitors as potential therapeutics. Reprinted by permission from The International Journal of Biochemistry & Cell Biology (Brook *et al.*, 2018)

Table 1-1: ABL, tyrosine-protein kinase ABL1; BCR, breakpoint cluster protein; CRPC, castration-resistant prostate cancer; mTOR, mammalian target of rapamycin; NGF, nerve growth factor; OS, overall survival; PFS, progression-free survival; RON, macrophage-stimulating 1 receptor; SRC, proto-oncogene tyrosine kinase SRC; SRE, skeletal-related event; [a]Has regulatory approval in the United States and/or Europe for use in patients with cancer or other indications as indicated. [b]Drug in phase III trials. [c]Drug in phase II trials. [d]Drug in phase I trials. [e]Drug investigated in preclinical studies. Adapted with permissions from Bone Metastases, Coleman *et al.* (2020), Nature Reviews Disease Primers volume 6, Article number 83 (Coleman *et al*., 2020b).

Drug	Targets	Results	Trial ID	Refs
Everolimus[a]	mTOR	Improvement in PFS in patients with breast cancer bone metastases Approved for treatment of metastatic breast cancer, renal cell carcinoma and neuroendocrine tumours	NCT00863655 (BOLERO II) NCT01783444 (BOLERO 6)	(Hortobagyi, 2015)
Dasatinib[a]	BCR–ABL and SRC	Inhibits bone turnover markers in patients with prostate cancer Responses in patients with prostate cancer seen on PET–CT imaging Approved for use in haematological malignancies	NCT00410813 NCT00918385	(Koreckij *et al*., 2009, Yu *et al*., 2015)
Romosozumab[a]	Sclerostin	Reduces osteolytic lesions in mouse models of breast cancer or multiple myeloma Approved for use in postmenopausal women with severe osteoporosis	Preclinical studies only for effects on cancer NCT01575834	(Cosman *et al*., 2016)
Tanezumab[b]	NGF	Attenuates cancer pain in animal models of prostate and breast cancer bone metastasis and sarcoma. Provides additional sustained analgesia in patients with metastatic bone pain who are taking opioids; failed to achieve the primary end point of lowering opioid usage	NCT00545129 NCT02609828	(Aiello *et al*., 2016)
Odanacatib[c]	Cathepsin K	Inhibits the formation of osteolytic lesions *in vivo*. Reduces bone resorption in the clinic Development halted owing to potential cardiac adverse events	NCT00399802	(Jensen *et al*., 2010, Liang *et al*., 2019)
Saracatinib[c]	SRC and BCR–ABL	Limited activity in solid tumours Minimal effects on bone pain	NCT00558272 NCT02085603	(Sousa and Clezardin, 2018)
BMS777607[d] or ASLAN002[d]	RON	Inhibits the formation of osteolytic lesions in animal models Reduces bone resorption in patients with advanced cancer	NCT01721148 NCT00605618	(Sousa and Clezardin, 2018)
IVD11[e]	Jagged or Notch	Inhibits osteoclastogenesis and bone metastasis formation *in vivo*	Preclinical only	(Sousa and Clezardin, 2018)

1.4.10 LIMITATIONS

Currently, metastatic BC is considered incurable and treatments for secondary relapse in the bone are palliative in nature, such as the reduction of bone resorption offered by the bisphosphonate zoledronic acid (Polascik, 2009). Standard therapy, such as chemotherapy and radiotherapy, fail to eradicate dormant DTCs as they act on rapidly dividing cells, while dormant cells are maintained in a non-dividing state and are therefore insensitive to conventional methods of intervention. An unclear understanding of the mechanisms supporting the induction and escape from dormancy in the bone underpins a lack of effective treatment options available that offer improved clinical endpoints (Wu and Lu, 2018). Elucidating this process would shed light on key molecules and cells involved in this disease state, leading to the identification of therapeutic candidates that may result in improved patient outcome.

1.5 DISSEMINATED TUMOUR DORMANCY - DEADLY PERSISTENT CANCER CELLS

During clinical remission, presenting no evidence of disease (NED) following treatment of the primary tumour, a subset of breast cancer patients consequently experience secondary recurrence at a distant site after a period of latency. This occult phase of dormancy is asymptomatic, while metastases stemming from aggravated overt outgrowth are often unresponsive to available treatments (Yadav *et al*., 2018).

Once DTCs localise to the bone, they may remain in a mitotically dormant state (Vishnoi *et al*., 2015). The mechanisms of current systemic identification methods and therapies require mitotically active cancer cells for efficacy; and as such render this phenotype challenging to identify, study and treat (Gelao *et al*., 2013). Within the perivascular and endosteal regions where dormant DTCs have been found to reside, it is proposed that these DTCs parasitize the hematopoietic stem cell (HSC) niche (Shiozawa *et al*., 2011). Mechanisms ascribed to micro-environmental and immunological factors present in the bone microenvironment that maintain HSCs in a mitotically quiescent state are also thought to play a role in maintaining DTCs in dormancy (Ghajar, 2015, Walker *et al*., 2016).

Metastases concurrent and asynchronous to primary tumour detection and treatment suggest variable kinetics in tumour cell dissemination, leading to identification of early and late disseminated cells, as well as dormancy. The rate of secondary site outgrowths is highly variable and dependent on tumour stratification, even within kindred organs of origin, suggesting a cell-intrinsic mechanism governing outgrowth (Gomis and Gawrzak, 2017). However, specific organotropism derived from primary organs and tissues may lend additional cell-extrinsic mechanisms governing these variable kinetics. As an example, breast cancer latency is classified as either medium or long-term latent disease compared to lung cancer presenting short latency (see Figure 1-6).

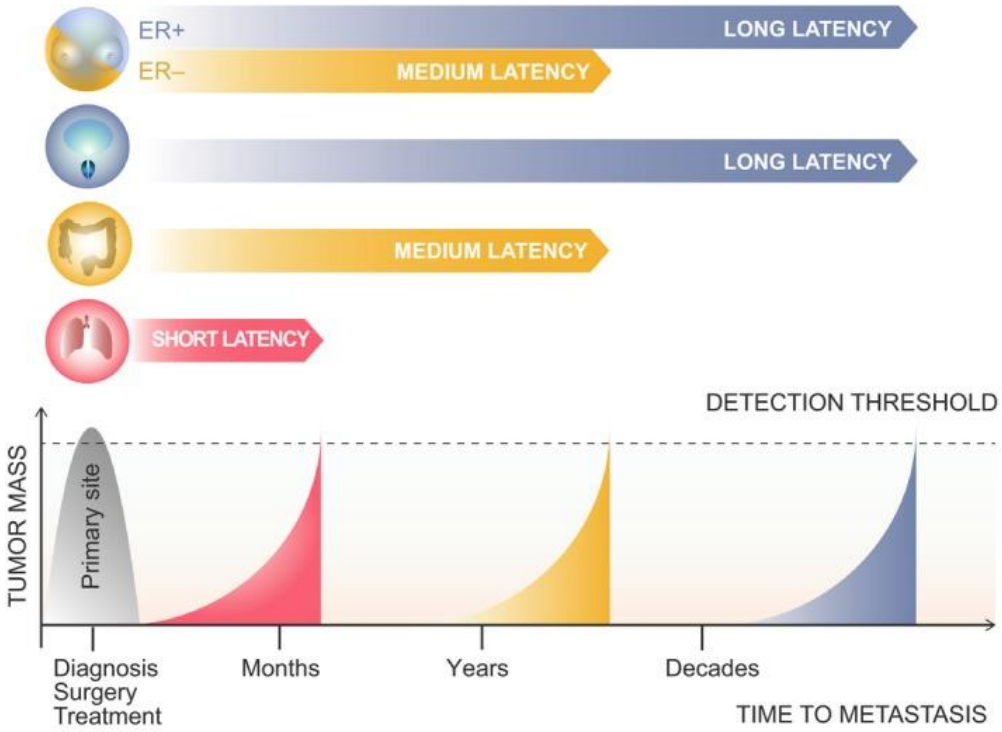

Figure 1-6: Rates of metastatic latency kinetics vary with site of primary tumour. Short latency presents as tumour mass surpassing detection threshold in months following treatment of primary site, medium latency presents as years and long latency as decades in time to metastasis from remission. Reprinted by permission from FEBSPRESS: Molecular Oncology (Gomis and Gawrzak, 2017)

1.5.1 Mechanisms of Dormancy

Tumour dormancy is widely divided into two broad categories, described as $Ki67^{+/low}$ indolent, where the rate of proliferation and apoptosis are at equilibrium, and $Ki67^{-}$ indolent where cells enter mitotic G0-G1 growth arrest via disruption of the ERK/p38 pathway, as well as alterations in the STAT family molecules and apoptosis-related molecules, such as BAX/BCL2 (Payne *et al*., 2016). Models for dormancy are further distributed into three categories: (i) cellular (intrinsic mechanisms that induce dormancy, such as mutations), (ii) angiogenic (cell cycle arrest induced due to nutrient deprivation) and (iii) immunological dormancy (immune-cell induced dormancy) (Yeh and Ramaswamy, 2015). The following section will discuss mechanisms of dormancy derived from experimental data obtained from both within, and outside the bone.

1.5.1.1 Cellular Dormancy

Cellular dormancy refers to cellular-intrinsic mechanisms that result in reduced cell cycling, with decreased mitogenic signalling and upregulation of autophagy pathways emergent as pivotal mechanisms. Disruption of the balance between the extracellular signal-regulated kinase (ERK) and p38 signalling pathways is central in effecting this phenotype. Upregulated p38 and downregulated ERK signalling has been profiled as the critical shift in signalling pathways to induce dormancy (Aguirre-Ghiso *et al*., 2003, Park and Nam, 2020). Further to this, downregulation of phosphatidylinositide 3-

kinase (PI3K) protein kinase B (PKB) and alteration of Ras-homologue gene family member A (RhoA) signalling are involved in the switch to reduced mitotic signalling (Quayle *et al*., 2015).

Cellular dormancy, though an intrinsically defined pathway, has various cell-intrinsic and extrinsic effector mechanisms to trigger the P38/ERK disbalance, such as from cellular stressors or microenvironmental cues. As such, cellular dormancy is often the cellular response to angiogenic or immune-mediated dormancy, not excluding microenvironmental signals that regulated cell cycling (Yeh and Ramaswamy, 2015). Table 1-2 lists the various cell extrinsic and intrinsic molecules and pathways proposed to be associated with cellular dormancy.

Table 1-2: Dormancy associated molecules and their function contributing to maintenance or escape from dormancy

Dormancy Associated Molecule	Function	Reference
P38/ERK	The key molecular pathway balance thought to determine entering quiescence or exit. Shift towards P38 signals dormancy	(Aguirre-Ghiso *et al*., 2003)
TGFβ	Induces cellular quiescence in hematopoietic stem cells (HSCs), but drives proliferation in malignantly transformed cells	(Colak and Ten Dijke, 2017, Fluegen *et al*., 2017, Wang *et al*.,
p21/p27	Induction of p21 leads to inhibition of cyclin dependent kinases and arrest of the cell cycle, promoting a dormant non-dividing state	(Xiong *et al*., 1993)
BMP7-BMPR2	BMP7 binds to BMPR2 and activates P38 MAPK and p21 leading to increased dormancy	(Kobayashi *et al*., 2011)
GAS6/AXL	GAS6/AXL axis has been found to induce dormancy, but not maintain it, suggesting a role in a network of factors	(Axelrod *et al*., 2019, Taichman *et al*., 2013)
NR2F1-RARβ1-SOX9	NR2F1 induces quiescence in bone DTCs through upregulation of pluripotency gene, Nanog, dependent on SOX9 and RARβ1	(Sosa *et al*., 2015)

1.5.1.2 ANGIOGENIC DORMANCY

Angiogenic dormancy stems from the maintenance of angiostasis in a growing tumour. Distinct populations of cells in a mass are limited to a size of approximately $1mm^3$ without a need for their own blood supply and increased microvasculature. To increase beyond this point would require angiogenesis to the mass of cells to provide adequate nutrition and clearance of waste for increased growth potential. Therefore, in areas of poor vasculature or attenuated potential for development of neovasculature, tumour cells are limited in size, reaching a population equilibrium-based dormancy.

Proliferation may occur in these instances, but it is matched by the rate of apoptosis. Pharmacological inhibition of angiogenesis has been shown to induce dormancy by driving increased rates of apoptosis while maintaining rates of proliferation in mouse models, as well as the association of hypoxia and accompanying transcriptional alterations with dormancy (Holmgren *et al*., 1995, O'Reilly *et al*., 1996). This paradigm has formed the basis for anti-cancer therapies widely used in the clinic, such as the monoclonal antibody bevacizumab and small molecule tyrosine-kinase inhibitor sunitinib which target the vascular endothelial growth factor (VEGF) pro-angiogenic signalling cascade (Jayson *et al*., 2016).

Within the body, several anti-angiogenic factors may act in a similar fashion to inhibit angiogenesis and induce angiogenic dormancy. These factors have been implicated in preventing the angiogenic switch and subsequent induction of dormancy in otherwise rapidly dividing cells (see Figure 1-7).

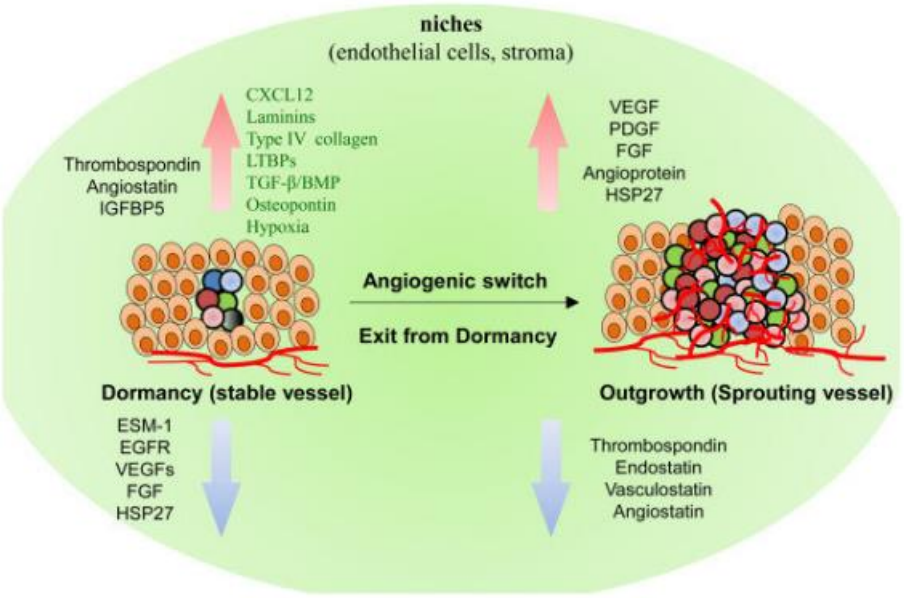

Figure 1-7: Angiogenic dormancy is characterised by the upregulation of anti-angiogenic factors and downregulation of pro-angiogenic factors. Escape from dormancy is correlated with a reversal of the expression of these genes. Reprinted by permission from Biomed Central: Experimental Hematology & Oncology (Wang and Lin, 2013)

Stromal and immune cells, such as tumour associated macrophages are known to play a key role in the generation of blood supply for tumours through the excretion of angiogenic factors and the release of matrix metalloproteinase (MMP) enzymes which aid in remodelling of the extracellular matrix subsequent to growth and metastasis. These cells have been implicated in resistance to anti-VEGFA therapy and may offer targets for understanding and exploiting angiogenic dormancy (Dalton *et al*., 2017). However, it is unknown whether these cells are recruited at the dormant phase to trigger sprouting of new blood vessels, or localise as a response to factors released by overtly outgrowing tumours.

The bone microenvironment presents a unique, hypoxic environment due to vascular heterogeneity, poor perfusion rates of blood vessels and high metabolic activity of hematopoietic stem cells (Guo and Wu, 2021). In experimental animal models of breast cancer dormancy within the bone, the perivascular niche has been shown to be an important factor in dormancy, as thrombospondin-1 has been shown to maintain DTC quiescence, whereas factors such as TGF-β1 and periostin promote outgrowth (Ghajar *et al*., 2013). This has led to the suggestion that stable microvasculature constitutes a dormant niche, which proceeds into micrometastatic outgrowth after sprouting neovasculature.

1.5.1.3 Immune-mediated Dormancy

The intricate process of stochastic events leading to metastasis is often abridged into simplified, broad steps, including; epithelial to mesenchymal transition, local invasion, intravasation, circulatory survival, extravasation, mesenchymal to epithelial transition and distant colonisation resulting in clinical manifestation. To survive this process, individual transformed cells must evade immune surveillance on their journey through non immune-privileged locations, suggesting mechanisms of evasion diverse to local immune-suppression.

Paul Ehrlich first proposed a tumour-suppressive role of the immune system in 1909, followed by Burnet and Thomas' hypothesis of immunosurveillance described in the 1950s, reviewed by (Dunn *et al.* (Dunn *et al*., 2004). However, the concept of an immuno-oncological axis fell out of favour amongst the scientific community, until the tripartite immune-editing model proposed by Dr. Schreiber in the early 2000s (Starling, 2017). Immuno-oncology now represents a significant arm of anti-cancer strategies, exemplified in incorporation into the hallmarks of cancer (Hanahan and Weinberg, 2011). Increased understanding of the immune-oncological axis has underpinned recent successes in clinical trials and FDA approval for immune checkpoint inhibitors and vaccines (Chiarella *et al*., 2018). Research centred on immune cell involvement in establishing and maintaining a dormant phenotype is gaining traction as novel treatment modalities are sought (Romero *et al*., 2014).

The immunoediting hypothesis encapsulates three distinct phases observed in immune-mediated targeting of tumour cells; (i) The *Elimination* phase, whereby immunogenic cells are targeted and eradicated by constituents of the innate and adaptive immune system present within the tumour microenvironment, followed by (ii) The *Equilibrium* phase**,** a sustained period of dormancy exists as the immune system suppresses, but does not entirely eliminate cancer cells. Lastly, the (iii) The *Escape* phase in which evolution of the immune population, reduction of immunogenic cells and epigenetic alterations disrupt the equilibrium phase, leading to overt tumour growth (see Figure 1-8) (Mittal *et al*., 2014).

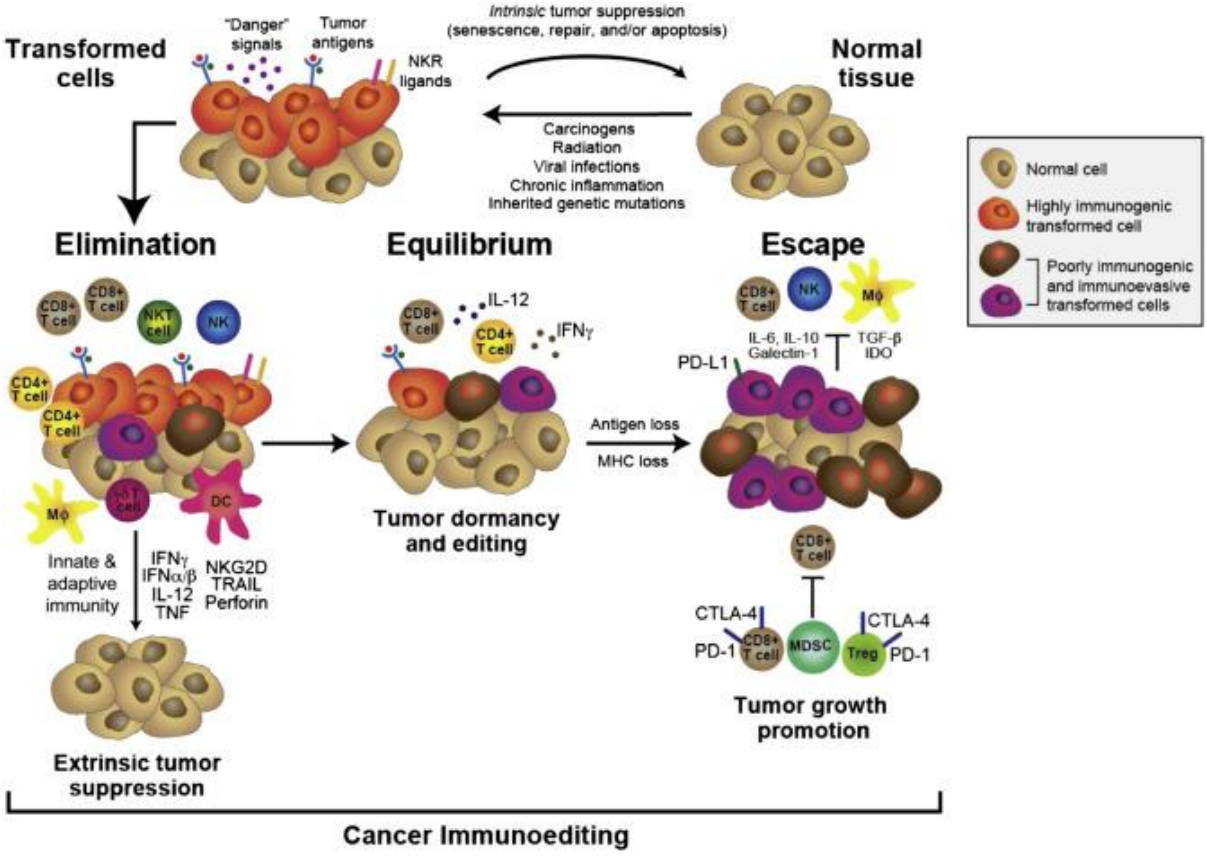

Figure 1-8: Cancer immunoediting highlighting the 3 Es - the role of the immune system in cancer suppression and promotion. Various cell types play contrasted roles in elimination or protection and subsequent escape through immunogenic mechanisms. Reprinted by permission from AAAS: Science (Schreiber *et al.*, 2011)

It is currently unknown what fraction of dormant tumour cells exist in an arrested state of proliferation in the G0 phase of the cell cycle or are held in population equilibrium through immunoediting.

Evidences for immune-mediated tumour cell dormancy in humans have come from tissue transplant cases, whereby recipients undergoing immunosuppressive regimens to prevent graft rejection have developed overt tumours that were genetically traced to donors that themselves did not display any clinical indications of cancer. Mackie and Reid (2003) reported a case concerning two different kidney transplant recipients received from the same donor, who had been discharged as tumour free 15 years after diagnosis and without clinical manifestation of cancer. Following immunosuppressive treatment, both recipients developed secondary melanoma traced back to the donor (MacKie *et al.*, 2003). Recurrence of these tumours was attributed to immunosuppressive treatments, suggesting the presence of tumour cells that had been held dormant by the immune system. A further 13 cases in 21 out of 26 organ recipients developing secondary melanoma supported this hypothesis (MacKie *et al.*, 2003). Transplant malignancies stemming from undiagnosed or cancer-remitted donors are not uncommon in immunosuppressed recipients in various cancer subtypes, linking the immune system with tumour suppression and dormancy (Teng *et al.*, 2008).

The opposite effect can also occur, where immune-supportive therapy has led to positive patient outcome. In one such example, immune reconstitution therapy facilitated spontaneous tumour regression in an AIDS patient with non-small cell lung carcinoma (NSCLC)(Menon and Eaton, 2015). Likewise, a study on leukaemia patients receiving autologous bone marrow transplants, showed 8 out of 18 patients possessing anti-tumour cytotoxic T-lymphocyte (CTL) precursors and no instance of relapse was recognised in these patients thereafter (Montagna *et al*., 2006).

A few immune associated molecules are of interest in cancer dormancy, and are particularly prevalent in literature and the basis for various immune-mediated dormancy models. However, the role of factors produced by the immune system in tumour dormancy has often proved unclear, such as that of IFN-γ. IFN-γ is a well-described molecule, being the only type 2 interferon and primarily secreted by natural killer (NK), natural killer T-cells (NKT), $CD4^+$ Th1 and $CD8^+$ CTLs. Evidence also exists for macrophage secretion under stimulation of IL-12 and IL-18 or M-CSF (Darwich *et al*., 2009). IFN-γ plays a dual role in the immune-tumour axis, being a mediator of anti-tumour immunity, but also playing a role in subsequent immune escape. Previously mentioned interactions between immune cells and dormant DTCs have shown a role for IFN-γ, particularly in CD8+ lymphocyte interactions (Koebel *et al*., 2007, Romero *et al*., 2014). Low dose IFN-γ has been shown to confer resistance to NK cells in a B16 melanoma model which facilitated higher lung colonisation than IFN-α/β, while inducing upregulation of MHC I molecules $H\text{-}2K^b$ and $H\text{-}2D^b$ (Mojic *et al*., 2017). MHC I loss has been linked with immune evasion, yet is also a marker of dormancy (Romero *et al*., 2014). IFN-γ is therefore implicated in eradication of cancer cells via STAT1, induction of dormancy via STAT3 and MHC I loss, potentially resulting in immune evasion (Kulling *et al*., 2018, Lin *et al*., 2017).

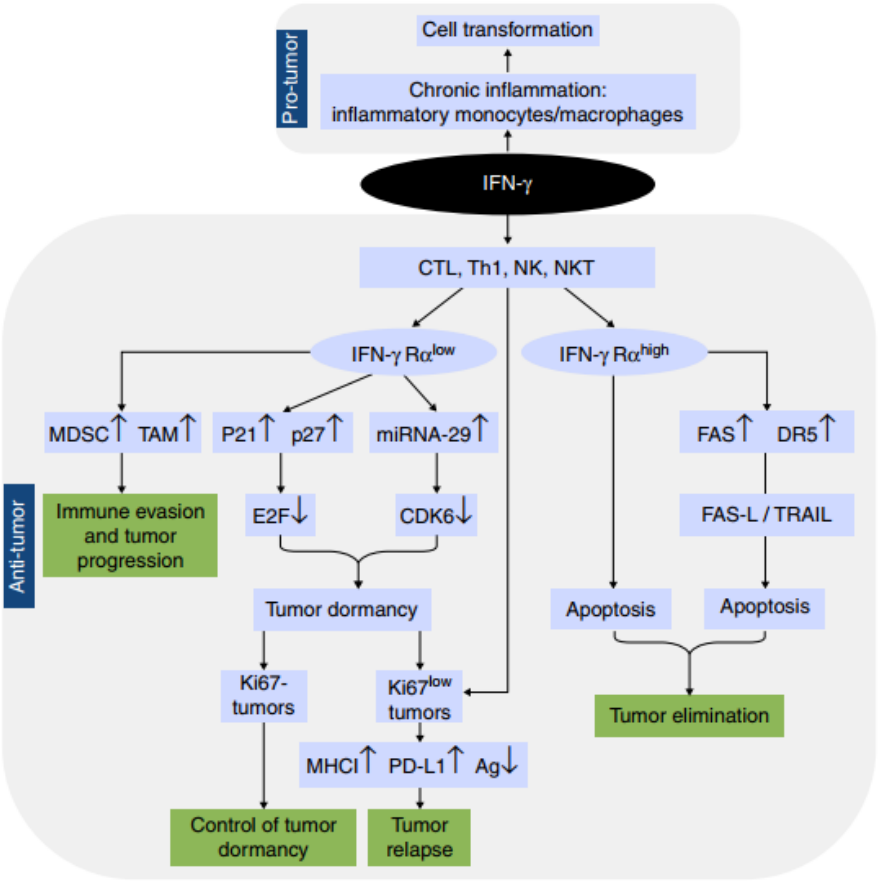

Figure 1-9: The role of IFN-γ in modulating tumour dormancy. Cellular cascades are representing leading to tumour dormancy through decreased cell-cycling molecules and increased expression of molecules associated with inhibition of the cell cycle. MHCI and PD-L1, also implicated in dormancy are further regulated through IFN- γ signalling. Reprinted by permission from Journal of Leukocyte Biology (Aqbi *et al.*, 2018).

Despite the bone being an immune-privileged site, the role of the immune system in dormancy has been observed in clinical samples and in animal models (Fujisaki *et al.*, 2011). Feurer *et al.* (2001) analysed the bone marrow of 90 breast cancer patients who were found to have an increased proportion of $CD4^+$ and $CD8^+$ T cells than healthy donors. Furthermore, the extent of memory T-cell increase was correlated with the size of the primary tumour, while those patients having disseminated tumour cells in their bone marrow had more $CD4^+$ T cells and $CD56^+$ $CD8^+$ cells, suggesting a role for the immune system in maintaining dormancy within the bone marrow (Feuerer *et al.*, 2001). Importantly, only some of these changes observed in the bone marrow were captured by changes in peripheral blood samples.

Further analysis of DTCs by Pantel and colleagues (1991) obtained from bone marrow aspirates of patients with various adenocarcinoma, including breast cancer, observed that these quiescent cells had a reduced MHC I expression, possibly preventing their eradication by $CD8^+$ T cells, highlighting the importance of the immune system in maintenance of dormancy(Pantel *et al.*, 1991).

In animal studies, Mahnke and colleagues found the presence of disseminated tumour cells in the bone marrow maintained a population of LacZ (Gal) $CD8^+$ memory cells within the bone marrow that retained their memory through up to four successive bone marrow transplants to recipients (Mahnke *et al.*, 2005). They also found that the bone marrow acted as a reservoir for these cells which could be recruited to the peritoneal cavity by vaccination and maintained anti-tumour activity *ex vivo.* Their work showed that a compartment of the immune system responds to DTCs within the bone marrow, maintaining a state of dormancy despite the immune privilege of the bone marrow.

Taken together, these examples provide evidence that the immune system plays a significant role in the maintenance of tumour dormancy, but whose role needs to be further elucidated.

1.5.1.4 MicroRNAs in Cancer Dormancy

Being derived from a rapidly dividing population, the switch to dormancy and subsequent relapse of DTCs has been partly attributed to epigenetic and gene regulatory mechanisms. These are mechanisms that regulate the transcription of DNA into mRNA (such as DNA methylation or histone acetylation) or translation of transcripts from mRNA to protein (such as mRNA inhibition or degradation mechanisms). The reduction in DNA metabolism suggests replication errors introducing mutations, such as in the form of single nucleotide polymorphisms (SNP), repeats and more severe chromosomal aberrations during cell division are unlikely to occur in a dormant, non-replicating cell. Microenvironments in which tumour cells reside, including that of bone, may be responsible for inducing epigenetic and gene regulatory alterations, such as DNA methylation, histone acetylation, alternative splicing and post-transcriptional modifications (Crea *et al*., 2015).

A particular form of gene expression regulation is found in micro RNAs (miRNA), which have recently been implicated in the field of cancer dormancy. MiRNAs are small non-coding RNAs responsible for the regulation of translation of transcribed mRNA, through translational suppression or degradation of transcripts by the RNA-induced silencing complex (RISC)n. MiRNA transcripts are generated through RNA polymerase 3, and processed by enzymes dicer and drosha and exported through the exportin-5 family of membrane channel proteins from the nucleus to the cytosol where they exert their effect (Wahid *et al*., 2010).

Transfer of miRNAs from the supporting microenvironment was shown by Makiko *et al.* who demonstrated the transfer of exosomes containing miR23-b by bone marrow mesenchymal stem cells into disseminated breast cancer tumour cells *in vivo,* which decreased expression of the target gene MARCKS, a promoter of cycling and motility, expression (Ono *et al*., 2014). This was further supported by clinical data showing an increased miR-23b expression in patient samples of bone-metastatic breast cancer.

A well-characterised dormancy-associated miRNA is miR-190 that targets a range of transcription factors, tumour suppressor genes and interferon response pathways to induce transcriptional changes leading to a state of dormancy (Almog *et al*., 2013). In the transformation of dormant DTCs into a fast-growing phenotype, Almog *et al.* showed a consensus of 19 miRs that governed this switch, primarily by the downregulation of dormancy associated miRs miR16,19, 190,580 and 588. Reconstitution of a single miRNA between 190, 580 and 588 reversed the fast growing phenotype to dormancy in a glioblastoma and osteosarcoma model, showing a novel means to potentially rescue a malignant tumour into an asymptomatic dormant state and demonstrating the potency of these molecules in facilitating an entire phenotypic switch (Almog *et al*., 2012). Pro-angiogenic factors TIMP-3, bFGF, TGFα were downregulated in miR-190 overexpression, and downregulation of Bv8. This change in

gene expression was correlated with decreased recruitment of bone-marrow derived CD11b+GR-1+ myeloid cells was an effect correlated with all pro-dormancy miRNAs.

In any form of dormancy, evasion of NK-mediated immune-surveillance is important for malignantly transformed cells due to downregulation of MHC-I (Codo *et al*., 2014). MiR20a has been found to downregulate MICA and MICB, components of the NK cell receptor NKG2D ligands and promoting evasion of NK cell cytotoxicity by breast cancer cells (Shen *et al*., 2017). This marks a critical step in maintaining dormant presence, as downregulation of MHC-I and evasion of NK-mediated tumour killing are necessary for prolonged existence within the body.

MiRNAs are potentially significant regulators of dormancy due to their ability to regulate clusters of proteins and potentially modify entire pathways. Further to this, the relative stability of miRNAs make them attractive targets for systemic serum-based diagnosis of potential dormant tumour cells.

Despite the identification of different classifications of dormancy; cellular, angiogenic and immunologic, it is highly likely that these work synchronously to create the phenomenon, due to the complex interplay of the microenvironment, representing angiogenic and immunologic dormancy, subsequently resulting in cellular intrinsic responses to initiate dormancy. For dormant, malignantly-transformed cells to survive in the body for any length of time, there must be an avoidance of the immune system, regardless of quiescence/indolence, slow cycling or population equilibrium, making the immune aspect essential for dormancy to occur. Furthermore, autophagy as a result of nutrient deprivation or stress signalling, is also observed in a significant proportion of dormant cells (Akkoc *et al*., 2021). However, the existence of individual dormant cells, significantly smaller than the angiogenic-inhibitory $1mm^3$ volume leads to questioning of its necessity. Specific spatio-temporal localization of individual cells, however, may indeed be in a nutrient-deprived immediate locality.

Epigenetic mechanisms are gaining tract as drivers for sustaining DTCs in a state of dormancy and mediating subsequent exit due to their relatively quick induction and the ability for cells in the microenvironment to transfer molecules associated with dormancy, such as the miRNAs.

1.5.2 Dormancy regulation in the Hematopoietic Stem Cell Niche

Of particular interest in relation to bone-disseminated tumour cells is the microenvironment that constitutes the hematopoietic stem cell (HSC) niche. The hematopoietic stem cell niche refers to spatio-temporal locations within the bone marrow where HSCs reside under physical and chemical cell cycle regulation by resident cellular populations, largely consisting of endothelial cells, osteoblastic cells, mesenchymal stem cells (MSCs), megakaryocytes, T-cells and bone marrow macrophages (Allocca *et al*., 2019b, Frisch, 2019, Riether *et al*., 2015).

The HSC niche in the bone marrow is hypothesised to be a site for localisation of dormant DTCs, (Ghajar, 2015). Mechanisms involved in the regulation of HSC stemness, dormancy and subsequent mobilisation during inflammation, tissue repair and localised stress events may be associated with regulating the same processes in dormant DTCs in the bone (Ghajar, 2015, Shiozawa *et al*., 2011, Sun

et al., 2005). Illuminating immune regulation of HSC quiescence and proliferation may therefore ostensibly reveal key players in DTC dormancy regulation within the context of the bone.

Furthermore, the bone microenvironment being an immune-privileged area due to the presence of immunomodulatory cells such as macrophage subsets and regulatory T-cells (T Regs), as well as areas of reduced vascularization make this an area with significant potential for all forms of dormancy. An immunosuppressive environment may hinder complete immune eradication of DTCs and thus create a setting favourable to immunosurveillance escape and overt growth. Bone marrow, being the primary site of hematopoiesis, renders it an immunosuppressive environment. Hirata, Furuhashi *et al*. (2018) showed that bone-homing $CD150^{high}$ $CXCR4^{+}$ $FoxP3^{+}$ T regs conferred immune privilege within the HSC niche (Hirata *et al*., 2018). T regs are further implicated in dampening the immune response via constitutive expression of the immune checkpoint molecule CTLA4 (Walker, 2013). The bone marrow stromal cells (BMSCs) are also implicated in immunosuppression by expression of PD-L1 and IL-6 secretion, which induce quiescence in effector $CD8^{+}$ CTLs that have been shown to induce tumour elimination and dormancy (Ara *et al*., 2009, Augello *et al*., 2005).

Implicated in microenvironmental regulation of HSC quiesence, TGF-β has been found to induce HSC cell cycle arrest through activation of smad and p57Kip2, while inhibiting lipid raft clustering, an essential feature of HSC cell cycle re-entry. This effect of TGF-β on HSC has been found to be mediated by non-myelinating Schwann cells within the bone marrow (Yamazaki and Nakauchi, 2014). Despite its purported role in HSC quiescence, TGF-β is a functionally diverse molecule, its exerting effects paradoxically in malignant tissue by promoting tumour outgrowth (Zhang *et al*., 2014b). Further to this enigma, is the differential effect of TGF-β isoforms on cancer cells, such as that of TGF-β, which induces cell cycling quiesence in prostate cancer cells. Nevertheless, this molecule is thought to play a primary role in the escape from dormancy, and is found in abundance in the bone cellular matrix. Disruption of this matrix, may release factors such as insulin-like growth factor (IGF)-1 and TGF-β in periods of increased resorption, triggering overt outgrowth of dormant tumour cells.

Megakaryocytes have been shown to play a key role in HSC quiesence. Bruns, *et al.* used 3D whole-mount imaging to demonstrate non-random co-localisation of HSCs and megakaryocytes and further strengthened this finding by inducing increased HSC expansion following megakaryocyte selective depletion (Bruns *et al*., 2014). Molecules regulating HSC dormancy, expansion, migration and mobilisation can be seen in Table 1-3.

Table 1-3: Molecules regulating hematopoietic stem cells

HSC-regulating associated molecule	Function	Cells secreting	Reference
CXCL4	HSC dormancy	Megakaryocytes	(Bruns *et al*., 2014)
Kit Ligand	HSC expansion	Stromal Cells	(Kent *et al*., 2008)
SDF-1/CXCL12	HSC migration	Mesenchymal stem cells, Osteoblasts	(Itkin and Lapidot, 2011)

G-CSF	HSC mobilisation	Endothelial cells, macrophages	(Petit *et al*., 2002)

1.6 Escape from Dormancy

Once DTCs have successfully colonised the bone and gone through a period of dormancy, they must escape this programming and enter into a state of increased proliferation, here referred to as escape from dormancy. Recent evidence from model systems have shown that the bone remodelling process may be one of the mechanisms that results in triggering proliferation of DTCs within the bone microenvironment (Ottewell *et al*., 2015). In particular, the role of osteoclast-induced increased bone resorption leading to overt outgrowth has developed and is an active area of research. Research by Ottewell *et al.* (2014) demonstrated that stimulating pre-osteoclasts into differentiation and into active bone resorption triggered the overt outgrowth of DTCs in *in vivo* models, and the inhibition of this process prevented outgrowth of DTCs in the long bones of mature mice(Ottewell *et al*., 2014a, Ottewell *et al*., 2014b).

1.6.1 Hypocalcemia-induced bone resorption

In a state of hypocalcemia, the parathyroid glands detect hypocalcemia in the serum and release parathyroid hormone, which act to increase bone resorption by increasing osteoclastogenesis via upregulation of RANKL or direct osteoclast stimulation (see Figure 1-10) (Datta, 2011). The resulting increased bone resorption may be sufficient to induce overt outgrowth in patients with disseminated tumour cells and initiate the vicious cycle, however this remains to be demonstrated.

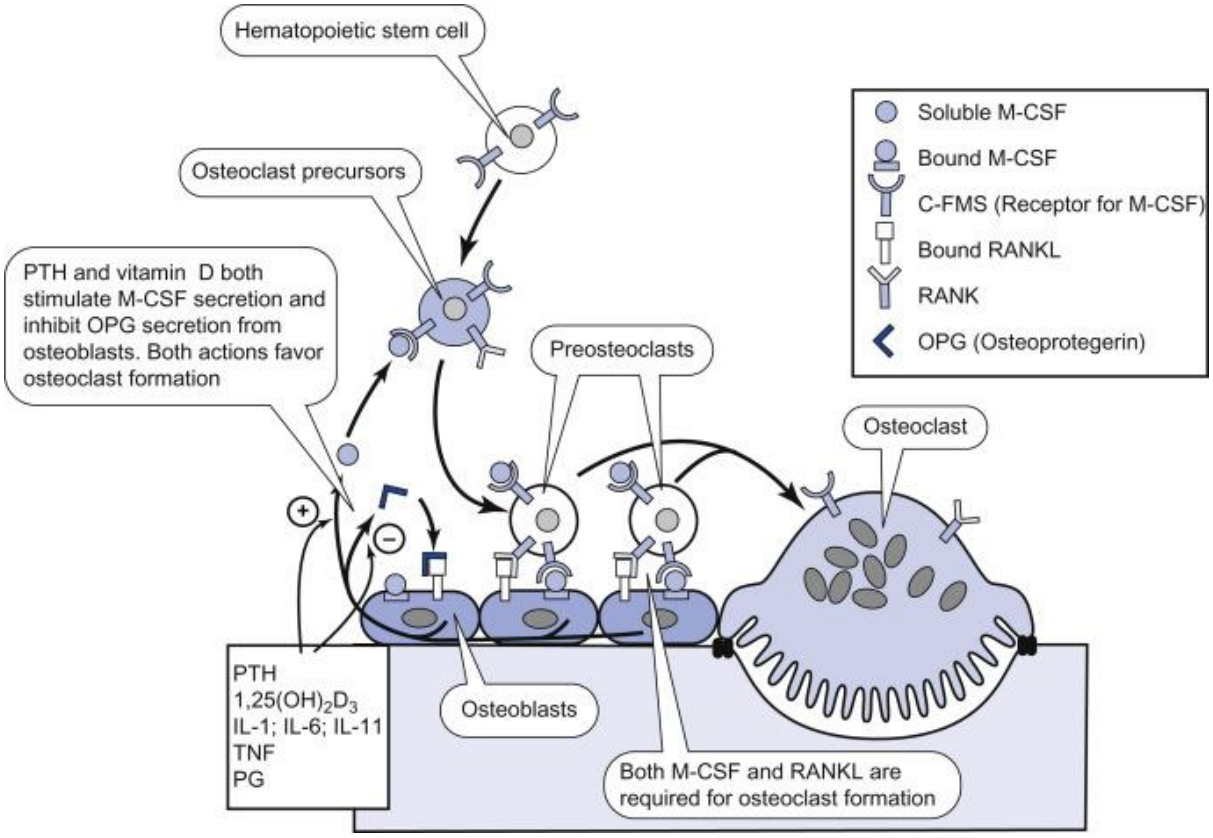

Figure 1-10: Parathyroid hormone acts on osteoclasts directly on PTH1 receptors on osteoclasts or indirectly by promoting increased RANKL and M-CSF expression and decreased OPG secretion by Osteoblasts. Reprinted by permission from Academic Press (Feher, 2017)

In addition to increased bone resorption, PTH may promote tumourigenesis through modulation of immunomodulatory chemicals. Of particular interest is Monocyte Chemoattractant Protein 1 (MCP-1) (CCL2) which is a protein involved in the chemotaxis of monocytes to areas of secretion. In the bone, it is primarily secreted by osteoblasts, and is an important factor in the localization and infiltration of monocyte progenitors which may subsequently differentiate into osteoclasts (Yadav *et al*., 2010). MCP-1 secretion is upregulated in the presence of PTH and is markedly correlated with osteoporotic bone in prostate cancer-induced bone resorption. The effects of MCP-1 are functionally dynamic, being reported to have dual effects. As with bone anabolic or catabolic effects of PTH being dependent on intermittent (anabolic) or continuous (catabolic) PTH secretion, MCP-1's effects is also dependent in a similar manner on the type of PTH secretion (Siddiqui and Partridge, 2017). MCP-1 has been correlated with an increase of pro-tumourigenic macrophage M2 polarisation, which would further As such, a state of hypocalcaemia leading to continuous PTH may lead to increased MCP-1 secretion, further affecting the immune-milieu of the bone microenvironment.

1.6.2 OESTROGEN AS A REGULATOR OF BONE TURNOVER

Another key player in the bone resorption axis is oestrogen, which exerts a bone-protective influence in the bone microenvironment. Oestrogen's effect on osteoblasts and osteoclasts is well characterised, as both express oestrogen receptors α and β. Oestrogen promotes osteoblast-mediated

bone formation and inhibits osteoclastogenesis (Krassas and Papadopoulou, 2001). During periods of normal oestrogen secretion, such as pre-menopause, bone resorption is inhibited by the downregulation of RANKL, and upregulation of osteoprotegerin secretion by osteoblasts (see Figure 1-11) (Wright and Guise, 2014). Furthermore, it limits the production of pro-osetoclastic cytokines such as TGFβ (Krassas and Papadopoulou, 2001). Although oestrogen's modulation of the bone vasculature is not well described, studies into 17β-estradiol have shown effects on subcutaneous tumour vasculature by increasing vessel density and maintenance of structure (Sharma *et al*., 2011). Furthermore, the link between osteogenesis and vasculogenesis suggests that oestrogen's influence on bone formation would indirectly affect vasculature within the bone (Sharma *et al*., 2011).

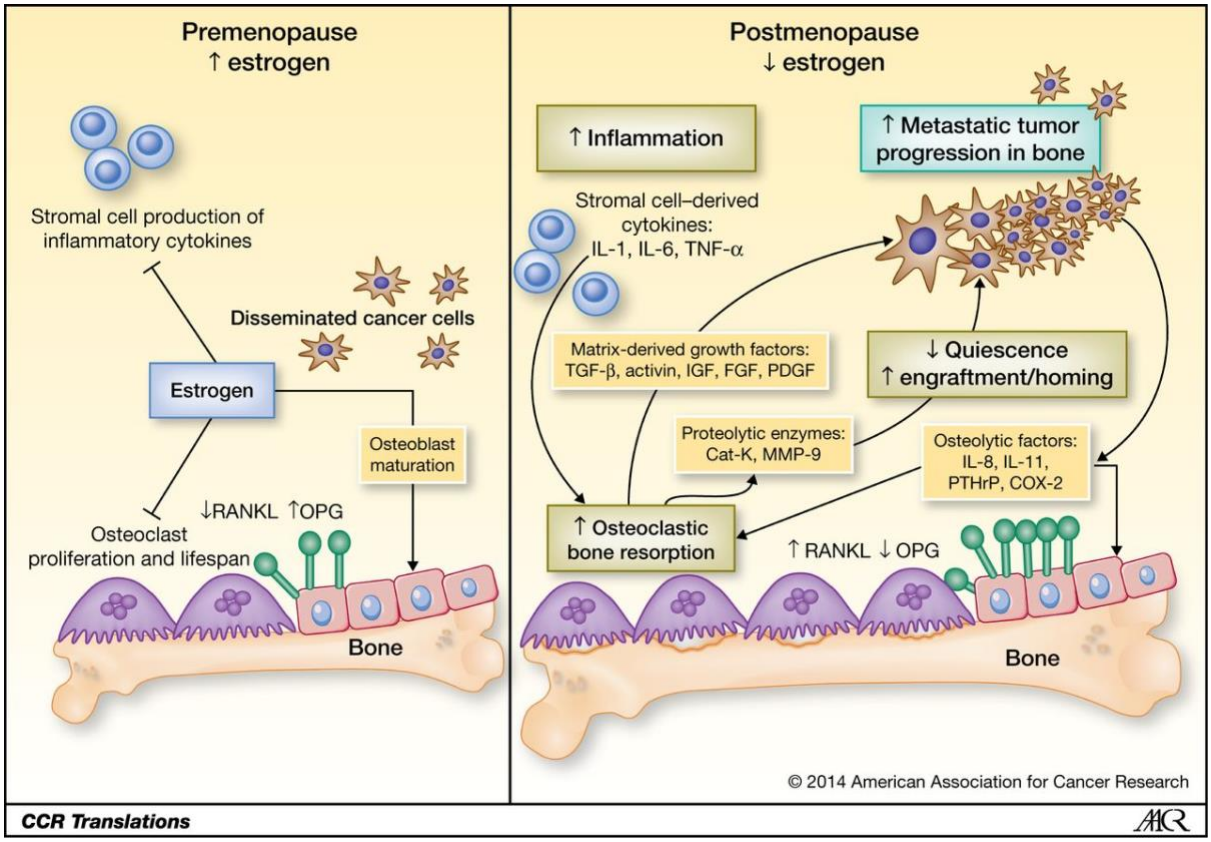

Figure 1-11: Oestrogen works to inhibit RANKL expression and increase OPG expression, preventing bone loss. Inflammatory cytokine production is further abrogated in the presence of oestrogen. Post-menopause, loss of oestrogen leads to increased inflammation and bone resorption that may be responsible for tumour recurrence in the bone. Reprinted by permission from Clinical Cancer Research (Wright and Guise, 2014)

During a state of low-oestrogen, such as post-menopause, the protective influence of oestrogen over the bone microenvironment may lead to increased bone resorption, facilitating an escape from dormancy through modulated osteoclast activity (Riggs, 2000). Oestrogen further modulates the immune system, inhibiting the secretion of pro-inflammatory cytokines, such as IL-6, TNFα and macrophage inhibitory factor by monocytes (Pelekanou *et al*., 2016). Loss of oestrogen may lead to a shift in an immune-equilibrium state to a pro-tumourigenic immune milieu, further implicating a loss of oestrogen to a pro-tumourigenic microenvironment (Khan and Ansar Ahmed, 2015). A key finding

from AZURE was that post-menopausal women had a survival advantage that was not linked to bone metastasis, further posing questions as to what role oestrogen status had on bone metastasis, resorption and disease progression (Coleman *et al*., 2014). This provides opportunity for investigation into hormone-bone interaction.

1.7 Challenges in Studying Dormancy

The poor understanding regarding underlying mechanisms responsible for dormancy is due to the relative complexity of detection and obtaining samples *ex vivo*. Availability of existing pre-clinical models make this a challenging phenotype to study in lab or clinic, as methods for detecting the presence of dormant tumour cells are lacking, particularly in the clinic. Current methods of tumour cell identification require size above detectable thresholds and/or proliferation and uptake of detectable markers, such as increased fluoro-deoxyglucose (FDG) uptake in positron emission tomography (PET) detection, which are significantly reduced in dormant cells. It is therefore poses a significant challenge to identify, isolate, and study the rare populations presented by dormant DTCs.

However, using dye retention, lost through cell division, to detect quiescent cells, has shown promise in recent findings, allowing researchers to isolate and characterise these cells in the lab (Quayle *et al*., 2018). This strategy would further allow the identification of the nature of dormancy; whether cell cycle arrested or at population equilibrium. However, this strategy is not feasible for clinical use, where not only identification of the presence of dormant DTCs would be valuable, but also further identifying the nature of dormancy may inform therapeutic strategies to be pursued in these cases.

The models used to study dormancy, especially those pertaining to the regulation of the bone microenvironment are still largely in infancy and require further insight and development in order to reliably inform clinical meaning.

1.8 RNA sequencing

Gene expression is the fundamental level at which the results of various genetic and regulatory programs are observable. Large scale quantification of mRNA abundance has fundamentally shifted from lower throughput techniques such as PCR, to microarrays and most recently to next generation sequencing in the form of RNA-sequencing. The ability to quantify the expression of transcripts across the entire transcriptome has provided unparalleled quantification of gene expression, leading to its wide-spread adoption in a wide range of fields from agriculture, to cancer research.

In addition to identifying dysregulated proteins in cancerous tissue RNA sequencing has been applied in the a wide range of areas including the discovery of previously unknown RNA species and phenomena such as microexons (Irimia *et al*., 2014), cryptic exons (Eom *et al*., 2013), so-called skiptic exons (Fratta *et al*., 2018), circular RNAs (Kim *et al*., 2015b, Salzman *et al*., 2012), enhancer RNAs (Kim *et al*., 2015b), fusion genes (Parker and Zhang, 2013), and so-called epitranscriptomics involving RNA

base modifications (Frye *et al*., 2018), greatly accelerating disease characterisation and drug discovery efforts.

Steps taken in a typical RNA sequencing experiment include the isolation of RNA from the tissue of interest, before creating a cDNA library based on the transcripts. This is an important as the sequencing process relies on DNA polymerase that requires DNA. The cDNA library then has adapters ligated to aid in binding to flow cells within the sequencer, and subsequently sequencing is performed. Reads from the sequencing experiment are then checked for read quality and aligned to a genome or transcriptome. These aligned reads can then be processed by counting in the case of differential gene expression, or analysed for splice variants and novel RNA sequences for discovery.

Computational Analysis

The first step in computational data analysis of RNA sequencing reads is to clean the raw sequencing file, often provided in the form of FASTQ files. Visual outputs of this quality control step reveal the quality of the sequencing, which then informs the discarding of low-quality reads, elimination of poor-quality bases and the trimming of adapter sequences. Tools frequently in this step include FASTQ/FASTQC (Krueger F, 2012), Trimmomatic (Bolger *et al*., 2014) and PRINSEQ (Schmieder and Edwards, 2011).

Cleaned reads are then mapped either to a genome or a transcriptome. Mapping tools currently available and frequently used include Tophat2 (Kim *et al*., 2013), HISAT2 (Kim *et al*., 2015a), STAR (Dobin *et al*., 2013), BWA (Li and Durbin, 2009) and Bowtie (Langmead *et al*., 2009). Following alignment, transcripts can be assembled using tools such as such as Cufflinks (Trapnell *et al*., 2010), StringTie (Pertea *et al*., 2015), Trinity (Grabherr *et al*., 2011), SOAPdenovoTrans (Hurgobin, 2016) and Trans-ABySS . Expression can be quantified at the gene, transcript and exon levels using tools including FeatureCount (Liao *et al*., 2014) and HTSeq-count (Anders *et al*., 2015). Alignment-free quantification tools exist that provide significantly lower computational requirements, such as Kallisto (Bray *et al*., 2016), Sailfish (Patro *et al*., 2014)and Salmon (Patro *et al*., 2017). Additional tools, such as DegNorm, have been developed to correct read counts for fragmented genes owing to low RNA integrity at extraction. After normalizing, an expression matrix is generated, and statistical methods can be used to identify differentially expressed genes using tools such as DESeq2 (Love *et al*., 2014) and edgeR (Robinson *et al*., 2010). A summary and visual illustration of this process can be seen in Figure 1-12.

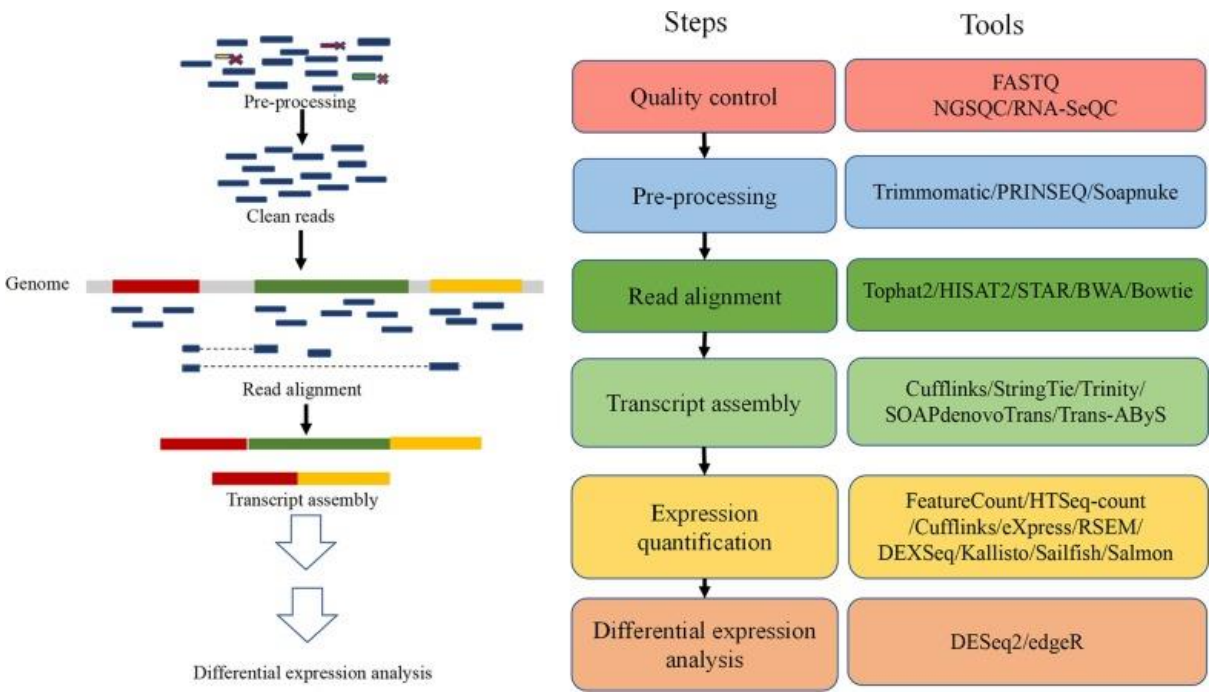

Figure 1-12: Processing pipeline for a typical RNA sequencing experiment. Reprinted with permissions from the Journal of Hematology & Oncology (Hong *et al*., 2020)

1.8.1 Cellular deconvolution of Bulk RNA sequencing

While RNA sequencing of tissues provides valuable information about altered transcripts within a tissue, this data only represents averaged expression levels of the heterogenous mixture of cells present (Haubruck *et al*., 2020, Huang *et al*., 2022). This can confound the interpretation of the expression of these genes, and masks shifts in cell type compositions that can drive disease without significantly affecting differential gene expression. Therefore it is important to understand the composition of cell types within samples, and especially in phenomena such as DTC dormancy where cells local to the dormant cell may be driving entry into or escape from dormancy of these DTCs without having an effect on transcript abundance when considering the entire tissue.

Methods to obtain information on individual cell populations exist, such as flow cytometry and single cell sequencing, with recent advances in spatial transcriptomics that can identify positional information in addition to transcriptomic information (Baccin *et al*., 2020). However, these methods are expensive and require significant time and expertise to perform. In addition, it is not possible to use these methods to obtain information on cellular composition when tissue has samples have been inappropriately processed, stored or have depleted nor can they be performed on tissues that a researcher would not have access to, such as publicly available data. In such cases, using computed cellular deconvolution methods to estimate cell type abundance within and between tissues can provide a quick, cheap and effective means of deriving insights into the cellular composition based on bulk RNA sequencing data (Finotello and Trajanoski, 2018). These methods use gene expression profiles from single cell gene expression quantification to provide an estimate of the cell type within

the bulk mixture (Finotello and Trajanoski, 2018). This is repeated for every cell in which a gene expression profile is available, thereby estimating the abundance of several cells from each sample which can be scored against

Deconvolution methods use a wide variety of statistical techniques to estimate cell type abundance, and are grouped into 3 main types; marker genes methods where marker gene and gene set enrichment analysis are used to estimate cell type abundance, partial deconvolution where present cell mixtures are estimated and complete deconvolution which simultaneously estimate the relative cell fractions and disentangle their expression profiles (Finotello and Trajanoski, 2018). Deconvolution methods utilising marker genes use the gene set enrichment analysis (ssGSEA) method with additional steps, such as averaging enrichment scores across gene sets belonging to a cell type, conversion of enrichment scores into abundance scores that are highly correlated with the true cell proportions. Examples of tools and algorithms that use this method include TIminer (Tappeiner *et al*., 2017), xCell (Aran *et al*., 2017) and MCP-counter (Becht *et al*., 2016).

Deconvolution of cell mixtures fall under the partial deconvolution and in essence formulate a system of equations that describe the expression of each gene in a heterogeneous sample as a linear combination of the expression levels of that gene across the different cell subsets present in the sample, weighted by their relative cell fractions based on a reasonable linearity assumption (Shen-Orr and Gaujoux, 2013). This can include using linear least square regression, constrained least squares, perturbation models, support vector regression and quadratic programming, given input gene expression mixture and cell gene signature matrices to obtain abundance estimates for cell fractions (Shen-Orr and Gaujoux, 2013). These are then normalised between 0 and 1 and therefore relative cell fractions. Tools utilising partial deconvolution include DeconRNASeq (Gong and Szustakowski, 2013), PERT (Qiao *et al*., 2012), CIBERSORT (Chen *et al*., 2018a), TIMER (Li *et al*., 2017), EPIC and quanTIseq (Plattner *et al*., 2020).

Complete deconvolution methods which simultaneously estimate relative cell fractions and disentangle their expression profiles, often using an unsupervised method, non-negative matrix factorization (NMF) (Venet *et al*., 2001). As it is an unsupervised method, the factorization may decompose the mixture matrix into components not related to the cell types of interest but may be constrained by the incorporation of prior knowledge of cell-specific marker genes. A tool utilising NMF methods is deconf (Repsilber *et al*., 2010), though other methods such as k-means clustering, maximum likelihood over the residual sum of squares and quadratic programming are used by tools such as MMAD (Liebner *et al*., 2014) and DSA to provide abundance estimates of cells and their expression profiles from bulk RNA sequencing data (Zhong *et al*., 2013).

Many of these cellular deconvolution methods have pre-curated and validated expression profiles for genes belonging to a set of selected cells in which the algorithm has been demonstrated to perform well. As such, it is common for users to select methods based not only on their function, but on the applicability of the curated list of available gene sets for the cell types they intend to estimate. A

summary of the aforementioned methods including available validated gene sets can be seen in Table 1-4.

Despite its utility, cellular deconvolution can be variable and different methods can provide vastly different estimates for the same dataset dependent on input gene signature matrix or number of cell types being simultaneously estimated, as well as a tendency to overestimate abundance of cell types with similar expression profiles (Finotello and Trajanoski, 2018). Extensive work has been done to benchmark methods, but these still remain experimental and indicative rather than conclusive (Avila Cobos *et al*., 2020, Decamps *et al*., 2021, Jin and Liu, 2021). However, an increase in the availability and quality of single cell sequencing data is improving the accuracy of bulk deconvolution methods (Finotello and Trajanoski, 2018). Cellular deconvolution still remains a valuable alternative to more specialist and expensive single cell profiling methods, especially when analysing historic and public data that did not provide single cell resolution data.

Table 1-4: Features of the computational tools for the quantification of constituent cells from transcriptomics data algorithm type (M = marker genes, P = partial deconvolution, C = complete deconvolution), main method, cell types quantified using the embedded gene sets or signature profiles, and code availability. Adapted with permissions from *Quantifying tumor-infiltrating immune cells from transcriptomics data*, Finotello and Trajanoski (2018), Cancer Immunol Immunother (Finotello and Trajanoski, 2018)

Tool	Type	Method	Cell types	Code availability	References
TIminer	M	PrerankedGSEA	Different gene sets with 31, 28, and 64 cell types	http://icbi.i-med.ac.at/software/timiner/timiner.shtml (Docker image)	(Tappeiner *et al.*, 2017)
xCell	M	ssGSEA	64 immune and non-immune cell types	http://xcell.ucsf.edu/ (R script, web tool)	(Aran *et al.*, 2017)
MCP-counter	M	Geometric mean of expression of marker genes	8 immune cells, fibroblasts, and endothelial cells	http://github.com/ebecht/MCPcounter (R script)	(Becht *et al.*, 2016)
DeconRNASeq	P	Constrained least square regression	–	DeconRNASeq package available on Bioconductor (R package)	(Gong and Szustakowski, 2013)
PERT	P	Non-negative maximum likelihood		Supplementary material in the original publication (Octave)	(Qiao *et al.*, 2012)
CIBERSORT	P	Nu support vector regression	22 immune cell types	https://cibersort.stanford.edu/ (R script, java executable, web tool)	(Newman *et al.*, 2015)
TIMER	P	Linear least square regression	6 immune cell types	https://cistrome.shinyapps.io/timer/ (web tool)	(Li *et al.*, 2016)
EPIC	P	Constrained least square regression	6 immune cell types, fibroblasts, endothelial cells, and uncharacterized cells	https://gfellerlab.shinyapps.io/EPIC_1-1 (R script, web-interface)	(Racle *et al.*, 2017)
quanTIseq	P	Constrained least square regression	10 immune cell types, uncharacterized cells	http://icbi.i-med.ac.at/software/quantiseq/doc/index.html (Docker image)	(Plattner *et al.*, 2020)
deconf	C	Non-negative matrix factorization	-	Supplementary material in the original publication (R package)	(Repsilber *et al.*, 2010)
DSA	C	Quadratic programming	–	https://github.com/zhandong/DSA (R package)	(Zhong *et al.*, 2013)
MMAD	C	Maximum likelihood over the residual sum of squares	–	http://sourceforge.net/projects/mmad/ (Matlab)	(Liebner *et al.*, 2014)

1.9 FURTHER RESEARCH

Breast cancer therefore remains a disease with significant societal impact. The frequency of incurable bone metastases, including dormant phenotypes warrants further investigation to alleviate unmet clinical needs despite the availability of various therapeutic options. Chemical interventions, including those that alter the endocrine status may have significant effects on numerous components in the bone microenvironment (Ubellacker *et al*., 2017).The significance of these alterations is not well understood and research may provide further insight into the strengths, weaknesses and opportunities of current therapies (Ubellacker *et al*., 2018). Current research points to the osteoclast and the rate of bone turnover playing an important role early in the escape of dormant, disseminated tumour cells (Ottewell *et al*., 2015). In addition, clinical trial data suggesting a role for oestrogen in the bone microenvironment through differences in treatment outcome based on menopausal status further highlight the need to understand the role of this molecule in the bone microenvironment (Coleman *et al*., 2014, Westbrook *et al*., 2016). Importantly, the dynamic interplay between dormant tumour cells and the bone microenvironment is poorly understood, and developing, assessing and improving current models is of significance. The advent of next-generation sequencing and increasing availability of public data are vital tools that can be employed to shed insight into the proposed research questions. I therefore framed my aims, hypothesis and objectives according to these insights.

1.10 Aims, Hypothesis and objectives

1.10.1 Aims

The body of work present in this thesis aims to use *in vivo* models to investigate and characterise the effect of the bone microenvironment, particularly increased bone resorption by osteoclasts or inhibition thereof, on tumour cell dormancy and overt outgrowth of disseminated breast cancer cells.

1.10.2 Hypotheses

The overarching hypothesis of this thesis is that:

> Altering the bone microenvironment to induce increased bone turnover triggers the outgrowth of dormant disseminated breast cancer cells

The following hypotheses are formed in relation to the overarching hypothesis of this thesis:

1. A low calcium diet is sufficient to trigger increased bone resorption by osteoclasts, resulting in the outgrowth of dormant, disseminated tumour cells within the bone
2. A higher rate of bone turnover leading to increased tumour growth, can be inhibited by repeated administrations of clinically relevant doses of Zoledronic acid
3. The effect of Zoledronic acid in reducing tumour growth within the bone microenvironment is impacted by altered tumour gene and protein expression
4. Decreasing oestrogen in the bone microenvironment through ovariectomy recapitulates transcriptional changes in the post-menopausal bone microenvironment

1.10.3 Objectives

Testing the above hypotheses will determine whether:

1. Subtle changes to the bone microenvironment can trigger the outgrowth of dormant, disseminated tumour cells
2. More frequent dosage of bone targeting agents in bone with higher turnover can inhibit the growth of steadily growing breast cancer cells within the bone microenvironment by altering resident cell populations
3. The effect of bone targeting agents in inhibiting tumour outgrowth in high-turnover bone is dependent on intra-tumoural protein composition
5. How accurate current mouse models for dormancy and menopausal status using ovariectomy recapitulate the clinic and can be used to model transcriptional changes

2 MATERIALS AND METHODS

2.1 MATERIALS

Table 2-1: Laboratory reagents

Reagent	Supplier
Dimethyl formamide	Sigma Aldrich
DMEM culture medium	Gibco
DMSO	Sigma-Aldrich
DPX mounting glue	VWR
EDTA	Sigma-Aldrich
Eosin	Atom Scientific
Gill's haematoxylin solution	Merck
Isoflourane	Abbott
Luciferin	Perkin Elmer
Naphthol AS-BI phosphate (sodium salt)	Sigma-Aldrich
Paraformaldehyde	Sigma-Aldrich
Pararosaniline	Sigma-Aldrich
PBS (*in vivo*)	Gibco
PBS tablets	Oxoid
RPMI culture medium	Gibco
Sodium acetate	Sigma Aldrich
Sodium Hydroxide	Fisher Scientific
Trypsin EDTA	Thermo Fisher
Vibrant-DiD cell membrane dye	Life Technologies
Zoledronic Acid	Novartis

Table 2-2: Disposable equipment

Item	Supplier
Bijoux tubes (5ml)	Starstedt
Cell strainer (70µm)	BD Biosciences
Conical centrifuge (falcon) tubes (15, 50ml)	
Cryovials (1ml)	Thermo Scientific
Filter tips (10, 20, 200 and 1000µl)	Starlab
Glass cover slips (22x40mm)	Menzel-Gläser
Insulin syringe (0.5 and 1ml) with needle (27G)	Terumo Europe
Microcentrifuge tubes (0.6 and 1.5ml) STARLAB	Starlab

Needle (25G)	Becton Dickinson
Pipette tips (10, 20, 200 and 1000µl)	Costar
Strippets (5, 10 and 25ml)	Costar
Syringe (1ml)	Terumo
T75 Tissue culture flasks	Nalgene Nunc Ltd
Universal containers	Starstedt

Table 2-3: Non-bioinformatic analysis software

Software Used	Vendor
CTAnalyser software	SkyScan, Burker microCT, CT-Analyser
OsteoMeasure7 version 4.2	OsteoMetrics
Prism version 8.x	GraphPad
Nrecon	OsteoMetrics

Table 2-4: Laboratory equipment

Laboratory equipment	Supplier
Benchtop Centrifuges	Thermo Fisher, MSE Mistral 2000
BX53 microscope	Olympus
Centrifuge	Beckman
Leitz DMRB microscope	Leica Microsystems
IVIS Lumina II	Perkin Elmer
pH meter	Mettler Toledo
SpectraMax 5Me plate reader	Molecular Devices
Vortexer	Hook&Tucker Instruments
Water bath	Grant JB Series
X-ray micro computed tomograph	SkyScan 1272, Bruker microCT

Table 2-5: Cell lines used

Cell line	Source	Description
MDA-MB-231-IV-GFP-Luc2	Dr Penelope Ottewell	Frequently used triple negative breast cancer cells selected for bone-homing properties , transfected with Green Fluorescent Protein and Luciferase II for *in vivo* and *ex vivo* detection
MDA-MB-231-TD-Tomato	Dr Victoria Cookson	Clone of MDA-MB-231-GFP-Luc2 selected for slower growth kinetics
MDA-MB-231-GIPC1ko-CAPGko	Dr Victoria Cookson	Clone of MDA-MB-231-GFP-Luc2 with the addition of GIPC1 and CAPG gene knockouts

2.2 *IN VITRO* METHODS

2.2.1 MDA-MB-231 AND MDA-MB-231-IV-GFP-LUC2

MDA-MB-231 is an epithelial metastatic mammary adenocarcinoma established from a pleural effusion derived from a Caucasian female (Cailleau *et al*., 1978). It is a highly aggressive, TNBC cell line lacking ER, PR and HER2 expression (Holliday and Speirs, 2011). Two lineages possessing genetic alterations enabling *in vivo* and *ex vivo* imaging were developed at the University of Sheffield; the IV cell line stably transfected with Firefly Luciferase and Green-Fluorescent Protein (GFP) and the td-Tomato cell line transfected with firefly luciferase.

2.2.2 MAINTENANCE OF CELL CULTURES

MDA-MB-231-IV cells were cultured in Gibco RPMI 1640 (1X) + GlutaMAX™ medium (Thermo Fisher Scientific, UK), supplemented with 10% Foetal Calf Serum (FCS)(Sigma Aldrich) in air-filtered T75 flasks. MDA-MB-231-td-Tomato cells were cultured in Gibco Dulbecco's Modified Eagle Medium (DMEM) (1X) containing GlutaMAX™, 4.5g/L D-Glucose and Pyruvate (Thermo Fisher Scientific, UK), further supplemented by adding 10% FCS within air-filtered T75 flasks. All cells were maintained in incubators at 37°C, relative humidity of 95% and 5% CO_2.

2.2.3 FREEZING OF CELLS

To freeze cells for later use at a similar passage, a single cell suspension was prepared by twice washing the cells with sterile PBS before dissociation with trypsin. The cells suspension was pelleted by spinning in a centrifuge (Beckman) at 800-1000rpm for 5 minutes, the supernatant discarded and cells resuspended in 10% DMSO in DMEM or RPMI medium, volume dependent on cell number (approximately $1x10^6$ cells/ml). Suspension of cells was aliquoted into labelled cryovials (Thermo Scientific), at a maximum of 1ml/vial and immediately stored at -80°C overnight awaiting transfer to liquid nitrogen storage by a responsible member of faculty.

2.2.4 THAWING OF CELLS

To thaw cells previously frozen in medium and DMSO, a fresh aliquot of the same medium used to freeze cells was warmed to ~37°C in a 15ml falcon centrifuge tube (Thermo Scientific). Cells were then removed from frozen storage, and quickly thawed at 37°C in a water bath (Grant). 1ml of thawed cell suspension was added to the 9ml cell suspension, before pelleting by centrifuging at 800rpm for 5 minutes in a centrifuge, the supernatant discarded and cells re-suspended in appropriate media and volume, according to cell concentration required.

2.2.5 CELL PASSAGING

To passage cells, old media (10ml) was discarded from ~80% confluent cells in T75 flasks and washed twice with 5ml sterile cell culture-grade Gibco phosphate buffered saline (PBS) (ThermoFisher, UK)

which was subsequently discarded. To detach cells, 1-2ml of Trypsin EthyleneDiamineTetraacetic Acid (EDTA)(Thermo Fisher Scientific) was added to the flask and incubated at 37°C for 3-5 minutes until complete detachment was achieved. 4-8ml of appropriate FCS-containing medium was added to inactivate the trypsin, cell suspension transferred to tubes and centrifuged at 800rpm for 5 minutes to form a pellet. Supernatant was discarded, and cells re-suspended in 10ml medium with FCS. Re-suspended cells were re-seeded in T75 flasks at densities of 5-20% of parent suspension and stored as per maintenance protocol.

2.2.6 Counting of Cells

Cells were prepared as per cell passaging protocol prior to seeding for counting. 10µl of cell suspension was pipetted into two sides of a haemocytometer with a cover slip. Four 4x4 square corners ($1x10^{-4}$ ml volume) were counted (see Figure 2-1) across two grids under a light microscope, a total of 8 4x4 square corners.

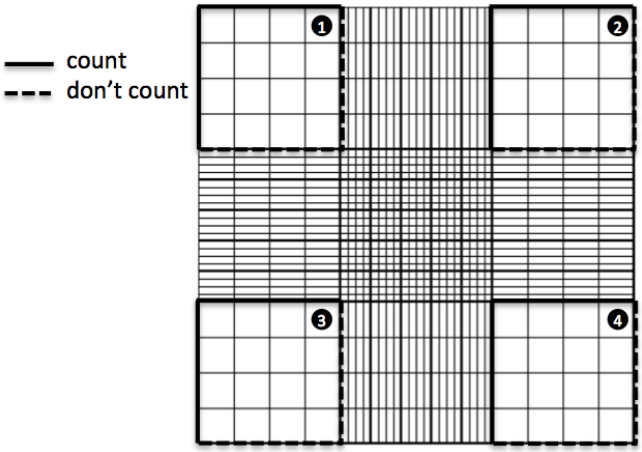

Figure 2-1: Haemocytometer counting squares 1-4 representing a single grid. Cells lying on borders of squares counted (thick lines) and not counted (dashed lines) represented. Image courtesy of Maria Fuentes (Fuentes, 2014)

To calculate total number of cells per ml, cell counts were totalled and averaged across all 8 squares (total count / number of squares counted) and multiplied by the volume factor $1x10^{4}$.

2.2.7 Preparation of cells for intra-cardiac injection

In experiments involving introducing cancer cells into mice, animals were injected with vybrant DiD labelled MDA-MB-231-IV cells via intra-cardiac injection. Vybrant DiD (Life Technologies, Paisley, UK) is a lipophilic membrane-bound dye that is lost through cell division and is used to track dormant cells that are quiescent or slow cycling.

$1x10^{6}$ cells or $5x10^{5}$ cells per ml were suspended in serum-free medium to a volume twice that required for each mouse to receive $1x10^{5}$ or $5x10^{5}$ cells in a 100µl volume. 5µL per ml of dye was added to the cell suspension in a single 15ml falcon tube, and incubated at 37°C in a water bath for 20 mins while protected from light by wrapping in foil. Cell suspensions were then centrifuged at 800rpm for 5 minutes, generating a blue pellet. Supernatant was discarded and an equivalent volume of PBS was added to re-suspend the cells, before being centrifuged at 800rpm for 5 minutes, with resuspensions and centrifugation repeated thrice. Finally, cells were suspended in an equivalent volume of ice-cold PBS and stored on ice to be injected into mice within 2 hours of initial trypsinisation.

2.3 *IN VIVO* METHODS

2.3.1 ANIMALS

12-week-old female Bagg and Albino (BALB)/c (CAnN.Cg-***Foxn1^{nu}***/Crl) nude (immunocompromised) and C57BL/6 (immunocompetent) mice were acquired from Charles River, UK. 12-week-old female BALB/c (OlaHsd-*Foxn1^{nu}*) nude (immunocompromised) mice were obtained from Envigo, UK. Upon arrival, mice were acclimatised in the Biological Services Unit (BSU) for a minimum of 7 days before procedures. Mice were aged for a further 2-3 weeks to obtain mice aged 14-15 weeks at the time of procedure, reflecting aged phenotypes.

All procedures performed were approved and carried out under Procedure Project Licence (PPL) 70/8964 and personal license PIL I62B58981 within the Biological Services Unit (BSU) under local guidelines and in accordance with Home Office regulations.

2.3.2 LOW CALCIUM DIET

Mineral adjusted chow (0.1% calcium) was obtained from Envigo, US. Animals were fed a low calcium diet in order to trigger increased bone resorption as a result of hypocalcaemia and the action of PTH. In *in vivo* experiments, mice were fed a low calcium diet for variable periods of time, following intra-cardiac injection of tumour cells where this was performed.

2.3.3 INTRA-CARDIAC INJECTION

Late-stage metastasis was mimicked by direct injection of Luc2+ve MDA-MB-231-IV cells into the circulation. To encourage bone metastases, 100µl of $1x10^5$ or $5x10^4$ cells suspended in PBS were injected directly into the left ventricle of mice under inhalation anaesthesia consisting of 2-3% isoflurane (Zoetis, UK). Mice were placed in an incubator at 32°C for 1-3 hours post-injection and monitored closely for adverse signs in the 24-hour period ensuing.

2.3.4 OVARIECTOMY

Bilateral resection of the ovaries by ovariectomy (OVX) is a surgical procedure that has been used to induce deprivation of hormones produced by the ovaries, with oestrogen a particular target of reduction. It has been performed on various animals, such as rodents and non-human primates (Brinton, 2012). In mice, the procedure entails access to the visceral cavity from the lumbar area of the mouse, to allow surgical resection of the ovaries. The procedures in my experiments were performed by Dr Penelope Ottewell, Mrs. Diane Lefley under the project license (PPL P99922A2E).

2.3.4.1 SURGICAL PROCEDURE

14-week-old female mice BALB/C were anaesthetised with isoflurane (2.5% vaporisation rate and oxygen flow of 1.5-2 L/min) followed by administration of 100µl analgesic (buprenorphine

(Vetergesic), CEVA Animal Health) (0.1mg/kg) and 100µl broad-spectrum antibiotic (enrofloxacin (Baytril), Bayer) (6.25mg/kg) via sub-cutaneous injection. Hair was removed from the lower third of the back using electric clippers before being swabbed with iodine to sterilise the operation site. A ~1.5cm longitudinal incision was made following the midline along the spine using a surgical scalpel blade. A gentle blunt dissection was used to detach skin from the muscle on both sides of the incision. Curved forceps were then used to produce a blunt dissection through the muscle wall immediately above the ovary, approximately 1cm from the spinal cord on each side. Using cat-spay forceps, the ovaries were located above the womb and removed using blunt dissection on each ovary. On successful removal of the ovaries, the internal wound was closed using absorbable sutures, and the external wound was closed suing non-absorbable polypropylene monofilament suture using a simple interrupted technique.

Following the procedure, all mice were left to recover in a veterinary incubator set at 25°C for four hours, before being transfered back to clean cages. Mice were given a second dose of analgesic and antibiotic sub-cutaneously 24 hours following the surgical procedure and closely monitored for adequate healing of the sutured incision on the back and fluctuations in weight until the experiment was completed.

2.3.5 *IN VIVO* IMAGING

To track tumour progress *in vivo,* animals injected with cancer cells expressing firefly luciferase were injected sub-cutaneously with 100µl of D-luciferin (30mg/kg) 5 minutes prior to imaging on both sides of the coronal plane (front and back) of the animal. Imaging was done in the *in vivo* imaging system (IVIS) LUMINA II (Caliper Life Sciences). This procedure was carried out under anaesthetic following administration of 2-4% isofluorane.

Living image software (version 4.1) was used to identify presence and quantify size of tumours by bioluminescent capture measured in photos/second and displayed on a scale with different colours representing varying intensities of luminescence. Both larger size and increased intensity of luminescence represent larger tumours (see Figure 2-2).

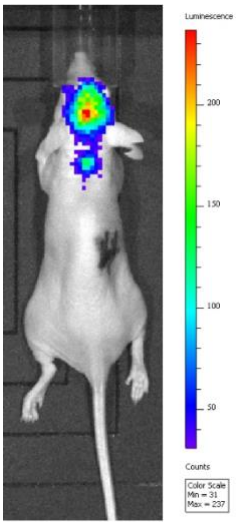

Figure 2-2: Bioluminescent imaging of MDA-MD-231 cells expressing firefly luciferase and subjected to luciferin. Scale on the right represents varying levels of intensity, blue hue representing approximately 50 units, and red representing more than 210 units.

2.4 Sample Collection and Preparation

2.4.1 Buffer Solution preparation

Solutions for tissue sample collection were prepared as below:

2.4.1.1 PBS

Phosphate-Buffered-Saline (PBS) solution was prepared by adding 1 tablet of PBS per 100ml of de-ionized water (dH_2O). Volumes typically prepared were 500ml, by adding 5 tablets to 500ml of dH_2O.

2.4.1.2 Fixation of tissue samples

Fixation is an important step in the preservation of tissues obtained from mice prior to use in microscopy or other techniques reliant on the preservation of proteins. For fixation, PFA solution (4% (*w/v*)) was typically prepared at 500ml. Within a chemical fume hood, 20g of paraformaldehyde (PFA)(Fisher Scientific) was weighed and added to 500ml of PBS solution in a glass bottle. A magnetic flea was then added, the bottle cap screwed on and placed on a magnetic stirrer at 50-65°C until fully dissolved. This was cooled down, aliquoted and stored refrigerated for short term use, or frozen (-80°C) for long term use.

2.4.1.3 Decalcification of skeletal tissue samples

Cutting of sections from samples to be mounted on slides for microscopy used in this project require sections ranging between 3-40µM. Such thin slides require sharp, thin, yet brittle blades, and the sections cut are fragile. To obtain such cuttings from bone, decalcification of mineralised bone is required to soften the bone sufficiently to aid the cutting process.

For decalcification, 14% (*w/v*) ethylenediaminetetraacetic acid (EDTA) (Fisher Scientific) was typically prepared in a final volume of 500ml. 70g of EDTA powder and 10g of NaOH (Fisher Scientific) (2% (*w/v*)) were added to 500ml PBS and stirred until clear before adjustment to pH 7.5 +/- 0.1 using HCl and stored at 2-8°C for up to 2 months.

Bones processed through decalcification are placed in 4-6ml of EDTA, with the solution changed 2-3 times a week for 4 weeks before processing for wax embedding

2.4.2 Sample collection from *in vivo* studies

At the end of experiments, mice were culled and tissues collected in the following formats.

2.4.2.1 WHOLE BLOOD EXTRACTION BY CARDIAC PUNCTURE

Whole blood was collected for use in down-stream analysis using techniques such as Enzyme-Linked Immuno-Sorbent Assay (ELISA) for the detection of markers, or for analysis of circulating cells in whole blood using hematological analysis.

Mice were placed under anaesthetic prior to the procedure with isoflurane (2.5% vaporisation rate and oxygen flow of 1.5-2 L/min) in a flow chamber. Subsequently, mice were transferred to a surgical pad extension of the anaesthetic device, with isoflurane delivery via nasal mask. Using 1ml syringes and 27 gauge needles (Terumo), needles were inserted ~1-2mm to the right of the sternum of mice and inserted until ~2-3cm of the needle was inserted. Syringes were pulled back to assess the presence of blood by inserting the needle in the heart, and once established 0.4-0.9ml of whole blood was obtained per mouse.

2.4.2.2 SERUM

Whole blood was extracted by cardiac puncture as described above and syringed into Eppendorf tubes and allowed to coagulate at room temperature. The samples were then spun at 8000 RPM for 10 minutes at 4°C, causing separation of the serum and blood cells. Serum (0.3-0.5ml/sample), transferred to a fresh Eppendorf tube and stored at -80°C preparatory for use in Enzyme-Linked Immuno-Sorbent Assay (ELISA) for serum markers.

2.4.2.3 WHOLE BLOOD FOR HEMATOLOGICAL ANALYSIS

Whole blood was extracted by cardiac puncture and 20µl of whole blood was pipetted into Eppendorf tubes containing 20µl of 14% (*w/v*) ethylenediaminetetraacetic acid (EDTA) (Fisher Scientific) to prevent coagulation prior to use in hematological analysis.

2.4.2.4 DISSECTION

The hind limbs of mice were samples obtained from every mouse, in particular the tibia and femur. To obtain these limbs, cuts through the pelvis were made in order to disconnect the entire hind limb from the main body for easier access and manipulation. Following securing the freedom of the limbs from the main body, hind limbs were then separated by cutting through joints with scissors to obtain individual bones prior to the removing of muscle and connective tissue with forceps.

After dissection, bones were processed in various ways dependent on downstream analysis. These are described in the following sections.

2.4.2.5 BONES FOR HISTOLOGY AND HISTOMORPHOMETRY

Immediately following dissection, tibias used for histology and histomorphometry were placed in 7ml bijous containing 5ml of 4% (*w/v)* paraformaldehyde (PFA) for 48-72 hours. These were then washed

3 times in ice-cold PBS and stored in PBS at 4°C pending µCT analysis. Once µCT scanning was complete, bones were placed in 14% (*w/v*) ethylenediaminetetraacetic acid (EDTA) for decalcification for 3 weeks before bone processing. Bones were subsequently paraffin-embedded (wax). To obtain sections for histological analysis, wax embedded tibias were cut at 3µm thickness, and 6 samples taken from 3 levels, 20-30µm apart before mounting on glass slides and storing at room temperature.

2.4.2.6 Bones for Gene Expression Analysis by PCR

Femurs were used for RNA extraction and subsequent PCR gene expression. Once obtained, they were placed in labelled foil and snap frozen in liquid nitrogen, before being stored at -80°C.

2.5 *Ex vivo* Analysis

2.5.1 Micro computed tomography imaging

Micro-computed tomography (µCT) performed on bones was performed in three steps; scanning, reconstruction and analysis. Scanning involves the projection of x-rays through a sample onto a detection plate to create an image representing mineralised bone. The sample is then partially rotated through a selected rotation range with smaller rotation steps with an x-ray-generated image created at each rotation step. The collection of images is subsequently collated and reconstructed to produce 3D images. Finally, 3D images are analysed to produce quantitative data on various bone physical parameters.

Scanning was performed using a Skyscan 1172 X-ray computed microtomography scanner (Bruker, Aartselaar, Belgium) which emits x-rays through an x-ray tube with voltage of 49kV and 200µA current. Control of the scanner was through Skyscan software, with settings of 0.5mm aluminium filter, 4.3µm pixel size and rotation step of 0.7° through a total rotation of 180°. Reconstruction of images was performed using NRecon software and analysis performed using CT Analyser (CTAn) software obtained from Bruker.

A description of the process of analysis data obtained from µCT is given below using the right tibia from a mouse in an *in vivo* experiment utilising immunocompromised BALB/C nude mice placed on a low calcium diet for 7 days or a normal diet. The sample label is CRT1.

2.5.1.1 ROI and reference selection

ROI selection was determined via analytic selection in the CTAn software. Offset value was 46, indicating a 0.198mm offset from the reference marker. Height of selection was 232, indicating a height of 0.998mm. This will be described in more detail below. Reference selection was based on a qualitative method; finding the point at which the spongy bridge on the trabecular bone had broken and using this to set the top of the growth plate. An example picture is shown below for TO2 sample CRT1.

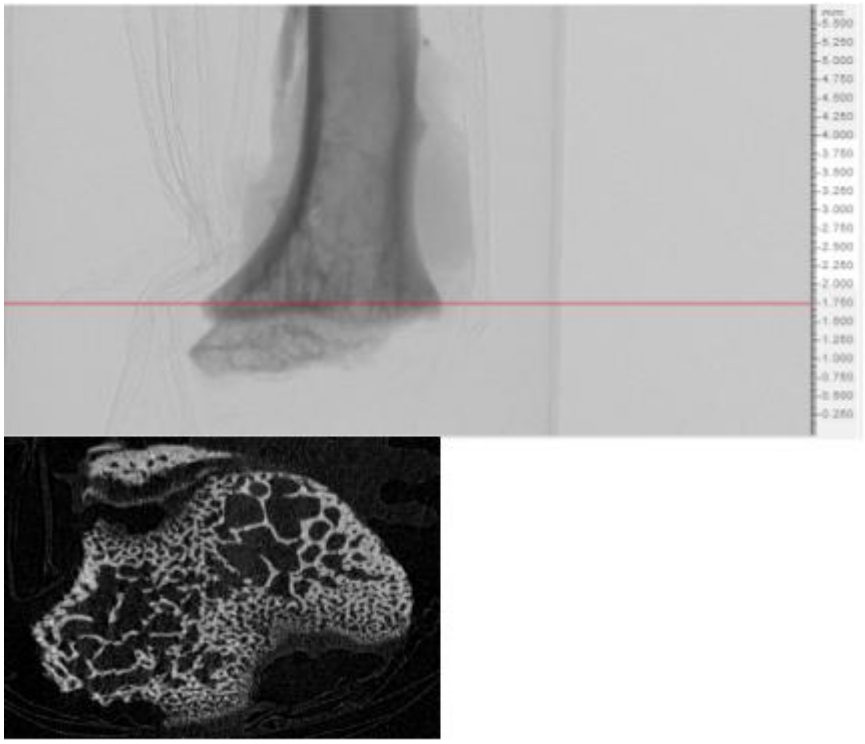

Figure 2-3: Reference selection picture 413 (CRT1__rec00000414). A.) Height of 1.776mm from bottom of picture scan. B.) Cross sectional view of reconstructed image from µCT scan of a tibia

Selecting a reference picture then offset the starting point for the collection of data by 0.198mm from the reference selection. At this point is the first location where the regions of interest are drawn. Region of interest included the inner trabecular bone, excluding the wall. An example is given below of TO2 sample CRT1.

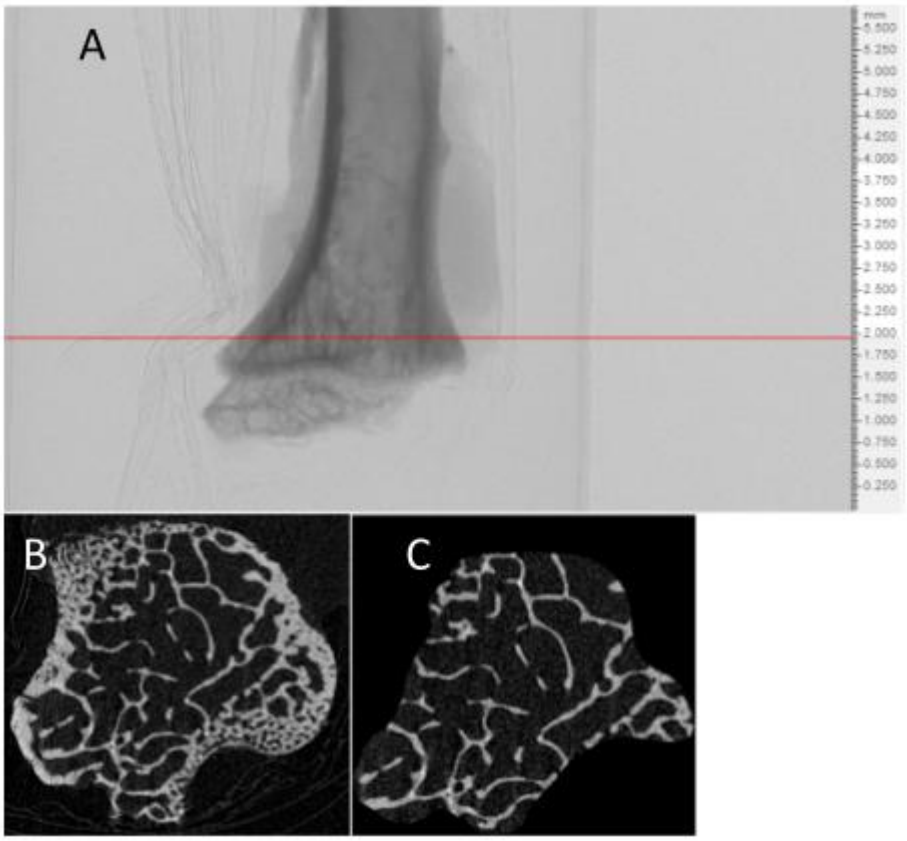

Figure 2-4: CRT1 first scanning picture 459 (Filename: CRT1__rec00000459). A.) Height of 1.974mm, 0.198mm offset from reference picture. B.) Cross section of last reference position. C.) Region of Interest from section B

The end of the region of interest was automatically set once selection of reference and first starting point were selected. A scanning height of 0.998mm input in the settings selected an image 0.998mm, or closest to this distance, from the first starting point.

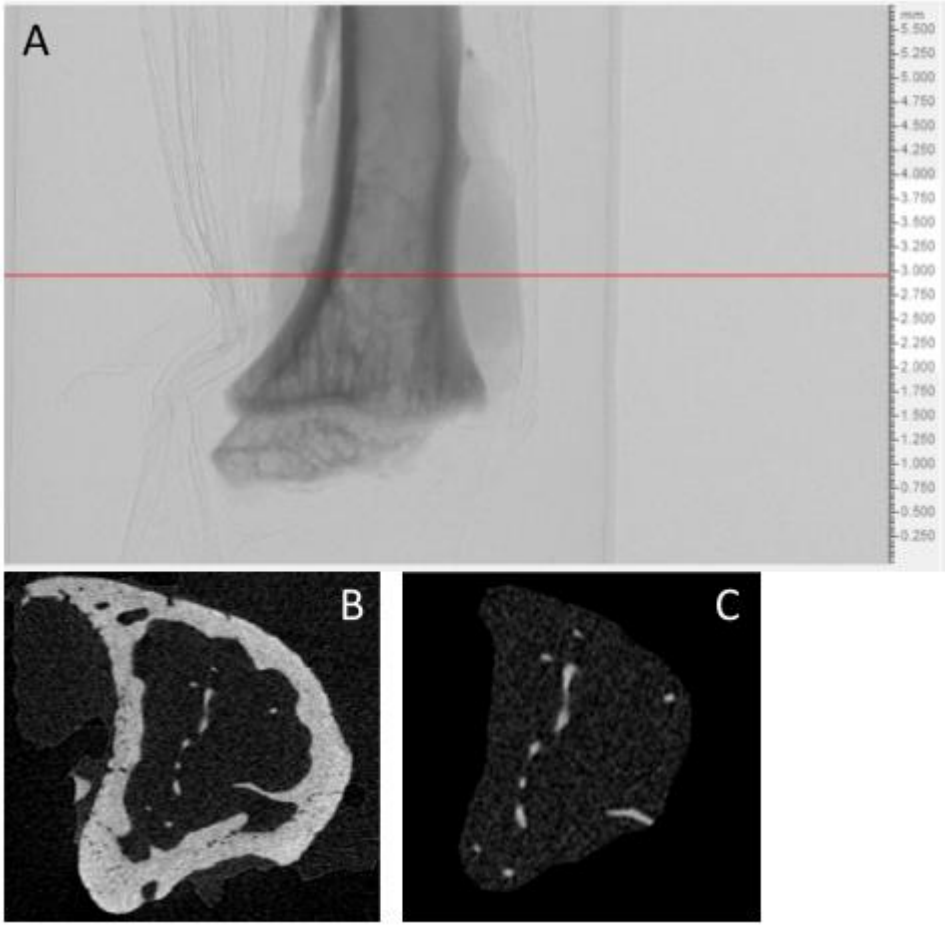

Figure 2-5: TO2 sample CRT1 last scanning picture 691 (Filename: CRT1__rec00000691). A.) Height of 2.971mm, 0.997mm height from first scan. B.) Cross section of last reference position. C.) Region of Interest from section B

Processing of ROIs was performed using batch manager within CTAn software using a lower grey threshold of 80-85 and an upper grey threshold of 255. Internal processing "Thresholding", "Despeckle" and "3D Analysis" were selected with the following paramters:

- Threshold values were set to 83 for lower and 255 for higher
- Despeckle was set to remove white speckles less than 10 voxels within the region of interest
- 3D analysis was performed for all basic values, as well as additional values structure model index, trabecular thickness and number, and trabecular separation

This technology would allow the analysis of physical bone parameters based on mineralised structures. In particular, the trabecular region was of interest for this study as it is the most dynamic area of the bone displaying the effect of changes in diet and bone remodelling in a relatively short time.

2.5.2 Histological Sectioning

To prepare bone samples for histological sectioning, tibias from mice were fixed in 4% PFA in bijoux containers for 24 hours at 4°C. The PFA was then emptied, bones washed thrice with PBS before being placed into 0.5M EDTA, which was changed thrice a week for 4 weeks to decalcify bone mineral and allow sufficient softening to cut. These were then placed in plastic embedding cassettes and processed by laboratory technicians. After processing, bones were placed in cast iron rectangular moulds and filled with wax ready for sectioning. Sections were taken across the sagittal plane of the tibias.

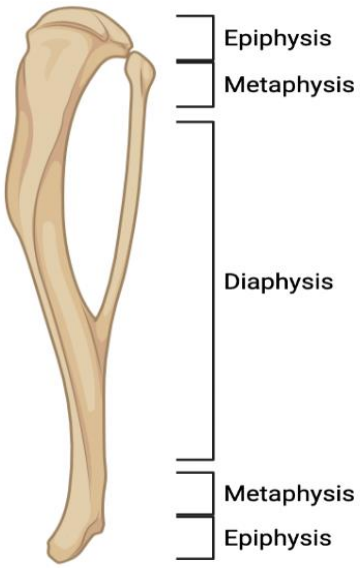

Figure 2-6: Diagrammatic representation of tibias used for histology. Sections obtained across sagittal plane

2.5.3 TRAP Staining

Tartrate-Resistant Acid Phosphatase (TRAP) staining is a histological stain that reveals osteoclast activity by the catalysis of a naphthol-AS-BI phosphate substrate by TRAP, a key enzyme in bone resorption. Presence of red product indicates areas of high TRAP activity, and thereby implicating presence of osteoclasts. This gives an indicator of the number and size, correlated with activity of osteoclasts within a given sample. Counterstaining with Gill's haematoxylin reveals purple nuclei and cell perimeters.

Paraffin-embedded slides, cut at 3µm, were dewaxed and immersed for 5 minutes in a pre-warmed acetate-tartrate buffer prepared by mixing sodium tartrate (2.18% (*w/v*)) into an acetate buffer of diluted acetic acid (1.2% acetic acid (*v/v*) in dH_2O) in H_2O (20% diluted acetic acid (*v/v*) in H_2O).

Solution A was prepared by adding 2% (w/v) naphthol AS-BI phosphate (Sigma-Aldrich) to dimethyl formamide (Sigma Aldrich), before diluting 50x in acetate-tartrate buffer. Sections were transferred into solution A for 30 mins at 37˚C.

Solution B was prepared by dissolving 4% (*w/v*) sodium nitrite in H_2O, which hexasotized when added to an equal amount of pararosaniline (Sigma Aldrich). Solution B was added to 20X volume acetate-tartrate buffer prior to incubating sections in the solution for 15 mins at 37˚C.

Sections were thoroughly rinsed in tapwater and counterstained for 20 seconds in Gil's haematoxylin (Merck) and blue before dehydration and mounted with DPX glue (VWR).

2.5.4 OsteoMeasure Analysis

To analyse the cellular response to bone remodelling, TRAP-stained bone sections were analysed on OsteoMeasure7 version 4.2 through a LEICA Leitz DMRB microscope at a 20X magnification.

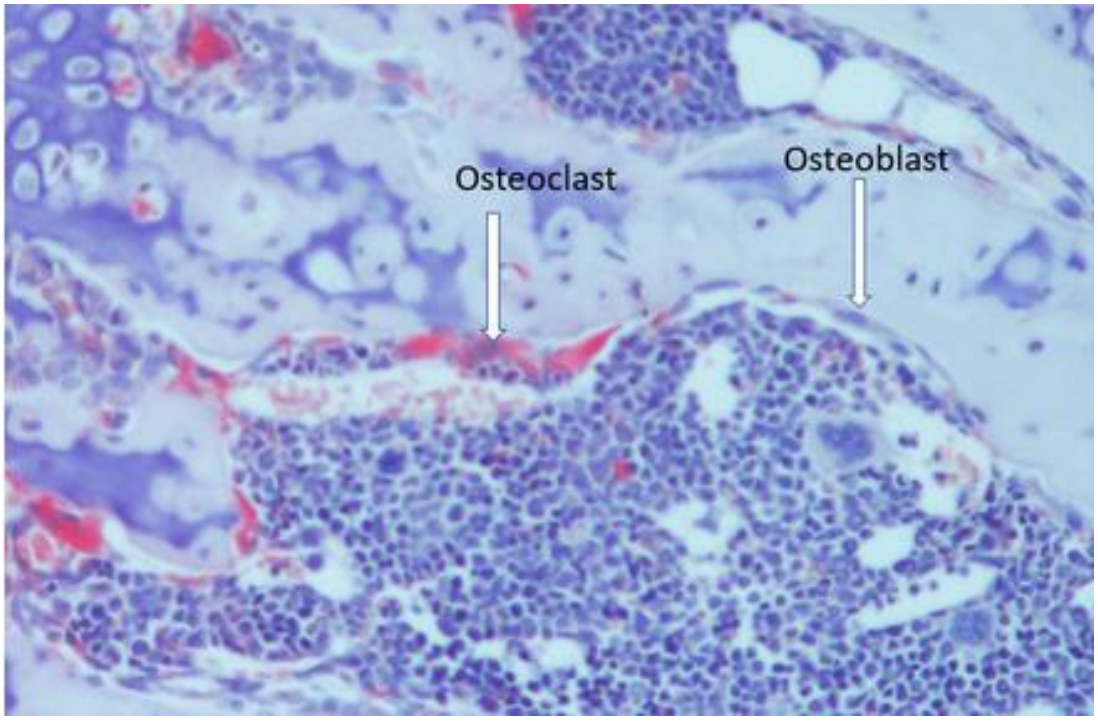

Figure 2-7: Pictorial view of TRAP positive osteoclasts (red, bone-lining) and osteoblasts (blue, rectangular, bone-lining). Image cropped from 20x magnification.

Entire cortical and trabecular surface below offset was measured. Cortical measurement offset was 250µm below chondrocytes and offset for trabecular measurements was 125µm (see Figure 2-8).

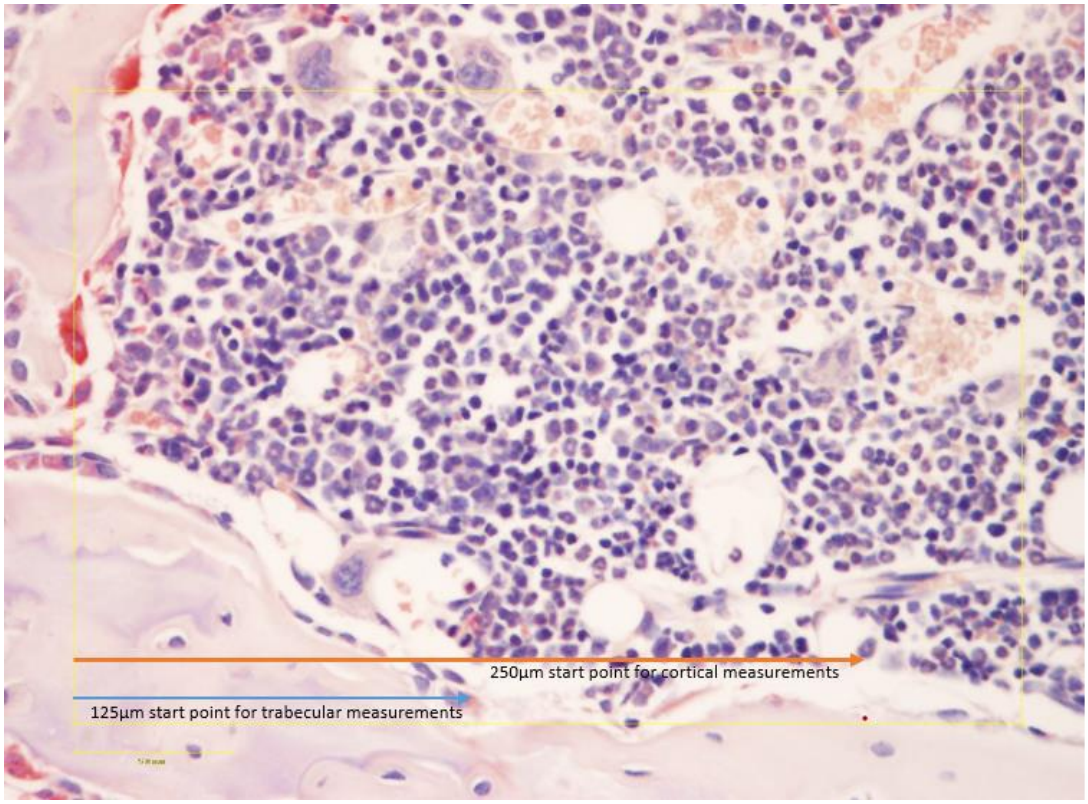

Figure 2-8: References to begin measurements on TRAP stained sections were based on the bottom of the chondrocytes for trabecular (blue arrow -125µm) and cortical (orange arrow - 250µm) start points

The number of osteoclasts (N.Oc), number of osteoblasts (N.Ob), osteoclast surface area(Oc.Pm) on bone, osteoblast surface (Ob.Pm) on bone and bone surface were measured.

2.6 Preparation of samples for Real time PCR

2.6.1 RNA extraction

For extraction of RNA from bones, a chloroform-based method was used with TRI-reagent (TRI-Zol) (Sigma). After obtaining hind-limbs from the dissection protocol and following snap-freezing, material was obtained from the bones by three different methods; scraping, crushing and flushing. These are described in the sections below.

2.6.1.1 Scraping

To obtain cellular material by the scraping method, the head of the bones were broken using hard tissue scissors, and bones split in half. With a teasing needle, bone marrow and bone lining cells were scraped into an Eppendorf tube with 500µl of PBS. These were then spun at 1-2000rpm for 3-4 minutes to obtain a pellet. The resulting supernatant was discarded and 1ml of TRI reagent was added to the pellet and re-suspended. RNA extraction then continued as per section 2.6.1.4.

2.6.1.2 CRUSHING

To obtain cellular material using the crushing method, a single whole bone was placed in a mortar with 1ml of TRI-reagent and crushed as fine as possible, ensuring sufficient homogenisation. RNA extraction then continued as per section 2.6.1.4.

2.6.1.3 FLUSHING

To flush bones, the head of bones were broken with teasing needle to reveal marrow cells and placed into a 0.2ml Eppendorf tube (Starlab, Germany) with a hole smaller than the bone to be flushed. The 0.2ml eppendorfs were subsequently placed in a 1.5ml Eppendorf to collect flushed material and spun at 6000rpm for 2 minutes before being suspended in 1ml of TRI reagent. RNA extraction then continued as per section 2.6.1.4.

2.6.1.4 EXTRACTION

Once tissue samples were obtained, for all the above methods, 200µl of chloroform was added to samples in 1ml of TRI reagent and shaken vigorously for approximately 15 seconds and left to incubate for 2 minutes at room temperature. Samples were then centrifuged for 15 minutes at 12000g (4°C or RT) at which point 3 layers containing protein, DNA and RNA were visible. The colourless phase of the upper layer containing RNA was removed (approximately 500µl) and pipetted into a new Eppendorf tube. 0.5ml isopropanol was added per 1ml of TRI reagent to precipitate RNA, vortexed for 30 seconds and incubated for 10 minutes at room temperature. Subsequent centrifugation of the sample was performed at 12000g for 15 minutes to form an RNA pellet. Supernatant was discarded, pellet re-suspended in 0.5ml 75% ethanol and vortexed at 7500g for 5 minutes. Supernatant was discarded and pellet was left to air dry at room temperature until as much alcohol was evaporated as possible. Pellets were finally re-suspended in 50µl molecular biology-grade water and analysed on the nanodrop for RNA quantity and quality.

2.6.1.5 NANODROP ANALYSIS OF RNA QUANTITY AND QUALITY

Following RNA extraction, RNA analysis was performed using a Nanodrop 2000 spectrophotometer (Thermo Scientific) with Nanodrop 2000/2000C software. Nucleic acids, RNA, dsDNA and ssDNA absorb at a wavelength of 260nm, and as such, a wavelength ratio of 260/280nm and 260/230nm is used to assess the quality of the RNA sample. Before scanning a sample, 1µl of diluent, molecular biology-grade water, was pipetted into the sample port and used as a blank. Subsequently, each sample of 1µl RNA was pipetted into the sample port and wavelengths measured. A ratio of ~2.0 at 260/280 and ~2.0-2.2 at 260/230 is generally accepted as pure for RNA. Furthermore, a smooth sigmoid-like curve on the scanning graph is used to determine scanning.

2.6.2 Polymerase Chain Reaction

Real-Time Polymerase chain reaction (RT-PCR) is both a fundamental biological reaction, as well as a routinely used tool in many biotechnological laboratories for the detection and quantification of DNA sequences and RNA transcripts. This technique relies on the native properties found in the enzyme polymerase, responsible for the duplication of DNA strands within both prokaryotic and eukaryotic cells coupled with a technique to capture duplication in real time for the purpose of quantifying transcript abundance. RT-PCR of RNA transcripts requires two broad steps i.) reverse-transcription of RNA into cDNA, ii.) real time amplification, detection and quantification of previously-transcribed cDNA.

2.6.2.1 Step i.) Reverse Transcription of RNA into cDNA

Reverse transcription of RNA into cDNA was performed using two separate kits and protocols; Quantitect Reverse Transcription Kit (Qiagen) and RevertAid RT Reverse Transcription Kit (Thermo Scientific).

2.6.2.1.1 Quantitect Reverse Transcription Protocol

Before reverse transcription, genomic DNA removal was performed by using the gDNA wipeout buffer provided. 2µl gDNA 7x wipeout buffer and 1µg template RNA were added to RNAse-free water up to a total volume of 14µl in an RNAse-free tube (Alpha Laboratories). Samples were incubated at 42°C for 2 minutes in a PTC-200 Peltier Thermo Cycler (MJ Research) and immediately placed on ice.

First-strand reverse synthesis was performed by adding 1µl Quantiscript Reverse Transcriptase, 4µl 5x Quantiscript RT Buffer and 1µl RT Primer Mix to 14µl of gDNA-free RNA with 1µg RNA from the previous step and incubated at 42°C for 15 minutes in a PTC-200 thermocycler.

2.6.2.1.2 RevertAid RT Reverse Transcription Protocol

Prior to reverse transcription using the RevertAid kit, RNA samples had genomic DNA removed by the use of DNase I using RevertAid DNase I kit (Thermo Scientific). Preparation of 1µg of RNA, 1µl of 10x reaction buffer with $MgCl_2$, 1µl (1U) DNase I, RNase-free was done in DEPC-treated water up to a final volume of 10µl in RNase-free Eppendorf tubes. Samples were incubated at 37°C for 30 mins in a PTC-200 Thermo Cycler. 1µl of 50mM EDTA was added to the tubes and incubated at 65°C for 10 mins in a PTC-200 Thermo Cycler. The prepared RNA, total volume 11µl, was then used as a template for reverse transcription.

To perform first-strand synthesis, 1µg template RNA from the genomic removal step had 0.5µl oligo $(dT)_{18}$ and 0.5µl random hexamer primers added to make a final volume of 12µl. The following components were added in order; 4µl of 5x reaction buffer, 1µl RiboLock RNase inhibitor (20U/µl), 2µl 10mM dNTP mix and 1µl RevertAid M-MuLV RT(200U/µl) for a final volume of 20µl in RNase-free Eppendorf tubes. These were then incubated at 25°C for 5 mins for random-hexamer primed

synthesis, followed by 42°C for 60 mins for first strand synthesis. Termination of reaction was accomplished by heating to 70°C for 5 mins. Synthesis steps were performed in a PTC-200 thermocycler.

2.6.2.2 STEP II.) REAL-TIME AMPLIFICATION OF CDNA TRANSCRIPTS

Samples for real-time detection were prepared using 2x PrecisionPLUS qPCR SYBR Green Master Mix (Primer Design) and added into 384-well PCR plates with 10µl per well. Each well contained 5µl 2x master mix, 0.5µl 300nM forward primer, 0.5µl 300nM reverse prime, 1µl template cDNA and 3µl RNase-free water. Each sample was repeated in triplicate.

Real-time amplification of cDNA transcripts was performed using Applied Biosystems PRISM HT-7900 sequence detection system (Thermo Scientific) using SDS 2.4 software (Thermo Scientific). To obtain quantitative values, Standard Curve (AQ) settings were used. Default thermal profile settings were used to run real-time PCR, with an added dissociation step for assessment of primer efficiency. SYBR Green was selected as a detector and applied to all wells, with ROX as a passive reference.

2.6.2.3 PRIMER DESIGN

Primers were designed using NCBI BLAST and further verified via MFE Primer 3.0 for predicted target specificity. Once primers were obtained, they were run on a PCR plate with cDNA synthesised from 1µg of RNA diluted at 1 in 2, 1 in 5, 1 in 10, 1 in 50, 1 in 100 and 1 in 1000 dilutions. When running the PCR using applied biosystem software, an additional fourth step in the PCR sequence, dissociation, was used to verify the specificity of the primer sequence and presence of primer dimerisation. The results from the dilutions were then plotted using a logarithmic scale representing the dilutions used, and plotted using a straight-line. The gradient of the straight line slope was then used in determining the primer efficiency

Molecule	Primer Sequence (5’ to 3’)
GAPDH *Fwd*	ACG TGC CGC CTG GAG A
GAPDH *Rev*	CCC TCA GAT GCC TGC TTC A
TBSP-1 *Fwd*	CCT CCC CTC TGC TTT CAC AA
TBSP-1 *Rev*	TAA CCG AGT TCT GGC AGT GAC
CXCL4 *Fwd*	CCCGAAGAAAGCGATGGAGAT
CXCL4 *Rev*	TTCTTCAGGGTGGCTATGAGCTG
Osteopontin *Fwd*	CTT TCA CTC CAA TCG TCC CTA
Osteopontin *Rev*	GCT CTC TTT GCA ATG CTC AAG
Osteoprotegerin *Fwd*	GTG TGG AAT AGA TGT CAC CCT GT
Osteoprotegerin *Rev*	CTT GTG AGC TGT GTC TCC GT

RANKL *Fwd*	CCCATCGGGTTCCCATAAAG
RANKL *Rev*	AGCAAATGTTGGCGTACAGG

2.6.3 ELISA

2.6.3.1 N-TERMINAL PROPEPTIDE OF TYPE I PROCOLLAGEN (P1NP)

Bone matrix is composed of between 70 and 90% mineral, with organic material constituting the rest. A large part of the organic material is composed of type I collagen, whose amino-terminal propeptide (PINP) and carboxy-terminal pro-peptide (PICP) constituents are cleaved during collagen synthesis. These are released into the circulation, and quantification in serum samples is often used as a biomarker for collagen synthesis within bone (Melkko *et al*., 1996; Seibel, 2005). In particular, commercial immunoassays detecting PINP are used as a surrogate for osteoblast activity and bone formation.

To detect and quantify PINP in serum samples extracted from mice, I used a rat/mouse enzyme-linked immunosorbent assay (ELISA) kit (Immunodiagnostics Systems, UK). The manufacturer's standard instructions were used, in which 50µl of calibrators (supplied) and controls (supplied) were added to a polyclonal rabbit anti-PINP antibody coated well plate (supplied) in duplicate. Sample mixture was then made by adding 5µl serum to 45µl sample diluent (supplied) and added to the same antibody coated plate in duplicate within 15 minutes of adding calibrators and controls in order to minimise drift. Using a multichannel pipette, 50µl biotin (supplied) was added to all wells before covering the plate with an adhesive plate sealer (supplied) and incubated on a microplate shaker (500-700rpm) at room temperature for one hour. Following incubation, liquid content was decanted by inverting sharply and 250µl of wash solution (supplied) was added to all wells, repeating for a total of 3 cycles and finally tapping the inverted plate on absorbent tissue to remove excess wash solution. 150µl enzyme conjugate (avidin - horseradish peroxidase (HRP)) (supplied) and allowed to incubate for 30 mins at room temperature, before repeating the triplicate wash step. 150µl chromogenic 3,3',5,5'-Tetramethylbenzidine (TMB) HRP substrate (supplied) was added to all wells, the plate sealed and incubated at room temperature for 30 minutes. The reaction was stopped by the addition of 50µl stop solution (HCl) (supplied). Optical absorbance was read at 450nm using a SpectraMax 5Me plate reader (Molecular Devices, UK).

2.6.3.2 TARTRATE-RESISTANT ACID PHOSPHATASE FORM 5B (TRACP 5B)

The tartrate-resistant acid phosphatase (TRAP) is part of the mammalian acid phosphatase group of enzymes expressed by various immune cells including macrophages and dendritic cells (Hayman, 2008). In particular, isoforms 5a and 5b have demonstrated different clinical significance, with 5a correlated with, and used as a measure of macrophage activation and chronic inflammation. In contrast, 5b has diagnostic relevance as a measure of osteoclast number and bone resorption, particularly in osteoporosis, cancers with bone metastasis and chronic renal failure (Janckila and Yam, 2009). TRAP 5b is secreted extracellularly by osteoclasts into the resorption lacunae where it subsequently escapes into peripheral circulation and where it be measured in serum as a biomarker

of bone resorption (Alatalo *et al*., 2003). In my experiments, to detect and quantify TRAcP 5b as a surrogate for bone resorption, a polyclonal antibody against recombinant mouse TRAcP 5b was used in an ELISA kit (Immunodiagnostic Systems, UK) in accordance with the manufacturer's instructions and reagents.

100µl of Anti-MouseTRAP antibody was added to the antibody-coated plate (supplied), and incubated at room temperature for 60 minutes on a plate shaker at approximately 150rpm. The contents were then decanted by sharp inversion, before dispensing 250µl of wash buffer (supplied) to the wells. Wash buffer was decanted and the previous step repeated for a total of 3 times. 100µl of calibrator (supplied) or control (supplied) were added to the antibody coated plate in duplicate, and 75 µl of 0.9% NaCl followed by 25µl of sample were added to appropriate wells. 25µl of releasing reagent (supplied) was added to all wells and the plate incubated at room temperature for 60 minutes on a plate shaker at approximately 150rpm. 100µl chromogenic substrate solution (supplied) was added to all wells, the plate covered with an adhesive plate sealer and incubated at 37°C for 2 hours. Subsequently, 25µl NaOH stop solution (supplied) was added to all wells to stop chromogenic development. Optical absorbance was read at 450nm using a SpectraMax 5Me plate reader (Molecular Devices, UK).

2.6.4 Hematological Analysis

Hematological analysis was used to determine the population abundance for circulating hematopoietic cells in mice using blood collected via cardiac puncture as described in section 2.4.2.1.

Upon culling, mice had their blood withdrawn through cardiac puncture, of which 20µl was placed into 500µl Eppendorf tubes containing 20µl of EDTA to prevent clotting, thoroughly mixed and stored at room temperature for up to 2 hours post-cull. These samples (10µl per sample) were then run through a Scil Vet abc Plus hematological analyzer (Horiba Medical) which measured total white blood cells (number per $10^3/mm^3$ blood), total red blood cells (number per $10^3/mm^3$ blood), lymphocytes (percentage(%) and number per $10^3/mm^3$ blood), monocytes (percentage(%) and number per $10^3/mm^3$ blood), granulocytes (percentage(%) and number per $10^3/mm^3$ blood), eosinophils (percentage(%) and number per $10^3/mm^3$ blood), hemoglobin (g/dL), hematocrit (percentage), mean corpuscular volume (μm^3), mean corpuscular hemoglobin (pg), mean corpuscular hemoglobin concentration (g/dL), red blood cell distribution width (percentage), platelets (number per $10^3/mm^3$ blood) and mean platelet volume (μm^3).

2.7 RNA Sequencing

2.7.1 Power Analysis

Statistical power is the probability that a statistical test will correctly reject the null hypothesis. A power analysis can be utilised to estimate the minimum sample size requires for an experiment given a desired significance level, effect size and statistical power, or can be used to estimate the statistical power for an experiment given significance level, effect size and sample size (Dumas-Mallet *et al*.,

2017). The statistical power for a given experiment is the inverse of the probability of a type II error (false negative), meaning that the higher the statistical power for a given experiment, the lower the probability of making a type II error, where the null hypothesis is, incorrectly, not rejected.

Statistical power is influenced by three main variables; the effect size, which is the quantified magnitude of a result present in the measured samples, the sample size, and the significance threshold, often set to 0.05 (Dumas-Mallet *et al*., 2017). In standard statistical analysis, a simple measure such as a student's t test power analysis can be used to estimate the power of a statistical test. However, for RNA-sequencing differential gene expression analysis, n-statistical tests are performed on n-genes present in the dataset, meaning a different approach is required to measure true statistical power (Yu *et al*., 2017).

2.7.2 Developing a method for isolation of high quality RNA from snap-frozen bone for RNA sequencing

Optimization of an RNA extraction method for high yield, purity and integrity RNA for RNA sequencing purposes was performed. The methods of dissociation and subsequent isolation utilised in optimisation steps are outlined below and discussed further in the results section.

2.7.2.1 Tissue dissociation and homogenisation

Dissociation of tissues were performed by three different methods; using a mortar and pestle, scraping and Fisherbrand Bead Mill 4 Homogenizer as described below.

2.7.2.2 Mortar and Pestle

To obtain dissociated tissue by mortar and pestle, 1ml of TRI reagent or 600µl of RLT lysis buffer (Qiagen RNeasy kit) was added to an empty mortar, before being crushed by pestle until sufficiently homogenised in the mortar. These were then transferred into empty 1.5ml Eppendorf tubes to complete the extraction processes dependent on the method used.

2.7.2.3 Scraping

To obtain dissociated material by the scraping method, the head of the bones were broken using surgical blades, and bones split in half. With a teasing needle, bone marrow and bone lining cells were scraped into an Eppendorf tube with 1ml of TRI reagent or 600µl of RLT lysis buffer (Qiagen RNeasy kit).

2.7.2.4 Bead Mill

Prior to being placed in the bead mill, bones were broken into 3 pieces using a teasing needle, ensuring fracturing along the length of the shaft. The bone fragments were then placed in bead mill vials, which come pre-loaded with beads, and 1ml of TRI reagent was added to each vial. Three different beads

were available and tested; metal, ceramic and glass. The speed settings are between 1 and 5, with 5 being the fastest, and 1 being the slowest.

2.7.2.5 EXTRACTION METHODS

Three extraction methods were used when aiming to extract RNA from homogenised tissue and are outlined in the following three sections; namely Trizol, RNEasy and Hybrid methods.

2.7.2.6 TRIZOL METHOD

The Trizol method of extraction is accordance with the commonly used lab protocol developed by Ms Diane Lefley, University of Sheffield.

The bone tissue is disrupted and homogenised by mortar and pestle in 1ml TRI reagent and placed into a 1.5ml Eppendorf tube. Then 200µl of chloroform is added and shaken gently for approximately 15 seconds and left to incubate for 2 minutes at ambient

temperature. The mixture is centrifuged for 15 minutes at 12000g at room temperature (RT). Chloroform separates protein, DNA and RNA in different layers. Three different layers are apparent after centrifuging. The colourless phase in the upper layer contains the RNA which is transferred to a new Eppendorf while being careful to not contaminate with any of the other layers. Subsequently, 500µl of pure isopropanol per 1 ml of TRIreagent initially used is added to the colourless upper phase to precipitate RNA. This is vortexed for 30 seconds and left to incubate for 10 minutes at room temperature before being centrifuged for 15 minutes at 12000g at RT. The Eppendorf is removed and has an equal amount of 75% ethanol diluted molecular biology-grade water added to it as a wash step. The pellet is then vortexed thoroughly to detach, before being centrifuged at 7500g for 5 mins to attach the pellet to the bottom of the tube. This supernatant is removed, avoiding discarding the pellet, and left to air dry for a few minutes at RT until as much liquid as possible evaporates. The final pellet air-dried is re-suspended in an appropriate volume of molecular-biology grade water for tissue volume (For ≤ 100µg starting tissue, use one 30-100µL elution volume, or for ≥ 100µg starting tissue, use 2-3 sequential 100µL elutions).

2.7.2.7 RNEASY METHOD

The RNeasy method of extraction is according to the Qiagen's supplied protocol with the RNeasy kit. Supplied materials are indicated and all buffers are provided in the kit. The protocol is outlined below:

The tissue was disrupted and homogenised in 600µl RLT buffer (supplied), before being centrifuged for 3 min at maximum speed. The supernatant was then transferred into a new Eppendorf before adding 1 volume of 70% ethanol to the lysate, and mixed well by pipetting. Up to 700 µl of the sample, including any precipitate that may have formed, was pipetted into an RNeasy Mini spin column in a 2 ml collection tube (supplied). The spin column with lysate was centrifuged at ≥8000 x *g* (≥10,000 rpm) for 15 s at room temperature and the flow-through discarded. Any excess lysate was pipetted into the

same RNeasy Mini spin column and centrifuged at ≥8000 x *g* (≥10,000 rpm) for 15 s and flow-through discarded. To the RNeasy Mini spin column, 700 µl Buffer RW1 was added before centrifuging for 15 s at ≥8000 x *g* (≥10,000 rpm) to wash the column and discarded the flow through. 500 µl Buffer RPE was then pipetted into the RNeasy Mini spin column before centrifuging for 15 s at ≥8000 x *g* (≥10,000 rpm) to wash the column and discarding the flow-through. Another 500 µl Buffer RPE was then added to the RNeasy Mini spin column before centrifuging for 2 min at ≥8000 x *g* (≥10,000 rpm) to dry the RNeasy Mini spin column membrane. The long centrifugation dries the spin column membrane, ensuring that no ethanol is carried over during RNA elution. Residual ethanol may interfere with downstream reactions. To ensure optimal drying, the RNeasy Mini spin column was placed into a new 2 ml collection tube (supplied), and discarded the old collection tube with the flow-through. This was centrifuged in a microcentrifuge at full speed for 1 min. This step was performed to eliminate any possible carryover of Buffer RPE or residual flow-through that may remain on the outside of the RNeasy Mini spin column. The RNeasy Mini spin column was then transferred to a new 1.5 ml collection tube (supplied). To elute the RNA, 50 µl RNase-free water was pipetted directly onto the RNeasy Mini spin column membrane before being centrifuged for 1 min at ≥8000 x *g* (≥10,000 rpm). The resulting flow through contained the eluted RNA and was used for downstream applications.

2.7.2.8 HYBRID METHOD

Due to bone's consistency, fat and collagen content, a hybrid method is often used when lysis with RLT buffer (RNeasy protocol) does not result in sufficient lysis of tissue. This method combines the phenol-based extraction of TRIzol with further purification using the RNeasy columns and buffers. Effectively, it combines the dissociation and homogenisation steps of the TRIzol method, which leads up to a solution with precipitated RNA, which is then placed into the RNeasy columns, continuing the columnar steps of the RNeasy protocol and is outlined below:

Disruption and homogenisation of the bone was achieved by breaking bone into approximately 3 pieces using a surgical blade, along the line of the shaft, before transferring into a bead mill tubes with ceramic beads with 1ml of TRI reagent. The tubes were then spun in the bead mill for 60 seconds at speed 3. 200µl of chloroform was then added and the mixture was shaken gently for about 15 seconds and left to incubate for 2 minutes on ice. The tubes were then centrifuged for 15 minutes at 12000g (4°C) in a microfuge. Chloroform separates protein, DNA and RNA in three different layers with the colourless phase in the upper layer containing the RNA. The colourless upper phase was transfered to a new Eppendorf with 500µl of pure isopropanol per 1 ml of TRI reagent added to colourless upper phase to precipitate RNA. 700µl of the sample, including any precipitate that may have formed, was transfered into a RNeasy Mini spin column in a 2 ml collection tube and centrifuged at ≥8000 x *g* (≥10,000 rpm) for 15 s at 4°C. The flow through was discarded and the rest of the sample transferred to the column before repeating the centrifugation step, discarding the flow-through again. 700µl of RW1 buffer was added to the RNeasy Mini spin column and centrifuged for 15 s at ≥8000 x *g* (≥10,000 rpm) to wash the column, discarding the flow-through. 500µl of RPE buffer was added into the RNeasy Mini spin column and centrifuged for 15 s at ≥8000 x *g* (≥10,000 rpm) to wash the column with flow-through discarded. Another 500µl of RPE buffer was added to the RNeasy Mini

spin column and centrifuged for 2 min at ≥8000 x *g* (≥10,000 rpm) to dry the RNeasy Mini spin column membrane, with flow through discarded. The RNeasy Mini spin column was then centrifuged at full speed (≥14,000 rpm) for 1 min to eliminate any possible carryover of Buffer RPE or if residual flow-through remained on the outside of the RNeasy Mini spin column. The RNeasy Mini spin column was transfered to a new 1.5 ml collection tube before adding 30–50 µl RNase-free water directly onto the RNeasy Mini spin column membrane and centrifuging for 1 min at ≥8000 x *g* (≥10,000 rpm) to elute the RNA.

2.7.2.9 Assessment of RNA Quality on Nanodrop

Following RNA extraction, RNA analysis was performed using a Nanodrop 2000 spectrophotometer. Before scanning a sample, 1µl of diluent, molecular biology-grade water, was pipetted into the sample port and used as a blank. Subsequently, each sample of 1µl RNA was pipetted into the sample port and wavelengths measured. A ratio of ~2.0 at 260/280 and ~2.0-2.2 at 260/230 is generally accepted as pure for RNA.

2.7.2.10 Assessment of RNA Quality via Agilent Bioanalyzer

Following successful extraction of RNA, yield and purity measurements by Nanodrop analysis, sample aliquots were taken to Matthew Wyles at Sheffield Institute for Translational Neuroscience (SITraN) who performed RNA integrity number analysis, and was supplied with the elution solvent to use as a blank (molecular biology grade water). Results were returned in PDF format, including RIN scores for each sample. RIN scores range from 1 (blank) to 10 (most optimum). Integrity scores above 7 are required for RNA-sequencing. Lower scores suggest fragmenting of RNA transcripts, but may also be skewed by impurities.

2.7.3 RNA extraction for RNA sequencing

2.7.3.1 Extraction

Left femurs from all mice had RNA extracted for RNA-sequencing according to the hybrid method detailed in section 2.7.2.8, with the addition of pre-cooling all tubes and reagents used to < 0 °C.

2.7.3.2 Removal of genomic DNA contamination

Prior to sequencing, RNA is converted into cDNA in order to be amplified by a polymerase chain reaction step. However, present genomic DNA will be co-amplified and would necessarily confound the subsequent analysis into upregulated transcripts. Despite obtaining the colourless aqueous upper phase containing RNA during the extraction with Trizol and chloroform, leaving sufficient clearance to the interphase, as well as obtaining 260/280 values ~2 as assessed by nanodrop, a further step for the digestion of genomic DNA was performed to ensure minimal DNA contamination.

To prepare DNase I stock solution before using the RNAse-Free DNase Set for the first time, the lyophilized DNase I (1500 Kunitz units) was dissolved in 550 µl of the RNAse-free water. To avoid loss

of DNase I, the vial was not opened, but RNAse-free water was injected into the vial using an RNAse-free needle and syringe and mixed by inverting. Subsequently, 11 aliquots of 50 µl were prepared for subsequent use to reduce freeze-thawing when stored at -25 °C.

To perform digestion, samples were adjusted to a volume of 100 µl with RNAse-free water and 350 µl Buffer RLT was added before mixing well. Next, 250 µl ethanol (99%) was added to the diluted RNA, and mixed well by pipetting. The sample (700 µl) was transfered to a RNeasy Mini spin column placed in a 2 ml collection tube (supplied), and centrifuged for 15 s at ≥8000 x g (≥10,000rpm) and flow-through discarded. To the mini-spin column, 350 µl Buffer RW1 was and centrifuged for 15 s at ≥8000 x g (≥10,000 rpm) to wash the spin column membrane. From previously prepared stock solution, 10 µl DNase I stock solution was added to 70 µl Buffer RDD and mixed by gently inverting the tube, centrifuging briefly (10s) to collect residual liquid from the sides of the tube to obtain a DNAse I incubation mix. 80 µl from the DNAse I incubation mix was pipetted directly to the RNeasy spin column membrane with RNA sample, and placed on the benchtop (20–30°C) for 15 min.

Following incubation, 350 µl Buffer RW1 was added to the RNeasy spin column that was centrifuged for 15 s at ≥8000 x g (≥10,000 rpm) and flow-through discarded. 500 µl Buffer RPE was added to the RNeasy spin column and centrifuged for 15 s at ≥8000 x g (≥10,000 rpm) to wash the spin column membrane. 500µl of RPE buffer was added into the RNeasy Mini spin column and centrifuged for 15 s at ≥8000 x *g* (≥10,000 rpm) to wash the column with flow-through discarded. Another 500µl of RPE buffer was added to the RNeasy Mini spin column and centrifuged for 2 min at ≥8000 x *g* (≥10,000 rpm) to dry the RNeasy Mini spin column membrane, with flow through discarded. The RNeasy Mini spin column was then centrifuged at full speed (≥14,000 rpm) for 1 min to eliminate any possible carryover of Buffer RPE or if residual flow-through remained on the outside of the RNeasy Mini spin column. The RNeasy Mini spin column was transfered to a new 1.5 ml collection tube before adding 30–50 µl RNase-free water directly onto the RNeasy Mini spin column membrane and centrifuging for 1 min at ≥8000 x *g* (≥10,000 rpm) to elute the RNA.

2.8 Computational Analysis

The below pipeline was used to pre-process RNA-sequencing transcripts:

Table 2-6: Processing pipeline for RNA-sequencing data

Process	Input File	Output File	Tools	Reference / Website
Quality check on raw reads	Fastq sequencing reads	HTML report	FastQC	(Krueger F, 2012)
Trim raw reads	Fastqc sequencing reads	Trimmed fastq files	Trimmomatic	(Bolger *et al.*, 2014)
Align raw reads to reference genome	Trimmed reads Reference genome gtf file	Sorted BAM files	STAR	(Dobin *et al.*, 2013)
Assemble gene expression from aligned reads	Sorted BAM Files	Adjusted read counts	DegNorm	(Xiong *et al.*, 2019)
Differential gene expression analysis	Counts CSV / Expression Set	List of differentially expressed genes	DESeq2	(Love *et al.*, 2014)
Gene Ontology Analysis	Differentially expressed gene list	Images/Tables	DAVID	(Dennis *et al.*, 2003)
Pathway Analysis	Differentially expressed gene list	Images/Tables	clusterProfiler	(Yu *et al.*, 2012)
Deconvolution of bulk expression	Counts CSV / Expression Set	Images/Tables	xCell	(Aran *et al.*, 2017)
Signature set scoring	Differentially expressed gene list. List of genes to score	Images/Tables	SingsScore	(Foroutan *et al.*, 2018)

2.8.1 RNA Sequencing

2.8.1.1 Power Analysis for RNA-seq

In high throughput experiments, such as RNA-seq, where many statistical tests are performed simultaneously several factors lead to complications in estimating the statistical power of an experiment, such as the choice of significance test correction, the incorporation of baseline expression, variability of both gene expression and magnitude of effect as well as sequencing depth (Yu *et al.*, 2017). The significance test correction is often solved by using the false discovery rate (FDR) as the method of significance, accounting for multiple statistical tests using the Benjamini-Hochberg

correction. In microarray data, the baseline is not of significant interest and can be assumed to be 0 without affecting generality or affecting type I or II errors. However, in RNA-seq, gene expressions are measured as counts and often modeled as Poisson or negative binomial distributions (Anders and Huber, 2010, Robinson *et al*., 2010, Wu *et al*., 2013). The variation in gene expression measurements comes from both the biological variation and the sequencing counting error. The relative importance of the counting error depends on the expression level; for genes with low counts, the variation owing to the counting process dominates the variance, whereas for genes with high counts, it is negligible (Wu *et al*., 2015). Therefore, the power in DE detection is affected by expression level in RNA-seq.

Owing to these complexities in estimating power for RNA-sequencing experiments, Wu *et al.* (2015) argue that it is no longer feasible to rely on one simple power versus sample size curve while treating all other factors as fixed input and holding strong assumptions such as exchangeability between genes and equating nominal error rate as actual error rate (Wu *et al*., 2015). As a result, they developed a simulation-based power evaluation that allows the construction of *in silico* datasets that resemble real RNA-seq data and allowing the evaluation of the actual error rate by comparing true and false discovery values from the dataset against computed simulations using the parameters and method of choice to be to be used in an experiment. This is provided as an R/Biodonductor package, PROspective Power Evaluation for RNAseq (PROPER) and is used for power analysis in chapter 5 (Wu *et al*., 2015).

2.8.2 Pre-processing of raw RNA-sequencing reads

Raw reads from sequencing were provided by amazon web services (AWS) S3 cloud storage as raw FASTQ files (n=8). These files were subsequently downloaded onto private storage on the Sheffield advanced research computer (ShARC) high performance computing (HPC) cluster under user storage ready for pre-processing.

2.8.2.1 Quality assessment of sequencing reads

Prior to pre-processing, adequate read quality was measured using TrimGalore, which is a wrapper around FastQC and Cutadapt, tools for quality checking and trimming respectively. FastQC is a tool designed to assess the quality of raw reads from a variety of sequencer, including the Illumina HiSeq™ 2500 used for these samples. FastQC is a java-based programme that can be used through the command line to assess quality metrics such as per base sequence quality, per tile sequence quality, per sequence quality scores, per base sequence content, per sequence GC content, per base N content, sequence length distribution, sequence duplication levels, overrepresented sequences, adapter content and kmer content. FastQC version 0.11.7 was used to assess the quality of the reads.

In addition to FastQC, MultiQC was used to produce summarised reports representing all samples, showing an overview of sequencing quality. MultiQC version 1.9 was used to aggregate sample quality metrics into a single html file for viewing. Important metrics and cutoffs can be seen in Table 2-7.

Table 2-7: Metrics covered by FastQC processing and their description

Measurement	Description	Importance/Cut off
Basic statistics	The summary of percentage duplications, percentage duplication and total sequences per sample.	Importance: Medium
Per base sequence quality	The mean quality value across each base position in the read across the sample, meant as a measure of the base calling quality for each base position within a read.	Importance: High **Cut off:** Lower quartile for any base < 10, median < 20
Per tile sequence quality	The average quality scores from each tile across all bases along parts of the flow cell to see if a loss of quality was associated with a part of the flow cell.	**Importance**: High but reduces towards end of read **Cut off:** Most frequently observed mean quality < 20
Per base sequence content	The proportion of each base position for which each of the four normal DNA bases has been called, which gives an overview as to which position in the read may have a bias for certain bases.	Importance: Low **Cut off:** Difference between A/T and G/C at any position is > 10%
Per base GC content	The distribution of percentage GC content of reads.	Importance: Medium **Cut off:** GC content of any base > 10% from the mean
Per base N content	The percentage of bases calls at each position for which the base caller could not identify a base with sufficient confidence.	Importance: Low **Cut off:** Any position shows N content of > 20%
Sequence length distribution	The distribution of fragment sizes (read lengths) sequenced.	Importance: Low **Cut off:** Sequences have zero length
Sequence duplication levels	The relative level of duplication found for every sequence.	Importance: Low **Cut off:** Non-unique sequences > 50% of total
Overrepresented sequences	The total amount of overrepresented sequences found in the sample library.	Importance: Low **Cut off:** Any sequence represents >1% of total

2.8.2.2 TRIMMING OF ADAPTER SEQUENCES AND LOW-QUALITY READS

During library preparation, adapters are ligated to sample RNA. These, as well as primers, need to be removed prior to aligning to the reference genome. TrimGalore version 0.6.6 was used to concurrently trim reads and provide quality metrics.

2.8.2.3 Alignment of reads to reference genome

To align RNA-seq reads to a reference genome prior to quantification, the commonly used alignment tool Spliced Transcripts Alignment to a Reference (STAR), which uses sequential maximum mappable seed search in uncompressed suffix arrays followed by a seed clustering and stitching procedure, was used.

STAR version 2.7.8a was initially used to index a reference genome, the gencode release M27 (GRCm39) using the comprehensive gene annotation Gene Transfer File (GTF) format which is the main annotation file for most users. This was used with the transcript sequences FASTA file containing the nucleotide sequences of all transcripts on the reference chromosomes to index a reference genome using the genomeGenerate function of STAR with a transcript overhang of 100, as a read length minus 1 is suggested for most cases whereby the transcripts used had 101 bases per read.

Following the generation of an indexed genome, trimmed sample FASTQ files were aligned to the genome using STAR with BAM SortedByCoordinate specified in the outSAMtype argument to generate sorted Binary Sequence Alignment Map (SAM) (BAM) files for the samples. These sorted BAM files would subsequently be used in the quantification step.

2.8.2.4 Quantification of aligned reads

The quality of RNA sequencing results is affected by RNA degradation, and is a significant factor that may bias the results from RNA-seq analysis. As the samples sequenced had RIN scores of <7, leading to the rRNA sequencing protocol being used, degradation would potentially be a source of bias in transcript abundance estimation. In order to reduce the bias and variability present due to degradation, DegNorm, a pipeline which adjusts read counts for transcript degradation on a gene-by-gene basis, while controlling for sequencing depth was used to quantify the aligned and sorted sample BAM files. Degnorm version 0.1.4 was used in conjunction with the gencode release M27 GTF annotation file to quantify BAM files, with 100 for the -nmf-iter argument resulting in 100 iterations per non-negative matrix factorisation (NMF) over-approximation (OA) algorithm approximations.

The output from quantification by DegNorm was a comma separated values (csv) file containing adjusted read counts. These adjusted read counts, adjusted for transcript degradation, were then used in subsequent downstream analyses.

2.9 Downstream Computational Analyses

Downstream analyses were performed in R version 4.0.4 (2021-02-15) through R Studio version 1.4.1106 unless otherwise stated.

2.9.1 Analysis of Differentially expressed genes

To obtain differentially expressed genes, the adjusted read counts in comma separated values (csv) file type obtained as an output from DegNorm counting were loaded into R studio, along with a file containing experimental metadata for each sample. Using the DESeq2 package version 1.30.1, the two files were combined into a DESeq DataSet object using the DESeqDataSetFromMatrix function, using the counts file with rounded integers as values as the countData argument, using the metadata file as the colData argument and the experimental condition (OVX or Sham) as the design argument in the function. The DESeq DataSet object was then used to create a new object with the function estimateSizeFactors in order to assess various quality control metrics, such as clustering and principal component analysis after a variance stabilising transform (VST). The original DESeq DataSet object was then finally used to obtain differentially expressed genes by the function DESeq performed on the expression and group data contained in the object.

2.9.2 Deconvolution of Bulk RNA sequencing reads

To obtain an estimation of cellular populations within the microenvironment of sequenced samples, bulk deconvolution was performed whereby cellular populations could be inferred by relative abundances of transcripts associated with cell-type signatures. For this, the xCell, a computational gene signature-based method employing a curve fitting approach for linear comparison of cell types and single sample gene set enrichment analysis (ssGSEA) was used. xCell provide a reference signature dataset for 64 immune and stromal types harmonised from 1822 human transcriptomes, validated by *in silico* analyses and cytometry immunophenotyping comparison consisting of the following cells; Adipocytes, Astrocytes, B-cells, Basophils, CD4+ T-cells, CD4+ Tcm, CD4+ Tem, CD4+ memory T-cells, CD4+ naive T-cells, CD8+ T-cells, CD8+ Tcm, CD8+ Tem, CD8+ naive T-cells, common lymphoid progenitors (CLP), common myeloid progenitors (CMP), Chondrocytes, Class-switched memory B-cells, dendritic cells (DC), Endothelial cells, Eosinophils, Epithelial cells, Erythrocytes, Fibroblasts, granulocyte-monocyte progenitor (GMP), HSC, Hepatocytes, Keratinocytes, Megakaryocyte–erythroid progenitor cell (MEP), Multi-Potent Progenitor (MPP), mesenchymal stem cells (MSC), Macrophages (total, M1 and M2 polarised), Mast cells, Megakaryocytes, Melanocytes, Memory B-cells, Mesangial cells, Monocytes, Myocytes, NK cells, natural killer T cells (NKT), Neuronal cells, Neutrophils, Osteoblasts, Pericytes, Plasma cells, Platelets, Preadipocytes, Sebocytes, Skeletal muscle, Smooth muscle, Gamma Delta T cells (Tgd), Th1 cells, Th2 cells, Tregs, activated dendritic cells (aDC), classical dendritic cells (cDC), interstitial dendritic cells (iDC), Endothelial cells, Endothelial cells, naive B-cells plasmacytoid dendritic cells (pDC) and pro B-cells.

As xCell uses human gene references for inference of cell types, samples from the mouse reference genome were converted to human orthologs using the biomaRt package version 2.46.3 and the ensembl mart within the getLDS function, successfully mapping 17,484 genes from mouse to human. These were retained and used in xCell within the xCellAnalysis function of the xCell package version 1.1.0. The output from this is a matrix consisting of of samples in columns and estimated cell types in rows with their relative fraction compared between samples.

2.9.3 Signature Scoring of RNA-sequencing reads

To assess dormancy signatures, a tool or method allowing for the supplying of a custom set of genes was required. Singscore is a rank-based single sample scoring method that scores the expression activities of specified gene sets at a single-sample level. Singscore version 1.10 was used, and as an input, genes mapped to human orthologs from the deconvolution step were used. Prior to scoring samples, the dataset was ranked using the rankGenes function which returns a rank matrix. This matrix was then supplied to the simpleScore function, with a list of upregulated genes as the upSet argument and a list of genes downregulated genes in the downSet argument, where upregulated and downregulated genes are genes altered in the signature of interested for the samples to be scored by. This returns a dataframe consisting of the scores and dispersion for the upregulated genes in isolation, the downregulated genes in isolation and the total score of both the upregulated and downregulated genes combined. These are then visualised to show dispersion and scores.

2.9.4 Identifying gene ontology terms

To identify altered terms according to gene ontology, he Database for Annotation, Visualization and Integrated Discovery (DAVID) v6.8 was used. Lists of up-regulated and down-regulated genes were uploaded into the Gene List Manager on the DAVID website (https://david.ncifcrf.gov/tools.jsp), whereby they were scored against DAVID's databases functional annotation by the Functional Annotation Tool. Gene Ontology (GO) and Kyoto Encyclopaedia of Genes and Genomes (KEGG) Pathways were used to derive altered terms and pathways, with associated FDR values and genes involved in the specified pathways.

2.9.5 Non-sequencing computational tools

2.9.5.1 Spearman correlation for matrix correlation of circulating hematopoietic cells

To assess correlation between measurements from hematological analysis and experimental conditions, spearman correlation was used in the programming language, *Python*, using the *Pandas* package. Correlation was performed on numeric data frames where all categorical data was coerced into numerical (0 or 1) in the case of two conditions in the parameter measured, such as whether they were treated with PBS (0) or Zoledronic acid (1). A correlation function was then used in pandas, version 1.1.2, by using the *dataframe.corr()* function, passing the method argument into the function to specify the correlation method used, such as the full function call was, as an example *dataframe.corr(method = 'spearman').* This function was used on the dataframe, which generated a correlation matrix, displaying correlations between -1 and 1. The closer to -1, shows a negative correlation, and closer to 1 shows a positive correlation, whereas closer to 0 indicates less correlation, either positive or negative. The output from this function was assigned to a variable to be used in generating a heatmap using visualisation package *Seaborn.*

Documentation for this function can be found at the following address:

https://pandas.pydata.org/pandas-docs/stable/reference/api/pandas.DataFrame.corr.html

2.9.5.2 Generation of heatmaps to plot correlation matrix results

Following the generation of a correlation matrix, *Seaborn* python package, version 0.11.0 was used to plot a heatmap using the *seaborn.heatmap()* function, where the variable representing the correlation matrix was used as an input into the heatmap function.

2.10 Statistical Analysis

Statistical tests performed between groups and samples was performed using Graphpad Prism versions 8.0 and 9.1 unless otherwise stated.

Comparisons between two conditions was performed using a two-tailed independent student's T-test with the below equation: as no sets of data were assumed to be dependent unless otherwise stated. Independent t-tests were used to compare the mean of two unrelated groups of samples such as mean expression difference of a gene tested by PCR in mice that had been fed either a low calcium or normal diet, as well as the mean percentage bone volume difference between mice that had undergone an ovariectomy and those that had undergone a sham operation.

Comparisons between multiple conditions was performed using a two-way analysis of variation (ANOVA), such as when testing for the effect of cell clone and treatment on tumour growth in chapter 4.

A p-value of 0.05 derived from these statistical tests was considered to be significant.

3 CHARACTERISING THE EFFECTS OF A LOW CALCIUM DIET *IN VIVO* – MODIFICATION OF THE BONE MICRO-ENVIRONMENT AND DISSEMINATED TUMOUR CELLS

3.1 SUMMARY

Tumour cell dormancy remains a significant challenge in the diagnosis and management of patients with breast cancer. Better understanding of the processes involved in the induction and escape of dormancy would provide better methods of improving clinical outcome for these patients. Bone, a key site of dissemination and dormancy, merits increased investigation.

In model systems, elevated bone turnover as a result of increased osteoclast activity following ovariectomy has been shown to confer tumour cell escape from dormancy (Ottewell *et al*., 2015, Brown *et al*., 2012). This effect was subsequently inhibited by OPG-Fc and Zoledronic acid, supporting a role for increased osteoclast activity as a mediator of outgrowth of disseminated tumour cells. The mechanism remains to be identified.

Modification of the bone microenvironment in mice following administration of a low calcium diet (0.006% - 0.1%) is shown to result in alteration of bone density and cell composition, correlating with an effect on tumour growth in some studies (Libouban and Chappard, 2017, Minematsu *et al*., 2001, Wang *et al*., 2017a, Zheng *et al*., 2008). Inducing increased bone turnover using a low calcium diet could therefore potentially trigger escape from dormancy of disseminated tumour cells.

I therefore characterised the effect of exposure to a low calcium diet (0.1%) for increasing periods of time on the bone microenvironment and turnover in 12-15 week old female immunocompetent (BALB/c and C57BL/6) and immunocompromised (BALB/c nude) mice. This resulted in minor alterations to the bone microenvironment, indicated by assessment of physical trabecular bone density and volume, bone gene expression, cellular composition and osteoblast and osteoclast activity, showing minor structural changes following 28 days of a low calcium diet. For tumour studies, 12-15 week-old BALB/c nude mice were injeccted with MDA-MB-231 human breast cancer cells and subsequently fed a low calcium diet to assess escape from dormancy and influence on tumour outgrowth. There was no significant difference in tumour growth in mice fed a low calcium diet and those on a normal diet. In summary, escape from dormancy in the ovariectomy-induced model was not recapitulated by using a low calcium diet.

In conclusion, the exposure to a low calcium diet with this formulation or concentration (0.1%) may be insufficient to trigger disseminated tumour cells into escape from dormancy in this model system. Alternative strategies to induce bone turnover and subsequent mechanistic analysis in the escape from dormancy would therefore need to be pursued.

3.2 INTRODUCTION

3.2.1 INDUCED BONE RESORPTION AND INCREASED PROLIFERATION OF DISSEMINATED TUMOUR CELLS

Bone is a highly mineralised tissue consisting of type I collagen fibres enamelled with hydroxyapatite, a composite of calcium and phosphate, and serves as the body's main store of these two minerals. In addition, the bone matrix is a rich store of proteins, and is a reservoir for growth factors transforming growth factor (TGF)-β, fibroblast growth factor (FGF), platelet derived growth factor (PDGF), bone morphogenetic proteins (BMP) and insulin-like growth factor (IGF)-1 amongst others (Mohan and Baylink, 1991, Tremollieres *et al*., 1991) . Osteoclasts are the only cell with the ability to degrade both mineralised contents of the bone and the organic matrix, which leads to release of ionic calcium and growth factors that promote cellular growth. Osteolytic cancers, such as disseminated breast cancer, rely on recruited osteoclasts and the vicious cycle to propagate tumour growth in response to increased bone turnover (Käkönen and Mundy, 2003).

Targeting the osteoclast in disseminated breast cancer has shown promise, and is a candidate for the investigation in the prevention of overt outgrowth of disseminated tumour cells mediated by increased bone resorption. The AZURE trial, a randomised open-label phase 3 trial of 3360 women investigated the adjuvant use of zoledronic acid, which inhibits osteoclast activity, in high-risk patients with early breast cancer. Zoledronic acid did not improve overall survival or distant recurrences, but reduced development of bone metastases (Coleman *et al*., 2014). Importantly, postmenopausal women achieved increased survival as compared to pre and perimenopausal women, linking the differential effects of the drug with age and menopausal status. These data, combined with experimental data reflecting the beneficial impact of using zoledronic acid for bone DTCs *in vivo*, shows promise in the targeting of the osteoclast in bone metastatic disease (Ottewell *et al*., 2015).

Several studies using *in vivo* models have outlined the impact of hormone deprivation on bone turnover and subsequent increased tumour proliferation within the bone. In particular, castration in the case of prostate cancer and ovariectomy in breast cancer models have resulted in a rapid and substantial effect on bone turnover. In adult mice with low bone turnover metastatic outgrowth was observed at very low frequency from tumour cells disseminated in bone and that castration or ovariectomy increased bone turnover which stimulated metastatic outgrowth of disseminated PC3 prostate and MDA-MB-231 breast cancer cells in mouse models. (see Table 3-1 for a summary of select studies demonstrating these effects). Thus, increased bone resorption has been shown to induce of escape from dormancy of disseminated tumour cells.

Animal Model / Strain / Age	Method of Increased Turnover	Tumour Cells Used	Effect on Tumour Growth / Bone Turnover	Author/Reference
12-week old male	Castration	PC3 human	Increased bone resorption and decreased bone volume. 70% of castrated mice had	(Ottewell *et al*., 2014b)

BALB/C nude mice		prostate cancer	outgrowth of disseminated tumour cells compared to 10% in sham controls.	
12-week old female BALB/C nude mice	Ovariectomy, inhibited by OPG-Fc	MDA-MB-231 human breast cancer	Increased bone loss in ovariectomy group. 78.5% animals in ovariectomy/saline compared to 17% sham/saline group. OPG-fc completely inhibited tumour growth in ovariectomy-induced group with no effect on sham.	(Ottewell *et al*., 2015)
12-week old female BALB/C nude mice	Ovariectomy, inhibited by Zoledronic Acid	MDA-MB-231 human breast cancer	Increased bone loss in ovariectomy group. 83% in ovariectomy group had tumours, compared to 17% in sham control. Effect completely inhibited by zoledronic acid.	(Ottewell *et al*., 2014a)

Table 3-1: A summary of hormone deprivation-induced increased tumour proliferation within bone

3.2.2 HYPOCALCEMIA- INDUCED BONE RESORPTION

In a state of hypocalcemia, where blood calcium falls below normal physiologically levels, the parathyroid glands respond by releasing parathyroid hormone (PTH), which acts to increase bone resorption by increasing osteoclastogenesis via upregulation of RANKL or direct osteoclast stimulation (Datta, 2011).

Considered the most important hormonal regulator of calcium homeostasis, PTH acts on the bone bi-modally, dependent on a continuous or intermittent release (Lotinun *et al*., 2002). Calcium sensing receptors located on parathyroid cell membranes, detect ionic calcium levels in extracellular fluid, which subsequently regulate secretion or inhibition of PTH (Liu *et al*., 2016b). In humans with regular consumption of food, PTH levels fluctuate in the course of a day, being inhibited following consumption of calcium-containing foods that subsequently increase plasma concentrations of calcium. A period of time without consumption of calcium containing foods results in a drop in plasma concentrations of calcium, detected by parathyroid cells, triggering the release of PTH. Thus, in a cycle of intermittent calcium consumption, an intermittent pattern of PTH release is achieved. In situations of poor calcium consumption however, PTH is released in a continuous state.

Being FDA approved for treatment of osteoporosis and hypoparathyroidism amongst other conditions, teriparatide, the N-terminal peptides 1-34 of PTH, is anabolic and stimulates bone formation following daily administration of 20μg/day for 18 months with a maximum stipulated duration of daily administration of 24 months (Cheng and Gupta, 2012). Conversely, continuous infusion is catabolic and has been shown to result in severe bone loss, showing that exposure to PTH causes increased bone turnover (Bodenner *et al*., 2007). Release of PTH following a low calcium diet may be sufficient to elicit increased bone turnover, which would subsequently trigger the escape from dormancy of disseminated tumour cells. In addition, the use of teriparatide in the treatment of patients with disseminated tumour cells within the bone may be explored for therapeutic benefit.

In a hypothetical clinical setting, increased bone resorption, leading to overt outgrowth of bone-disseminated dormant tumour cells, may occur in a state of hypocalcemia where serum levels of calcium are insufficient, possibly resulting from inadequate dietary intake of calcium or inadequate vitamin D which facilitates efficient calcium intake. Increased bone turnover as a response to a low calcium diet has been demonstrated in a number of studies where mice have undergone chronic inducement of hypocalcemia following medium to long term low calcium diets resulting in bone catabolic effects (see Table 3-2 for a summary of various studies utilising a low calcium diet to trigger increased bone turnover). These effects have been described in a variety of mouse strains, ages, tumour models, calcium concentrations and periods of time on the diet. In general, the studies demonstrate that placing mice on a low calcium diet increases bone turnover mediated by osteoclast activity.

The calcium sensing receptor (CaSR), is a G-Protein coupled receptor and is expressed in the parathyroid glands and kidneys and responsible for triggering events leading to modulating serum calcium is also expressed on bone cells and regulates skeletal homeostasis (Saidak *et al*., 2009). The role of CaSR in the bone may be enigmatic, as activation of CaSR on osteoclasts contributes to enhanced bone anabolism in young animals by inhibiting bone resorption, but in older animals increases the expression of RANKL by osteoblasts and subsequent osteoclast-mediated bone resorption (Goltzman and Hendy, 2015). Similar to the enigmatic role played by CaSR in bone regulation, it also has differential effects on tumours, dependent on primary tissue; exhibiting oncogenic properties in breast cancer cells, while functioning to inhibit proliferation in colon and parathyroid cancers (Saidak *et al*., 2009). Its exact role in cancer may be linked to the relationship of the primary tissue with calcium, as calcium reduces the activity of parathyroid-secreting glands (Yano *et al*., 2000). In normal breast tissue, CaSR activation couples to $G\alpha_i$ acting to inhibit cAMP and PTHrP, but in cancerous breast tissue binds to $G\alpha_s$ resulting in an increase of cAMP and PTHrP, subsequently inducing increased proliferation (Kim and Wysolmerski, 2016). Therefore, in addition to the activity of parathyroid hormone in hypocalcemia-induced increased cancer cell proliferation in the bone, CaSR warrants investigation in this setting.

Table 3-2: Summary of studies utilising a low calcium diet in the presence or absence of tumours and subsequent effects

Animal Model / Strain /Age	Low Calcium Diet	Tumour Cells Used	Effect on Tumour Growth / Bone Turnover	Author/Reference
4-week old female BALB/C nu/nu	0.1% Calcium for 14 days, inhibited by OPG	Tx-SA (MDA-MB-231 variant) human breast cancer	Tumour-induced lytic lesion, tumour area and proliferation increased by 43%, 24% (completely inhibited by OPG) and 24% respectively (reduced by OPG).	(Zheng *et al*., 2007)
5-week old female ICR mice	0.006%	None	Mechanical strength, ash content and dry bone to weight ratio significantly reduced.	(Minematsu *et al*., 2001)

	Following ovariectomy for 140 days			
9-month old female BALB/C mice	0.008% for 14 days	4-T1 mouse mammary carcinoma	Increased cortical osteolysis, periosteal woven bone formation and tumour cell infiltration into muscle.	(Wang *et al.*, 2017b)
6-8 week old female C57BL/KaLwRij mice	0.05% for 6, 8 and 10 weeks	5T2MM mouse multiple myeloma	Tumour-induced trabecular bone loss and decreased cortical thickness at 10 weeks. Increased osteoclast number at 6 weeks.	(Libouban and Chappard, 2017)
4-week old female BALB/C nu/nu mice	0.1% for 17, 35 or 60 days inhibited by OPG	MDA-MB-231 and MCF7 human breast cancer	Increased tumour size in low calcium diet for both MDA-MB-231(24%) and MCF7 (71%). OPG reduced tumour size in both MDA-MB-231 and MCF7 (46% and 67% respectively).	(Zheng *et al.*, 2008)

Importantly, using a low calcium diet to induce outgrowth of dormant disseminated tumour cells has not been demonstrated as in the case of ovariectomy. Thus placing mice on a low calcium diet to induce bone resorption and subsequently trigger outgrowth of disseminated tumour cells is a novel approach to establish whether increased osteoclast activity can mediate escape from dormancy. Ovariectomy and low-calcium-diet induced bone turnover both occur through osteoclastic activity, and inhibition of this bone turnover would therefore be through similar interventions. Furthermore, as estrogen can have an effect on tumour cells, using a low calcium diet would cement a direct and sole-sufficient role for osteoclasts in re-awakening of dormant disseminated tumour cells.

Hypothesis and Aims

The hypothesis underpinning the work in this chapter is that ***feeding mice a low calcium diet stimulates increased bone resorption which subsequently triggers the proliferation of dormant disseminated tumour cells*** and will be assessed by the following aims:

1) Characterise the effects of a low calcium diet on the bone micro-environment in C57BL/6, BALB/c immunocompetent mice and BALB/c nude immunocompromised mice by measuring trabecular bone volume by uCT, gene expression by rtPCR, osteoclast and osteoblast size and numbers by bone histomorphometry with corresponding activity assessed by ELISA for TRAP and P1NP.

2) Assess the effect of a low calcium diet on the outgrowth of dormant, disseminated tumour cells by introducing MDA-MB-231 cells into immunocompromised BALB/c mice followed by a low calcium diet and monitoring for differences in outgrowth compared to mice fed a normal diet.

The effect of a low calcium diet will be compared using immunocompetent and immunocompromised mice. Immunocompromised mice are necessary for the inoculation and monitoring of allogeneic human breast cancer cells which are rapidly rejected by immunocompetent hosts prior to tumour establishment. A low calcium diet may have differential effects in immunocompetent mice, therefore these shall be used to identify any model-specific variations in response to hypocalcaemia.

3.3 MATERIALS AND METHODS

A summary of methods used in this chapter. Extended descriptions can be found in chapter 2: Materials and Methods.

Method	Parameters analysed	Materials / Equipment / Software
Low Calcium Diet		
Low Calcium diet	-	Mineral adjusted chow (0.1% calcium), Envigo, US
Bone mineralised content		
Microcomputed tomography (μCT)	-Trabecular bone volume (BV/TV in %) -Trabecular number (TB.N. in mm-1) -Trabecular thickness (Tb.Th. in mm) Trabecular Spacing (in mm)	-SkyScan 1172/1272 scanner (SkyScan) -NRecon software -CTAn software

Gene expression		
Quantitative PCR	RNA transcript abundance relative to housekeeping gene	Applied Biosystems PRISM HT-7900 sequence detection system (Thermo Scientific)
Histological assessment		
Tartrate-resistant acid phosphatase staining (TRAP)	-Osteoclast number per mm of trabecular bone surface -Osteoclast size (in mm)	-OsteoMeasure software (OsteoMetrics) -LeicaDMRB upright microscope
Haematoxylin and Eosin staining (H&E)	-Osteoblast number per mm trabecular bone surface -Osteoblast size (in mm)	-OsteoMeasure software (OsteoMetrics) -Leica DMRB upright microscope -Olympus BX53 microscope
Tumour cell homing to bone and tumour development		
IVIS *in vivo* imaging	-Presence of tumour cells in live mice and tissue *ex vivo*	(IVIS) LUMINA II (Caliper Life Sciences).
Enzymatic analysis		
Mouse TRAP Enzyme Immunoassay	-Osteoclast activity	-MouseTRAP Assay from immunodiagnostic systems (SB-TR103)
Rat/Mouse PINP Enzyme immunoassay	-Osteoblast activity	-Rat/Mouse PINP Enzyme immunoassay for the quantitative determination of N-terminal propeptide of type I procollagen from immunodiagnostic systems
Statistical analysis		
Statistical analysis	-Experimental datasets	-PrismGraphPad version 8.1

3.3.1 ANIMALS

Six and 12-week-old female Bagg and Albino (BALB)/c (CAnN.Cg-***Foxn1^{nu}***/Crl) nude (immunocompromised), BALB/c (immunocompetent) and C57BL/6 (immunocompetent) mice were acquired from Charles River, UK. 12-week-old female BALB/c (OlaHsd-*Foxn1^{nu}*) nude (immunocompromised) mice were obtained from Envigo, UK. Upon arrival, mice were acclimatised in the Biological Services Unit (BSU) for a minimum of 7 days before procedures. Mice were aged for a

further 2-3 weeks to obtain mice aged 14-15 weeks at time of procedure, reflecting aged phenotypes previously shown to support tumour cell dormancy.

All procedures performed were approved and carried out under Programme Project Licence (PPL) 70/8964 and personal license PIL I62B58981 within the Biological Services Unit (BSU) under local guidelines and in accordance with Home Office regulations.

3.3.2 LOW CALCIUM DIET

Mineral adjusted chow (0.1% calcium) was obtained from Envigo, US. Animals were fed a low calcium diet in order to trigger increased bone resorption as a result of hypocalcaemia and the action of PTH. In *in vivo* experiments, mice were fed a low calcium diet for variable periods of time, following intra-cardiac injection of tumour cells where this was performed. Control animals were fed chow containing 1.01% calcium (Harlan Laboratories, UK).

3.3.3 INTRA-CARDIAC INJECTION

Late-stage metastasis was mimicked by direct injection of MDA-MB-231-IV *Luc2* positive human breast cancer cells into the circulation. To encourage bone metastases, 100µl of $1x10^5$ or $5x10^4$ of cells suspended in PBS were injected directly into the left ventricle of mice under inhalation anaesthesia consisting of 2-3% isoflurane (Zoetis, UK). Mice were placed in an incubator at 32°C for 1-3 hours post-injection and monitored closely for adverse signs in the 24-hour period ensuing.

3.3.4 *IN VIVO* IMAGING

To track tumour progress *in vivo,* animals injected with cancer cells expressing firefly luciferase were injected sub-cutaneously with 100µl of D-luciferin (30mg/kg) 5 minutes prior to imaging on both sides of the coronal plane (front and back) of the animal. Imaging was done in the *in vivo* imaging system (IVIS) LUMINA II (Caliper Life Sciences). This procedure was carried out under anaesthetic following administration of 2-4% isofluorane.

Living image software (version 4.1) was used to identify presence and quantify size of tumours by bioluminescent capture measured in photos/second and displayed on a scale with different colours representing varying intensities of luminescence. Both larger size and increased intensity of luminescence represent larger tumours (see Figure 2-2).

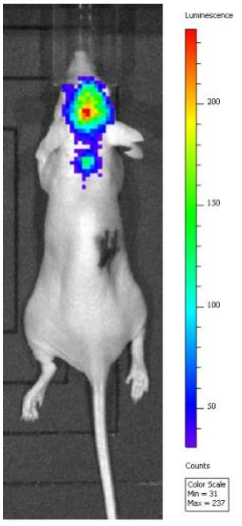

Figure 3-1: Bioluminescent imaging of MDA-MD-231 cells expressing firefly luciferase and subjected to luciferin. Scale on the right represents varying levels of intensity, blue hue representing approximately 50 units, and red representing more than 210 units.

3.3.5 *Ex vivo* analysis

3.3.5.1 Bones for histology and histomorphometry

Immediately following dissection, tibias used for histology and histomorphometry were placed in 4% (*w/v)* paraformaldehyde (PFA) for 48-72 hours. These were then washed 3 times in ice-cold PBS and stored in PBS at 4°C pending µCT analysis. Once µCT scanning was complete, bones were placed in 14% (*w/v*) ethylenediaminetetraacetic acid (EDTA) for decalcification. This solution was changed twice a week for 3 weeks before bone processing. Bones were subsequently paraffin-embedded (wax). To obtain sections for histological analysis, wax embedded tibias were cut at 3µm thickness, and 6 samples taken from 3 levels, 20-30µm apart before mounting on glass slides and stored at room temperature.

3.3.5.2 Osteomeasure Analysis

To analyse the cellular response to bone remodelling, TRAP-stained bone sections were analysed on OsteoMeasure7 version 4.2 through a LEICA Leitz DMRB microscope at a 20X maginification.

Entire cortical and trabecular surface below offset was measured. Cortical measurement offset was 250µm below chondrocytes and offset for trabecular measurements was 125µm (see Figure 2-8).

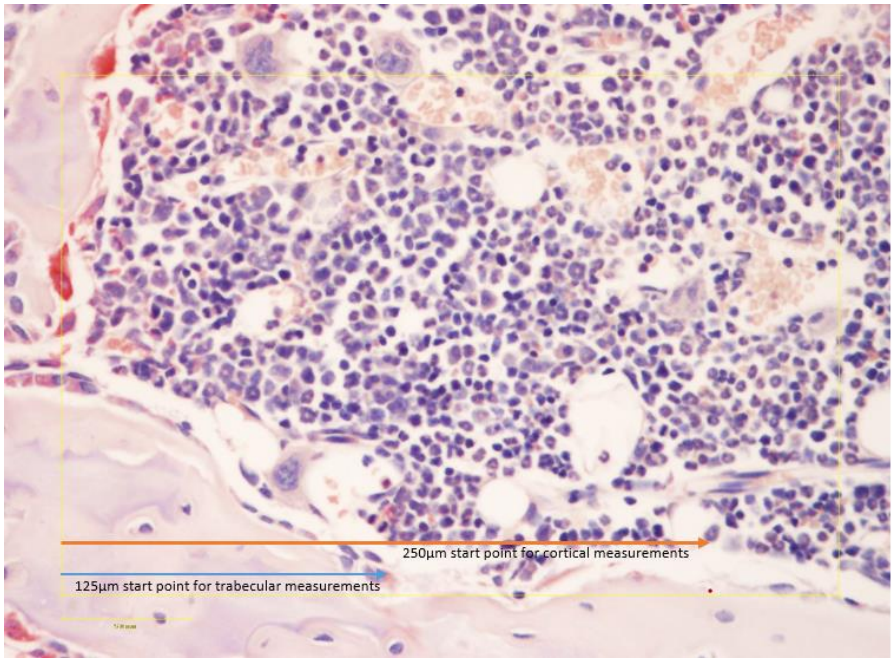

Figure 3-2: References to begin measurements on TRAP stained sections were based on the bottom of the chondrocytes for trabecular (blue arrow -125µm) and cortical (orange arrow - 250µm) start points

The number of osteoclasts (N.Oc), number of osteoblasts (N.Ob), osteoclast surface area (Oc.Pm) on bone, osteoblast surface (Ob.Pm) on bone and bone surface were measured.

3.3.5.2.1 Reverse Transcription

Femurs were used for RNA extraction and subsequent PCR gene expression. Once obtained, they were placed in labelled foil and snap frozen in liquid nitrogen, before being stored at -80°C. Reverse transcription was performed as per section 2.6.2.1 of the materials and methods.

3.3.5.3 Real-time amplification of cDNA transcripts

Samples for real-time detection were prepared using 2x PrecisionPLUS qPCR SYBR Green Master Mix (Primer Design) and added into 384-well PCR plates with 10µl per well. Each well contained 5µl 2x master mix, 0.5µl 300nM forward primer, 0.5µl 300nM reverse prime, 1µl template cDNA and 3µl RNase-free water. Each sample was repeated in triplicate.

Real-time amplification of cDNA transcripts was performed using Applied Biosystems PRISM HT-7900 sequence detection system (Thermo Scientific) using SDS 2.4 software (Thermo Scientific). To obtain quantitative values, Standard Curve (AQ) settings were used. Default thermal profile settings were used to run real-time PCR, with an added dissociation step for assessment of primer efficiency. SYBR Green was selected as a detector and applied to all wells, with ROX as a passive reference.

Primer sequences used can be found in section 2.6.2.3 of the materials and methods.

3.4 Results

3.4.1 Profiling the bone microenvironment in immunocompetent mice following 7 days of a low calcium diet

In characterising an immunocompetent model of dormancy and subsequent relapse, a low calcium (0.1) diet was selected as a trigger of increased bone resorption. The aim of using a low calcium diet was to stimulate increased bone resorption through the action of continuous PTH secretion followed by assessing the effects of this increased bone resorption on the wider bone microenvironment *ex vivo.*

The basis of these studies was earlier unpublished studies carried by Dr Hannah Brown and Professor Ingunn Holen, which had found that placing mice on a low calcium diet for 1 or 5 days increased the onset of the outgrowth on disseminated tumour cells, compared to a control group receiving a normal

diet (see Figure 3-5 and Figure 3-6).

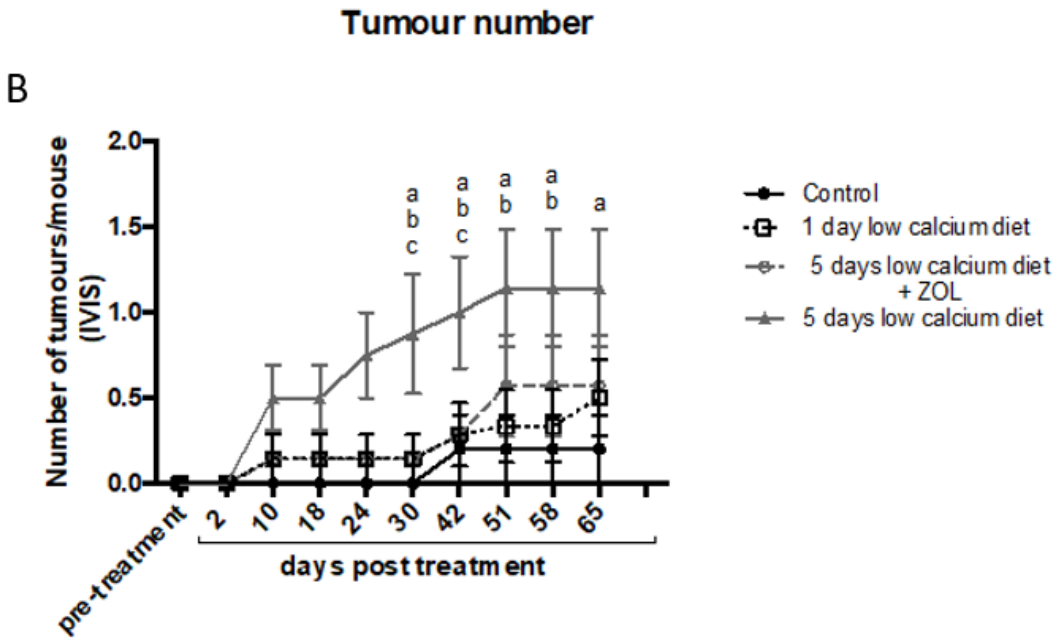

Figure 3-3: Experiment carried out by Dr. Hannah Brown to characterise the effects of a low calcium diet on tumour outgrowth in immunocompromised mice (unpublished). A.) Experimental outline. Four groups (n=8 per group) of 16-17 week old female BALB/c nude mice were injected with 1x105 DiD+ labelled MDA-MB-231-tomato cells before being randomised to either receive i.) a single dose of 100µg/kg of Zoledronic acid on day 18, 3 days prior to a low calcium diet on day 21, which lasted 5 days from day 21 to 25, ii.) a low calcium diet for 5 days from day 21 to 25, iii.) a low calcium diet for 1 days from day 21 to 22, or iv.) a normal diet. B.) Mice were monitored for up to 65 days by *in vivo* imaging for tumour growth, with the number of tumours in skeletal sites quantified in each group.

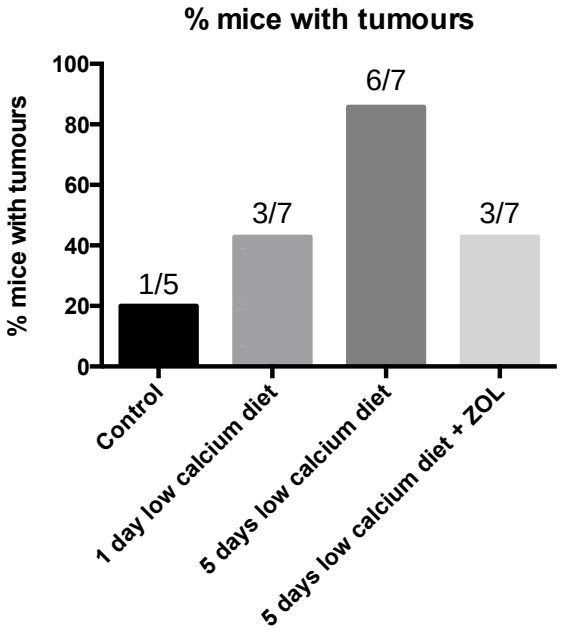

Figure 3-4: Final summary results by Dr. Hannah Brown (unpublished) showing 5 days of a low calcium diet induced a majority of mice to develop hind limb tumours within 65 days, which was attenuated with a single dose of Zoledronic Acid

To assess the effect of low calcium diet on the bone microenvironment of mature, immunocompetent mice, naïve 15-week old female C57BL/6 mice (n=10) were randomly assigned to 2 groups (n=5/group) that received either a normal diet or low calcium diet for 7 days (see Figure 3-5). The duration of the low calcium diet was selected based on previous pilot studies that showed changes in the frequency of tumour growth in mice between 5-7 days following a low calcium diet, and initial small-scale studies to optimise the diet and duration, a small number of animals were used.

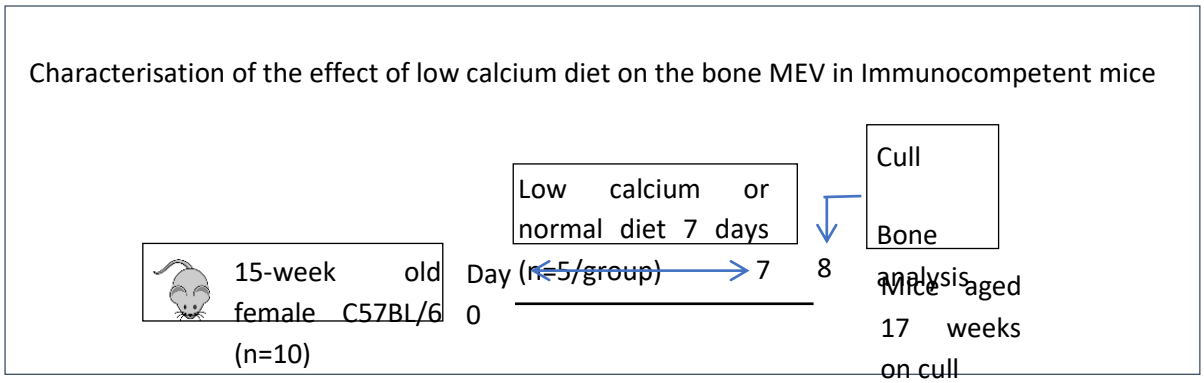

Figure 3-5: Experimental outline to assess the effect of a low calcium diet (0.1%) on the bone microenvironment. On day 0, mice were randomised to receive a low calcium diet for 7 days or a normal diet. On day 8, mice were culled and tissues harvested for analysis.

Tissues were then extracted to perform gene expression analysis by rtPCR and bone architecture by µCT.

3.4.2 µCT – Physical effects of a low calcium diet on the bone microenvironment

µCT was performed on the trabecular region of right tibias obtained from this experiment to determine whether exposure to the low calcium diet modified bone volume and structure, as assessed by measurement of physical structural parameters. Hind limbs were isolated and subjected to *ex vivo* µCT analysis allowing the assessment of tissue volume, bone volume, percent bone volume, trabeculae thickness, trabecular number and trabecular spacing as described in section 2 in the materials and methods chapter. This data demonstrates that exposure to 7 days on a low calcium diet does not result in significant change in physical bone parameters as a result of increased bone resorption.

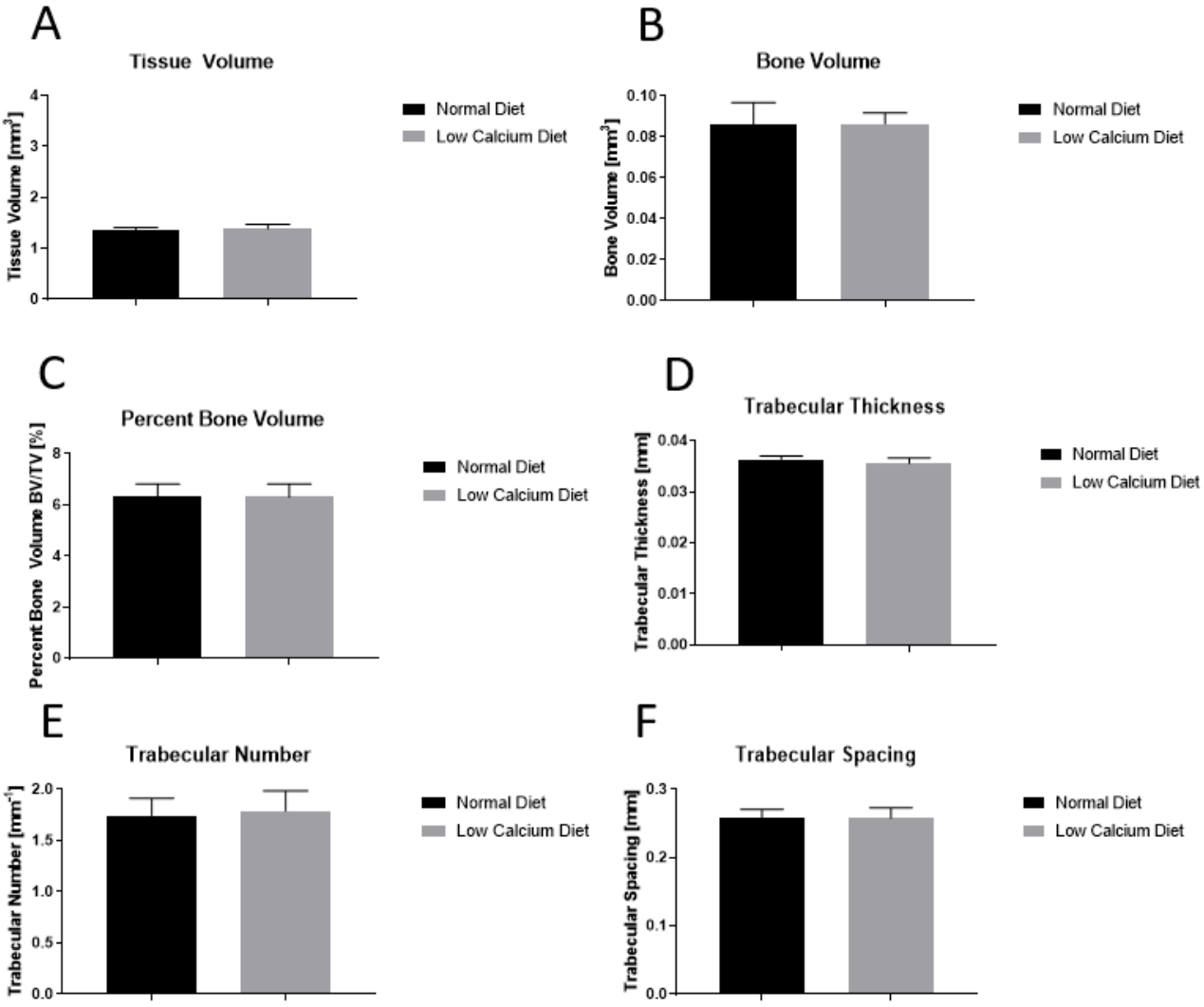

Figure 3-6: Right tibias were analysed by µCT on animals from the entire study with n=5 normal diet, n=5 low calcium diet. Unpaired T-test was performed for each parameter measured A.) Tissue Volume, B.) Bone Volume, C.) Percent Bone Volume, D.) Trabecular Thickness, E.) Trabecular Number, F.) Trabecular Spacing. No significant differences were detected.

Data from µCT analysis performed on trabecular bone from right tibias: Measured mean tissue volume (TV) (measured in mm^3) for the low calcium diet group (n=5) was 1.39 (± 0.08042 SEM) and 1.355 (± 0.0527 SEM) for the normal diet group (n=5), with a non-significant p-value of 0.7325 (A). Average measured bone volume (BV) (measured in mm^3) was at 0.08649 (± 0.005221 SEM) for the low calcium group (n=5) and 0.0863 (± 0.01051 SEM) for the normal diet group (n=5) with a non-significant p-value of 0.9874 (panel B). Percent bone volume measured as (BV/TV %) yielded an average of 6.303 (± 0.5219 SEM) for the low calcium diet group (n=5) and 6.304 (± 0.5158 SEM) for the normal diet group (n=5) with a non-significant p-value of 0.9987 (panel C). Average trabecular thickness (measured in mm) for the low calcium diet group (n=5) was 0.03559 (± 0.001095 SEM) whereas the normal diet group (n=5) measured 0.03637 (± 0.0006858 SEM), with a non-significant p-value of 0.5678 (panel D). Average trabecular number (measured in mm^{-1}) was 1.79 (± 0.1952 SEM) for the low calcium diet

group (n=5) and 1.744 (± 0.1704 SEM) for the normal diet group (n=5) with a non-significant p-value of 0.8634 (panel E). Mean trabecular spacing (measured in mm) was 0.2578 (± 0.01496 SEM) and 0.2574 (± 0.01343 SEM) for the low calcium diet (n=5) and normal diet (n=5) groups respectively with a non-significant p-value of 0.9868 (panel F). These data did not show any detectable difference in bone mineral composition between mice fed a low calcium diet for 7 days and those on a normal diet.

3.4.2.1 PCR – Gene expression profiling of genes reflecting bone turnover and HSC quiescence

Studies into the effect of a low calcium diet on bone structure integrity were accompanied by assessments on the change of gene expression for Kit Ligand, RANKL, CXCL4, OPG, OPN and TBSP-1 to assess for genes associated with altered bone turnover (RANKL, OPN, OPG), increased HSC quiescence (CXCL4, TBSP-1) and expansion (Kit Ligand) on RNA extracted from the right femurs of animals. RNA was obtained using the flush method from right femurs as described in section 2.4.2.6 of the materials and methods section.

Table 3-3: Table 3 3: Summary of genes analysed, role and the cells expressing these genes

Primer/Protein	Role	Cells Expressing
Osteopontin (OPN)	Hypocalcemia indicator Anchors osteoclast and develops ruffled border, cellular adhesion	Osteoclast/blast progenitors, immune cells including macrophages, neutrophils, dendritic cells, and T and B cells
Osteoprotegerin (OPG)	Molecular decoy for RANKL	Osteoblasts
Thrombospondin-1 (TBSP-1)	Inhibitor of neovascularization and tumorigenesis, metastasis (MET), cellular adhesion	Megakarytocytes/platelets fibroblasts, macrophages, neutrophils
RANK Ligand (RANKL)	Master regulator of Osteoclast differentiation through NFκβ signalling	Osteocytes, Osteoblasts, Th17
CXCL4	Heparin binder – blood vessel integrity Chemotactic for $CD11b^{+}Ly6G^{+}$ myeloid cells	Megakaryocytes and α granules of platelets
Kit ligand (KitL)	Binds to c-kit on hematopoietic stem cells triggering differentiation	HSC niche stromal cells
Tartrate-Resistant Acid Phosphatase (TRAP)	Enzyme involved in dephosphorylation of osteopontin / bone sialoprotein involved in bone resorption	Osteoclasts
Procollagen type 1 N Propeptide (P1NP)	N-terminal end of procollagen cleaved during formation of type 1 collagen in bone – marker of increased bone formation	Osteoblasts

Osteopontin, TRAP and RANKL would be expected to be elevated directly due to increased bone resorption in response to the low calcium diet. Kit Ligand would be expected to be increased indirectly due to increased HSC expansion following bone resorption to replenish myeloid progenitor populations which have been reduced due to differentiation into osteoclasts. Osteoprotegerin and P1NP would be expected to be elevated in animals not readily undergoing resorption. CXCL4 and TBSP1 would concurrently be expected to be increased in these animals due to angiogenic and hematopoietic homeostasis.

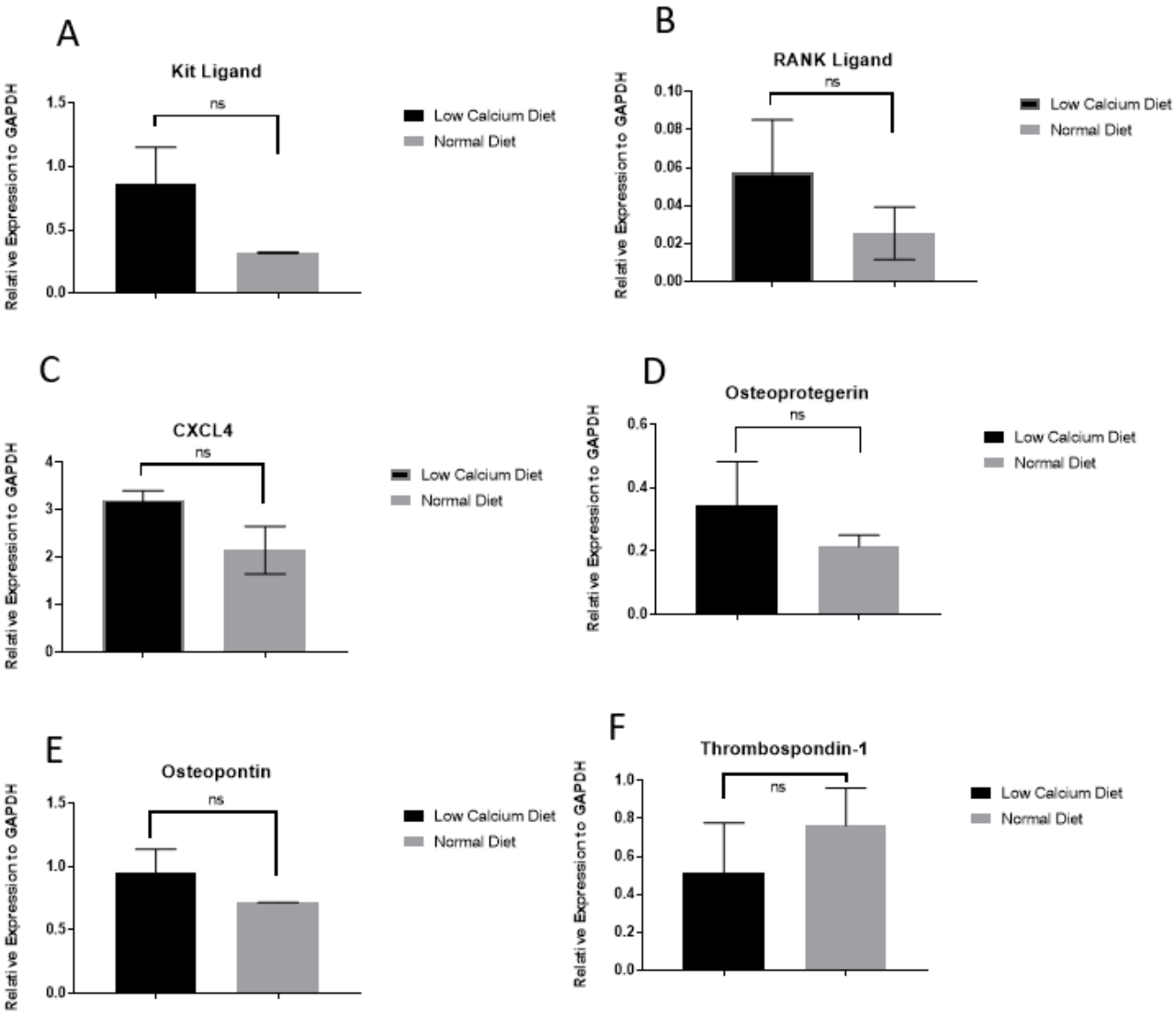

Figure 3-7: Gene expression analysis by PCR was performed on animals from the entire study with n=5 normal diet, n=5 low calcium diet. Unpaired T-test was performed for each gene measured A.) Kit Ligand, B.) RANK Ligand, C.) CXCL4, D.) Osteoprotegerin, E.) Osteopontin, F.) Thrombospondin-1. No significant differences were detected . Each biological replicate was run in triplicate.

Gene expression relative to housekeeping gene detected by PCR for six genes selected as indicating altered bone resorption and HSC regulation. Difference between means was reported as normal diet group – low calcium diet group ± SEM. Unpaired T-test was used for statistical inference. There was considerable variation, and in some cases, significant outliers were removed prior to statistical analysis and graph plotting. See Figure 3-7 for accompanying visualisation of results. Kit Ligand (A) expression in the low calcium diet group (n=4) was 0.859 versus an expression level of 0.320 for the normal calcium diet group (n=4) with a difference between the means of -0.540 (± 0.291 SEM). Despite suggesting a trend in higher expression from the low calcium diet group, the level of variance in the low-calcium diet group was high, with a non-significant p-value of 0.165 between the groups. RANKL

expression (B) was 0.025 (n=3) for the normal diet group in comparison to 0.058 for the low calcium diet group (n=3) with a difference between means of -0.032 (± 0.031 SEM), suggesting a non-significant trend towards an increased expression in the low calcium diet group. CXCL4 (C) expression had a mean of 2.151 for the low-calcium diet group (n=3) and 3.207 (n=2) for the normal diet group, with a difference between means of -1.057 ± (0.539 SEM). This indicates a trend in decreased CXCL4 expression following a low calcium diet, but similarly to Kit Ligand, a non-significant p-value of 0.161 may be attributed to variance both groups. OPG average expression (D) in the low calcium group (n=3) was 0.343 compared to 0.214 for the normal diet group (n=2) with a difference between the mean of -0.129 (± 0.085 SEM) and a non-significant p-value of 0.251. OPN expression (E) for the low calcium diet group (n=2) was 0.947 in contrast to 0.715 the normal diet group (n=2) and a difference between the means of -0.232 (± 0.193 SEM). P-value for OPN expression was non-significant at 0.442. TBSP1 (F) expression for the low calcium diet group (n=3) was 0.514 in comparison to 0.7630 for the normal diet group (n=3) with a difference between the means of 0.249 (± 0.329 SEM) and a non-significant p-value of 0.494.

These data suggest an increased gene expression in all the tested genes in the low-calcium diet group, excluding TBSP1. However, variances between biological replicates lead to statistically non-significant results. In agreement with the minor changes detected in bone structure and volume in response to the low ca diet, there was also no significant change in genes analysed associated with bone turnover or HSC expansion or quiescence.

3.4.3 PROFILING THE BONE MICROENVIRONMENT IN IMMUNOCOMPROMISED MICE FOLLOWING 7 DAYS OF A LOW CALCIUM DIET

The initial experiment assessing the effect of a low calcium diet for 7 days in immunocompetent mice described above was followed by an experiment investigating the effect of a low calcium diet on the bone microenvironment in immunocompromised BALB/c nude mice. This model was chosen to allow subsequent investigations in tumour cell dormancy escape. To characterise the effect of a low-calcium diet on the bone microenvironment, 15-week old female BALB/c nude mice (n=10) were randomised to either receive a low calcium diet for 7 days (n=5) or a normal diet (n=5) see Figure 3-8.

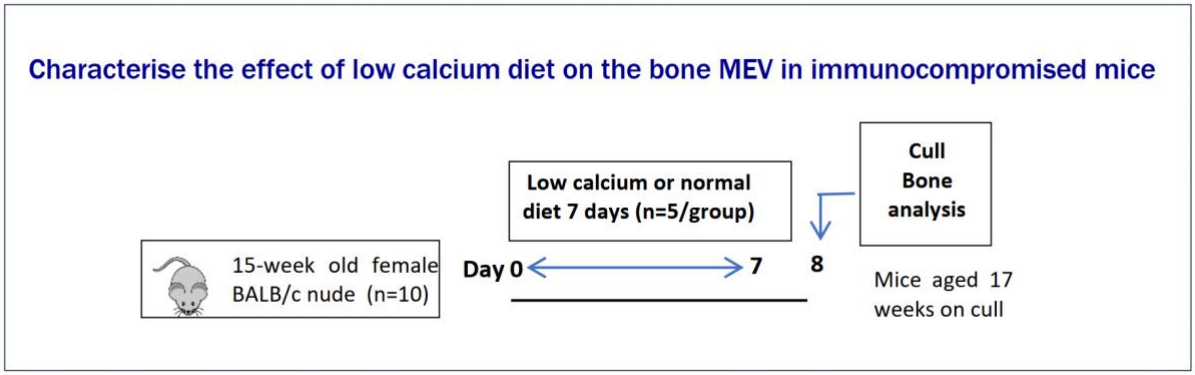

Figure 3-8: Overview of experimental plan for characterising the bone microenvironment following 7 days of a low calcium diet in immunocompromised animals

Tissues were then extracted to perform gene expression analysis by rtPCR, bone architecture by µCT and cellular analyses on osteoblasts and osteoclasts by TRAP staining and bone histomorphometry.µCT – Physical effects of a low calcium diet on the bone microenvironment

To assess whether a low calcium diet significantly modified bone volume and structure in the immunocompromised bone microenvironment, µCT was performed on right tibias obtained from this experiment. Hind limbs were isolated and subjected to *ex vivo* µCT analysis allowing the assessment of tissue volume, bone volume, percent bone volume, trabeculae thickness, trabecular number and trabecular spacing as described in section 2 in the materials and methods chapter. This data, similarly to data from immunocompetent models shown earlier, demonstrates that exposure to 7 days on a low calcium diet does not result in significant change in physical bone parameters as a result of increased bone resorption.

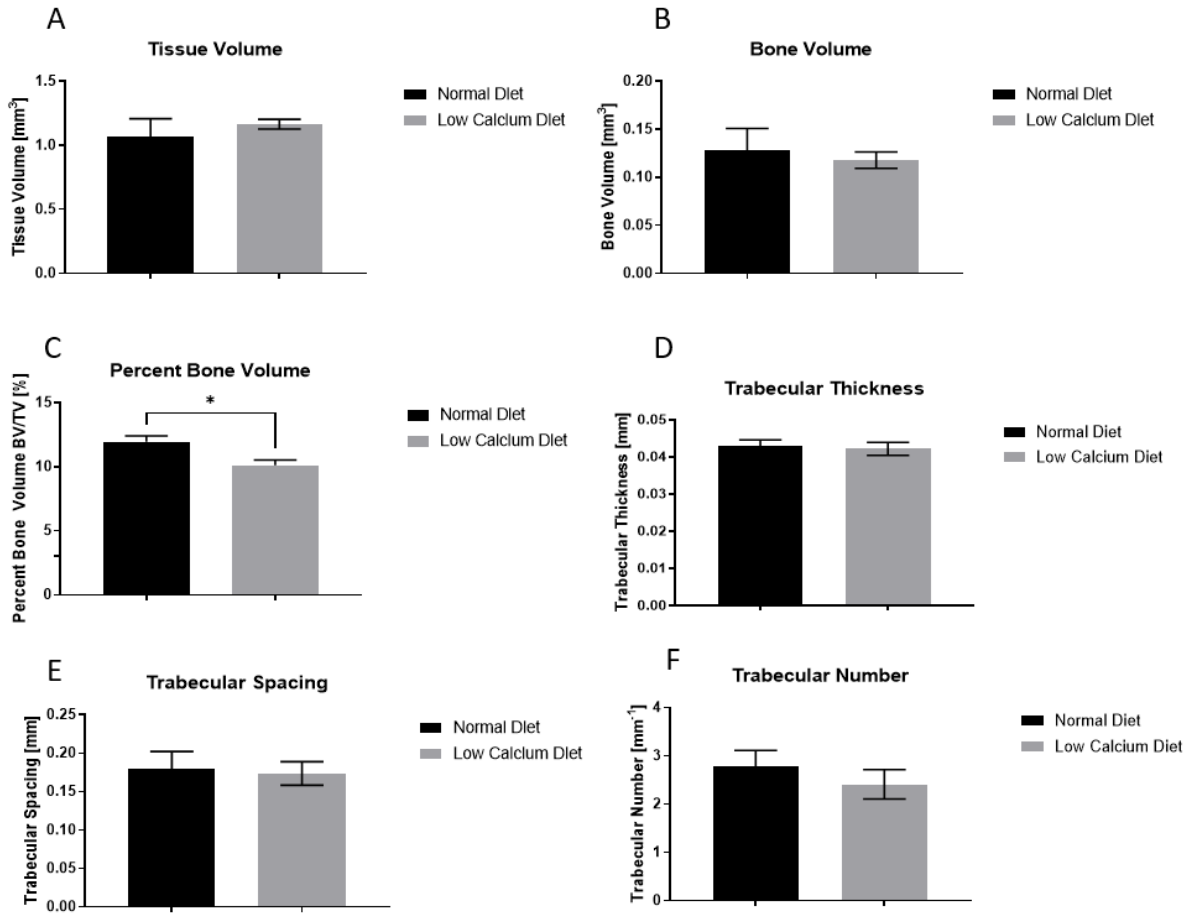

Figure 3-9 Right tibias were analysed by µCT on animals from the entire study with n=5 normal diet, n=5 low calcium diet. Unpaired T-test was performed for each parameter measured A.) Tissue Volume, B.) Bone Volume, C.) Percent Bone Volume p=0.0136, D.) Trabecular Thickness, E.) Trabecular Spacing, F.) Trabecular Number. No other significant differences were detected aside Percent Bone Volume (C).

Unpaired T-test was used for statistical inference. Measured mean tissue volume (TV) (measured in mm^3) (A) for the normal diet group (n=5) was 1.069 (± 0.062 SEM) and 1.166 ± (0.017 SEM) for the low-calcium diet group (n=5), with a non-significant p-value of 0.2005. Average measured bone volume (BV) (measured in mm3) (B) was 0.102 (± 0.003 SEM) for the low calcium group (n=5) and (0.111 ± 0.010 SEM) for the normal diet group (n=5) with a non-significant p-value of 0.442. Percent bone volume measured as (BV/TV %)(C) yielded an average of 8.765 (± 0.310 SEM) for the low calcium diet group (n=5) and 10.27 (± 0.360 SEM) for the normal diet group (n=5) with a 1.506% (± 0.475) reduction in percent bone volume affirmed by a significant p-value of 0.0136. Average trabecular thickness (measured in mm) (D) for the low calcium diet group (n=5) was 0.0384 ± (0.001 SEM) whereas the normal diet group (n=5) measured 0.040 (± 0.001 SEM) with a non-significant p-value of 0.325. Average trabecular number (measured in mm-1) (E) was 2.296 (± 0.128 SEM) for the low calcium diet group (n=5) and 2.6 (± 0.127 SEM) for the normal diet group (n=5) with a non-significant p-value of 0.130. Mean trabecular spacing (measured in mm) (F) was 0.245 (± 0.007 SEM) and (0.236 ± 0.009 SEM) for the low calcium diet (n=5) and normal diet (n=5) groups respectively with a non-significant p-value of 0.447. Taken together, these data show no changes in increased bone resorption

in the low-calcium diet group, with a minor, yet statistically significant difference in percent bone volume.

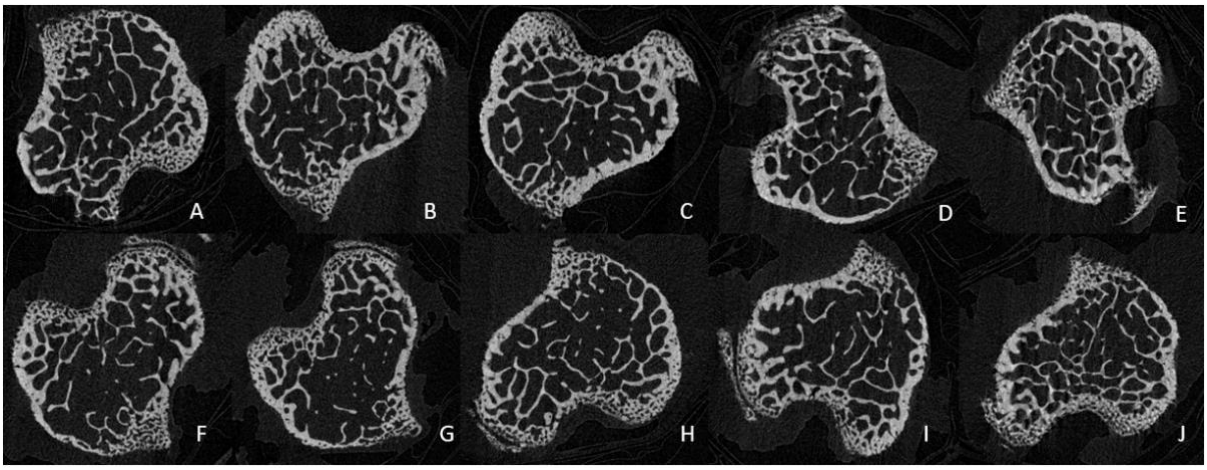

Figure 3-10: µCT figures of the first positions of scanning of bones from BALB/c nude mice fed a control (A-E) and a low calcium (F-J) diet for 7 days

3.4.3.1 PCR – GENE EXPRESSION PROFILING OF GENES REFLECTING BONE TURNOVER AND HSC QUIESCENCE

Similarly to the study on immunocompetent mice, the bone microenvironment gene expression was measured for genes associated with altered bone metabolism (RANKL, OPG, OPN) and HSC quiescence (CXCL4, TBSP1) and expansion (KitL) in order to ascertain microenvironmental influences on potential dormancy and subsequent escape. RNA was obtained using the flush method from right femurs. See Figure 3-11 for a summary view of the results.

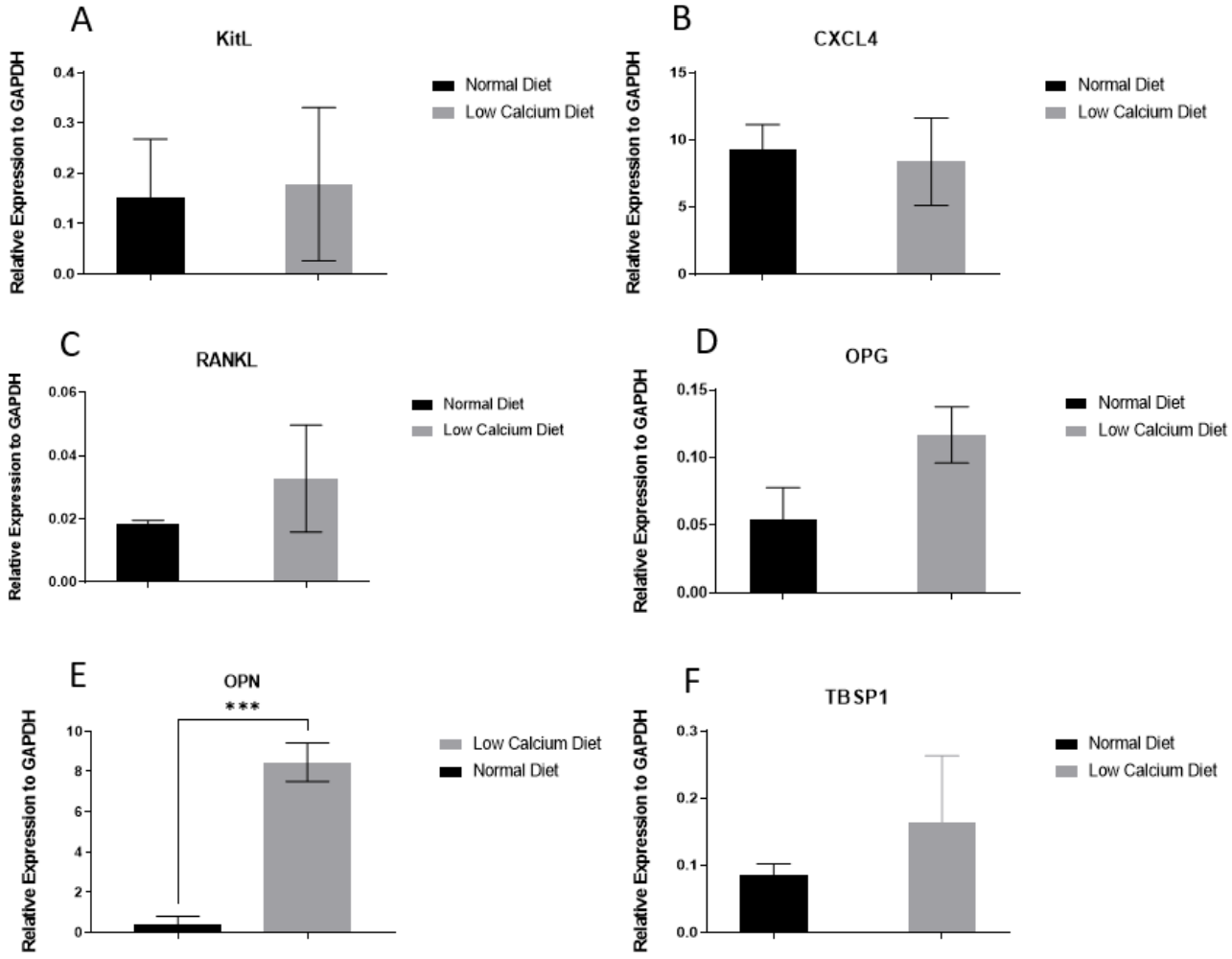

Figure 3-11: Gene expression analysis by PCR was performed on animals from the entire study with n=5 normal diet, n=5 low calcium diet. Unpaired T-test was performed for each gene measured A.) Kit Ligand, B.) CXCL4, C.) RANK Ligand, D.) Osteoprotegerin, E.) Osteopontin *** = p < 0.001, F.) Thrombospondin-1. All measurements taken in relation to housekeeping gene GAPDH.

PCR-measured expression of genes associated with altered bone turnover and HSC activity. Un-paired t-test was used for statistical inference. KitL gene expression (A) was 0.1786 ± 0.0878 in the low calcium diet group (n=3) and 0.152 (± 0.0670 SEM) in the normal diet group (n=3) with a non-significant p-value of 0.822. CXCL4 (B) expression for the low calcium diet group (n=2) was 8.37 (± 2.301 SEM) and 9.306 (± 1.293 SEM) with a non-significant p-value of 0.765. RANKL (C) expression within the low calcium diet group (n=3) was 0.0328 (± 0.010 SEM) and 0.01838 (± 0.001 SEM) for the normal diet group (n=2) with a non-significant p-value of 0.2786. OPG (D) expression was 0.117 (± 0.0121 SEM) for the low calcium diet group (n=3) and 0.0541 ± 0.01673 for the normal diet group (n=2) with a non-significant p-value of 0.0911. OPN (E) expression was 8.465 (± 0.674 SEM) for the low calcium diet group (n=2) and 0.371 ± 0.251 for the normal diet (n=3) group respectively with a significant p-value of 0.001. TBSP1 (F) expression was 0.165 (± 0.057 SEM) for the low-calcium diet group (n=3) in contrast to 0.0860 ± 0.010 for the normal diet group (n=3) with a non-significant p-value of 0.299. Gene expression was measured as relative expression to housekeeping gene GAPDH,

using the delta CT method ((Gene Ct value – housekeeping Ct value)$^{-2}$). Difference between means was reported as normal diet group – low calcium diet group ± SEM.

Despite potentially significant results, such as for OPN, there was a trend towards non-significance derived from variance in biological replicates and omission of values that could impact the significance of the reported results. I therefore repeated the PCR analysis of these samples in order to evaluate the validity of the findings (see Figure 3-12.)

This data shows inconclusive trends in gene expression for genes involved in increased bone resorption and HSC quiescence. Furthermore, the data is divergent in comparison to the first PCR analysis for this experiment. Very close CT values between technical triplicates, and varying CT values between biological replicates suggest variations between samples as the attributive cause for non-significant statistical values.

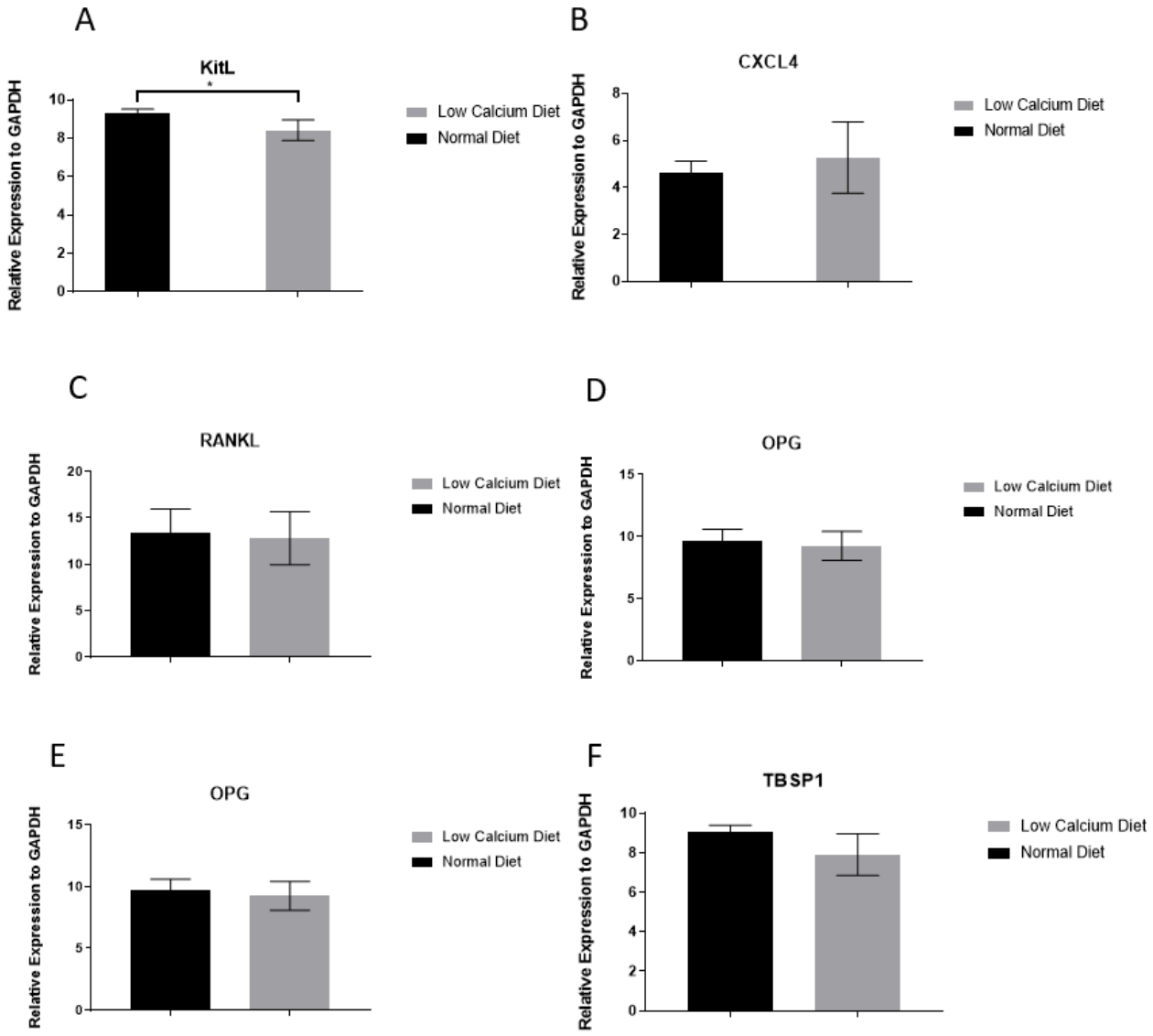

Figure 3-12: Gene expression analysis by PCR was performed a second time on animals from the entire study with n=5 normal diet, n=5 low calcium diet. Unpaired T-test was performed for each gene measured A) Kit Ligand, B) CXCL4, C) RANK Ligand, D) Osteoprotegerin, E) Osteopontin, F) Thrombospondin 1. Measurements in reference to housekeeping gene GAPDH.

Due to the high variability, a repeat of the PCR analysis of bone samples isolated from immunocompetent mice fed a low calcium or normal diet for 7 days was performed. Genes of interest involved in HSC quiescence and expansion, as well as altered bone turnover were analysed. Unpaired t-test was used for statistical inference. KitL expression (A) was 8.423 for the low calcium diet group (n=5) in comparison to 9.326 for the normal diet group (n=5) with a difference between means of 0.904 (± 0.258 SEM). The difference between groups was statistically significant with a p-value of 0.017. CXCL4 expression (B) was 5.271 for the low calcium diet group (n=5) and 4.604 for the normal diet group, with a difference between the means of (-0.666 ± 0.742 SEM) being statistically non-significant with a p-value of 0.408. For RANKL (C), the low calcium diet group (n=4) had an expression

level of 12.82, in contrast to 13.42 for the normal diet group (n=4) with a difference between the means of (0.599 ± 1.919 SEM) and a non-significant p-value of 0.768. Similarly, OPG (D) expression was non-significant with a p-value of 0.500 with a gene expression level of 9.256 for the low calcium diet group (n=5) and 9.709 for the normal diet group (n=5), the difference between the means being 0.4537 (± 0.656 SEM). OPN (E) expression of 8.657 for the low calcium diet group (n=3) and 6.569 for the normal diet group (n=5) with a difference between the means of -2.088 (± 1.449 SEM) but a non-significant p-value of 0.275. The low calcium diet group (n=5) expressed TBSP1 (F) at 7.912 in contrast to 9.037 by the normal diet group (n=5) with a difference between the means of 1.125 (± 0.500 SEM) and a non-significant p-value of 0.075. These results show that there was no significant change in gene expression for any of the selected genes in mice given a low calcium diet compared to those on a normal diet.

3.4.3.2 HISTOMORPHOMETRIC ANALYSIS OF BALB/C NUDE MICE FED A NORMAL DIET OR LOW CALCIUM DIET FOR 7 DAYS

Although µCT detects large-scale changes in bone structure, changes at a cellular molecular level preparatory to this are not detected. Furthermore, changes in gene expression may be transient and may mask changes at a cellular level. To investigate whether changes in osteoclast or osteoblast numbers and size occurred, I performed histomorphometry on TRAP-stained tibias obtained from the experiment.

Right tibias of BALB/c nude mice were extracted, fixed in PFA and decalcified, embedded in wax and cut before TRAP staining followed by histomorphometric analysis of osteoblast and osteoclast quantity and size (see Figure 3-13). A low calcium diet for 7 days did not have an effect on osteoclast density or size, or osteoblast size, but showed a trend to decrease osteoblast numbers.

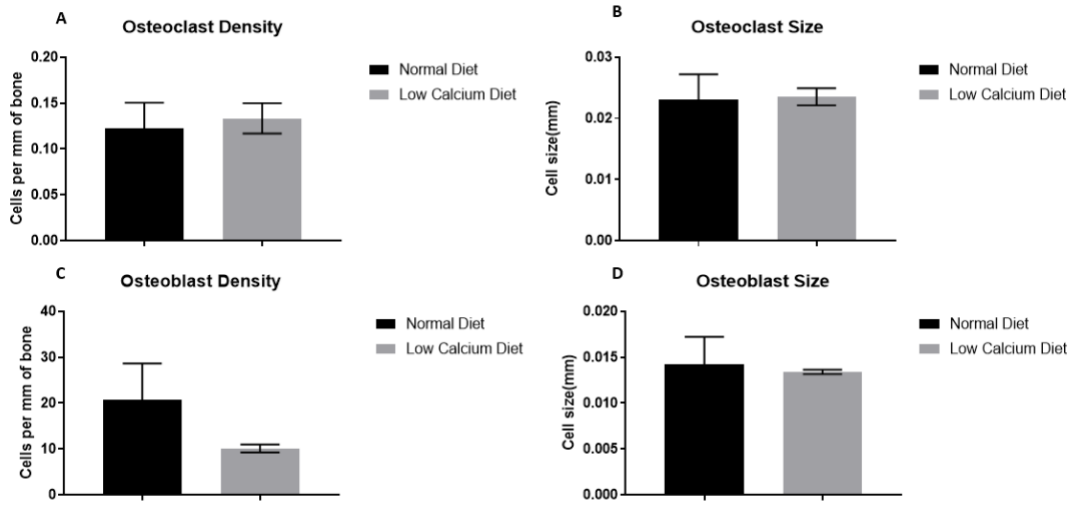

Figure 3-13: Histomorphometric analysis of right tibias from mice fed a normal diet (n=5) or a low calcium diet (n=5). Osteoclast (A) and osteoblast (C) density refers to the number of cells per mm of bone, osteoclast (B) and osteoblast (D) size refers to the cell width in contact with bone in mm. Each bone was scored at 3 different levels at least 20µm apart. Unpaired T-test was performed on each parameter. No significant differences were detected.

3.4.4 Assessing the effects of a low calcium diet over a period of 28 days

As the previous experiments demonstrated that a 7-day exposure to a low calcium (0.1%) diet was insufficient to trigger significant change in bone architecture, cellular composition and gene expression, further analysis of an optimal time to place mice on a low calcium diet was undertaken through a time course experiment. To gain a better understanding of the effects of a low calcium diet over a period of time, in the absence of cancer cells, 15-week old BALB/c (n=40) mice were placed on a low calcium diet for up to 28 days with matched controls fed a normal diet. Mice were culled at day 2, 3, 7, 14, and 28 (n=4 per time point, per group). No adverse effects were noted in mice receiving a low calcium diet as indicated by normal behavioural patterns and no weight loss. As cited previously, studies have shown a low calcium diet up to 140 days produced no detrimental effects on mice, even in the presence of ovariectomy (Minematsu *et al*., 2001). As expected, as my study used a higher calcium content and reduced time on the diet, no detrimental effects were noted.

Tissues were collected and analysed *ex vivo* to characterise the effects of the low calcium diet on the bone microenvironment by µCT (right tibias), and PCR gene expression (right femurs).

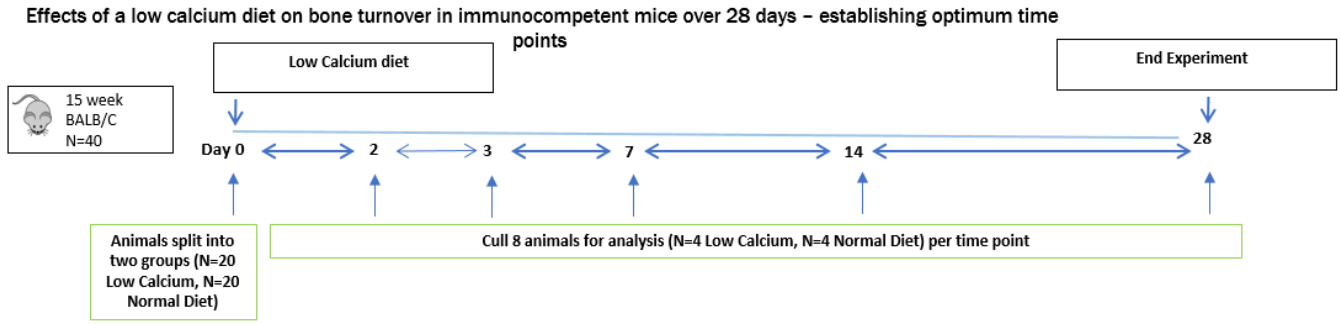

Figure 3-14: Experimental overview of the experimental plan to assess the effects of a low calcium diet for up to 28 days.

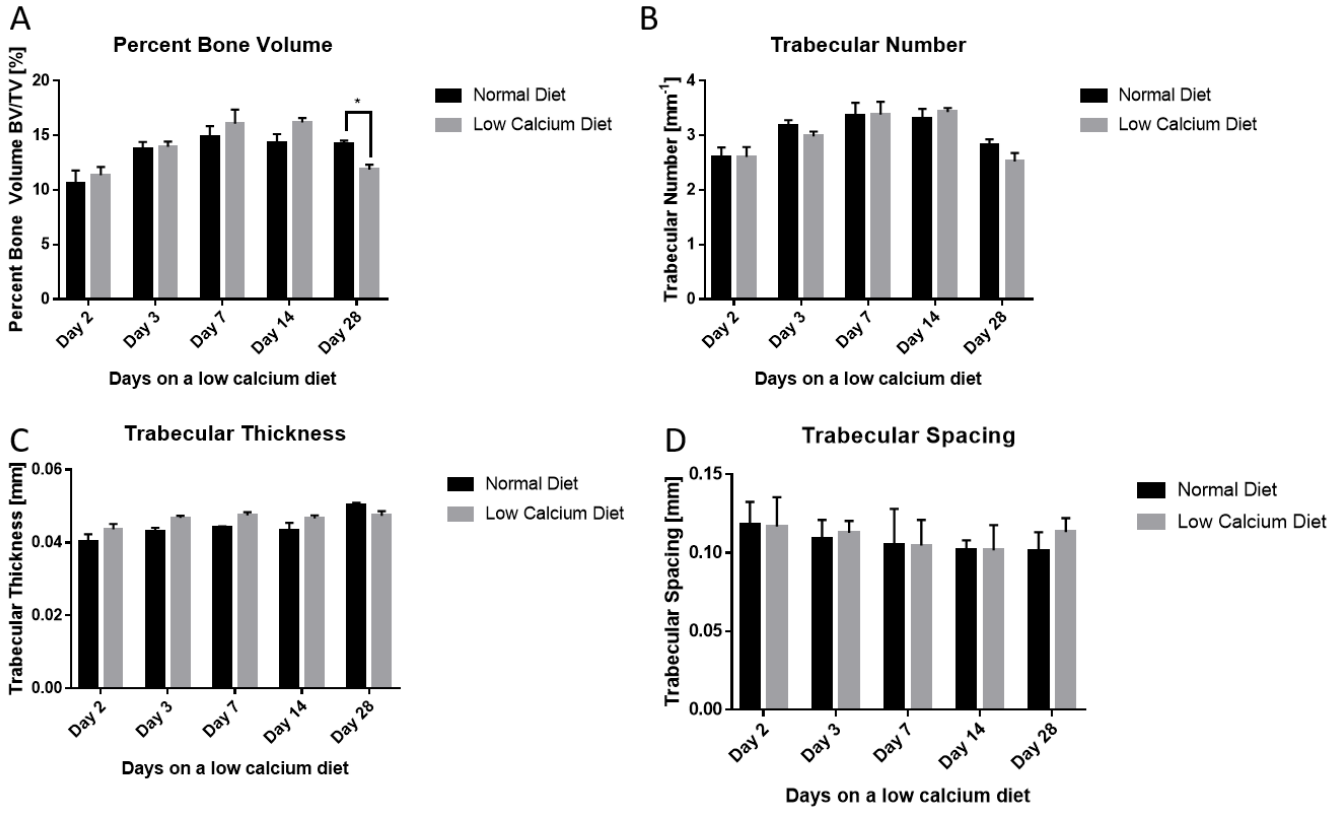

Figure 3-15: µCT analyses of each time point and statistical results of the (A) percent bone volume, (B) trabecular number, (C) trabecular number and (D) trabecular spacing of the right tibias of mice placed on a low calcium diet with matched controls for each time point (n=4 per time point per group).

Right tibias from all mice were subjected to µCT analysis, which showed no significant difference in trabecular number, thickness or spacing, between animals fed a low calcium diet and those on a normal diet (see Figure 3-15). The only statistically significant result was a decrease in percent bone volume on day 28 in the low calcium diet group ($p = 0.006$), suggesting that the low calcium diet would show differences after prolonged periods on the low calcium diet, and that any change at cellular or transcriptional level prior to day 28 could not be detected by µCT.

PCR analyses were subsequently followed up to assess the expression of genes involved in HSC quiescence (CXCL4) and expansion (Kit L), as well as regulators of osteoclast-driven bone resorption (RANKL and OPG) (see Figure 3-16) in samples from day 2 and 28 as these were the two most extreme periods on a low calcium in the time-course. A high inter-individual variation meant that there were no statistically significant results that could be compared across different days.

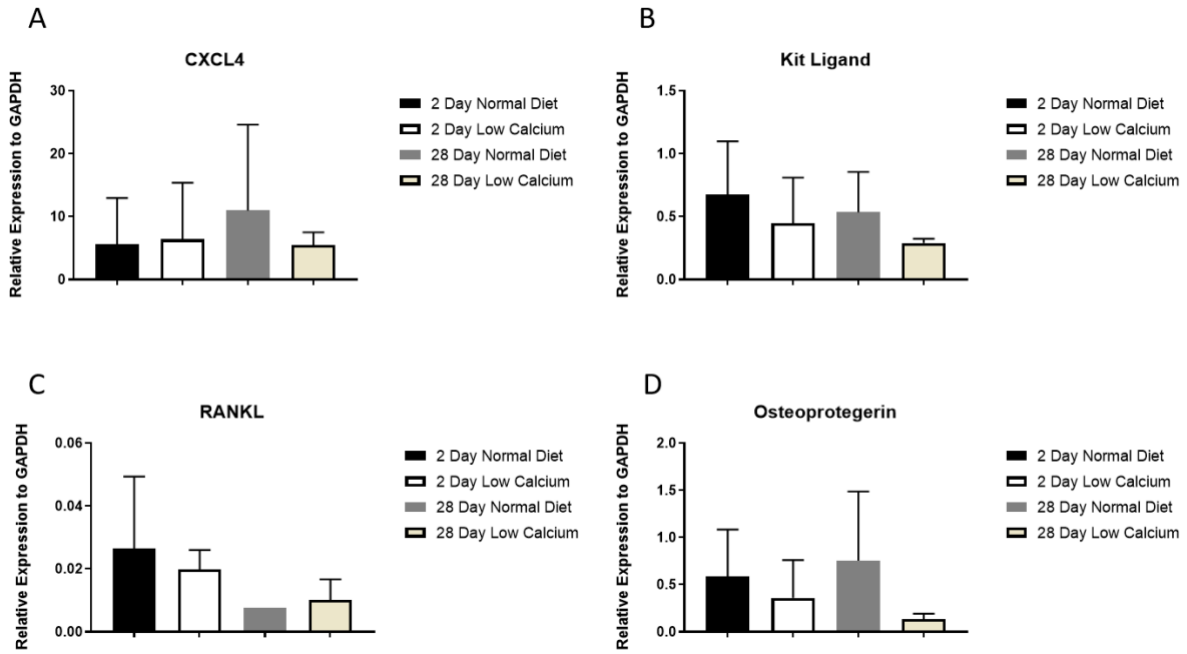

Figure 3-16: PCR analysis of bone marrow obtained from right femurs of mice placed on a low calcium diet for 2 days or 28 days (n=4 per expression set) for A) CXCL4, B) Kit Ligand, C) Rank Ligand and D) Osteoprotegerin. Unpaired T-test was performed for each time-point for each gene.

In order to assess whether there was a response to the low calcium diet at a molecular level that was not detectable at a cellular level or through physical bone parameters, serum was collected from mice at each timepoint was then analysed for bone turnover markers TRAP and PINP by ELISA (Figure 3-17). TRAP levels were marginally increased at day 2 and day 28 in mice fed a low calcium diet, but significantly increased at day 7 and 14. PINP showed a trend of decrease on days 7 and 14 of a low calcium diet, which was on a trend to normal by day 28, showing that the low calcium diet had an effect on osteoblast activity detectable on days 7 and 14. This confirmed the findings of a lower osteoblast number after 7 days of a low calcium diet in Figure 3-13.

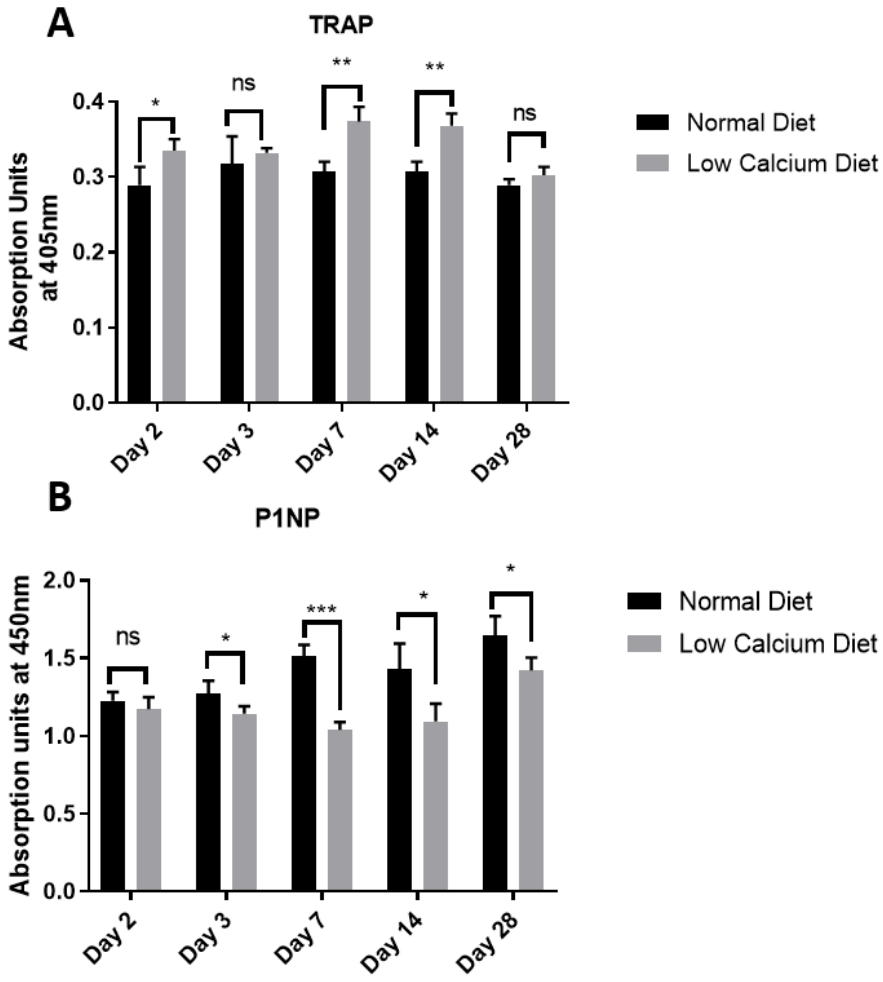

Figure 3-17: Optical density absorption units at 450nm of anti-TRAP (A) and anti-P1NP (B) ELISA of serum from of mice fed a low calcium diet or normal diet for up to 28 days (n=4 per time point indicated per group). Unpaired T-test was performed per marker per time-point.

Unpaired t-test was used for statistical inference. (A) optical density of TRAP ELISA; day 2 mean of normal diet 0.290 and mean of low calcium diet 0.3353 (p=0.018), day 3 mean of normal diet 0.317 and mean of low calcium diet 0.3325 (p=0.522); day 7 mean of normal diet 0.308 and mean of low calcium diet 0.374 (p=0.001), day 14 mean of normal diet 0.3076 and mean of low calcium diet 0.3687 (p= 0.001), day 28 mean of normal diet 0.289 and mean of low calcium diet 0.303 (p= 0.100). (B) optical density of P1NP ELISA; day 2 mean of normal diet 1.226 and mean of low calcium diet 1.172 (p=0.306), day 3 mean of normal diet 1.271 and mean of low calcium diet 1.142 (p=0.037); day 7 mean of normal diet 1.512 and mean of low calcium diet 1.039 (p=0.000043), day 14 mean of normal diet 1.427 and mean of low calcium diet 1.094 (p=0.0163), day 28 mean of normal diet 1.645 and mean of low calcium diet 1.422 (p=0.0244).

Changes in bone turnover are the result of the difference between osteoclast and osteoblast activity, as measured by TRAP and P1NP, respectively. I therefore plotted the percentage change in osteoclast and osteoblast activity on a single graph to better visualise the changes in both osteoclast and osteoblast activity at each timepoint. To summarize the effects of a low calcium diet on TRAP and PINP

over time, a percentage difference in the low calcium diet – generated by dividing the difference between the two groups over the normal diet and multiplying by 100 – was plotted to provide a visual reference as to changes over time in TRAP and PINP (see Figure 3-18). TRAP trended to increase to a peak by day 7 and 14, whereas PINP trended to decrease at a peak on the same days. The µCT data showing differences in percentage bone volume on day 28 show that there is a delay between increased expression of TRAP and reduction of PINP and detectable difference in the physical structure by µCT.

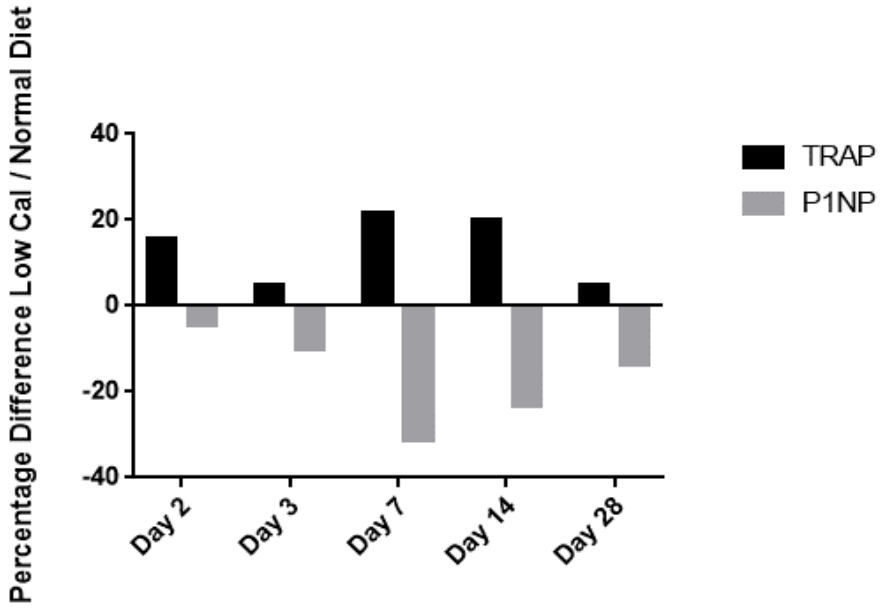

Figure 3-18: Representative percentage increase or decrease in optical density measurements of TRAP or PINP of animals fed a low calcium diet compared to a normal diet.

After assessing the bone mineral and cellular composition, as well as gene and protein expression after placing mice on a low calcium diet for various time points, 7 day and 14 day low-calcium diet were optimum in inducing effects at the cellular and protein levels. However, these effects may not have been detected by changes in bone mineral composition until day 28. By 28, there seemed to be an attenuation of the increased bone turnover that may have been the result of compensatory mechanisms. Therefore, for studies involving tumour cells, a 7 or 14 day low calcium diet has been established as the optimum time to induce the molecular triggers that may stimulate outgrowth.

3.4.5 CHARACTERISING THE EFFECT OF BONE TURNOVER FOLLOWING A LOW CALCIUM DIET ON THE OUTGROWTH OF BONE-DISSEMINATED TUMOUR CELLS

I next wanted to investigate the effect of altered bone turnover caused by the low calcium diet on the outgrowth of disseminated tumour cells. This required using a model whereby disseminated human breast cancer cells were present in the hind limbs of animals, described in the following section.

Following the characterisation of the bone microenvironment after a 7-day low calcium diet, non-significant changes in the physical bone parameters and genetic level led to the extension of the low calcium diet to 14 days in the subsequent experiments.

15-week old BALB/C nude mice were injected with $1x10^5$ GFP+ and Luc2+ transfected MDA-MB-231-IV cells labelled with Vybrant DiD lipophilic dye via intra-cardiac injection. Cells were labelled with Vybrant Did in order to facilitate tracking of cells for downstream analysis. Mice were subsequently monitored for 21 days post injection, with a lack of tumour outgrowth indicating that tumour cells remain dormant in bone. At day 21, mice with detectable tumour growth were removed from the experimental group, while non-skeletal tumour-bearing mice, predicted to have dormant, disseminated tumour cells based on previous studies (Ottewell *et al*., 2015) , were randomised 50/50 to receive either a low-calcium diet or a normal diet for 14 days. Mice were monitored for signs of overt tumour growth and comparisons between the low calcium diet and normal diet would be made relating to the rate of overt tumour growth in the two conditions (see Figure 3-19).

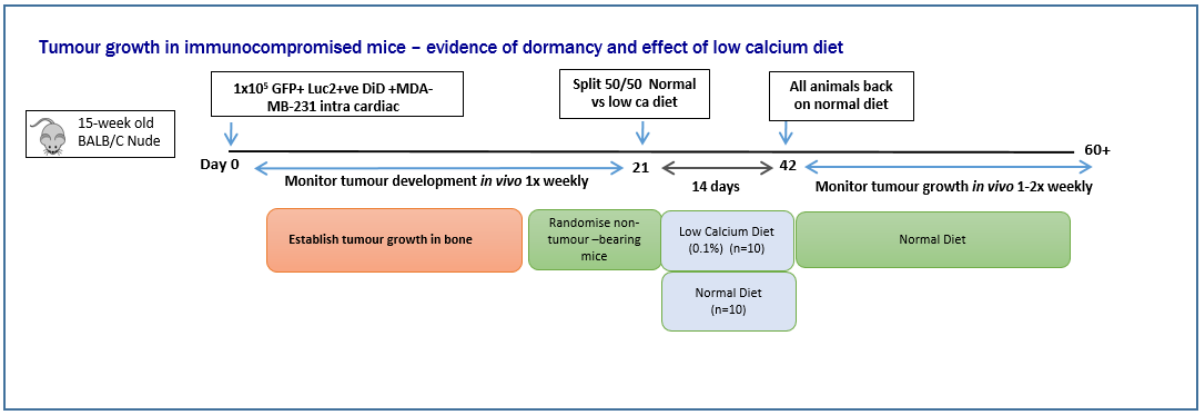

Figure 3-19: Experimental overview of *in vivo* experiment to assess the effect of a low calcium diet for 14 days on the outgrowth of disseminated tumour cells

In this experiment, three animals were culled shortly after intra-cardiac injection due to hind limb paralysis, seizures and lung tumours, leaving n=17 for the remainder of the experiment. Unexpectedly, *in vivo* IVIS imaging revealed 15 out of 17 animals developed skeletal tumours by day 21, thereby confounding subsequent results in attributing growth of tumour to alteration of diet. The experiment was therefore re-designed at this point and animals randomised to either the low calcium diet (n=9) or controlled with normal diet (n=8) for 14 days. Animals were culled and tissues harvested for *ex vivo* analysis to assess the potential effects of the low calcium diet on increasing tumour outgrowth, for

14 days. The model did not mimic dormancy as expected due to the early onset of tumours in the skeletal sites of the mice.

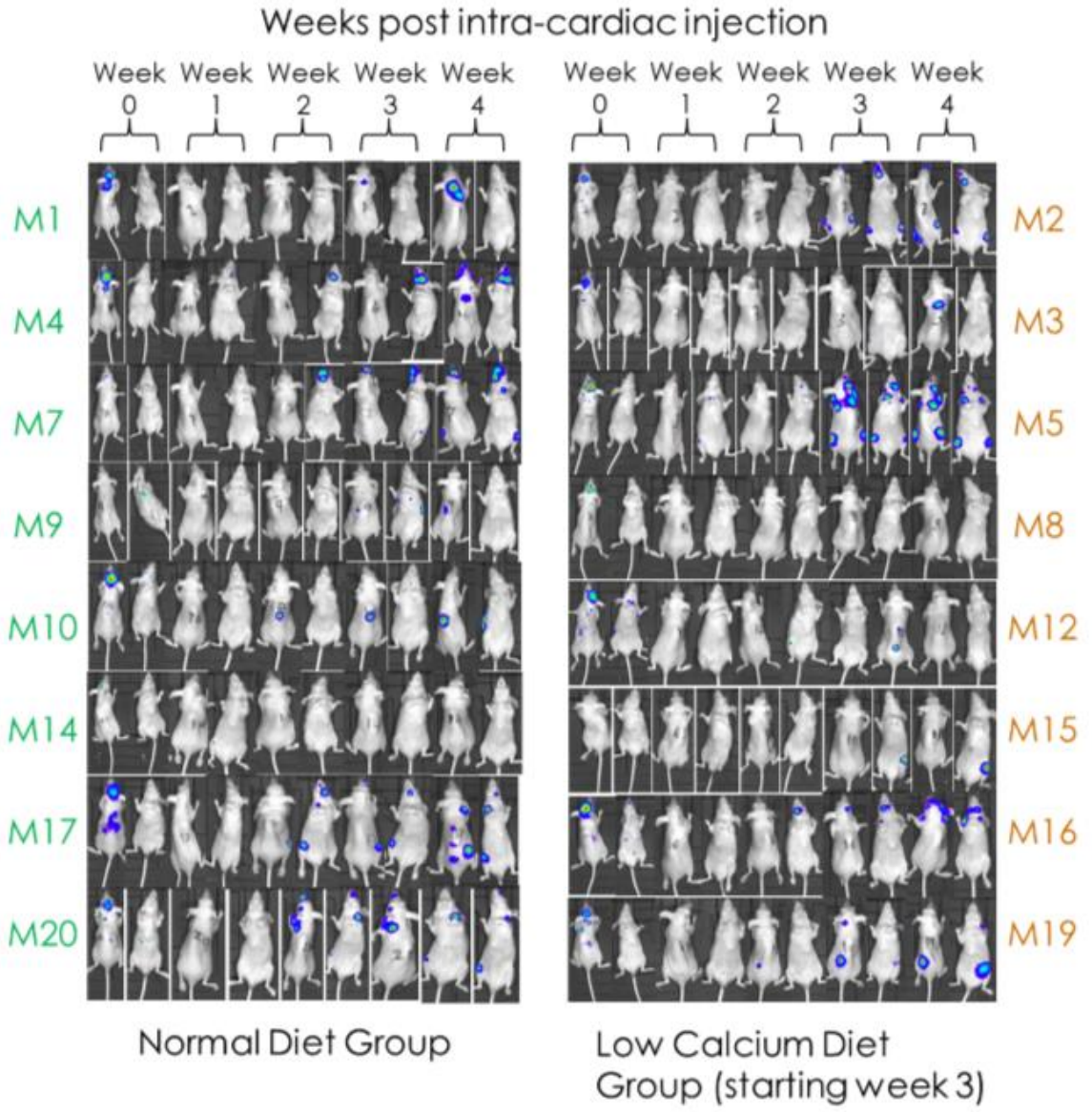

Figure 3-20: ***In vivo*** **(IVIS) images of mice injected with MDA-MB-231 -GFP+-Luc2+ cells and randomised after 3 weeks to be fed either a low calcium diet for 14 days or a left on a normal diet . Left, green text, normal diet. Right, orange text, low calcium diet. Each row represents a different mouse (M#). Each set of two photos (ventral and dorsal) from left to right represents a subsequent, 1-week incremental time point**

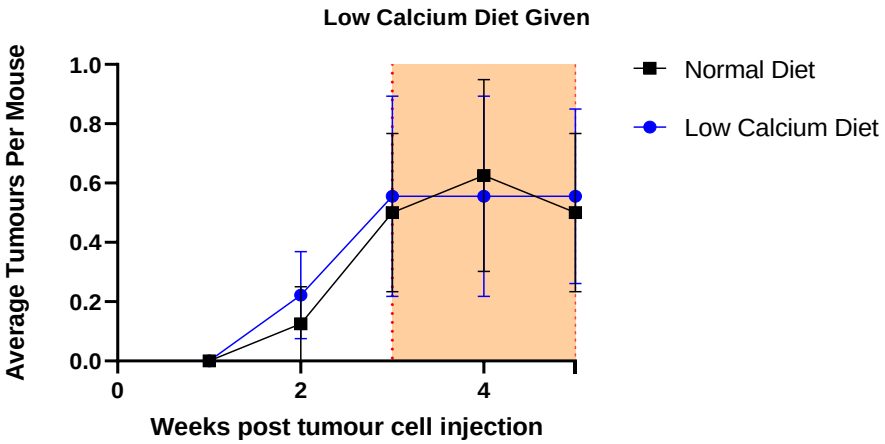

Figure 3-21: Average number of hind limb tumours in mice placed on a low calcium diet or normal diet on week 3 following intra-cardiac injection with MDA-MB-231 cells. Exposure to low calcium diet for animals randomised to receive it indicated by orange vertical column.

The tumours per mouse were calculated as the total number of skeletal size tumours in the group divided by the number of mice in the group that completed the experiment. Skeletal tumours were the prevalent site of metastasis and therefore no soft tissue metastases were observed during viable imaging. There was no observable significant difference in site or number of metastases.

3.4.5.1 µCT – Physical effects of a low calcium diet on the bone microenvironment

Following 14 days of low-calcium diet, mice were culled and right tibias obtained for use in µCT to ascertain the effect of the low-calcium diet for 14 days on trabecular bone. There was no significant difference between mice fed a low calcium diet and those on a normal diet on trabecular bone physical parameters as measured by µCT (see Figure 3-22).

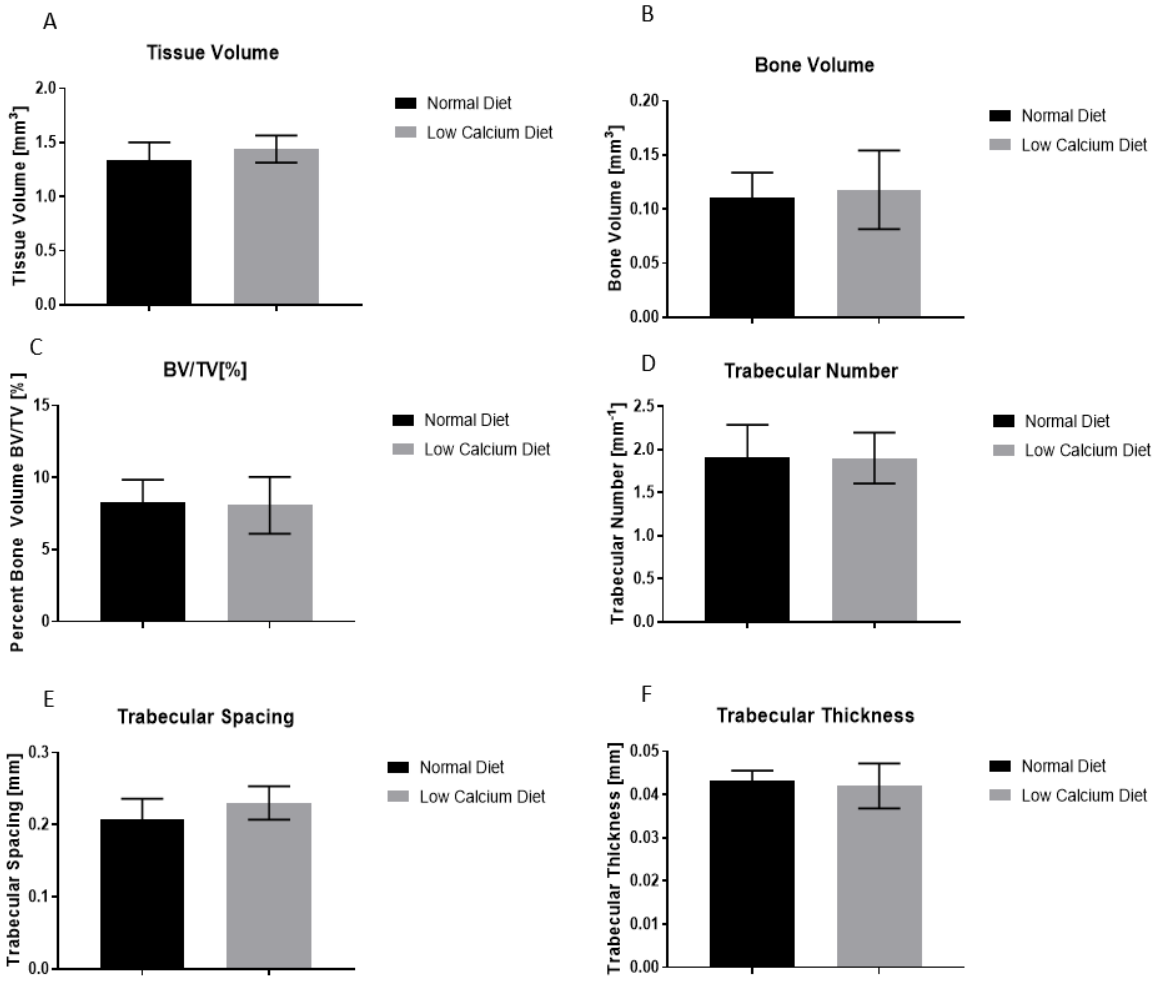

Figure 3-22: Right tibias were analysed by µCT on animals from the entire study with n=8 normal diet, n=9 low calcium diet. Unpaired T-test was performed for each parameter measured A.) Tissue Volume, B.) Bone Volume, C.) Percent Bone Volume, D.) Trabecular Thickness, E.) Trabecular Spacing , F.) Trabecular Number.

Measured mean tissue volume (TV) (measured in mm3) for the normal diet group (n=8) was 1.440 and 1.337 for the low-calcium diet group (n=9), a difference between the mean of 0.1033 (± 0.07514 SEM) with a non-significant p-value of 0.1968. Average measured bone volume (BV) (measured in mm3) was 0.1178 for the low calcium group (n=9) and 0.1108 for the normal diet group (n=8), a difference between the means of 0.006974 ± 0.01489 with a non-significant p-value of 0.0.6470. Percent bone volume measured as (BV/TV %) yielded an average of 8.064 for the low calcium diet group (n=9) and 8.297 for the normal diet group (n=8) with difference between the means of -0.2327 ± 0.8754 SEM and non-significant p-value of 0.7942. Average trabecular thickness (measured in mm) for the low calcium diet group (n=9) was 0.04199 whereas the normal diet group (n=8) measured 0.04334, a difference between the means of -0.001352 ± 0.001925 SEM with a non-significant p-value of 0.4966. Average trabecular number (measured in mm-1) was 1.903 for the low calcium diet group (n=9) and 1.919 for the normal diet group (n=8), a difference between the means of -0.01612 ± 0.1711 SEM, with a non-significant p-value of 0.9266. Mean trabecular spacing (measured in mm) was 0.2301 and

0.2073 for the low calcium diet (n=9) and normal diet (n=8) groups respectively, a difference between the means of 0.02286 ± 0.01331 with a non-significant p-value of 0.1127.

Taken together, these data reflect a largely non-significant trend in increased bone resorption in the low-calcium diet group compared to control, but no significant differences in tumour size or site of metastasis outgrowth were observed. Due to the early onset of tumour growth in in this experiment, the effect on escape from dormancy could not be ascertained, therefore requiring a repeat with the same experimental plan with exception of fewer cells inoculated into mice, 50,000 cells injected per mouse instead of 100,000, in order to have a slower rate of tumour growth.

3.4.6 Characterising the effect of bone turnover following a low calcium diet on the outgrowth of bone-disseminated tumour cells

Due to the unexpected early onset of tumour growth in mice injected with MDA-MBD-231 cells prior to being placed on a low calcium diet, a repeat experiment was carried reducing the number of breast cancer cells injected per mouse in order to extend the time to detectable tumour growth.

15-week old BALB/c nude mice were injected with $5x10^4$ GFP+ and Luc2+ transfected MDA-MB-231-IV cells labelled with Vybrant DiD lipophilic dye via intra-cardiac injection. Mice were subsequently monitored for 21 days post injection for tumour growth, with a lack of tumour indicating dormant cells. At day 21, mice with detectable tumours by bioluminescent imaging were removed from the experimental group, while non-skeletal tumour-bearing mice were planned randomised 50/50 to receive either a low-calcium diet or a normal diet for 14 days. Mice were monitored for signs of overt tumour growth and comparisons between the low calcium diet and normal diet would be made relating to the rate of overt tumour growth in the two conditions

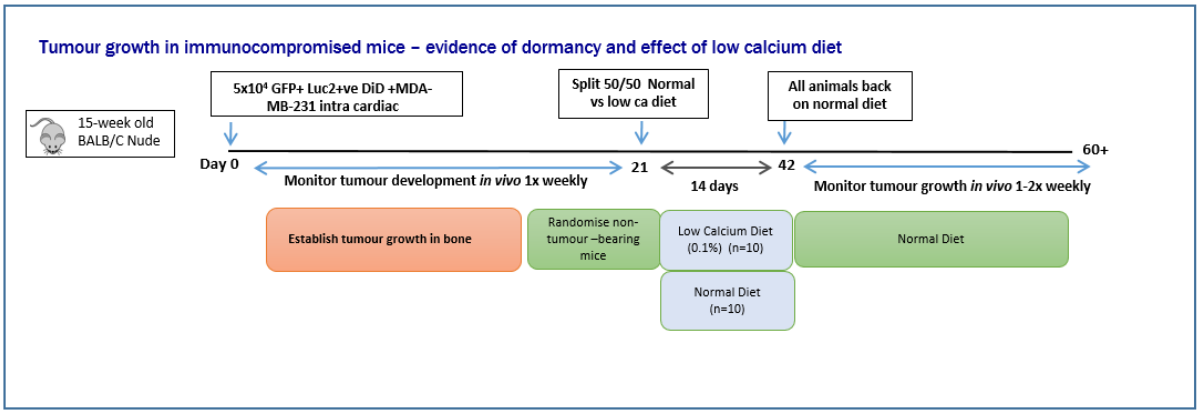

Figure 3-23: Experimental overview of the repeat experiment of the effect of a low calcium diet on the outgrowth of tumours from DTC-bearing mice

Similarly to the previous experiment, a large proportion of the animals (n=10/20) developed tumours in their hind limbs or other skeletal sites prior to randomising on day 21 to receive a low calcium diet. In order to examine whether placement on a low calcium diet for different periods of time would

result in variable rates of outgrowth, these animals, and one more from the group not bearing tumours, were randomised to receive a low calcium diet (n=2) or normal diet (n=2) for 2 days, a low calcium diet (n=4) or normal diet for 3 days (n=3). The tumour-free animals were randomised to receive either a normal diet (n=4) or low-calcium diet (n=5) for 14 days. This randomisation would be similar to results found in preliminary studies in our lab whereby placing mice on a low calcium diet for 3 days had an impact on overt tumour growth (data unpublished).

Following alteration of diet, 1 animal developed hind limb tumours on the normal diet and 1 animal from the low-calcium di*et al*so developed hind-limb tumours. See Figure 3-24 and Figure 3-25 for graphical summaries of the development of tumours over time in mice given a low calcium diet for 2, 3 or 14 days.

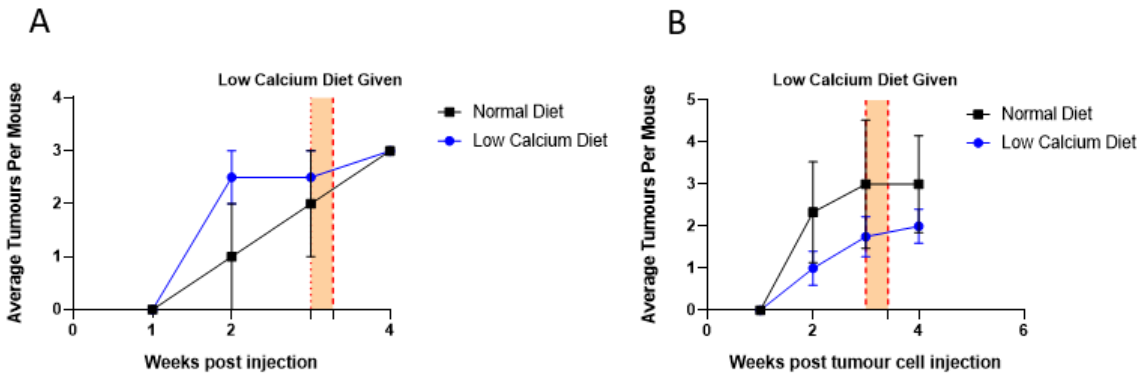

Figure 3-24: Mice randomised to receive either a low calcium diet or continue a normal diet 3 weeks post tumour cell injection for 2 days (A) – low calcium (n=2), normal diet (n=2) or 3 days (B) – low calcium (n=3), normal diet (n=2) as indicated by orange vertical bars.

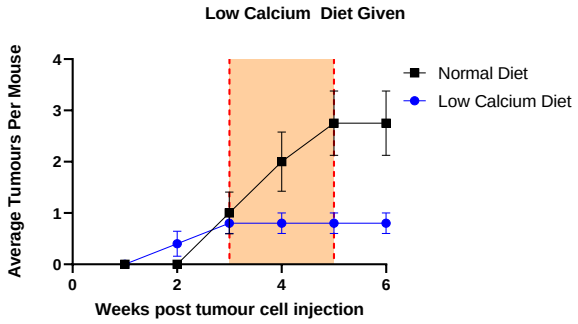

Figure 3-25: Mice fed a low calcium diet 3 weeks post injection for 14 days and randomised to receive either a low calcium diet (n=5) or a normal diet (n=4) for 14 days as indicated by orange vertical.

Placing mice on a low calcium diet for either 2, 3, or 14 days did not have a significant effect on the number of skeletal tumours in mice as compared with controls. However, the low calcium diet's effect

may have been attenuated by increased calcium mobilisation from osteolytic tumours already present in skeletal sites. It must be noted, however, a small proportion of animals (n=4) without any skeletal tumours did not proceed to develop any skeletal metastases following exposure to a low calcium diet for up to 14 days. In my experiments, the animals were culled shortly following the low calcium diet. In other studies, however, mice were monitored for a longer period of time following inducement of bone turnover through hormone deprivation or low calcium. Subsequent studies would therefore utilise a longer period of monitoring following the low calcium diet, albeit with tumour burden presenting a constraining factor.

3.4.7 Assessing the growth of MDA-MB-231-TD-tomato cells in 12-week old BALB/C nude mice

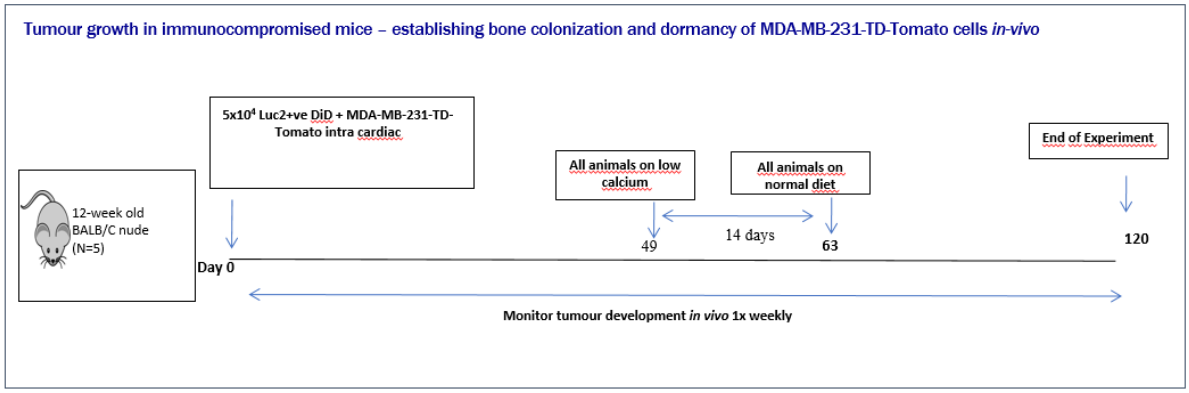

Figure 3-26: Experimental outline of an experiment investigating the effect of a low calcium diet on disseminated MDA-MB-231-TD-Tomato cells

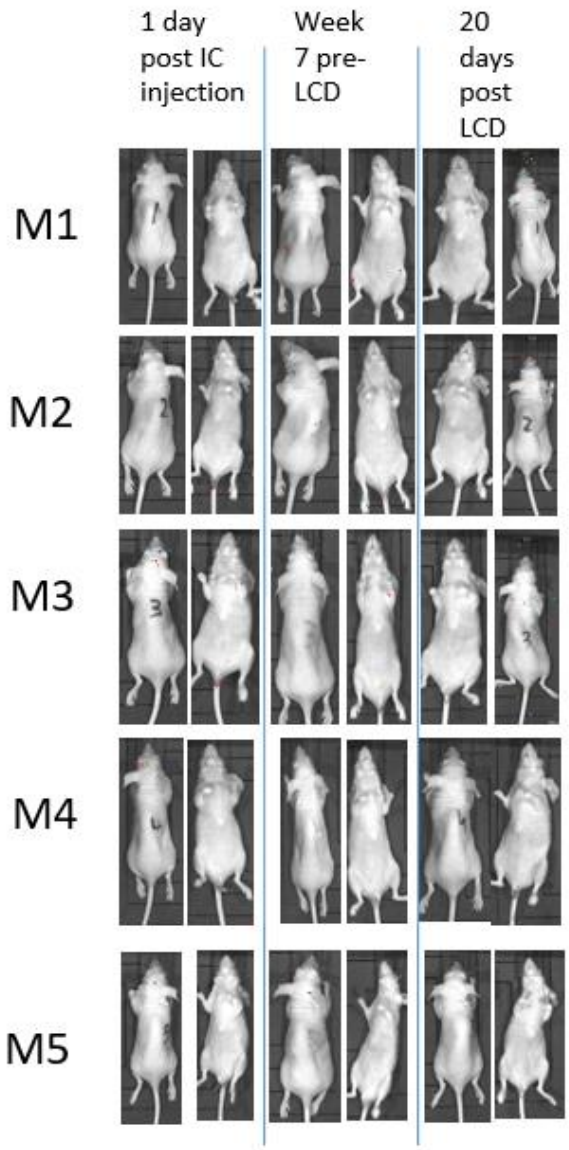

Following rapid outgrowth of injected MDA-MB-231 cells in prior experiments, it was decided to repeat the experiment using a different clone of the human breast cancer cell line; MDA-MB-231-TD-Tomato cells transfected with red fluorescent protein (RFP), with a slower cycling time. Twelve week old mice were injected intra-cardiac with 5x10^4 cells and were left to develop signs of tumour growth or dormancy and monitored via IVIS (see Figure 3-26). Following a period of 7 weeks without any signs of outgrowth, mice were subsequently placed on a low calcium diet for 28 days, following which period they were placed back on a normal diet for a further 20 days (see Figure 3-27). Post-dissection imaging further showed no signs of tumour in any skeletal sites. It was decided to not pursue this intervention further as it was not possible to recapitulate the dormancy model.

Figure 3-27: Mice were injected with MDA-MB-231-TD-Tomato cells and images represent: column 1 - 1 day following intra-cardiac injections; column 2 - 7 weeks following intra-cardiac injections; and column 3 - 20 days after cessation of the low calcium diet

3.5 DISCUSSION

Cancer cell dormancy represents a significant aspect of breast cancer, the understanding of which may contribute to therapies preventing or delaying metastatic relapse. Breast cancer is the most frequently diagnosed cancer, whose most common site of dissemination is the bone, where disseminated cells may reside dormant for many years or even decades before incurable secondary relapse (Gomis and Gawrzak 2016). Understanding how the bone microenvironment contributes to the mechanisms underlying this phenotypic change into dormancy and subsequent exit is the basis of my project.

In particular, the regulation of dormancy within the bone metastatic niche by microenvironmental signals, including HSC expansion in response to increased bone turnover, is of interest to my project, as this is the mechanism under investigation as to the induction and exit from dormancy for disseminated tumour cells. Increasing bone turnover through a low calcium diet, subsequently accelerating escape from dormancy would provide a potential for utilising dietary interventions to induce tumour outgrowth in models where other methods would be permanent or confound experimental plans.

3.5.1 Characterisation of the bone microenvironment following a low calcium diet for 7 days in immunocompetent and immunocompromised mice

I initially performed a number of studies to establish the effects of a low calcium diet on bone turnover in immunocompromised and immunocompetent mice. The results of these experiments would then be used as a foundation to explore the effect of increased bone turnover following a low calcium diet on the exit from dormancy and subsequent overt outgrowth of disseminated tumour cells residing in the bone. The basis of these studies was earlier unpublished studies carried out in the group, which had found that placing mice on a low calcium diet for 1 or 5 days increased the onset of the outgrowth on disseminated tumour cells, compared to a control group (see Figure 3-3, Figure 3-4). Furthermore, the pro-tumourigenic effect was significantly increased after 5 days of a low calcium diet, compared to 1 day, and was attenuated with the use of the bisphosphonate zoledronic acid, which acts by reducing bone resorption. This suggested that the effect of a low-calcium diet on outgrowth of disseminated tumour cells was attributed to the increase in bone resorption. After consultation with Professor Ingunn Holen and Dr Hannah Brown, who had conducted these studies, it was decided a period of 7 days on a low calcium diet would facilitate adequate bone resorption to trigger outgrowth of disseminated tumour cells.

Conducting these experiments on tumour-free mice would allow for the assessment of the changes of the microenvironment that would precede tumour outgrowth. The presence of overt tumours in the bone microenvironment may have confounded any relevant analysis, such as bone turnover and gene expression. Therefore, these experiments would allow for analysis of the effect that a low-calcium diet was having on the microenvironment, and allow for mechanistic identification. Furthermore, prior studies had been carried out on immunocompromised mice, yet the adaptive immune system plays a significant role in cancer, and taking this into account in an experiment would be more representative of a clinical setting. Therefore, also using an immunocompetent mouse model would allow for the assessment of the role of the immune system in the outgrowth of DTCs in the bone marrow, whether there would be a difference and what causative factors may be attributed to this difference.

After placing mice on a low calcium diet for 7 days, I found that there was no significant difference as a result of the low calcium diet on bone structure and composition and select gene expression as measured by µCT and PCR analyses.

When used on bone, µCT can be, and is often, used to infer the physical structural characteristics based on volume and density of minerals, specifically that of calcium (Nazarian *et al.* 2008). Increases or decreases in bone volume or density can be attributed to bone anabolic or catabolic activity respectively, attributed to the activity of osteoblasts in the formation of bone, and osteoclasts in the degradation. The trabecular region of bone is the primary site of osteoclast localisation and activity, and so measurements of this area would be more sensitive in detecting changes in bone resorption (Nordin *et al.* 1984). Data from µCT analysis of the trabecular region measuring percent bone volume, trabecular number, trabecular thickness or trabecular spacing did not show any

significant difference between the two groups tested. This suggests minimally altered mineral composition of bone samples between animals placed on a low calcium diet for 7 days and those on a normal diet, as any significant increase in bone resorption that may have occurred could not be detected nor confirmed by µCT analysis.

Studies by Alloca *et al.* showed that DTCs in the bone marrow localise to niches occupied by HSCs. This localisation was also shown to increase when the CXCR4-antagonist AMD3100 (Plerixafor) was used to dislodge HSCs from the bone marrow into circulation (Allocca *et al.* 2019). As the HSC niche is under investigation as to the induction and subsequent escape from dormancy, molecules associated with HSC quiescence (CXCL4, (Bruns *et al*., 2014)) and HSC expansion (Kit L, (Katayama *et al*., 1993, Wilson *et al*., 2007)) were selected as candidate genes to investigate microenvironmental control of HSCs. Inference may be made as to the microenvironmental mechanisms of control of HSC quiescence and expansion similarly regulating DTCs in a similar manner, should a correlation be found. Further to this, the rate of increased bone resorption under investigation led to genes involved in increased osteoclast differentiation and activity (RANKL, (Teitelbaum and Ross, 2003)) as well as increased bone resorption (Osteopontin,), or decreased RANKL signalling (Osteoprotegerin (Teitelbaum and Ross, 2003)) being selected as indicators of increased bone resorption (Kostenuik 2005; Luukkonen *et al.* 2019). Increased bone resorption would lead to release of growth factors and calcium, triggering the exit of DTCs from dormancy and provide a plausible explanation should gene expression correlate with increased bone resorption and subsequent DTC escape from dormancy. As restriction of overt outgrowth can be attributed in part to nutrient deprivation from inhibited angiogenesis and blood supply, the anti-angiogenic molecule Thrombospondin 1, significantly expressed in the bone by megakaryocytes, was also selected as a candidate gene (McLaren 1983; Ghajar *et al.* 2013).

To evaluate whether any significant differences in genes regulating hematopoietic stem cell quiescence or bone resorption between mice placed on a low calcium diet and those on a normal diet, despite no changes observed in the bone mineral composition, PCR was used to quantify selected transcripts and the effect of a low calcium diet on their regulation. In order to assess the effect of a low calcium diet on the expression of Kit L, CXCL4, RANKL, Osteoprotegerin, Osteopontin and Thrombospondin 1, PCR experiments were run using samples from flushed bone marrow, with primers specific for these genes. The PCR data did not show significant differences in expression of Kit L, CXCL4, RANKL, Osteopontin, Osteoprotegerin or Thrombospondin 1 beteween the treatment and control groups. The technical replicates of each sample were of satisfactory precision, but the difference between biological replicates seemed to be the cause of variance in plotted data, and therefore non-significant statistical results.

The biological variation may be due to individual differences in mechanisms such as decreased renal excretion of calcium, effected by PTH, leading to differences in gene expression between mice on low calcium diet and control diet (Caniggia *et al.* 1976). The small group sizes (n=5 per group) was a potential limitation, but due to unexpected variability between tumour-free mice, a large number of mice was not used. Furthermore, increased bone resorption, and associated genes, in particular, RANKL, may be expected to be seen in immunocompetent mice due to the presence of Th17 cells

which further express RANKL in the presence of continuous PTH secretion (Pacifici 2016). In this case, through personal communication with Dr. Penelope Ottewell, it was suggested that the C57BL/6 strain has been noted to be resistant to bone resorption following ovariectomy, and this may be why there was no statistically significant difference in gene expression. However, this does not account for the similar insignificant response to bone resorption seen in the BALB/C nude strain.

3.5.2 Establishment of the bone microenvironment following a low calcium diet over a period of 28 days in immunocompetent mice

After finding minimal effects in mice given a low calcium diet for 7 days, a time course was set up to assess the effects of a low calcium diet over a period of time up to 28 days to obtain an optimal time point on which to place animals with disseminated tumour cells. Samples were analysed by µCT (bone architecture), rtPCR (gene expression) and ELISA (bone turnover markers P1NP and TRAP). The findings showed no significant difference in gene expression, owing to inter-individual variations within the groups. Furthermore, bone architecture did not change over 14 days, but there was a small statistically significant decrease in bone volume in the low calcium diet group by day 28. Serum assessment of bone turnover markers showed that there was indeed a difference in bone turnover, having a decrease in P1NP, a marker for bone formation, and an increase in TRAP, a marker for bone resorption, in mice fed a low calcium diet across all time points.

Histomorphometric analyses of bones from animals fed a low calcium diet for 7 days showed that there was no difference in osteoclasts number, but a decrease in osteoblast numbers. The effect of PTH, altered by a low calcium-diet, on osteoblast population has been demonstrated in a study by Brown *et. al* (2018), who found that 5-days of treatment with PTH on 12-week old BALB/c nude mice had no effect on trabecular bone volume, width or number as measured by µCT, as compared with untreated controls when measured between 5 and 15 days post-treatment. However, PTH-treated animals had increased osteoblast numbers and increased PINP on days 5 and 7 (Brown *et al*., 2018). In contrast to these findings, I found that following a 7-day low calcium diet, there was a significant decrease in PINP and an increase in TRAP as measured by ELISA, as well as a decrease in osteoblast numbers. Significantly, Brown *et. Al* administered a single daily dose of PTH, reflecting an intermittent release of PTH in contrast to the chronic, continuous release of PTH that should arise as a result of a constant state of hypocalcaemia, and thus have a differential, catabolic effect, as was shown after 7 days of a low calcium diet (Lotinun *et al*., 2002).

This increase in osteoblast numbers may be less of a direct effect of PTH on osteoblasts, but may be attributed to indirect effects of osteoclasts in the promotion of osteoblast differentiation and expansion (Mansour *et al*., 2012). Osteoclasts have been implicated in the formation of HSC niches due to the activation of osteoblasts following osteoclast activity. As observed in subjecting mice to a low calcium diet, after 7 and 14 days there was an increase in osteoclast activity as measured by ELISA, but without a correlated increase in osteoclast size or numbers as measured by histomorphometry. This correlated with a decrease in osteoblast numbers as would be expected.

Similar findings of attenuation of low calcium effects after a given period of time have been found by other researchers. In a mouse model of multiple myeloma, Libouban and Chappard injected two groups of C57BL/KaLwRij mice with 5T2MM cells accompanied by either a normal diet (0.8% calcium) or a low calcium diet (0.05%) and were monitored at 6, 8 and 10 weeks (Libouban and Chappard 2017). Osteoclast numbers from the endosteal region of tibiae showed an increase at 6 weeks in the low calcium diet, but this effect was attenuated by week 8 and 10, suggesting a time-sensitive fluctuation in response to a low calcium diet. This suggests that bone turnover in response to a low calcium diet does indeed have feedback mechanisms to regulate calcium homeostasis and balance in bone turnover.

The results of my experiment elucidating the effects of a low calcium diet over 28 days suggested between 7 and 14 days was optimal to elicit the most cellular and molecular changes in comparison to 2, 3 or 28 days.

3.5.3 Effects of a low calcium diet on the bone microenvironment and influence on dormancy escape

To investigate the effect of a low calcium diet on subsequent disseminated tumour cell escape from dormancy, studies were carried out which aimed to seed mammary carcinoma cells in a dormant state within the bone, before placing a portion of the animals on a low calcium diet to observe the effect of the escape from dormancy. Previously published studies have demonstrated that a low calcium diet increases disseminated breast cancer tumour cell growth in bone (Zheng *et al.* 2008; Wang *et al.* 2017). Furthermore, in a study by Zheng *et al*, the increased tumour growth from a low calcium diet was attenuated by administration of Osteoprotegerin, suggesting a mechanism involving increased osteoclast activity was responsible for low-calcium mediated increased tumour growth (Zheng *et al.* 2008). However, these studies used a low calcium (0.1%) diet prior to, or relatively shortly following tumour cell seeding and the effect of tumour outgrowth, not as a potential trigger of escape from dormancy. The studies I carried out aimed to mimic the escape from dormancy, whereby animals would not develop skeletal tumours after a prolonged period of time, before being placed on a low calcium diet.

Cancer cell dormancy is characterised by a period of restrained outgrowth through decreased cell cycling, restrained outgrowth due to nutrient deprivation or immune editing (Gao *et al.* 2017). Previously published studies from our lab have showed that a proportion of mature BALB/c nude mice aged 12-weeks old injected with 75,000 MDA-MB-231 cells had detectable dormant tumour cells in bone (Allocca *et al.* 2019). However, this was not reflected in my experiments where BALB/c nude mice injected with 100,000 or 50,000 cells per mouse, were expected to show a very limited number of detectable metastases at 21 days and therefore considered to harbour dormant cells. A significant proportion of mice developed hind-limb or skeletal tumours within 14 days of tumour cell injection, which contribute to accelerated cancer-induced bone resorption, thereby possibly increasing serum calcium and confounding any effects a low-calcium diet may have on modulating bone resorption.

It is therefore expected that serum bone resorption markers would have been elevated both in mice on low-calcium and normal diets due to the development of cancer-induced bone disease. This was reflected in the second experiment in section 3.4.6 whereby a change of diet did not result in a difference in tumour growth in the hind limbs. This could be due to the presence of excess calcium in serum from distant skeletal sites negatively regulating the release of PTH; and thereby inhibiting its bone catabolic action on osteoclasts. Levels of PTH and bone resorption markers would ordinarily be measured in serum samples, but presence of osteolytic lesions prior to adjustment of diet would confound the results.

I proceeded to use a slower-growing MDA-MB-231-Td-Tomato clone, which did appear to recapitulate the dormancy model, without tumour outgrowth for up to 7-weeks post-injection ($5x10^4$-$7.5x10^4$ cells per mouse in 6-week and 12-week old mice). However, when consequently given a low calcium diet for 28 days, before being placed back on a normal diet and monitored for tumour outgrowth, no tumours were detected in skeletal sites even up to a period of 3 months post-injection. Thus there was no effect of exposure to low calcium diet in mice expected to have disseminated tumour cells in their long bones. Lack of access to previously available multiphoton microscopy meant verification of the presence of disseminated tumour cells could not be demonstrated in the same manner as in the previously published studies (Allocca *et al*., 2019b) hence it cannot be ruled out that tumour cells failed to reach and/or were eliminated from skeletal sites in my studies.

These findings did not recapitulate the results achieved by hormone deprivation in castration/ovariectomy induced bone loss studies (Ottewell *et al*., 2015). Decreased expression of OPG expression by osteoblasts due to hormone deprivation induces a rapid, sustained loss of bone (Bord *et al*., 2003). In contrast PTH released in response to hypocalcemia, induces bone resorption, to increase serum calcium, but also increases the efficiency of calcium absorption in the gastrointestinal tract and re-uptake in the kidneys, leading to stabilised serum calcium levels. This then attenuates PTH in a negative feedback loop, which then also reduces bone turnover (Fleet, 2017, Mundy and Guise, 1999). As was seen across different time points in my studies, TRAP and P1NP levels fluctuated and were attenuated at different time points, possibly to this mechanism, and hence, may be why a dramatic loss of bone is not detected as a result of a low calcium diet in contrast to hormone deprivation.

3.6 Conclusions, limitations and future work

Preliminary work in our lab has shown the use of a low calcium diet may influence exit from dormancy in immunocompromised BALB/C nude mice. Recapitulation of these results has been unsuccessful in initial experiments and lead to revision of the experimental plans. The low calcium chow used to place the mice on a low calcium diet was the same batch from the same supplier, the mice used of the same strain and age and so no obvious explanation has been found to explain the discrepancy. A low calcium (0.1%) diet has shown changes in cellular number of osteoblasts and increase of activity in osteoclasts, with minor yet statistically significant effects on percentage bone volume after 28 days of a low calcium diet. However, in pilot studies, this has not translated to any difference in tumour growth in

both 6 week-old 12 week-old mice. Concerns about mice obtaining calcium from the drinking water still exist, although an increase in TRAP and decrease in PINP by day 7 and 14 on a low calcium diet show that it is not significant enough to completely attenuate the effect of the low calcium diet. Levels of RANKL and OPG, key molecules involved in the regulation of bone turnover, has not been shown to be significantly different between mice placed on a low calcium diet and those on a normal diet. However, similar to bone turnover having fluctuations, it may also be the case that the molecules involved in their regulation have similar fluctuations within shorter spaces of time. Statistically significant results could not be obtained due to high inter-individual variations in the expression of these genes within each treatment group. This may be attributed to fluctuations in the up- or downregulation of these genes across individuals at different times.

Despite fluctuations in bone turnover, the low calcium diet (28 days) has not shown any effects on DTC outgrowth as shown in *in vivo* experiments utilising MDA-MB-231-TD-Tomato which display a dormant phenotype . An explanation of the lack of response may be due to the slower cycling of these cells, as is seen in the experiments where outgrowth was delayed for at least 5 weeks post-injection, compared to MDA-MB-231-IV cell lines which displayed rapid outgrowth on average 2 weeks following intra-cardiac injection. A low calcium diet's effect on bone turnover may be insufficient to trigger rapid expansion of tumour cells, as µCT scans showed no significant difference in bone architecture up to day 28, which then had a statistically significant difference, yet of low magnitude. An approach that confers increased bone turnover in a more aggressive manner, such as an ovariectomy, may be a more appropriate approach to guarantee increased bone turnover, and therefore stimulation of overt growth from dormant, disseminated tumour cells, which has previously been shown to be the case by Ottewell *et. al (Ottewell et al., 2015).*

Studies using a low calcium diet in models using tumour cells, and those without, have not shown dramatic differences in initial outgrowth of tumour cells or bone architecture, but rather show differences in proliferation over a longer period of time on the diet (Zheng *et al*., 2007). Along with my findings, this suggests that a low calcium diet may not invoke as rapid a change in bone turnover as seen in hormone deprivation, and so may not be sufficient, in isolation, to trigger the outgrowth of disseminated tumour cells.

3.6.1 LIMITATIONS OF THE STUDY AND FURTHER WORK

A limitation to attributing escape from dormancy following a low calcium diet, is that PTH type 1 receptor (PTH1R) activation may directly affect tumour dormancy. The PTH-related protein (PTHrP), which binds to PTH1R has been reported to negatively regulate pro-dormancy genes (Johnson *et al.* 2018). The similarity between PTH and PTHrP would need to be examined as to exclude the downregulation of pro-dormancy genes causes an escape from dormancy, rather than the micro-environmental effects following increased bone resorption. Utilising ovariectomy-induced bone resorption leading to dormancy escape may give an indicator that this effect is, indeed, independent of PTH1R activation on the cancer cells and has been shown by our group in published studies (Ottewell *et al.* 2015; Brown *et al.* 2018).

A further limitation to this study is that bone loss was only measured in the hind limbs by µCT, which may have missed detection of skeletal-wide changes yet at a lower detectable levels in the hind limbs alone. PTH's actions are not limited to the hind limbs, but induce bone resorption in areas with particularly higher trabecular bone, such as the spinal vertebrae. A whole-mouse scan may have revealed differences not detected by µCT. This is further suggested by the significant increase in serum TRAP levels, yet corresponding cellular and bone-mineral changes were not detected when analysing the hind limbs in isolation. This increase in serum turnover markers may be reflecting slight increases in bone turnover across numerous sites in the skeleton rather than significant, dramatic changes in the hind limbs alone.

Direct effects of extracellular calcium on cancer cells is a key consideration on the effect of a low-calcium diet on disseminated tumour cells. The Calcium Sensing Receptor (CaSR) is implicated in promoting proliferation and inhibiting apoptosis in conditions of high extracellular calcium concentrations . This is mediated by reduction of $p27^{kip1}$ levels, induced by the actions of PTHrP, leading to the reduction of nuclear concentration of Apoptosis Inducing Factor (AIF). Furthermore, endogenously expressed CaSR on metastatic breast cancer cells has been found to regulate tumour cell secretion of IL-6, a pro-tumour inflammatory cytokine. Pharmacological inhibition of CaSR engages a Rab11a-dependent attenuation of IL-6 secretion via PI3K/AKT and PKC signalling pathways. On the contrary, using an inverse antagonist promoting constitutive activity of CaSR resulted in an increased secretion of IL-6 through Gαs/PKC, MEK1/2 and mTORC1 signaling pathways (Hernandez-Bedolla *et al.* 2016). CaSR activation would therefore promote tumourigenesis in disseminated tumour cells following an increase in extracellular ionic calcium. As local calcium concentrations of in the bone microenvironment are enriched following bone turnover, it would be expected to further promote overt outgrowth instead of diminishing proliferation. As no increased outgrowth in skeletal sites was present in mice with disseminated tumour cells displaying latent dormant phenotypes, it can be deduced that either the proximity of the tumour cells to areas of increased bone turnover was not sufficient to elicit a response to increased presence of soluble growth factors and calcium released from the organic and mineralised bone matrix, or the cells did not colonise the bone as expected.

Other molecules of interest:

In addition to increased bone resorption and direct effects on cancer cells, PTH may affect tumorigenesis through regulation of immunomodulatory chemicals. Of particular interest is Monocyte Chemoattractant Protein 1 (MCP-1) (CCL2) which is a protein involved in the chemotaxis of monocytes to areas of secretion. In the bone, it is primarily secreted by osteoblasts, and is an important factor in the localization and infiltration of monocyte progenitors which may subsequently differentiate into osteoclasts (Yadav *et al.* 2010). MCP-1 secretion is upregulated in the presence of PTH and is markedly correlated with osteoporotic bone in prostate cancer-induced bone resorption. The effects of MCP-1 are functionally dynamic, being reported to have dual effects. As with bone anabolic or catabolic effects of PTH being dependent on intermittent (anabolic) or continuous (catabolic) PTH secretion, MCP-1's effects is also dependent in a similar manner on the type of PTH

secretion (Siddiqui and Partridge 2017). A state of hypocalcaemia leading to continuous PTH may lead to increased MCP-1 secretion, further affecting the immune-milieu of the bone microenvironment. The immune population is therefore worthy of consideration in assessing the effects of PTH on DTC outgrowth in a setting of hypocalcaemia.

4 CHARACTERISING THE EFFECTS OF ZOLEDRONIC ACID ON TUMOUR GROWTH AND CELLS OF THE BONE MICROENVIRONMENT IN YOUNG MICE

4.1 SUMMARY

Data from model systems have led to bone turnover increasingly being implicated in the establishment of secondary tumour metastases from dormant, disseminated tumour cells in this organ. As a result, the potential of bone-targeted agents (BTAs) reducing skeletal metastasis has been investigated in laboratory studies as well as in clinical trials.

A commonly used BTA is Zoledronic acid (Zol), a nitrogen-containing bisphosphonate which is a pseudo-specific drug against osteoclasts due to its distribution in the body and high affinity for bone surface hydroxyapatite crystals. Due to its potent anti-resorptive actions Zol inhibits progression of osteolytic bone lesions, figuring prominently in the treatment of cancer-induced bone disease. Its role in preventing or slowing development of secondary bone metastases is under investigation and has so far yielded inconclusive results. Previous studies using murine models of breast cancer bone metastasis have shown that models with higher bone turnover (following ovariectomy, a low calcium diet or using young - 6-week old - mice) have a higher frequency of tumour growth compared to mature mice with low bone turnover. Interventions to reduce bone turnover, such as use of anti-resorptive agents, inhibit the metastatic outgrowth of tumour cells in bone shown in mature (12-20 week-old) mice, demonstrating a link between the levels of bone turnover, in particular osteoclast activity, and tumour growth in bone. However, the precise interplay between the bone microenvironment in a state of high bone turnover and colonised tumour cells, and how this is modified by of anti-resorptive agents in altering the rate of tumour outgrowth, requires further elucidation.

I therefore set out to characterise the effect of repeated Zol treatment on the bone microenvironment in young mice (6-week old, high bone turnover) and subsequent outgrowth of two different clones of triple negative breast cancer cells. The effect of Zol on circulating hematopoietic cells was also assessed to assess the extent of Zol activity on bone and bone-derived populations.

uCT analysis showed that 4 weeks of weekly Zol administration induced a significant increase in trabecular bone volume and number and significant decrease in trabecular spacing, but importantly, not affecting trabecular thickness, indicating a reduction in osteoclast-mediated bone resorption rather than increased bone growth. Interestingly, this was not followed by a significant reduction in osteoclasts by Zol, but a trend to increase osteoclast numbers. Nevertheless, this increase in osteoclasts still resulted in increased trabecular bone content, suggesting inactive osteoclasts or a high rate of apoptosis to match osteoclast formation.

Despite having a major impact on the bone structure, Zol treatment did not reduce the rate of growth or number of skeletal tumours compared to control treatments, supporting clinical observations and pre-clinical *in vivo* studies that show that Zol has bone protective effects but does not significantly

impact tumour growth. This result was consistent across two different MDA-MB-231 human breast cancer cell clones used.

Circulating hematopoietic cell populations were largely unaltered by Zol treatment, but showed a trend to increase eosinophil and granulocyte numbers in both tumour-free and tumour-bearing animals. In addition, the presence of skeletal tumours similarly did not alter the circulating hematopoietic population, suggesting that the skeletal sites that remained tumour free were sufficient to maintain the circulating population(s).

Although Zol had a significant effect on trabecular bone, it did not affect tumour growth nor hematopoietic cells in circulation.

4.2 INTRODUCTION

4.2.1 BONE TURNOVER AND TUMOUR GROWTH

Breast cancer bone metastasis is characterised by osteolytic lesions within the bone caused by the activity of osteoclasts. As described in chapter 3 section 3.2.1, increased bone turnover leads to the release of minerals and growth factors stored within the bone matrix that support the growth of tumour cells within the bone microenvironment. In addition, accompanying skeletal-related events (SREs) still pose significant morbidity in patients with osteolytic bone metastases (Coleman, 1997a).

Murine model systems have been widely used to study bone metastases, including immunocompetent and immunocompromised models where tumour cells implanted into the mammary fat pad spontaneously metastasise, including to bone (Tulotta *et al*., 2019). Alternatively, intraosseous and intracardiac injection models where tumour cells are injected into the circulation before engraftment in the bone or directly injected into the bone, are used to mimic the metastatic setting (Jinnah *et al*., 2018). Upon engraftment, interventions introducing alterations to the bone microenvironment, such as through ovariectomy or diets consisting of low calcium content, often inducing increased bone turnover, are used to reflect the osteolytic nature of breast cancer metastases.

The use of animals of different ages, young (approximately 6-week), or mature (12-week old and upwards) have been used to study different aspects of tumour-bone interaction (Dutta and Sengupta, 2016). Younger mice have an immature bone structure and as such, display high levels of bone turnover indicated by high osteoblast and osteoclast activity, resulting in a tumour growth permissive bone microenvironment. In comparison, mature mice display lower levels of bone turnover and have shown a DTC dormancy-supportive microenvironment (Jilka, 2013).

These model systems provide opportunities to investigate the different stages of bone metastases and the role of the microenvironment in affecting the rate of tumour growth in bone. Bone targeted agents, including bisphosphonates, haven been widely used in these models, and have been shown to induce osteoclast apoptosis, thereby reducing bone turnover, modulate hematopoietic populations, and inhibit the outgrowth of disseminated tumour cells induced into overt outgrowth through increased bone turnover (Fournier *et al*., 2010).

4.2.2 USE OF ZOLEDRONIC ACID IN CANCER

Zoledronic acid has been shown to decrease breast tumour cell proliferation and invasion *in vitro* (Mahmood *et al*., 2020). However, due to its strong affinity for bone and rapid clearance from circulation, direct effects *in vitro* are often not reflected *in vivo.* Despite having the potential to directly affect tumour cells following repeated high dosing *in vitro*, any observed anti-tumour effects *in vivo* are likely to be indirect following inhibition of osteoclast activity and release of bone-associated growth factors. Research into Zol in the cancer setting has therefore focused on its effect on the bone microenvironment which would indirectly influence tumour growth.

Zol is used in three different breast cancer settings; 1) in patients with confirmed bone metastases to prevent development of skeletal-related events and improve quality of life, 2) as adjuvant therapy in post-menopausal patients with early breast cancer to prevent recurrence and improve survival and 3) to prevent cancer treatment-induced bone loss (such as from aromatase inhibitors).

Zol is used routinely to reduce skeletal complications in patients who have established skeletal metastasis and has shown superior efficacy compared to other bisphosphonates. This was demonstrated in a phase III randomised trial investigating the effect of 90mg of pamidronate (Pam), every 3-4 weeks for 12 months, compared to 4mg or 8mg Zol at the same frequency and duration on the reduction of skeletal events in 1130 breast cancer patients who had bone metastases (Rosen *et al*., 2003). Though proportions of SRE occurrence between treatment groups was comparable (43% in 4mg Zol treated vs 45% in Pam-treated), among patients with at least 1 osteolytic lesion at study enrolment, Zol showed a reduction in the proportion with SREs (48% Zol vs 58% Pam) though not significant ($p = 0.058$). Time to first SRE was longer amongst the group treated with Zol compared with Pam (median, 310 vs 174 days; $p=0.013$) as well as showing a 30% reduction in the risk of developing SREs amongst the osteolytic subset ($p=0.037$)(Rosen *et al*., 2003).

Adjuvant Zol is also used in post menopausal patients with early breast cancer to prevent recurrence and improve survival. A major analysis into the adjuvant use of Zol in cancer was performed in the AZURE trial, a randomised open-label phase 3 trial of 3360 women investigating the adjuvant use of Zol in high-risk patients with stage II/III breast cancer. In the overall population, Zol did not improve overall survival or distant recurrences, but reduced development of bone metastases (Coleman *et al*., 2014). Significantly, in women who were at least 5 years past menopause, Zol improved invasive disease-free survival (DFS), but there was no benefit in other menopausal groups. Significantly, this effect was observed regardless of tumour estrogen receptor status, suggesting a role for estrogen in the microenvironment altering the actions of Zol.

The cellular and molecular mechanisms responsible for the differential effect of Zol in pre vs post menopausal women remain to be established, including the impact of the different endocrine environments in bone in these settings. Following on from the AZURE study, a number of *in vivo* model studies were instigated to try and determine how Zol affects bone and bone metastasis, mimicking the pre- and post-menopausal setting.

One such preclinical investigation was carried out by Ottewell, *et al.* who used 12-week-old female BALB/c-nude mice with disseminated MDA-MB-231 breast cancer cells characterised by a dormant phenotype, before performing ovariectomy or sham surgery and treating with Zol or control. Their results showed that ovariectomised mice had increased bone turnover and 83% of animals had detectable tumours, compared with 17% of those which underwent a sham operation (Ottewell *et al*., 2015). Importantly, the ovariectomy-induced growth of DTCs was completely prevented by the use of Zol, whereas growth of DTCs in the sham-operated animals were unaffected. These results demonstrated that OVX-induced tumour growth was driven by osteoclast activity. The same results were achieved by using OPG-Fc to prevent osteoclast expansion and activation, suggesting that Zol

acted on DTCs by reducing bone turnover (Ottewell *et al*., 2015). Combining these observations with results from clinical trial data reflect the beneficial impact of using Zol for early bone metastatic disease in post menopausal women (Coleman *et al*., 2014), and suggests the link between Zol and estrogen being in part due to bone turnover induced by osteoclasts.

The interaction between the tumour and the bone microenvironment at different stages of tumour growth is incompletely understood. Work by Ottewell *et al.* (2015) used a single dose of Zol, prior to subsequent injection of cells which prevented the outgrowth of disseminated tumour cells by increased bone turnover in an ovariectomised model. Despite this success, there are unanswered questions as to the tumour-bone interactions at different stages of tumour growth, and how Zol may affect later stages of tumour growth. Current NICE guidelines indicate monthly dosing for adult patients who are at risk of SREs in advanced malignancies (myeloma, secondary bladder, breast and prostate cancer) involving bone (BNF, 2020).

4.2.3 Zoledronic Acid as an immunomodulator and effects on hematopoiesis

Increasing evidence shows that Zol affects more hematopoietic subsets than just osteoclasts, including various immune subsets (George *et al*., 2020). What effect Zol may have on the immune compartment within the bone microenvironment is still under investigation and may elucidate the intricate mechanism of action exerted by Zol on immune cells (Liu *et al*., 2016a). A number of cells of the immune system have been well characterised as modulated by Zol, and further investigations into different subsets are still pending. Some of these will be summarised below.

An immune cell population well characterised as a target of Zol-mediated immunomodulation are γδ T cells. Inhibition of the mevalonate pathway by N-BPs result in an accumulation of metabolic intermediates from the pathway, such as isopentenyl pyrophosphate (IPP). IPP is then secreted extracellularly and is a potent activator of circulating γδ T cells (Gober *et al*., 2003b, Tanaka *et al*., 1995). Activation of this T-cell subset by N-BPs including Zol has been demonstrated in humans and in cancer models, which typically leads to increased anti-cancer activity (Altvater *et al*., 2012, Correia *et al*., 2013, Gober *et al*., 2003a, Hewitt *et al*., 2005, Kunzmann *et al*., 2000). Another facet of Zol's immunomodulatory role is its effects on macrophages. The functionally enigmatic role of tumour-infiltrating macrophages is attributed to their polarization, generally categorized as either tumour suppressive and immune promoting (M1) or tumour promoting and immune-suppressive phenotype (M2), although these represent parts of a wide spectrum (Lanciotti *et al*., 2014, Zhang *et al*., 2014a). Zol has been demonstrated to increase M1 polarisation in tumour associated macrophages and as such, may have an influence on the anti-tumour immune response (Kaneko *et al*., 2018, Rogers and Holen, 2011). Recent advances in immunotherapy have cemented a significant role for the immune system in the development of cancer, therefore the immunomodulatory effect of Zol warrants investigation.

In addition to immune cells, hematopoietic populations are affected by the use of Zol. Ubellacker *et al.* (2017), demonstrated that a single, clinically relevant dose of Zol induced transient changes in the

numbers of hematopoietic stem cells, myeloid-biased and lymphoid-biased progenitor cells, which also inhibited breast tumour growth in bone in 6 to 7 week-old mice. Interestingly, the tumour suppressive effect was maintained past the timepoint at which progenitor cells returned to base line (Ubellacker *et al*., 2017). An interpretation of these findings could conclude that these changes may be attributed to the fact that endosteal and vascular niches, which are significantly modified by changes in bone turnover, are important for hematopoietic homeostasis, and so attenuation of bone turnover by inhibiting osteoclast activity may directly affect the numbers of hematopoietic stem cells and progenitor cells.

Table 4-1: Immunomodulatory mechanisms of Zoledronic acid in humans and mice

Organism	Cells	Effect	Result	Dose/ Frequency	Reference
Human-based experiments					
Human	T-regs	Co-localization of the nuclear factor of activated T cells (NFAT) and forkhead box P3 (FOXP3) diminished by Zol treatment	Increased proliferation of T cells and NK cells	Single overnight 10µM *in vitro* incubation	(Sarhan *et al*. 2017)
Human	Natural Killer / Dendritic Cells	Depletion of endogenous prenyl pyrophosphates in Dendritic Cells and increased secretion of IL-1β and IL-18	Increased expansion of NK cells and secretion of IFN-γ	Single 10 or 30µM *in vitro* incubation for 20 hours	(Nussbaumer *et al*. 2011)
Mouse-based experiments					
Mouse	Thymocytes	Increased response to flu-HA protein in aged mice compared to young	Enhanced host response to immunisation and increased survival	Single dose 100µg/kg	(Melissa *et al*. 2011)
Mouse	CD4+CD25+ T-regs	Downregulated CCR4, CTLA4, PD-1 and RANKL on T-regs	Attenuated T-reg enhanced breast cancer migration rate	Single 24-hour 100µM *in vitro* incubation	(Liu *et al*. 2016)
Mouse	Myeloid progenitors	Myeloid/Osteoclast Progenitors numbers reduced with Zol	Reduced tumour growth	Single dose 100µg/kg single	(Ubellacker *et al*. 2018)

Mouse	Hematopoietic Stem cells (HSCs), myeloid-biased and lymphoid-biased progenitor cells	Transient increase in myeloid-biased and lymphoid-biased progenitor cells concurrent with increase in HSCs	Tumour outgrowth was inhibited by Zol administration	Single dose 100µg/kg	(Ubellacker *et al*. 2017)

Further hematopoietic alterations and immunomodulatory functions attributed to Zol in various settings; *in vitro* and *in vivo*, in human and mouse can be seen in Table 4-1. Importantly, the *in vivo* studies included in the table have used a single, clinically relevant dose of Zol, thereby providing evidence that even limited exposure to this drug can result in altered hematological and immune populations either through abundance or function.

Therefore, the hematopoietic and immune-modulatory effects of Zol warrant further investigation to establish what cell populations Zol treatment alters in the bone microenvironment other than osteoclasts, that sustain a tumour suppressive microenvironment.

GIPC1 and CAPG

Specific proteins that potentially influence the response to Zol and may be used as biomarkers to select patients that may or may not benefit are not well characterised, but a few have been identified. Two such proteins are macrophage-capping protein (CAPG) and PDZ domain-containing protein GIPC1 (GIPC1), two novel biomarker candidates which have been identified for bone-metastasis in MDA-MB-231 cells (Westbrook *et al*., 2016). In proteomic analyses from the AZURE trial, it was found that high tumour expression of both proteins led to an increased chance of developing first distant recurrence in bone in patients not treated with Zol, compared to patients with a lower expression of the proteins. In contrast, patients with high expression of both proteins that were treated with Zol, had a 10-fold reduction in the hazard ratio for first distant recurrence in bone compared to control (Westbrook *et al*., 2016). This report identifies GIPC1/CAPG as promising therapeutic targets, but whether inhibition or deletion of these proteins in conjunction with Zol administration would affect tumour growth rate *in vivo* needs to be established. I therefore carried out a pilot study to determine if breast cancer cells where CAPG and GIPC had been silenced formed tumours in bone following intra-cardiac injection in young animals and whether their subsequent growth was affected by Zol treatment.

4.2.4 HYPOTHESIS AND AIMS

The hypothesis underpinning the work in this chapter is that Zoledronic acid reduces bone turnover, affecting bone mass, tumour growth and the hematopoietic milieu in young mice.

The main aims of this chapter were as follows:

1) Characterise the BMEV and growth of TNBC cells in the bone of young (6-week old) mice
2) Investigate how tumour growth is affected by Zol and whether this effect is influenced by silencing expression of GIPC1 and CAPG in the tumour cells
3) Determine how weekly Zol modifies the bone microenvironment and influences tumour growth

4.3 MATERIALS AND METHODS

Method	Parameters analysed	Materials / Equipment / Software
Bone mineralised content		
Microcomputed tomography (µCT)	-Trabecular bone volume (BV/TV in %) -Trabecular number (TB.N. in mm-1) -Trabecular thickness (Tb.Th. in mm) Trabecular Spacing (in mm)	-SkyScan 1172/1272 scanner (SkyScan) -NRecon software -CTAn software
Circulating Blood Cells		
Hematological Analysis	Circulating erythrocytes, thrombocytes, leukocytes, hemoglobin and all erythrocyte-indices in absolute quantity and relative percentage	Scil Vet abc Plus hematological analyzer (Horiba Medical)
Histological assessment		
Tartrate-resistant acid phosphatase staining (TRAP)	-Osteoclast number per mm of trabecular bone surface -Osteoclast size (in mm)	-OsteoMeasure software (OsteoMetrics) -LeicaDMRB upright microscope
Haematoxylin and Eosin staining (H&E)	-Osteoblast number per mm trabecular bone surface -Osteoblast size (in mm)	-OsteoMeasure software (OsteoMetrics) -Leica DMRB upright microscope -Olympus BX53 microscope
Tumour growth in bone		

IVIS *in vivo* imaging	-Presence of tumour cells in live mice and tissue *ex vivo*	(IVIS) LUMINA II (Caliper Life Sciences).
Statistical analysis		
Statistical analysis	-Experimental datasets	-Prism GraphPad -Python 3.7.4 : pandas package version 1.12 and seaborn package version 0.11.0

4.3.1 CELLS

For this experiment, two MDA-MB-231 clones were used. An MDA-MB-231 *Luc2* positive cell line, (referred to as control cells) and MDA-MB-231 cell line with CRISPR-Cas9 mediated knockout of two genes, CAPG and GIPC1, (referred to as DKO). Cells were modified by and obtained from Dr Victoria Cookson (University of Sheffield) who also found that there was no difference in proliferation rate or cell cycle distribution *in vitro* between control and DKO cells (unpublished). Analysis have shown that patients with breast tumours expressing GIPC1 and CAPG are more likely to develop a first distant recurrence in bone but that this is also associated with better response to Zol (Westbrook *et al*., 2016).

4.3.2 ANIMALS

Six-week-old female Bagg and Albino (BALB)/c (CAnN.Cg-***Foxn1^{nu}***/Crl) nude (immunocompromised), mice were acquired from Charles River, UK. Upon arrival, mice were acclimatised in the Biological Services Unite (BSU) for a minimum of 7 days before procedures.

All procedures performed were approved and carried out under Procedure Project Licence (PPL) 70/8964 and personal license PIL I62B58981 within the Biological Services Unit (BSU) under local guidelines and in accordance with Home Office regulations.

4.3.3 ZOLEDRONIC ACID

Zol was prepared to by diluting 10µl of stock 10µg/ml Zol solution 1/500 in 4990µl of PBS. Assuming an average weight of 20g per mouse, this dilution would yield 100µg/kg when injected at 100µl per mouse intra-peritoneally.

4.3.4 INTRA-CARDIAC INJECTION OF MDA-MB-231 CELLS

Late-stage metastasis was mimicked by intra-cardiac injection of MDA-MB-231 human breast cancer. To establish bone metastases, 100µl of $1x10^5$ cells from either clone, suspended in PBS were injected directly into the left ventricle of 32 mice under inhalation anaesthesia consisting of 2-3% isoflurane (Zoetis, UK). Subsequently, 16 mice were randomised to receive control cells, and 16 to receive double knockout (DKO) cells. Mice were in groups of 4 per cage and were randomised to ensure two mice per

cage were injected with either cell line to control for cage-mediated differences. All mice were injected on the same day by two operators alternating per mouse to control day-mediated or operator-induced differences in cell engraftment in each treatment group. Mice were placed in an incubator at 32°C for 1-3 hours post-injection and monitored closely for adverse signs in the 24-hour period ensuing.

4.3.5 *IN VIVO* IMAGING

To track tumour progress *in vivo,* animals injected with cancer cells expressing firefly luciferase were injected sub-cutaneously with 100µl of D-luciferin (30mg/kg) 5 minutes prior to imaging on both sides of the coronal plane (front and back) of the animal. Imaging was done in the *in vivo* imaging system (IVIS) LUMINA II (Caliper Life Sciences). This procedure was carried out under anaesthetic following administration of 2-4% isofluorane.

Living image software (version 4.1) was used to identify presence and quantify size of tumours by bioluminescent capture measured in photos/second and displayed on a scale with different colours representing varying intensities of luminescence. Both larger size and increased intensity of luminescence represent larger tumours.

4.3.6 INTRA-PERITONEAL INJECTION OF ZOLEDRONIC ACID OR PBS

Seven days post intra-cardiac injection of MDA-MB-231 cells, mice from both the control and DKO group were randomised to receive either PBS (n=8 per group) or Zol (n=8/group). Zol, prepared at 100µg/kg per mouse per 100µl or PBS were injected at a volume of 100µl per mouse once per week for four weeks. Injections were performed intraperitoneally on opposite sides of the sagittal plane relative to the previous injection, injected in the left or right segment of the peritoneum.

4.3.7 *EX VIVO* ANALYSIS

4.3.7.1 HEMATOLOGICAL ANALYSIS

Upon culling, mice had their blood withdrawn through cardiac puncture, of which 20µl was placed into 500µl Eppendorf tubes containing 20µl of EDTA to prevent clotting, thoroughly mixed and stored at room temperature for up to 2 hours post-cull. These samples (10µl per sample) were then run through a Scil Vet abc Plus hematological analyzer (Horiba Medical) which measured total white blood cells (number per $10^3/mm^3$ blood), total red blood cells (number per $10^3/mm^3$ blood), lymphocytes (percentage (%) and number per $10^3/mm^3$ blood), monocytes (percentage (%) and number per $10^3/mm^3$ blood), granulocytes (percentage (%) and number per $10^3/mm^3$ blood), eosinophils (percentage (%) and number per $10^3/mm^3$ blood), hemoglobin (g/dL), hematocrit (percentage), mean corpuscular volume (μm^3), mean corpuscular hemoglobin (pg), mean corpuscular hemoglobin concentration (g/dL), red blood cell distribution width (percentage), platelets (number per $10^3/mm^3$ blood) and mean platelet volume (μm^3).

4.3.7.2 Preparation of samples for histology and bone histomorphometry

Immediately following dissection, tibias used for histology and histomorphometry were placed in 4% (*w/v)* paraformaldehyde (PFA) for 48-72 hours. These were then washed 3 times in ice-cold PBS and stored in PBS at 4°C pending µCT analysis. Once µCT scanning was complete, bones were placed in a PBS 14% (*w/v*) ethylenediaminetetraacetic acid (EDTA) solution for decalcification. This solution was changed twice a week for 3 weeks before bone processing. Bones were subsequently paraffin-embedded (wax). To obtain sections for histological analysis, wax embedded tibias were cut at 3µm thickness, and 6 samples taken from 3 levels, 20-30µm apart before mounting on glass slides and stored at room temperature.

4.3.7.3 Microcomputed tomography

Micro-computed tomography (µCT) performed on bones was performed in three steps; scanning, reconstruction and analysis. Scanning involves the projection of x-rays through a sample onto a detection plate to create an image representing mineralised bone using a SkyScan 1172/1272 scanner . The sample is then partially rotated through a selected rotation range with smaller rotation steps with an x-ray-generated image created at each rotation step. The collection of images is subsequently collated and reconstructed to produce 3D images. Finally, 3D images are analysed to produce quantitative data on various bone physical parameters.

4.3.8 Statistical Analysis

Graphpad prism 8.0.2 was used to derive statistical analysis, running singular or multiple t-tests where appropriate, analysing both row factor (treatment), column factor (tumour status) and row x column factor (treatment given tumour status) t-tests.

Correlation plots were drawn using Python 3.7.4 using Pandas package 1.1.2 correlation plot with the spearman correlation parameter, and Seaborn package 0.11.0 heatmap to visualise results.

4.4 Results

4.4.1 Cell clone bioluminescence

Bioluminesence as observed during *in vivo* imaging relies on the production of exogenously incorporated luciferase, expressed by tumour cells, and their subsequent metabolism of D-luciferin to produce photons that are detected, quantified and displayed by Living Image software as photons per second. The expression of luciferase and rate of uptake of luciferin may be different between clones and can therefore affect the rate of release of photons per cell. This may lead to incorrect measurements and comparisons of tumour size, and therefore tumour growth rate. As I used 2 different MDA-MB-231 breast cancer cell clones in this experiment (control cells and DKO cells where CAPG and GIPC1 had been silenced), it was possible that their Luc2 expression may have been different, and would have confounded *in vivo* estimation of tumour size using bioluminescent capture.

Fewer cells with a stronger bioluminescent output could therefore appear a similar size to a higher number of cells with a lower expression of Luc2.

To assess whether clone type impacted observable bioluminescence, cells from each clone were suspended in 1ml of media at different densities ($5x10^5$, $1x10^5$, $5x10^4$ and $1x10^4$ cells per well) in a 12-well plate, incubated with 10µl of D-luciferin (6mg/ml) and exposed in (IVIS) LUMINA II for 60 seconds. Control cells showed a higher bioluminescence than DKO cells (see Figure 4-1). These results demonstrate that an equal number of cells from each clone yields different bioluminescence intensity, hence making it a challenge to accurately compare tumour size from the different clones based on bioluminescent signal *in vivo.*

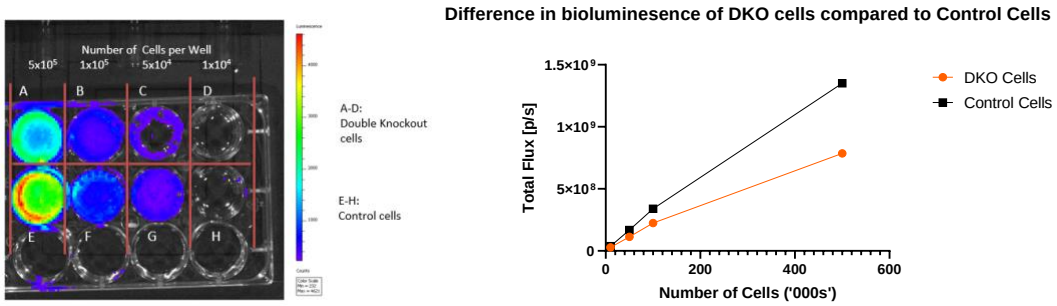

Figure 4-1: Left: Bioluminescent analysis of different clone types seeded at different densities in 1ml medium, incubated with 10µl luciferin and exposed for 60 seconds . Top: MDA-MB-231-GIPC1/CAPG double-knockout cells; A.) 5x105, B.) 1x105, C.) 5x104 and D.)1x104 cells per well. Bottom: MDA-MB-231 control cells; E.) 5x105, F.) 1x105, G.) 5x104 and H.) 1x104 cells per well. Right: Bioluminesence of the two MDA-MB-231 clones used in this experiment at different cell densities

4.4.2 EXPERIMENTAL OUTLINE

To assess the effect of Zol on the bone microenvironment and tumour growth in bone of young, immunocompromised mice, 6-week old female BALB/C nude mice (n=32) were randomised into two groups of n=16 injected with $1x10^5$ either control or DKO MDA-MB-231 cancer cell clones, before being randomly assigned to one of two groups (n=8/treatment group/cell type) that received four consecutive weekly treatments with either PBS (control) or Zol (100µg/kg) (see Figure 4-2).

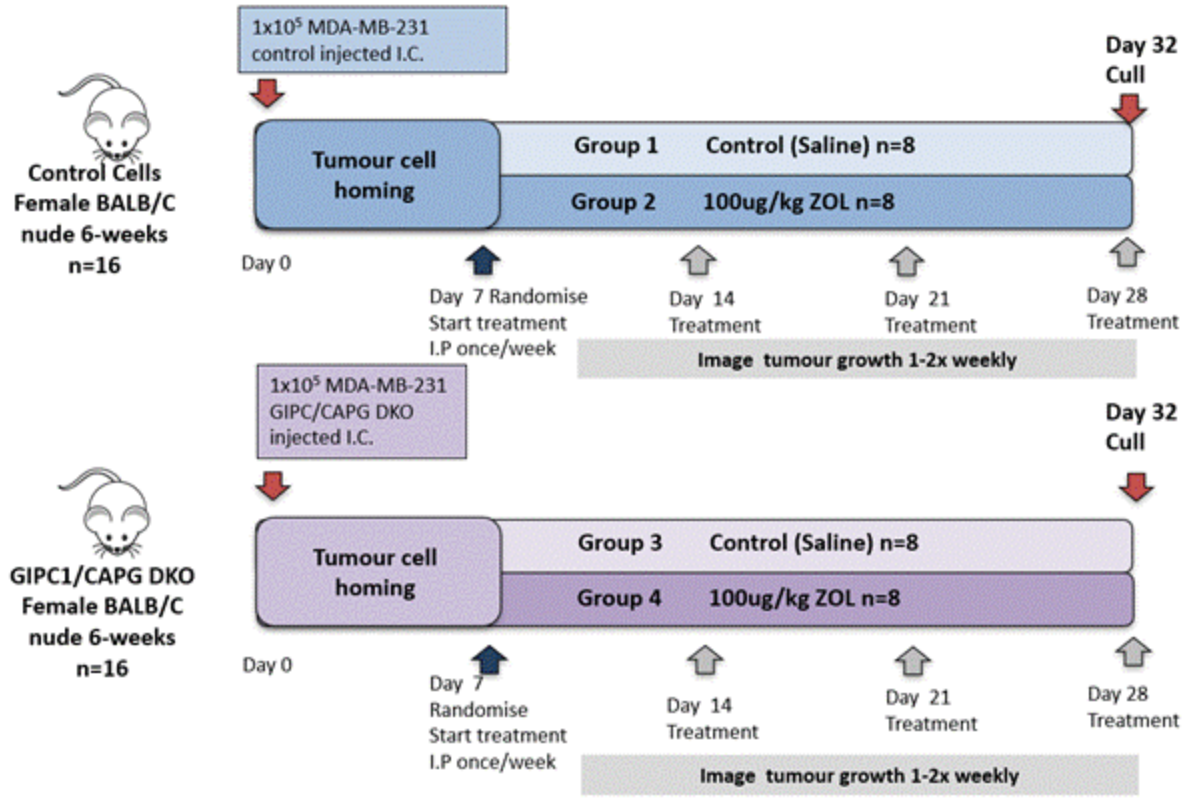

Figure 4-2: Experimental outline to assess the effect of Zoledronic acid on the bone microenvironment and circulating immune cells. On day 0, all mice (n=32) were injected intra-cardiac with 1x10^5 MDA-MB-231 cancer cells in 100µl suspension and randomised on day 7 to receive either PBS or Zoledronic acid once weekly for 4 weeks before subsequently being culled on day 32.

Randomisation was performed according to strength of bioluminescent signal in the skull as imaged 24 hours following injection with cells, a measure of the success of intra-cardiac injections, to ensure both treatment groups in both cell clone groups were similar in cancer cell uptake profile (see Figure 4-3). After four once-weekly treatments, mice were culled on day 32. Two mice in the PBS-treated developed hind limb paralysis, one shortly after intra-cardiac injection, and the other two weeks later and were subsequently culled due to humane endpoints, resulting in final numbers of n=16 in the Zol group and n=14 in the PBS control group. See Table 4-2 for a more detailed breakdown of randomisation and tumour growth per stratified group.

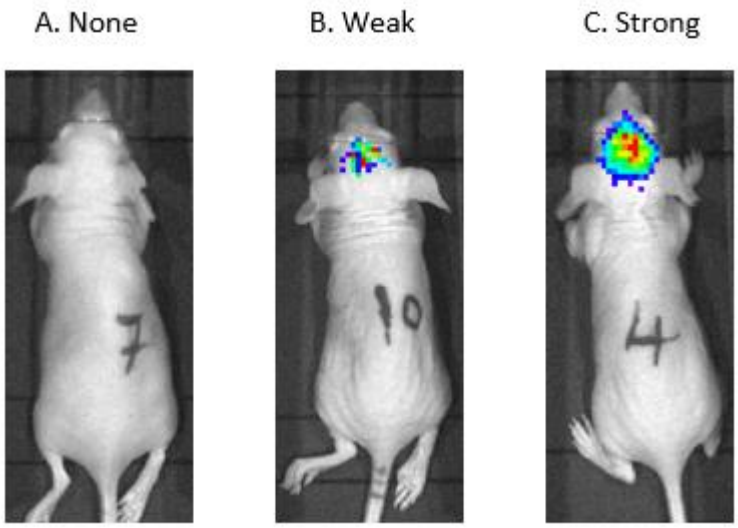

Figure 4-3: Example bioluminescent imaging 24 hours following intra-cardiac injection as an indicator of injection success. A.) Left, mouse 7, an example of no signal. B.) Middle, mouse 10, an example of weak signal. C.) Right, mouse 4, an example of strong signal.

Table 4-2: Stratification of animals into different groups according to signal strength and subsequent skeletal tumour development with percentage figures. W; Weak signal, S; Strong signal, N; No signal in the skull 24 hours following intra-cardiac injection with cancer cells.

	Total Number of Mice			Total Number of Mice with Tumours			Percentage mice with tumours		
Cell type	W total	S total	N total	W total	S total	N total	W%	S%	N%
Total DKO	4	2	10	4	2	4	100	100	40
DKO Zol	2	1	5	2	1	3	100	100	60
DKO PBS	2	1	5	2	1	1	100	100	20
Total CTRL	2	6	7	2	6	5	100	100	71.43
CTRL Zol	0	3	5	0	3	3	-	100	60
CTRL PBS	2	3	2	2	3	2	100	100	100

Mice with any signal 24 hours post intra-cardiac injection were defined as positive, whereas mice with no signal were defined as negative. As can be seen in Table 4-2, 100% of the mice with a detectable bioluminescent signal in the skull 24 hours following intra-cardiac injection went on to develop skeletal tumours. Mice with no signal were a higher percentage (62.5% in DKO and 46% in control groups with no signal, compared with 25% DKO and 13% control with weak signal and 12.5% DKO and 40% control with strong signal), and fewer developed tumours (40% in DKO and 71.4% compared to 100% of both weak and strong signal in both clone groups groups) than those with weak or strong signal. The resultant animals not bearing tumours were all from the group with no signal and therefore it is

assumed that the lack of tumour development was due to poor cell uptake in this group, rather than due to treatment effects.

To assess whether first time to metastasis was affected by treatment, analysis was done of the time it took to achieve first observable metastasis within the hind limbs *in vivo* as detected by a bioluminescence signal. As can be seen in Figure 4-4, within animals receiving the control cells, the use of Zol appeared to reduce the time to first observable metastasis, whereas it significantly delayed the time to metastasis in DKO cells (p 0.0059 as measured by two-way ANOVA).

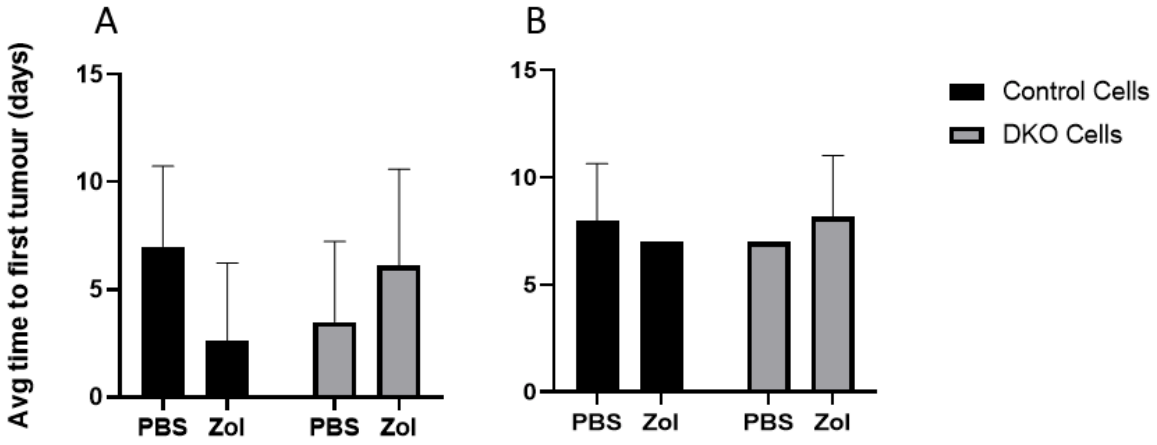

Figure 4-4: A.) Average time to first tumour as stratified by treatment and cell type. Difference between means of Zol and PBS treated animals was 1.375 days, p 0.3128, whereas difference between cell type was 0.5 days p 0.7113. However, combined ANOVA identified a mixed difference of 1.1 days, with a p value of 0.0173 as analysed by a two-way ANOVA.B.) Average time to first observable tumour when omitting animals that did not go on to develop any tumours. Treatment difference p-value 0.9392, cell-type p-value of 0.9392 and mixed effect analysis p-value of 0.3286 as assessed by a two-way ANOVA. No significant differences were observed

Further analysis into time to first tumour identified 9 animals that did not develop any tumours, which all belonged to the cohort of animals with no signal in the skull 24 hours following injection of tumour cells. These were omitted from analysis as they were assumed to not have had tumour cells of sufficient quantity injected into their circulation. Including them in the analysis would bias the effects of treatment on preventing tumour growth as only animals with engrafted tumour cells should be considered. Omitting these animals from analyses, the differences between cell types and treatments became less apparent and showed only minor effects with a mixed factor analysis p value of 0.3286.

4.4.3 Assessing the effects of Zoledronic acid on tumour growth

Mice were monitored weekly by *in vivo* imaging for tumour growth. As can be seen in Figure 4-5, the number of animals with skeletal tumours, and their growth, were comparably similar between the Zol-treated and PBS-treated groups. Attenuation of tumour growth by Zol was not observed as the individually tracked mice and the grouped analyses both reflected a relatively similar rate of tumour growth in skeletal sites.

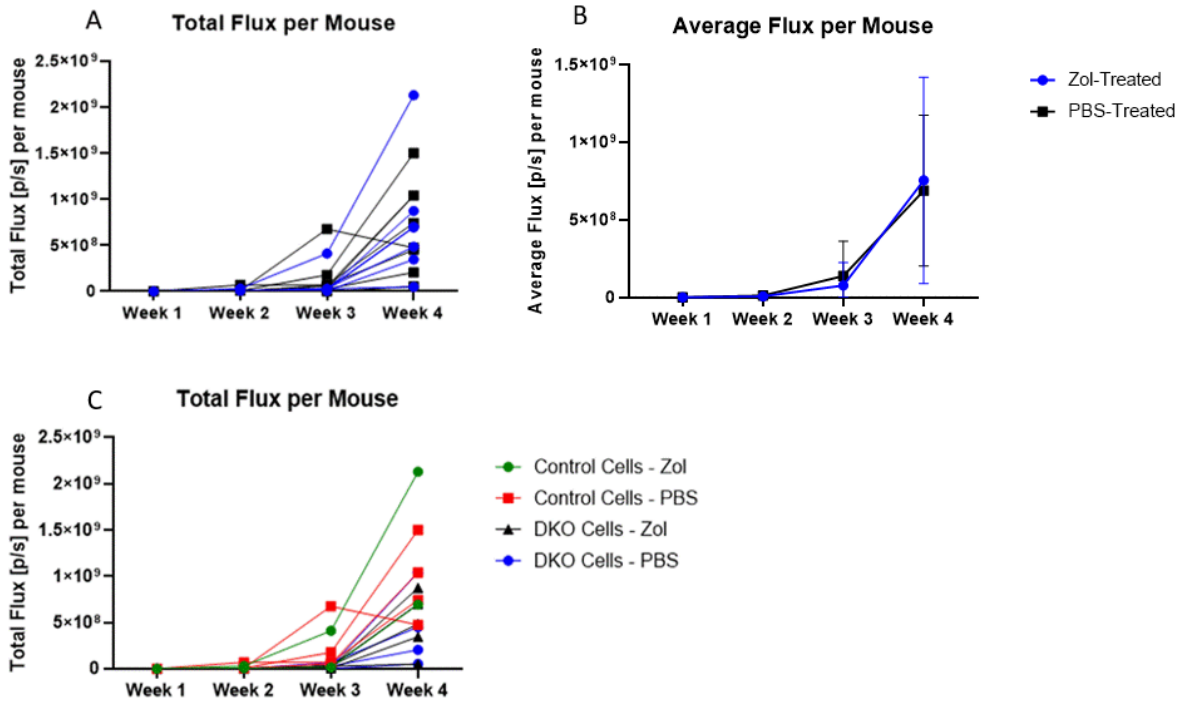

Figure 4-5: The total flux per individual mouse measured on all skeletal sites bearing tumours over time distinguished by A.) treatment only for individual mice, including both cell types B.) treatment only for group averages C.) treatment and clone type for individual mice.

No significant trend was observed into the attenuation of tumour growth by either PBS or Zol, nor did the clone type have significant differences on tumour growth rate. Control cells appeared more luminescent in *in vitro* assessment, and as such, appear more luminescent in these graphs. However, the difference between control and DKO cells varied with cell count, making it difficult to normalise the *in vivo* derived bioluminescence without knowing the cell count.

10 out of 15 (66.7%) of PBS-treated animals and 8 out of 16 (50%) Zol-treated animals developed tumours in the hind limb by the first week, rising to 11 out of 14 (78.6%) and 9 out of 16 (56.25%) treated with PBS and Zol, respectively, by the second week. Eight out of 16 in DKO-injected animals and 10 out of 15 (66.7%) in control-injected animals developed tumours by week 2. Overall, there was no significant difference in tumour growth rate or first time to tumour between the different clones injected, nor did Zol treatment affect tumour growth rate. Animals from both cell clone groups and both treatments within those groups displayed a range of tumour numbers and sites (hind limb, spinal and front limb), as well as rates of growth which were not characteristic of any single treatment/cell clone stratification and seemed random (see Figure 4-6:). As a result of this variability, conclusions as to the effect of the clone type or treatment could not be firmly made.

The quantification of the number of animals bearing skeletal tumours were used in the subsequent results.

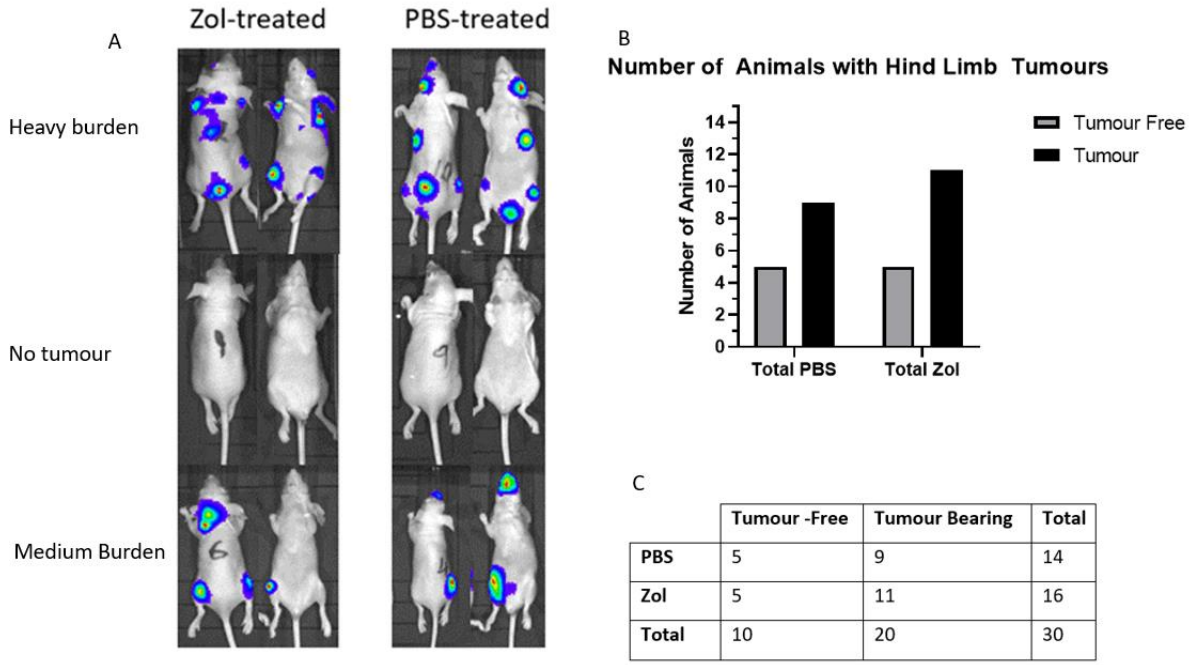

C

	Tumour -Free	Tumour Bearing	Total
PBS	5	9	14
Zol	5	11	16
Total	10	20	30

Figure 4-6: A. (Left) Example images of tumour growth in both Zol-treated and PBS-treated animals. A.) variety of tumour growth characteristics from none (no tumour), small number of site engraftment (medium burden) and widespread tumour growth (heavy burden) can be seen in both groups. B.) (Top Right) The number of animals with hind-limb skeletal tumours. Tumour-free PBS treated n=5, tumour-free Zol treated n=5, tumour bearing PBS treated n=9, tumour-bearing Zol-treated n=11. C.) (Bottom Right) (Right) Summary table of number of animals per treatment group across treatments and tumour status.

4.4.4 Effects of Zoledronic Acid on Trabecular Bone

Zol is a potent anti-resorptive agent that reduces bone turnover. Trabecular bone has a higher rate of turnover than cortical bone (Ott, 2018), effects of Zol would be most pronounced in trabecular bone and analyses were therefore focussed on this area. As the mice injected were young (age 6-7 weeks at the start of Zol treatment), a relatively high rate of bone turnover was assumed. Osteoclast inhibition would therefore lead to increased trabecular bone and be a reliable indicator into the effect of Zol. To establish this, µCT analysis was performed on the trabecular region of tumour-free tibias from all mice with at least one tumour-free tibia (n=28).

Figure 4-7 illustrates the differences between Zol-treated and PBS-treated animals, showing that 4 weeks of weekly Zol treatment has a dramatic effect on bone architecture, increasing the amount, but not the thickness, of trabecular bone. These results were quantified in detail (Figure 4-8)

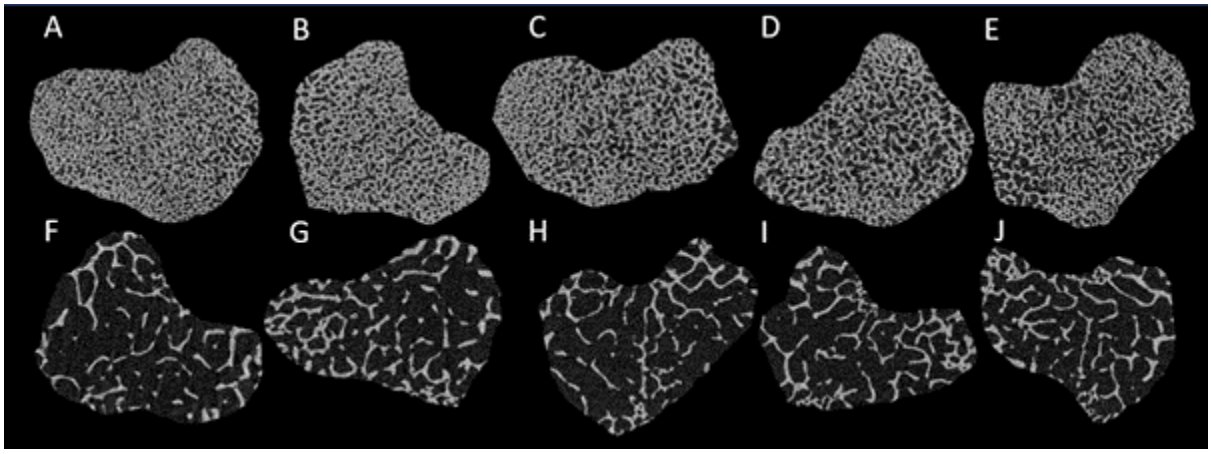

Figure 4-7: Example first scanning region of interest from 5 different mice treated with four weekly doses of Zol (A-E) and or with four weekly doses of PBS (F-J).

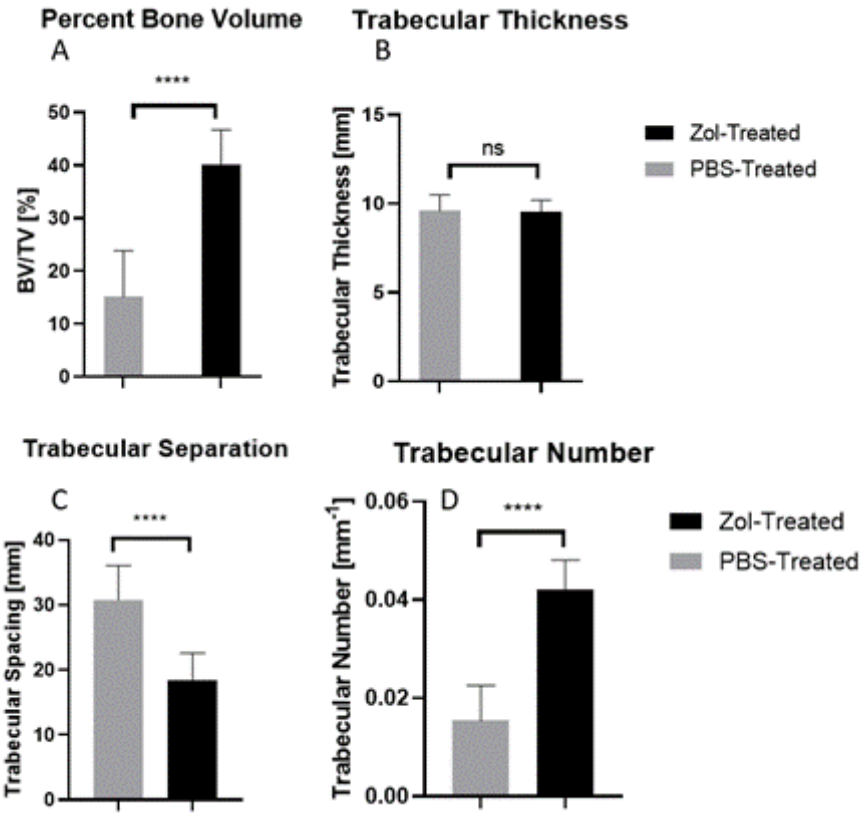

Parameter	PBS-treated mean	Zol-treated mean	Difference between means ± SEM	P Value

Percent Bone Volume (%)	15.14	40.15	25.01 ± 3.101	< 0.0001
Trabecular Thickness (mm)	9.60	9.55	0.05 ± 0.312	0.8845
Trabecular Separation (mm)	30.77	18.47	12.30 ± 1.907	< 0.0001
Trabecular Number (mm^{-1})	0.015	0.042	0.27 ± 0.003	< 0.0001

Figure 4-8: Effects of Zoledronic Acid on bone structure and integrity in the absence of tumour. Quantification of A.) trabecular bone volume (BV) per tissue Volume (TV) (BV/TV%), B.) Trabecular Thickness, C.) Trabecular Separation and D.) Trabecular Number for animals (n=28) given four once weekly doses of 100µg/kg Zoledronic Acid (n=16) or PBS (n=14). Two-tailed t-test with Welch's correction performed for significance. ** indicates a p-value of <0.0001.**

As shown in Figure 4-8, percentage bone volume and trabecular number were all significantly increased and trabecular separation significantly increased in Zol-treated mice compared to control. In contrast, trabecular thickness was unchanged between groups. As osteoclasts are responsible for bone resorption, results show that Zol significantly reduced osteoclast activity.

4.4.5 BONE HISTOMORPHOMETRY

To assess the effect of Zol on bone resident populations, TRAP staining (allowing detection of active osteoclasts stained red in the following figures) was performed on tibias from mice treated with four-weekly 100µg/kg doses of Zol (n=6); with (n=3) and without (n=3) tumours, and from mice treated with four-weekly injections of PBS (n=6); with (n=3) and without (n=3) tumours.

This experiment was completed in March 2020, at the commencement of the national lockdown, and samples were subsequently stored in PBS after being fixed with 4% PFA for 24 hours. However, at the time, it was not known how long lockdown would last. The samples were subsequently left in PBS for 5 months, which is postulated to be responsible for causing dispersion of the bone marrow cellular content specifically around the trabecular region. Most samples displayed this condition, which involved dispersion of bone marrow cellular content, as well as the compression of bone marrow cells against the trabecular bone (see Figure 4-9 for dispersion compared to a reference image in Figure 4-10 without dispersion).

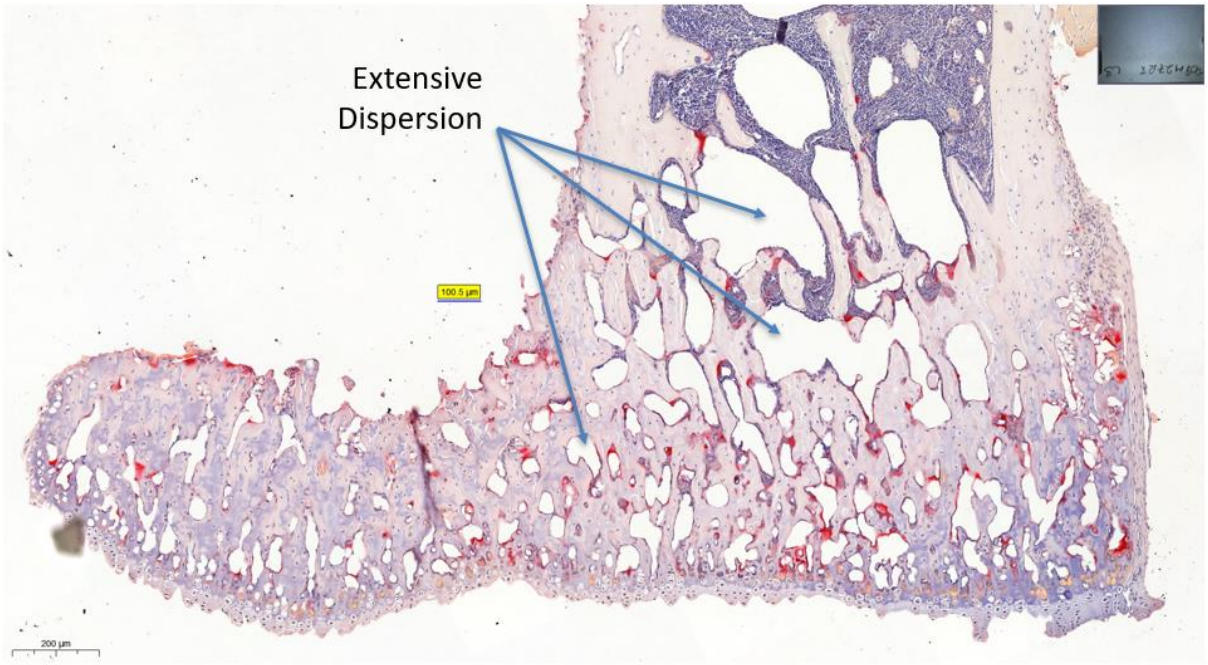

Figure 4-9: 10x magnification of zol-treated tibia showing dispersion of marrow cells around the trabecular region. Empty spaces can be seen where bone marrow cells would normally be expected to be filled.

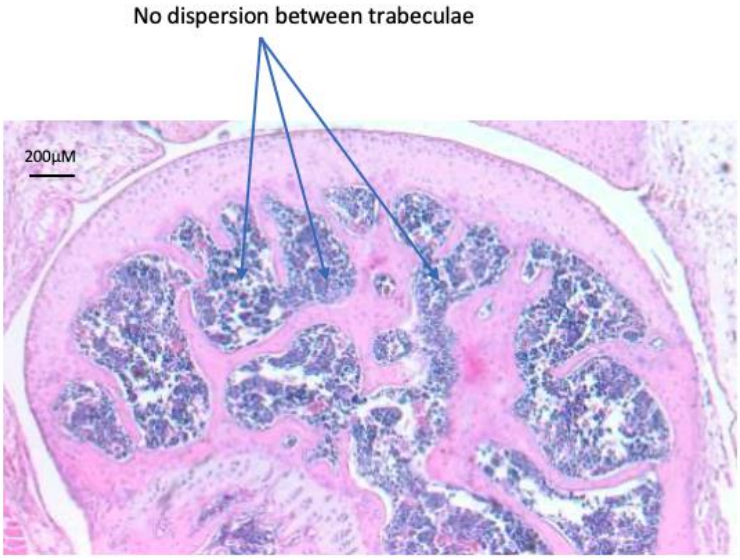

Figure 4-10: Reference bone with no dispersion of cells between trabeculae

These effects made it difficult to accurately identify osteoblasts, which appear cuboidal and flat compared to other bone resident cells. The compressed marrow cells developed a flattened appearance, making them difficult to distinguish from osteoblasts that were stained a similar colour by Gill's haematoxylin, in contrast to the red-stained osteoclasts (see Figure 4-11). As a result, osteoblast quantification could not be performed on these samples and analyses focused on osteoclasts (in red).

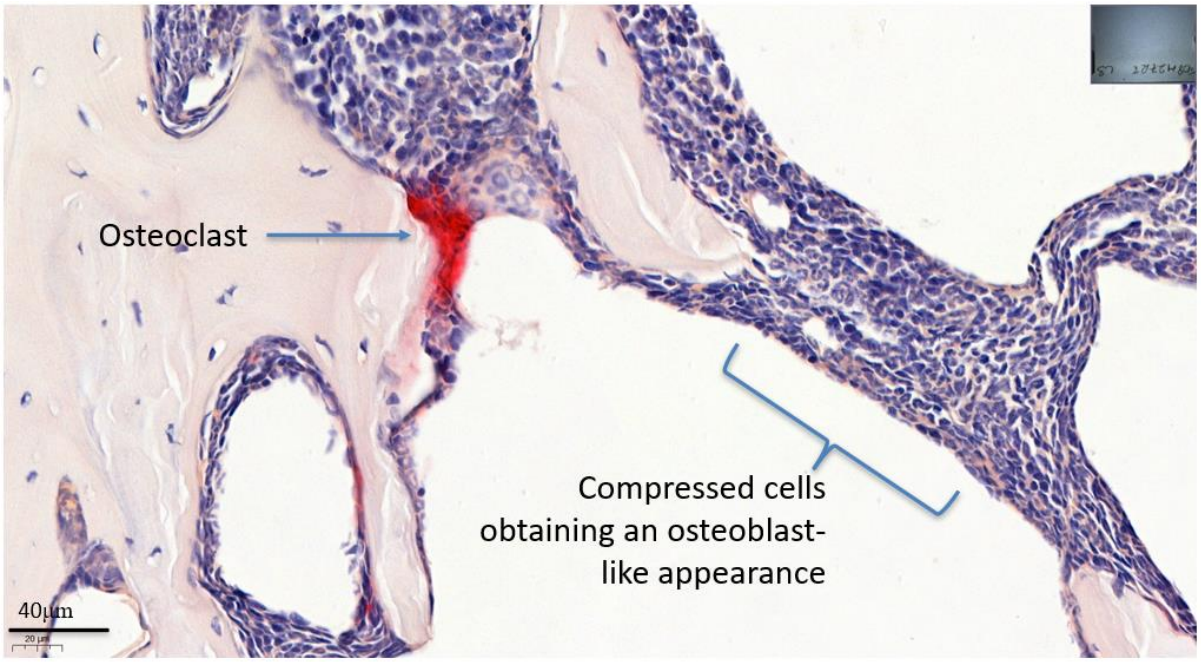

Figure 4-11:40x magnification of Zol-treated tibia showing dispersion and compression of cells against trabecular bone. Red stained osteoblasts can be easily identified, but accurate osteoblast measurements are difficult.

In representative images, the volume of trabecular bone between Zol-treated and PBS-treated tibias could be visualised, with Zol treated tibias showing an increased volume of trabecular bone. Some tibias with tumour cells had significantly reduced trabecular bone due to extensive tumour growth filling the marrow cavity (see Figure 4-12).

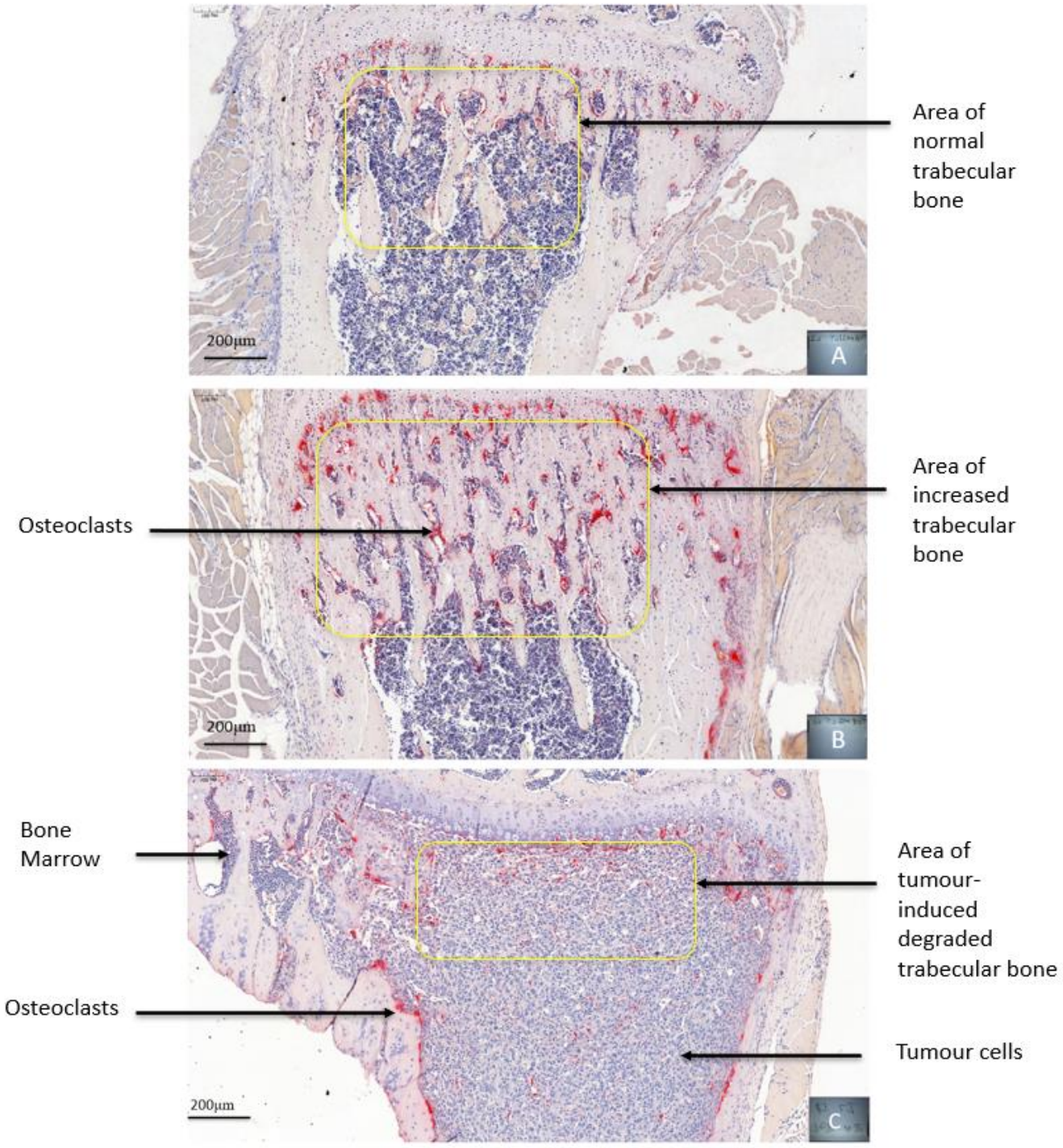

Figure 4-12: 8.7x magnification of representative tibias A) PBS-treated tibia showing trabeculae and number of osteoclasts (top), and B) Zol-treated tibia showing trabeculae and number of osteoclasts (middle), and C) PBS-treated tibia bearing tumour

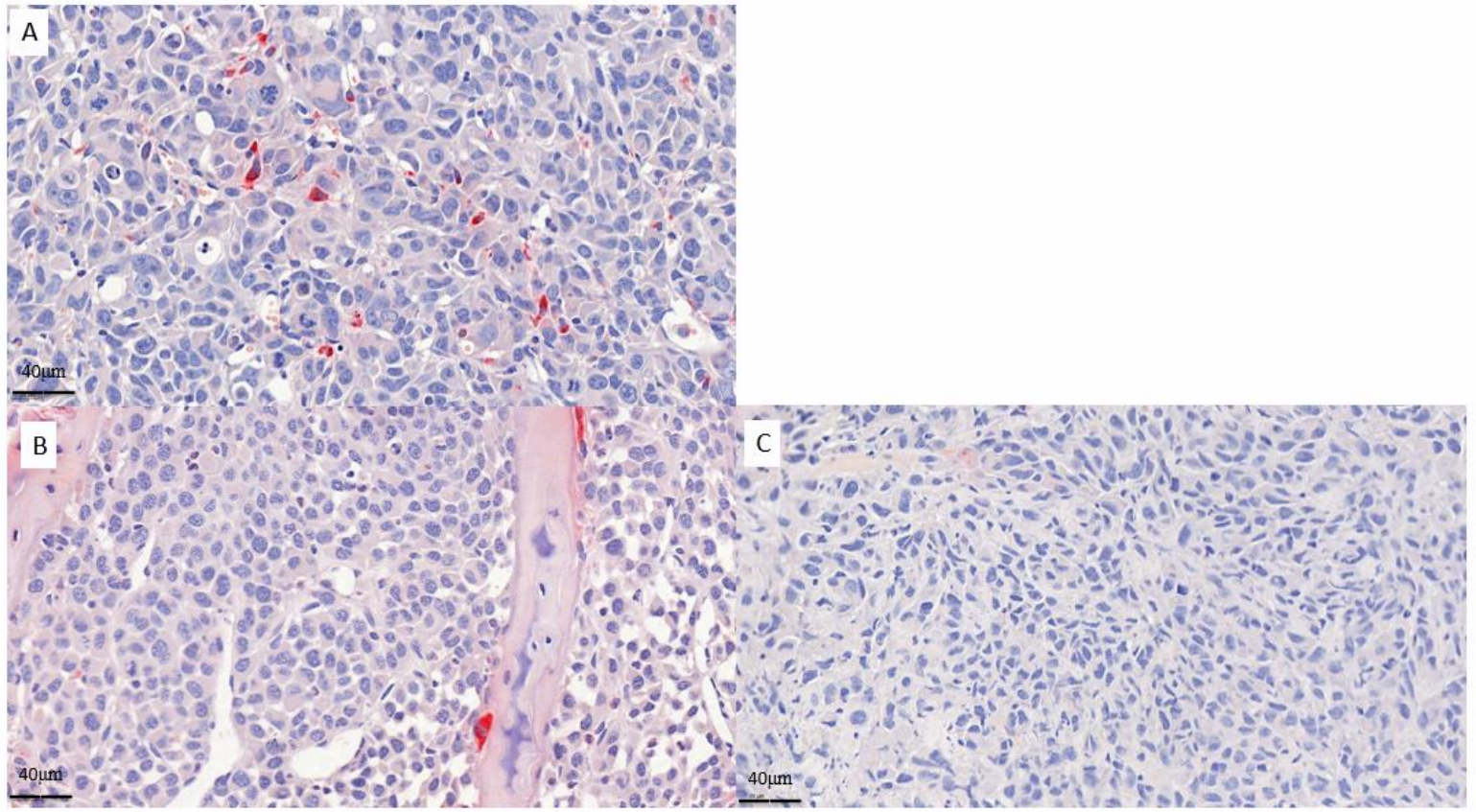

Figure 4-13: 40x magnification of *ex vivo* tibia sections with tumour cells, either DKO or control, following four once-weekly treatments of PBS or 100µg/kg Zol. A.) Control tumour cells treated with PBS, B.) DKO cells treated with PBS, C.) DKO cells treated with Zol. Control cells treated with zol missing due to sample degradation

Tumour cells within the bone retained a squamous epithelial morphology with a larger cell size than most cells within the bone marrow and positive TRAP staining within the tumour. Tumour cells from the control group appeared larger and showed a more spindle-like morphology than DKO cells, whereas the DKO cells appear smaller and rounder in morphology.

Treatment with Zol did not seem to change the general morphology of the DKO tumour cells as could be detected by microscope.

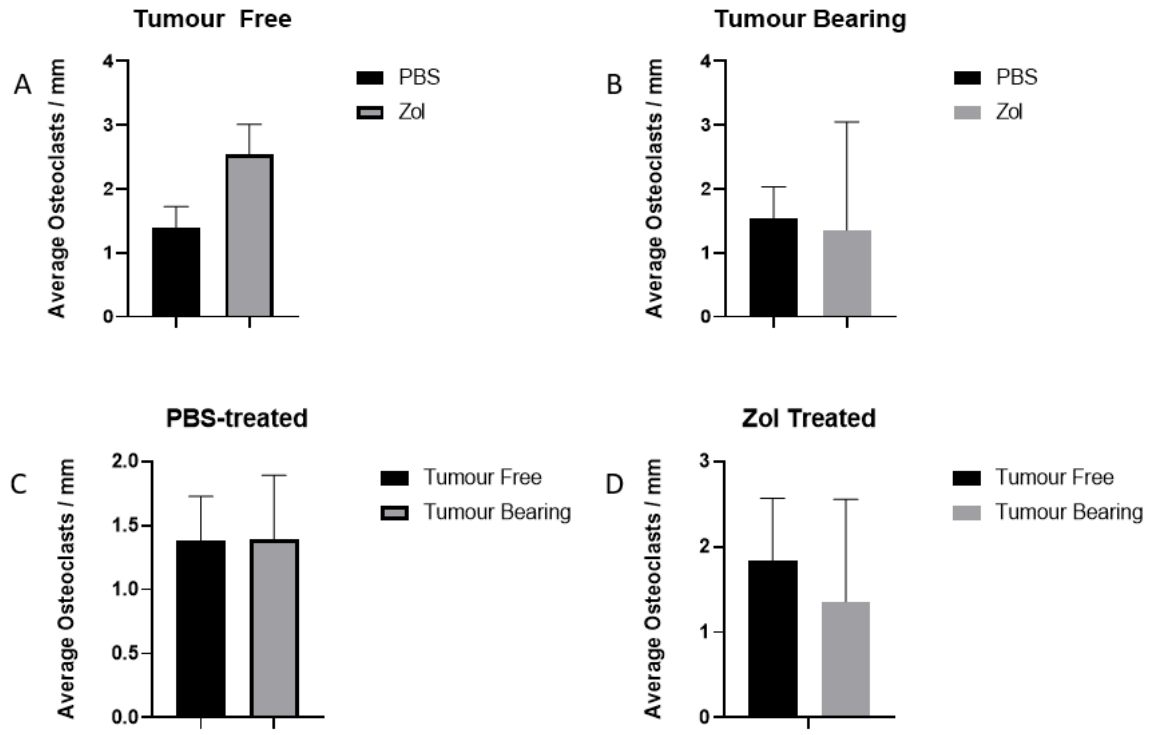

Condition	PBS-treated mean	Zol-treated mean	Difference between means ± SEM	P Value
Panel A - Tumour Free Only	1.385	2.544	1.160 ± 0.4092	0.1052
Panel B - Tumour Bearing Only	1.536	1.359	-0.1773 ± 0.9659	0.8660
Condition (with & without tumour)	**Tumour Free Mean**	**Tumour Bearing Mean**	**Difference between means ± SEM**	**P Value**
Panel C – PBS Treated	1.385	1.389	0.004572 ± 0.4038	0.9915
Panel D – Zol-treated	9.60	9.55	0.05 ± 0.312	0.8845

Figure 4-14: The average number/mm of osteoclasts in the trabecular area of tibias in animals treated with PBS or Zol and stratified by the presence or absence of tumours in the tibia measured. A) tumour free tibias, treated with Zol (n=3) or PBS (n=3), B) tumour bearing, treated with Zol (n=3) or PBS (n=3), C) tibias treated with PBS with (n=3) and without (n=3) tumours, and D) tibias treated with Zol with (n=3) and without (n=3) tumours in measured tibias. The table shows group means, differences between the means and P value. No significant differences were observed.

When accounting for all tibias with and without the presence of tumours, the number of osteoclasts is significantly increased in the Zol treated animals compared to PBS treated animals (see Figure 4-15).

This difference seems to be driven mainly by an increase in the number of osteoclasts in tumour free tibias treated with Zol with a difference between means (compared to PBS) of 1.160 (p=0.1052). However, separate analysis of the tumour-free tibias did not reveal a significant difference when comparing treatments, and the increased significance when combining tumour free and tumour bearing tibias may be a facet of increased numbers and therefore more likely significance in statistical tests. Indeed, this increase in osteoclast number in tibias from Zol treated mice was also seen in histology slides (see Figure 4-12).

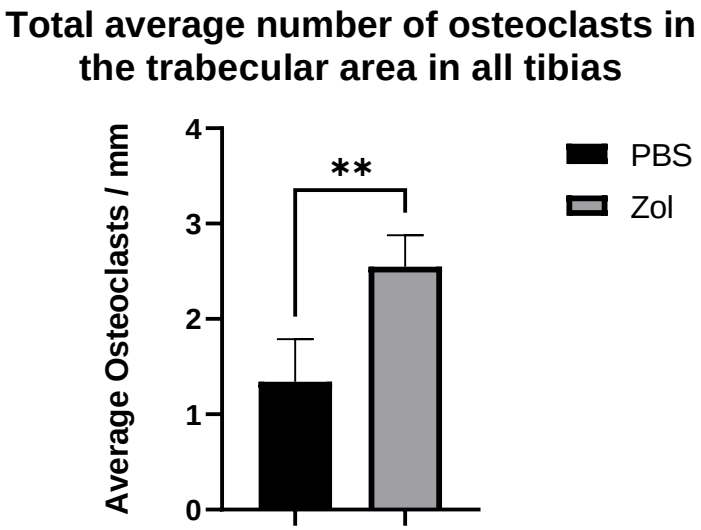

Figure 4-15: The average number of osteoclasts in the trabecular for all tibias with and without tumours, stratified y treatment .Average number of osteoclasts per mm for PBS 1.34, compared with Zol, 2.55. Difference between means (SEM) 1.208 ± 0.2767and p = 0.0058.

4.4.6 Characterising the effects of Zoledronic Acid on circulating blood cells

Due to the major impact of Zol treatment seen in the µCT analysis, the question was raised as to whether reduced physical space may have an effect on other cells in the niche, such as terminally differentiated progeny that are more numerous than their bone-resident progenitor cells, nor whether this can be identified in the circulating milieu (Ubellacker *et al.*, 2017).

To characterise the effects of weekly Zol administration on circulating hematopoietic cells, hematological analysis was carried out on 10µl of blood diluted 1:1 in EDTA from all mice (n=30). Animals were classified as tumour free or tumour bearing on the basis of having detectable skeletal

tumours (luc 2 signal) by IVIS following cull and *ex vivo* imaging of hind limbs and samples were collected 2 hours after the last Zol administration.

As shown in Figure 4-16 Zol treatment did not cause significant changes to circulating hematopoietic cell populations compared to control. There was also no significant difference in these cells between tumour-free and tumour-bearing animals. Multiple t tests measured the difference between tumour status (tumour free vs tumour bearing), treatment (Zol-treated vs PBS-treated) and cross-testing of tumour status incorporating treatment using two way analysis of variation (ANOVA). These yielded non-significant results and the group averages did not show a trend in any direction. However, eosinophils had a trend to increase with Zol treatment regardless of tumour status, as can be seen with a lower p-value of 0.1149 when taking into account treatment effects only, but a higher p-value of 0.7359 when taking into account tumour status only, suggesting Zol had a minor effect on circulating eosinophils. Granulocytes also showed a similar trend, although not as strong as Eosinophils, with a treatment only p-value of 0.2686 and a tumour status p-value of 0.7494.

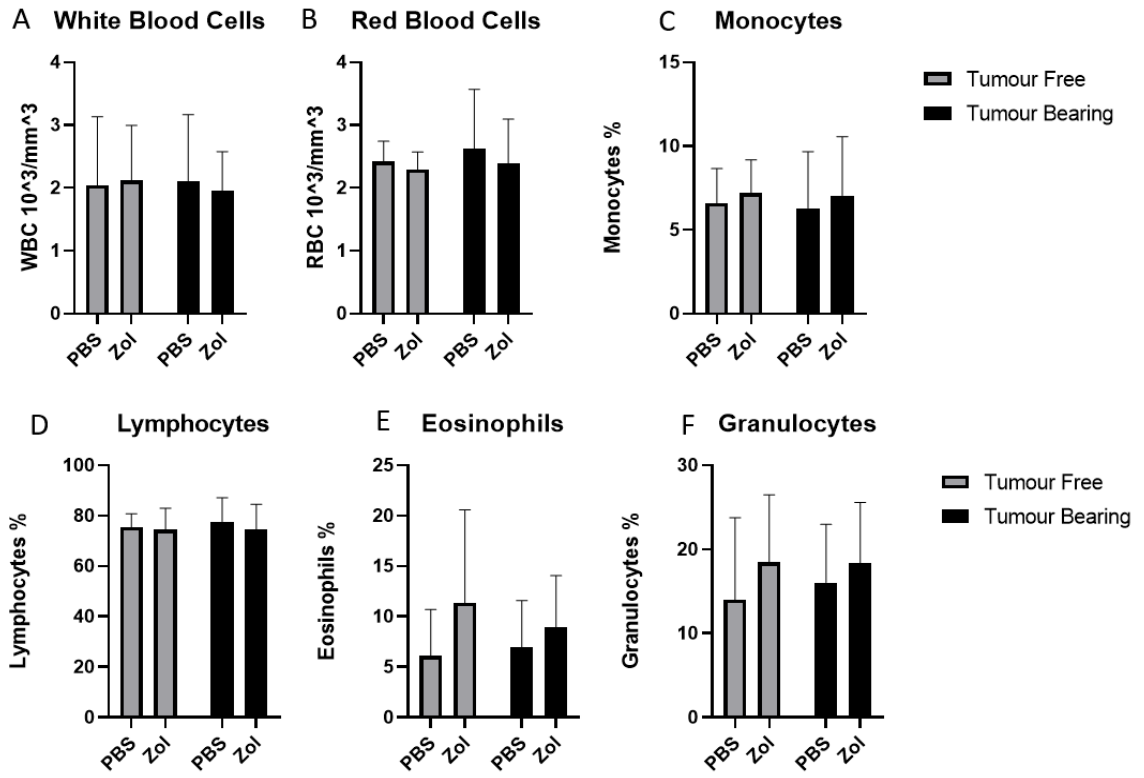

		Mean values				Factor P-values		
		Tumour-free		Tumour-bearing				
	Cell Type	PBS	Zol	PBS	Zol	Treatment	Tumour Status	Tumour x Treatment
A	WBCs per mm^3	2.04	2.12	2.111	1.955	0.9745	0.8533	0.7465
B	RBCs per mm^3	2.422	2.296	2.623	2.391	0.4134	0.7111	0.8616
C	Monocytes %	6.6	7.18	6.3	7.045	0.4784	0.9285	0.9973
D	Lymphocytes %	75.42	74.36	77.66	74.63	0.4944	0.7359	0.7291
E	Eosinophils %	6.08	11.34	6.922	8.955	0.1149	0.7432	0.4663
F	Granulocytes %	13.98	18.46	16.04	18.33	0.2686	0.7494	0.7164

Figure 4-16: The effects of Zoledronic Acid on circulating hematopoietic cells in animals bearing tumours and tumour-free animals. Actual values and p-value results can be seen in table

To visualise correlations between the treatment type and effects on measured parameters from circulating hematopoietic cells, a correlation plot using pandas and seaborn within python were used. To obtain a correlation with treatment type, treatments had to be converted into numerical encoding; 1 for PBS-treated animals and 0 for Zol-treated animals. As such, negative correlation with treatment indicates a correlation of increased number with Zol treatment, and a positive correlation indicates decreased correlation with Zol-treatment (see Figure 4-17). Areas of high

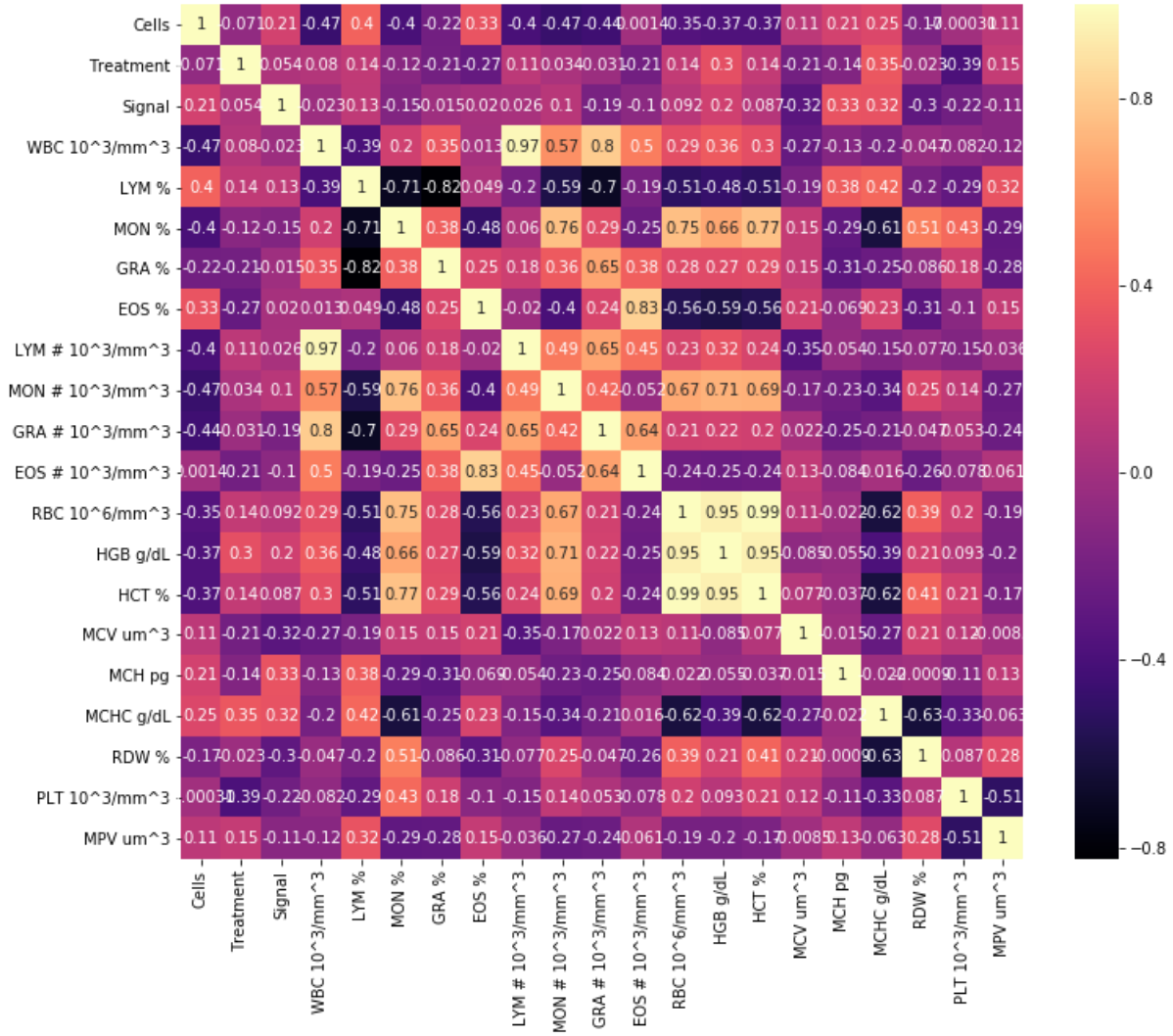

Figure 4-17: Correlation plot showing correlation between different parameters analysed by hematological analysis using spearman correlation; positive values (from 0-1) indicate positive correlations with an increasing value, negative values (from 0 to -1) indicate negative correlations and 0 represents no correlation. Areas of high positive correlation have colour tending towards bright yellow with increasing positive correlation. Areas of high negative correlation tend towards black colour with decreasing negative correlation value (and therefore increased negative correlation). Areas of no correlation tend towards purple/red at 0.

The correlation plot shows minor correlations with the treatment column, suggesting that treatment had a weak effect on circulating hematopoietic cells. Interestingly, granulocyte percentage and eosinophil percentage had correlations of -0.21 and -0.27 respectively, suggesting an increase of eosinophils and granulocytes as a result of Zol treatment. This confirms data shown in Figure 4-16 which, although insignificant, show a trend towards increasing eosinophil and granulocyte percentages with Zol treatment.

4.5 Discussion

4.5.1 General Overview

In this chapter, I explored how Zol affects skeletal metastases growth in young animals, through the modulation of the microenvironment. Included in this analysis was whether the cancer cell clone type had a significant effect on growth characteristics when Zol was administered, whether the hematopoietic milieu was altered, both in the bone marrow and in the circulation, as well as how repeated administration compared to results reported by literature following administration of a single dose.

4.5.2 Dosing concentration and schedule

The clinical dosing regimen for Zol is a dose of 4mg given every 3-4 weeks in patients with confirmed bone metastases. The *in vivo* dose of 100µg/kg used in this project is equivalent to that given in the clinic and several studies have investigated the effects of single doses of Zol (Brown *et al*., 2012, Haider *et al*., 2014, Ottewell *et al*., 2008, Ottewell *et al*., 2015) , therefore I sought to characterise the effect of multiple clinically relevant doses at an increased frequency. Although the cumulative effect of weekly administration is significantly higher than the clinical administration given once every 3-4 weeks, my dosing regimen maintained the clinical relevance at single doses, and was selected to ensure maximal suppression of osteoclast activity. This would allow investigation into the impact of inhibition of osteoclastic activity on bone structure, hematopoeisis and tumour growth in bone. Furthermore, the rate of cancellous bone turnover is higher in mice (0.7% per day as measured in the distal femur) compared to humans (0.1% per day as measured in the iliac crest), and a more frequent dosing is therefore commonly used in murine models (Jilka, 2013).

4.5.1 Effect of Zoledronic Acid on Bone structure

The effect of Zol on trabecular bone showed a dramatic effect, increasing the amount, but not the thickness, of trabecular bone. Zol primarily inhibits osteoclasts, leading to a reduction in bone resorption, and as a consequence, it is expected that there would be an increase in bone volume and alterations in the trabecular structure, but not an alteration in thickness which would suggest an increase of osteoblastic function. The major increase in bone volume following repeated Zol dosing is likely to affect multiple bone niches with potential implications for their resident cell populations such as HSCs and the bone microvascular network.

My findings are in agreement with previous studies showing that administrations of Zol have significant impact on trabecular bone parameters; percent bone volume, trabecular number and reduction in trabecular separation. These effects have been observed consistently in both young (6-week old) and mature (12+-week old) mice (Brown *et al*., 2012, Haider *et al*., 2014, Ottewell *et al*., 2008, Ottewell *et al*., 2015). In all these studies, Zol was shown to increase bone volume percentage and improve bone structural integrity compared to control, but did not significantly alter tumour growth on its own, despite beginning Zol treatment prior to the injection of cells in young (4-7 week

old) mice. However, Zol showed enhanced anti-tumour efficacy when combined with a standard of care treatment, such as Doxorubicin compared to the standard of care alone (Ottewell *et al*., 2008). In agreement with the previously published studies I found using Zol as a single agent enhanced bone structural integrity, but without antitumour activity. These data support the combination of Zol with a chemotherapy over a single agent in osteolytic bone disease.

Interestingly, at the cellular level, Zol did not significantly alter the number of osteoclasts in trabecular bone when stratified by the presence or absence of tumour, nor did it significantly alter the number of osteoclasts when comparing tibias that were tumour bearing and tumour free. As Zol primarily targets osteoclasts, this was a surprising result. However, it must be noted that in several tumour-bearing bone samples had their trabecular bone completely replaced by tumour, and as osteoclasts tend to be located along the bone surfaces, this may have led to a false negative result. Ubellacker and colleagues (2017), found that a single dose of Zol induced a 7-fold decrease in the number of osteoclasts after a single dose of Zol at 100 µg/kg (Ubellacker *et al*., 2017). It may be that the quantity of osteoclasts is proportionate to the increased trabecular bone area in young mice with higher rates of hematopoiesis, as Zol induces apoptosis in actively resorbing osteoclasts at a higher rate than inactive precursors. This however, is contradictory to findings by Ubellacker and other results in mature mice. The increased osteoclast number in Zol-treated animals could be seen in histology slides. Furthermore, this was driven by increased numbers of osteoclasts in Zol-treated in tumour free animals than those without tumours, suggesting that the presence of tumour cells did not drive an increase in osteoclasts. It must be noted, however, that although there was an increase in osteoclast numbers, they were less active as, seen in histology slides and µCT data, showing a significant increase in trabecular bone in Zol-treated animals. Unfortunately, the osteoblast numbers could not be accurately determined in these samples, whose numbers may have shed light on the population balance between Zol-treated and PBS-treated tibias. Serum bone turnover markers for osteoclast and osteoblast activity, TRAP and P1NP respectively, would be more accurate measurements of dynamic changes in bone turnover, but would be still limited to end-point measurement. Ultimately, Zol still produced the same increase in trabecular bone as expected.

4.5.2 Effect of Zoledronic Acid on Circulating Hematopoietic populations

The BALB/c Nude mice used in this study carry a mutation in the transcription factor Forkhead box protein N1 gene, Fox N1 (former name: Whn or Hfh11) (Schorpp *et al*., 1997). The mutation in the gene coding for this pleiotropic protein is responsible for hairlessness and athymia which is a typical phenotype of mice carrying mutations in this gene (Schorpp *et al*., 1997). The result is an immunodeficient status due to significant reductions in T-cells that mature in the thymus (Flanagan, 1966). As I carried out haematological analysis of these T-cell depleted mice, lymphocytes were identified as being the largest population of circulating immune cells. Despite lacking T-cells, athymic nude mice possess comparable B-cell compartment, in terms of abundance and diversity, to wild-type BALB/C Foxn1$^{+/+}$ mice and are the cell type responsible for the abundance of circulating lymphocytes (Cancro and Klinman, 1980, Quintáns and Lefkovits, 1973). Notwithstanding the lack of T-cell

compartments, athymic nude mice produce other immune subsets , which have been reported to be altered by Zol, as well as a range of hematopoietic cells.

Ubellacker *et al.* (2017) demonstrated that by administering a single dose of Zol at the concentration I used (100µg/kg) in the same mouse strain (BALB/C Nude) and age (6-7 weeks) altered the hematopoietic population as estimated by flow cytometry of flushed bone marrow from femurs. In particular, hematopoietic stem cells (HSC) (day 3) and common myeloid progenitors (CMP) (days 3 and 5) were increased after Zol administration, but common lymphoid progenitors (CLP) (day 5) were reduced following Zol administration compared to PBS-treated mice. Therefore, a significant alteration of these progenitor cells which give rise to immune cells was mediated by a single dose of Zol. In addition, megakaryocyte/erythroid progenitors (MEPs, which give rise to megakaryocytes, erythrocytes and platelets) were also significantly increased at day 5 post-Zol treatment (Ubellacker *et al*., 2017). Importantly, all of these progenitor cells populations returned to near-baseline levels by day 10 following Zol administration, suggesting a transient change that is restored after a period of time. Whether repeated doses of Zol would sustain a significant change in these cells over time, or whether cells would be de-sensitised to repeat Zol exposure, is still unanswered.

My analysis of hematological cells circulating in peripheral blood vessels showed no significant alteration in the daughter cells that differentiate from the aforementioned progenitor cells. Lymphoid- and myeloid-derived immune cells, as well as red blood cells and platelets showed no significant changes in animals treated with Zol compared to those treated with PBS. Ubellacker *et al.* (2017) also followed up their findings of altered hematopoietic stem and progenitor cells, measured through flow cytometry, with hematological analysis of peripheral circulating hematopoietic cells, and similarly found no significant changes in circulating hematopoietic cells in BALB/C Nude mice following a single dose of Zol, but a slight trend towards reduced neutrophil and monocytes in these animals compared to vehicle-treated control. Of note, Ubellacker *et al.* (2017) treated C57BL/6 mice with Zol and found alterations in the hematopoietic stem and progenitor milieu in the bone marrow, similar to that in BALB/c Nude mice treated with Zol, but also found a corresponding significant increase in circulating monocytes and neutrophils (day 3 and 5), as well as platelets (day 5) after Zol treatment. This altered population was back to baseline levels after 10 days following Zol treatment, again suggesting a transient increase in circulating monocytes, neutrophils and platelets similar to the transient nature observed in the stem and progenitor cells in the bone marrow. Their findings suggest that hematopoietic stem and progenitor cells are significantly altered by Zol within the bone marrow, yet mice lacking an intact, complete immune system do not display a corresponding significant change in differentiated circulating cells.

The findings from Ubellacker *et al.* (2017) showed that the most significant alteration in the hematopoietic cells were detected between 3 and 5 days post Zol treatment. As my analyses were carried out within four days of the last Zol administration, they were within the window of time showing the largest difference in these cell types between control and Zol treated animals, and any changes to circulating cells would not be expected to have returned to homeostasis within this time. Therefore, it can be concluded that there were no significant changes to circulating hematopoietic

cells even after four repeated weekly doses of Zol. This is in agreement with findings by Ubellacker *et al.* (2017) which show that immunocompromised mice do not exhibit significant changes in the circulating milieu as a result of repeated weekly exposure to Zol. Importantly, progenitor cells appeared to recover their function in-between repeated treatments, and this may be a basis as to why the circulating population was maintained.

Despite having a significant effect on the physical bone structure as demonstrated by the uCT results, my analyses confirmed that Zol did not appear to have a significant effect on circulating immune cells. Hematological analysis showed no significant difference in the circulating hematopoietic population measured, which is in agreement with previously published data (Ubellacker *et al*., 2017). Questions still remain as to the tightly controlled homeostasis of circulating hematopoietic cells. The immune landscape is known to transform in the presence of tumours, yet the presence or absence of tumours in PBS-treated animals did not appear to have a significant difference on circulating hematopoietic cells either. Furthermore, the lack of resolution into immune subsets may have played a role in a seeming lack of difference in immune types, as Zol has been shown to polarise or induce differentiation in subsets of immune cells in specific tissue locations, rather than alter their abundance (Clarke *et al*., 2018, Comito *et al*., 2017, Coscia *et al*., 2010, Veltman *et al*., 2010). Still, previous data showing alterations in circulating immune cells in mice with a fully intact immune compartment suggest that the presence and/or activity of T-lymphocytes plays a significant role into the effect of Zol on circulating immune subsets of hematopoietic cells.

Routine clinical use of Zol reflects the single administration given to mice by Ubellacker *et al.* (2017) and assessed within 3 weeks, compared to the weekly doses I used in my studies, which was at a higher dosage and intensity than the most frequent dose of 4mg every 3-4 weeks (BNF, 2020). No change in circulating hematological populations in mice at either a clinically-relevant dosing regimen used by Ubellacker *et al.* or an increased frequency used in my studies, is consistent with clinical guidance in which disturbances of the hematological compartment are limited to uncommon (haematuria, leucopenia and thrombocytopenia) and rare or very rare (pancytopenia) side effects with the use of Zol (BNF, 2020). My findings are in agreement with those from the AZURE trial which placed patients on a frequent dosage of 4mg/3-4 weeks for six doses, then every 3 months for eight doses, followed by every 6 months for five doses, for a total of 5 years of treatment, monitored hematological function of women enrolled on the study and did not report significant effects that altered hematological function while on Zol, illustrating the minimal impact of Zol on circulating hematopoietic abundance (Coleman *et al*., 2014).

4.5.3 The effect of Zol on tumour growth in bone and young animals

Although Zol had a significant effect on the bone structure, this did not translate into significant effects on the rate of tumour growth. There was no significant difference in tumour growth rate between animals treated with Zol and those treated with PBS, regardless of tumour cell clone.

Tumour growth is increased by growth factors released during accelerated bone turnover, but also induce bone turnover through the vicious cycle, meaning that micro-metastases size at time of treatment may be important in establishing the success of Zol as an intervention (Chirgwin and Guise, 2000, Guise and Chirgwin, 2003). Furthermore, tumours may reach a size and become microenvironment-independent such that inhibition of osteoclasts does not significantly affect tumour growth.

Considering this, the size of established tumours at the point when Zol treatment was initiated has the potential to affect its ultimate effect on controlling tumour growth. Previous studies from our lab have shown bone colonisation rates of a few dozen cells per bone, but this was in mature (aged 12 weeks+) mice (Allocca *et al*., 2019a). This rate may be significantly higher in young mice (age 6-8 weeks), but it assumed similarly small clusters of a few cells would form and colonise the bone microenvironment even though ultimately numbers may be higher. At this size, the microenvironment would have a significant effect on the replicative ability of tumour cells. A week after I injected the tumour cells, a significant number of mice (n=18) had already developed a detectable tumour in a skeletal site. Through examining the cells' bioluminescent profile (see Figure 4-3), at a count of 10^4 cells, there was barely any signal identified. Therefore, detectable tumours would be assumed to contain cells exceeding this number, and especially considering the location of the tumours underneath tissues that occlude a significant portion of signal. It can thus be stated that by the time Zol was introduced, many of the animals had tumours that may have had capacity to grow, at least partially independent of the microenvironment, thus any alterations by Zol may have been insignificant for tumour growth.

Previous studies which used Zol after the introduction of tumour cells administered Zol at an earlier time point and further used a chemotherapy combination to inhibit tumour growth (Brown *et al*., 2012, Ottewell *et al*., 2008). An example is work done by Brown *et al.* (2012) using 6-week old BALB/c nude mice with inoculation of a similar number of MDA-MB-231 cells as I used ($1x10^5$), followed by a single PBS, Zol (100µg/kg) or Doxorubicin (Dox) (2mg/kg) administration 24 hours later. A subset of the animals received Zol treatment 24 hours following Dox injection (Brown *et al*., 2012). In these studies, the use of Zol alone did not alter tumour growth when assessed on day 15 and 23, whereas the combination of Zol with Dox did result in attenuating the growth of the tumours. Breast tumour cells grow in organs outside the bone, indeed the primary tissue is distinct, where osteoclasts and the vicious cycle are not present. As such, it is to be expected that osteoclast-independent growth can continue even in the presence of osteoclast inhibitors like Zol.

The effect of Zol alone on inhibiting tumour growth has been shown in a few studies, but these have used a significantly higher dose of Zol compared to the clinically-relevant dose, which is limited due renal toxicity at higher doses. Croucher *et al.* used 120µg/kg Zol twice weekly for 12 weeks to prevent osteolytic myeloma bone disease in 6-week old C57 mice (Croucher *et al.* 2003) and Corey *et al.* used 200µg/kg twice weekly over a period of 4 to 9 weeks in order to also reduce osteolytic lesions from metastatic prostate cancer cells in 4-8 week old male Fox chase SCID mice (Corey *et al*., 2003, Croucher *et al*., 2003). Despite having an increased dosing frequency of Zol in my studies, I did not manage to

recapitulate the findings in the studies. However, although the mice were similar ages to my studies, they were different strains and the dosages of Zol were 2-4 times greater than that I used, in addition to being tumours of different tissue origin. Therefore, it is not surprising to obtain different results. Interestingly, using a B02/GFP breast cancer model, Daubiné *et al.* (2007) reported that more frequent daily and weekly dosages, amounting to 100µg/kg/3-4 weeks accumulated dose, did reduce skeletal tumour burden (Daubiné *et al*., 2007). However, this was measured by the size and incidence of osteolytic tumour lesions, which, although reducing bone osteolysis, does not necessarily mean a reduced tumour burden within the bone.

4.5.4 Differential effect of Zoledronic Acid in GIPC1 and CAPG knockout cells

A limitation with many of the published studies of effects of Zol on tumour growth in bone is that they used a single cell line model, most commonly a version of the TNBC MDA-MB-231 line (Dai *et al*., 2017). The results from these studies could therefore to some degree be cell line specific, applicable only to the particular line used. By combining my studies with ongoing work on a complementary project, I had the opportunity to directly compare Zol effects on tumours derived from 2 different clones of MDA-MB-231 cells within the same experiment. The clones differ only in their expression of two proteins; GIPC1 and CAPG, and have been shown to have similar growth rate *in vitro (see* Figure 4-18*)*.

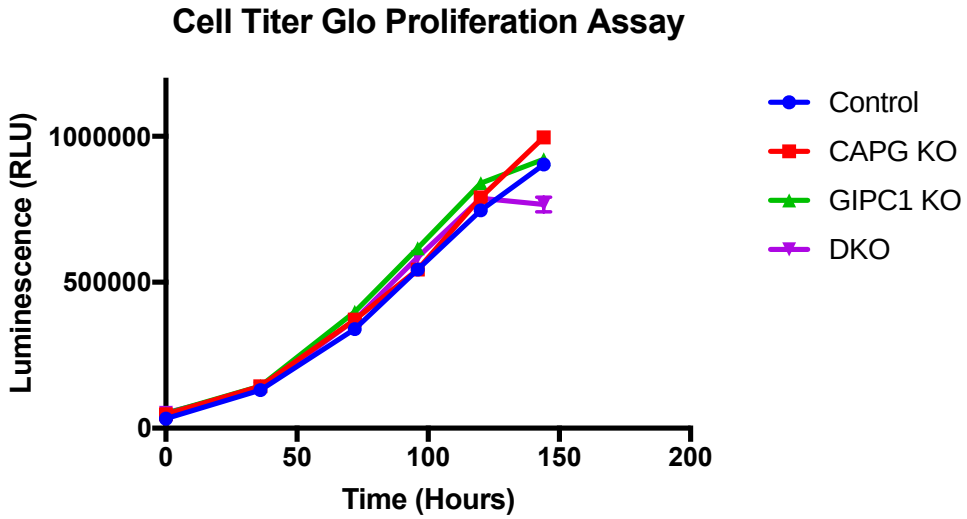

Figure 4-18: Unpublished data generated by Dr Victoria Cookson comparing growth rates of control cells compared to CAPG KO, GIPC1 KO and DKO as measured by *in vitro* bioluminesence

The effect of clonal difference was investigated in the context as to whether cells not expressing GIPC1 and CAPG would have a significant difference to tumour outgrowth. Work done by Westbrook *et al.* (2016) revealed a poorer prognosis in time to distant recurrence when these proteins were highly expressed in tumours of breast cancer patients not treated with Zol, yet high expression of these proteins was correlated with a reduced time to distant recurrence in patients treated with Zol (Westbrook *et al*., 2016). Therefore, it would be expected that clones expressing GIPC1 and CAPG

would have a faster time to metastasis in PBS-treated animals compared to the DKO, but would show the opposite in a reduced time to metastasis in Zol-treated animals, a differential response to Zol. The data suggests high tumour cell expression of GIPC1/CAPG is correlated with a better response to Zol, and as such, DKO tumour cells should in theory have a weaker response to Zol than the parental cell line they were derived from.

Initial analysis of time to first observable metastasis in animals showed similar results to findings by Westbrook *et al.* (2016) in which cells expressing a higher level of GIPC1 and CAPG (control cells) had a faster time to metastasis those with a lower level (DKO cells). However, 10 of the 30 animals did not have signal in their skull 24 hours following intra-cardiac injection (positive signal in the skull), and did not go on to develop tumours at any site. Therefore, these were omitted from the analysis due to poor injection success, leaving 20 out of 30 animals available for the tumour progression analysis. Upon re-assessment, there was no significant difference between cell type nor treatment in time to first metastasis, which did not support the published literature. What remains unclear is whether the animals that did not have any detectable bioluminescence signal indeed had any colonization of disseminated cancer cells in bone which simply did not grow out. The lack of availability of a multiphoton microscope for my use further prevented assessment of whether this was the case, as tumour cells would have to be established in growth and be at least 10^4 cells to be identified by IVIS imaging. I therefore opted to discount these animals from analyses relating to differences between clones as tumour colonisation of bone could not be confidently assumed although some animals not showing any signal in the skull 24 hours following intra-cardiac injection went on to develop metastases.

It must be noted that GIPC1 and CAPG are involved in cellular motility and the clinical endpoints they affected were time to distant recurrence, inferring a role in the process of metastasis. Considering this, Zol treatment commenced one week following the injection of tumour cells when colonisation of bone would have already taken place. This may explain why there was no difference in the growth rate between the clones, as cells were already in suspension and in the circulation, potentially masking the effect of motility proteins in progressing the tumour to a motile phenotype. GIPC1 and CAPG may still therefore have a significant influence on time to metastasis in a model where cells are injected at the primary site breast tissue and have to undergo processes to induce motility through epithelial to mesenchymal transition (EMT). Indeed, DKO cells exhibited a different morphology, appearing smaller and less epithelial-like than the control cells, which suggests there may be a corresponding difference in motility. This is supported by unpublished data generated by Dr Victoria Cookson. It is also important to note that the AZURE trial used Zol in the neoadjuvant setting, whereas my studies focused on the metastatic setting with Zol as a singular agent, and therefore differences in treatment regime may account for differences in observations.

4.5.5 Further Questions and Research

Further questions still remain surrounding the use of Zol in the bone-tumour microenvironment. In particular, too few tumours of consistent size developed to accurately identify differences between

the potential differential response of GIPC1/CAPG DKO cells and control cells to Zol. I would repeat this experiment with bigger numbers to ensure sufficient number and onset of tumours occur. Although my experiment involved investigating the differential effect of Zol based on CAPG/GIPC1 expression by knockout of CAPG and GIPC1 in MDA-MB-231 cells, an alternative method of investigation would be to induced overexpression of these proteins in the cell lines, as differential expression of GIPC1 and CAPG can be induced by overexpression. Indeed, inducing overexpression in contrast to knockout cells with a wild type control would yield the best conditions to investigate the effect of these two proteins on differential response to Zol. It may be overexpression is required to have any observable effects.

Zol has been shown to induce changes in bone cellular populations, specifically osteoclasts and progenitor cells (Ubellacker *et al*., 2018, Ubellacker *et al*., 2017). However, although Zol had a potent effect on the bone structure, the effects on the circulating cells and on osteoclasts were uncharacteristic and different to previous findings. Whether frequent repeat doses would have an unforeseen and unexpected effect on the bone marrow populations is unknown. Repeating this experiment with its dosing regimen and re-quantifying the cellular and circulating hematopoietic and bone resident populations using more sensitive measurement methods, such as flow cytometry, would further elucidate whether there is an underlying, unseen mechanism, as the literature is sparse on frequently repeated doses in young mice.

The vicious cycle is a well characterised mechanism used to explain the interaction between osteolytic tumour cells in the bone and osteoclasts. Furthermore, the initiation of the vicious cycle has also been shown to initiate and increase the rate of tumour growth within the bone. Despite this, inhibition of osteoclast activity and therefore the disruption of the vicious cycle has not shown a significant impact on tumour growth within the bone. In particular, the DCARE trial, an international, multicentre, randomised, placebo-controlled phase 3 trial of 4509 women with stage II or II breast cancer investigated the effects of denosumab, a significantly more-potent inhibitor of osteoclasts than Zol, with adjuvant chemotherapy (Coleman *et al*., 2020a). The findings showed that there was no benefit in disease-related outcomes for women with high-risk early breast cancer from osteoclast inhibition by denosumab. This is similar to findings in the AZURE trial, which found no significant overall benefit in the use of Zol in patients of a similar cohort. However, stratification of patients in the AZURE trial revealed a benefit for women post-menopause compared to peri or pre menopausal women. This suggests that, unlike Denosumab which is highly targeted to osteoclasts, Zol has an effect on the bone microenvironment in conjunction with decreased oestrogen presence. Work by Ottewell and colleagues showed the use of Zol in mature mice prevented the outgrowth of dormant, disseminated, tumour cells, which were not in an acquired growth phase. Therefore, understanding the bone microenvironment in the early stage of the initiation of bone turnover and how the bone microenvironment changes in response to bone turnover needs to be better understood in order to provide more suitable targets for therapy.

5 TRANSCRIPTOMIC PROFILING OF THE BONE MICROENVIRONMENT COMPARING OVARIECTOMISED AND SHAM OPERATED MICE

5.1 SUMMARY

How the bone microenvironment regulates disseminated breast cancer cells remains an active area of research. Animal models aim to recapitulate the bone microenvironment in various clinical situations by introducing various perturbations to the bone microenvironment in the presence of tumour cells. In particular, modelling the post-menopausal, oestrogen-deprived bone microenvironment involves the excising ovaries of mature (12+ week-old) mice, and in combination with inoculation with tumour cells, provides a window into the dynamic interplay between the cancer cells and bone microenvironment. Published research has demonstrated the link between oestrogen deprivation via ovariectomy and the outgrowth of dormant, disseminated tumour cells in ovariectomised mice compared to sham operated mice. Inhibition of osteoclasts in conjunction with ovariectomy has been shown to prevent this overt outgrowth. However, what early transcriptional events occur within the bone microenvironment to trigger this outgrowth, and whether these changes can be therapeutically targeted outside osteoclast inhibition still remain to be further elucidated. To what extent the ovariectomised mouse bone microenvironment reflects the aged post-menopausal bone microenvironment is a question that also needs further analysis.

I therefore set out to characterise the early transcriptional landscape of the bone microenvironment in mature (14 week-old) mice following ovariectomy by RNA-Sequencing flushed whole bone marrow 14 days following ovariectomy. Selected publicly available datasets were used to assess the similarity between the post-menopausal human bone microenvironment and ovariectomised mouse bone microenvironment.

µCT analysis showed a decrease in bone volume and trabecular thickness in ovariectomised mice compared to sham, at levels consistent with published research of a similar model, indicating cellular and transcriptional changes within the bone. Circulating hematopoietic cells as measured by hematological analysis were largely unaltered by ovariectomy, although there was a trend to decrease red blood cell count, with a corresponding decrease in expression of erythropoietic genes EPB41 and EPB42 as measured by RNA-Seq. Homeostatic mechanisms are thought to have returned circulating cells to baseline by the time of measurement.

Differential expression testing of RNA-Seq data revealed 82 genes were significantly downregulated and 75 significantly upregulated, with altered pathways including ECM-receptor interaction and focal adhesion amongst those upregulated in ovariectomised mice. From a comparative dataset generated by Farr *et al.* (2015), young women were found to also have cell adhesion and extra cellular matrix organisation upregulated relative to older women, with increased angiogenic pathways in addition.

Genes of interest upregulated in ovariectomised mice included THBS1, SPP1, MMP2 and POSTN, soluble proteins secreted into the microenvironment that were upregulated in ovariectomised mice, altered by age in human datasets as well being differentially expressed in bone metastases compared to brain, liver and lung, with SPP1 and THBSP1 contributing to significantly reduced DMFS in large-scale public data.

Scoring gene expression from mice against established cancer dormancy signatures generated by Kim *et al.* (2012) did not reveal any differences between ovariectomised and sham-operated animals, indicating dormancy signatures are difficult to apply to generic populations in a rapidly dividing tissue.

Overall, the ovariectomised bone microenvironment induced transcriptional changes consistent with those found altered by age. However, these changes take on similarities to both old women and young women, thereby supporting the need for caution in extrapolating comparisons of the mouse ovariectomised bone microenvironment with the human post-menopausal bone microenvironment. Further development of models that recapitulate the bone microenvironment in old, post-menopausal women is needed to better represent the clinical situation.

5.2 Introduction

Oestrogen is the most abundant form of the oestrogen family of steroidal hormones found in women and is a major hormonal regulator of bone metabolism. The effects of oestrogen on cells requires the presence and homo- or hetero-dimerisation of two subsets of oestrogen receptors (ER), alpha (ERα) and beta (ERβ). A number of cell types within the bone microenvironment express these receptors including hematopoietic stem cells, osteoclasts and osteoblasts, whose activation leads to various outcomes dependent on cell location and type, quantity and subtype of oestrogen receptor expressed, and nature of ER-dependent promoter regulatory sequences (Manolagas *et al*., 2013, Martin-Millan *et al*., 2010). An example of this differential effect is the extension of osteoblastic-lineage cells by ERβ activation, contrasted to reduction of osteoclast longevity by ERα (Bradford *et al*., 2010, Hughes *et al*., 1996, Martin-Millan *et al*., 2010). The precise mechanisms through which oestrogen influences various cell types within the bone microenvironment is still an area of active research. In particular, the impact of reduced levels of oestrogen on the bone microenvironment and how this may affect disseminated cancer cells, remains to be established and is the focus of the research within this this chapter.

5.2.1 Oestrogen and Bone Turnover

A major role played by oestrogen within the bone microenvironment is that of regulating bone metabolism, primarily through ERα (Sims *et al*., 2003). Clinically, it is well established women past menopause experience dramatic increases in bone loss, frequently leading to conditions such as osteoporosis. Lindsay *et al* demonstrated that metacarpal mineral content loss in oophorectomized women could be completely attenuated by treatment with synthetic oestrogen, demonstrating its central role in the regulation of bone metabolism (Lindsay *et al*., 1976).

Studying the effects of oestrogen-induced bone loss on cancer progression in humans is difficult, as menopausal status in clinical trials is often self-reported, as well as variable definitions of pre-menopause or post-menopause across studies (Wright and Guise, 2014). Modelling ovarian failure in pre-clinical *in vivo* studies eliminates this variability and can be precisely timed in order to capture and rightly attribute early events in microenvironment modification from oestrogen deprivation.

Various studies in mice have detailed an increase in bone loss in response to ovariectomy. One such study, done by Streicher and colleagues, performed selective deletion of ERα or inhibition of RANKL in hematopoietic and mesenchymal cells in 16-week old αERKO and huRANKL-KI mice from a C57BL/6 genetic background. Their results identified suppression of RANKL expression by bone lining cells as a prominent mechanism through which oestrogen protects the bone from degradation, whereas ERα-mediated signalling in hematopoietic cells and RANKL derived from hematopoietic sources in ovariectomised mice did not have an impact on physiological bone turnover (Streicher *et al*., 2017).

5.2.2 Ovariectomy in Dormancy

Ovariectomy-induced reduction of oestrogen has been shown to increase tumour growth in murine models of breast cancer, mediated through changes in the bone microenvironment.

However, its role in inducing dormant, disseminated tumour cells into overt outgrowth was demonstrated by Ottewell and colleagues, who developed a murine model to mimic pre and post-menopausal status in order to study the differential effects of oestrogen deprivation on tumour growth *in vivo*. In their model, they used twelve week old BALB/c-nude female mice that underwent ovariectomy or sham operations for between 1 to 8 weeks prior to assessment of ovariectomy-induced bone effects in the absence of tumour. In addition, another cohort of mice were ovariectomised or had a sham operation performed 7 days prior to inoculation with triple negative breast cancer cells, that are not known to be affected by direct oestrogenic influence, to assess tumour growth driven by changes in the microenvironment in response to oestrogen deprivation (Ottewell *et al*., 2014a). OVX was shown to induce a rapid loss of bone volume and induced the outgrowth of dormant, disseminated tumour cells in the long bones of mice within 4 weeks of procedure, whereas sham-operated animals did not display significant outgrowth. Ottewell *et al*. went on to demonstrate the differential effects of the anti-resorptive agent Zoledronic acid on cancer progression in ovariectomised compared to sham operated mice, which had an effect on mice in the OVX group but not the sham operated group. These experiments showed that the effects of OVX on the outgrowth of DTCs was due to the effects of oestrogen, and that inhibition of osteoclasts attenuated the resulting outgrowth, suggesting a central role of increased osteoclast activity under oestrogen deprivation in influencing tumour outgrowth.

These findings linked their studies to the AZURE trial which found that women who were postmenopausal for at least 5 years prior to entry into the study had a significantly reduced risk of disease-free progression (DFS) and risk of death from any cause (Coleman *et al*., 2014, Ottewell *et al*., 2014a). This differential response to anti-resorptive agents dependent on menopausal status/age was also observed in other trials including NSABP-34 which showed increased DFS in women over 50 receiving clodronate, as well as an increased survival in women over age 40 who received Zoledronic acid therapy in the ABCSG-12 trial (Gnant *et al*., 2011). In follow up studies, Ottewell and colleagues showed that the attenuation of tumour growth in ovariectomised mice can be recapitulated by the use of RANKL-decoy, OPG-Fc, further strengthening the hypothesis that prevention of outgrowth is achieved by inhibition of osteoclast-mediated bone resorption (Ottewell *et al*., 2015). However, the

precise molecular mechanisms underpinning the differential effects of anti-resorptive agents in the pre- vs the post-menopausal setting remain to be established.

5.2.3 Early events and genes affected by Ovariectomy.

Studies assessing the role of oestrogens in tumour progression and outgrowth from dormancy have demonstrated that the attenuation of bone turnover by osteoclast inhibition plays a significant role in reducing morbidity and disease progression. However, the early events played by oestrogen loss in altering the bone microenvironment to adopt a conducive landscape for osteoclast differentiation and increased bone resorption is still unclear. Furthermore, whether these changes induced by rapid and dramatic loss in oestrogen and subsequent increase in bone loss can be translated to menopausal changes in women needs to be further established.

Limited candidate gene expression studies by Ottewell *et al.* showed that a number of genes involved in osteoclast-mediated bone turnover were upregulated in ovariectomised mice compared with sham controls, including MMP2 and SPP1 (Ottewell *et al*., 2014a). However, the use of zoledronic acid in bone metastases has not been successful in completely stopping tumour growth, compared to the early use of Zol in ovariectomised mice. A comprehensive analysis of the transcriptional landscape, comparing the bone microenvironment in OVX vs Sham operated mice, may further elucidate gene regulation may provide a more thorough picture and alternative mechanisms of early events that trigger tumour cell escape from dormancy leading to subsequent tumour outgrowth dictated by the microenvironment.

5.2.4 RNA-Seq profiling of the oestrogen-deprived bone microenvironment

Increased use of gene expression profiling by sequencing has vastly increased the insights into transcriptional alterations within cells and can be utilised to increase our understanding of how loss of oestrogen modifies the bone microenvironment. Furthermore, various computational tools validated by experimental results have been developed to further illuminate gene expression data, such as to detail the cellular landscape based on bulk RNA-Seq deconvolution and identify altered signatures and pathways.

The advent of next-generation sequencing has produced vast amounts of data which are available in public databases for the use of researchers, and provided unparalleled depth of information in regards to genetic coding and gene expression in samples sequenced. These publicly available data are invaluable to modern day researchers as they provide freely usable information and a plethora of methods that can be performed on them.

Of particular relevance to my work, a study performed by Farr, *et al.* (2015) on the Effects on Age and Oestrogen on Skeletal Gene Expression in Humans Assessed by RNA Sequencing, is publicly available for analysis through the Gene Expression Omnibus. In this study, 58 women, 19 young (mean age 30.3 +/- 5.4 years), 19 older women (mean age 73.1 +/- 6.6 years) and 20 old women treated with 3 weeks

of Oestrogen Therapy (mean age 70.5 +/- 5.2 years) had samples from their bone marrow sequenced (Farr *et al*., 2015). In this study, it was found that aging altered a total of 678 genes and 12 pathways, which included a subset characterized in regulation of bone metabolism, such as Notch. Furthermore, the Wnt/β-catenin signaling pathway, with downstream transcription factor *LEF1,* whose binding sites were significantly enriched in the promoter regions of differentially expressed genes, was found to be upregulated in the old versus young women. Supplemental oestrogen in older women for 3 weeks restored 21 unique genes, including *INHBB* (encodes beta B polypeptide inhibin), a gonadal peptide member of the TGF-β super family which was restored to levels seen in young women (Farr *et al*., 2015). This study demonstrated that hormonal-regulated changes in gene expression responsible for bone turnover were among the major changes induced by age, some of which were rescued by short term oestrogen therapy.

The availability of methods to deconvolute bulk expression data to identify the relative abundance of immune and stromal cells, as well as methods to identify pathways, genes, and signatures altered make this a valuable resource to understand the changes that occur with age, and those directly affected by oestrogen. This dataset coincides with research into the effects of ovariectomy (and thus oestrogen loss)-induced increased bone turnover and may provide further insight into bone-turnover induced escape from dormancy of disseminated tumour cells. Thus, combining data from this human study, with RNA-Sequencing data from ovariectomized mice would allow the deconvolution of cell-specific and transcriptome-wide changes that may contribute to tumour escape within the bone microenvironment.

5.3 HYPOTHESIS AND AIMS

The hypothesis underpinning the work in this chapter is that ***ovariectomy in mice induces early transcriptional events that lead to increased bone turnover***, altering the cellular and molecular landscape to recapitulate the clinical setting where oestrogen alters the bone microenvironment according to menopausal status.

The main aims of this chapter are as follows:

1. Establish how the loss of oestrogen drives changes within the bone microenvironment that induces dormant cancer cells into overt outgrowth
2. Determine whether these changes are consistent with those reported in women according to their menopausal status

The main objectives of this chapter are as follows:

1. Develop an optimal method of RNA extraction from bone for RNA-Sequencing purposes
2. Carry out RNA-Seq on samples extracted from ovariectomised and sham operated mice
3. Establish a pipeline for analysis of raw RNA-Seq FASTQ files into file formats to be used in R for differential expression, signature scoring, gene network inferring and bulk deconvolution

4. Use transcriptomic profiling to assess the effects of ovariectomy compared to a sham operation on the bone microenvironment of mature mice
5. Compare the effects of ovariectomy on the bone microenvironment of mature mice with relevant publicly available human datasets

5.4 MATERIALS AND METHODS

Method	Parameters analysed / Purpose	Materials / Equipment / Software
Ovariectomy		
Mice either ovariectomised or undergone a sham operations.	-	-
Bone mineralised content		
Microcomputed tomography (μCT)	-Trabecular bone volume (BV/TV in %) -Trabecular number (TB.N. in mm-1) -Trabecular thickness (Tb.Th. in mm) Trabecular Spacing (in mm)	-SkyScan 1172/1272 scanner (SkyScan) -NRecon software -CTAn software
Circulating Blood Cells		
Hematological Analysis	Circulating erythrocytes, thrombocytes, leukocytes, hemoglobin and all erythrocyte-indices in absolute quantity and relative percentage	Scil Vet abc Plus hematological analyzer (Horiba Medical)
Histological assessment		
Tartrate-resistant acid phosphatase staining (TRAP)	-Osteoclast number per mm of trabecular bone surface -Osteoclast size (in mm)	-OsteoMeasure software (OsteoMetrics) -LeicaDMRB upright microscope
Haematoxylin and Eosin staining (H&E)	-Osteoblast number per mm trabecular bone surface -Osteoblast size (in mm)	-OsteoMeasure software (OsteoMetrics) -Leica DMRB upright microscope -Olympus BX53 microscope
Statistical analysis		
Spearman correlation	Spearman correlation of parameters analysed by hematological analysis	Python 3.7.4 : pandas package version 1.12 and seaborn package version 0.11.0

Unpaired t-tests	Unpaired t-tests of column analyses	Graphpad Prism 9.1.0
RNA extraction		
Hybrid extraction method with pre-cooled equipment	Extraction of high yield, purity and integrity RNA	Trizol RNeasy Mini Kit (Qiagen)
Genomic DNA contamination digestion	Removal of genomic contamination from RNA samples	Lyophilised DNAse (Qiagen) RNeasy Mini Kit (Qiagen)
RNA sequencing		
rRNA depletion	Deplete rRNA prior to sequencing	
Library preparation	Library preparation for RNA-Sequencing	
Sequencing	Single end sequencing at 37.5 million reads per samplDAVIDe	Illumina HiSeq™ 2500
Pre-processing of RNA-Sequencing reads		
Trimming of raw reads	Trim adapter sequences from raw RNA-Seq reads	Cutadapt 3.4 (wrapped through TrimGalore 0.4.1)
Quality assessment of raw reads	Assess quality of raw and trimmed RNA-Seq reads	FastQC (wrapped through TrimGalore 0.4.1) 0.11.7
Alignment of reads	Align the reads to GRCm39 mouse reference genome	STAR Aligner 2.7.8a
Counting of aligned reads	Count reads aligned to reference genome taking into account RNA degradation indexes	DegNorm 0.1.4
Processing of RNA-Sequencing data within the R framework		
Differential expression testing	Quantifying significantly altered genes across conditions	DESeq2 1.30.1
Identification of altered pathways and networks		DAVID 6.8
Signature scoring	Scoring samples for selected signatures using gene counts	Singscore 1.10.0
Deconvolution of Bulk RNA-Seq	Quantifying stromal and immune cellular populations from bulk sequencing data	xCell 1.1.0

5.4.1 ANIMALS

Twelve-week-old female Bagg and Albino (BALB)/c (immunocompetent) mice were purchased from Charles River, UK. Upon arrival, mice were acclimatised in the Biological Services Unite (BSU) for 14 days before procedures beginning when the mice were aged 14 weeks old.

All procedures performed were approved and carried out under Procedure Project Licence (PPL) PPL P99922A2E within the Biological Services Unit (BSU) under local guidelines and in accordance with Home Office regulations.

5.4.2 OVARIECTOMY

Mice were randomised into two groups to undergo either an ovariectomy or a sham control (whereby identical surgical procedures to ovariectomy were followed, with the exception of the removal of ovaries) as described in detail in section 2.3.4.12.3.4 of the materials and methods section. This would ensure any experimental differences observed would be due to the loss of ovaries and not due to systemic effects of surgical procedures. The surgery was carried out by Dr Penelope Ottewell, Mrs. Diane Lefley under the project license (PPL P99922A2E).

5.4.3 *EX VIVO* ANALYSIS

5.4.3.1 HEMATOLOGICAL ANALYSIS

Upon culling, mice had their blood withdrawn through cardiac puncture, of which 20µl was placed into 500µl Eppendorf tubes containing 20µl of EDTA to prevent clotting, thoroughly mixed and stored at room temperature for up to 2 hours post-cull. These samples (10µl per sample) were then run through a Scil Vet abc Plus hematological analyzer (Horiba Medical) which measured the following as % and number per $10^3/mm^3$ blood; total white blood cells, total red blood cells, the following as % and number per $10^3/mm^3$ blood; lymphocytes, monocytes, granulocytes, hematocrit (percentage), mean corpuscular volume (μm^3), mean corpuscular hemoglobin (pg), mean corpuscular hemoglobin concentration (g/dL), red blood cell distribution width (percentage), platelets (number per $10^3/mm^3$ blood) and mean platelet volume (μm^3).

5.4.3.2 PREPARATION OF SAMPLES FOR HISTOLOGY AND BONE HISTOMORPHOMETRY

Immediately following dissection, tibias that were used for histology and histomorphometry were placed in 4% (*w/v)* paraformaldehyde (PFA) for 48-72 hours. These were then washed 3 times in ice-cold PBS and stored in PBS at 4°C pending µCT analysis. Once µCT scanning was complete, bones were placed in a PBS 14% (*w/v*) ethylenediaminetetraacetic acid (EDTA) solution for decalcification. This solution was changed twice a week for 3 weeks before bone processing. Bones were subsequently paraffin-embedded (wax). To obtain sections for histological analysis, wax embedded tibias were cut at 3µm thickness, and 6 samples taken from 3 levels, 20-30µm apart before mounting on glass slides and stored at room temperature.

5.4.3.3 MICROCOMPUTED TOMOGRAPHY

Micro-computed tomography (µCT) performed on bones was performed in three steps; scanning, reconstruction and analysis. Scanning involves the projection of x-rays through a sample onto a detection plate to create an image representing mineralised bone. The sample is then partially rotated through a selected rotation range with smaller rotation steps with an x-ray-generated image created at each rotation step. The collection of images is subsequently collated and reconstructed to produce 3D images. Finally, 3D images are analysed to produce quantitative data on various bone physical parameters.

5.4.4 EXTRACTING MATERIAL FOR RNA SEQUENCING

Femurs of mice were dissociated by being placed in Trizol and spun in a bead mill for 60 seconds, according to the bead mill protocol in section 2.7.2.4 and RNA extracted using the Hybrid method as detailed in section 2.7.3.1. Genomic contamination was then removed as detailed in section 2.7.3.1, before RNA quality was assessed using Nanodrop as detailed in 2.7.2.9. Eight of the highest quality RNA samples were then delivered to Dr Timothy Wright at the Sheffield Diagnostic Genetics Service of the Sheffield Children's NHS Foundation Trust on dry ice.

The sequencing of raw reads was subsequently performed by Dr Timothy Wright at the Sheffield Diagnostic Genetics Service. Eight samples, consisting of four samples per group (OVX n=4, Sham n=4) were prepared for sequencing using the NEBNext rRNA depletion kit protocol. Sequencing was performed using an Illumina Hiseq Rapid 100bp single read flow cell providing 300 million reads, with samples sequenced at 37.5 million reads per sample.

5.4.5 PRE-PROCESSING OF RAW RNA-SEQUENCING READS

Raw reads from sequencing were provided by amazon web services (AWS) S3 cloud storage as raw FASTQ files (n=8). These files were subsequently downloaded onto personal researcher storage on the Sheffield Advanced Research Computer (ShARC) high performance computing (HPC) cluster under user storage ready for pre-processing.

5.4.5.1 QUALITY ASSESSMENT OF SEQUENCING READS

Prior to pre-processing, adequate read quality was measured using TrimGalore, which is a wrapper around FastQC and Cutadapt, tools for quality checking and trimming respectively. FastQC is a tool designed to assess the quality of raw reads from a variety of sequencer, including the Illumina HiSeq™ 2500 used for these samples. FastQC is a java-based programme that can be used through the command line to assess quality metrics such as per base sequence quality, per tile sequence quality, per sequence quality scores, per base sequence content, per sequence GC content, per base N content, sequence length distribution, sequence duplication levels, overrepresented sequences, adapter content and kmer content. FastQC version 0.11.7 was used to assess the quality of the reads.

In addition to FastQC, MultiQC was used to produce summarised reports representing all samples, showing an overview of sequencing quality. MultiQC version 1.9 was used to aggregate sample quality metrics into a single html file for viewing.

5.4.5.2 TRIMMING OF ADAPTER SEQUENCES AND LOW-QUALITY READS

During library preparation, adapters were ligated to sample RNA. These, as well as primers, needed to be removed prior to aligning to the reference genome. TrimGalore version 0.6.6 was used to concurrently trim reads and provide quality metrics.

5.4.5.3 ALIGNMENT OF READS TO REFERENCE GENOME

To align RNA-Seq reads to a reference genome prior to quantification, the commonly used alignment tool Spliced Transcripts Alignment to a Reference (STAR), which uses sequential maximum mappable seed search in uncompressed suffix arrays followed by a seed clustering and stitching procedure, was used.

STAR version 2.7.8a was initially used to index a reference genome, the gencode release M27 (GRCm39) using the comprehensive gene annotation Gene Transfer File (GTF) format which is the main annotation file for most users. This was used with the transcript sequences FASTA file containing the nucleotide sequences of all transcripts on the reference chromosomes to index a reference genome using the genomeGenerate function of STAR with a transcript overhang of 100, as a read length minus 1 is suggested for most cases whereby the transcripts used had 101 bases per read.

Following the generation of an indexed genome, trimmed sample FASTQ files were aligned to the genome using STAR with BAM SortedByCoordinate specified in the outSAMtype argument to generate sorted Binary Sequence Alignment Map (SAM) (BAM) files for the samples. These sorted BAM files would subsequently be used in the quantification step by a quantification tool.

5.4.5.4 QUANTIFICATION OF ALIGNED READS

The quality of RNA sequencing results is affected by RNA degradation, and is a significant factor that may bias the results from RNA-Seq analysis. As the samples sequenced had RIN scores of <7, leading to the rRNA sequencing protocol being used, degradation would potentially be a source of bias in transcript abundance estimation. In order to reduce the bias and variability present due to degradation, DegNorm, a pipeline which adjusts read counts for transcript degradation on a gene-by-gene basis, while controlling for sequencing depth was used to quantify the aligned and sorted sample BAM files. Degnorm version 0.1.4 was used in conjunction with the gencode release M27 GTF annotation file to quantify BAM files, with 100 for the -nmf-iter argument resulting in 100 iterations per non-negative matrix factorisation (NMF) over-approximation (OA) algorithm approximations.

The output from quantification by DegNorm was a comma separated values (csv) file containing adjusted read counts. These adjusted read counts, adjusted for transcript degradation, were then used in subsequent downstream analyses.

5.4.6 Analysis of Differentially expressed genes

Analyses downstream from obtaining adjusted read counts were performed in R version 4.0.4 (2021-02-15) through R Studio version 1.4.1106 unless otherwise stated.

To obtain differentially expressed genes, the adjusted read counts in csv file types obtained as an output from DegNorm counting were loaded into R studio, along with a file containing experimental metadata for each sample.

Differential gene expression was next performed. Differential gene expression is often performed using three main packages in the R/Bioconductor language and package ecosystem; limma, edgeR and DESeq2 (Dillies *et al*., 2013, Liu *et al*., 2021, Ritchie *et al*., 2015). DESeq2 and edgeR both use the negative binomial distribution, and perform geometric and a weighted mean of log ratios-based normalisation methods respectively, both initially assuming no genes are differentially expressed (Love *et al*., 2014, Robinson *et al*., 2010). In contrast limma uses a linear model to calculate gene expression statistics, using quantile normalisation to attempt the matching of gene count distributions across samples in the dataset (Ritchie *et al*., 2015). While DESeq2 and edgeR are frequently used in RNA-seq analysis, limma is more commonly used for microarray analysis (Liu *et al*., 2021). Schurch, *et al.* (2016) showed that when fewer than 12 replicates are used, edgeR and DESeq2 have a superior combination of increasing true positive and reducing false positive performance, whereas DESeq2 marginally outperforms the other tools when minimising the false positives are more important with more replicates (Schurch *et al*., 2016). Due to superior performance across these metrics, as well as ease of use, DESeq2 was selected as the most optimal tool to perform differential gene expression, though edgeR could have also been used.

Using the DESeq2 package version 1.30.1, the two files were combined into a DESeq DataSet object using the DESeqDataSetFromMatrix function, using the counts file with rounded integers as values as the countData argument, using the metadata file as the colData argument and the experimental condition (OVX or Sham) as the design argument in the function. The DESeq DataSet object was then used to create a new object with the function estimateSizeFactors in order to assess various quality control metrics, such as clustering and principal component analysis after a variance stabilising transform (VST). The original DESeq DataSet object was then finally used to obtain differentially expressed genes by the function DESeq performed on the expression and group data contained in the object.

5.4.6.1 Power analysis

Statistical power refers to the probability that a hypothesis test leads to the correct rejection of the null hypothesis when a specific alternative hypothesis is true, and is influenced by significance

criterion, magnitude of effect and sample size of the statistical test (Lenth, 2007). In RNA sequencing experiments, it is common to run simulations with representative data to analyse the statistical power of an experiment given number of genes tested, sample size and significance criterion (Yu *et al*., 2017).

To perform power analysis for RNA-seq, PROspective Power Evaluation for RNAseq (PROPER) Bioconductor package version 1.30.0 was used. Briefly, PROPER runs simulations on finding differentially expressed genes in an RNA seq, with the option to select a dataset of choice to more-accurately reflect experimental conditions being modelled (Wu *et al*., 2015).

Simulations were performed on the Bottomly (2011) dataset which consists of consisting of 11 replicates of striatal tissue from DBA/2J mice, and 10 replicates of striatal tissue from C57BL/6J mice (Bottomly *et al*., 2011). This dataset is representative of the ovariectomy and sham dataset and therefore would be used instead of data from human RNA-seq samples as there is less dispersion in gene expression with inbred mice compared to unrelated human individuals, and this dataset would be more representative of the data it is modelling. To model the experimental conditions, a dataset consisting of 28,000 was selected with 20 repeat simulations with a log2 fold change greater than 0.5. Furthermore, false discovery rates (FDR) of 0.05 and 0.1 were explored as well as 3, 4,8 and 12 samples per group to assess the effect of altering the significance threshold as well as sample number on statistical power.

5.4.7 Deconvolution of Bulk RNA sequencing reads

To obtain an estimation of cellular populations within the microenvironment of sequenced samples, bulk deconvolution was performed whereby cellular populations could be inferred by relative abundances of transcripts associated with cell-type signatures. For this, the xCell, a computational gene signature-based method employing a curve fitting approach for linear comparison of cell types and single sample gene set enrichment analysis (ssGSEA) was used. xCell provide a reference signature dataset for 64 immune and stromal types harmonised from 1822 human transcriptomes, validated by *in silico* analyses and cytometry immunophenotyping comparison consisting of the following cells; Adipocytes, Astrocytes, B-cells, Basophils, CD4+ T-cells, CD4+ Tcm, CD4+ Tem, CD4+ memory T-cells, CD4+ naive T-cells, CD8+ T-cells, CD8+ Tcm, CD8+ Tem, CD8+ naive T-cells, common lymphoid progenitors (CLP), common myeloid progenitors (CMP), Chondrocytes, Class-switched memory B-cells, dendritic cells (DC), Endothelial cells, Eosinophils, Epithelial cells, Erythrocytes, Fibroblasts, granulocyte-monocyte progenitor (GMP), HSC, Hepatocytes, Keratinocytes, Megakaryocyte–erythroid progenitor cell (MEP), Multi-Potent Progenitor (MPP), mesenchymal stem cells (MSC), Macrophages (total, M1 and M2 polarised), Mast cells, Megakaryocytes, Melanocytes, Memory B-cells, Mesangial cells, Monocytes, Myocytes, NK cells, natural killer T cells (NKT), Neuronal cells, Neutrophils, Osteoblasts, Pericytes, Plasma cells, Platelets, Preadipocytes, Sebocytes, Skeletal muscle, Smooth muscle, Gamma Delta T cells (Tgd), Th1 cells, Th2 cells, Tregs, activated dendritic cells (aDC), classical dendritic cells (cDC), interstitial dendritic cells (iDC), Endothelial cells, Endothelial cells, naive B-cells plasmacytoid dendritic cells (pDC) and pro B-cells.

As xCell uses human gene references for inference of cell types, samples from the mouse reference genome were converted to human orthologs using the biomaRt package version 2.46.3 and the ensembl mart within the getLDS function, successfully mapping 17,484 genes from mouse to human. These were retained and used in xCell within the xCellAnalysis function of the xCell package version 1.1.0. The output from this is a matrix consisting of samples in columns and estimated cell types in rows with their relative fraction compared between samples.

5.4.8 Signature Scoring of RNA-Sequencing reads

To assess dormancy signatures, a tool or method allowing for the supplying of a custom set of genes was required. Singscore is a rank-based single sample scoring method that scores the expression activities of specified gene sets at a single-sample level. Singscore version 1.10 was used, and as an input, genes mapped to human orthologs from the deconvolution step were used. Prior to scoring samples, the dataset was ranked using the rankGenes function which returns a rank matrix. This matrix was then supplied to the simpleScore function, with a list of upregulated genes as the upSet argument and a list of genes downregulated genes in the downSet argument, where upregulated and downregulated genes are genes altered in the signature of interested for the samples to be scored by. This returns a dataframe consisting of the scores and dispersion for the upregulated genes in isolation, the downregulated genes in isolation and the total score of both the upregulated and downregulated genes combined. These are then visualised to show dispersion and scores.

5.4.9 Identifying gene ontology terms

To identify altered terms according to gene ontology, the Database for Annotation, Visualization and Integrated Discovery (DAVID) v6.8 was used. Lists of up-regulated and down-regulated genes were uploaded into the Gene List Manager on the DAVID website (https://david.ncifcrf.gov/tools.jsp), whereby they were scored against DAVID's databases functional annotation by the Functional Annotation Tool. Gene Ontology (GO) and Kyoto Encyclopaedia of Genes and Genomes (KEGG) Pathways were used to derive altered terms and pathways, with associated FDR values and genes involved in the specified pathways.

5.5 Results

5.5.1 Developing a method for isolation of high-quality RNA from snap-frozen bone for RNA sequencing

Prior to RNA-Sequencing, high quality RNA material needed to be extracted from the bone tissue, as assessed by a high RNA Integrity Number (RIN) which measures the degradation index of RNA as compared to ribosomal 28s and 60s subunit RNA. A score of 10 is the highest measure undegraded, intact RNA, whereas a score of 1 is completely fragmented RNA. For RNA sequencing by polyA enrichment workflow, an RNA integrity score of > 7 is recommended for Illumina sequencers, whereas RNA showing a lower degradation score require an rRNA-depletion workflow.

Bone contains a large amount of platelets, adipose tissue, collagen and minerals that make it a particularly challenging tissue to extract high integrity RNA from. Prior efforts in our lab did not yield RNA integrity above RIN 4 despite being able to produce high RNA yields and purity. I therefore needed to optimise a method that would yield RNA of higher quality for sequencing. The outline of this processes is shown in Figure 5-1.

Figure 5-1: An outline of methods and steps taking to extract RNA from bone with an improved yield, purity and integrity for the purpose of RNA-Sequencing.

The first step was to carry out RNA extraction using the Trizol method, which yielded high concentrations of RNA, but low purity and integrity (see Figure 5-2).

Subsequently, the RNeasy kit was purchased and RNA-extracted using the manufacturer's protocol. However, this yielded poor results and lysis failed to occur adequately for these samples using the manufacturer's lysis buffer, and the results were very poor yields for the material expected in bone.

Following poor results from the RNeasy method, I attempted lysing with TRI reagent instead of RLT buffer and following subsequent steps using the RNeasy protocol. This hybrid method started yielding better results, yet the RIN scores were poor. To troubleshoot this, I first pre-cooled all the tubes to ensure any residual RNase activity was slowed down, and the results increased (see Figure 5-2).

However, results were still variable, though improved. Subsequently, I tested different methods of RNA dissociation to identify whether lysis steps were causing fragmentation, and found using ceramic beads for 60 seconds at speed 3 was optimal (see Figure 5-2)

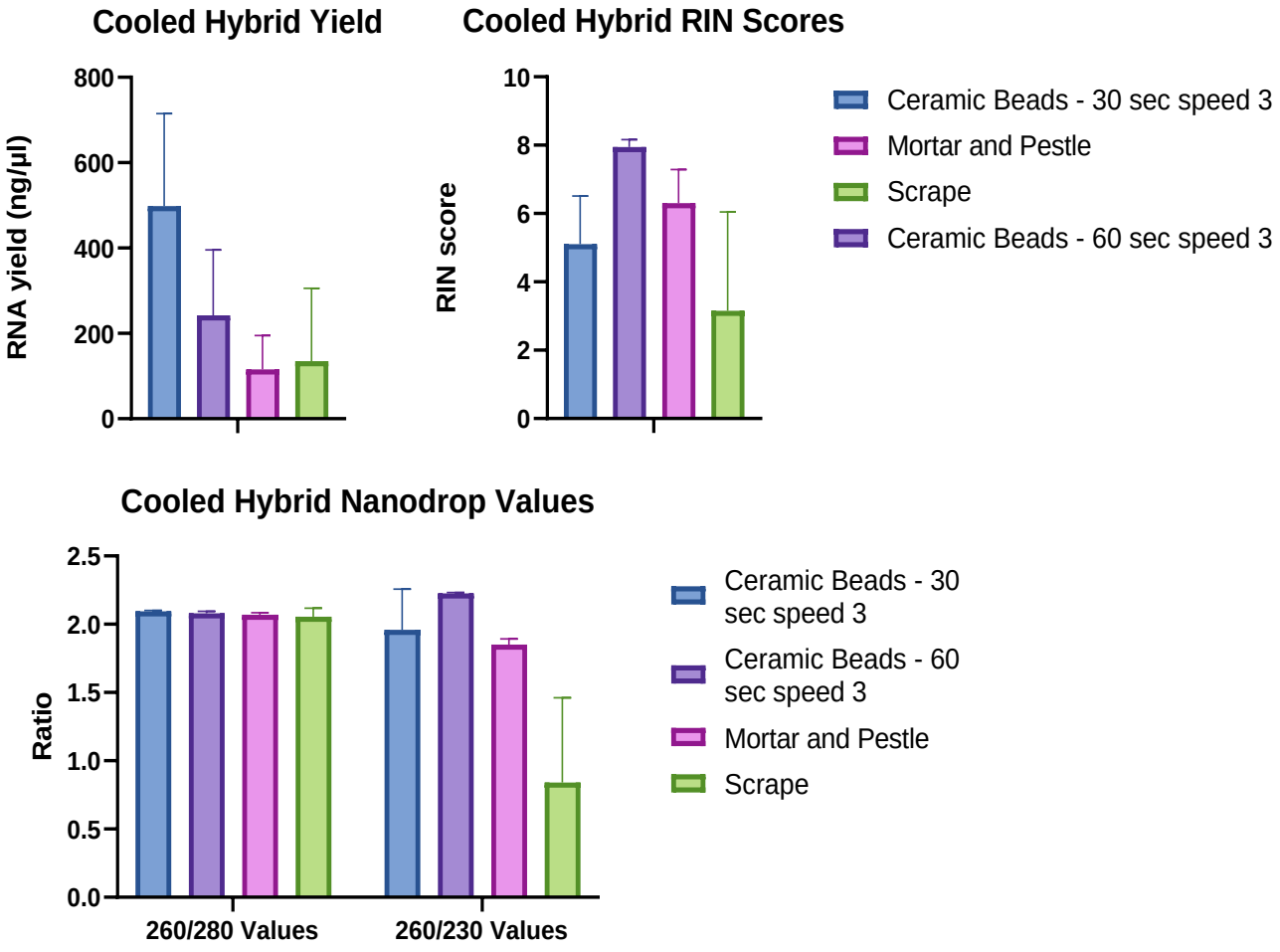

Figure 5-2: Different dissociation methods and their impact on yield, nanodrop values (purity) and RIN scores (integrity).

I therefore used the cooled hybrid method, with a dissociation method of ceramic beads at speed 3 for 60 seconds during subsequent RNA extraction from snap frozen femurs isolated from OVX or sham operated mice.

5.5.2 Experimental overview

To assess the effect of ovariectomy on the early events within the bone microenvironment that could trigger the overt outgrowth of disseminated, dormant tumour cells, 14-week immunocompetent BALB/C mice (n=12) were randomised into two groups of n=6 to receive either a OVX or a sham operation as control for 14 days (see Figure 5-3). Following 14 days under procedure, mice were culled and had both femurs snap frozen in liquid nitrogen for RNA extraction for the purpose of transcriptomic profiling by RNA-Seq. Both tibias were fixed in PFA for 48 hours before performing µCT analysis, and then being decalcified and embedded in paraffin wax for histology. Blood was extracted

from the mice for haematological analysis and serum extracted for analysis of systemic soluble proteins.

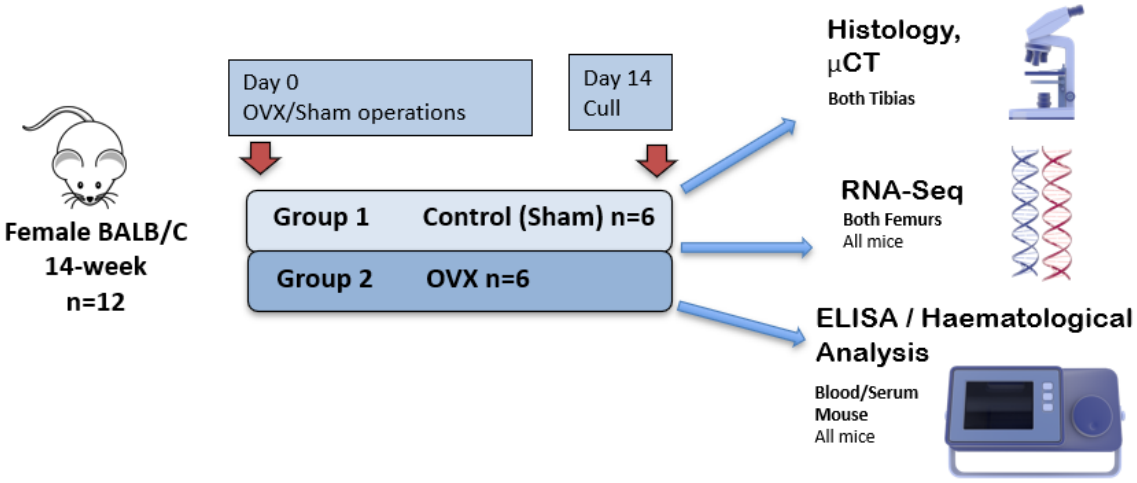

Figure 5-3: Experimental outline. On day 0, animals were randomised to undergo either a sham control (n=6) operation or ovariectomy (n=6) and subsequently culled on day 14 when tissues were collected for downstream processing.

5.5.3 Assessing the effects of ovariectomy-induced bone resorption

Oestrogen is a potent modulator of the bone microenvironment. Several decades ago, Fuller Albright observed an association between oestrogen deficiency and bone loss and osteoporosis (Albright *et al.*, 1946). Lindsay *et al.* solidified this role for oestrogen by completely preventing the loss of metacarpal calcium mineral content over 5 years in oophorectomized women treated with a synthetic oestrogen mestranol compared to sustained loss by those without this supplemental oestrogen (Albright *et al.*, 1946, Khosla *et al.*, 2011, Lindsay *et al.*, 1976). Since then, the role of oestrogen in bone loss has now been established by significant basic and clinical research (Khosla *et al.*, 2012). One mechanism through which, oestrogen affects the bone is through inducing the secretion of OPG, subsequently sequestering soluble RANKL and leading to reduced osteoclastogenesis. Deprivation of oestrogen would lead to reduced OPG secretion, increased osteoclast formation and activity, resulting in bone loss. I therefore set out to establish the effect of oestrogen deprivation by OVX on the trabecular region of the tibias of mice that had undergone OVX procedure compared to those that undergone a sham operation.

As trabecular bone has a higher rate of turnover than cortical bone, effects of OVX would be most pronounced in trabecular bone, especially within the relatively short time frame under this experiment of 14 days, and analyses were therefore focussed on this area. As the mice were mature (age 14 weeks at the time of procedure), a relatively low rate of bone turnover and bone mineral constancy was assumed. Decreased oestrogen resulting in increased osteoclast activity would

therefore lead to decreased trabecular bone and be a reliable indicator that sufficient effect on the bone microenvironment had occurred to affect bone structure. To establish this, µCT analysis was performed on the trabecular region of one tibia from all mice (n=10) (see Figure 5-4).

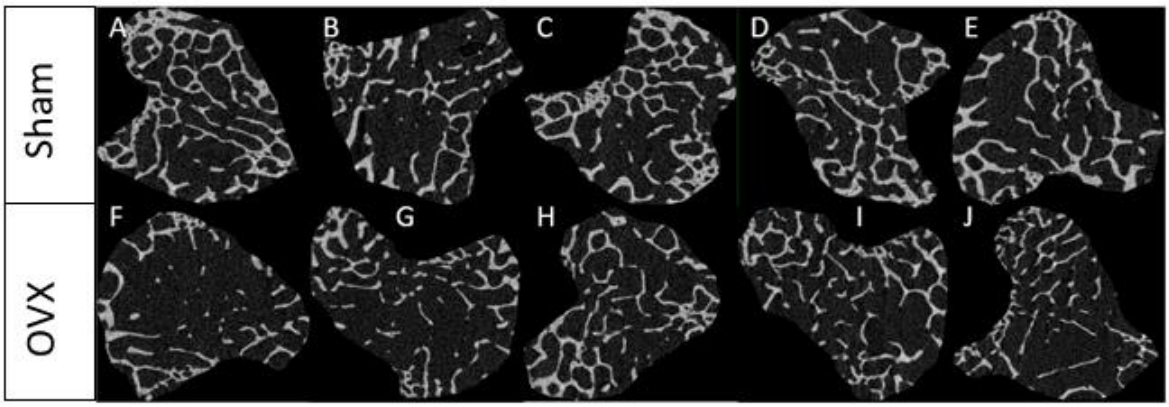

Figure 5-4: Example first µCT scanning region of interest of trabecular cross sections of proximal tibia from 5 different mice from the Sham (A-E) and OVX (F-J) groups.

As shown in Figure 5-5 percentage bone volume and trabecular thickness were significantly decreased in OVX-operated mice compared to sham-operated controls. Trabecular number also decreased, although not significantly, a p value of 0.0720 is close to significance. Thus a longer gap between OVX and subsequent culling may have resulted in significant changes as alterations to the physical bone takes place over a period of time.

In contrast, trabecular spacing was unchanged between groups. As osteoclasts are responsible for bone resorption, increased osteoclast activity would result in a decrease in trabecular bone, but an unchanged trabecular spacing suggests distances between the trabeculae are unchanged, possibly due to incomplete degradation of individual trabeculae. These results show that OVX had a significant effect on osteoclast activity as shown by a decrease in trabecular bone.

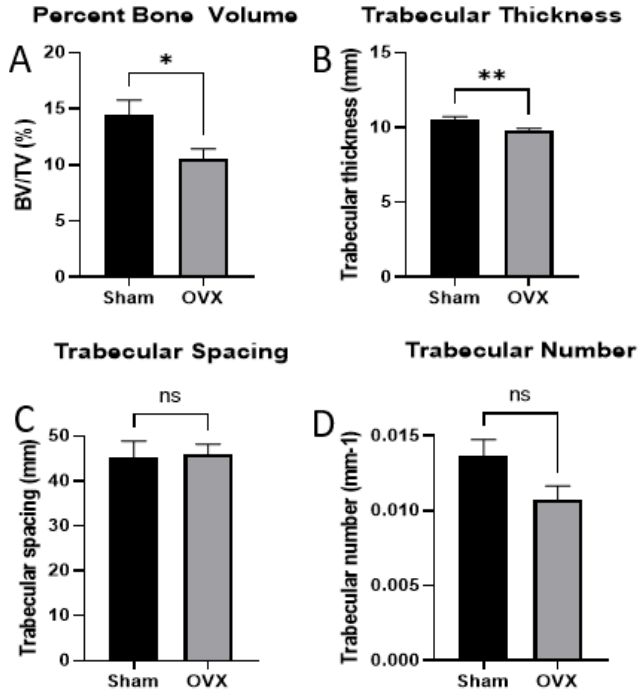

Parameter	Sham mean	OVX mean	Difference between means ± SEM	P-value
BV/TV(%)	14.49	10.55	3.934 ± 1.555	0.0353
Trabecular Thickness (mm)	10.56	9.841	0.7173 ± 0.209	0.0090
Trabecular Spacing (mm)	45.37	45.96	0.5949 ± 4.228	0.8916
Trabecular number (mm-1)	0.01367	0.01074	0.002932 ± 0.001415	0.0720

Figure 5-5: Effects of OVX on bone structure and integrity. Quantification of A.) trabecular bone volume (BV) per tissue Volume (TV) (BV/TV%), B.) Trabecular Thickness, C.) Trabecular Separation and D.) Trabecular Number for animals (n=8) that underwent sham or ovariectomy procedures (n=4/group). Unpaired two-tailed t-test with Welch's correction performed for significance. * indicates a p-value < 0.05, ** < 0.01

5.5.4 Assessing the effects of ovariectomy-induced oestrogen deprivation on circulating hematopoietic cells

Major alterations in the bone microenvironment by oestrogen deprivation by OVX may impact hematopoietic populations due to the regulation of the endosteal and vascular niches by bone turnover and direct effects of oestrogen. As oestrogen can affect a variety of cells in the hematopoietic lineage in mammalian organisms, such as leading to increased HSC self-renewal, or oestrogen deficiency resulting in dysfunctional haematopoiesis, I sought to characterise whether such changes may be evident in the circulating population (Nakada *et al.*, 2014, Qiu *et al.*, 2012).

To characterise the effects of OVX on circulating hematopoietic cells, analysis was carried out on 10µl of blood diluted 1:1 in EDTA from all mice (n=11) measuring total white blood cells, total red blood cells, lymphocytes, monocytes, granulocytes and eosinophils.

As shown in Figure 5-6, OVX did not cause significant changes to circulating hematopoietic cell populations compared to a sham operation. Significance was calculated using t-test via GraphPad Prism version 9.1. These yielded non-significant results and the group averages did not show an overall trend in any direction. However, red blood cell count had a trend to decrease in the OVX group, as can be seen with a p-value close to significance of 0.0879, suggesting OVX had a minor effect on red blood cell count. Eosinophils also showed a marginal trend, although not as strong as the change in red blood cell count, with a p-value of 0.3145.

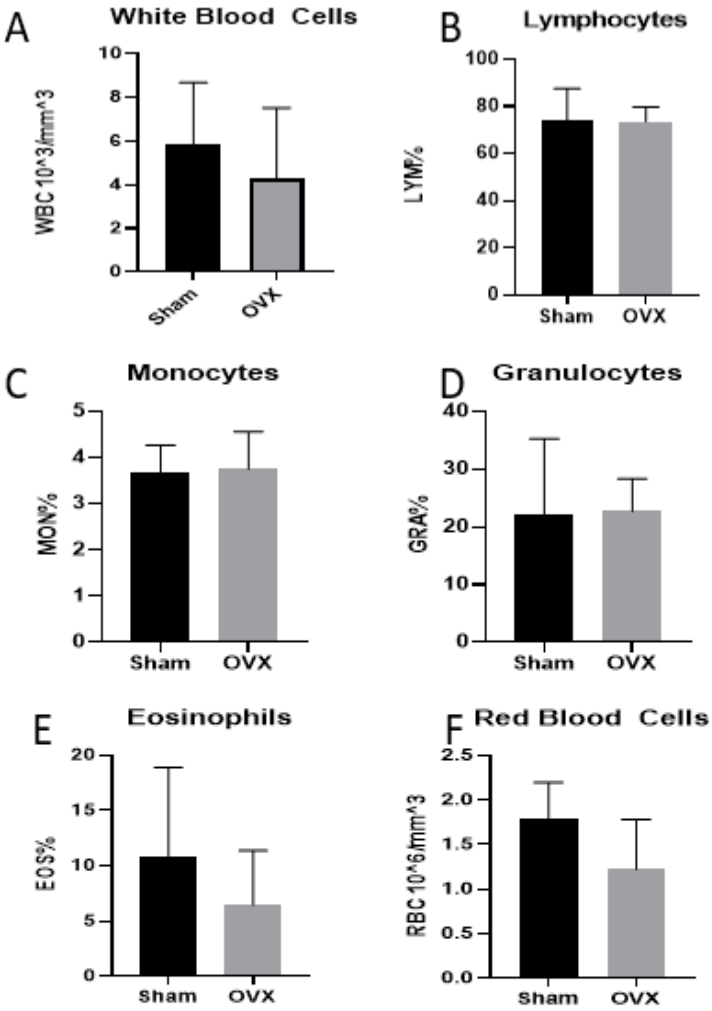

Parameter	Sham mean	OVX mean	Difference between means ± SEM	P-value
WBC 10^3/mm^3	5.833	4.300	1.533 ± 1.831	0.4240
LYM %	74.03	73.50	0.5333 ± 6.583	0.9372
MON %	3.683	3.760	0.07667 ± 0.4224	0.8600
GRA %	22.28	22.74	0.4567 ± 6.314	0.9439
EOS %	10.87	10.87	4.387 ± 4.118	0.3145
RBC 10^6/mm^3	1.783	1.222	0.5613 ± 0.2933	0.0879

Figure 5-6: The effects of OVX on circulating hematopoietic cells A.) White blood cells, B.) Lymphocytes, C.) Monocytes, D.) Granulocytes, E.) Eosinophils, F.) Red blood cells from animals (n=8) that underwent sham or ovariectomy procedures (n=4/group). Unpaired two-tailed t-test with Welch's correction performed for significance. No values found significant

To visualise correlations between the operation and effects on measured parameters from circulating

hematopoietic cells, a correlation plot using pandas and seaborn within python were used. To obtain a correlation with operation, treatments had to be converted into numerical encoding; 1 for OVX-intervention and 0 for Sham-intervention. As such, positive correlation with intervention indicates an increase with ovariectomy, and a negative correlation indicates a decrease in the parameter with OVX-operated animals (see Figure 5-7). A correlation close to 0 indicates no strong trend to either increase or decrease with either sham or OVX.

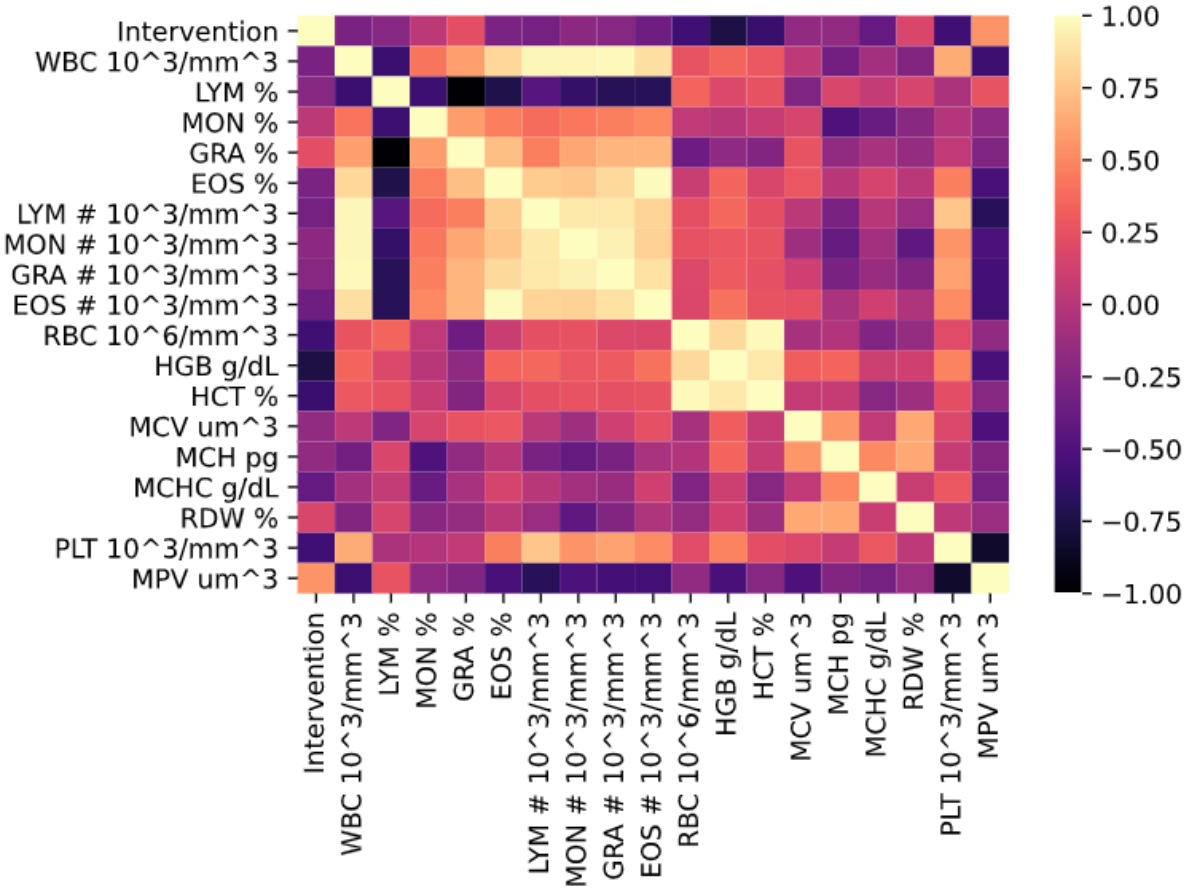

Figure 5-7: Spearman correlation of Hematological parameters measured following ovariectomy or sham operation. Intervention refers to surgical procedure applied to mice converted into binary digits (0 for sham, 1 for ovariectomy) to allow numerical correlation with other features in the data.

5.6 PRE-PROCESSING OF RNA SEQ DATA

To assess transcriptomic changes in the early stage of OVX-induced bone turnover, whole femur marrow samples from 11 mice were extracted using a hybrid extraction technique involving pre-chilling materials and using Qiagen's RNeasy kit once tissues were homogenised in a Bead Mill 4 (Thermo Fisher) for 60 seconds, in Trizol to achieve lysing of cells. The RNA extracted from the samples was dissolved in molecular biology-grade water and delivered to Dr Timothy Wright at the Sheffield Diagnostic Genetics Service of the Sheffield Children's NHS Foundation Trust in dry ice.

The sequencing of raw reads was subsequently performed by Dr Timothy Wright at the Sheffield Diagnostic Genetics Service. Eight samples, consisting of four samples per group (OVX n=4, Sham n=4) were prepared for sequencing using the NEBNext rRNA depletion kit protocol. Sequencing was performed using an Illumina Hiseq Rapid 100bp single read flow cell providing 300 million reads, with samples sequenced at 37.5 million reads per sample.

Sequenced reads in the standard format of FASTQ were then hosted on Amazon Web Services (AWS) S3 storage facilities before being downloaded into storage on the University of Sheffield's HPC Sheffield Advanced Research Computer (ShARC) cluster ready for pre-processing.

5.6.1 PRE-PROCESSING OF RAW RNA-SEQUENCING READS

Prior to differential expression and other downstream analysis, raw reads must be assessed for quality, have adapters trimmed, aligned to the genome and aligned reads be counted before obtaining a final count file to be used for downstream analysis, performed in a HPC cluster due to processing and memory requirements. Pre-processing started with raw FASTQ files, containing multiple sequence reads 100 base pairs long, with information regarding base sequence, base quality scores and flow cell location for the reads. These reads were then aligned to mouse reference genome GRCm39 using STAR, producing aligned and sorted BAM files. These were then subsequently quantified using DegNorm, which accounts for degraded transcripts in its counting algorithm. The output from this was the adjusted read counts file, a comma-separated value (CSV) file, containing an expression matrix consisting of samples as columns, genes as rows with their estimated count per transcript. This CSV file could then be used in the R programming language for further downstream analysis, such as differential expression testing leading to gene ontology and pathway analysis.

Figure 5-8 outlines the pre-processing steps taken to pre-process the raw files into the final count files

Figure 5-8: Workflow for RNA-Sequencing pre-processing. Briefly, raw reads are obtained from the sequencing facility and transferred to a high-performance computing environment. These raw reads are subsequently checked for quality, trimmed and quality reassessed post-trimming, before being aligned to a reference genome and subsequently quantification of aligned reads leads to a counts file output that is used in assessment of differential gene expression and further downstream processing.

5.6.2 Quality Assessment and Trimming of Raw Reads

To assess the quality of the raw reads, TrimGalore, developed by Babraham Bioinformatics was used (https://www.bioinformatics.babraham.ac.uk/projects/fastqc/). TrimGalore is a wrapper around frequently used tools FastQC (quality assessment) and Cutadapt (trimming) (Martin, 2011) with html reports as outputs for each sample. Following the trimming of reads, multiQC, a tool that summarises multiple fastQC reports into a single, summarised report was used to summarise the quality reports (Ewels *et al.*, 2016). The FastQC tool assesses basic statistics, per base sequence quality, per tile sequence quality, per base sequence content, per base GC content, per base N content, sequence length distribution, sequence duplication, overrepresented sequences and adapter content.

Table 5-1: Metrics covered by FastQC processing and their description

Measurement	Description	Importance/Cut off
Basic statistics	The summary of percentage duplications, percentage duplication and total sequences per sample.	Importance: Medium
Per base sequence quality	The mean quality value across each base position in the read across the sample, meant as a measure of the base calling quality for each base position within a read.	Importance: High **Cut off:** Lower quartile for any base < 10, median < 20
Per tile sequence quality	The average quality scores from each tile across all bases along parts of the flow cell to see if a loss of quality was associated with a part of the flow cell.	**Importance**: High but reduces towards end of read **Cut off:** Most frequently observed mean quality < 20
Per base sequence content	The proportion of each base position for which each of the four normal DNA bases has been called, which gives an overview as to which position in the read may have a bias for certain bases.	Importance: Low **Cut off:** Difference between A/T and G/C at any position is > 10%
Per base GC content	The distribution of percentage GC content of reads.	Importance: Medium **Cut off:** GC content of any base > 10% from the mean
Per base N content	The percentage of bases calls at each position for which the base caller could not identify a base with sufficient confidence.	Importance: Low **Cut off:** Any position shows N content of > 20%
Sequence length distribution	The distribution of fragment sizes (read lengths) sequenced.	Importance: Low **Cut off:** Sequences have zero length
Sequence duplication levels	The relative level of duplication found for every sequence.	Importance: Low

		Cut off: Non-unique sequences > 50% of total
Overrepresented sequences	The total amount of overrepresented sequences found in the sample library.	Importance: Low **Cut off:** Any sequence represents >1% of total
Adapter content	The cumulative percentage count of the proportion of the library which has seen each of the adapter sequences at each position.	Importance: Low **Cut off:** Any k-mer enriched more than 10 fold at any individual base position

MultiQC reports for the sequencing data showed normal results for base statistics, per base sequence quality, per tile sequence quality and adapter content for all samples, showing good sequencing quality and successful adapter trimming (see Figure 5-9). However, per base sequence content, per base N content and sequence duplication all showed very unusual results for all samples, and per sequence GC content, sequence length distribution and overrepresented sequences showed a mix of slightly unusual and very unusual results.

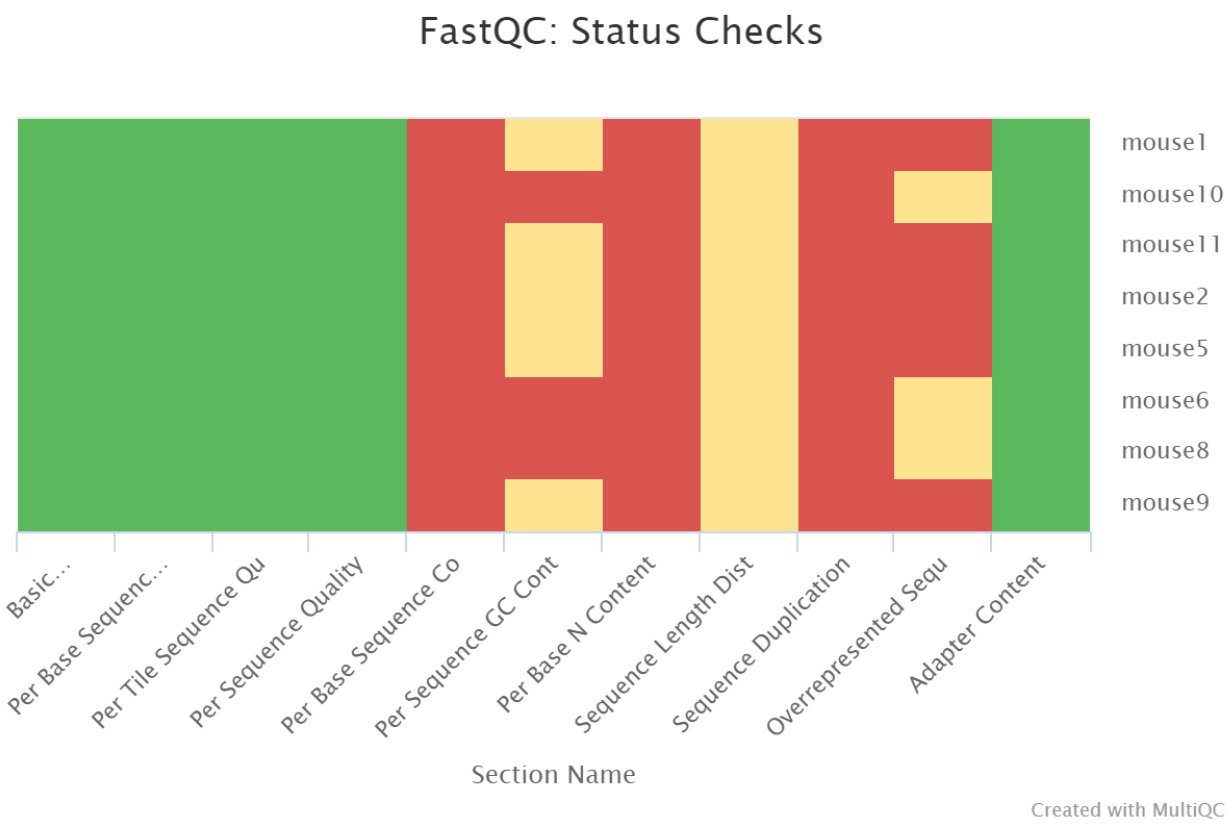

Figure 5-9: Summary plot created with multiQC summarising sample scores for each of the metrics. Green indicates normal results, orange indicates slightly abnormal and red indicates very unsual as would be expected from a typical RNA-Seq sequence

It must be noted, however, that normal results used for this benchmarking are based on a typical RNA-Sequence experiment that uses poly A selection methods in the RNA isolation, meaning only mature, coding mRNA species are selected. The RNA sequencing flow used for these samples was rRNA depletion, which meant various other RNA species, such as long non-coding and shorter fragmented RNA are also present in the sample. This leads to an inconsistent sequence length distribution, resulting in a higher per base N content when fragments are shorter, less heterogeneity in sequences resulting in more overrepresented sequences, and skewed GC content. The unusual results shown can largely be explained by the presence of a variety of RNA species in the sequencer due to sequencing workflow.

5.6.3 Alignment of reads to a reference genome

Once the quality of the raw reads was established, the reads were aligned to a reference genome. For this, the STAR aligner was used, which aligns reads to a reference genome, by first creating an index from the reference index and then mapping reads to the index. Mouse release M27 (GRCm39) from Gencode was used as the latest release, using a comprehensive gene annotation with all regions. The index was successfully created with STAR and all sample reads were mapped to the same index successfully, producing sorted BAM files for use in counting.

5.6.4 Counting of Aligned Reads

As the reads were based on RNA transcripts exhibiting mild degradation, with RIN scores between 6 and 7, degradation bias may be introduced in transcript and gene quantification. DegNorm is a pipeline tool that adjusts read counts on by accounting for transcript degradation heterogeneity on a gene-by-gene basis while simultaneously controlling for sequencing depth.

5.7 Downstream analysis

5.7.1 Workflow

To understand molecular and cellular changes within the bone microenvironment of ovariectomised mature mice, pre-processed RNA-Seq data was analysed with differential gene expression, deconvolution of bulk sequencing, pathway analysis, signature scoring and correlation with public datasets was performed (see Figure 5-10).

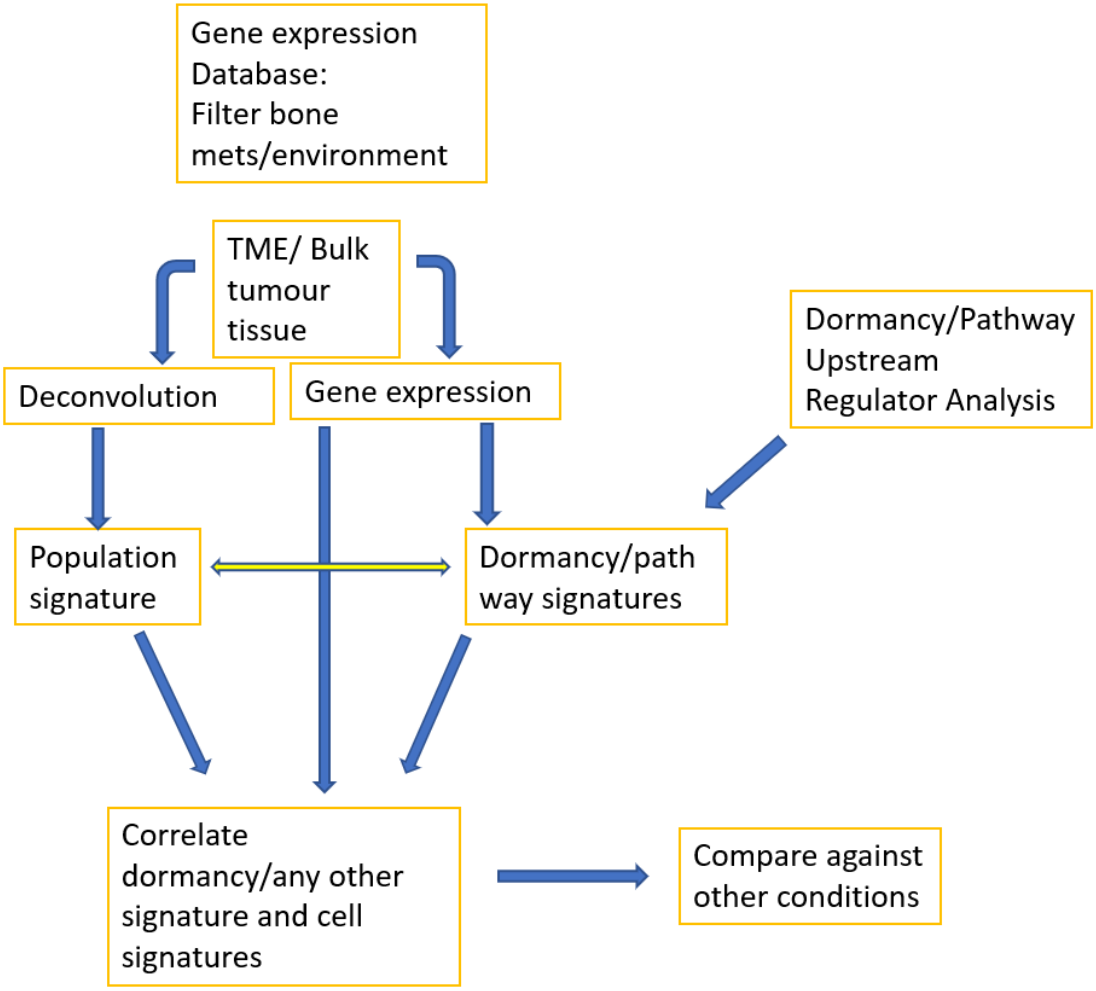

Figure 5-10: Workflow for analysing RNA sequencing against publicly available datasets

The following sections will detail the results from the corresponding analyses performed.

5.7.2 Quality Control of Adjusted read counts

Prior to differential expression gene testing, sample correlations and distancing were assessed to understand how closely the genes from each sample were clustering together. In order to accurately quantify sample distances, data usually needs to be transformed to possess the same range of variance across different ranges of the mean values and achieve homoscedasticity (constant/close range of variation across all values) . However, with RNA-Seq counts, the expected variance grows with the mean, meaning genes with higher counts across samples are expected to have a larger variation in those counts than those with lower counts. A frequently used transformation to prepare RNA-Seq data for clustering and principal component analysis is the variance stabilising transform (VST) utilised by the DESeq2 package.

Following the VST transform on the data, samples and relative distances were calculated using hierarchical clustering from the DESeq2 package, and plotted using pheatmap package which plots a heatmap of the distances between samples in a heatmap configuration (see Figure 5-11).

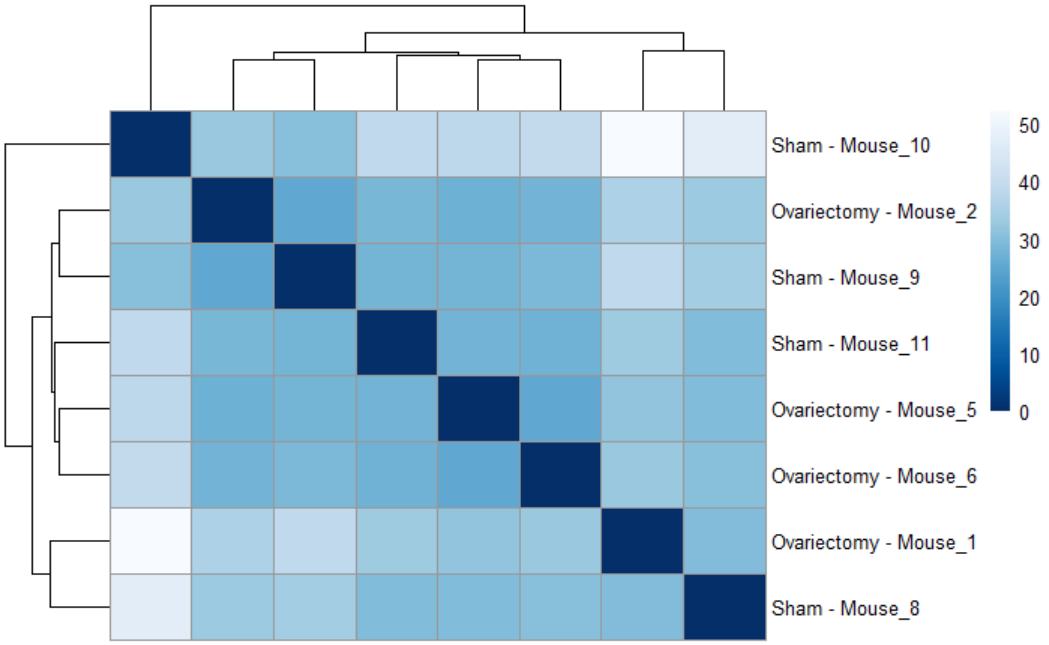

Figure 5-11: Relative sample distances as calculated by hierarchical clustering using the DESeq2 dist function. A distance of 0 indicates perfect concord between samples, whereas higher numbers equate to larger distances between samples. Samples are also clustered on the axes according to relative distances, with adjacent samples on the axes being closer than distant samples.

The results showed a relative clustering of the sham and OVX groups. However, two samples, mouse 8 (sham) and mouse 2 (OVX) appeared to cluster closer to their opposite treatment groups and were deemed outliers.

The transformed data then underwent principal component analysis, which shows the strength of separation between different groups of samples. In RNA-seq, principal component analysis uses linear combinations to derive eigenvalues of the gene expression values to define a new set of unrelated variables principal components (Chen *et al*., 2020b). The new variables are orthogonal to each other, eliminating redundant information allowing the description of data sets and their variance with a reduced number of variables. As similarities between data sets are correlated to the distances in the projection of the space defined by the principal components, PCA can also be used to identify outliers with respect to the principal components. The variance in RNA-Seq data usually grows with the expression mean meaning PCA on the matrix of normalised read counts will often lead to principal components that are dominated by the variance of a few highly expressed genes (Chen *et al*., 2020b). DESeq2 calculates a variance stabilizing transformation (VST) from the fitted dispersion-mean relation(s) and then transforms the count data (normalized by division by the size factors or normalization factors), which normalises the high random noise of low count data (Love *et al*., 2014). Therefore, the VST transform is performed prior to PCA. The first principal component (PC1) accounts

for the largest difference between the groups, and the second principal component (PC2) accounts for the second largest explanation of variation between the groups. When performed on the VST transformed data, the samples did not show a distinct separation, suggesting little difference between the groups (see Figure 5-12).

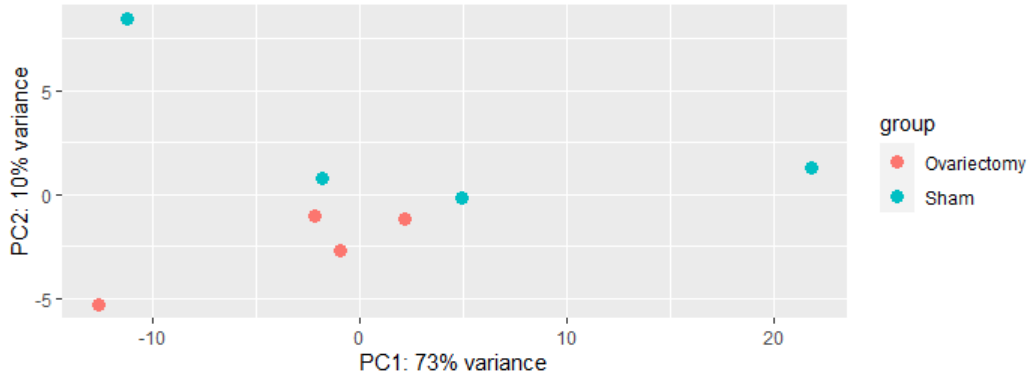

Figure 5-12: Principal component plotting of VST transformed data

Therefore, prior to differential expression testing, outliers identified in the previous hierarchical clustering, mouse 2 and mouse 8 were removed in order to achieve greater separation between the groups, leaving 3 samples per group. Upon omitting the outlier samples, hierarchical clustering was performed and showed more distinct clustering, though one other sample from the OVX group clustered closer the sham group (see Figure 5-13).

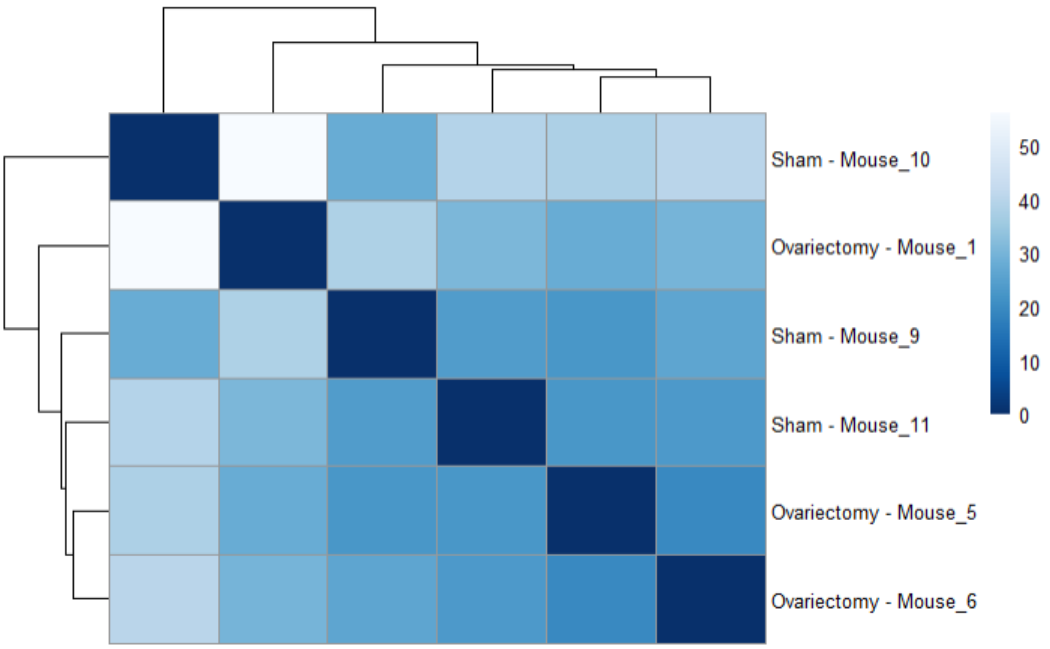

Figure 5-13: Heatmap plot of hierarchical clustering of samples with outliers removed. Mouse 1 from OVX group clusters closer to the sham group

PCA analysis following the removal of outliers showed clearer separation between the sham and OVX groups (see Figure 5-14).

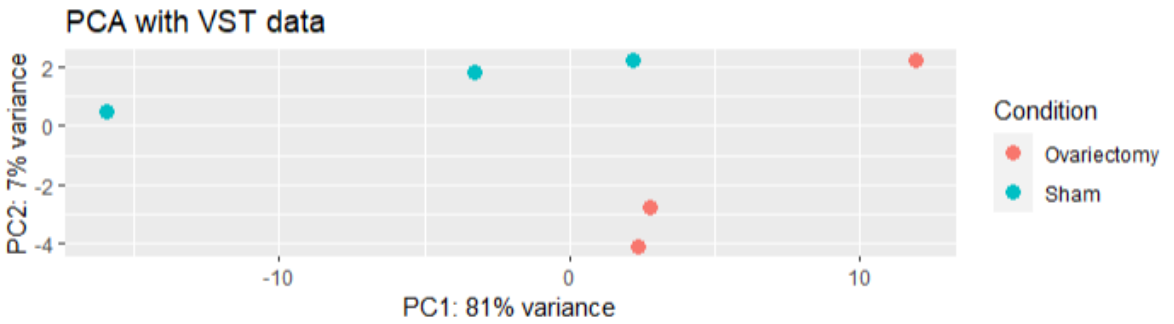

Figure 5-14: Principal component analysis of reduced sample, showing more distinct separation than with all samples present

Despite one sample from OVX clustering closer to the sham group, the separation was deemed sufficient to perform differential expression testing, as with 3 samples per group, more samples could not be removed to maintain a triplicate biological repeat.

Selecting the most variable genes was considered as a possible avenue to better assess difference between the groups. The 6000 most variable genes as ranked by standard deviation were selected and PCA with 8 components according to sample number was performed. The first component accounted for 60% of the variance, and the second component accounted for approximately 17% of the variance (see Figure 5-15). Despite accounting for a significant portion of the variance, the first two components did not linearly separate the two groups. Components 2 and 3 (accounting for approximately 8% of variance) separated the two groups marginally better than component 1 and 2. However, it was deemed a more appropriate strategy to remove outliers as shown in previous figures.

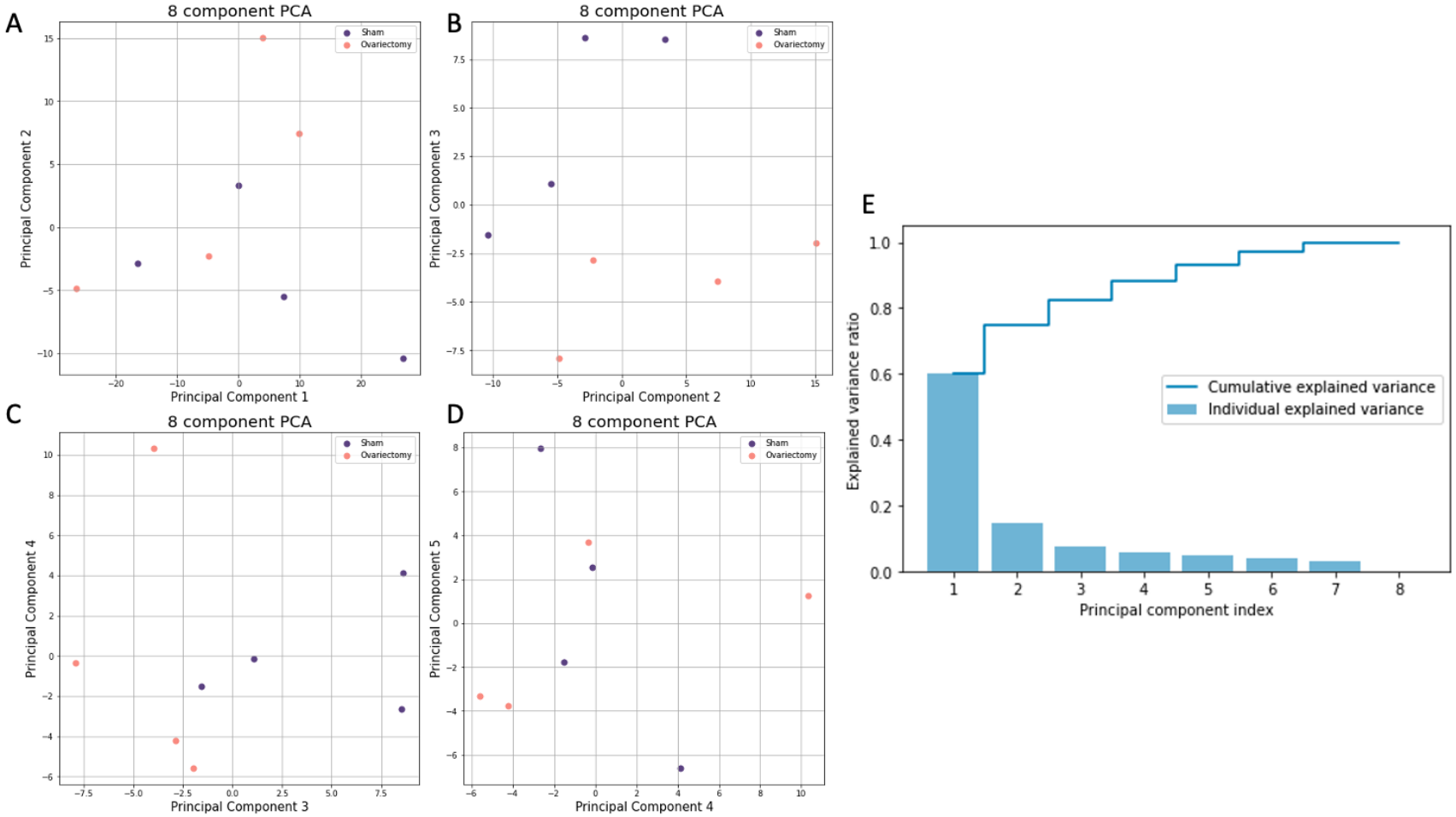

Figure 5-15: PCA performed on the 6000 most variable genes as ranked by standard deviation. PCA was performed using 8 components. A.) First 2 components, B.) second and third components, C.) third and fourth components, D.) fourth and fifth components, E.) individual explained variance per principal component and cumulative explained variance. Purple dots: Sham operated samples, Orange dots: Ovariectomised samples. Selecting the 6000 most variable genes in isolation showed a lower separation compared to removing outliers

5.7.3 DIFFERENTIAL GENE EXPRESSION TESTING

Differential expression analysis identifies genes whose expression are significantly differentially expressed between at least two distinct sample groups. Common tools for statistical analysis of differential expression perform univariate comparisons, comparing each gene across samples individually, producing a score that relates to the fold change between one group compared to another. This allows easy interpretation and comparisons of genes whose transcript expression are orders of magnitude apart. For my analyses, I used DESeq2, a frequently cited tool in the R/Bioconductor ecosystem that uses shrinkage estimation for dispersions and fold changes to produce differential expression estimates between samples.

Differential expression testing omitted genes with a zero read count in more than 3 samples, meaning testing was performed on 27,999 genes with non-zero read count and used a Benjamini-Hochberg correction to adjust significance rates for the amount of tests being performed, referred to as adjusted p-value or false discovery rate (FDR). Out of 27,999 genes with non-zero read count, at an FDR value of < 0.1 and log fold changes > 0, 82 genes were found to be significantly downregulated in the OVX group, and 75 were found to be significantly upregulated in the OVX group (see Figure 5-16 and Table 5-2).

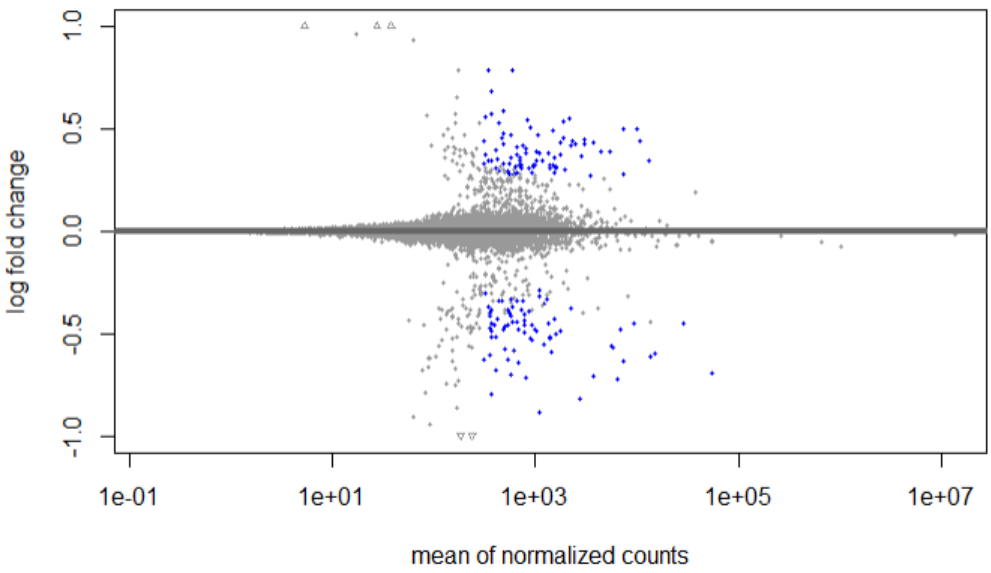

Figure 5-16: MA plot of differential expression testing, y-axis showing the log2 fold change of genes, and x-axis showing the statistical significance value of the differential expression. Blue colour indicates significantly altered genes.

Table 5-2: Complete list of genes significantly downregulated and upregulated in the OVX group vs sham according to DESeq2 differential expression testing

Condition	Genes
Downregulated in OVX	ABCB10, ALAS2, ARRB1, BSDC1, BTNL10, CAR2, CD177, CLN8, CREG1, CTSE, DCAF12, DMTN, DSTN, E2F4, EIF2AK1, EPB41, EPB42, ERMAP, FAM117A, FZR1, GAS5, GDA, GPX1, GYPA, GYPC, H2AX, H2BC9, HBA-A1, HBA-A2, HBB-BT, HEMGN, HMBS, KEL, LCN2, LMO2, MARCHF8, MKI67, MKRN1, ODC1, OLFM4, PABPC1, PIGQ, PPOX, PRDX2, PRTN3, RAB3IL1, RANBP10, RHD, SLC16A10, SLC25A37, SLC43A1, SLC4A1, SLFN14, SMOX, SNCA, SPECC1, SPIRE1, SPTA1, ST3GAL5, TAL1, TENT5C, TFDP2, TMCC2, TRIM10, TRIM59, UBE2O, XPO7
Upregulated in OVX	MAN2A2, 1110002E22RIK (C4orf54 ortholog), ABLIM1, ACTN3, AGL, AK1, AMPD1, ATP1B1, ATP2A1, CACNA2D1, CAMK2A, CAMK2D, CKM, CMYA5 COL11A1, COL12A1 COL1A1, COL1A2, COL3A1, COL5A1, COL5A2, CPE, DMPK, FSD2, GJA1, GPD1, HSPA9, IDH3B, IGFN1, IRS1, JPH1, KLHL24, LUM, MAF, MAP7D1, MMP2, MYBPC2, YH4, MYL1, MYLK4, MYOZ1, MYPN, PDLIM3, PINK1, POSTN, PRKAA2, PVALB, PYGM, RORA, SELENOW, SH3PXD2A, SPARC, SPP1, SUCLA2, THBS2, TMEM38A, TNN, TOB1, TPM1, TRDN, TXNIP

When plotting the expression value Z scores for the differentially expressed genes, the groups clustered well for both the upregulated and downregulated genes (see Figure 5-17), showing samples generally correlated within their groups. Including previously excluded samples (mouse 8 from the sham group and mouse 2 from the ovariectomy group) showed contrasting gene expression to their own groups and further justified their exclusion from downstream analysis. Although general correlation was shown in sample groups, variations of the strength of expression overall were also present. Mouse 10 (sham) and mouse 1 (ovariectomy) showed very strong contrast with both upregulated and downregulated gene sets, whereas mouse 11 (sham) showed weak correlation in both upregulated and downregulated gene sets. Mouse 5 (ovariectomy) showed a weak correlation for downregulated genes, but good correlation for the upregulated genes.

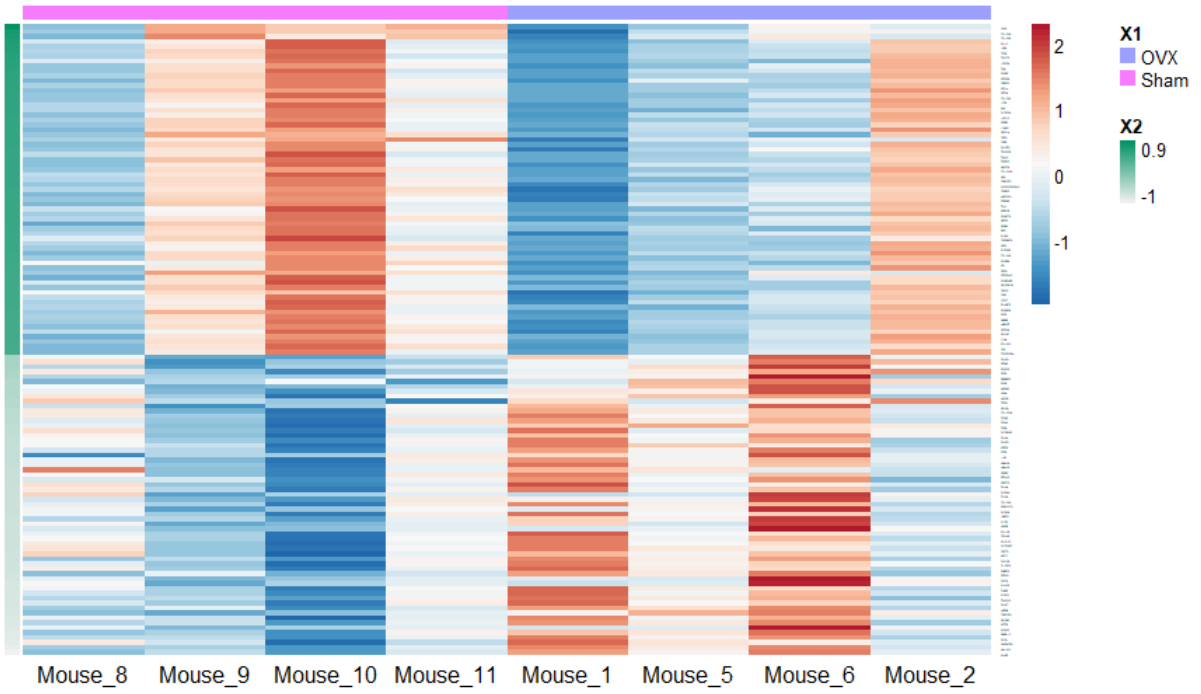

Figure 5-17: Scale: Z score of gene expression values. Top bar; pink represents Sham operated animals (mouse 8 -11), purple represents OVX (mouse 1-6) operated animals. Left green bar: Log2Foldchange of genes in sham compared to ovariectomy, dark green upregulated, light green downregulated. Produced using NMF version 0.23.0 aheatmap function

5.7.3.1 POWER ANALYSIS

Power analysis for RNA-seq requires the running of simulations to simulate the expected power for a given sample size, count of genes and specified FDR. A standard acceptable power is 80%. To accomplish this, simulations were run on the Bottomly (2011) dataset consisting of inbred mice using the PROPER Bioconductor package (Bottomly *et al*., 2011, Wu *et al*., 2015). Simulations were carried out to assess the expected power for an experiment investigating 28,000 genes, either a 0.1 or 0.05 FDR and 3, 4, 8, or 12 samples per group for 20 simulations. Results can be seen in Table 5-3 and show that for this experiment with 3 samples per group after omitting outliers, with a nominal FDR of 0.1, a marginal power of 0.73 was obtained, with a false discovery cost of 0.19, meaning 19% of genes discovered as differentially expressed, 19% would be falsely discovered as so. Increasing samples to 4 would increase the power to 0.77, whereas reducing nominal FDR to 0.05 would reduce the marginal power to 0.7. To achieve a power of over 0.8 (80%), the sample size would have to be 8 or over in the range of sample sizes simulated.

Table 5-3: Effect of group sample size and FDR on statistical power as generated by the PROPER R package. Nominal FDR – False Discovery Rate selected as cut-off for discovery of genes. SS1 & 2 – sample size of group 1 (control) and group 2 (test). TD – True discoveries, FD – False discoveries, FDC - False discovery cost, defined as the number of FD divided by the number of TD.

SS1	SS2	Nominal FDR	Actual FDR	Marginal power	Average number of TD	Average number of FD	FDC
3	3	0.05	0.09	0.7	348	47	0.14
4	4	0.05	0.08	0.75	375	44	0.12
8	8	0.05	0.05	0.83	418	35	0.08
12	12	0.05	0.05	0.86	435	34	0.08
3	3	0.1	0.13	0.73	360	69	0.19
4	4	0.1	0.11	0.77	384	68	0.18
8	8	0.1	0.09	0.84	425	65	0.15
12	12	0.1	0.09	0.87	441	65	0.15

The low sample count significantly contributes to a lower power, as well as the heterogenous nature of the samples used and lack of technical replicates. The power of this experiment was below the minimally expected threshold of 0.8. However, to increase the power, the samples sequenced would have to be doubled. Within financial constraints, technical and biological replicates could be performed, but the major limiting factor was the number of samples that could be sequenced remaining at 4 per group. Therefore increasing power above 0.8 could not be done and the experiment would be considered as exploratory with findings to be verified with follow up sufficiently powered analyses.

As the expected number of true discoveries with this experimental setup was 360 and false discoveries being 69 (see Table 5-3), the number of differentially expressed genes was expected to be 429. However, the number of differentially expressed genes was 157, which is significantly less than expected. It must be taken into account that the Bottomly (2011) dataset compared two different mouse strains, C57BL/6J and DBA/2J (Bottomly *et al*., 2011), therefore more genes would be expected to be differentially expressed compared to observing groups based on the same strain. Furthermore, as the experiment was designed to capture early events following ovariectomy, subtle changes, rather than drastic would be expected.

Importantly, the discovery of 157 genes out of 27,999 falls below the threshold set for the false discovery rate of 0.05. Therefore a careful consideration of the genes must be made when making any inference with respect to biological expectation; emphasising genes and pathways expected to be upregulated or downregulated in ovariectomy or sham operated mice according to previous experiments within the lab and in literature.

5.7.4 ALTERED PATHWAYS

In order to understand the wider landscape of transcriptomic changes, pathway analysis was performed in the selected genes from the Farr *et al.* dataset and the one I generated following ovariectomy of mature mice. This would help identify further correlations of process pathways altered as different genes can contribute to a singular pathway, thereby potentially obscuring these pathways when comparing genes in isolation. To achieve this, lists of upregulated genes in the ovariectomy group, as well as the list of upregulated genes in young women compared to old were uploaded into the Database for Annotation, Visualization and Integrated Discovery (DAVID) and gene ontology terms assessed, with statistical analyses performed for significance (see Table 5-4 and Table 5-5).

Table 5-4: Gene ontology terms altered from genes upregulated in ovariectomised mice, with their gene counts, significance (FDR - adjusted p-value) and genes contributing to the pathway/process

Term	Gene Count	FDR	Genes
ECM-receptor interaction	9	0.0000009	COL1A1, COL3A1, COL1A2, COL5A1, TNN, COL11A1, COL5A2, SPP1, THBS2
Focal adhesion	11	0.0000024	COL1A1, COL3A1, COL1A2, ACTN3, COL5A1, TNN, COL11A1, COL5A2, SPP1, THBS2, MYLK4
Protein digestion and absorption	8	0.0000071	COL1A1, COL3A1, COL1A2, COL5A1, COL11A1, COL12A1, COL5A2, ATP1B1
PI3K-Akt signaling pathway	11	0.00015	COL1A1, COL3A1, COL1A2, PRKAA2, COL5A1, TNN, IRS1, COL11A1, COL5A2, SPP1, THBS2
Platelet activation	7	0.00069	COL1A1, COL3A1, COL1A2, COL5A1, COL11A1, COL5A2, MYLK4
Proteoglycans in cancer	6	0.044	COL1A1, CAMK2D, COL1A2, LUM, MMP2, CAMK2A

Table 5-5: Gene ontology terms altered from genes upregulated in young women compared to old, with their gene counts, significance (FDR - adjusted p-value) and genes contributing to the pathway/process

Term	Gene count	FDR	Genes
Angiogenesis	39	8.90E-14	CCL2, DAB2IP, EGFL7, RAPGEF3, SOX17, SOX18, ANGPTL4, ANGPTL6, CAV1, COL4A2, COL15A1, CYP1B1, DLL4, EMCN, EPAS1, ECSCR, FGF1, FGFR2, GJA5, HSPG2, HEY1, HIF3A, ID1, LEP, MMP19, MCAM, MMRN2, NRXN1, NRP1, NOS3, PIK3CG, PGF, PTPRB, RAMP2, ROBO4, SRPX2, THSD7A, TMEM100, TIE1
Cell adhesion	47	1.70E-08	CCL2, CX3CL1, CD34, CD36, EGFL7, KIAA1462, NUAK1, PDZD2, AOC3, B4GALT1, CDH11, CDH5, COL6A1, COL6A2, COL7A1, COL15A1, COL28A1, CYP1B1, EMP2, FERMT1, LGALS4, HES1, ISLR, ITGA7, ITGB4, ITGBL1, ICAM3, LAMA3, LAMA4, LAMB1, LAMB2, LAMC1, LSAMP, LYVE1, MCAM, MAG, NLGN4X, PARVA, PGM5, PKP1, PODXL, PTPRF, PCDH18, PCDHGC3, SORBS1, TINAGL1, VWF

Extracellular matrix organization	25	2.30E-05	APBB2, B4GALT1, COL2A1, COL4A1, COL4A2, COL5A3, COL6A1, COL6A2, COL7A1, FGF2, HSPG2, ITGA7, ITGB4, ICAM3, JAM2, LAMA3, LAMA4, LAMB1, LAMB2, LAMC1, NR2E1, OLFML2A, OLFML2B, VWA1, VWF
Vasculogenesis	12	1.10E-03	EGFL7, EPHA2, SOX17, SOX18, TEAD2, YAP1, CAV1, FZD4, HEG1, RAMP2, TMEM100, TIE1
Positive regulation of angiogenesis	16	2.70E-03	CX3CL1, CD34, GATA2, RAPGEF3, ANGPTL4, AQP1, CMA1, CCBE1, CYP1B1, FGF1, FGF2, NOS3, NR2E1, PGF, RAMP2, TMIGD2

Cell adhesion and extra cellular matrix organisation pathways were commonly altered between the two datasets, with blood vessel formation-inducing genes occurring more significantly in young women than ovariectomised mice. Many of the processes significantly upregulated in the dataset I generated were driven by collagen genes, thrombospondin-2 (THBS2), osteopontin (SPP1) and Tenascin-N precursor (TNN). These genes and processes were expected, taking into account biological results of increased bone resorption and disruption of the extra-cellular matrix.

5.7.5 IDENTIFYING A DORMANCY SIGNATURE

Identification of individual genes regulating dormancy has revealed that dormancy is a phenomenon of transcriptional signature alterations, rather than being primarily driven by individual genes, though usually acting through critical signalling nodes for dormancy induction, such as NR2F1. Much research has involved finding clusters of genes that drive dormancy within tumour cells. In particular, research by Segall and colleagues into transcriptional signatures associated with dormancy derived from various cancer types and applied to breast cancer cell lines revealed a number of genes that were upregulated and also others that were downregulated in ER+ positive cell lines (see Figure 5-18) (Kim *et al*., 2012). Among them, inhibition of BHLHE41 and NR2F1 were shown to increase *in vivo* growth of ER+ MCF7 cells.

Status in Dormant Cells	**Gene Symbols**
Up-regulated	ACVR1, ADAM10, AMOT, BHLHE41, COL1A1, COL4A5, CTSD, DDR1, EPHA5, GATA6, HIST1H2BK, IGFBP5, MMP2, NR2F1, P4HA1, SOX9, SREBF1, STAT3, TGFB2, THBS1, TP53, TPM1
Down-regulated	APEX1, ASNS, ATF3, ATF4, BUB1, BUB1B, CDKN3, CEBPG, CKS2, DNMT1, DTYMK, EGFR, EGR1, ESM1, FOSL1, FOXD1, FOXM1, IGF1R, IL8, JUN, MMP1, NT5E, ODC1, PIK3CB, PLAT, TIMP3, TK1

Figure 5-18: Upregulated and downregulated genes in dormant cancer cell lines as identified by Kim *et al*. (Kim *et al*., 2012).

To investigate the predictive value of these genes within the bone microenvironment, I used a dataset from a study published by Cawthorn *et al.* (2009). In this, bone marrow biopsies were collected from breast cancer patients with either metastatic tumour growth within the bone marrow (MTC), or with confirmed presence of disseminated tumour cells without overt outgrowth (DTC) (Cawthorn *et al*., 2009). This data consisted of genes detected by microarray and their relative expression amongst a cohort of 13 patients, 6 MTC and 7 DTC samples. These data were scored for their relative expression of the up-regulated and the down-regulated gene sets as discovered by Kim *et al.* (2012) in breast cancer cell lines using SingScore, an R/Bioconductor package for quantifying concordance between sample transcriptomes and selected molecular signatures (Foroutan *et al*., 2018). The scoring of these samples produced a plot of score on the x-axis, and dispersion on the y-axis, where the score is an arbitrary unit signifying the concordance of the abundance of selected genes in the signature present in the sample, whereas dispersion is a factor of the rank of the genes within the samples. Scores are provided for upregulated genes, downregulated genes and the total combined (see Figure 5-19).

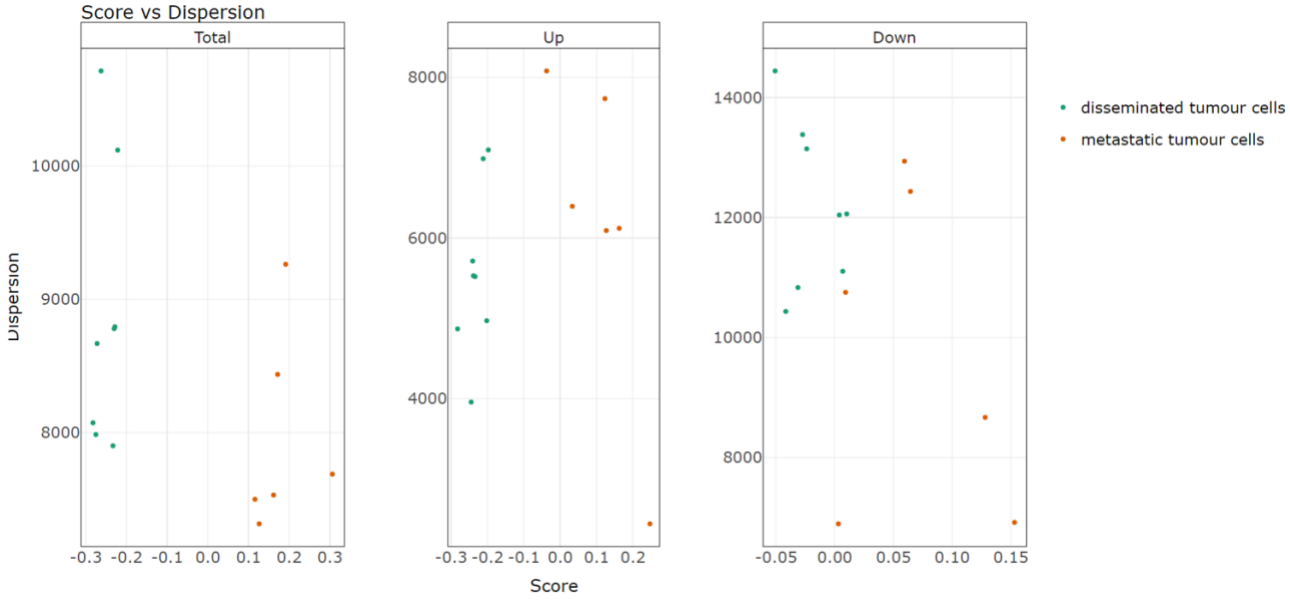

Figure 5-19: The score and dispersion of the total across up- and down-regulated gene scores and dispersion, the up-regulated and the downregulated gene sets from ER+ breast cancer cell lines scored against samples of bone marrow biopsies from women with either disseminated tumour cells or metastatic tumour cells (Cawthorn *et al*., 2009). Higher score reflects higher relative gene expression of gene set, high dispersion reflects higher variation in expression of genes in gene set.

Scoring this dataset yielded interesting results. In both the up-regulated and down-regulated gene sets, the samples from the metastatic tumour cells showed a higher score, whereas isolated disseminated tumour cells had a low score despite similar dispersion. This indicates that the metastatic tumour cell samples had a higher resemblance in transcriptomic profile to the dormant cell lines than did the isolated disseminated tumour cells.

Samples from the ovariectomised mice were also subsequently scored, showing an inconsistent scoring of genes across the sample groups with poor separation (see Figure 5-20).

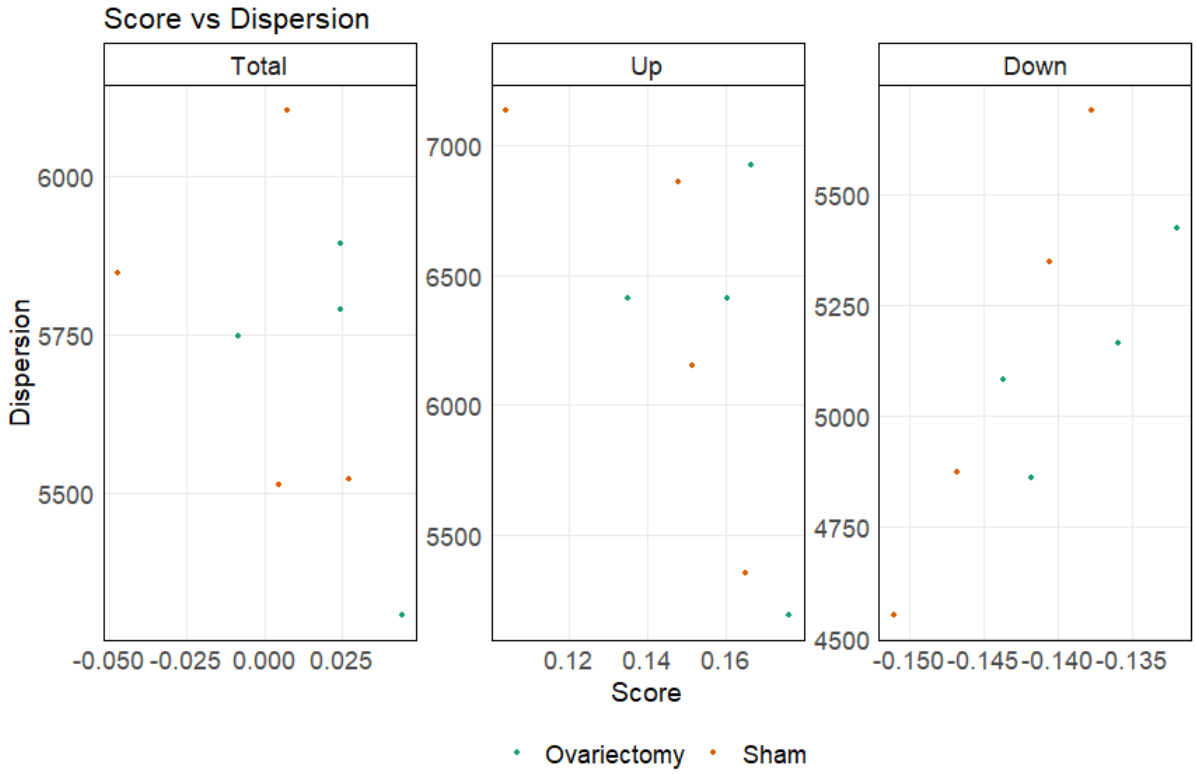

Figure 5-20: The score and dispersion of the total across up- and down-regulated gene scores and dispersion, the up-regulated and the downregulated gene sets from ER+ breast cancer cell lines scored against samples from ovariectomised and sham operated mice. Higher score reflects higher relative gene expression of gene set, high dispersion reflects higher variation in expression of genes in gene set.

	Treatment	Total Score	Total Dispersion	Up Score	Up Dispersion	Down Score	Down Dispersion
Mouse 1	OVX	0.044218	5308.82	0.176137	5193.548	-0.13192	5424.092
Mouse 2	OVX	-0.00839	5746.558	0.135223	6412.245	-0.14362	5080.87
Mouse 5	OVX	0.024332	5788.812	0.160256	6413.728	-0.13592	5163.896
Mouse 6	OVX	0.024676	5894.076	0.166473	6928.19	-0.1418	4859.963
Mouse 8	Sham	0.027203	5522.685	0.164916	5356.634	-0.13771	5688.736
Mouse 9	Sham	0.007528	6103.123	0.148037	6859.99	-0.14051	5346.256
Mouse 10	Sham	-0.04707	5845.892	0.104014	7138.719	-0.15109	4553.065
Mouse 11	Sham	0.004502	5513.419	0.151265	6154.273	-0.14676	4872.565

The results show poor separation between the groups regarding the dormancy signature. To identify whether individual genes may have been altered, key genes Kim *et al*. (2012) identified as being critical to dormancy and leading to inhibition of dormancy when inhibited, BHLHE41 and NR2F1 were isolated from the adjusted read counts and plotted to show the difference between groups. In addition, thrombospondin 1, TGFB2, STAT3 and SOX9, were also plotted to show the difference between groups (see Figure 5-21).

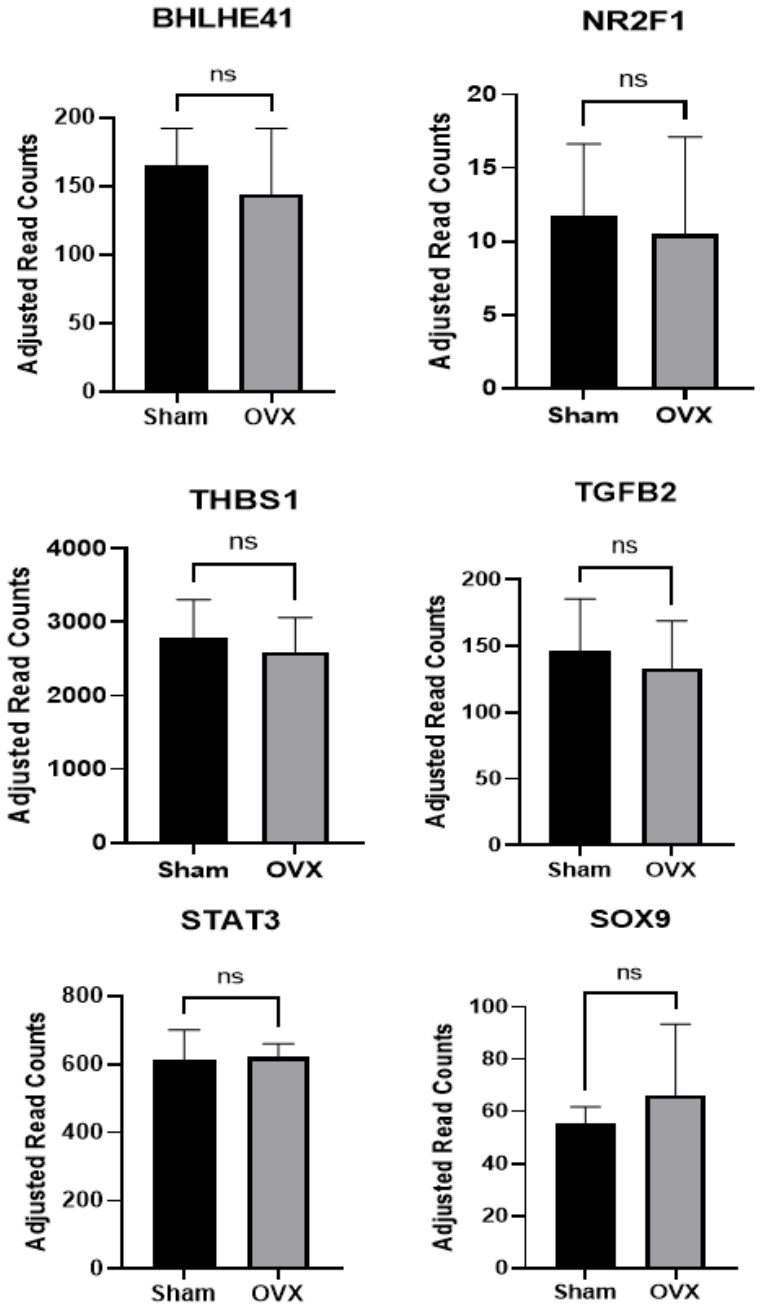

Figure 5-21: Adjusted read counts of significant genes implicated in cancer dormancy. BHLHE41 sham mean 165.4, OVX mean 144.3, difference between means (± SEM) 21.08(± 27.42) p=0.4711. NR2F1 sham mean 11.72, OVX mean 10.49, difference between means (± SEM) 1.230(± 4.131) p=0.7760. THBS1 sham mean 2795, OVX mean 2600, difference between means (± SEM) 195.1 (± 346.4) p=0.5936. TGFB2 sham mean 146.1, OVX mean 133.4, difference between means (± SEM) 12.67(± 26.61) p=0.6509. STAT3 sham mean 614.8, OVX mean 622.8, difference between means (± SEM)8.032(± 47.09) p=0.4737. SOX9 sham mean 55.67, OVX mean 66.32, difference between means (± SEM) 10.65(± 13.94) p=0.4711.

Consistent with poorly resolved scoring of the dormancy signature between the two groups, none of the individual genes plotted revealed significant differences between the two groups.

To further assess whether age or oestrogen treatment would have an impact on the dormancy score, the dataset from Farr *et al.* (2015) was scored and displayed according to status (young woman, old woman, old woman with oestrogen therapy) (see Figure 5-22).

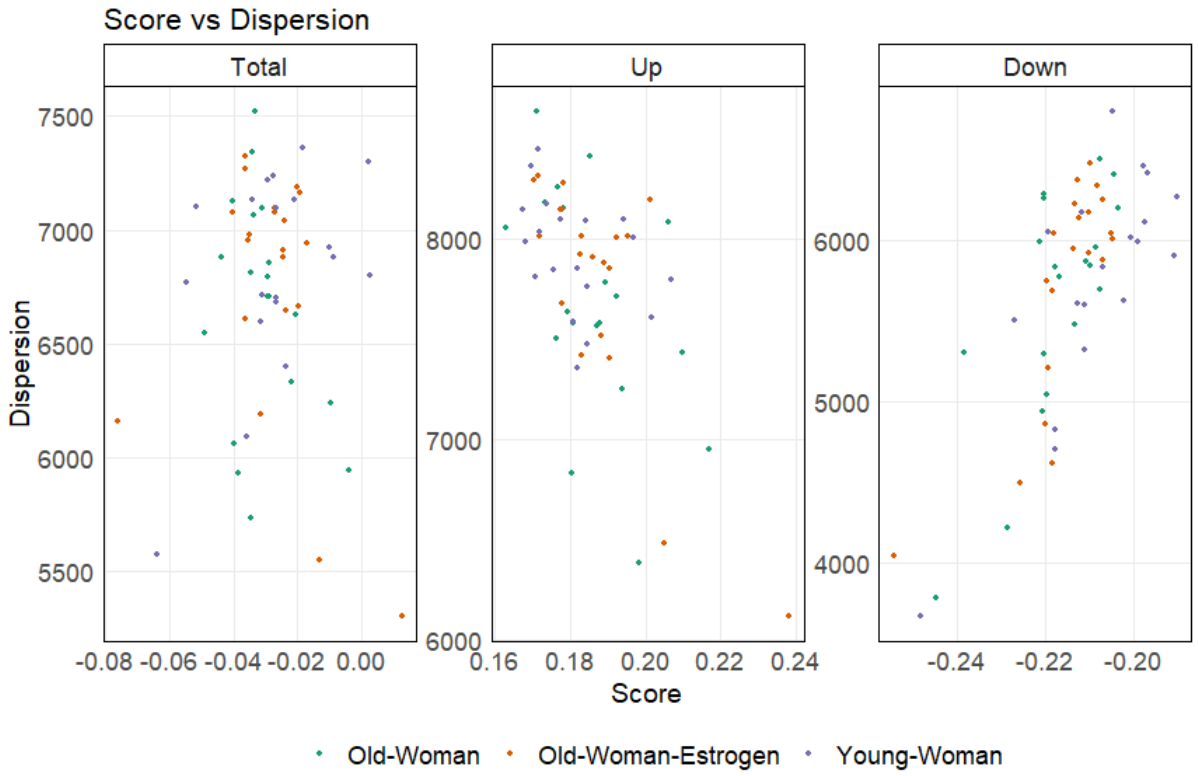

Figure 5-22: The score and dispersion of the total across up- and down-regulated gene scores and dispersion, the up-regulated and the downregulated gene sets from ER+ breast cancer cell lines against samples of young (~30 years old) women, old women (~73 years old) and old women (~70 years old) treated with 3 weeks of oestrogen therapy. Higher score reflects higher relative gene expression of gene set, high dispersion reflects higher variation in expression of genes in gene set.

Similarly to the dataset based on OVX or sham operated mice, there did not seem to be any strong correlation in status with dormancy score, whether the up-regulated, down-regulated or total score was measured. Using the dormancy scoring signature against whole bone or bone marrow bulk sequences did not show significant differences in treatment groups.

5.7.6 Deconvolution of Bulk Sequencing

To estimate cell type abundance within the bone marrow in order to infer the changes in the cellular landscape, xCell, a tool that estimates the abundance of 64 different cell types from bulk RNA-Seq data was used on the sequencing data from both the comparison between sham and ovariectomised mice as well as the data reported in Farr *et al.* (2015) on the effects of age and oestrogen on human skeletal gene expression. Cell type estimates included Adipocytes, Astrocytes, B-cells, Basophils, CD4+ T-cells, CD4+ Tcm, CD4+ Tem, CD4+ memory T-cells, CD4+ naive T-cells, CD8+ T-cells, CD8+ Tcm, CD8+ Tem, CD8+ naive T-cells, common lymphoid progenitors (CLP), common myeloid progenitors (CMP), Chondrocytes, Class-switched memory B-cells, dendritic cells (DC), Endothelial cells, Eosinophils, Epithelial cells, Erythrocytes, Fibroblasts, granulocyte-monocyte progenitor (GMP), HSC, Hepatocytes, Keratinocytes, Megakaryocyte–erythroid progenitor cell (MEP), Multi-Potent Progenitor (MPP), mesenchymal stem cells (MSC), Macrophages (total, M1 and M2 polarised), Mast cells, Megakaryocytes, Melanocytes, Memory B-cells, Mesangial cells, Monocytes, Myocytes, NK cells, natural killer T cells (NKT), Neuronal cells, Neutrophils, Osteoblasts, Pericytes, Plasma cells, Platelets, Preadipocytes, Sebocytes, Skeletal muscle, Smooth muscle, Gamma Delta T cells (Tgd), Th1 cells, Th2 cells, Tregs, activated dendritic cells (aDC), classical dendritic cells (cDC), interstitial dendritic cells (iDC), Endothelial cells, Endothelial cells, naive B-cells plasmacytoid dendritic cells (pDC) and pro B-cells. Analysis of data obtained from mice that underwent a sham or OVX treatment revealed a relatively unchanged cellular landscape, with only class switched memory B-cells as significantly increased in the OVX group ($p = 0.026$) (see Figure 5-23). Interestingly, pro-B cells, despite not being significantly altered, were increased at a significance value marginally above significance ($p=0.0536$).

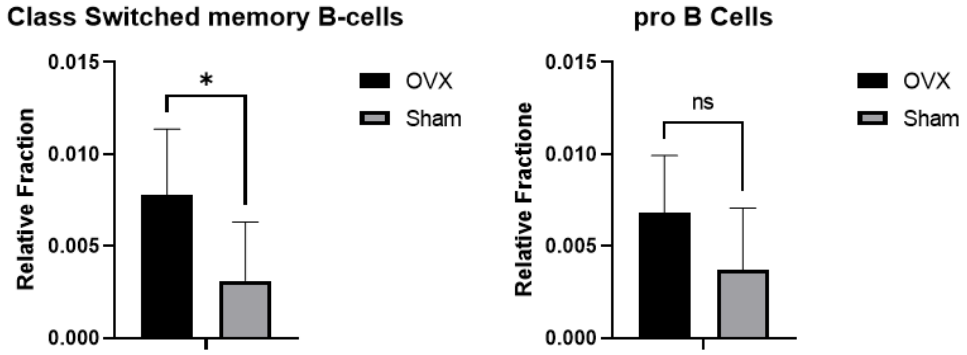

Figure 5-23: Relative fraction estimates of cell type abundances for mice that underwent sham vs OVX procedures.

These cells were assessed for significant changes in the Farr *et al.* (2015) dataset deconvoluted results, but did not show a significantly altered estimation of either Class Switched memory B-cells or pro B cells as assessed by ANOVA ($p=0.6032$ and $p=0.4803$ respectively).

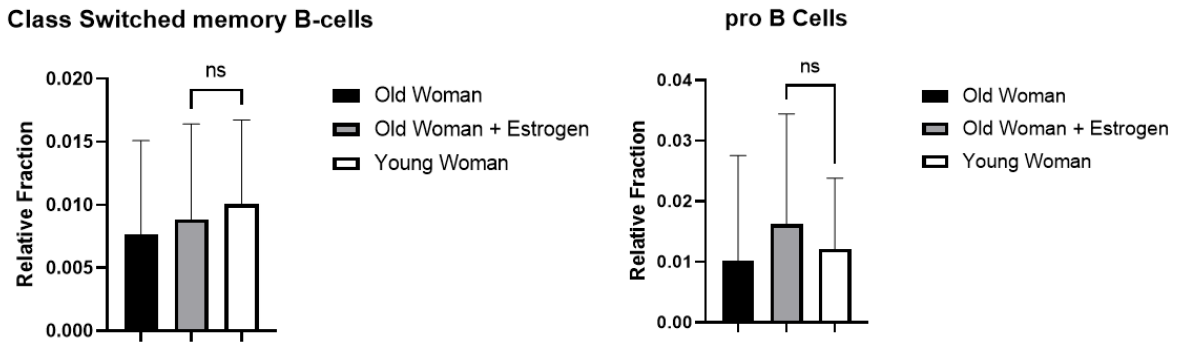

Figure 5-24: Relative fraction estimates of cell type abundances for samples from the Farr *et al*. (2015) dataset.

To further hone cells of interest, the results from the deconvolution were correlated with the dormancy score for the samples in the Farr *et al.* (2015) dataset. Cells having a correlation of > 0.3 or <-0.3 indicating either positive or negative correlation were retained, showing that basophils, chondrocytes, endothelial cells, fibroblasts, HSCs, monocytes, neutrophils and osteoblasts had correlation with the dormancy score, and thus are cells that may influence dormancy either negatively or positively (see Figure 5-25).

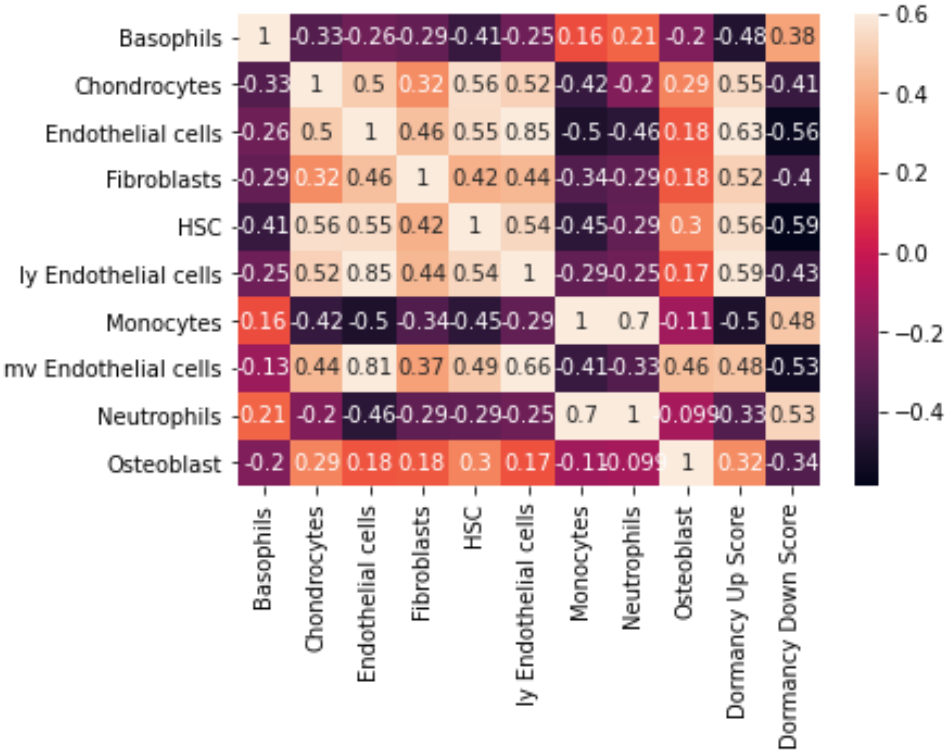

Figure 5-25: Spearman correlation plot of estimated cell type abundance with either a correlation of >0.3 or <-0.3 for both the dormancy up score and the dormancy down score regardless of group (young women, old women or old women treated with oestrogen)

The resulting correlation showed a negative correlation with dormancy for basophils, and monocytes, suggesting their presence is associated with a lower expression of dormancy promoting genes,

whereas chondrocytes, endothelial cells, fibroblasts, HSCs and osteoblasts were positively correlated with the dormancy signature genes, suggesting their presence is associated with a higher expression of dormancy promoting genes.

The expression of these individual cell types was assessed in the deconvoluted dataset for both the Farr *et al.* (2015) dataset (see Figure 5-26) and for mice that underwent sham vs OVX (see Figure 5-27).

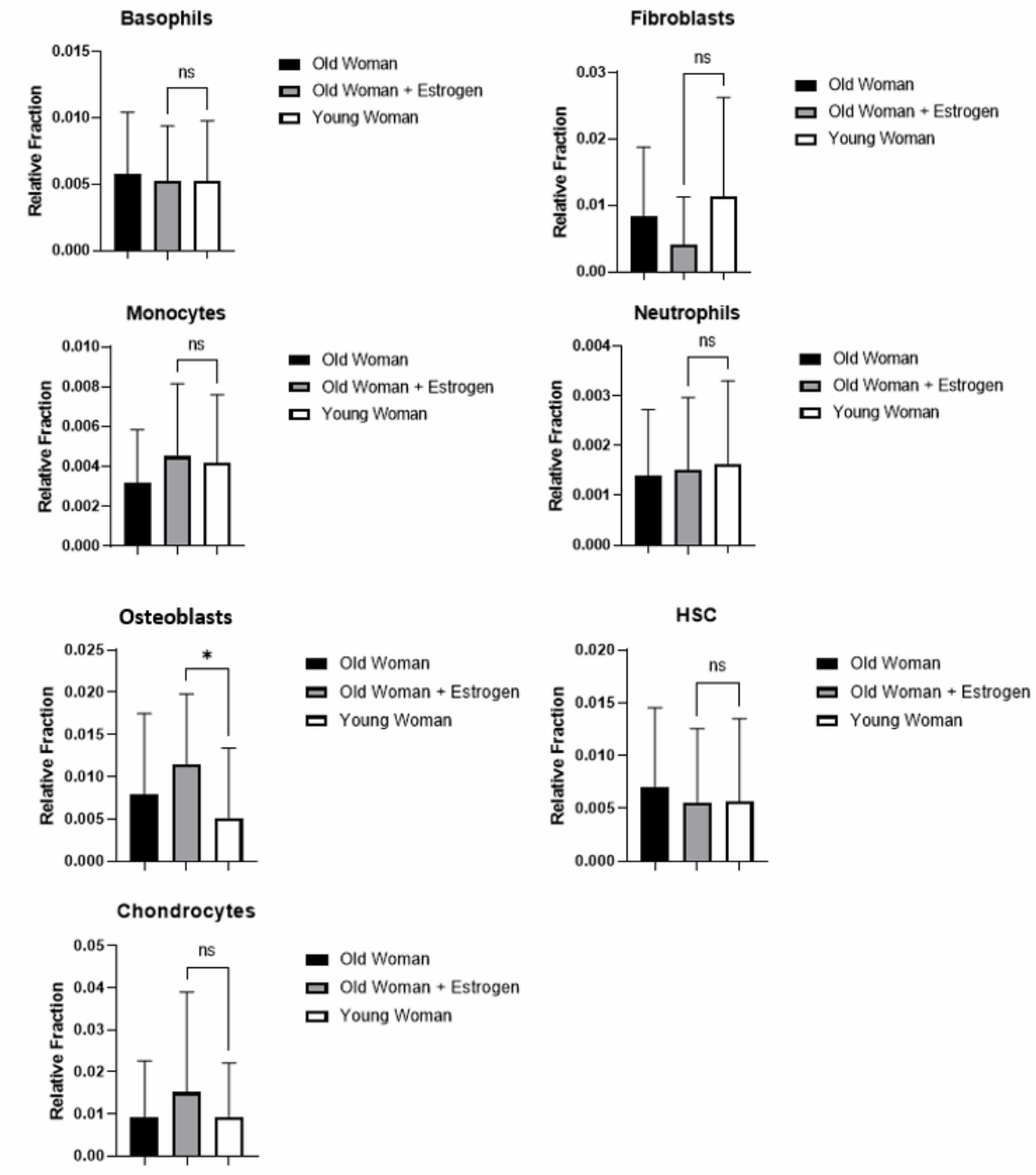

Figure 5-26: Cell type abundance estimates from the Farr *et al*. (2015) dataset. No significant difference in cell abundance between Old Woman vs Old Woman + Oestrogen, Old Woman vs Young Woman and Old Woman + Oestrogen vs Young Woman for all cells tested by unpaired t-test with welch's correction

In the Farr *et al.* (2015) dataset, there was a largely unchanged landscape of the cell types isolated between the different groups. However, osteoblast numbers were significantly increased in old women treated with oestrogen compared to young women. The difference was not significant between old women and any of the other groups. This result is not unexpected, as oestrogen mediates the differentiation of parental bipolar stromal cells towards osteoblasts (Okazaki *et al*., 2002).

The same cells were analysed in the sham vs OVX dataset (see Figure 5-27).

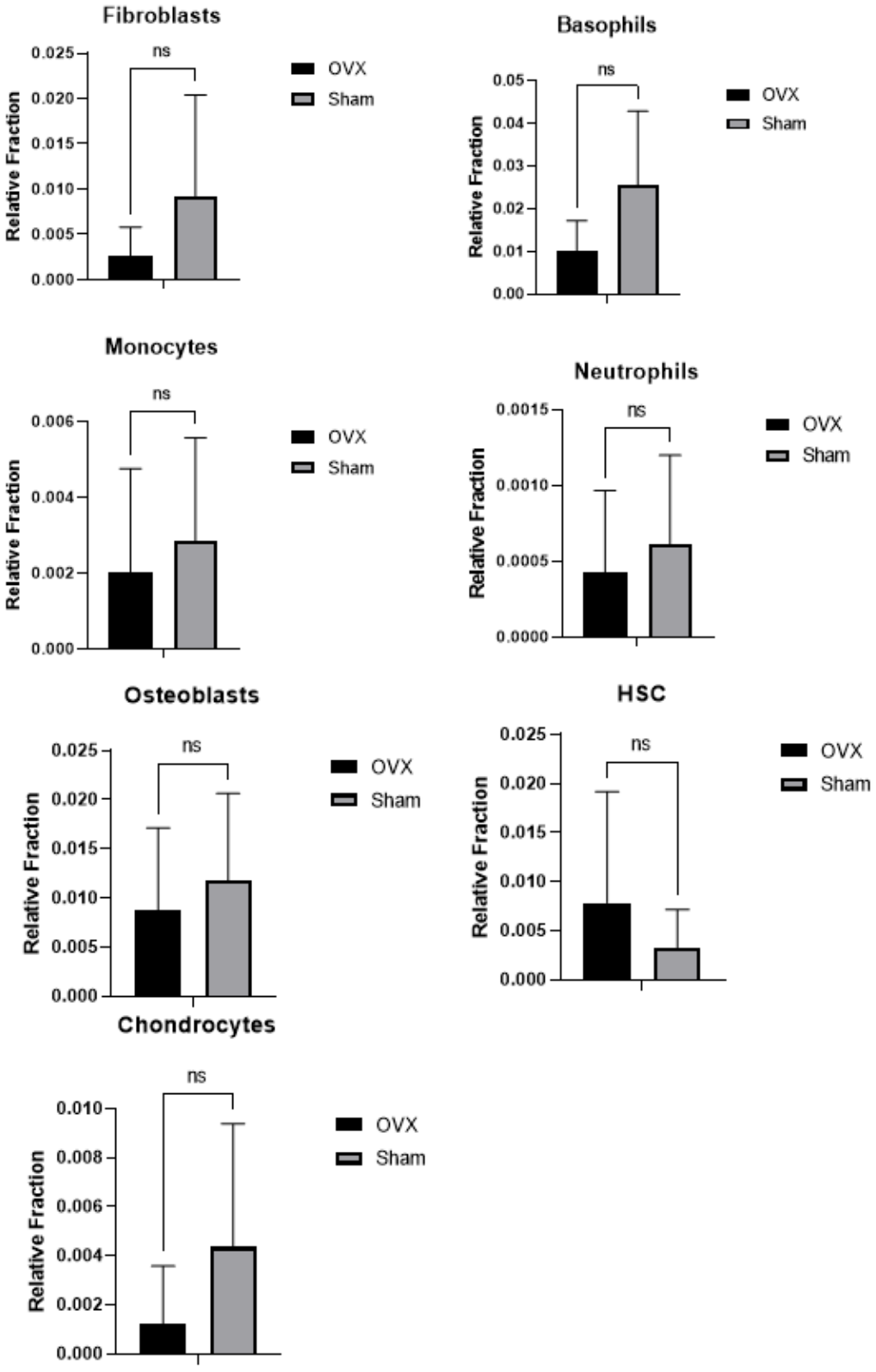

Figure 5-27: Cell type abundance estimates from mice that have undergone either sham or OVX. No significant difference found between all cells tested between OVX and sham.

Similarly to the Farr *et al.* (2015) dataset, there were no significant differences between the groups, with a general tendency to decrease all cell types in the OVX group. Interestingly, cells correlated with a decrease in dormancy promoting genes, monocytes and basophils, were reduced on average, though non-significantly. However, other cells associated with an increase in dormancy promoting genes appeared to be likewise decreased, meaning a trend could not be established. Overall, a correlation between pro-dormancy genes could not be established in the conditions belonging to the datasets, neither could a correlation between cell types and the dormancy-promoting signature be established. The limited number of animals used for this study and sample variability may mask important correlations, and repeating this experiment with increased sample numbers would significantly improve comparisons between the datasets.

5.7.6.1 Human Cancer Metastasis Database correlation

To investigate the clinical value of the altered transcriptional landscape detected in my sample set, the top two enriched pathways upregulated in ovariectomised mice were used to identify potential genes of interest to query in clinical datasets. The top two enriched pathways, ECM receptor interaction and focal adhesion, contained various genes belonging to the collagen super family as well as SPP1, THBS2 and TNN were upregulated in both enriched pathways. Therefore, these genes, SPP1 and THBS2 were selected to be further investigated. In addition, MMP2, which was altered in the Ottewell *et al.* (2015) dataset, the Farr *et al.* dataset, as well as in ovariectomised mice was further investigated.

As gene expression data from metastatic sites are limited, analyses were focused on the effect of these genes expressed in the primary breast cancer on time to metastasis using distant metastasis free survival (DMFS), as well as correlation with the expression of these genes with the site of metastasis. DMFS was assessed in KM-plotter using gene symbols as input (SPP1, THBS2, MMP2 and POSTN) with default parameters, searching across all breast cancer subtypes and treatments, using the auto-select best cut-off feature, which selected the best separation value between the upper and lower expression thresholds for separation of high-expressing and lower-expressing patients. This was combined with expression data of these genes from breast cancer metastases to different organ sites based on data from the Human Cancer Metastasis Database (HCMDB) generated by Zhang *et al.* (2009. Zhang which profiled 58 breast cancer metastases from different organs (bone, liver, lung and brain) under Gene Expression Omnibus (GEO) accession number GSE14020 split across 2 datasets (Zhang *et al*., 2009). Data from the HCMBD also included genes co-expressed with the selected gene.

Analysis of SPP1 expression in breast tumours that metastasised to different sites showed an increased expression in the bone compared to brain liver and lung in both HCMBD analysed (p=0.013) (see Figure 5-28). In addition, analysis of DMFS across breast cancer patients found higher expression of SPP1 to be significantly correlated with decreased DMFS across breast cancer subtypes or sites of metastasis with a hazard ratio of 1.83 (logrank p = 4.4×10^{-14}). Similarly, THBS2 expression was found to be significantly increased in tumours that metastasised to bone compared to the brain and lung in both HCMBD datasets analysed (p=2.086×10^{-3} and 1.167×10^{-3}), and was also found to be significantly

correlated with difference in DMFS outcome, though with lower effect compared to SPP1 with hazard ratio of 1.27 (p=0.005) (see Figure 5-29). MMP2 was also found to be upregulated in tumours that metastasised to the bone compared to brain and lung in both datasets HCMDB datasets selected (p= $7.038x10^{-3}$ and $8.883x10^{-3}$ but had an insignificant change in risk of distant metastasis in high expressing patients (logrank p =0.09) (see Figure 5-30) . Similarly to MMP2, POSTN expression was significantly increased in tumours that metastasised to bone compared to brain and lung (p= $3.30x10^{-3}$ and $4.44x10^{-3}$) but risk of metastasis of high expressing patients vs low expressing patients was insignificant (logrank p =0.28) (see Figure 5-31).

A

Gene name	Correlation coef
LINC00312	0.437469644528499
ANKRD10-IT1	0.400440784231457
KDM2A	0.570940492026582
CLCF1	0.568493322788331
MYO1C	0.568016531564356
SPHK1	0.554639791718219
RBM41	0.550502128729591
GNL3L	0.545646825298727
CDC27	0.544826788819597
C1orf61	0.54437261249166
ZBTB7A	0.537642183163772

B

Gene name	Correlation coef
LINC00312	0.437469644528499
ANKRD10-IT1	0.400440784231457
KDM2A	0.570940492026582
CLCF1	0.568493322788331
MYO1C	0.568016531564356
SPHK1	0.554639791718219
RBM41	0.550502128729591
GNL3L	0.545646825298727
CDC27	0.544826788819597
C1orf61	0.54437261249166

C

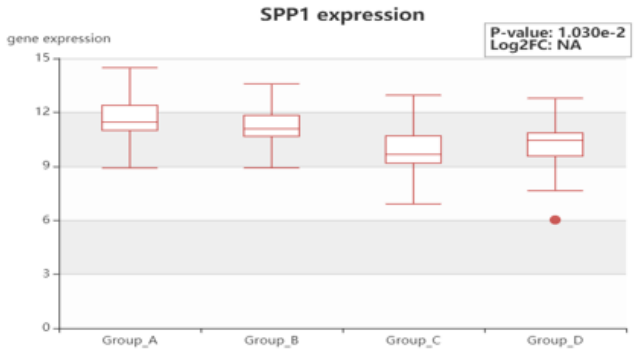

D

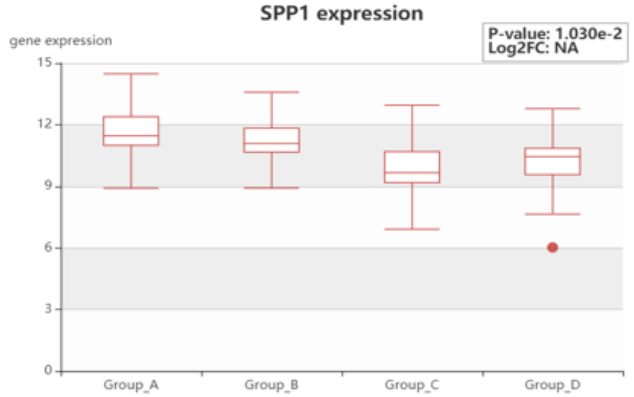

E

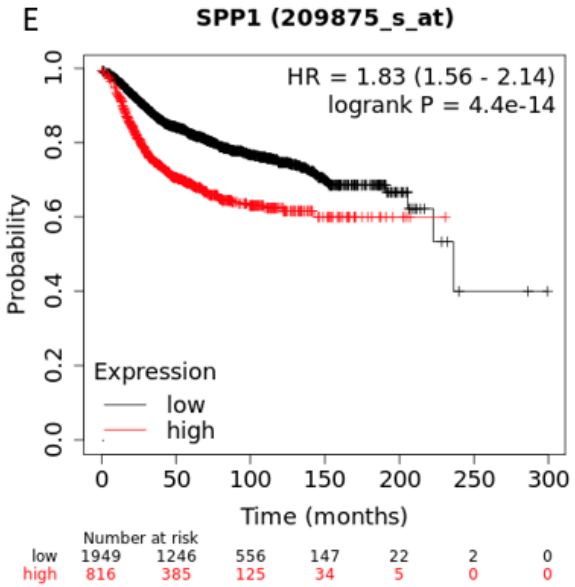

Figure 5-28: A and B co-expression correlation of genes with SPP1 in both datasets; C and D; Expression values for SPP1 in tumours that metastasised to Bone (Group A), Brain (Group B), Liver(Group C) and Lung (Group D) showing significantly increased expression of SPP1 in tumours that metastasized to bone in both datasets selected (p- 0.013); E DMFS of high expressing patients vs low expressing patients showing significantly increased risk of distant metastasis in high expressing patients (logrank p 4.4e-14)

A

Gene name	Correlation coef
MIR100HG	0.790781248784855
LINC01279	0.771729826141916
MAGI2-AS3	0.723973542772236
ITGB2-AS1	0.688779533031069
RUNX1-IT1	0.671696103654635
LINC01505	0.637587513982077
LEF1-AS1	0.622653574695807
MIR22HG	0.605060643918423

B

Gene name	Correlation coef
MIR100HG	0.79654934902786
LINC01279	0.749145768283235
MAGI2-AS3	0.732745278323251
RUNX1-IT1	0.678241063216498
ITGB2-AS1	0.655761412368406
LINC01505	0.642089785860454
LEF1-AS1	0.634853630215284
MIR22HG	0.594952362288112

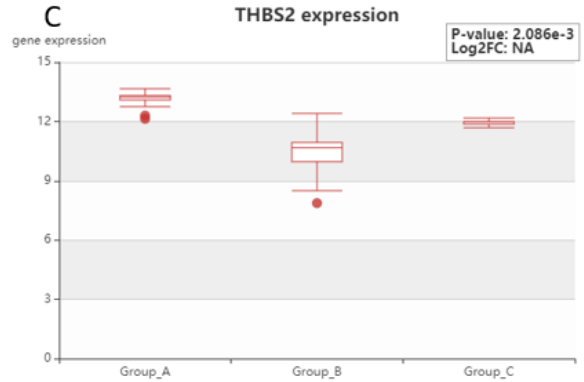

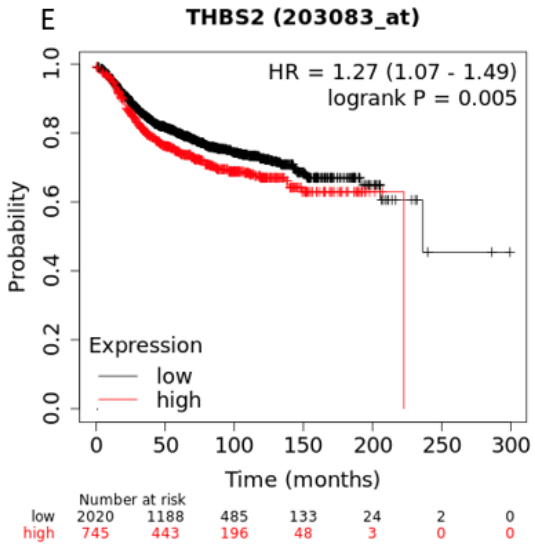

Figure 5-29: A and B co-expression correlation of genes with THBS2 in both datasets; C and D; Expression values for SPP1 in tumours that metastasised to Bone (Group A), Brain (Group B), Lung(Group C) showing significantly increased expression of THBS2 in tumours that metastasized to bone in both datasets selected (p- $2.086x10^{-3}$ and $1.167x10^{-3}$); E DMFS of high expressing patients vs low expressing patients showing slight yet significantly increased risk of distant metastasis in high expressing patients (logrank p =0.005)

A

Gene name	Correlation coef
LINC01279	0.858798994755511
RUNX1-IT1	0.786169655795695
ITGB2-AS1	0.748144232835978
MAGI2-AS3	0.731747955207507
MIR100HG	0.665855293834471
LEF1-AS1	0.66456008345109
LINC01505	0.656121400838047
MIR22HG	0.612397046449654

B

Gene name	Correlation coef
LINC01279	0.871939615566135
RUNX1-IT1	0.78345079960508
ITGB2-AS1	0.76950994342698
MAGI2-AS3	0.729491126701105
MIR100HG	0.661171636376021
LEF1-AS1	0.660472054396938
LINC01505	0.652510095090469
MIR22HG	0.616928915531161

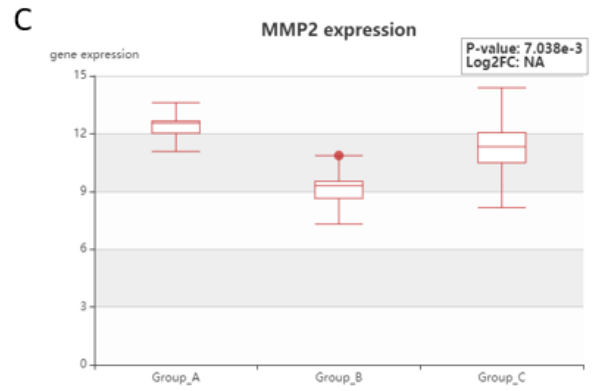

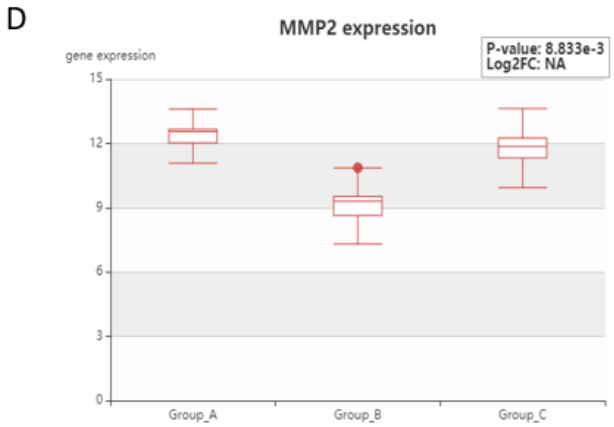

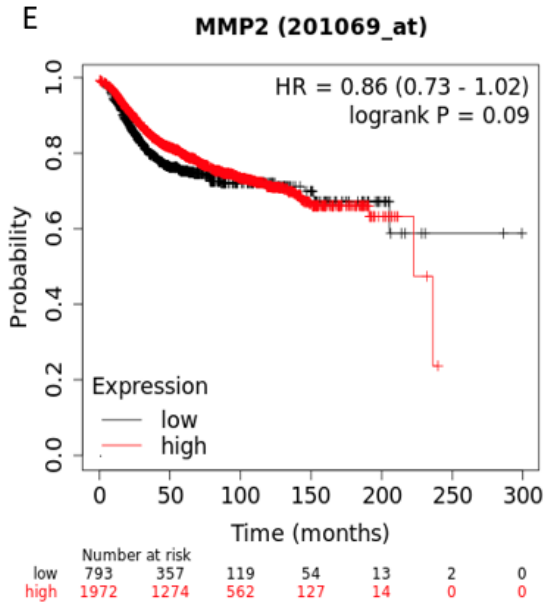

Figure 5-30: A and B co-expression correlation of genes with MMP2 in both datasets; C and D; Expression values for MMP2 in tumours that metastasised to Bone (Group A), Brain (Group B), Lung(Group C) showing significantly increased expression of MMP2 in tumours that metastasized to bone in both datasets selected (p= 7.038e-3 and 8.883e-3); E DMFS of high expressing patients vs low expressing patients showing an insignificant change in risk of distant metastasis in high expressing patients (logrank p =0.09)

A

Gene name	Correlation coef
LINC01279	0.728118500802019
MIR100HG	0.66135608760938
MAGI2-AS3	0.624114768085918
SNHG18	0.608833946533727
FZD10-AS1	0.601208479175225
MIR22HG	0.578308058259925
PAXIP1-AS2	0.568606598157891

B

Gene name	Correlation coef
LINC01279	0.72725225186974
MIR100HG	0.650564497891785
MAGI2-AS3	0.609284079150758
SNHG18	0.606381106762579
FZD10-AS1	0.579308408698384
MIR22HG	0.578348521124433

C

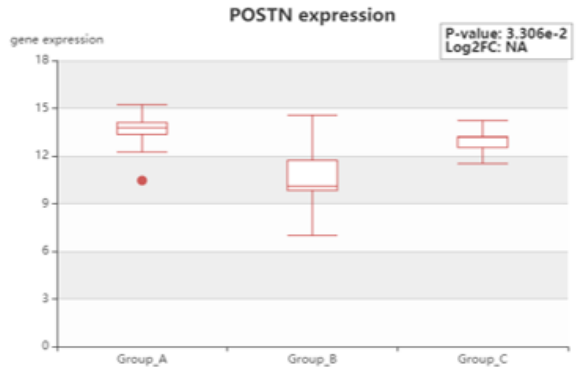

D

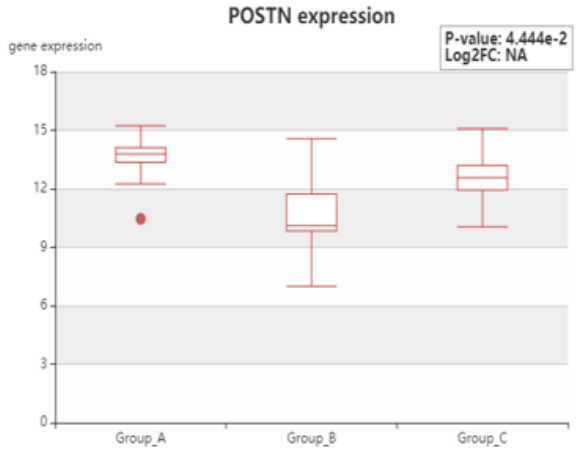

E

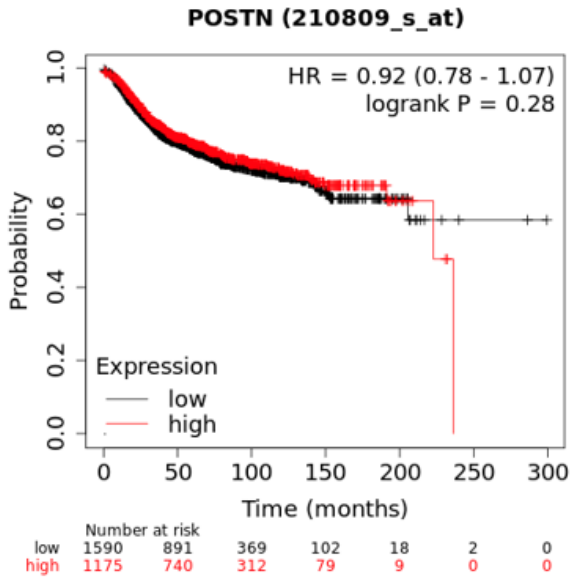

Figure 5-31: A and B co-expression correlation of genes with POSTN in both datasets; C and D; Expression values for POSTN in tumours that metastasised to Bone (Group A), Brain (Group B), Lung(Group C) showing significantly increased expression of POSTN in tumours that metastasized to bone in both datasets selected (p- 3.306e-3 and 4.444e-3); E DMFS of high expressing patients vs low expressing patients showing an insignificant change in risk of distant metastasis in high expressing patients (logrank p =0.28)

5.8 DISCUSSION

The bone microenvironment plays a significant role in the homing and engraftment of disseminated breast cancer cells, as well as their subsequent maintenance in a dormant state or overt outgrowth. Understanding the complicated interplay between genes and cells of the microenvironment with disseminated tumour cells under different conditions may allow more accurate recapitulation of clinical events in research models, as well as provide potential targets for therapeutic or prognostic purposes.

In particular, ovariectomy has been shown to alter the bone microenvironment leading to the overt outgrowth of dormant, disseminated tumour cells (DTCs) in the long bones of mice (Ottewell *et al*., 2015). Outgrowth of DTCs to form overt tumours has also been inhibited in mouse models by therapeutically targeting osteoclasts, even in the absence of cancer-targeting therapies (Ottewell *et al*., 2008).

However, these results have only been demonstrated in pre clinical models and remain difficult to extrapolate to the clinical setting. The AZURE trial showed that the use of the anti-resorptive Zol in the adjuvant setting was not sufficient to prevent progressive secondary disease within the bone of women with breast cancer (Coleman *et al*., 2014). Stratification of results based on menopausal status did show that Zol benefit was influenced by menopausal status, with increased invasive disease free survival (IDFS) and overall survival (OS) with Zol treatment, but only in women 5 years or more into menopause. These findings suggest that the influence of oestrogen on the bone microenvironment of post-menopausal women may have played a significant role in disease prevention with Zol. Combined with preclinical data on oestrogen deprivation leading to overt outgrowth of disseminated tumour cells (Ottewell *et al*., 2015), this shows that oestrogen may play a key role in the progression of cancer within the bone in both the presence or absence of bone targeting agents.

Previously, Ottewell *et al.* (2014) inoculated mature (12week old) BALB/C nude mice with MDA-MB-231 breast cancer cells before waiting for dormancy to be established after 8 weeks. Animals were divided into two groups, to undergo either an ovariectomy or sham operation, and tumour growth monitored. Importantly, mice which underwent an ovariectomy operation had a significant increase in tumour cells in the long bones, approximately 80% of the ovariectomised animals developed outgrowth of DTCs (n=7). In contrast, the sham operated animals had a lower rate of outgrowth of DTCs in the long bones, approximately 30% (n=7) (Ottewell *et al*., 2015). Understanding the changes that occur in the absence of tumours would allow for the assessment of the changes to the microenvironment that would precede and subsequently support tumour growth. I therefore carried out a comprehensive study to investigate the composition of the bone microenvironment following oestrogen deprivation by ovariectomy in the absence of tumours, in order to determine the changes to the early transcriptional landscape leading to overt outgrowth od DTCs. To this end, 14-week old immunocompetent BALB/C mice underwent either a sham operation or ovariectomy and analyses of the BMEV carried out after 2 weeks to capture the changes. Bones and tissue from these mice were then collected to analyse the physical bone structure, circulating hematopoietic cells and RNA-

Sequencing to comprehensively characterise and compare the cellular and molecular composition under these conditions.

5.8.1 Physical Bone Structure

Ovariectomy-mediated deprivation of oestrogen within the bone microenvironment leads to a reduction of OPG and increased production of RANKL by osteoblasts (Eghbali-Fatourechi *et al*., 2003, Hofbauer *et al*., 1999), increasing bone turnover and subsequent bone resorption that can be detected by µCT. Consistent with this, I found a significant reduction in bone volume and trabecular thickness in animals that had undergone ovariectomy procedure. The change was not dramatic and could be marginally observed in reconstructed images, but was significant according to measurements taken from the trabecular region. Ottewell *et al.* (2014) showed that 2 weeks following ovariectomy, bone volume as measured by µCT was statistically significantly reduced by approximately 3%, which is similar to the results I obtained (Ottewell *et al*., 2014a). These µCT data indicate that the ovariectomy procedure induced the expected effect that could be detected at the structural level, therefore implicating changes at the cellular and transcript level.

5.8.2 Circulating hematopoietic cells

Whole blood was collected from the mice for analysis of the hematopoietic milieu in the circulation. A significant difference in circulating cells could not be observed following alteration of the bone microenvironment by OVX compared to Sham. Interestingly, red blood cells were reduced in the OVX group compared to Sham, though not significantly (p=0.0879). This, in conjunction with a reduction of erythropoietic genes EPB41 and EPB42 in the OVX group as well as in older women according to the Farr *et al.* (2015) dataset, may indicate that oestrogen influences erythropoiesis and may potentially impact on red blood cell numbers. However, further research is required to establish this indication.

Regulation of haematopoiesis may return cellular populations to homeostatic levels following Sham/OVX within the 2-week time frame between operation and sample collection. Although various stressors, including DNA damage, inflammation, metabolic stress, obesity and ovariectomy can directly influence HSC regulation and function, quiescent HSCs that have been activated by stress can return to the quiescent state within a few weeks, as well as returning downstream progeny to baseline levels (Poller *et al*., 2020). It is therefore likely that cells within the peripheral circulation would return to homeostatic cell levels within the time frame of my experiment.

Circulating cells may also appear to be unchanged between OVX and sham animals due to the systemic effect that surgery, performed on both groups, has on inflammation and hematopoiesis. Krall and colleagues (2018) described an *in vivo* model of surgery-induced systemic inflammation that led to the escape of tumour cells in immune-mediated dormancy (Krall *et al*., 2018). Analysis of circulating hematopoietic cells revealed an elevated level of $Ly6C^{hi}$ monocytes and neutrophils with a corresponding increase in G-CSF and CCL2 in surgically-wounded mice, which reflect leukocyte pertubations following surgery in breast cancer patients (Bartal *et al*., 2010). Therefore the surgery

experienced in both groups may be a confounding factor that would result in greater alterations in circulating hematopoietic cells than oestrogen deprivation alone and may mask an changes observed through oestrogen deprivation on circulating hematopoietic cells.

5.8.3 RNA-Sequencing

To further elucidate the bone microenvironment in sham-operated and ovariectomised mice, whole femurs from the mice were used for RNA-Sequencing. This required the optimisation and development of a hybrid protocol which allowed extraction of RNA with sufficient integrity. However, due to the limitations on the extraction protocol, the whole bone could not be digested, and fragments of the bone were not processed. It must be noted that bone lining cells may not have been dislodged in sufficient quantity to produce their expressed genes in the data.

The extracted RNA was then sequenced at 37.5 million reads per sample in single end sequencing. Although paired end sequencing and higher reads per sample yield more accurate and robust results, due to constrains on budget and the need to sequence at least 4 samples for comparison between conditions, through consultation with Dr Timothy Wright at the Sheffield Diagnostic Genetics Service and Dr Lewis Quayle, it was decided that this sequencing protocol would be sufficient for the conditions and budget.

The processing pipeline of RNA sequencing reads can significantly impact the results. Therefore, methods chosen for pre-processing were chosen as they are well established and cited in the literature, such as FastQC for quality control, Trimmomatic for adapter trimming and STAR for read alignment, with the latest reference genome for mouse at the time of processing, GRCm39 used as a reference genome for alignment and for quantification (Callari *et al*., 2018, Conesa *et al*., 2016, Dobin *et al*., 2013). The method used for quantification, DegNorm, was selected as it was deemed optimal for the quantification of potentially degraded transcripts and would produce read counts adjusted for transcript degradation(Xiong *et al*., 2019).

5.8.4 Differentially Expressed Genes

Out of 27,999 genes with non-zero read count, at an FDR value of < 0.1 and log fold changes > 0, a total of 157 genes were found to be significantly altered between the sham and OVX group. This is a relatively small number, as in the Farr *et al.* (2015) dataset that compared young women (~30 years old) with old women (~73 years old), a total of 678 genes were found to be significantly altered. This suggests a more moderate difference in physiology between mice that have had an ovariectomy compared to sham operated animals. Considering the timeframe in which the animals were under procedure, 2 weeks, it is not surprising that the resultant differentially expressed genes were moderate in number. In the Farr *et al.* (2015) dataset, when older women were compared with those who had 3 weeks of oestrogen therapy, only 21 genes were found to be differentially expressed between the two groups, again indicating significant changes in gene expression within the bone may occur through sustained supplementation or loss of oestrogen over greater periods of time. This slight

alteration in physiology is also suggested by µCT analysis which showed a slight, yet significant, reduction in trabecular bone volume in ovariectomised mice.

One of the ways proposed that oestrogen exerts bone protective mechanisms is attributed to an increase in OPG and decrease in RANKL signalling by osteoblasts leading to reduced osteoclastogenesis (Streicher *et al*., 2017). Therefore, it may be expected to see a change in the transcripts, but these were not significantly altered by ovariectomy compared to sham. However, a large proportion of the genes upregulated in the ovariectomised group are involved in the remodelling of the extracellular matrix and cellular adhesion, notably with MMP2, osteopontin (SPP1), periostin and various collagen coding genes upregulated. These indicate an increased bone remodelling cycle of degradation and formation by osteoclast and osteoblasts respectively and were also found by Ottewell *et al.* (2015) when identifying differentially expressed genes by rtPCR. The increased osteoclast activity as indicated by decreased trabecular bone volume measurements by µCT assessment would subsequently involve increased osteoblast activity through the tight coupling of bone degradation and formation. Therefore the findings are in harmony with what would be expected with increased bone turnover.

The relatively low number of genes found to be differentially expressed from such a large sample has the potential to be misleading, as even with the use of Benjamini-Hochberg correction for multiple hypothesis testing, there can still be a significant proportion of genes randomly predicted as differentially expressed when such low numbers are identified. In addition to this, with low sample numbers, inference must be made with caution due to low statistical power. However, as discussed prior, the differentially expressed genes were in in broad agreement with what would be expected in a bone microenvironment with higher bone turnover, and it can be safely assumed that the genes predicted as differentially expressed are indeed that.

Although fewer genes and pathways than expected were significantly altered in ovariectomised mice, they were consistent with expected results, showing a changes to collagen and cellular adhesion molecules, as would be expected to be observed in a microenvironment with increased turnover. There was also poor overlap with genes found by Ottewell *et al.* (2014) using a very similar experimental procedure. The timepoint analysed, 14 days following ovariectomy may have been a time point when initial transcriptional changes had already occurred and several genes had return to homeostasis. Indeed, Ottewell *et al* (2014) found 27 significantly altered genes by PCR 7 days following ovariectomy, of which one was found altered across both datasets (MMP2). Interestingly though, MMP2 was upregulated in my dataset of ovariectomised mice, yet Ottewell *et al.* (2014) found this gene to be downregulated. Furthermore, they found a number of genes involved in osteoclast function, such as RANKL, TRAP (inducers of osteoclast differentiation and function) and OPG (inhibitor of osteoclast function), significantly altered, which did not appear to be differentially expressed in my dataset. However, decreased bone volume as measured by µCT and changes in various genes related to extra cellular matrix reorganisation, osteoblast function (collagen genes) and osteoclast-mediated bone resorption (osteopontin) were detected to indicate that, although the exact gene overlaps were small in number, the physiology was similar. It is important to consider that the Ottewell *et al.* (2014)

study performed the analysis of genes 7 days following ovariectomy and it is not clear whether a subset of genes that were initially increased in transcription could have returned to base line through equilibrating mechanisms and therefore were not differentially expressed in my dataset (analysed at day 14). Furthermore, as the optimised method for RNA isolation for RNA-Seq I used may not have sufficiently extracted cells from the trabecular region where osteoclasts are concentrated, it may have meant that several genes indicating altered osteoblast or increased osteoclast activity would have been disproportionate to the actual expression levels in the trabecular region. Therefore there may be an underestimation of the transcriptional changes in genes from these bone lining cells.

5.8.5 Altered Pathways

Pathway analysis using differentially expressed genes showed that pathways involved in cellular adhesion, platelet activation and proteoglycans in cancer were generally increased in ovariectomised mice, driven in a large part by genes involved in collagen formation. Although overall the bone volume decreased, the tight coupling between bone resorption by osteoclasts and formation by osteoblasts in the bone remodelling cycle would indicate that increased collagenous genes produced by osteoblasts would be expected. The increase in extra cellular matrix remodelling are in agreement with results from the Farr *et al.* (2015) dataset, where young women have an increase in genes involved in pathways relating to cell adhesion and extra cellular matrix reorganisation, driven significantly by collagen and laminin genes. In contrast, pathways involved in angiogenesis and vascular formation were also upregulated in young women compared to old, which did not feature significantly in the pathways I found to be upregulated in ovariectomised mice. The short duration from OVX/Sham to sample collection may in part account for the lack of altered angiogenic pathways altered in the ovariectomised mice.

5.8.6 Genes of interest

Several genes altered in ovariectomised mice were of interest as to the potential regulation of tumour cell outgrowth, and a subset discussed in the following sections may be candidates for further research.

MKI67, widely used as a marker for increased proliferation, was found to be upregulated in ovariectomised mice, reflecting a general increase in cell cycling within the bone marrow. The downregulation of cell cycle repressors E2F4 and TFDP2 in ovariectomised mice further revealed a microenvironment supportive of increased proliferation (Chen and Lodish, 2014, Hsu *et al*., 2019). Additionally, TAL1, an important player in leukemogenesis and haematopoiesis that maintains the multipotency and quiescence of HSCs, an important factor in upregulating c-KIT, was found to be downregulated in ovariectomised mice, suggesting that cells within the HSC niche and progenitor cells were activated into proliferation (Vagapova *et al*., 2018). TAL1 is also upregulated in 60% of T-cell acute lymphoblastic leukemia and mutant forms of TAL1 are present in approximately 20% of patients diagnosed with lymphoid and myeloid leukemia (Begley *et al*., 1989, Ferrando *et al*., 2002). Therefore TAL1 would potentially be an interesting target for understanding the regulation of dormancy and

cancer progression in the bone. However, as a transcription factor, it is unclear as to whether it is a driver of quiescence or a downstream effector of dormancy-inductive cues. Furthermore, it is difficult to speculate as to how the microenvironment would induce aberrant expression of TAL1 in resident tumour cells without upstream signalling and may thus prove an indicator rather than driver of the entry into and exit from dormancy.

Growth arrest specific 5 (GAS5) is a long non-coding RNA which was downregulated in ovariectomised mice. GAS5 has been demonstrated to play a role in quiescence-inductive cues in CD133+ pancreatic tumour initiating cancer stem cells, that are characterised by quiescence and are responsible for tumour relapse (Sharma *et al*., 2019). In their study, Sharma and colleagues (2019) demonstrated that the emergence of CD133+ pancreatic cancer cells coincided with upregulation of GAS5, further characterised with routed metabolites, such as the shunting of biosynthetic pathways such as the pentose phosphate pathway, reducing nucleic acid synthesis. On inhibition of GAS5 in this population, release from cell cycle arrest occurred, increasing proliferation and nucleic acid synthesis. This study demonstrated that altering GAS5 alone was able to regulate quiescence in tumour cells, showing its significance in tumour cell dormancy. Furthermore, as a long non-coding RNA, it is possible for its transfer between cells in exosome-mediated signalling, and thus can potentially be a molecule used to transfer quiescent inductive signals within the microenvironment (Han *et al*., 2020, Kogure *et al*., 2013).

The histone subunit H2AX plays a critical part in double strand break repair and H2AX phosphorylation is used as a marker for DNA damage (Redon *et al*., 2010). H2AX was found to be downregulated in ovariectomised mice compared to sham operated animals. Oestrogn receptor α-mediated transcription has been shown to induce cell cycle-dependent DNA double-strand breaks (DSBs) in human MCF-7 breast cancer cells response to 17β-estradiol. Although ovariectomised mice had a transcriptional signature suggesting an increase in cell cycling, and therefore more potential for DSBs to occur, Williamson and Lees-Miller showed that the increase in DSBs was through the action of oestrogen-inducible genes (Williamson and Lees-Miller, 2011). Therefore, in the absence of oestrogen, increased proliferation may be accompanied by fewer DSBs. Further research is needed to establish the correlation of H2AX in therapeutically-induced dormancy in cancer.

Amongst genes selected for additional analysis were MMP2, POSTN, THBS2 and SPP1, all upregulated in ovariectomised mice. These were chosen due to their secretion into the microenvironment and inclusion in the two most-enriched pathways in ovariectomised mice (ECM receptor interaction and focal adhesion – THBS2 and SPP1), being significantly altered in all three datasets of interest; the Farr *et al.* (2015) and Ottewell *et al.* (2015) datasets, as well as upregulated in ovariectomised mice (MMP2). In addition, POSTN was included as a significantly overexpressed gene in ovariectomised with well studied effects within the bone (Bonnet *et al*., 2016). To establish the potential clinical relevance of the upregulation of these genes in cancer is limited by the lack of available datasets; publicly available clinical gene expression data are largely derived from in primary tumours without corresponding expression data from metastatic sites or the associated microenvironment. Current large scale tumour-derived clinical data, combined with smaller data from metastatic sites, were

therefore used to suggest how the genes influence the site of metastasis and time to metastasis. Although metastatic recurrence is an imperfect measure in this context, a large proportion of patients who die from metastatic breast cancer will have skeletal involvement, suggesting a key role of the bone microenvironment in metastatic progression.

Analysis of SPP1, THBS2, MMP2 and POSTN expression at metastatic sites from the HCMDB showed a significantly increased expression in the bone compared to brain, liver or lung, implying their significance within the bone microenvironment compared to the other sites. In addition, the top co-expressed genes with MMP2 and THBS2 showed high similarity, with POSTN showing similarity, albeit less and even less so with SPP1. These genes included MIR100HG, LINC01279, MIR22HG and MAGI2-AS3, all non-coding RNAs highly co-expressed with MMP2, THBS2 and POSTN implicated in modulating cancer disease progression MAGI2-AS3 and MIR22HG showing tumour-suppressive characteristics and MIR100HG and LINC01279 tumour-promoting (Chen *et al*., 2020a, Meng *et al*., 2021, Shu and Wang, 2020, Xu *et al*., 2021). High similarity with co-expression of genes further suggests complicated interplay between genes and regulatory RNAs that may be upstream of several of these genes and may offer attractive targets. However, it must be noted that these non-coding RNAs were not found to be significantly altered in my dataset from ovariectomy or sham operated mice, despite the form of RNA selection (rRNA depletion), in contrast to poly-A selection, making possible the discovery of these non-coding RNAs. The co-expression of these other non-coding RNAs in this case, only highlight the importance of exploring regulatory networks in addition to directly comparing altered genes.

Analysis of expression of MMP2, SPP1, THBS2 and POSTN in large scale clinical data from breast cancer primary sites relating to DMFS through KM Plotter showed a significant reduction in time to metastasis in patient cohorts with a high expression of SPP1, with a marginal, yet still significantly reduced time to metastasis in patients with a high expression of THBS2. High expression of MMP2 and POSTN did not significantly change time to metastasis progression when highly expressed by the primary site. A lack of resolution to stratify by metastatic site may be confounding the possibility of site-specific increased metastatic risk, but it may be reasoned when taking into account data from metastases that SPP1 is important in both the metastasis from the primary tumour to the bone, where it continues to play a significant role, whereas MMP2, THBS2 and POSTN are more important in the bone microenvironment in driving metastasis progression. The proteins coded by these genes are therefore targets of interest for further research and therapeutic development as they were significantly altered in the oestrogen-deprived microenvironment across datasets, while their co-expressed non-coding RNAs potentially provide therapeutic potential upstream of the signalling cascades that lead to the expressions of these proteins.

5.8.7 Cellular Deconvolution

The cellular deconvolution using the xCell package inferred relative abundance of 64 different cell types within the bone microenvironment. The only significant differences in cell types identified by deconvolution of the dataset I generated was in class-switched memory B cells, being increased in ovariectomised mice. Interestingly, pro B cells were similarly were also increased in ovariectomised

mice, although not statistically significantly increased with a p value of 0.0536, marginally above the significance threshold. This change in B cells however was not observed when comparing between young women, old women and old women supplemented with oestrogen therapy. Oestrogen receptors α and β are both present on B cells and lymphoid progenitors (Sanchez-Aguilera and Mendez-Ferrer, 2016), and as such could reasonably be thought to be altered due to changes in oestrogen presence. Published research has suggested an increase in B cell activation and reduced apoptosis in response to oestrogen, which is contrary to the findings that they increase in ovariectomised mice, which have reduced oestrogen, compared to sham operated mice (Grimaldi *et al*., 2002). It must be noted, that these changes in B cell activation in response to oestrogen have largely been carried out using *in vitro* models, or settings where bone turnover were not present. Bone remodelling alters and is altered by the cellular landscape, in part by increasing osteoclast and osteoblast numbers and activity. It may therefore reasonably be expected that other cells in the hematopoietic and mesenchymal lineage are affected in response to changes in bone remodelling (Compston, 2002). The genes significantly altered in response to ovariectomy did not further support alterations in B cell populations. Indeed, TAL1 (SCL), a gene that has been shown to function as a cell cycle activator in myeloid and lymphoid progenitors, was downregulated in ovariectomised mice, suggesting that this would lead to increases in B cell numbers (Souroullas *et al*., 2009). Although deconvolution showed a significant alteration in class switched memory B cells, there were no other indicators in gene expression nor in hematopoietic analysis to support this conclusion.

Although a number of analyses of cells showed statistically significant changes in cell abundance between ovariectomised mice and sham in addition to B cells, they had a majority (more than or equal to 2) of samples with zero scores for that specific cell type, which would significantly alter the average. These cell types were discarded from analyses, but it is possible that these were true positives and were discarded due to caution. Greater sample numbers would allow for more robust analysis and handling of outliers.

Deconvolution in the Farr *et al.* (2015) dataset only showed osteoblasts as significantly altered between young women and old women supplemented with oestrogen. Oestrogen influences osteoblast numbers and function, and therefore observing an increase in osteoblast numbers is appropriate for women treated with oestrogen. Coinciding with this, on average, women treated with oestrogen experienced a 55.4% (+/- 27.4%) increase in serum PINP over the three weeks of supplementation, compared to changes of 2.1 (+/- 22.4%) in old women, while data on changes in PINP were unavailable for young women. However, it is surprising to observe significant changes in osteoblast numbers in old women supplemented with oestrogen compared to young women, but not compared to other old women. Neither was there a significant difference in osteoblast numbers between old women and young women, where would be expected to observe the greatest differences. The genes in young women presented higher levels of osteoblast-associated genes, yet they had a lower average number of osteoblasts, although this difference was not significant. Furthermore, the genes altered by oestrogen supplementation in older women did not include genes associated with osteoblasts. Therefore, even though osteoblast function may be what oestrogen deprivation or supplementation is altering, these results do seem inconclusive despite statistical

significance and any inference based on them must be done so with caution. It must be noted that there is potential for a disconnect between gene expression and cell numbers, as not just cell numbers, but relative activity is also important, meaning that each measure in isolation may mask significant changes. Furthermore, the data was obtained at a point in time and therefore do not reflect the biological changes that would have taken place over years when comparing expression between young and old groups.

Overall, deconvolution of bulk RNA-Sequencing data by xCell was not conclusive despite some statistically significant results. The bone microenvironment, being the site of haematopoiesis and also a site that contains a heterogeneous population of cells, may be particularly difficult to resolve computationally. Furthermore, converting mouse genes to human genes prior to deconvolution resulted in the loss of a portion of genes that may have contributed to better resolving the cellular population.

5.8.8 Dormancy Scoring

Using singscore, a R/Bioconductor package that allows scoring of custom gene sets, was used to score samples against the dormancy signature developed by Kim *et al.* (2012) derived from cancer cell lines, providing both up and down regulated genes in dormant cancer cells. A dormancy signature from cancer cells was used, as, although it is derived from tumour cells and not the microenvironment, dormancy signatures are not well elucidated and this provided an experimentally-verified signature. Applying this to gene expression in the bone microenvironment would therefore potentially identify transcriptional signatures in the microenvironment that may induce dormancy within the microenvironment, and therefore, tumour cells that may be present within it.

Scoring ovariectomised mice compared to sham operated mice did not reveal any distinction between the groups in the gene signature tested. Analysis of expression values of NR2F1 and BHLHE41, key genes whose inhibition led to exit from dormancy, did not reveal any significant differences between ovariectomised and sham operated mice. Interestingly, two genes, MMP2 and COL1A1, genes found upregulated in dormant cancer cells, were upregulated in ovariectomised mice. However, their function may be enigmatic and may coincide with a phenotypical switch into dormancy when accompanied by the other genes within the signature. These genes were not considered significant by Kim *et al.* (2012). Having a small sample number poses difficulty in resolving signatures scored on genes that were not necessarily differentially expressed and may have been why the signature did not clearly distinguish the groups. Scoring the Farr *et al.* (2015) dataset, however, also showed poor resolution between the different groups of women, with a heterogenous score for all the groups, suggesting that increased numbers would not necessarily lead to a better resolution in the presence or absence of oestrogen and with age.

It must be noted, however, that these two datasets involved the sequencing of entire bone marrow with heterogenous cell populations. The bone marrow is a site of continuous haematopoiesis, where quiescence is reserved for distinct cellular populations and would therefore contain a significant

portion of actively dividing cells, confounding the ability to resolve quiescent transcriptional programmes in a specific population of cells. Therefore, a dormancy signature may not exist in a heterogenous population but rather within a specific cell population. This is supported by the testing of the dataset from Cawthorn *et al.* (2009), where tumour cells were isolated from the bone marrow prior to sequencing, and despite sample numbers closer to the dataset I generated, it distinguished the dormancy signature between the two groups (DTCs vs MTCs) more significantly. Importantly, the signature was generated from tumour cells, which frequently have distinct transcriptional programmes to other cells. This may also be why the Cawthorn *et al.* dataset showed better resolution between the two groups tested for this tumour cell dormancy signature. Therefore, the application for this dormancy signature, and others derived from lineages of distinct populations, may not be suitable for application in heterogenous cell populations distinct from the cell types the signatures were derived from and in which a significant fraction of the population is actively dividing. There is a need to establish dormancy signatures relating to the bone microenvironment, and even cellular compartments within this microenvironment as these signatures vary from tissue and cell type. Further research into dormancy within the microenvironment must be underpinned by robust, validated dormancy signatures within clear cellular compartments.

To further analyse whether any cell types could be correlated with samples that scored highly with the dormancy transcriptional signature, spearman correlation between the samples' dormancy score and cellular population as inferred through deconvolution, was performed. The results revealed a subset of cells which had either a positive or negative correlation with the dormancy-associated upregulated genes score, and a corresponding opposite effect on the dormancy associated downregulated genes score. These cells were selected by using a cut off of a correlation either <0.3 (positive) or > -0.3 (negative) correlation in either the up or down score. Basophils, neutrophils and monocytes were subsequently negatively correlated with the dormancy signature, whereas chondrocytes, endothelial cells, fibroblasts, HSCs and osteoblasts had a positive correlation with the dormancy signature. A positive correlation between HSCs and the dormancy signature is reasonable as HSCs are the resident quiescent cells within the bone marrow (Passegue and Wagers, 2006). Furthermore, osteoblasts, fibroblasts and endothelial cells are also implicated in cancer dormancy (Dai *et al*., 2021, Indraccolo *et al*., 2009, Yu-Lee *et al*., 2018). However, their presence and function is enigmatic and have also been implicated in tumourigenesis. Although immune cells are implicated in various cancers, their role in regulation of tumour dormancy is still undefined (Wang *et al*., 2019). Therefore, although the correlation between cells estimated through deconvolution and dormancy scores provide some interesting results, they remain inconclusive without further analysis.

5.8.9 Comparability between the ovariectomised mouse and post-menopausal bone microenvironments

Pre clinical models provide some recapitulation of clinical (human) features, though limited. The ovariectomy model has been used to attempt to model the bone microenvironment of post-menopausal women due to the loss of oestrogen. The availability of an RNA-Seq dataset from Farr *et al.* (2015) including bone marrow samples from young women, old women and old women treated

with oestrogen provided a good opportunity to assess in some part, the veracity and degree of biological inference from an established ovariectomy model to the clinical situation it is attempting to recapitulate (Diaz Brinton, 2012, Koebele and Bimonte-Nelson, 2016). The lack of tumour cells and control for clinical parameters that would affect the bone microenvironment, such as levels of FSH and vitamin D, allowed for a robust, controlled experiment, and of a good sized data set (n=20 per group)(Farr *et al*., 2015).

Comparing ovariectomised mice to the human dataset revealed a larger overlap in gene expression between ovariectomised mice and young women than ovariectomised mice and old women. The presence of collagenous genes and pathways relating to ECM remodelling were similar between young women and ovariectomised mice. However, angiogenic pathways seemed to be increased in young women, whereas ovariectomised mice did not reveal signatures linked with these pathways, but rather had THBSP2, an inhibitor of angiogenesis upregulated, suggesting a more similar angiogenic profile to older women. The overlap between ovariectomised mice and young women presented a complex landscape in which some features resemble the bone younger women, such as ECM remodelling, while other features are contrasted, such as the loss of oestrogen and angiogenic signals. It should be taken into account, however, that there was not a significant overlap between transcriptional profiles of ovariectomised mice from my dataset and those generated by ovariectomy by Ottewell *et al.* (2014) either. This may present anomalous results in my dataset, but it must be noted that Ottewell *et al.* (2008, 2014, 2015) showed the efficacy of the use of osteoclast-targeting agents in preventing overt outgrowth of disseminated tumour cells, which has not been observed in clinical trials of Zol or Denosumab, potent osteoclast inhibitors. However, with the use of Zol in the AZURE trial, women who were 5 years into menopause had an invasive disease free survival (IDFS) of 78.2% and overall survival (OS) at 5 years of 85.6% treated with Zol compared to 71% IDFS and 78.7% OS in the control arm. Importantly, women that were rendered post-menopausal due to chemotherapy did not benefit from bisphosphonates, suggesting menopausal status at the initiation of treatment was important. In that case, a preclinical mouse model of ovariectomy may better recapitulate the post-menopausal bone microenvironment after a significant period of time, and the time of genetic analysis may be the causative factor in the limited overlap between these datasets. Indeed, oestrogen therapy for 3 weeks in old women altered the bone microenvironment significantly less extensively than the effect age had, and it is uncertain whether cellular and transcriptional changes were more impacted by an aged hematopoietic lineage than by oestrogen (de Haan and Lazare, 2018, Kim *et al*., 2008, Mejia-Ramirez and Florian, 2020). Indeed, the age of the mature mice used in these studies is more comparable to young women with stable bone homeostasis, rather than aged mice whose bone microenvironment may better recapitulate that of old women. Therefore, this highlights the current limitation of extrapolating results from pre clinical ovariectomy mouse model to the clinic and any such inferences must be done so with caution and careful consideration of what aspects are truly similar to the clinical setting being inferred.

5.8.10 LIMITATIONS OF THE STUDY

A number of limitations in this study may have impacted conclusions that could be drawn from this research. Importantly, low numbers of samples were used in each tested group. This would present significant influences of outliers on the results, and such small numbers may not present a representative sample of the population but should be considered a pilot study. This could be observed when removing two samples from the differential expression testing resulting in better resolution on PCA analysis separation. However, this represented 25% of the samples, a significant portion to omit. Furthermore, the sequencing depth of 37.5 million single end reads per sample is on the lower end of published research, which often uses 50 million paired end reads per sample and above. Limited funding placed restrictions on the study design and number of samples to be sequenced and the strategy designed was optimal for the budget after consultation with Dr Timothy Wright and Dr Lewis Quayle.

The analysis pipeline chosen would also heavily influence gene expression estimation and downstream prediction (Tong *et al*., 2020). The tools used individually and jointly impact the accuracy of gene expression estimation. Although the pipeline was carefully chosen as the industry standard tools or for the particular considerations for my experiment, such as DegNorm for degraded transcripts, using a different pipeline would have resulted in potentially significantly different gene expression estimation as benchmarking of tools is often done in limited combination, validation and with samples distinct to those I was using. In addition, the presence of non-coding RNA species may have impacted the alignment and subsequent abundance estimation of transcript reads. However, analysis of differentially expressed genes revealed genes expected and as such confidence can be placed on the tools and pipeline used.

How transcriptional signatures in the bone microenvironment change in response to oestrogen, and whether this is evolves over time is also an important consideration. Differences in differentially expressed genes between my dataset, in which mice were ovariectomised for 14 days prior to analysis and the dataset from Ottewell *et al.* (2014), in which mice were ovariectomised 7 days prior to analysis, may indicate a potential evolution of genes over time in the absence of oestrogen, and so the timing of the experiment may have produced different results. However, this change in gene expression over time is not well elucidated.

Changes to the post-menopausal bone microenvironment include effects greater than those attributable to oestrogen deprivation. An aged hematopoietic lineage confers many age-related characteristics independent of the effects attributed purely oestrogen deprivation, including shifts from osteolineage to adipolineage differentiation bias of MSCs (Kim *et al*., 2008). This results in decreased bone formation and increased adipocytes, altered vasculature such as reduced frequency of arterioles and transitional vessels, higher reactive oxygen species presence (ROS), decreased arteriolar innervation, increased CCL5 expression leading to myeloid bias (Poller *et al*., 2020). Therefore, extrapolating results from the mature, oestrogen-deprived mouse bone to human post-

menopausal bone must be done with caution and improved models are needed to capture the biological complexity of the aged, post-menopausal bone.

5.8.11 Conclusion and further work/experiments

Further investigation is necessary in order to elucidate the early transcriptional and cellular changes in the bone microenvironment of ovariectomised mice to uncover clinically relevant mechanisms that may be exploited in patients at high risk of developing secondary breast cancer in the bone at a more favourable, early stage.

Analysis of upstream regulators for genes altered by ovariectomy, as well as those altered in dormancy may yield further insight into the correlation between maintenance of dormancy and metastatic outgrowth of DTCs within bone following ovariectomy in mice, with upstream regulators in dormant cancer cells. Preliminary investigation into upstream regulators using the eXpression2Kinase upstream protein-protein kinase and transcription factor prediction (Clarke *et al*., 2018), show potential correlation between regulatory kinases that interacting with transcription factors regulating genes that were upregulated in dormant cancer cell lines (Kim *et al.,* 2012) and those downregulated in ovariectomised bone, as well as correlation between those downregulated in dormant cancer cell lines (Kim *et al.,* 2012) and those upregulated in ovariectomised mice. This correlation would suggest similarities between mature naïve mouse bone and pro-dormancy cancer transcriptional regulatory landscapes, as well as similarities between ovariectomised mouse bone and cancer cell outgrowth, and appear worthy of further investigation (see appendix 1).

It is not clear whether genes altered by oestrogen deprivation or therapy would vary over time, which is likely as bone is a dynamic system. In the Farr *et al.* (2015) dataset, the effect of age was much more pronounced than the transcriptional changes elicited by short term oestrogen supplementation in older women. Furthermore, a majority of genes found to be transcriptionally altered in mice following 7 days of ovariectomy by Ottewell *et al.* (2014) were not differentially expressed in my dataset based on mice being under ovariectomy procedure for 14 days before analysis. A time course in ovariectomised mice, including analysis at shorter time spans from ovariectomy (up to 7 days) and extended time following ovariectomy (up to 12 months) would allow for better resolution as to the evolution of the transcriptional landscape and any equilibrium and homeostatic reverse of gene expression. Furthermore, the current ovariectomy models use 12-14 week old mice are more comparable in relative age and physiology to young women than the older women included in the clinical studies. A more robust approach would be to use aged mice with aged stem cells that more appropriately respond to oestrogen deprivation as old women.

The studies performed focused on the tumour free bone microenvironment. Therefore, necessary next steps would involve the presence of disseminated tumour cells, to study how the cellular and transcriptional landscape evolves with tumour cells in the early stages of growth. It is important to focus on the early stages, as even in pre-clinical mouse models, once overt tumours are detectable, their growth is not stopped by osteoclast inhibition alone. Use of chemotherapy combined with bone

targeted agents has shown more promise in pre-clinical models and it would be important to further investigate the early mechanisms and the impact of chemotherapy on the bone microenvironment that may significantly contribute to the success or failure of a therapeutic regimen.

A limitation posed by my experiment is that of RNA transcripts that were partially degraded, with RIN scores less than 7, as well as probable insufficient lysis of bone lining cells. Downstream analysis, such as read alignment and differential expression may have been impacted by the presence of degraded transcripts and shorter non-coding nucleic acid sequences as rRNA depletion was used, instead of the industry standard poly A selection for RNA sequencing on which most standard tools are benchmarked. Therefore, further optimisation of a protocol that would include sufficient material from bone lining cells and allow for sufficient RNA integrity for the use of poly A selection in the RNA sequencing workflow would contribute to the robustness of results.

Computational imputation of genes and cellular constituents is statistically based and can on occasion produce erroneous results. Often, the exact method used for computational inference can have an impact on the resulting outputs which may be incorrect without further validation, as observed in benchmarking studies (Avila Cobos *et al.*, 2020). Without validating genes and proteins they encode by PCR and cells by histology or flow cytometry, false positive and equally false negatives may be inferred.

6 DISCUSSION

Cancer remains a significant contributor to mortality accounting for approximately one third of deaths in the UK (UK, 2018). Breast cancer incidence is amongst the highest, with 15% of new cancer cases in 2015 from breast cancer, where 60-80% of cancers spread to the bone (Ahn *et al*., 2013, Coleman, 1997b, Yousefi *et al*., 2018). A major challenge facing therapeutic intervention and monitoring in breast cancer is tumour cell dormancy, which is characterised by long periods (5+ years) of undetectable tumour cells following remission from the primary tumour, whereby metastatic relapse subsequently occurs that is often incurable (Pan *et al*., 2017). It is currently not possible to detect and monitor tumour dormancy in patients, as the cells are often in small clusters or are not cycling and cannot be detected by conventional methods, such as using radioactively-labelled glucose (5-FDG) that allow for detection of concentrated cells with increased glucose metabolism (Xi *et al*., 2014). Understanding the regulation of dormancy and subsequent escape is important for developing new therapeutic strategies to improve the outcome for patients with breast cancer.

Dormancy is characterised into three broad types; immune, angiogenic and cellular, which have differing physiological characteristics, such as cell cycle arrest in cellular dormancy, or the rate of immune destruction of a dividing population at equilibrium with the rate of multiplication in immune-mediated dormancy (Yeh and Ramaswamy, 2015). It is currently difficult to establish the type of dormancy in a clinical setting, and it is likely a combination of all three types. Therefore, murine models have been developed that reflect known types of dormancy.

The microenvironment plays an important role in the establishment and maintenance of dormancy (Sosnoski *et al*., 2015). In immunologic dormancy, the immune cells are the key in maintaining an equilibrium between tumour cell proliferation and immune-induced apoptosis (Teng *et al*., 2008). However, the microenvironment is also important in angiogenic and cellular dormancy. Angiogenic dormancy is induced by nutrient deprivation owing to distance from blood vessels. Various cells, such as macrophages and fibroblasts, and molecules, such as VEGF, MMPs and THBSP-1, in the microenvironment are implicated in angiogenesis (Benzekry *et al*., 2014, Naumov *et al*., 2009). An imbalance in these cells and molecules within the microenvironment can either maintain angiogenic dormancy, or lead to a pro-angiogenic switch, leading to outgrowth of dormant DTCs.

Bone is a highly mineralised tissue and is also a rich store of proteins that promote cellular growth. In addition, various cells and molecules residing within the bone microenvironment, including immune cells from a hematopoietic lineage, as well as cells from a mesenchymal lineage, also directly induce dormancy (Bruns *et al*., 2014, Gustafsson and Welsh, 2016, Wilson *et al*., 2008). The dynamic interplay between these niches, cells and molecules create a complex picture in which breast cancer cells metastasise to, are held dormant and subsequent escape into overt outgrowth (Sosnoski *et al*., 2015). Elucidating the contribution of the bone microenvironment to cancer progression is therefore important in order to provide therapeutic, actionable targets.

The quiescent and proliferative state of HSCs are informed by cells and molecules locally resident within the bone microenvironment. It is postulated that disseminated tumour cells may be located in locations within the HSC niche and be similarly regulated (Allocca *et al*., 2019a, Bruns *et al*., 2014).

In particular, osteoclasts are the only cell with the ability to degrade both mineralized contents of the bone and the organic matrix, leading to release of ionic calcium and growth factors that promote cellular growth. Osteolytic cancers, such as disseminated breast cancer, rely on recruited osteoclasts and the vicious cycle to propagate tumour growth in response to increased bone turnover (Käkönen and Mundy, 2003). In model systems of breast cancer, targeting the osteoclast has shown promise, and is a candidate approach for the prevention of overt outgrowth of disseminated tumour cells mediated by increased bone resorption (Ottewell *et al*., 2015).

Various methods and protocols are used to study dormancy and tumour progression in bone. Lipophilic membrane dyes which are subsequently lost during replication can be used in conjunction with multiphoton microscopy to image dormant, disseminated tumour cells within the bone. In one such study, Allocca *et al.* (2019) showed that a proportion of mature BALB/C nude mice injected with MDA-MB-231 cells had detectable dormant tumour cells in the bone, as detected by the retention of lipophilic membrane dyes. Unreliability of the multiphoton microscope available meant it could not be used in my studies to confirm the presence of dormant, disseminated tumour cells. Therefore, my studies defined dormancy in an *in vivo* setting as undetectable tumours by *in vivo* IVIS imaging after a period of 3 weeks (21 days) following injection with between 5-10x10^4 cells via intra-cardiac injection.

Hematopoietic populations have been shown to be affected by the use of the anti-resoptive agent Zol. Ubellacker *et al.* (2017), demonstrated that a single, clinically relevant dose of Zol induced transient changes in the numbers of hematopoietic stem cells, myeloid-biased and lymphoid-biased progenitor cells, generating tumour-suppresive bone marrow populations which inhibited breast tumour growth in bone when injected into recipient 6 to 7 week-old mice. Interestingly, the tumour suppressive effect was maintained past the timepoint at which the number of progenitor cells returned to baseline levels (Ubellacker *et al*., 2017). The alteration of this niche may therefore affect tumour dormancy and growth within the bone and requires further investigation. Studies investigating the effects of Zol alone on tumour growth have often used a single, clinically relevant dose of 100µg/kg, yet have not found significant benefit to preventing tumour outgrowth in bone. Daubiné *et al.* (2007), however, found a reduction in tumour-induced bone lesions and tumour burden when using a daily and weekly cumulative doses, providing justification for exploring more frequent doses than a single administration for my studies.

Ottewell *et al.* (2015) demonstrated that triggering dramatic changes to the bone microenvironment by ovariectomy was sufficient to stimulate dormant, disseminated breast cancer cells into overt outgrowth, but that this process could be inhibited by administering mice with OPG-Fc or Zol prior to ovariectomy. Though Zol monotherapy has shown inhibition in rate of tumour growth, there have been limited results in preventing tumour growth. Understanding the exact changes in the microenvironment at an early stage is necessary to provide clinically-actionable targets. Preliminary data from our lab has also suggested that a low calcium diet may be able to induce the overt outgrowth of dormant, disseminated tumour cells, highlighting the need to understand the role of a microenvironment in a state of high turnover on the progression of cancer.

My studies aimed to explore the effect of alterations in the bone microenvironment on the regulation of disseminated breast cancer cells within bone by i.) characterising the effect of a low calcium (0.1%) diet on the bone microenvironment and whether this could trigger subsequent escape from dormancy of disseminated tumour cells, ii.) characterising the effects of repeated administration of the anti-resorptive agent Zoledronic Acid on the bone microenvironment and development of bone metastases in mice with high bone turnover, and iii.) profiling early transcriptional and cellular changes by RNA-seq in the bone microenvironment of ovariectomised mice, which procedure has been previously shown to trigger the outgrowth of dormant, disseminated tumour cells.

6.1 The Effect of a Low Calcium Diet on the Bone Microenvironment and the Outgrowth of Disseminated Tumour Cells

In chapter 3, I explored the effect of a low calcium diet on the bone microenvironment and how this alteration would subsequently affect the outgrowth of dormant, disseminated tumour cells *in vivo*. The proposed mechanism would be that a low calcium diet, leading to hypocalcaemia would induce the secretion of parathyroid hormone, whose effect is to increase osteoclast-mediated bone resorption in a bid to release calcium stored within bone, by upregulating RANKL and decreasing OPG secretion by osteoblasts (Silva and Bilezikian, 2015). This increase in bone resorption would also trigger changes in the bone microenvironment, such as release of growth factors embedded in the bone matrix, that would subsequently lead to dormancy escape of dormant DTCs. Published studies exploring the effect of a low calcium diet in mice have focused on the alteration of the rate of tumour growth (Libouban and Chappard, 2017, Wang *et al*., 2017a, Zheng *et al*., 2007). Collectively, these studies provide evidence that changes to the BMEV that occur due to a low calcium diet are sufficient to affect the rate of tumour outgrowth. However, my experiments were novel in using a low calcium diet to accelerate bone resorption to induce the overt outgrowth of dormant, disseminated breast cancer cells.

That changes in bone turnover can trigger outgrowth of DTCs is supported by studies that have used other methods to accelerate bone resorption. Ottewell and colleagues demonstrated that increasing osteoclast activity in the presence of DTCs through ovariectomy triggered the outgrowth of the DTCs, whereas inhibition of osteoclast activity by Zol or OPG-Fc was sufficient to significantly inhibit this outgrowth (Ottewell *et al*., 2015, Ottewell *et al*., 2014a).

I initially placed immunocompromised BALB/C nude mice as well as immunocompetent C57/BL6 mice on a low calcium diet for 7 days and assessed the effects a low calcium diet had on the bone microenvironment in the absence of tumours. Suprisingly, there was no detectable change in bone structure in either mouse strain as assessed by µCT, neither did PCR analysis of genes involved in HSC expansion (Kit Ligand), quiescence (CXCL4), osteoclast differentiation and activity (RANK Ligand, Osteopontin), osteoclast inhibition (Osteoprotegerin), and anti-angiogenic markers (Thrombospondin 1) reveal significant differences between mice fed a low calcium diet and those fed a normal diet, despite earlier pilot studies in our lab showing the low calcium diet induced bone loss.

A time-course experiment placing mice on a low calcium diet with cohorts culled and analyses carried at days 2, 3, 7, 14 and 28 was then conducted, to establish whether changes in the bone microenvironment could be detected at different points in time after the change in diet. I found that the bone structure of isolated tibiae was statistically significantly reduced at day 28 as assessed by μCT, with no significant change at any other time point, yet this change was minor compared to control. Analysis of Kit L, CXCL4, Osteopontin, RANKL, THBSP1 and OPG by PCR from whole femurs also showed no significant difference at all time points. Analysis of serum TRAP (a marker for osteoclast-induced bone destruction) and P1NP (a marker for bone formation by osteoblasts), displayed an increase in bone destruction, with a decrease in bone formation on days 7 and 14 of the low calcium diet, shifting the balance towards bone resorption. This effect had returned to baseline by day 28. These experiments suggested that the low calcium diet did not have a strong effect on the bone microenvironment, even after 4 weeks. However, it is still possible that the subtle changes detected could be sufficient to alter the bone metastatic niches and affect DTCs. It is also important to consider that genes analysed were not a comprehensive selection, and that changes to the bone microenvironment may have occurred at the transcriptional level that were not captured due to a limited number of genes analysed.

To analyse the effect of the low calcium diet on the outgrowth of dormant, disseminated tumour cells, 15-week old BALB/C nude mice were injected with $1x10^5$ GFP+ and Luc2+ transfected MDA-MB-231-IV cells via intra-cardiac injection. Mice were subsequently monitored for 21 days post injection, with a lack of tumour outgrowth indicating that tumour cells remain dormant in bone. At day 21, mice with detectable tumour growth were removed from the experiment, while tumour free mice, predicted to have dormant, disseminated tumour cells in bone, were randomised 50/50 to receive either a low-calcium diet or a normal diet for 14 days. Unexpectedly, a significant proportion of mice developed hind-limb or skeletal tumours within 14 days of tumour cell injection, with 15 out of 17 surviving mice developing skeletal metastases by day 21. At this point, the experimental design was adapted and the tumour-bearing mice were randomised to receive either a low calcium diet to assess whether I could detect accelerated tumour growth as reported by other studies. Mice received the low calcium diet for 2, 3, or and 14 days, however no significant effect on tumour growth was observed, which did not agree with previously published data showing an increase in tumour growth rate (Libouban and Chappard, 2017, Wang *et al*., 2017a, Zheng *et al*., 2007). Possible explanations for the lack of agreement with previous studies could be that the calcium content (0.1%) was not low enough to induce significant bone loss in mature (12-week old) mice, as a variety of mouse strains, ages and tumour types were used to demonstrate the effects of a low calcium diet on the bone microenvironment (Libouban and Chappard, 2017, Minematsu *et al*., 2001, Wang *et al*., 2017a, Zheng *et al*., 2008, Zheng *et al*., 2007). Other studies that demonstrated significant bone loss using a 0.1% calcium diet used young (4-week old) mice with a different rate of natural bone growth and therefore an increased requirement for calcium (Zheng *et al*., 2008, Zheng *et al*., 2007). Several studies used diets with a calcium content lower than 0.05, with those using mature mice (12+ week old) using diets of 0.008% (Wang *et al*., 2017a).

As the MDA-MB-231 IV cells caused a rapid progression of tumours in bone, precluding studies of longer-term exposure to low calcium, I proceeded to repeat the experiment using a slower-growing MDA-MB-231-TD-Tomato clone in fewer animals of differing ages (6- and 12-week old female BALB/C nude mice). Use of these cells did appear to recapitulate the dormancy model, with no evidence of tumour outgrowth for up to 7-weeks post-injection (50,000-75,000 cells per mouse in 6-week and 12-week old mice). However, when subsequently given a low calcium diet for 28 days, before being placed back on a normal diet, no tumours were detected in skeletal sites even up to a period of 3 months post- tumour cell injection. Thus, there was no effect of exposure to low calcium diet in mice expected to have disseminated tumour cells in their long bones. Lack of access to previously available multiphoton microscopy meant verification of the presence of disseminated tumour cells in the apparently tumour-free mice could not be demonstrated in the same manner as in previous studies carried out in our team (Allocca *et al*., 2019b).

Studies using a low calcium diet in models using tumour cells, and those without, have not shown dramatic differences in initial outgrowth of tumour cells or bone architecture, but rather show difference in proliferation over a longer period of time on the diet (Zheng *et al*., 2007) (Minematsu *et al*., 2001) (Wang *et al*., 2017b) (Libouban and Chappard, 2017) (Zheng *et al*., 2008). Along with my findings, this demonstrated that a low calcium diet may not invoke as rapid a change in bone turnover as seen in hormone deprivation, and so may not be sufficient, in isolation, to trigger the outgrowth of disseminated tumour cells.

6.2 The Effect of Zoledronic Acid on the Bone Microenvironment in Young Mice

In chapter 4, I explored how repeated, weekly administration of Zol affects skeletal metastasis growth in young animals, through the modulation of the microenvironment. Included in this analysis was whether the cancer cell clone type had a significant effect on growth characteristics when Zol was administered, whether the hematopoietic milieu was altered, both in the bone marrow and in the circulation, as well as whether an increased frequency of administration would lead to differences in results reported by literature based on single administrations.

Murine model systems have been widely used to study breast cancer bone metastases, and upon engraftment, interventions inducing alterations to the bone microenvironment are introduced to trigger the outgrowth of dormant, disseminated tumour cells or aggravate existing metastatic outgrowths, such as through ovariectomy or low calcium diets. Animals of different ages, young (approximately 6 weeks) or mature (12+ weeks old) have been used to study different aspects of tumour-bone interaction, as younger mice experience higher levels of bone turnover with increased osteoblast and osteoclast activity compared to mature mice, whose lower levels of bone turnover have shown a DTC dormancy-supportive microenvironment (Jilka, 2013). There has been considerable debate as to whether Zol-mediated inhibition of bone resorption is sufficient to inhibit tumour growth in bone, with *in vivo* studies showing limited effect in reducing tumour growth using Zol alone. Despite research from Daubiné *et al.* (2007) suggesting that Zol administration reduces the tumour burden in

mice with breast cancer metastases to the bone, other research performed by Ottewell *et al.* (2008), Ubellacker *et al.* (2017), Brown *et al.* (2012) has shown limited effects of Zol alone on tumour burden, but have highlighted significant efficacy in reducing tumour burden, and hence tumour progression, when Zol is co-administered with chemotherapy than chemotherapy or Zol alone (Ottewell *et al*., 2008).

In my studies, I investigated the effect of Zol on tumour growth in young (~6 week old) mice. Published studies have mostly used a single 100µg/kg dose of Zol (Brown *et al*., 2012, Haider *et al*., 2014, Ottewell *et al*., 2008, Ubellacker *et al*., 2017); in contrast I used a once-weekly 100µg/kg dose for four consecutive weeks to determine whether more frequent dosing would have a larger effect on the bone microenvironment, and subsequent tumour growth. The frequent dosing was selected as patients with cancer induced bone disease receive Zol every 3-4 weeks, and as mice have a higher rate of bone turnover, an even more frequent schedule was chosen. In addition, research from Daubiné *et al.* (2007) showed that repeated dosing, of daily, weekly or single dosage had differential effects on reducing tumour burden, 87%, 53% and 16% reduction respectively (Daubiné *et al*., 2007). As this study suggested increased frequency of Zol administration reduces tumour burden, frequency of dose was considered as a variable that may alter tumour response to Zol administration and may explain the lack of research supporting reduced tumour burden as such studies frequently use a single dose.

Furthermore, proteomic analysis of tumour samples derived from the AZURE trial indicated a potential role for two proteins in the differential effect of Zol, macrophage-capping protein (CAPG) and PDZ domain-containing protein GIPC1 (GIPC1). Patients with higher expression of CAPG and GIPC1 in primary tumours were more likely to develop first distant recurrence when not treated with Zol. However, if patients had a high expression of both of these proteins, Zol administration was correlated with a 10-fold reduction in hazard ratio for first time to distant recurrence (Westbrook *et al*., 2016)(Lovero *et al*., 2021). This work suggested that a higher expression of GIPC1/CAPG in tumour cells (control cells) would correlate with slower growth in response to Zol, than cells with low expression (GIPC1/CAPG double knockout (DKO)). The study suggested that the expression of GIPC/CAPG in the primary tumour could be a biomarker for response to Zol.

Access to two different MDA-MB-231 clones (control and DKO) generated by Dr Vicky Cookson provided me with the opportunity to explore whether these did display a different growth pattern in bone and response to Zol, reflecting the clinical findings. I therefore designed an experiment where mice were divided into two groups to receive either the control or DKO cells by i.c. injection to generate tumours in bone. Each group was further divided into 2 groups receiving either PBS control or 100µg/kg Zol once weekly for 4 consecutive weeks, starting 7 days after injection with tumour cells, prior to cull and downstream analysis.

My experiments showed that four weeks of weekly Zol treatment had a significant effect on trabecular bone, increasing the bone volume, trabecular thickness and trabecular number in Zol-treated animals compared to control. However, there was no effect of Zol on the circulating hematopoietic cells measured at endpoint, nor did it alter the rate of tumour growth, whether analysed stratifying clones

or irrespective of clone type. This showed that in young mice, Zol does not slow down the rate of tumour growth, providing further evidence that effective targeting of OC activity is not sufficient to eliminate growth of bone metastases. It's important to note that, as a significant portion of animals did not show any tumour growth, the sample size comparing tumour growth was smaller than originally planned. In addition, there was significant variability between the groups and therefore consistent outcomes could not be established. Larger groups would reduce the impact of variability and allow for consistent measures of treatment groups.

My findings do not reflect those reported by Ubellacker *et al.* (2017), who showed significant alteration in hematopoietic cells following a single, clinically relevant dose of 100µg/kg of Zol in tumour-free, mature BALB/C nude mice. In that study, hematopoietic stem cells, megakaryocyte/erythroid progenitors and common myeloid progenitors were increased whereas common lymphoid progenitors were reduced, with the most dramatic changes detected between 3 and 5 days following Zol treatment before returning to homeostasis. As my analyses were carried out within four days of the last Zol treatment, I expected to detect similar changes. However, my analyses were carried out after the fourth successive dose, by which time any changes in the hematopoietic lineage cells may have returned to homeostasis or experienced diminished returns after such frequent dosing. Furthermore, the presence of tumours may have impacted the circulating cell fraction and confounded any potential changes that may have developed as a result of Zol administration. However, comparing circulating cells in tumour free animals also did not show any, significant difference, and when taking into account both treatment (Zol vs PBS) as well as presence of tumours in hind limbs (tumour free vs tumour bearing), there was no significant difference in any combination of conditions. Therefore, it is likely that the effects exerted by Zol had diminished by the fourth administration, 4 weeks after the initial dose, and thus may be the greatest factor in obtaining results dissimilar to Ubellacker *et al.* (2017).

My investigations showed that repeated administrations of a clinically relevant dose of Zol did not affect the rate of tumour growth despite significantly altering the bone microenvironment in the absence of tumours in young mice. Data from several clinical trials and preclinical studies also support the findings that Zol does not inhibit tumour growth but still plays a role in preventing skeletal related events in secondary breast cancer in the bone (Hitron and Adams, 2009). Zol has been shown to induce the reduction of osterix-positive osteoprogenitors due to the expansion of mesenchymal lineage cells and differentiation into osteoblasts (Hughes *et al*., 2019). Osteoblasts may be diverted from synthesising new matrix into secreting cytokines that promote breast cancer cell maintenance and change in osteoblast numbers and reduction in osteoprogenitors may have an impact on tumour growth that offsets a reduction in osteoclast-induced bone destruction (Kolb *et al*., 2019).

In contrast to the findings of Westbrook *et al* (Westbrook *et al*., 2016), there was no differential effect on tumour growth in tumour cell clones lacking expression of GIPC1 and CAPG (DKO), either with Zol or control treatment. It is important to note that the data correlating improved outcome with Zol in high GIPC1 and CAPG expressing tumours was generated through analysis of primary breast tumour samples only, as bone metastases are difficult to obtain in human studies. In addition, my experiments

focused on clones which had low/no CAPG/GIPC1 expression compared to control cells with average expression, exploring the effect a difference of expression had on tumour growth in the presence or absence of Zol. This overexpression may induce phenotypic differences that alter tumour growth kinetics in the presence or absence of Zol that my experimental design did capture. Clinical observations of the differential response to Zol with samples with overexpression of GIPC1 and CAPG showed differences in distant recurrences. Subsequently, GIPC1 and CAPG, involved in tubulin formation and cellular motility may be important in the process of metastasis, but not in a difference in growth kinetics of established metastases which may explain why no difference was observed between DKO and control cells with the use of PBS or Zol. Interestingly, DKO cells assumed a more spindle-like, thinner and smaller morphology than control cells, suggesting a change to phenotype with a double knockout, yet no measurable alteration in growth kinetics.

Taken together, my studies confirmed that Zol has major effects on the bone microenvironment in young mice, that appear to be mainly driven by reduced osteoclast activity. However, even repeated dosing for 4 weeks did not inhibit tumour growth in bone, irrespective of the tumour cell clone used, supporting that therapeutic targeting of bone alone is insufficient to inhibit progression of bone metastases.

6.2.1 TRANSCRIPTOMIC PROFILING OF THE BONE MICROENVIRONMENT COMPARING OVARIECTOMISED AND SHAM OPERATED MICE

Ottewell *et al.* (2014, 2015) demonstrated that the ovariectomy procedure in mature mice triggers the outgrowth of dormant, disseminated tumour cells within the bone microenvironment. In my studies in chapter 5, I investigated whether the changes in the bone microenvironment in response to ovariectomy showed a change in genes attributed to dormancy and to what extent the bone microenvironment in a murine ovariectomy model reflects the bone microenvironment in women past menopause. RNA-seq was used to analyse changes in the transcriptomic landscape at an early time point (14 days) following ovariectomy, to identify genes and pathways that could contribute to the triggering of overt outgrowth of dormant, disseminated tumour cells that may also be potential therapeutic targets.

To investigate this, 12-week old female BALB/C mice were randomised into 2 groups to either undergo an ovariectomy procedure or sham procedure, before being culled on day 14 and hind limb bones (tibia and femur) extracted for *ex vivo* analysis. µCT analysis of tibia showed a significant decrease in bone volume and trabecular spacing, indicating that the loss of oestrogen affected the molecular, cellular and physical landscape of the bone microenvironment as expected. This is in agreement with the previous studies by Ottewell that showed a decrease in bone volume following ovariectomy (Ottewell *et al*., 2014a).

Out of the 12 mice, 4 from each group had RNA extracted from femurs through a protocol I had optimised for extraction of sufficient quality RNA from bone, before being sequenced at the Sheffield Diagnostic Genetics Service of the Sheffield Children's NHS Foundation. The sequencing data was then

analysed for differentially expressed genes, scored against a dormancy signature and deconvoluted to identify cellular populations within the bone microenvironment. Quality control analyses were performed on the output data, which was visualised using principal component analysis and hierarchical clustering. Initially, poor clustering was observed between the two groups (Sham vs OVX), but following informed removal of two samples, the distinction between groups improved. The use of publicly available reference datasets was limited to human datasets, as comparable datasets based on murine bone are extremely scarce.

Dormancy Signature

While dormancy can be attributed to the function of specific genes, such as NR2F1, it is often characterised by a signature in which multiple genes are upregulated and downregulated in order to maintain cell cycle arrest (Kim *et al*., 2012). However, these signatures are not well defined and consistency between different cell and tissue types is unclear. A dormancy signature derived by Kim *et al.* (2012) from various cancer cell lines and applied specifically to ER+ breast cancer cell lines was used to compare the bone microenvironment in sham operated and ovariectomy operated mice. Although this signature is derived from tumour cells, it is one of a limited number of validated dormancy signatures, and it was used to shed light on whether these signatures are universal and can be observed in different conditions within the bone microenvironment. This signature was also compared to the dataset derived by Farr *et al.* (2015) which primarily assessed the changes in the bone microenvironment of women in response to age and oestrogen. I found that although the dormancy signature separated dormant cells in breast cancer cell lines, it did not separate between ovariectomised and sham operated mice, neither did it separate young (~30 years old) women from old (~73 years old) women or old women treated with oestrogen therapy (~70 years old). Applied to a third dataset based on microarray gene expression data from Cawthorn *et al.* (2009) who analysed metastatic deposits and isolated disseminated tumour cells from the bone marrow of breast cancer patients, a separation between the two groups based on dormancy score was found. My investigations showed that translation of dormancy gene expression signatures from isolated cell lines, must be approached with caution when applying findings to a population of heterogenous non-cancer cells. The development of a dormancy signature that can be applied to a heterogeneous cell population has yet to be defined, and does not seem plausible. It is currently more profitable to assess dormancy signatures in singular cell populations isolated from a heterogenous population. Further analysis of pathways, though, may reveal distinct pathways resulting in dormancy that could be compared despite differences in gene expression.

Bulk Deconvolution of bulk RNA-seq

The bulk RNA-seq data from mouse samples as well as the bulk sequencing from the Farr *et al.* (2015) dataset were deconvoluted through the use of xCell, a deconvolution algorithm developed by Aran, Hu and Butte (2017) from the University of California, San Francisco. Briefly, cell type enrichment analysis was performed from gene expression data for 64 immune and stromal cell types to estimate the abundance of these cell types present in the bulk deconvolution data. Abundance estimates of cell

types did not show significantly altered cell types in sequenced mice data. The Farr *et al* (2015) dataset showed a statistically significant increase of osteoblasts in old women treated with oestrogen compared to young women, but did not show any significant difference in other cell types analysed. The use of bulk deconvolution did not provide meaningful insight into cellular alterations within the bone microenvironment and other methods, such as flow cytometry, would have provided better insight into alterations to the hematopoietic milieu within the bone microenvironment.

Genes altered by ovariectomy

Amongst the genes upregulated in ovariectomised mice that may provide therapeutic interest was TAL1, a transcription factor involved in maintaining the multipotency and quiescence of HSCs, which was found to be downregulated in ovariectomised mice compared to sham, suggesting an increased proliferation of HSCs and potentially cells that would reside the HSC niche, such as DTCs. Growth arrest specific 5, a long non-coding RNA which has been demonstrated to play a role in quiescence-inductive cues in CD133+ pancreatic tumour initiation cancer stem cells was also found to be downregulated in ovariectomised mice, suggesting the potential for less quiescence-inductive cues in the ovariectomised bone microenvironment.

Amongst genes selected for additional analysis were MMP2, POSTN, THBS2 and SPP1. These were selected due to their secretion into the microenvironment inclusion in the two most-enriched pathways in ovariectomised mice (ECM receptor interaction and focal adhesion – THBS2 and SPP1), being significantly altered in all three datasets of interest; the Farr *et al.* (2015) and Ottewell *et al.* (2015) datasets, as well as upregulated in ovariectomised mice (MMP2). POSTN was also included as a significantly overexpressed gene in ovariectomised with well studied effects within the bone (Bonnet *et al*., 2016). These were analysed on data from the human cancer metastasis database (HMCDB) from breast cancer tumours that had metastasised to the bone compared to brain, liver and lung. All four genes were found to be significantly upregulated in cells that had metastasised to the bone compared to the other sites, suggesting a site-specific expression of these genes. Furthermore, many long non-coding RNAs were found co-expressed with these genes, such as MIR100HG, LINC01279, MIR22HG and MAGI2-AS3, suggesting common regulatory elements involved in the expression of these genes. Analysis of the effect of MMP2, POSTN, THBS2 and SPP1 expressed by primary breast cancer tissue on disease metastasis free survival was also carried out on large scale samples through KM Plotter, without discriminating metastatic site however. Patient cohorts with a high expression of SPP1 showed a significant reduction in time to metastasis. Patients overexpressing THBS2 also had a reduction in time to metastasis, albeit a slight one. High expression of MMP2 or POSTN did not correlate with a change in time to metastasis. Taken together, this data suggests that SPP1 has a significant effect on both metastasis and on tumour progression within the bone, whereas MMP2, THBS2 and POSTN are implicated in a more site-specific role within the bone.

Zol benefits and time on menopause

My investigations in chapter 5 found a significant similarity between young women and ovariectomised mice, which have been used as a model to study the bone microenvironment in women past menopause. The AZURE trial, analysing the use of Zol in women with breast cancer showed no improved survival in the overall population (Coleman *et al*., 2014). However, upon further stratification of study subjects, it was found that women past menopause gained a significant benefit in invasive disease free survival (IDFS) and overall survival (OS) when treated with Zol, whereas premenopausal and peri-menopausal women did not benefit. Further analysis of data from the AZURE trial suggested that time under menopause was an important factor in determining whether IDFS and OS would be altered, as only women 5+ years past menopause, and not women who experienced treatment-induced menopause had a benefit in these clinical endpoints. As such, pre-clinical modelling of the post-menopausal bone microenvironment may require lengthier durations under ovariectomy than are currently used. Ovariectomy does induce the outgrowth of disseminated tumour cells, but is limited in reflecting the menopausal bone microenvironment and therefore any extrapolation would be limited.

Conclusion

My pilot study demonstrated that it is possible to carry out RNA-Seq from mouse bone to compare early transcriptional changes resulting from ovariectomy that could lead to increased tumour growth. However, a larger experiment is required to establish a signature of the dormancy supporting (sham) and tumour growth promoting (OVX) BMEV, to allow detection of key molecular drivers/pathways that in turn represent potential therapeutic pathways.

Overall, analysis of genes between young women and ovariectomised mice found an overlap between genes upregulated in young women compared to old women and those in ovariectomised mice. In particular, genes coding for collagen fragments were upregulated in young women as well as ovariectomised mice. However, genes relating to angiogenesis were upregulated in young women but not in ovariectomised mice. These experiments demonstrate that extrapolation of pre-clinical findings to clinical settings needs to be approached with caution, as there was overlap between the microenvironment of mature, ovariectomised mice, and that of young women. Further research is needed to accurately capture the clinical features and optimise the model in order to provide clearer guidance into extrapolation of results into the clinic.

6.3 CONCLUSIONS AND FUTURE WORK

My studies explored how modification of the bone microenvironment using a dietary approach (low calcium, a surgical intervention (ovariectomy) and pharmacological inhibition of bone resorption (Zol) impacted on breast tumour development and progression *in vivo*.

Low Calcium Diet

In my investigations, a low calcium diet had a minor impact on the bone microenvironment in the absence of tumours, slightly reducing percentage bone volume after 28 days, as well as increasing the levels of TRAP and decreasing P1NP, suggesting an increase in osteoclast and decrease in osteoblast activity though not altering their numbers. These changes to the bone microenvironment in the absence of tumours did not translate to changes in the outgrowth of dormant disseminated tumour cells. Although the low calcium diet has shown influence over rate of tumour growth, it does not appear to have significant effects on the outgrowth of dormant, disseminated tumour cells, as the changes may not be dramatic enough to cause a switch into cycling.

Studies using a low calcium diet in models using tumour cells, and those without, have not shown dramatic differences in initial outgrowth of tumour cells or bone architecture, but rather show difference in proliferation over a longer period of time on the diet (Zheng *et al*., 2007). Along with my findings, this suggests that a low calcium diet may not invoke as rapid a change in bone turnover as seen in hormone deprivation, and so may not be sufficient, in isolation, to trigger the outgrowth of disseminated tumour cells.

Zol

The use of Zol in young mice significantly altered trabecular bone, significantly increasing trabecular percent bone volume, trabecular number and reduced trabecular separation. Interestingly, this was not followed by an alteration in the number of osteoclasts either in the presence or absence of tumour cells. It also did not significantly alter circulating hematopoietic populations as it did in other research done by Ubellacker *et al.* (2017) which showed an alteration in monocytes, neutrophils, platelets and progenitor cells 3-5 days following treatment (Ubellacker *et al*., 2017). This discrepancy with my findings may be explained by cellular homeostasis, which was observed by Ubellacker approximately 10 days after initial treatment. As populations were assessed 28 days after the initial dose, repeated doses of Zol may not have affected the hematopoietic milieu after initial return to homeostasis.

My results are in agreement with existing literature that shows Zol administration alone, though significantly increasing trabecular bone, is not sufficient to prevent or significantly delay the outgrowth of tumours in the bone microenvironment with rapid turnover. Repeated dosing in short timescales does not significantly change the cellular landscape neither does it improve Zol's efficacy against outgrowing tumours, independent of tumour clone. Further research is required, and indeed,

is ongoing to elucidate the effect of Zol on the bone microenvironment under conditions that have suggested differential effects in clinical trials, namely in menopausal states.

Ovariectomy

Ottewell *et al.* (2014, 2015) demonstrated that ovariectomy is sufficient to induce the outgrowth of dormant DTCs, yet use of anti-osteoclastic agents, such as Zol and OPG-Fc, is sufficient to prevent the outgrowth of these DTCs. As targeting osteoclasts has been demonstrated to have limited anti-tumour activity in established tumours, the early events following ovariectomy as key in driving the outgrowth of dormant DTCs must therefore be important as the prevention of outgrowth by these agents (Barton, 2011, Biver, 2019, Steger and Bartsch, 2011, van der Pluijm, 2011). I therefore sought to characterise the early transcriptional changes that occur leading to overt outgrowth by profiling the bone microenvironment at 14 days following ovariectomy.

Validating findings with publicly available datasets proved challenging as few datasets exist that capture the bone microenvironment in relevant altered states of turnover without confounding factors, such as exogenous therapeutics, neither are there many datasets containing gene expression within the bone microenvironment. In addition, established dormancy gene signatures not derived from cancer cell lines are sparse and often unverified, or tissue specific. Therefore, analysis had to combine different datasets to provide as full a picture as possible with limited data available. Despite this, genes of interest POSTN, MMP2, THBS2 and OPN were found and explored, showing relevance in publicly available datasets, and are genes of active research within bone biology and tumour progression.

To be able to comprehensively profile the bone microenvironment and further elucidate its role in cancer progression, more transcriptomic data in base and altered states is required from both *in vivo* and clinical samples. Current databases such as the HCMDB collect and curate metastatic data, and as the cost of sequencing decreases and more datasets become available, more robust inference will be possible from the available data. Current efforts to elucidate the bone microenvironment at a single cell resolution will also identify transcriptional signals that can provide more accurate deconvolution of bulk samples.

Short term

As my experiments have focused on altering the bone microenvironment in order to model clinical settings, such as the post-menopausal bone microenvironment, future work would involve analysing and refining these models. Clinical trials, such as the AZURE and ABCSG-12, have shown that not only menopausal status, but time in menopause is important in determining the anti-cancer effects of agents targeting the bone microenvironment as women 5+ years into menopause had differential response to bone targeted treatments compared to women induced into menopause through treatment. Added to this, my experiments showed a significant overlap in genes and pathways between ovariectomised mice and young women, rather than old women whom the ovariectomy

model attempts to model. Therefore, understanding how time affects the gene expression of the ovariectomy model would provide important insights in modelling the post-menopausal bone microenvironment in old women. In the short term, investigations would involve performing ovariectomy on mature mice over a time course, sequencing at each time point and analysing the extent of overlap with older women based on the Farr *et al.* (2015) dataset in order to identify the time period that most strongly reflects the post-menopausal bone microenvironment. Time periods would ideally be 2, 3, 7, 14 and 28 days, 2, 3 and 6 months in order to capture the evolution of the bone microenvironment over time. In experiments involving the use of Zol by Ubellacker *et al.* (2018), and my experiments involving the low calcium diet, homeostasis of changes to the bone microenvironment occurred after approximately 7-14 days and 28 days respectively. In addition, Ottewell *et al.* (2015) also found 27 differentially expressed genes through PCR analysis 7 days following ovariectomy, of which I found only 3 differentially expressed when investigating at 14 days despite similar mouse strains. Therefore, it is plausible that homeostatic mechanisms may have altered the gene expression between day 7 and day 14, of which a time course would elucidate. Assessing the bone microenvironment of young (6 week-old), ovary-intact mice, as well as old (18+ months) ovariectomised mice, in comparison to mature, ovariectomised mice by RNA-seq and comparing changes with the Farr *et al.* (2015) dataset comparing young women and old women would provide further insight into the utility of these models in comparing them to young and old bone microenvironments.

Assessing cellular populations altered by ovariectomy using hematological analysis and deconvolution of bulk RNA-seq data did not show any significant changes. However, the cells in the peripheral circulation are not the same population as in the bone marrow, and deconvolution methods often produce differing results, suggesting the likelihood of inaccuracies. To analyse which cells are present in the bone microenvironment, flow cytometry would be used as it is directly quantitative, more accurate due to antibody technology and can provide a deeper resolution of cells of interest.

Long term

Current models in our laboratory to study dormant, disseminated tumour cells *in vivo* involve the injection of slowly cycling MDA-MB-231-TD-Tomato cells that may have an inherent transcriptional switch to a more dormant state. While these can be used to study the escape from dormancy, they do not provide strong insights into the role of the microenvironment in inducing cells into dormancy. Currently injecting MDA-MB-231 cells that do not inherently cycle slowly into mature mice leads to rapid engraftment and outgrowth within 14 days as observed in chapters 3 and 4. Therefore, developing a model that induces rapidly dividing cells into dormancy may provide insight into the dormancy-inductive cells and microenvironmental signals. Inoculation of mice with tumour cell particulates prior to the introduction of live tumour cells has been shown to induce immune-mediated tumour cell dormancy (Farrar *et al*., 1999, Khazaie *et al*., 1994, Uhr and Marches, 2001). Dormancy established through vaccination and engagement of the immune system primarily involves tumoricidal activity of the immune system at the same rate as proliferation and may thereby confound the analysis of pro-dormancy signals from the microenvironment. However, combining this with

lipophilic membrane dyes that get diluted with replication would allow the assessment of individual cells that have been induced into dormancy despite a population of rapidly dividing cells that is in equilibrium with immune-mediated tumour cell killing. Indeed, this may be a more accurate reflection of the occurrence of dormancy in the clinical setting as immune evasion must occur for cells to remain dormant for a period of time. Slow cycling stem cells have been demonstrated to have a lower expression of MHC I molecules and associated immune avoidance (Agudo *et al*., 2018), and so any dormant tumour cells would likely evade the immune destruction other rapidly dividing tumour cell clones would have. As this population would come from a rapidly dividing population, it would allow the assessment of dormancy-inductive cues.

To also further understand the role of the bone microenvironment in regulating tumour dormancy, the use of single-cell sequencing with spatial transcriptomics would be optimal in revealing the molecular, cellular and spatial bone marrow niche organisation surrounding tumour cells. Indeed Baccin *et al.* (2020) performed a series of experiments harmonising fluorescence microscopy and single-cell sequencing with spatial transcriptomics of the bone microenvironment to elucidate genes expressed by 32 different cell types, as well as computationally resolving cell niche locations, cell-cell signalling and physical interactions (Baccin *et al*., 2020). Such a strategy would be comprehensive and elucidate signalling cues provided by the microenvironment that support a pro-dormancy state.

Figure 6-1 is a diagrammatic summary of the findings, and conclusions from this thesis.

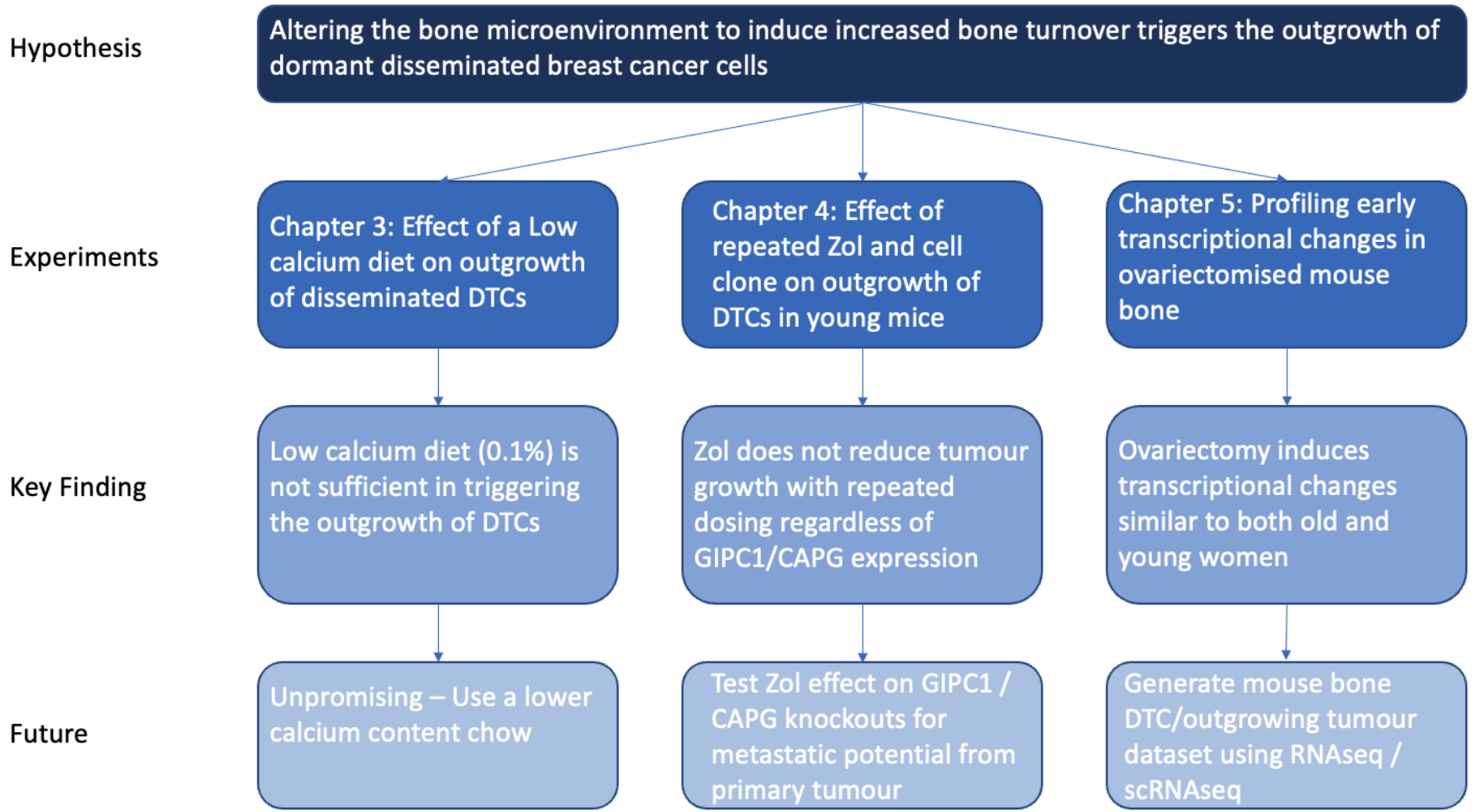

Figure 6-1: Diagrammatic summary of findings and conclusions in this thesis

7 APPENDIX

7.1 APPENDIX 1

Upstream analysis using X2K (Chen *et al.*, 2012; Clarke *et al.*, 2018) of genes upregulated in cancer cell lines with a dormant phenotype as found by Kim *et al.* (2012).

7.1.1 TRANSCRIPTION FACTOR ENRICHMENT ANALYSIS.

Predicted transcription factors that regulate the input gene list, using gene set enrichment analysis using various transcription factor – gene set libraries as determined by ChIP-seq experiments (Clarke *et al.*, 2018). A ranked list of transcription factors is produced, ranked by genes in the query set regulated and p-value (See Figure 7-1, Figure 7-2, Figure 7-3, Figure 7-4 for transcription factors enriched in dormant cancer cell lines, downregulated in ovariectomised mouse bone, downregulated in dormant cancer cell lines and enriched in ovariectomised mouse bone respectively). Transcription factors show marginal correlation between those predicted to be involved in dormant cancer cell lines (Figure 7-1) and those downregulated in ovariectomy (Figure 7-2)

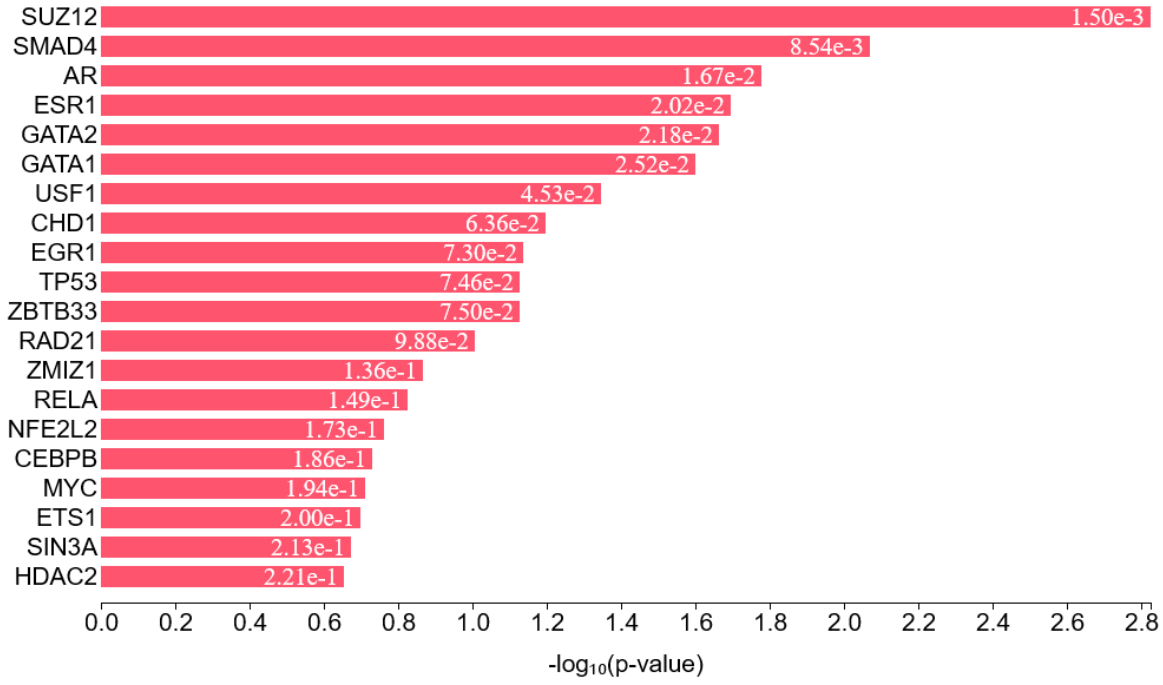

Figure 7-1: Transcription factor analysis of genes upregulated in dormant cancer cell lines (Kim *et al.*, 2012)

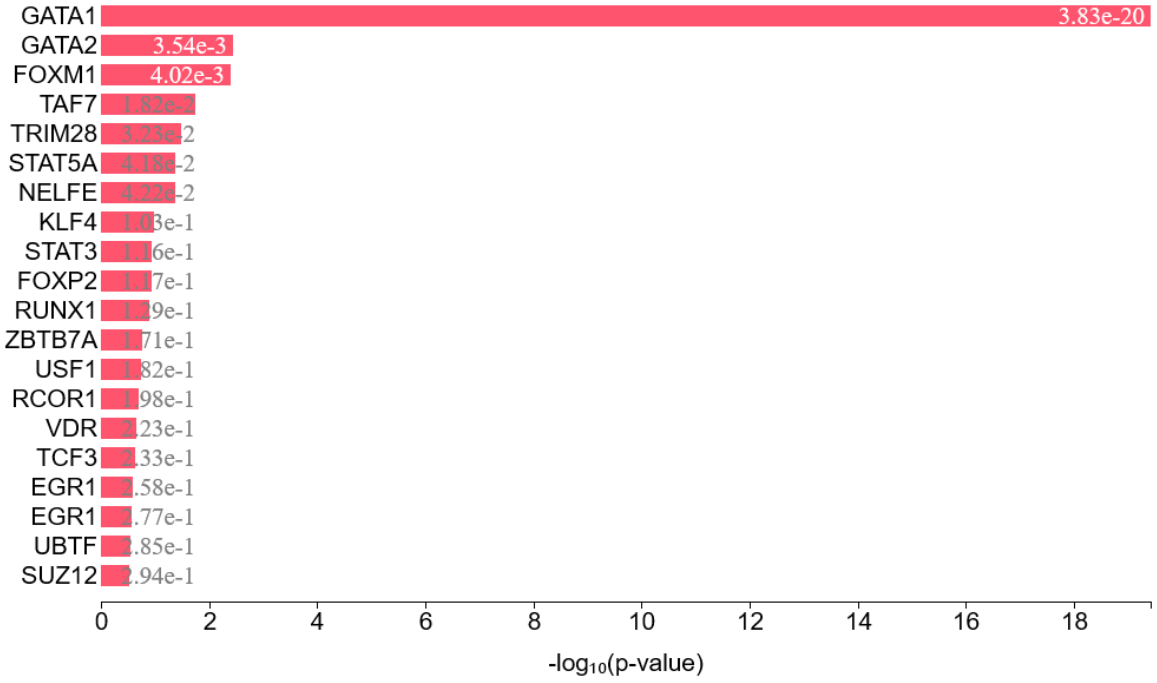

Figure 7-2: Transcription factor analysis of genes downregulated in ovariectomised mouse bone

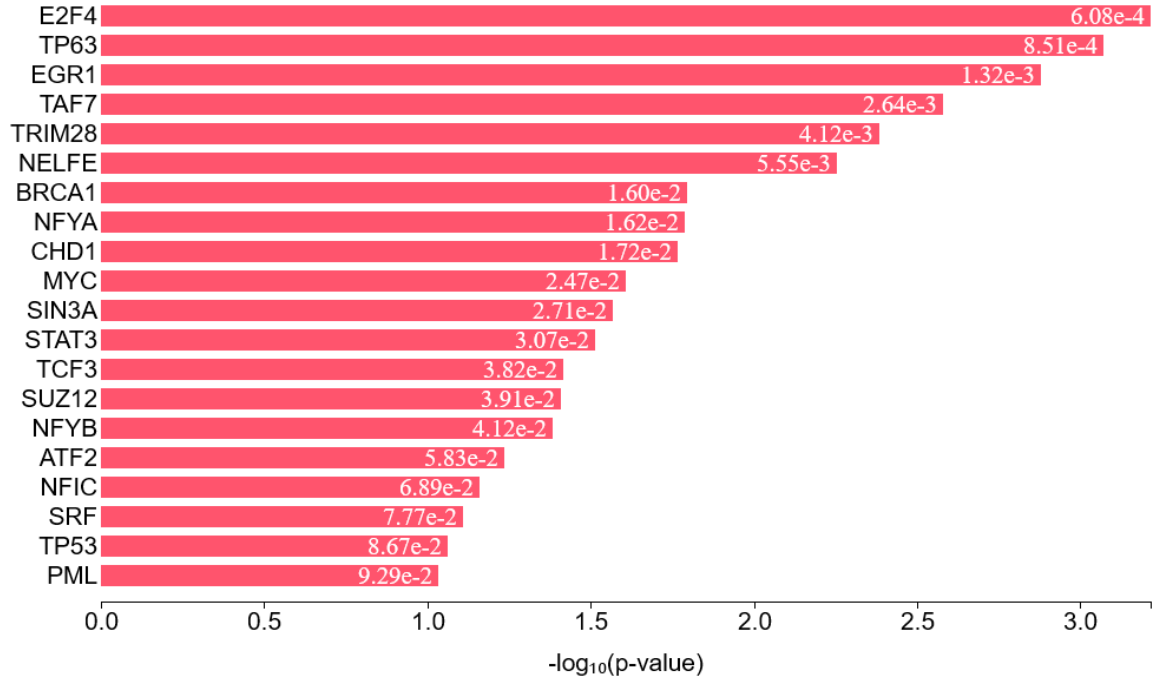

Figure 7-3: Transcription factor analysis of genes downregulated in dormant cancer cell lines (Kim *et al.*, 2012)

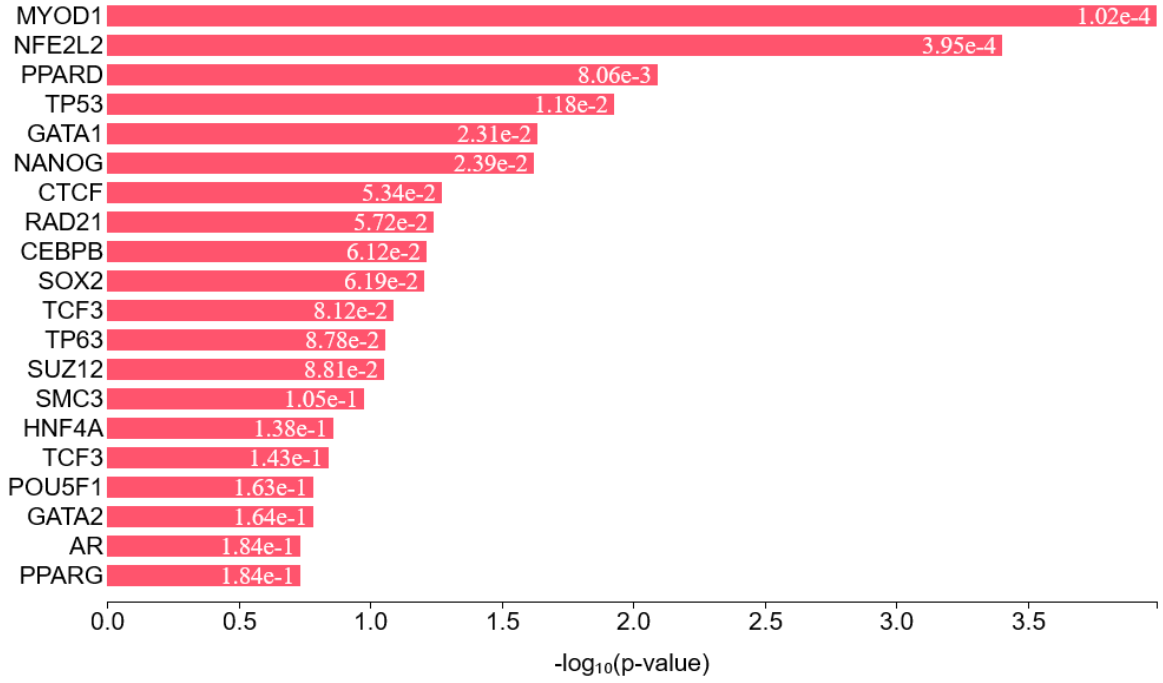

Figure 7-4: Transcription factor analysis of genes upregulated ovariectomised mouse bone

7.1.2 Kinase Enrichment Analysis

Predicted transcription factors from the transcription factor enrichment analysis are then used as inputs into protein-protein interactions based on the predicted transcription factors present in the list. **Kinase Enrichment Analysis** then predicts protein kinases that are the likely regulators of the expanded protein-protein interaction network, using gene set libraries from kinase-substrate interaction databases (Clarke *et al.*, 2018). Some marginal overlap found in top ranking predicted enriched kinases such as MAPK1, CDK1 and GSK3-β can be seen upstream of genes upregulated in dormant cancer cell lines (Figure 7-5) as well as those downregulated in ovariectomised mouse bone (Figure 7-6). However, some overlap can also be observed between datasets and controlling for these overlaps would provide more granularity into important upstream kinases that are enriched in these conditions in order to further assess correlation between ovariectomy and escape from dormancy.

(See for kinases enriched in dormant cancer cell lines, downregulated in ovariectomised mouse bone, downregulated in dormant cancer cell lines and enriched in ovariectomised mouse bone respectively).

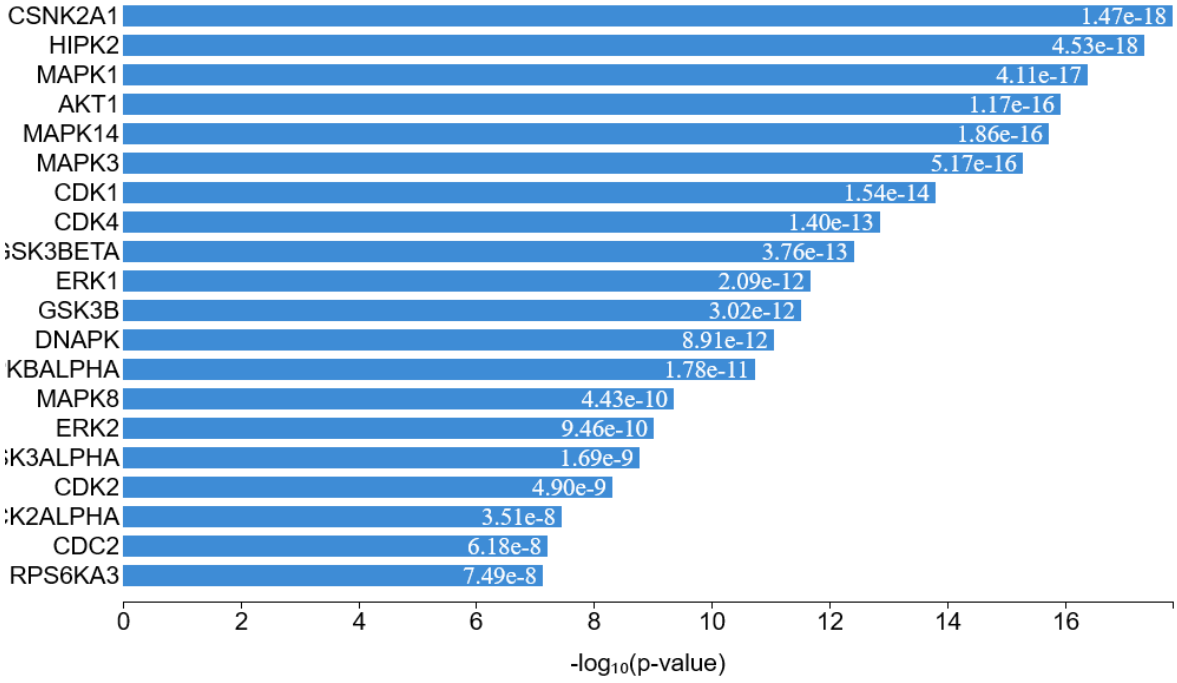

Figure 7-5: Kinase enrichment analysis of genes upregulated in dormant cancer cell lines (Kim *et al.*, 2012)

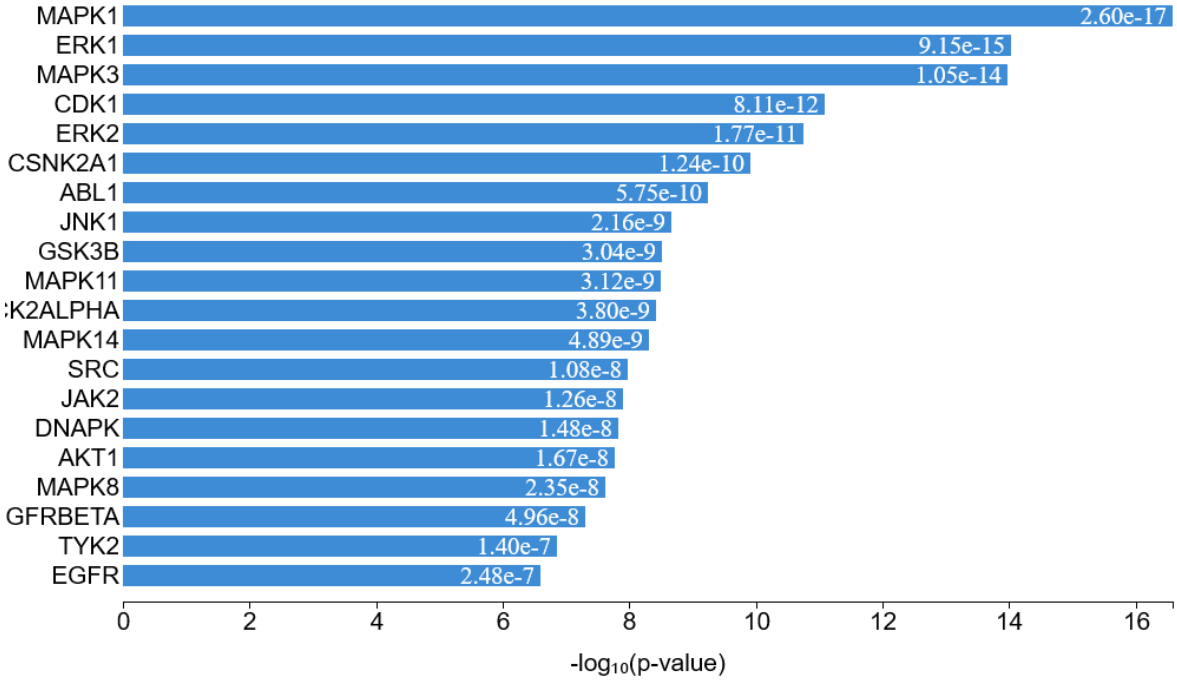

Figure 7-6: Kinase enrichment analysis of genes downregulated in ovariectomised mouse bone

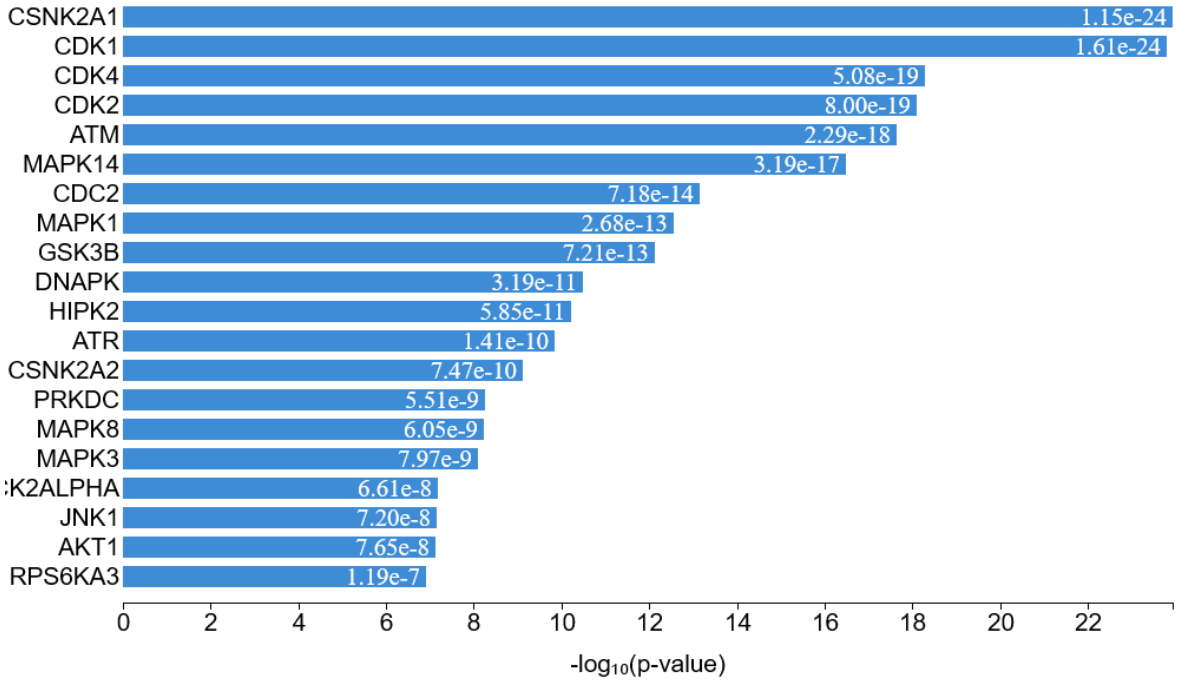

Figure 7-7: Kinase enrichment analysis of genes downregulated in dormant cancer cell lines (Kim *et al.*, 2012)

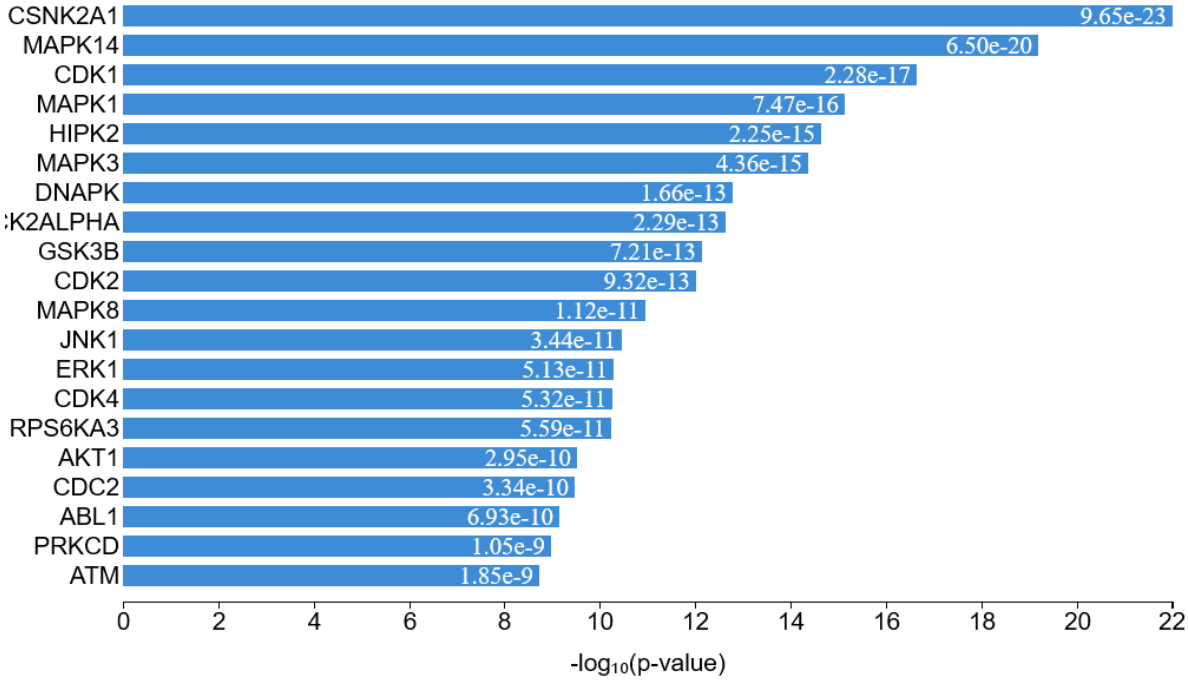

Figure 7-8: Kinase enrichment analysis of genes upregulated in ovariectomised mouse bone

8 REFERENCES

ADEEGBE, D. O. & NISHIKAWA, H. 2013. Natural and induced T regulatory cells in cancer. *Front Immunol,* 4**,** 190.

AGUDO, J., PARK, E. S., ROSE, S. A., ALIBO, E., SWEENEY, R., DHAINAUT, M., KOBAYASHI, K. S., SACHIDANANDAM, R., BACCARINI, A., MERAD, M. & BROWN, B. D. 2018. Quiescent Tissue Stem Cells Evade Immune Surveillance. *Immunity,* 48**,** 271-285 e5.

AGUIRRE-GHISO, J. A., ESTRADA, Y., LIU, D. & OSSOWSKI, L. 2003. ERK(MAPK) activity as a determinant of tumor growth and dormancy; regulation by p38(SAPK). *Cancer Res,* 63**,** 1684-95.

AHN, S. G., LEE, H. M., CHO, S. H., LEE, S. A., HWANG, S. H., JEONG, J. & LEE, H. D. 2013. Prognostic factors for patients with bone-only metastasis in breast cancer. *Yonsei Med J,* 54**,** 1168-77.

AIELLO, F., CARULLO, G., BADOLATO, M. & BRIZZI, A. 2016. TRPV1-FAAH-COX: The Couples Game in Pain Treatment. *ChemMedChem,* 11**,** 1686-94.

AKKOC, Y., PEKER, N., AKCAY, A. & GOZUACIK, D. 2021. Autophagy and Cancer Dormancy. *Front Oncol,* 11**,** 627023.

ALATALO, S. L., PENG, Z., JANCKILA, A. J., KAIJA, H., VIHKO, P., VAANANEN, H. K. & HALLEEN, J. M. 2003. A novel immunoassay for the determination of tartrate-resistant acid phosphatase 5b from rat serum. *J Bone Miner Res,* 18**,** 134-9.

ALBRIGHT, F., REIFENSTEIN, E. C., JR. & FORBES, A. P. 1946. Effect of stilbestrol in post-menopausal osteoporosis. *Trans Conf Metab Asp Conval***,** 99-101.

ALLOCCA, G., HUGHES, R., WANG, N., BROWN, H. K., OTTEWELL, P. D., BROWN, N. J. & HOLEN, I. 2019a. The bone metastasis niche in breast cancer-potential overlap with the haematopoietic stem cell niche. *J Bone Oncol,* 17**,** 100244.

ALLOCCA, G., HUGHES, R., WANG, N., BROWN, H. K., OTTEWELL, P. D., BROWN, N. J. & HOLEN, I. 2019b. The bone metastasis niche in breast cancer-potential overlap with the haematopoietic stem cell niche *in vivo*. *J Bone Oncol,* 17**,** 100244.

ALMOG, N., BRIGGS, C., BEHESHTI, A., MA, L., WILKIE, K. P., RIETMAN, E. & HLATKY, L. 2013. Transcriptional changes induced by the tumor dormancy-associated microRNA-190. *Transcription,* 4**,** 177-91.

ALMOG, N., MA, L., SCHWAGER, C., BRINKMANN, B. G., BEHESHTI, A., VAJKOCZY, P., FOLKMAN, J., HLATKY, L. & ABDOLLAHI, A. 2012. Consensus micro RNAs governing the switch of dormant tumors to the fast-growing angiogenic phenotype. *PLoS One,* 7**,** e44001.

ALTVATER, B., PSCHERER, S., LANDMEIER, S., KAILAYANGIRI, S., SAVOLDO, B., JUERGENS, H. & ROSSIG, C. 2012. Activated human gammadelta T cells induce peptide-specific CD8+ T-cell responses to tumor-associated self-antigens. *Cancer Immunol Immunother,* 61**,** 385-96.

ANDERS, S. & HUBER, W. 2010. Differential expression analysis for sequence count data. *Genome Biol,* 11**,** R106.

ANDERS, S., PYL, P. T. & HUBER, W. 2015. HTSeq--a Python framework to work with high-throughput sequencing data. *Bioinformatics,* 31**,** 166-9.

AQBI, H. F., WALLACE, M., SAPPAL, S., PAYNE, K. K. & MANJILI, M. H. 2018. IFN-gamma orchestrates tumor elimination, tumor dormancy, tumor escape, and progression. *J Leukoc Biol*.

ARA, T., SONG, L., SHIMADA, H., KESHELAVA, N., RUSSELL, H. V., METELITSA, L. S., GROSHEN, S. G., SEEGER, R. C. & DECLERCK, Y. A. 2009. Interleukin-6 in the bone marrow microenvironment promotes the growth and survival of neuroblastoma cells. *Cancer Res,* 69**,** 329-37.

ARAN, D., HU, Z. & BUTTE, A. J. 2017. xCell: digitally portraying the tissue cellular heterogeneity landscape. *Genome Biol,* 18**,** 220.

ATSUTA, I., LIU, S., MIURA, Y., AKIYAMA, K., CHEN, C., AN, Y., SHI, S. & CHEN, F. M. 2013. Mesenchymal stem cells inhibit multiple myeloma cells via the Fas/Fas ligand pathway. *Stem Cell Res Ther,* 4**,** 111.

AUGELLO, A., TASSO, R., NEGRINI, S. M., AMATEIS, A., INDIVERI, F., CANCEDDA, R. & PENNESI, G. 2005. Bone marrow mesenchymal progenitor cells inhibit lymphocyte proliferation by activation of the programmed death 1 pathway. *Eur J Immunol,* 35**,** 1482-90.

AUGSTEN, M. 2014. Cancer-associated fibroblasts as another polarized cell type of the tumor microenvironment. *Front Oncol,* 4**,** 62.

AVILA COBOS, F., ALQUICIRA-HERNANDEZ, J., POWELL, J. E., MESTDAGH, P. & DE PRETER, K. 2020. Benchmarking of cell type deconvolution pipelines for transcriptomics data. *Nat Commun,* 11**,** 5650.

AXELROD, H. D., VALKENBURG, K. C., AMEND, S. R., HICKS, J. L., PARSANA, P., TORGA, G., DEMARZO, A. M. & PIENTA, K. J. 2019. AXL Is a Putative Tumor Suppressor and Dormancy Regulator in Prostate Cancer. *Mol Cancer Res,* 17**,** 356-369.

BACCIN, C., AL-SABAH, J., VELTEN, L., HELBLING, P. M., GRUNSCHLAGER, F., HERNANDEZ-MALMIERCA, P., NOMBELA-ARRIETA, C., STEINMETZ, L. M., TRUMPP, A. & HAAS, S. 2020. Combined single-cell and spatial transcriptomics reveal the molecular, cellular and spatial bone marrow niche organization. *Nat Cell Biol,* 22**,** 38-48.

BAKEWELL, S. J., NESTOR, P., PRASAD, S., TOMASSON, M. H., DOWLAND, N., MEHROTRA, M., SCARBOROUGH, R., KANTER, J., ABE, K., PHILLIPS, D. & WEILBAECHER, K. N. 2003. Platelet and osteoclast beta3 integrins are critical for bone metastasis. *Proc Natl Acad Sci U S A,* 100**,** 14205-10.

BARTAL, I., MELAMED, R., GREENFELD, K., ATZIL, S., GLASNER, A., DOMANKEVICH, V., NAOR, R., BEILIN, B., YARDENI, I. Z. & BEN-ELIYAHU, S. 2010. Immune perturbations in patients along the perioperative period: alterations in cell surface markers and leukocyte subtypes before and after surgery. *Brain Behav Immun,* 24**,** 376-86.

BARTON, M. K. 2011. Denosumab an option for patients with bone metastasis from breast cancer. *CA Cancer J Clin,* 61**,** 135-6.

BASELGA, J., CERVANTES, A., MARTINELLI, E., CHIRIVELLA, I., HOEKMAN, K., HURWITZ, H. I., JODRELL, D. I., HAMBERG, P., CASADO, E., ELVIN, P., SWAISLAND, A., IACONA, R. & TABERNERO, J. 2010. Phase I safety, pharmacokinetics, and inhibition of SRC activity study of saracatinib in patients with solid tumors. *Clin Cancer Res,* 16**,** 4876-83.

BECHT, E., GIRALDO, N. A., LACROIX, L., BUTTARD, B., ELAROUCI, N., PETITPREZ, F., SELVES, J., LAURENT-PUIG, P., SAUTES-FRIDMAN, C., FRIDMAN, W. H. & DE REYNIES, A. 2016. Estimating the population abundance of tissue-infiltrating immune and stromal cell populations using gene expression. *Genome Biol,* 17**,** 218.

BEGLEY, C. G., APLAN, P. D., DAVEY, M. P., NAKAHARA, K., TCHORZ, K., KURTZBERG, J., HERSHFIELD, M. S., HAYNES, B. F., COHEN, D. I., WALDMANN, T. A. & *ET AL*. 1989. Chromosomal translocation in a human leukemic stem-cell line disrupts the T-cell antigen receptor delta-chain diversity region and results in a previously unreported fusion transcript. *Proc Natl Acad Sci U S A,* 86**,** 2031-5.

BENZEKRY, S., GANDOLFI, A. & HAHNFELDT, P. 2014. Global dormancy of metastases due to systemic inhibition of angiogenesis. *PLoS One,* 9**,** e84249.

BI, L. K., ZHOU, N., LIU, C., LU, F. D., LIN, T. X., XUAN, X. J., JIANG, C., HAN, J. L., HUANG, H., ZHANG, C. X., DONG, W., LIU, H., HUANG, J. & XU, K. W. 2014. Kidney cancer cells secrete IL-8 to activate Akt and promote migration of mesenchymal stem cells. *Urol Oncol,* 32**,** 607-12.

BIDWELL, B. N., SLANEY, C. Y., WITHANA, N. P., FORSTER, S., CAO, Y., LOI, S., ANDREWS, D., MIKESKA, T., MANGAN, N. E., SAMARAJIWA, S. A., DE WEERD, N. A., GOULD, J., ARGANI, P., MOLLER, A., SMYTH, M. J., ANDERSON, R. L., HERTZOG, P. J. & PARKER, B. S. 2012. Silencing of Irf7 pathways in breast cancer cells promotes bone metastasis through immune escape. *Nat Med,* 18**,** 1224-31.

BISWAS, S., NYMAN, J. S., ALVAREZ, J., CHAKRABARTI, A., AYRES, A., STERLING, J., EDWARDS, J., RANA, T., JOHNSON, R., PERRIEN, D. S., LONNING, S., SHYR, Y., MATRISIAN, L. M. & MUNDY, G. R. 2011. Anti-transforming growth factor ss antibody treatment rescues bone loss and prevents breast cancer metastasis to bone. *PLoS One,* 6**,** e27090.

BISWAS, S. K., GANGI, L., PAUL, S., SCHIOPPA, T., SACCANI, A., SIRONI, M., BOTTAZZI, B., DONI, A., VINCENZO, B., PASQUALINI, F., VAGO, L., NEBULONI, M., MANTOVANI, A. & SICA, A. 2006. A distinct and unique transcriptional program expressed by tumor-associated macrophages (defective NF-kappaB and enhanced IRF-3/STAT1 activation). *Blood,* 107**,** 2112-22.

BIVER, E. 2019. [Bone effects of bisphosphonates and denosumab treatments in breast or prostate cancer]. *Rev Med Suisse,* 15**,** 824-830.

BLOISE, E., CIARMELA, P., DELA CRUZ, C., LUISI, S., PETRAGLIA, F. & REIS, F. M. 2019. Activin A in Mammalian Physiology. *Physiol Rev,* 99**,** 739-780.

BNF 2020. Zoledronic Acid.

BODENNER, D., REDMAN, C. & RIGGS, A. 2007. Teriparatide in the management of osteoporosis. *Clin Interv Aging,* 2**,** 499-507.

BOLGER, A. M., LOHSE, M. & USADEL, B. 2014. Trimmomatic: a flexible trimmer for Illumina sequence data. *Bioinformatics,* 30**,** 2114-20.

BONNET, N., GARNERO, P. & FERRARI, S. 2016. Periostin action in bone. *Mol Cell Endocrinol,* 432**,** 75-82.

BORD, S., IRELAND, D. C., BEAVAN, S. R. & COMPSTON, J. E. 2003. The effects of estrogen on osteoprotegerin, RANKL, and estrogen receptor expression in human osteoblasts. *Bone,* 32**,** 136-41.

BOTTOMLY, D., WALTER, N. A., HUNTER, J. E., DARAKJIAN, P., KAWANE, S., BUCK, K. J., SEARLES, R. P., MOONEY, M., MCWEENEY, S. K. & HITZEMANN, R. 2011. Evaluating gene expression in C57BL/6J and DBA/2J mouse striatum using RNA-Seq and microarrays. *PLoS One,* 6**,** e17820.

BOYCE, B. F. & XING, L. 2007. The RANKL/RANK/OPG pathway. *Curr Osteoporos Rep,* 5**,** 98-104.

BOYCE, B. F., XING, L., YAO, Z., YAMASHITA, T., SHAKESPEARE, W. C., WANG, Y., METCALF, C. A., 3RD, SUNDARAMOORTHI, R., DALGARNO, D. C., IULIUCCI, J. D. & SAWYER, T. K. 2006. SRC inhibitors in metastatic bone disease. *Clin Cancer Res,* 12**,** 6291s-6295s.

BRADFORD, P. G., GERACE, K. V., ROLAND, R. L. & CHRZAN, B. G. 2010. Estrogen regulation of apoptosis in osteoblasts. *Physiol Behav,* 99**,** 181-5.

BRAY, N. L., PIMENTEL, H., MELSTED, P. & PACHTER, L. 2016. Near-optimal probabilistic RNA-seq quantification. *Nat Biotechnol,* 34**,** 525-7.

BROOK, N., BROOK, E., DHARMARAJAN, A., DASS, C. R. & CHAN, A. 2018. Breast cancer bone metastases: pathogenesis and therapeutic targets. *Int J Biochem Cell Biol,* 96**,** 63-78.

BROWN, H. K., ALLOCCA, G., OTTEWELL, P. D., WANG, N., BROWN, N. J., CROUCHER, P. I., EATON, C. L. & HOLEN, I. 2018. Parathyroid Hormone (PTH) Increases Skeletal Tumour Growth and Alters Tumour Distribution in an *In vivo* Model of Breast Cancer. *Int J Mol Sci,* 19.

BROWN, H. K., OTTEWELL, P. D., EVANS, C. A., COLEMAN, R. E. & HOLEN, I. 2012. A single administration of combination therapy inhibits breast tumour progression in bone and modifies both osteoblasts and osteoclasts. *J Bone Oncol,* 1**,** 47-56.

BRUNS, I., LUCAS, D., PINHO, S., AHMED, J., LAMBERT, M. P., KUNISAKI, Y., SCHEIERMANN, C., SCHIFF, L., PONCZ, M., BERGMAN, A. & FRENETTE, P. S. 2014. Megakaryocytes regulate hematopoietic stem cell quiescence through CXCL4 secretion. *Nat Med,* 20**,** 1315-20.

BUENROSTRO, D., PARK, S. I. & STERLING, J. A. 2014. Dissecting the role of bone marrow stromal cells on bone metastases. *Biomed Res Int,* 2014**,** 875305.

BURT, L. M., YING, J., POPPE, M. M., SUNEJA, G. & GAFFNEY, D. K. 2017. Risk of secondary malignancies after radiation therapy for breast cancer: Comprehensive results. *Breast,* 35**,** 122-129.

CAILLEAU, R., OLIVE, M. & CRUCIGER, Q. V. 1978. Long-term human breast carcinoma cell lines of metastatic origin: preliminary characterization. *In vitro,* 14**,** 911-5.

CALLARI, M., BATRA, A. S., BATRA, R. N., SAMMUT, S. J., GREENWOOD, W., CLIFFORD, H., HERCUS, C., CHIN, S. F., BRUNA, A., RUEDA, O. M. & CALDAS, C. 2018. Computational approach to discriminate human and mouse sequences in patient-derived tumour xenografts. *BMC Genomics,* 19**,** 19.

CALVO, F., EGE, N., GRANDE-GARCIA, A., HOOPER, S., JENKINS, R. P., CHAUDHRY, S. I., HARRINGTON, K., WILLIAMSON, P., MOEENDARBARY, E., CHARRAS, G. & SAHAI, E. 2013. Mechanotransduction and YAP-dependent matrix remodelling is required for the generation and maintenance of cancer-associated fibroblasts. *Nat Cell Biol,* 15**,** 637-46.

CANCER RESEARCH, U. 2016. *Breast Cancer Mortality* [Online]. Available: https://www.cancerresearchuk.org/health-professional/cancer-statistics/statistics-by-cancer-type/breast-cancer#heading-Two [Accessed November 2018].

CANCRO, M. P. & KLINMAN, N. R. 1980. B cell repertoire diversity in athymic mice. *J Exp Med,* 151**,** 761-6.

CAWTHORN, T. R., AMIR, E., BROOM, R., FREEDMAN, O., GIANFELICE, D., BARTH, D., WANG, D., HOLEN, I., DONE, S. J. & CLEMONS, M. 2009. Mechanisms and pathways of bone metastasis: challenges and pitfalls of performing molecular research on patient samples. *Clin Exp Metastasis,* 26**,** 935-43.

CHEN, B., KHODADOUST, M. S., LIU, C. L., NEWMAN, A. M. & ALIZADEH, A. A. 2018a. Profiling Tumor Infiltrating Immune Cells with CIBERSORT. *Methods Mol Biol,* 1711**,** 243-259.

CHEN, B., WANG, Y., KANE, S. E. & CHEN, S. 2008. Improvement of sensitivity to tamoxifen in estrogen receptor-positive and Herceptin-resistant breast cancer cells. *J Mol Endocrinol,* 41**,** 367-77.

CHEN, C. & LODISH, H. F. 2014. Global analysis of induced transcription factors and cofactors identifies Tfdp2 as an essential coregulator during terminal erythropoiesis. *Exp Hematol,* 42**,** 464-76 e5.

CHEN, F. Y., ZHOU, Z. Y., ZHANG, K. J., PANG, J. & WANG, S. M. 2020a. Long non-coding RNA MIR100HG promotes the migration, invasion and proliferation of triple-negative breast cancer cells by targeting the miR-5590-3p/OTX1 axis. *Cancer Cell Int,* 20**,** 508.

CHEN, W., HOFFMANN, A. D., LIU, H. & LIU, X. 2018b. Organotropism: new insights into molecular mechanisms of breast cancer metastasis. *NPJ Precis Oncol,* 2**,** 4.

CHEN, X., ZHANG, B., WANG, T., BONNI, A. & ZHAO, G. 2020b. Robust principal component analysis for accurate outlier sample detection in RNA-Seq data. *BMC Bioinformatics,* 21**,** 269.

CHENG, M. L. & GUPTA, V. 2012. Teriparatide - Indications beyond osteoporosis. *Indian J Endocrinol Metab,* 16**,** 343-8.

CHIARELLA, P., VERMEULEN, M., MONTAGNA, D. R., VALLECORSA, P., STRAZZA, A. R., MEISS, R. P., BUSTUOABAD, O. D., RUGGIERO, R. A. & PREHN, R. T. 2018. Improvement of Antitumor Therapies Based on Vaccines and Immune-Checkpoint Inhibitors by Counteracting Tumor-Immunostimulation. *Front Oncol,* 8**,** 6.

CHIRGWIN, J. M. & GUISE, T. A. 2000. Molecular mechanisms of tumor-bone interactions in osteolytic metastases. *Crit Rev Eukaryot Gene Expr,* 10**,** 159-78.

CLARKE, D. J. B., KULESHOV, M. V., SCHILDER, B. M., TORRE, D., DUFFY, M. E., KEENAN, A. B., LACHMANN, A., FELDMANN, A. S., GUNDERSEN, G. W., SILVERSTEIN, M. C., WANG, Z. & MA'AYAN, A. 2018. eXpression2Kinases (X2K) Web: linking expression signatures to upstream cell signaling networks. *Nucleic Acids Res,* 46**,** W171-W179.

CLEMONS, M., GELMON, K. A., PRITCHARD, K. I. & PATERSON, A. H. 2012. Bone-targeted agents and skeletal-related events in breast cancer patients with bone metastases: the state of the art. *Curr Oncol,* 19**,** 259-68.

CLEZARDIN, P. & TETI, A. 2007. Bone metastasis: pathogenesis and therapeutic implications. *Clin Exp Metastasis,* 24**,** 599-608.

CODO, P., WELLER, M., MEISTER, G., SZABO, E., STEINLE, A., WOLTER, M., REIFENBERGER, G. & ROTH, P. 2014. MicroRNA-mediated down-regulation of NKG2D ligands contributes to glioma immune escape. *Oncotarget,* 5**,** 7651-62.

COLAK, S. & TEN DIJKE, P. 2017. Targeting TGF-β Signaling in Cancer. *Trends Cancer,* 3**,** 56-71.

COLEMAN, M. P., FORMAN, D., BRYANT, H., BUTLER, J., RACHET, B., MARINGE, C., NUR, U., TRACEY, E., COORY, M., HATCHER, J., MCGAHAN, C. E., TURNER, D., MARRETT, L., GJERSTORFF, M. L., JOHANNESEN, T. B., ADOLFSSON, J., LAMBE, M., LAWRENCE, G., MEECHAN, D., MORRIS, E. J., MIDDLETON, R., STEWARD, J., RICHARDS, M. A. & GROUP, I. M. W. 2011. Cancer survival in Australia, Canada, Denmark, Norway, Sweden, and the UK, 1995-2007 (the International Cancer Benchmarking Partnership): an analysis of population-based cancer registry data. *Lancet,* 377**,** 127-38.

COLEMAN, R., CAMERON, D., DODWELL, D., BELL, R., WILSON, C., RATHBONE, E., KEANE, M., GIL, M., BURKINSHAW, R., GRIEVE, R., BARRETT-LEE, P., RITCHIE, D., LIVERSEDGE, V., HINSLEY, S., MARSHALL, H. & INVESTIGATORS, A. 2014. Adjuvant zoledronic acid in patients with early breast cancer: final efficacy analysis of the AZURE (BIG 01/04) randomised open-label phase 3 trial. *Lancet Oncol,* 15**,** 997-1006.

COLEMAN, R., DE BOER, R., EIDTMANN, H., LLOMBART, A., DAVIDSON, N., NEVEN, P., VON MINCKWITZ, G., SLEEBOOM, H. P., FORBES, J., BARRIOS, C., FRASSOLDATI, A., CAMPBELL, I., PAIJA, O., MARTIN, N., MODI, A. & BUNDRED, N. 2013. Zoledronic acid (zoledronate) for postmenopausal women with early breast cancer receiving adjuvant letrozole (ZO-FAST study): final 60-month results. *Ann Oncol,* 24**,** 398-405.

COLEMAN, R., FINKELSTEIN, D. M., BARRIOS, C., MARTIN, M., IWATA, H., HEGG, R., GLASPY, J., PERIANEZ, A. M., TONKIN, K., DELEU, I., SOHN, J., CROWN, J., DELALOGE, S., DAI, T., ZHOU, Y., JANDIAL, D. & CHAN, A. 2020a. Adjuvant denosumab in early breast cancer (D-CARE): an international, multicentre, randomised, controlled, phase 3 trial. *Lancet Oncol,* 21**,** 60-72.

COLEMAN, R. E. 1997a. Skeletal complications of malignancy. *Cancer,* 80**,** 1588-1594.

COLEMAN, R. E. 1997b. Skeletal complications of malignancy. *Cancer,* 80**,** 1588-94.

COLEMAN, R. E., CROUCHER, P. I., PADHANI, A. R., CLEZARDIN, P., CHOW, E., FALLON, M., GUISE, T., COLANGELI, S., CAPANNA, R. & COSTA, L. 2020b. Bone metastases. *Nat Rev Dis Primers,* 6**,** 83.

COLEMAN, R. E. & RUBENS, R. D. 1987. The clinical course of bone metastases from breast cancer. *Br J Cancer,* 55**,** 61-6.

COMITO, G., PONS SEGURA, C., TADDEI, M. L., LANCIOTTI, M., SERNI, S., MORANDI, A., CHIARUGI, P. & GIANNONI, E. 2017. Zoledronic acid impairs stromal reactivity by inhibiting M2-macrophages polarization and prostate cancer-associated fibroblasts. *Oncotarget,* 8**,** 118-132.

COMPSTON, J. E. 2002. Bone marrow and bone: a functional unit. *J Endocrinol,* 173**,** 387-94.

CONESA, A., MADRIGAL, P., TARAZONA, S., GOMEZ-CABRERO, D., CERVERA, A., MCPHERSON, A., SZCZESNIAK, M. W., GAFFNEY, D. J., ELO, L. L., ZHANG, X. & MORTAZAVI, A. 2016. A survey of best practices for RNA-seq data analysis. *Genome Biol,* 17**,** 13.

COREY, E., BROWN, L. G., QUINN, J. E., POOT, M., ROUDIER, M. P., HIGANO, C. S. & VESSELLA, R. L. 2003. Zoledronic acid exhibits inhibitory effects on osteoblastic and osteolytic metastases of prostate cancer. *Clin Cancer Res,* 9**,** 295-306.

CORREIA, D. V., LOPES, A. & SILVA-SANTOS, B. 2013. Tumor cell recognition by gammadelta T lymphocytes: T-cell receptor vs. NK-cell receptors. *Oncoimmunology,* 2**,** e22892.

COSCIA, M., QUAGLINO, E., IEZZI, M., CURCIO, C., PANTALEONI, F., RIGANTI, C., HOLEN, I., MONKKONEN, H., BOCCADORO, M., FORNI, G., MUSIANI, P., BOSIA, A., CAVALLO, F. & MASSAIA, M. 2010. Zoledronic acid repolarizes tumour-associated macrophages and inhibits mammary carcinogenesis by targeting the mevalonate pathway. *J Cell Mol Med,* 14**,** 2803-15.

COSMAN, F., CRITTENDEN, D. B., ADACHI, J. D., BINKLEY, N., CZERWINSKI, E., FERRARI, S., HOFBAUER, L. C., LAU, E., LEWIECKI, E. M., MIYAUCHI, A., ZERBINI, C. A., MILMONT, C. E., CHEN, L., MADDOX, J., MEISNER, P. D., LIBANATI, C. & GRAUER, A. 2016. Romosozumab Treatment in Postmenopausal Women with Osteoporosis. *N Engl J Med,* 375**,** 1532-1543.

CREA, F., NUR SAIDY, N. R., COLLINS, C. C. & WANG, Y. 2015. The epigenetic/noncoding origin of tumor dormancy. *Trends Mol Med,* 21**,** 206-11.

CROUCHER, P. I., DE HENDRIK, R., PERRY, M. J., HIJZEN, A., SHIPMAN, C. M., LIPPITT, J., GREEN, J., VAN MARCK, E., VAN CAMP, B. & VANDERKERKEN, K. 2003. Zoledronic acid treatment of 5T2MM-bearing mice inhibits the development of myeloma bone disease: evidence for decreased

osteolysis, tumor burden and angiogenesis, and increased survival. *J Bone Miner Res,* 18**,** 482-92.

DAI, L., LI, M., ZHANG, W. L., TANG, Y. J., TANG, Y. L. & LIANG, X. H. 2021. Fibroblasts in cancer dormancy: foe or friend? *Cancer Cell Int,* 21**,** 184.

DAI, X., CHENG, H., BAI, Z. & LI, J. 2017. Breast Cancer Cell Line Classification and Its Relevance with Breast Tumor Subtyping. *J Cancer,* 8**,** 3131-3141.

DALTON, H. J., PRADEEP, S., MCGUIRE, M., HAILEMICHAEL, Y., MA, S., LYONS, Y., ARMAIZ-PENA, G. N., PREVIS, R. A., HANSEN, J. M., RUPAIMOOLE, R., GONZALEZ-VILLASANA, V., CHO, M. S., WU, S. Y., MANGALA, L. S., JENNINGS, N. B., HU, W., LANGLEY, R., MU, H., ANDREEFF, M., BAR-ELI, M., OVERWIJK, W., RAM, P., LOPEZ-BERESTEIN, G., COLEMAN, R. L. & SOOD, A. K. 2017. Macrophages Facilitate Resistance to Anti-VEGF Therapy by Altered VEGFR Expression. *Clin Cancer Res,* 23**,** 7034-7046.

DAR, H. Y., AZAM, Z., ANUPAM, R., MONDAL, R. K. & SRIVASTAVA, R. K. 2018. Osteoimmunology: The Nexus between bone and immune system. *Front Biosci (Landmark Ed),* 23**,** 464-492.

DARVIN, P., TOOR, S. M., SASIDHARAN NAIR, V. & ELKORD, E. 2018. Immune checkpoint inhibitors: recent progress and potential biomarkers. *Exp Mol Med,* 50**,** 1-11.

DARWICH, L., COMA, G., PEÑA, R., BELLIDO, R., BLANCO, E. J., ESTE, J. A., BORRAS, F. E., CLOTET, B., RUIZ, L., ROSELL, A., ANDREO, F., PARKHOUSE, R. M. & BOFILL, M. 2009. Secretion of interferon-gamma by human macrophages demonstrated at the single-cell level after costimulation with interleukin (IL)-12 plus IL-18. *Immunology,* 126**,** 386-93.

DATTA, N. S. 2011. Osteoporotic fracture and parathyroid hormone. *World J Orthop,* 2**,** 67-74.

DAUBINÉ, F., LE GALL, C., GASSER, J., GREEN, J. & CLÉZARDIN, P. 2007. Antitumor effects of clinical dosing regimens of bisphosphonates in experimental breast cancer bone metastasis. *J Natl Cancer Inst,* 99**,** 322-30.

DE HAAN, G. & LAZARE, S. S. 2018. Aging of hematopoietic stem cells. *Blood,* 131**,** 479-487.

DECAMPS, C., ARNAUD, A., PETITPREZ, F., AYADI, M., BAURES, A., ARMENOULT, L., CONSORTIUM, H., ESCALERA, S., GUYON, I., NICOLLE, R., TOMASINI, R., DE REYNIES, A., CROS, J., BLUM, Y. & RICHARD, M. 2021. DECONbench: a benchmarking platform dedicated to deconvolution methods for tumor heterogeneity quantification. *BMC Bioinformatics,* 22**,** 473.

DEL FATTORE, A. & TETI, A. 2012. The tight relationship between osteoclasts and the immune system. *Inflamm Allergy Drug Targets,* 11**,** 181-7.

DEMICHELI, R., MICELI, R., MOLITERNI, A., ZAMBETTI, M., HRUSHESKY, W. J., RETSKY, M. W., VALAGUSSA, P. & BONADONNA, G. 2005. Breast cancer recurrence dynamics following adjuvant CMF is consistent with tumor dormancy and mastectomy-driven acceleration of the metastatic process. *Ann Oncol,* 16**,** 1449-57.

DENNIS, G., JR., SHERMAN, B. T., HOSACK, D. A., YANG, J., GAO, W., LANE, H. C. & LEMPICKI, R. A. 2003. DAVID: Database for Annotation, Visualization, and Integrated Discovery. *Genome Biol,* 4**,** P3.

DEVIGNES, C. S., ASLAN, Y., BRENOT, A., DEVILLERS, A., SCHEPERS, K., FABRE, S., CHOU, J., CASBON, A. J., WERB, Z. & PROVOT, S. 2018. HIF signaling in osteoblast-lineage cells promotes systemic breast cancer growth and metastasis in mice. *Proc Natl Acad Sci U S A,* 115**,** E992-E1001.

DIAZ BRINTON, R. 2012. Minireview: translational animal models of human menopause: challenges and emerging opportunities. *Endocrinology,* 153**,** 3571-8.

DIEFENBACH, A., JENSEN, E. R., JAMIESON, A. M. & RAULET, D. H. 2001. Rae1 and H60 ligands of the NKG2D receptor stimulate tumour immunity. *Nature,* 413**,** 165-71.

DILLIES, M. A., RAU, A., AUBERT, J., HENNEQUET-ANTIER, C., JEANMOUGIN, M., SERVANT, N., KEIME, C., MAROT, G., CASTEL, D., ESTELLE, J., GUERNEC, G., JAGLA, B., JOUNEAU, L., LALOE, D., LE GALL, C., SCHAEFFER, B., LE CROM, S., GUEDJ, M., JAFFREZIC, F. & FRENCH STATOMIQUE, C. 2013. A comprehensive evaluation of normalization methods for Illumina high-throughput RNA sequencing data analysis. *Brief Bioinform,* 14**,** 671-83.

DOBIN, A., DAVIS, C. A., SCHLESINGER, F., DRENKOW, J., ZALESKI, C., JHA, S., BATUT, P., CHAISSON, M. & GINGERAS, T. R. 2013. STAR: ultrafast universal RNA-seq aligner. *Bioinformatics,* 29**,** 15-21.

DOUGALL, W. C. 2012. Molecular pathways: osteoclast-dependent and osteoclast-independent roles of the RANKL/RANK/OPG pathway in tumorigenesis and metastasis. *Clin Cancer Res,* 18**,** 326-35.

DRAKE, M. T., CLARKE, B. L. & KHOSLA, S. 2008. Bisphosphonates: mechanism of action and role in clinical practice. *Mayo Clin Proc,* 83**,** 1032-45.

DUDA, D. G., DUYVERMAN, A. M., KOHNO, M., SNUDERL, M., STELLER, E. J., FUKUMURA, D. & JAIN, R. K. 2010. Malignant cells facilitate lung metastasis by bringing their own soil. *Proc Natl Acad Sci U S A,* 107**,** 21677-82.

DUMAS-MALLET, E., BUTTON, K. S., BORAUD, T., GONON, F. & MUNAFO, M. R. 2017. Low statistical power in biomedical science: a review of three human research domains. *R Soc Open Sci,* 4**,** 160254.

DUNFORD, J. E., THOMPSON, K., COXON, F. P., LUCKMAN, S. P., HAHN, F. M., POULTER, C. D., EBETINO, F. H. & ROGERS, M. J. 2001. Structure-activity relationships for inhibition of farnesyl diphosphate synthase *in vitro* and inhibition of bone resorption *in vivo* by nitrogen-containing bisphosphonates. *J Pharmacol Exp Ther,* 296**,** 235-42.

DUNN, G. P., OLD, L. J. & SCHREIBER, R. D. 2004. The immunobiology of cancer immunosurveillance and immunoediting. *Immunity,* 21**,** 137-48.

DUTTA, S. & SENGUPTA, P. 2016. Men and mice: Relating their ages. *Life Sci,* 152**,** 244-8.

EARLY BREAST CANCER TRIALISTS' COLLABORATIVE, G. 2015. Adjuvant bisphosphonate treatment in early breast cancer: meta-analyses of individual patient data from randomised trials. *Lancet,* 386**,** 1353-1361.

EGHBALI-FATOURECHI, G., KHOSLA, S., SANYAL, A., BOYLE, W. J., LACEY, D. L. & RIGGS, B. L. 2003. Role of RANK ligand in mediating increased bone resorption in early postmenopausal women. *J Clin Invest,* 111**,** 1221-30.

EOM, T., ZHANG, C., WANG, H., LAY, K., FAK, J., NOEBELS, J. L. & DARNELL, R. B. 2013. NOVA-dependent regulation of cryptic NMD exons controls synaptic protein levels after seizure. *Elife,* 2**,** e00178.

EWELS, P., MAGNUSSON, M., LUNDIN, S. & KALLER, M. 2016. MultiQC: summarize analysis results for multiple tools and samples in a single report. *Bioinformatics,* 32**,** 3047-8.

FANG, Y., CHEN, Y., YU, L., ZHENG, C., QI, Y., LI, Z., YANG, Z., ZHANG, Y., SHI, T., LUO, J. & LIU, M. 2013. Inhibition of breast cancer metastases by a novel inhibitor of TGFbeta receptor 1. *J Natl Cancer Inst,* 105**,** 47-58.

FARR, J. N., ROFORTH, M. M., FUJITA, K., NICKS, K. M., CUNNINGHAM, J. M., ATKINSON, E. J., THERNEAU, T. M., MCCREADY, L. K., PETERSON, J. M., DRAKE, M. T., MONROE, D. G. & KHOSLA, S. 2015. Effects of Age and Estrogen on Skeletal Gene Expression in Humans as Assessed by RNA Sequencing. *PLoS One,* 10**,** e0138347.

FARRAR, J. D., KATZ, K. H., WINDSOR, J., THRUSH, G., SCHEUERMANN, R. H., UHR, J. W. & STREET, N. E. 1999. Cancer dormancy. VII. A regulatory role for CD8+ T cells and IFN-gamma in establishing and maintaining the tumor-dormant state. *J Immunol,* 162**,** 2842-9.

FEHER, J. 2017. Target Tissues and Integrated Control. *In:* FEHER, J. (ed.) *Calcium and Phosphorus Homeostasis II.* Academic Press.

FERRANDO, A. A., NEUBERG, D. S., STAUNTON, J., LOH, M. L., HUARD, C., RAIMONDI, S. C., BEHM, F. G., PUI, C. H., DOWNING, J. R., GILLILAND, D. G., LANDER, E. S., GOLUB, T. R. & LOOK, A. T. 2002. Gene expression signatures define novel oncogenic pathways in T cell acute lymphoblastic leukemia. *Cancer Cell,* 1**,** 75-87.

FEUERER, M., ROCHA, M., BAI, L., UMANSKY, V., SOLOMAYER, E. F., BASTERT, G., DIEL, I. J. & SCHIRRMACHER, V. 2001. Enrichment of memory T cells and other profound immunological changes in the bone marrow from untreated breast cancer patients. *Int J Cancer,* 92**,** 96-105.

FINOTELLO, F. & TRAJANOSKI, Z. 2018. Quantifying tumor-infiltrating immune cells from transcriptomics data. *Cancer Immunol Immunother,* 67**,** 1031-1040.

FLANAGAN, S. P. 1966. 'Nude', a new hairless gene with pleiotropic effects in the mouse. *Genet Res,* 8**,** 295-309.

FLEET, J. C. 2017. The role of vitamin D in the endocrinology controlling calcium homeostasis. *Mol Cell Endocrinol,* 453**,** 36-45.

FLUEGEN, G., AVIVAR-VALDERAS, A., WANG, Y., PADGEN, M. R., WILLIAMS, J. K., NOBRE, A. R., CALVO, V., CHEUNG, J. F., BRAVO-CORDERO, J. J., ENTENBERG, D., CASTRACANE, J., VERKHUSHA, V., KEELY, P. J., CONDEELIS, J. & AGUIRRE-GHISO, J. A. 2017. Phenotypic heterogeneity of disseminated tumour cells is preset by primary tumour hypoxic microenvironments. *Nat Cell Biol,* 19**,** 120-132.

FOROUTAN, M., BHUVA, D. D., LYU, R., HORAN, K., CURSONS, J. & DAVIS, M. J. 2018. Single sample scoring of molecular phenotypes. *BMC Bioinformatics,* 19**,** 404.

FOURNIER, P. G., STRESING, V., EBETINO, F. H. & CLÉZARDIN, P. 2010. How do bisphosphonates inhibit bone metastasis *in vivo*? *Neoplasia,* 12**,** 571-8.

FRANCISCO, L. M., SALINAS, V. H., BROWN, K. E., VANGURI, V. K., FREEMAN, G. J., KUCHROO, V. K. & SHARPE, A. H. 2009. PD-L1 regulates the development, maintenance, and function of induced regulatory T cells. *J Exp Med,* 206**,** 3015-29.

FRATTA, P., SIVAKUMAR, P., HUMPHREY, J., LO, K., RICKETTS, T., OLIVEIRA, H., BRITO-ARMAS, J. M., KALMAR, B., ULE, A., YU, Y., BIRSA, N., BODO, C., COLLINS, T., CONICELLA, A. E., MEJIA MAZA, A., MARRERO-GAGLIARDI, A., STEWART, M., MIANNE, J., CORROCHANO, S., EMMETT, W., CODNER, G., GROVES, M., FUKUMURA, R., GONDO, Y., LYTHGOE, M., PAUWS, E., PESKETT, E., STANIER, P., TEBOUL, L., HALLEGGER, M., CALVO, A., CHIO, A., ISAACS, A. M., FAWZI, N. L., WANG, E., HOUSMAN, D. E., BARALLE, F., GREENSMITH, L., BURATTI, E., PLAGNOL, V., FISHER, E. M. & ACEVEDO-AROZENA, A. 2018. Mice with endogenous TDP-43 mutations exhibit gain of splicing function and characteristics of amyotrophic lateral sclerosis. *EMBO J,* 37.

FRISCH, B. J. 2019. The hematopoietic stem cell niche: What's so special about bone? *Bone,* 119**,** 8-12.

FRYE, M., HARADA, B. T., BEHM, M. & HE, C. 2018. RNA modifications modulate gene expression during development. *Science,* 361**,** 1346-1349.

FUENTES, M. 2014. *Hemocytometer protocol* [Online]. Available: https://www.hemocytometer.org/hemocytometer-protocol/ [Accessed June 2019].

FUJISAKI, J., WU, J., CARLSON, A. L., SILBERSTEIN, L., PUTHETI, P., LAROCCA, R., GAO, W., SAITO, T. I., LO CELSO, C., TSUYUZAKI, H., SATO, T., COTE, D., SYKES, M., STROM, T. B., SCADDEN, D. T. & LIN, C. P. 2011. *In vivo* imaging of Treg cells providing immune privilege to the haematopoietic stem-cell niche. *Nature,* 474**,** 216-9.

FULCINITI, M., TASSONE, P., HIDESHIMA, T., VALLET, S., NANJAPPA, P., ETTENBERG, S. A., SHEN, Z., PATEL, N., TAI, Y. T., CHAUHAN, D., MITSIADES, C., PRABHALA, R., RAJE, N., ANDERSON, K. C., STOVER, D. R. & MUNSHI, N. C. 2009. Anti-DKK1 mAb (BHQ880) as a potential therapeutic agent for multiple myeloma. *Blood,* 114**,** 371-9.

GARRIDO, C., PACO, L., ROMERO, I., BERRUGUILLA, E., STEFANSKY, J., COLLADO, A., ALGARRA, I., GARRIDO, F. & GARCIA-LORA, A. M. 2012. MHC class I molecules act as tumor suppressor genes regulating the cell cycle gene expression, invasion and intrinsic tumorigenicity of melanoma cells. *Carcinogenesis,* 33**,** 687-93.

GASPARETTO, C. 2004. Stem cell transplantation for multiple myeloma. *Cancer Control,* 11**,** 119-29.

GELAO, L., CRISCITIELLO, C., FUMAGALLI, L., LOCATELLI, M., MANUNTA, S., ESPOSITO, A., MINCHELLA, I., GOLDHIRSCH, A. & CURIGLIANO, G. 2013. Tumour dormancy and clinical implications in breast cancer. *Ecancermedicalscience,* 7**,** 320.

GEORGE, C. N., CANUAS-LANDERO, V., THEODOULOU, E., MUTHANA, M., WILSON, C. & OTTEWELL, P. 2020. Oestrogen and zoledronic acid driven changes to the bone and immune environments: Potential mechanisms underlying the differential anti-tumour effects of zoledronic acid in pre- and post-menopausal conditions. *J Bone Oncol,* 25**,** 100317.

GHAJAR, C. M. 2015. Metastasis prevention by targeting the dormant niche. *Nat Rev Cancer,* 15**,** 238-47.

GHAJAR, C. M., PEINADO, H., MORI, H., MATEI, I. R., EVASON, K. J., BRAZIER, H., ALMEIDA, D., KOLLER, A., HAJJAR, K. A., STAINIER, D. Y., CHEN, E. I., LYDEN, D. & BISSELL, M. J. 2013. The perivascular niche regulates breast tumour dormancy. *Nat Cell Biol,* 15**,** 807-17.

GNANT, M., MLINERITSCH, B., STOEGER, H., LUSCHIN-EBENGREUTH, G., HECK, D., MENZEL, C., JAKESZ, R., SEIFERT, M., HUBALEK, M., PRISTAUZ, G., BAUERNHOFER, T., EIDTMANN, H., EIERMANN, W., STEGER, G., KWASNY, W., DUBSKY, P., HOCHREINER, G., FORSTHUBER, E. P., FESL, C., GREIL, R., AUSTRIAN, B. & COLORECTAL CANCER STUDY GROUP, V. A. 2011. Adjuvant endocrine therapy plus zoledronic acid in premenopausal women with early-stage breast cancer: 62-month follow-up from the ABCSG-12 randomised trial. *Lancet Oncol,* 12**,** 631-41.

GOBER, H. J., KISTOWSKA, M., ANGMAN, L., JENO, P., MORI, L. & DE LIBERO, G. 2003a. Human T cell receptor gammadelta cells recognize endogenous mevalonate metabolites in tumor cells. *J Exp Med,* 197**,** 163-8.

GOBER, H. J., KISTOWSKA, M., ANGMAN, L., JENÖ, P., MORI, L. & DE LIBERO, G. 2003b. Human T cell receptor gammadelta cells recognize endogenous mevalonate metabolites in tumor cells. *J Exp Med,* 197**,** 163-8.

GOLTZMAN, D. & HENDY, G. N. 2015. The calcium-sensing receptor in bone--mechanistic and therapeutic insights. *Nat Rev Endocrinol,* 11**,** 298-307.

GOMIS, R. R. & GAWRZAK, S. 2017. Tumor cell dormancy. *Mol Oncol,* 11**,** 62-78.

GONG, T. & SZUSTAKOWSKI, J. D. 2013. DeconRNASeq: a statistical framework for deconvolution of heterogeneous tissue samples based on mRNA-Seq data. *Bioinformatics,* 29**,** 1083-5.

GRABHERR, M. G., HAAS, B. J., YASSOUR, M., LEVIN, J. Z., THOMPSON, D. A., AMIT, I., ADICONIS, X., FAN, L., RAYCHOWDHURY, R., ZENG, Q., CHEN, Z., MAUCELI, E., HACOHEN, N., GNIRKE, A., RHIND, N., DI PALMA, F., BIRREN, B. W., NUSBAUM, C., LINDBLAD-TOH, K., FRIEDMAN, N. & REGEV, A. 2011. Full-length transcriptome assembly from RNA-Seq data without a reference genome. *Nat Biotechnol,* 29**,** 644-52.

GRANNEMAN, J. G. & MOORE, H. P. 2008. Location, location: protein trafficking and lipolysis in adipocytes. *Trends Endocrinol Metab,* 19**,** 3-9.

GRANNEMAN, J. G., MOORE, H. P., GRANNEMAN, R. L., GREENBERG, A. S., OBIN, M. S. & ZHU, Z. 2007. Analysis of lipolytic protein trafficking and interactions in adipocytes. *J Biol Chem,* 282**,** 5726-35.

GRIMALDI, C. M., CLEARY, J., DAGTAS, A. S., MOUSSAI, D. & DIAMOND, B. 2002. Estrogen alters thresholds for B cell apoptosis and activation. *J Clin Invest,* 109**,** 1625-33.

GUISE, T. A. 2002. The vicious cycle of bone metastases. *J Musculoskelet Neuronal Interact,* 2**,** 570-2.

GUISE, T. A. & CHIRGWIN, J. M. 2003. Transforming growth factor-beta in osteolytic breast cancer bone metastases. *Clin Orthop Relat Res***,** S32-8.

GUO, W. & WU, C. 2021. Detection of Hypoxic Regions in the Bone Microenvironment. *Methods Mol Biol,* 2230**,** 345-356.

GUSTAFSSON, K. & WELSH, M. 2016. Maintenance of hematopoietic stem cell dormancy: yet another role for the macrophage. *Stem Cell Investig,* 3**,** 46.

HAEMMERLE, G., LASS, A., ZIMMERMANN, R., GORKIEWICZ, G., MEYER, C., ROZMAN, J., HELDMAIER, G., MAIER, R., THEUSSL, C., EDER, S., KRATKY, D., WAGNER, E. F., KLINGENSPOR, M., HOEFLER, G. & ZECHNER, R. 2006. Defective lipolysis and altered energy metabolism in mice lacking adipose triglyceride lipase. *Science,* 312**,** 734-7.

HAIDER, M. T., HOLEN, I., DEAR, T. N., HUNTER, K. & BROWN, H. K. 2014. Modifying the osteoblastic niche with zoledronic acid *in vivo*-potential implications for breast cancer bone metastasis. *Bone,* 66**,** 240-50.

HAN, S., QI, Y., LUO, Y., CHEN, X. & LIANG, H. 2020. Exosomal Long Non-Coding RNA: Interaction Between Cancer Cells and Non-Cancer Cells. *Front Oncol,* 10**,** 617837.

HANAHAN, D. & WEINBERG, R. A. 2011. Hallmarks of cancer: the next generation. *Cell,* 144**,** 646-74.

HARPER, J. & SAINSON, R. C. 2014. Regulation of the anti-tumour immune response by cancer-associated fibroblasts. *Semin Cancer Biol,* 25**,** 69-77.

HAUBRUCK, P., COLBATH, A. C., LIU, Y., STONER, S., SHU, C. & LITTLE, C. B. 2020. Flow Cytometry Analysis of Immune Cell Subsets within the Murine Spleen, Bone Marrow, Lymph Nodes and Synovial Tissue in an Osteoarthritis Model. *J Vis Exp*.

HAYMAN, A. R. 2008. Tartrate-resistant acid phosphatase (TRAP) and the osteoclast/immune cell dichotomy. *Autoimmunity,* 41**,** 218-23.

HEWITT, R. E., LISSINA, A., GREEN, A. E., SLAY, E. S., PRICE, D. A. & SEWELL, A. K. 2005. The bisphosphonate acute phase response: rapid and copious production of proinflammatory

cytokines by peripheral blood gd T cells in response to aminobisphosphonates is inhibited by statins. *Clin Exp Immunol,* 139**,** 101-11.

HIGHFILL, S. L., RODRIGUEZ, P. C., ZHOU, Q., GOETZ, C. A., KOEHN, B. H., VEENSTRA, R., TAYLOR, P. A., PANOSKALTSIS-MORTARI, A., SERODY, J. S., MUNN, D. H., TOLAR, J., OCHOA, A. C. & BLAZAR, B. R. 2010. Bone marrow myeloid-derived suppressor cells (MDSCs) inhibit graft-versus-host disease (GVHD) via an arginase-1-dependent mechanism that is up-regulated by interleukin-13. *Blood,* 116**,** 5738-47.

HIRATA, Y., FURUHASHI, K., ISHII, H., LI, H. W., PINHO, S., DING, L., ROBSON, S. C., FRENETTE, P. S. & FUJISAKI, J. 2018. CD150(high) Bone Marrow Tregs Maintain Hematopoietic Stem Cell Quiescence and Immune Privilege via Adenosine. *Cell Stem Cell,* 22**,** 445-453 e5.

HIRBE, A. C., RUBIN, J., ULUCKAN, O., MORGAN, E. A., EAGLETON, M. C., PRIOR, J. L., PIWNICA-WORMS, D. & WEILBAECHER, K. N. 2007. Disruption of CXCR4 enhances osteoclastogenesis and tumor growth in bone. *Proc Natl Acad Sci U S A,* 104**,** 14062-7.

HITRON, A. & ADAMS, V. 2009. The pharmacological management of skeletal-related events from metastatic tumors. *Orthopedics,* 32**,** 188.

HOFBAUER, L. C., KHOSLA, S., DUNSTAN, C. R., LACEY, D. L., SPELSBERG, T. C. & RIGGS, B. L. 1999. Estrogen stimulates gene expression and protein production of osteoprotegerin in human osteoblastic cells. *Endocrinology,* 140**,** 4367-70.

HOLLIDAY, D. L. & SPEIRS, V. 2011. Choosing the right cell line for breast cancer research. *Breast Cancer Res,* 13**,** 215.

HOLMGREN, L., O'REILLY, M. S. & FOLKMAN, J. 1995. Dormancy of micrometastases: balanced proliferation and apoptosis in the presence of angiogenesis suppression. *Nat Med,* 1**,** 149-53.

HONG, M., TAO, S., ZHANG, L., DIAO, L. T., HUANG, X., HUANG, S., XIE, S. J., XIAO, Z. D. & ZHANG, H. 2020. RNA sequencing: new technologies and applications in cancer research. *J Hematol Oncol,* 13**,** 166.

HORTOBAGYI, G. N. 2015. Everolimus plus exemestane for the treatment of advanced breast cancer: a review of subanalyses from BOLERO-2. *Neoplasia,* 17**,** 279-88.

HSU, J., ARAND, J., CHAIKOVSKY, A., MOONEY, N. A., DEMETER, J., BRISON, C. M., OLIVERIO, R., VOGEL, H., RUBIN, S. M., JACKSON, P. K. & SAGE, J. 2019. E2F4 regulates transcriptional activation in mouse embryonic stem cells independently of the RB family. *Nat Commun,* 10**,** 2939.

HUANG, R., WANG, X., YIN, X., ZHOU, Y., SUN, J., YIN, Z. & ZHU, Z. 2022. Combining bulk RNA-sequencing and single-cell RNA-sequencing data to reveal the immune microenvironment and metabolic pattern of osteosarcoma. *Front Genet,* 13**,** 976990.

HUDIS, C. A. & GIANNI, L. 2011. Triple-negative breast cancer: an unmet medical need. *Oncologist,* 16 Suppl 1**,** 1-11.

HUGHES, D. E., DAI, A., TIFFEE, J. C., LI, H. H., MUNDY, G. R. & BOYCE, B. F. 1996. Estrogen promotes apoptosis of murine osteoclasts mediated by TGF-beta. *Nat Med,* 2**,** 1132-6.

HUGHES, R., CHEN, X., HUNTER, K. D., HOBBS, J. K., HOLEN, I. & BROWN, N. J. 2019. Bone marrow osteoprogenitors are depleted whereas osteoblasts are expanded independent of the osteogenic vasculature in response to zoledronic acid. *FASEB J,* 33**,** 12768-12779.

HURGOBIN, B. 2016. Short Read Alignment Using SOAP2. *Methods Mol Biol,* 1374**,** 241-52.

INDRACCOLO, S., MINUZZO, S., MASIERO, M., PUSCEDDU, I., PERSANO, L., MOSERLE, L., REBOLDI, A., FAVARO, E., MECAROZZI, M., DI MARIO, G., SCREPANTI, I., PONZONI, M., DOGLIONI, C. & AMADORI, A. 2009. Cross-talk between tumor and endothelial cells involving the Notch3-Dll4 interaction marks escape from tumor dormancy. *Cancer Res,* 69**,** 1314-23.

IRIMIA, M., WEATHERITT, R. J., ELLIS, J. D., PARIKSHAK, N. N., GONATOPOULOS-POURNATZIS, T., BABOR, M., QUESNEL-VALLIERES, M., TAPIAL, J., RAJ, B., O'HANLON, D., BARRIOS-RODILES, M., STERNBERG, M. J., CORDES, S. P., ROTH, F. P., WRANA, J. L., GESCHWIND, D. H. & BLENCOWE, B. J. 2014. A highly conserved program of neuronal microexons is misregulated in autistic brains. *Cell,* 159**,** 1511-23.

ITKIN, T. & LAPIDOT, T. 2011. SDF-1 keeps HSC quiescent at home. *Blood,* 117**,** 373-4.

IYER, S. P., BECK, J. T., STEWART, A. K., SHAH, J., KELLY, K. R., ISAACS, R., BILIC, S., SEN, S. & MUNSHI, N. C. 2014. A Phase IB multicentre dose-determination study of BHQ880 in combination with anti-myeloma therapy and zoledronic acid in patients with relapsed or refractory multiple myeloma and prior skeletal-related events. *Br J Haematol,* 167**,** 366-75.

JACOBS, J. F., IDEMA, A. J., BOL, K. F., NIERKENS, S., GRAUER, O. M., WESSELING, P., GROTENHUIS, J. A., HOOGERBRUGGE, P. M., DE VRIES, I. J. & ADEMA, G. J. 2009. Regulatory T cells and the PD-L1/PD-1 pathway mediate immune suppression in malignant human brain tumors. *Neuro Oncol,* 11**,** 394-402.

JANCKILA, A. J. & YAM, L. T. 2009. Biology and clinical significance of tartrate-resistant acid phosphatases: new perspectives on an old enzyme. *Calcif Tissue Int,* 85**,** 465-83.

JAYSON, G. C., KERBEL, R., ELLIS, L. M. & HARRIS, A. L. 2016. Antiangiogenic therapy in oncology: current status and future directions. *Lancet,* 388**,** 518-29.

JEGANATHAN, S., FIORINO, C., NAIK, U., SUN, H. S. & HARRISON, R. E. 2014. Modulation of osteoclastogenesis with macrophage M1- and M2-inducing stimuli. *PLoS One,* 9**,** e104498.

JENSEN, A. B., WYNNE, C., RAMIREZ, G., HE, W., SONG, Y., BERD, Y., WANG, H., MEHTA, A. & LOMBARDI, A. 2010. The cathepsin K inhibitor odanacatib suppresses bone resorption in women with breast cancer and established bone metastases: results of a 4-week, double-blind, randomized, controlled trial. *Clin Breast Cancer,* 10**,** 452-8.

JILKA, R. L. 2013. The relevance of mouse models for investigating age-related bone loss in humans. *J Gerontol A Biol Sci Med Sci,* 68**,** 1209-17.

JIN, H. & LIU, Z. 2021. A benchmark for RNA-seq deconvolution analysis under dynamic testing environments. *Genome Biol,* 22**,** 102.

JINNAH, A. H., ZACKS, B. C., GWAM, C. U. & KERR, B. A. 2018. Emerging and Established Models of Bone Metastasis. *Cancers (Basel),* 10.

KÄKÖNEN, S. M. & MUNDY, G. R. 2003. Mechanisms of osteolytic bone metastases in breast carcinoma. *Cancer,* 97**,** 834-9.

KANEKO, J., OKINAGA, T., HIKIJI, H., ARIYOSHI, W., YOSHIGA, D., HABU, M., TOMINAGA, K. & NISHIHARA, T. 2018. Zoledronic acid exacerbates inflammation through M1 macrophage polarization. *Inflamm Regen,* 38**,** 16.

KARNOUB, A. E., DASH, A. B., VO, A. P., SULLIVAN, A., BROOKS, M. W., BELL, G. W., RICHARDSON, A. L., POLYAK, K., TUBO, R. & WEINBERG, R. A. 2007. Mesenchymal stem cells within tumour stroma promote breast cancer metastasis. *Nature,* 449**,** 557-63.

KATAYAMA, N., SHIH, J. P., NISHIKAWA, S., KINA, T., CLARK, S. C. & OGAWA, M. 1993. Stage-specific expression of c-kit protein by murine hematopoietic progenitors. *Blood,* 82**,** 2353-60.

KEARNS, A. E., KHOSLA, S. & KOSTENUIK, P. J. 2008. Receptor activator of nuclear factor kappaB ligand and osteoprotegerin regulation of bone remodeling in health and disease. *Endocr Rev,* 29**,** 155-92.

KENNECKE, H., YERUSHALMI, R., WOODS, R., CHEANG, M. C., VODUC, D., SPEERS, C. H., NIELSEN, T. O. & GELMON, K. 2010. Metastatic behavior of breast cancer subtypes. *J Clin Oncol,* 28**,** 3271-7.

KENT, D., COPLEY, M., BENZ, C., DYKSTRA, B., BOWIE, M. & EAVES, C. 2008. Regulation of hematopoietic stem cells by the steel factor/KIT signaling pathway. *Clin Cancer Res,* 14**,** 1926-30.

KHAN, D. & ANSAR AHMED, S. 2015. The Immune System Is a Natural Target for Estrogen Action: Opposing Effects of Estrogen in Two Prototypical Autoimmune Diseases. *Front Immunol,* 6**,** 635.

KHAZAIE, K., PRIFTI, S., BECKHOVE, P., GRIESBACH, A., RUSSELL, S., COLLINS, M. & SCHIRRMACHER, V. 1994. Persistence of dormant tumor cells in the bone marrow of tumor cell-vaccinated mice correlates with long-term immunological protection. *Proc Natl Acad Sci U S A,* 91**,** 7430-4.

KHOSLA, S., MELTON, L. J., 3RD & RIGGS, B. L. 2011. The unitary model for estrogen deficiency and the pathogenesis of osteoporosis: is a revision needed? *J Bone Miner Res,* 26**,** 441-51.

KHOSLA, S., OURSLER, M. J. & MONROE, D. G. 2012. Estrogen and the skeleton. *Trends Endocrinol Metab,* 23**,** 576-81.

KIM, D., LANGMEAD, B. & SALZBERG, S. L. 2015a. HISAT: a fast spliced aligner with low memory requirements. *Nat Methods,* 12**,** 357-60.

KIM, D., PERTEA, G., TRAPNELL, C., PIMENTEL, H., KELLEY, R. & SALZBERG, S. L. 2013. TopHat2: accurate alignment of transcriptomes in the presence of insertions, deletions and gene fusions. *Genome Biol,* 14**,** R36.

KIM, L. C., SONG, L. & HAURA, E. B. 2009. Src kinases as therapeutic targets for cancer. *Nat Rev Clin Oncol,* 6**,** 587-95.

KIM, M. J., KIM, M. H., KIM, S. A. & CHANG, J. S. 2008. Age-related Deterioration of Hematopoietic Stem Cells. *Int J Stem Cells,* 1**,** 55-63.

KIM, R. S., AVIVAR-VALDERAS, A., ESTRADA, Y., BRAGADO, P., SOSA, M. S., AGUIRRE-GHISO, J. A. & SEGALL, J. E. 2012. Dormancy signatures and metastasis in estrogen receptor positive and negative breast cancer. *PLoS One,* 7**,** e35569.

KIM, T. K., HEMBERG, M. & GRAY, J. M. 2015b. Enhancer RNAs: a class of long noncoding RNAs synthesized at enhancers. *Cold Spring Harb Perspect Biol,* 7**,** a018622.

KIM, W. & WYSOLMERSKI, J. J. 2016. Calcium-Sensing Receptor in Breast Physiology and Cancer. *Front Physiol,* 7**,** 440.

KMIECIAK, M., PAYNE, K. K., IDOWU, M. O., GRIMES, M. M., GRAHAM, L., ASCIERTO, M. L., WANG, E., WANG, X. Y., BEAR, H. D. & MANJILI, M. H. 2011. Tumor escape and progression of HER-2/neu negative breast cancer under immune pressure. *J Transl Med,* 9**,** 35.

KMIECIAK, M., PAYNE, K. K., WANG, X. Y. & MANJILI, M. H. 2013. IFN-gamma Ralpha is a key determinant of CD8+ T cell-mediated tumor elimination or tumor escape and relapse in FVB mouse. *PLoS One,* 8**,** e82544.

KOBAYASHI, A., OKUDA, H., XING, F., PANDEY, P. R., WATABE, M., HIROTA, S., PAI, S. K., LIU, W., FUKUDA, K., CHAMBERS, C., WILBER, A. & WATABE, K. 2011. Bone morphogenetic protein 7 in dormancy and metastasis of prostate cancer stem-like cells in bone. *J Exp Med,* 208**,** 2641-55.

KOEBEL, C. M., VERMI, W., SWANN, J. B., ZERAFA, N., RODIG, S. J., OLD, L. J., SMYTH, M. J. & SCHREIBER, R. D. 2007. Adaptive immunity maintains occult cancer in an equilibrium state. *Nature,* 450**,** 903-7.

KOEBELE, S. V. & BIMONTE-NELSON, H. A. 2016. Modeling menopause: The utility of rodents in translational behavioral endocrinology research. *Maturitas,* 87**,** 5-17.

KOGURE, T., YAN, I. K., LIN, W. L. & PATEL, T. 2013. Extracellular Vesicle-Mediated Transfer of a Novel Long Noncoding RNA TUC339: A Mechanism of Intercellular Signaling in Human Hepatocellular Cancer. *Genes Cancer,* 4**,** 261-72.

KOLB, A. D., SHUPP, A. B., MUKHOPADHYAY, D., MARINI, F. C. & BUSSARD, K. M. 2019. Osteoblasts are "educated" by crosstalk with metastatic breast cancer cells in the bone tumor microenvironment. *Breast Cancer Res,* 21**,** 31.

KORECKIJ, T., NGUYEN, H., BROWN, L. G., YU, E. Y., VESSELLA, R. L. & COREY, E. 2009. Dasatinib inhibits the growth of prostate cancer in bone and provides additional protection from osteolysis. *Br J Cancer,* 101**,** 263-8.

KRALL, J. A., REINHARDT, F., MERCURY, O. A., PATTABIRAMAN, D. R., BROOKS, M. W., DOUGAN, M., LAMBERT, A. W., BIERIE, B., PLOEGH, H. L., DOUGAN, S. K. & WEINBERG, R. A. 2018. The systemic response to surgery triggers the outgrowth of distant immune-controlled tumors in mouse models of dormancy. *Sci Transl Med,* 10.

KRAMAN, M., BAMBROUGH, P. J., ARNOLD, J. N., ROBERTS, E. W., MAGIERA, L., JONES, J. O., GOPINATHAN, A., TUVESON, D. A. & FEARON, D. T. 2010. Suppression of antitumor immunity by stromal cells expressing fibroblast activation protein-alpha. *Science,* 330**,** 827-30.

KRASSAS, G. E. & PAPADOPOULOU, P. 2001. Oestrogen action on bone cells. *J Musculoskelet Neuronal Interact,* 2**,** 143-51.

KRUEGER F, A. S. 2012. *FastQC* [Online]. Babraham Institute. Available: https://www.bioinformatics.babraham.ac.uk/projects/fastqc/ [Accessed].

KULLING, P. M., OLSON, K. C., HAMELE, C. E., TORO, M. F., TAN, S. F., FEITH, D. J. & LOUGHRAN, T. P. 2018. Dysregulation of the IFN-γ-STAT1 signaling pathway in a cell line model of large granular lymphocyte leukemia. *PLoS One,* 13**,** e0193429.

KUNZMANN, V., BAUER, E., FEURLE, J., WEISSINGER, F., TONY, H. P. & WILHELM, M. 2000. Stimulation of gammadelta T cells by aminobisphosphonates and induction of antiplasma cell activity in multiple myeloma. *Blood,* 96**,** 384-92.

LANCIOTTI, M., MASIERI, L., RASPOLLINI, M. R., MINERVINI, A., MARI, A., COMITO, G., GIANNONI, E., CARINI, M., CHIARUGI, P. & SERNI, S. 2014. The role of M1 and M2 macrophages in prostate cancer in relation to extracapsular tumor extension and biochemical recurrence after radical prostatectomy. *Biomed Res Int,* 2014**,** 486798.

LANGMEAD, B., TRAPNELL, C., POP, M. & SALZBERG, S. L. 2009. Ultrafast and memory-efficient alignment of short DNA sequences to the human genome. *Genome Biol,* 10**,** R25.

LE GALL, C., BELLAHCENE, A., BONNELYE, E., GASSER, J. A., CASTRONOVO, V., GREEN, J., ZIMMERMANN, J. & CLEZARDIN, P. 2007. A cathepsin K inhibitor reduces breast cancer induced osteolysis and skeletal tumor burden. *Cancer Res,* 67**,** 9894-902.

LE GALL, C., BONNELYE, E. & CLEZARDIN, P. 2008. Cathepsin K inhibitors as treatment of bone metastasis. *Curr Opin Support Palliat Care,* 2**,** 218-22.

LENTH, R. V. 2007. Statistical power calculations. *J Anim Sci,* 85**,** E24-9.

LETO, G. 2010. Activin A and bone metastasis. *J Cell Physiol,* 225**,** 302-9.

LETO, G., INCORVAIA, L., BADALAMENTI, G., TUMMINELLO, F. M., GEBBIA, N., FLANDINA, C., CRESCIMANNO, M. & RINI, G. 2006. Activin A circulating levels in patients with bone metastasis from breast or prostate cancer. *Clin Exp Metastasis,* 23**,** 117-22.

LI, B., SEVERSON, E., PIGNON, J. C., ZHAO, H., LI, T., NOVAK, J., JIANG, P., SHEN, H., ASTER, J. C., RODIG, S., SIGNORETTI, S., LIU, J. S. & LIU, X. S. 2016. Comprehensive analyses of tumor immunity: implications for cancer immunotherapy. *Genome Biol,* 17**,** 174.

LI, H. & DURBIN, R. 2009. Fast and accurate short read alignment with Burrows-Wheeler transform. *Bioinformatics,* 25**,** 1754-60.

LI, T., FAN, J., WANG, B., TRAUGH, N., CHEN, Q., LIU, J. S., LI, B. & LIU, X. S. 2017. TIMER: A Web Server for Comprehensive Analysis of Tumor-Infiltrating Immune Cells. *Cancer Res,* 77**,** e108-e110.

LI, Y., DRABSCH, Y., PUJUGUET, P., REN, J., VAN LAAR, T., ZHANG, L., VAN DAM, H., CLEMENT-LACROIX, P. & TEN DIJKE, P. 2015. Genetic depletion and pharmacological targeting of alphav integrin in breast cancer cells impairs metastasis in zebrafish and mouse xenograft models. *Breast Cancer Res,* 17**,** 28.

LIANG, W., WANG, F., CHEN, Q., DAI, J., ESCARA-WILKE, J., KELLER, E. T., ZIMMERMANN, J., HONG, N., LU, Y. & ZHANG, J. 2019. Targeting cathepsin K diminishes prostate cancer establishment and growth in murine bone. *J Cancer Res Clin Oncol,* 145**,** 1999-2012.

LIAO, Y., SMYTH, G. K. & SHI, W. 2014. featureCounts: an efficient general purpose program for assigning sequence reads to genomic features. *Bioinformatics,* 30**,** 923-30.

LIBOUBAN, H. & CHAPPARD, D. 2017. Altered bone microarchitecture and gene expression profile due to calcium deficiency in a mouse model of myeloma. *Micron,* 96**,** 77-85.

LIEBNER, D. A., HUANG, K. & PARVIN, J. D. 2014. MMAD: microarray microdissection with analysis of differences is a computational tool for deconvoluting cell type-specific contributions from tissue samples. *Bioinformatics,* 30**,** 682-9.

LIMA, Z. S., GHADAMZADEH, M., ARASHLOO, F. T., AMJAD, G., EBADI, M. R. & YOUNESI, L. 2019. Recent advances of therapeutic targets based on the molecular signature in breast cancer: genetic mutations and implications for current treatment paradigms. *J Hematol Oncol,* 12**,** 38.

LIN, C. F., LIN, C. M., LEE, K. Y., WU, S. Y., FENG, P. H., CHEN, K. Y., CHUANG, H. C., CHEN, C. L., WANG, Y. C., TSENG, P. C. & TSAI, T. T. 2017. Escape from IFN-γ-dependent immunosurveillance in tumorigenesis. *J Biomed Sci,* 24**,** 10.

LINDAU, D., GIELEN, P., KROESEN, M., WESSELING, P. & ADEMA, G. J. 2013. The immunosuppressive tumour network: myeloid-derived suppressor cells, regulatory T cells and natural killer T cells. *Immunology,* 138**,** 105-15.

LINDSAY, R., HART, D. M., AITKEN, J. M., MACDONALD, E. B., ANDERSON, J. B. & CLARKE, A. C. 1976. Long-term prevention of postmenopausal osteoporosis by oestrogen. Evidence for an increased bone mass after delayed onset of oestrogen treatment. *Lancet,* 1**,** 1038-41.

LIU, C., ZHAO, Q. & YU, X. 2020. Bone Marrow Adipocytes, Adipocytokines, and Breast Cancer Cells: Novel Implications in Bone Metastasis of Breast Cancer. *Front Oncol,* 10**,** 561595.

LIU, H., WANG, S. H., CHEN, S. C., CHEN, C. Y., LO, J. L. & LIN, T. M. 2016a. Immune modulation of CD4(+)CD25(+) regulatory T cells by zoledronic acid. *BMC Immunol,* 17**,** 45.

LIU, S., WANG, Z., ZHU, R., WANG, F., CHENG, Y. & LIU, Y. 2021. Three Differential Expression Analysis Methods for RNA Sequencing: limma, EdgeR, DESeq2. *J Vis Exp*.

LIU, S., ZHU, W., LI, S., MA, J., ZHANG, H., LI, Z., ZHANG, L., ZHANG, B., LI, Z., LIANG, X. & SHI, W. 2016b. Bovine parathyroid hormone enhances osteoclast bone resorption by modulating V-ATPase through PTH1R. *Int J Mol Med,* 37**,** 284-92.

LIU, X. H., KIRSCHENBAUM, A., YAO, S. & LEVINE, A. C. 2005. Cross-talk between the interleukin-6 and prostaglandin E(2) signaling systems results in enhancement of osteoclastogenesis through effects on the osteoprotegerin/receptor activator of nuclear factor-{kappa}B (RANK) ligand/RANK system. *Endocrinology,* 146**,** 1991-8.

LOGSDON, D. K., BEEGHLY, G. F. & MUNSON, J. M. 2017. Chemoprotection Across the Tumor Border: Cancer Cell Response to Doxorubicin Depends on Stromal Fibroblast Ratios and Interstitial Therapeutic Transport. *Cell Mol Bioeng,* 10**,** 463-481.

LOTINUN, S., SIBONGA, J. D. & TURNER, R. T. 2002. Differential effects of intermittent and continuous administration of parathyroid hormone on bone histomorphometry and gene expression. *Endocrine,* 17**,** 29-36.

LOVE, M. I., HUBER, W. & ANDERS, S. 2014. Moderated estimation of fold change and dispersion for RNA-seq data with DESeq2. *Genome Biol,* 15**,** 550.

LOVERO, D., D'ORONZO, S., PALMIROTTA, R., CAFFORIO, P., BROWN, J., WOOD, S., PORTA, C., LAURICELLA, E., COLEMAN, R. & SILVESTRIS, F. 2021. Correlation between targeted RNAseq signature of breast cancer CTCs and onset of bone-only metastases. *Br J Cancer*.

M. AKLILU, A. H., C.P. EVANS, R.A. HANNON, A. LIPTON, M. DIMAIRO, J. YU, P. ZOBEL, F.M. TORTI, R.D. FINKELMAN 2011. A phase II, randomized, open-label, pilot study to evaluate the safety and the effects on bone resorption of saracatinib (AZD0530) in patients with prostate cancer or breast cancer with metastatic bone disease. *Bone,* 48**,** S17.

MACKIE, R. M., REID, R. & JUNOR, B. 2003. Fatal melanoma transferred in a donated kidney 16 years after melanoma surgery. *N Engl J Med,* 348**,** 567-8.

MAHMOOD, N., ARAKELIAN, A., KHAN, H. A., TANVIR, I., MAZAR, A. P. & RABBANI, S. A. 2020. uPAR antibody (huATN-658) and Zometa reduce breast cancer growth and skeletal lesions. *Bone Res,* 8**,** 18.

MAHNKE, Y. D., SCHWENDEMANN, J., BECKHOVE, P. & SCHIRRMACHER, V. 2005. Maintenance of long-term tumour-specific T-cell memory by residual dormant tumour cells. *Immunology,* 115**,** 325-36.

MANOLAGAS, S. C., O'BRIEN, C. A. & ALMEIDA, M. 2013. The role of estrogen and androgen receptors in bone health and disease. *Nat Rev Endocrinol,* 9**,** 699-712.

MANSOUR, A., ABOU-EZZI, G., SITNICKA, E., JACOBSEN, S. E., WAKKACH, A. & BLIN-WAKKACH, C. 2012. Osteoclasts promote the formation of hematopoietic stem cell niches in the bone marrow. *J Exp Med,* 209**,** 537-49.

MANSOUR, A., MEZOUR, M. A., BADRAN, Z. & TAMIMI, F. 2017. (*) Extracellular Matrices for Bone Regeneration: A Literature Review. *Tissue Eng Part A,* 23**,** 1436-1451.

MARTIN, M. 2011. Cutadapt removes adapter sequences from high-throughput sequencing reads. *2011,* 17**,** 3.

MARTIN, S. & PARTON, R. G. 2006. Lipid droplets: a unified view of a dynamic organelle. *Nat Rev Mol Cell Biol,* 7**,** 373-8.

MARTIN-MILLAN, M., ALMEIDA, M., AMBROGINI, E., HAN, L., ZHAO, H., WEINSTEIN, R. S., JILKA, R. L., O'BRIEN, C. A. & MANOLAGAS, S. C. 2010. The estrogen receptor-alpha in osteoclasts mediates the protective effects of estrogens on cancellous but not cortical bone. *Mol Endocrinol,* 24**,** 323-34.

MARVEL, D. & GABRILOVICH, D. I. 2015. Myeloid-derived suppressor cells in the tumor microenvironment: expect the unexpected. *J Clin Invest,* 125**,** 3356-64.

MAYER, E. L., BAURAIN, J. F., SPARANO, J., STRAUSS, L., CAMPONE, M., FUMOLEAU, P., RUGO, H., AWADA, A., SY, O. & LLOMBART-CUSSAC, A. 2011. A phase 2 trial of dasatinib in patients with advanced HER2-positive and/or hormone receptor-positive breast cancer. *Clin Cancer Res,* 17**,** 6897-904.

MEJIA-RAMIREZ, E. & FLORIAN, M. C. 2020. Understanding intrinsic hematopoietic stem cell aging. *Haematologica,* 105**,** 22-37.

MENDOZA-REINOSO, V., MCCAULEY, L. K. & FOURNIER, P. G. J. 2020. Contribution of Macrophages and T Cells in Skeletal Metastasis. *Cancers (Basel),* 12.

MENG, S., DOLO, P. R., GUO, P., HONG, J., LI, C., ZHU, X. & ZHOU, D. 2021. Expression of long non-coding RNA LINC01279 in gastric adenocarcinoma and its clinical significance. *Asian J Surg*.

MENON, M. P. & EATON, K. D. 2015. Spontaneous regression of non-small-cell lung cancer in AIDS after immune reconstitution. *J Thorac Oncol,* 10**,** e1-2.

MINEMATSU, A., YOSHIMURA, O., YOTSUJI, H., ICHIGO, H., KOBAYASHI, R., SASAKI, H., TANAKA, S., KANEMURA, N., SHIRAHAMA, K. & MIYAMOTO, H. 2001. Time course of influence by ovariectomy and calcium diet on bone properties in mice. *J Jpn Phys Ther Assoc,* 4**,** 19-23.

MITTAL, D., GUBIN, M. M., SCHREIBER, R. D. & SMYTH, M. J. 2014. New insights into cancer immunoediting and its three component phases--elimination, equilibrium and escape. *Curr Opin Immunol,* 27**,** 16-25.

MOHAN, S. & BAYLINK, D. J. 1991. Bone growth factors. *Clin Orthop Relat Res*, 30-48.

MOJIC, M., TAKEDA, K. & HAYAKAWA, Y. 2017. The Dark Side of IFN-γ: Its Role in Promoting Cancer Immunoevasion. *Int J Mol Sci,* 19.

MONTAGNA, D., MACCARIO, R., LOCATELLI, F., MONTINI, E., PAGANI, S., BONETTI, F., DAUDT, L., TURIN, I., LISINI, D., GARAVAGLIA, C., DELLABONA, P. & CASORATI, G. 2006. Emergence of antitumor cytolytic T cells is associated with maintenance of hematologic remission in children with acute myeloid leukemia. *Blood,* 108**,** 3843-50.

MUKAIDA, N., ZHANG, D. & SASAKI, S. I. 2020. Emergence of Cancer-Associated Fibroblasts as an Indispensable Cellular Player in Bone Metastasis Process. *Cancers (Basel),* 12.

MUNDY, G. R. & GUISE, T. A. 1999. Hormonal control of calcium homeostasis. *Clin Chem,* 45**,** 1347-52.

NAKADA, D., OGURO, H., LEVI, B. P., RYAN, N., KITANO, A., SAITOH, Y., TAKEICHI, M., WENDT, G. R. & MORRISON, S. J. 2014. Oestrogen increases haematopoietic stem-cell self-renewal in females and during pregnancy. *Nature,* 505**,** 555-8.

NAKAMURA, I., TAKAHASHI, N., JIMI, E., UDAGAWA, N. & SUDA, T. 2012. Regulation of osteoclast function. *Mod Rheumatol,* 22**,** 167-77.

NAUMOV, G. N., FOLKMAN, J. & STRAUME, O. 2009. Tumor dormancy due to failure of angiogenesis: role of the microenvironment. *Clin Exp Metastasis,* 26**,** 51-60.

NEWMAN, A. M., LIU, C. L., GREEN, M. R., GENTLES, A. J., FENG, W., XU, Y., HOANG, C. D., DIEHN, M. & ALIZADEH, A. A. 2015. Robust enumeration of cell subsets from tissue expression profiles. *Nat Methods,* 12**,** 453-7.

NISHIKAWA, H. & SAKAGUCHI, S. 2010. Regulatory T cells in tumor immunity. *Int J Cancer,* 127**,** 759-67.

NOSTER, R., RIEDEL, R., MASHREGHI, M. F., RADBRUCH, H., HARMS, L., HAFTMANN, C., CHANG, H. D., RADBRUCH, A. & ZIELINSKI, C. E. 2014. IL-17 and GM-CSF expression are antagonistically regulated by human T helper cells. *Sci Transl Med,* 6**,** 241ra80.

O'REILLY, M. S., HOLMGREN, L., CHEN, C. & FOLKMAN, J. 1996. Angiostatin induces and sustains dormancy of human primary tumors in mice. *Nat Med,* 2**,** 689-92.

OKAZAKI, R., INOUE, D., SHIBATA, M., SAIKA, M., KIDO, S., OOKA, H., TOMIYAMA, H., SAKAMOTO, Y. & MATSUMOTO, T. 2002. Estrogen promotes early osteoblast differentiation and inhibits adipocyte differentiation in mouse bone marrow stromal cell lines that express estrogen receptor (ER) alpha or beta. *Endocrinology,* 143**,** 2349-56.

ONO, M., KOSAKA, N., TOMINAGA, N., YOSHIOKA, Y., TAKESHITA, F., TAKAHASHI, R. U., YOSHIDA, M., TSUDA, H., TAMURA, K. & OCHIYA, T. 2014. Exosomes from bone marrow mesenchymal stem cells contain a microRNA that promotes dormancy in metastatic breast cancer cells. *Sci Signal,* 7**,** ra63.

OTT, S. M. 2018. Cortical or Trabecular Bone: What's the Difference? *Am J Nephrol,* 47**,** 373-375.

OTTEWELL, P. D., DEUX, B., MÖNKKÖNEN, H., CROSS, S., COLEMAN, R. E., CLEZARDIN, P. & HOLEN, I. 2008. Differential effect of doxorubicin and zoledronic acid on intraosseous versus extraosseous breast tumor growth *in vivo*. *Clin Cancer Res,* 14**,** 4658-66.

OTTEWELL, P. D., WANG, N., BROWN, H. K., FOWLES, C. A., CROUCHER, P. I., EATON, C. L. & HOLEN, I. 2015. OPG-Fc inhibits ovariectomy-induced growth of disseminated breast cancer cells in bone. *Int J Cancer,* 137**,** 968-77.

OTTEWELL, P. D., WANG, N., BROWN, H. K., REEVES, K. J., FOWLES, C. A., CROUCHER, P. I., EATON, C. L. & HOLEN, I. 2014a. Zoledronic acid has differential antitumor activity in the pre- and postmenopausal bone microenvironment *in vivo*. *Clin Cancer Res,* 20**,** 2922-32.

OTTEWELL, P. D., WANG, N., MEEK, J., FOWLES, C. A., CROUCHER, P. I., EATON, C. L. & HOLEN, I. 2014b. Castration-induced bone loss triggers growth of disseminated prostate cancer cells in bone. *Endocr Relat Cancer,* 21**,** 769-81.

PAN, H., GRAY, R., BRAYBROOKE, J., DAVIES, C., TAYLOR, C., MCGALE, P., PETO, R., PRITCHARD, K. I., BERGH, J., DOWSETT, M., HAYES, D. F. & EBCTCG 2017. 20-Year Risks of Breast-Cancer Recurrence after Stopping Endocrine Therapy at 5 Years. *N Engl J Med,* 377**,** 1836-1846.

PANTEL, K., SCHLIMOK, G., KUTTER, D., SCHALLER, G., GENZ, T., WIEBECKE, B., BACKMANN, R., FUNKE, I. & RIETHMULLER, G. 1991. Frequent down-regulation of major histocompatibility class I antigen expression on individual micrometastatic carcinoma cells. *Cancer Res,* 51**,** 4712-5.

PARK, S. Y. & NAM, J. S. 2020. The force awakens: metastatic dormant cancer cells. *Exp Mol Med,* 52**,** 569-581.

PARKER, B. C. & ZHANG, W. 2013. Fusion genes in solid tumors: an emerging target for cancer diagnosis and treatment. *Chin J Cancer,* 32**,** 594-603.

PASSEGUE, E. & WAGERS, A. J. 2006. Regulating quiescence: new insights into hematopoietic stem cell biology. *Dev Cell,* 10**,** 415-7.

PATERSON, A. H., ANDERSON, S. J., LEMBERSKY, B. C., FEHRENBACHER, L., FALKSON, C. I., KING, K. M., WEIR, L. M., BRUFSKY, A. M., DAKHIL, S., LAD, T., BAEZ-DIAZ, L., GRALOW, J. R., ROBIDOUX, A., PEREZ, E. A., ZHENG, P., GEYER, C. E., SWAIN, S. M., COSTANTINO, J. P., MAMOUNAS, E. P. & WOLMARK, N. 2012. Oral clodronate for adjuvant treatment of operable breast cancer (National Surgical Adjuvant Breast and Bowel Project protocol B-34): a multicentre, placebo-controlled, randomised trial. *Lancet Oncol,* 13**,** 734-42.

PATRO, R., DUGGAL, G., LOVE, M. I., IRIZARRY, R. A. & KINGSFORD, C. 2017. Salmon provides fast and bias-aware quantification of transcript expression. *Nat Methods,* 14**,** 417-419.

PATRO, R., MOUNT, S. M. & KINGSFORD, C. 2014. Sailfish enables alignment-free isoform quantification from RNA-seq reads using lightweight algorithms. *Nat Biotechnol,* 32**,** 462-4.

PAYNE, K. K., KEIM, R. C., GRAHAM, L., IDOWU, M. O., WAN, W., WANG, X. Y., TOOR, A. A., BEAR, H. D. & MANJILI, M. H. 2016. Tumor-reactive immune cells protect against metastatic tumor and induce immunoediting of indolent but not quiescent tumor cells. *J Leukoc Biol,* 100**,** 625-35.

PELEKANOU, V., KAMPA, M., KIAGIADAKI, F., DELI, A., THEODOROPOULOS, P., AGROGIANNIS, G., PATSOURIS, E., TSAPIS, A., CASTANAS, E. & NOTAS, G. 2016. Estrogen anti-inflammatory activity on human monocytes is mediated through cross-talk between estrogen receptor ERalpha36 and GPR30/GPER1. *J Leukoc Biol,* 99**,** 333-47.

PERTEA, M., PERTEA, G. M., ANTONESCU, C. M., CHANG, T. C., MENDELL, J. T. & SALZBERG, S. L. 2015. StringTie enables improved reconstruction of a transcriptome from RNA-seq reads. *Nat Biotechnol,* 33**,** 290-5.

PETIT, I., SZYPER-KRAVITZ, M., NAGLER, A., LAHAV, M., PELED, A., HABLER, L., PONOMARYOV, T., TAICHMAN, R. S., ARENZANA-SEISDEDOS, F., FUJII, N., SANDBANK, J., ZIPORI, D. & LAPIDOT, T. 2002. G-CSF induces stem cell mobilization by decreasing bone marrow SDF-1 and up-regulating CXCR4. *Nat Immunol,* 3**,** 687-94.

PLATTNER, C., FINOTELLO, F. & RIEDER, D. 2020. Deconvoluting tumor-infiltrating immune cells from RNA-seq data using quanTIseq. *Methods Enzymol,* 636**,** 261-285.

POLASCIK, T. J. 2009. Bisphosphonates in oncology: evidence for the prevention of skeletal events in patients with bone metastases. *Drug Des Devel Ther,* 3**,** 27-40.

POLLER, W. C., NAHRENDORF, M. & SWIRSKI, F. K. 2020. Hematopoiesis and Cardiovascular Disease. *Circ Res,* 126**,** 1061-1085.

QIAN, B. Z. & POLLARD, J. W. 2010. Macrophage diversity enhances tumor progression and metastasis. *Cell,* 141**,** 39-51.

QIAO, W., QUON, G., CSASZAR, E., YU, M., MORRIS, Q. & ZANDSTRA, P. W. 2012. PERT: a method for expression deconvolution of human blood samples from varied microenvironmental and developmental conditions. *PLoS Comput Biol,* 8**,** e1002838.

QIU, X., YUAN, X. G., JIN, X. L., HE, X., ZHU, L. & ZHAO, X. Y. 2012. Oestrogen-deficiency inducing haematopoiesis dysfunction via reduction in haematopoietic stem cells and haematopoietic growth factors in rats. *Int J Exp Pathol,* 93**,** 179-87.

QUANTE, M., TU, S. P., TOMITA, H., GONDA, T., WANG, S. S., TAKASHI, S., BAIK, G. H., SHIBATA, W., DIPRETE, B., BETZ, K. S., FRIEDMAN, R., VARRO, A., TYCKO, B. & WANG, T. C. 2011. Bone marrow-derived myofibroblasts contribute to the mesenchymal stem cell niche and promote tumor growth. *Cancer Cell,* 19**,** 257-72.

QUATRINI, L., MARIOTTI, F. R., MUNARI, E., TUMINO, N., VACCA, P. & MORETTA, L. 2020. The Immune Checkpoint PD-1 in Natural Killer Cells: Expression, Function and Targeting in Tumour Immunotherapy. *Cancers (Basel),* 12.

QUAYLE, L., OTTEWELL, P. D. & HOLEN, I. 2015. Bone Metastasis: Molecular Mechanisms Implicated in Tumour Cell Dormancy in Breast and Prostate Cancer. *Curr Cancer Drug Targets,* 15**,** 469-80.

QUAYLE, L. A., OTTEWELL, P. D. & HOLEN, I. 2018. Chemotherapy resistance and stemness in mitotically quiescent human breast cancer cells identified by fluorescent dye retention. *Clin Exp Metastasis,* 35**,** 831-846.

QUINTÁNS, J. & LEFKOVITS, I. 1973. Precursor cells specific to sheep red cells in nude mice. Estimation of frequency in the microculture system. *Eur J Immunol,* 3**,** 392-7.

RACLE, J., DE JONGE, K., BAUMGAERTNER, P., SPEISER, D. E. & GFELLER, D. 2017. Simultaneous enumeration of cancer and immune cell types from bulk tumor gene expression data. *Elife,* 6.

REDON, C. E., NAKAMURA, A. J., ZHANG, Y. W., JI, J. J., BONNER, W. M., KINDERS, R. J., PARCHMENT, R. E., DOROSHOW, J. H. & POMMIER, Y. 2010. Histone gammaH2AX and poly(ADP-ribose) as clinical pharmacodynamic biomarkers. *Clin Cancer Res,* 16**,** 4532-42.

REPSILBER, D., KERN, S., TELAAR, A., WALZL, G., BLACK, G. F., SELBIG, J., PARIDA, S. K., KAUFMANN, S. H. & JACOBSEN, M. 2010. Biomarker discovery in heterogeneous tissue samples -taking the in-silico deconfounding approach. *BMC Bioinformatics,* 11**,** 27.

RIETHER, C., SCHURCH, C. M. & OCHSENBEIN, A. F. 2015. Regulation of hematopoietic and leukemic stem cells by the immune system. *Cell Death Differ,* 22**,** 187-98.

RIGGS, B. L. 2000. The mechanisms of estrogen regulation of bone resorption. *J Clin Invest,* 106**,** 1203-4.

RITCHIE, M. E., PHIPSON, B., WU, D., HU, Y., LAW, C. W., SHI, W. & SMYTH, G. K. 2015. limma powers differential expression analyses for RNA-sequencing and microarray studies. *Nucleic Acids Res,* 43**,** e47.

ROBINSON, M. D., MCCARTHY, D. J. & SMYTH, G. K. 2010. edgeR: a Bioconductor package for differential expression analysis of digital gene expression data. *Bioinformatics,* 26**,** 139-40.

ROGERS, T. L. & HOLEN, I. 2011. Tumour macrophages as potential targets of bisphosphonates. *J Transl Med,* 9**,** 177.

ROMERO, I., GARRIDO, F. & GARCIA-LORA, A. M. 2014. Metastases in immune-mediated dormancy: a new opportunity for targeting cancer. *Cancer Res,* 74**,** 6750-7.

ROSEN, L. S., GORDON, D., KAMINSKI, M., HOWELL, A., BELCH, A., MACKEY, J., APFFELSTAEDT, J., HUSSEIN, M. A., COLEMAN, R. E., REITSMA, D. J., CHEN, B. L. & SEAMAN, J. J. 2003. Long-term efficacy and safety of zoledronic acid compared with pamidronate disodium in the treatment of skeletal complications in patients with advanced multiple myeloma or breast carcinoma: a randomized, double-blind, multicenter, comparative trial. *Cancer,* 98**,** 1735-44.

ROY, L. D., GHOSH, S., PATHANGEY, L. B., TINDER, T. L., GRUBER, H. E. & MUKHERJEE, P. 2011. Collagen induced arthritis increases secondary metastasis in MMTV-PyV MT mouse model of mammary cancer. *BMC Cancer,* 11**,** 365.

RUSSELL, R. G. 2006. Bisphosphonates: from bench to bedside. *Ann N Y Acad Sci,* 1068**,** 367-401.

SAAD, F. 2005. Zoledronic acid: past, present and future roles in cancer treatment. *Future Oncol,* 1**,** 149-59.

SAIDAK, Z., MENTAVERRI, R. & BROWN, E. M. 2009. The role of the calcium-sensing receptor in the development and progression of cancer. *Endocr Rev,* 30**,** 178-95.

SALZMAN, J., GAWAD, C., WANG, P. L., LACAYO, N. & BROWN, P. O. 2012. Circular RNAs are the predominant transcript isoform from hundreds of human genes in diverse cell types. *PLoS One,* 7**,** e30733.

SANCHEZ-AGUILERA, A. & MENDEZ-FERRER, S. 2016. Regulation of hematopoietic progenitors by estrogens as a basis for new antileukemic strategies. *Mol Cell Oncol,* 3**,** e1009728.

SATO, K., SUEMATSU, A., OKAMOTO, K., YAMAGUCHI, A., MORISHITA, Y., KADONO, Y., TANAKA, S., KODAMA, T., AKIRA, S., IWAKURA, Y., CUA, D. J. & TAKAYANAGI, H. 2006. Th17 functions as an osteoclastogenic helper T cell subset that links T cell activation and bone destruction. *J Exp Med,* 203**,** 2673-82.

SCHMIEDER, R. & EDWARDS, R. 2011. Quality control and preprocessing of metagenomic datasets. *Bioinformatics,* 27**,** 863-4.

SCHORPP, M., HOFMANN, M., DEAR, T. N. & BOEHM, T. 1997. Characterization of mouse and human nude genes. *Immunogenetics,* 46**,** 509-15.

SCHOTT, A. F., BARLOW, W. E., VAN POZNAK, C. H., HAYES, D. F., MOINPOUR, C. M., LEW, D. L., DY, P. A., KELLER, E. T., KELLER, J. M. & HORTOBAGYI, G. N. 2016. Phase II studies of two different schedules of dasatinib in bone metastasis predominant metastatic breast cancer: SWOG S0622. *Breast Cancer Res Treat,* 159**,** 87-95.

SCHREIBER, R. D., OLD, L. J. & SMYTH, M. J. 2011. Cancer immunoediting: integrating immunity's roles in cancer suppression and promotion. *Science,* 331**,** 1565-70.

SCHURCH, N. J., SCHOFIELD, P., GIERLINSKI, M., COLE, C., SHERSTNEV, A., SINGH, V., WROBEL, N., GHARBI, K., SIMPSON, G. G., OWEN-HUGHES, T., BLAXTER, M. & BARTON, G. J. 2016. How many biological replicates are needed in an RNA-seq experiment and which differential expression tool should you use? *RNA,* 22**,** 839-51.

SEDER, R. A. & AHMED, R. 2003. Similarities and differences in CD4+ and CD8+ effector and memory T cell generation. *Nat Immunol,* 4**,** 835-42.

SHARMA, M., AFRIN, F., SATIJA, N., TRIPATHI, R. P. & GANGENAHALLI, G. U. 2011. Stromal-derived factor-1/CXCR4 signaling: indispensable role in homing and engraftment of hematopoietic stem cells in bone marrow. *Stem Cells Dev,* 20**,** 933-46.

SHARMA, N. S., GNAMLIN, P., DURDEN, B., GUPTA, V. K., KESH, K., GARRIDO, V. T., DUDEJA, V., SALUJA, A. & BANERJEE, S. 2019. Long non-coding RNA GAS5 acts as proliferation "brakes" in CD133+ cells responsible for tumor recurrence. *Oncogenesis,* 8**,** 68.

SHEMANKO, C. S., CONG, Y. & FORSYTH, A. 2016. What Is Breast in the Bone? *Int J Mol Sci,* 17.

SHEN, J., PAN, J., DU, C., SI, W., YAO, M., XU, L., ZHENG, H., XU, M., CHEN, D., WANG, S., FU, P. & FAN, W. 2017. Silencing NKG2D ligand-targeting miRNAs enhances natural killer cell-mediated cytotoxicity in breast cancer. *Cell Death Dis,* 8**,** e2740.

SHEN-ORR, S. S. & GAUJOUX, R. 2013. Computational deconvolution: extracting cell type-specific information from heterogeneous samples. *Curr Opin Immunol,* 25**,** 571-8.

SHIOZAWA, Y., PEDERSEN, E. A., HAVENS, A. M., JUNG, Y., MISHRA, A., JOSEPH, J., KIM, J. K., PATEL, L. R., YING, C., ZIEGLER, A. M., PIENTA, M. J., SONG, J., WANG, J., LOBERG, R. D., KREBSBACH, P. H., PIENTA, K. J. & TAICHMAN, R. S. 2011. Human prostate cancer metastases target the hematopoietic stem cell niche to establish footholds in mouse bone marrow. *J Clin Invest,* 121**,** 1298-312.

SHU, J. & WANG, D. 2020. Functional characterization of the long noncoding RNA MIR22HG as a tumour suppressor in cervical cancer by targeting IGF2BP2. *Eur Rev Med Pharmacol Sci,* 24**,** 7953-7962.

SIDDIQUI, J. A. & PARTRIDGE, N. C. 2017. CCL2/Monocyte Chemoattractant Protein 1 and Parathyroid Hormone Action on Bone. *Front Endocrinol (Lausanne),* 8**,** 49.

SIERRA-FILARDI, E., NIETO, C., DOMINGUEZ-SOTO, A., BARROSO, R., SANCHEZ-MATEOS, P., PUIG-KROGER, A., LOPEZ-BRAVO, M., JOVEN, J., ARDAVIN, C., RODRIGUEZ-FERNANDEZ, J. L., SANCHEZ-TORRES, C., MELLADO, M. & CORBI, A. L. 2014. CCL2 shapes macrophage polarization by GM-CSF and M-CSF: identification of CCL2/CCR2-dependent gene expression profile. *J Immunol,* 192**,** 3858-67.

SILVA, B. C. & BILEZIKIAN, J. P. 2015. Parathyroid hormone: anabolic and catabolic actions on the skeleton. *Curr Opin Pharmacol,* 22**,** 41-50.

SIMS, N. A., CLEMENT-LACROIX, P., MINET, D., FRASLON-VANHULLE, C., GAILLARD-KELLY, M., RESCHE-RIGON, M. & BARON, R. 2003. A functional androgen receptor is not sufficient to allow estradiol to protect bone after gonadectomy in estradiol receptor-deficient mice. *J Clin Invest,* 111**,** 1319-27.

SINN, H. P. & KREIPE, H. 2013. A Brief Overview of the WHO Classification of Breast Tumors, 4th Edition, Focusing on Issues and Updates from the 3rd Edition. *Breast Care (Basel),* 8**,** 149-54.

SOSA, M. S., PARIKH, F., MAIA, A. G., ESTRADA, Y., BOSCH, A., BRAGADO, P., EKPIN, E., GEORGE, A., ZHENG, Y., LAM, H. M., MORRISSEY, C., CHUNG, C. Y., FARIAS, E. F., BERNSTEIN, E. & AGUIRRE-GHISO, J. A. 2015. NR2F1 controls tumour cell dormancy via SOX9- and RARβ-driven quiescence programmes. *Nat Commun,* 6**,** 6170.

SOSNOSKI, D. M., NORGARD, R. J., GROVE, C. D., FOSTER, S. J. & MASTRO, A. M. 2015. Dormancy and growth of metastatic breast cancer cells in a bone-like microenvironment. *Clin Exp Metastasis,* 32**,** 335-44.

SOTTNIK, J. L., DAI, J., ZHANG, H., CAMPBELL, B. & KELLER, E. T. 2015. Tumor-induced pressure in the bone microenvironment causes osteocytes to promote the growth of prostate cancer bone metastases. *Cancer Res,* 75**,** 2151-8.

SOUROULLAS, G. P., SALMON, J. M., SABLITZKY, F., CURTIS, D. J. & GOODELL, M. A. 2009. Adult hematopoietic stem and progenitor cells require either Lyl1 or Scl for survival. *Cell Stem Cell,* 4**,** 180-6.

SOUSA, S. & CLEZARDIN, P. 2018. Bone-Targeted Therapies in Cancer-Induced Bone Disease. *Calcif Tissue Int,* 102**,** 227-250.

STARLING, S. 2017. MHC molecules: Immune editing shapes the cancer landscape. *Nat Rev Immunol,* 17**,** 729.

STEGER, G. G. & BARTSCH, R. 2011. Denosumab for the treatment of bone metastases in breast cancer: evidence and opinion. *Ther Adv Med Oncol,* 3**,** 233-43.

STOPECK, A. T., LIPTON, A., BODY, J. J., STEGER, G. G., TONKIN, K., DE BOER, R. H., LICHINITSER, M., FUJIWARA, Y., YARDLEY, D. A., VINIEGRA, M., FAN, M., JIANG, Q., DANSEY, R., JUN, S. & BRAUN, A. 2010. Denosumab compared with zoledronic acid for the treatment of bone metastases in patients with advanced breast cancer: a randomized, double-blind study. *J Clin Oncol,* 28**,** 5132-9.

STREICHER, C., HEYNY, A., ANDRUKHOVA, O., HAIGL, B., SLAVIC, S., SCHULER, C., KOLLMANN, K., KANTNER, I., SEXL, V., KLEITER, M., HOFBAUER, L. C., KOSTENUIK, P. J. & ERBEN, R. G. 2017. Estrogen Regulates Bone Turnover by Targeting RANKL Expression in Bone Lining Cells. *Sci Rep,* 7**,** 6460.

SUGIYAMA, T., KOHARA, H., NODA, M. & NAGASAWA, T. 2006. Maintenance of the hematopoietic stem cell pool by CXCL12-CXCR4 chemokine signaling in bone marrow stromal cell niches. *Immunity,* 25**,** 977-88.

SUN, Y. X., SCHNEIDER, A., JUNG, Y., WANG, J., DAI, J., COOK, K., OSMAN, N. I., KOH-PAIGE, A. J., SHIM, H., PIENTA, K. J., KELLER, E. T., MCCAULEY, L. K. & TAICHMAN, R. S. 2005. Skeletal localization and neutralization of the SDF-1(CXCL12)/CXCR4 axis blocks prostate cancer metastasis and growth in osseous sites *in vivo*. *J Bone Miner Res,* 20**,** 318-29.

TAICHMAN, R. S., PATEL, L. R., BEDENIS, R., WANG, J., WEIDNER, S., SCHUMANN, T., YUMOTO, K., BERRY, J. E., SHIOZAWA, Y. & PIENTA, K. J. 2013. GAS6 receptor status is associated with dormancy and bone metastatic tumor formation. *PLoS One,* 8**,** e61873.

TANAKA, Y., MORITA, C. T., NIEVES, E., BRENNER, M. B. & BLOOM, B. R. 1995. Natural and synthetic non-peptide antigens recognized by human gamma delta T cells. *Nature,* 375**,** 155-8.

TAPPEINER, E., FINOTELLO, F., CHAROENTONG, P., MAYER, C., RIEDER, D. & TRAJANOSKI, Z. 2017. TIminer: NGS data mining pipeline for cancer immunology and immunotherapy. *Bioinformatics,* 33**,** 3140-3141.

TEITELBAUM, S. L. & ROSS, F. P. 2003. Genetic regulation of osteoclast development and function. *Nat Rev Genet,* 4**,** 638-49.

TEIXEIRA, A. F., TEN DIJKE, P. & ZHU, H. J. 2020. On-Target Anti-TGF-beta Therapies Are Not Succeeding in Clinical Cancer Treatments: What Are Remaining Challenges? *Front Cell Dev Biol,* 8**,** 605.

TENG, M. W., SWANN, J. B., KOEBEL, C. M., SCHREIBER, R. D. & SMYTH, M. J. 2008. Immune-mediated dormancy: an equilibrium with cancer. *J Leukoc Biol,* 84**,** 988-93.

THOMAS, D., HENSHAW, R., SKUBITZ, K., CHAWLA, S., STADDON, A., BLAY, J. Y., ROUDIER, M., SMITH, J., YE, Z., SOHN, W., DANSEY, R. & JUN, S. 2010. Denosumab in patients with giant-cell tumour of bone: an open-label, phase 2 study. *Lancet Oncol,* 11**,** 275-80.

TONG, C. W. S., WU, M., CHO, W. C. S. & TO, K. K. W. 2018. Recent Advances in the Treatment of Breast Cancer. *Front Oncol,* 8**,** 227.

TONG, L., WU, P. Y., PHAN, J. H., HASSAZADEH, H. R., CONSORTIUM, S., TONG, W. & WANG, M. D. 2020. Impact of RNA-seq data analysis algorithms on gene expression estimation and downstream prediction. *Sci Rep,* 10**,** 17925.

TRAPNELL, C., WILLIAMS, B. A., PERTEA, G., MORTAZAVI, A., KWAN, G., VAN BAREN, M. J., SALZBERG, S. L., WOLD, B. J. & PACHTER, L. 2010. Transcript assembly and quantification by RNA-Seq reveals unannotated transcripts and isoform switching during cell differentiation. *Nat Biotechnol,* 28**,** 511-5.

TREMOLLIERES, F. A., STRONG, D. D., BAYLINK, D. J. & MOHAN, S. 1991. Insulin-like growth factor II and transforming growth factor beta 1 regulate insulin-like growth factor I secretion in mouse bone cells. *Acta Endocrinol (Copenh),* 125**,** 538-46.

TULOTTA, C., GROENEWOUD, A., SNAAR-JAGALSKA, B. E. & OTTEWELL, P. 2019. Animal Models of Breast Cancer Bone Metastasis. *Methods Mol Biol,* 1914**,** 309-330.

UBELLACKER, J. M., BARYAWNO, N., SEVERE, N., DECRISTO, M. J., SCENEAY, J., HUTCHINSON, J. N., HAIDER, M. T., RHEE, C. S., QIN, Y., GREGORY, W. M., GARRIDO-CASTRO, A. C., HOLEN, I., BROWN, J. E., COLEMAN, R. E., SCADDEN, D. T. & MCALLISTER, S. S. 2018. Modulating Bone Marrow Hematopoietic Lineage Potential to Prevent Bone Metastasis in Breast Cancer. *Cancer Res,* 78**,** 5300-5314.

UBELLACKER, J. M., HAIDER, M. T., DECRISTO, M. J., ALLOCCA, G., BROWN, N. J., SILVER, D. P., HOLEN, I. & MCALLISTER, S. S. 2017. Zoledronic acid alters hematopoiesis and generates breast tumor-suppressive bone marrow cells. *Breast Cancer Res,* 19**,** 23.

UHR, J. W. & MARCHES, R. 2001. Dormancy in a model of murine B cell lymphoma. *Semin Cancer Biol,* 11**,** 277-83.

UK, C. R. 2016. *The 20 Most Common Causes of Cancer Deaths, UK, 2016* [Online]. Available: https://www.cancerresearchuk.org/health-professional/cancer-statistics/mortality/common-cancers-compared#heading-Zero [Accessed 21-Nov-2018 2018].

UK, C. R. 2018. Available: https://www.cancerresearchuk.org/health-professional/cancer-statistics/statistics-by-cancer-type/breast-cancer#heading-Seven [Accessed October 2018].

VAGAPOVA, E. R., SPIRIN, P. V., LEBEDEV, T. D. & PRASSOLOV, V. S. 2018. The Role of TAL1 in Hematopoiesis and Leukemogenesis. *Acta Naturae,* 10**,** 15-23.

VAN DER PLUIJM, G. 2011. Breast cancer bone metastases: denosumab or zoledronic acid? *Nat Rev Endocrinol,* 7**,** 134-5.

VELTMAN, J. D., LAMBERS, M. E., VAN NIMWEGEN, M., HENDRIKS, R. W., HOOGSTEDEN, H. C., HEGMANS, J. P. & AERTS, J. G. 2010. Zoledronic acid impairs myeloid differentiation to tumour-associated macrophages in mesothelioma. *Br J Cancer,* 103**,** 629-41.

VENET, D., PECASSE, F., MAENHAUT, C. & BERSINI, H. 2001. Separation of samples into their constituents using gene expression data. *Bioinformatics,* 17 Suppl 1**,** S279-87.

VISHNOI, M., PEDDIBHOTLA, S., YIN, W., A, T. S., GEORGE, G. C., HONG, D. S. & MARCHETTI, D. 2015. The isolation and characterization of CTC subsets related to breast cancer dormancy. *Sci Rep,* 5**,** 17533.

VITETTA, E. S., TUCKER, T. F., RACILA, E., HUANG, Y. W., MARCHES, R., LANE, N., SCHEUERMANN, R. H., STREET, N. E., WATANABE, T. & UHR, J. W. 1997. Tumor dormancy and cell signaling. V. Regrowth of the BCL1 tumor after dormancy is established. *Blood,* 89**,** 4425-36.

WAHID, F., SHEHZAD, A., KHAN, T. & KIM, Y. Y. 2010. MicroRNAs: synthesis, mechanism, function, and recent clinical trials. *Biochim Biophys Acta,* 1803**,** 1231-43.

WALKER, L. S. 2013. Treg and CTLA-4: two intertwining pathways to immune tolerance. *J Autoimmun,* 45**,** 49-57.

WALKER, N. D., PATEL, J., MUNOZ, J. L., HU, M., GUIRO, K., SINHA, G. & RAMESHWAR, P. 2016. The bone marrow niche in support of breast cancer dormancy. *Cancer Lett,* 380**,** 263-71.

WANG, H. F., WANG, S. S., HUANG, M. C., LIANG, X. H., TANG, Y. J. & TANG, Y. L. 2019. Targeting Immune-Mediated Dormancy: A Promising Treatment of Cancer. *Front Oncol,* 9**,** 498.

WANG, J., LOBERG, R. & TAICHMAN, R. S. 2006. The pivotal role of CXCL12 (SDF-1)/CXCR4 axis in bone metastasis. *Cancer Metastasis Rev,* 25**,** 573-87.

WANG, R. F. 2006. Regulatory T cells and innate immune regulation in tumor immunity. *Springer Semin Immunopathol,* 28**,** 17-23.

WANG, S. H. & LIN, S. Y. 2013. Tumor dormancy: potential therapeutic target in tumor recurrence and metastasis prevention. *Exp Hematol Oncol,* 2**,** 29.

WANG, W., GORDON, J. L., PHILBRICK, K. A., YANG, X., BRANSCUM, A. J., LOHR, C. V., HASCHEK, W. M., TURNER, R. T., IWANIEC, U. T. & HELFERICH, W. G. 2017a. Low calcium diet increases 4T1 mammary tumor carcinoma cell burden and bone pathology in mice. *PLoS One,* 12**,** e0180886.

WANG, W., GORDON, J. L., PHILBRICK, K. A., YANG, X., BRANSCUM, A. J., LÖHR, C. V., HASCHEK, W. M., TURNER, R. T., IWANIEC, U. T. & HELFERICH, W. G. 2017b. Low calcium diet increases 4T1 mammary tumor carcinoma cell burden and bone pathology in mice. *PLoS One,* 12**,** e0180886.

WANG, X., DONG, F., ZHANG, S., YANG, W., YU, W., WANG, Z., WANG, J., MA, S., WU, P., GAO, Y., DONG, J., TANG, F., CHENG, T. & EMA, H. 2018. TGF-β1 Negatively Regulates the Number and Function of Hematopoietic Stem Cells. *Stem Cell Reports,* 11**,** 274-287.

WESTBROOK, J. A., CAIRNS, D. A., PENG, J., SPEIRS, V., HANBY, A. M., HOLEN, I., WOOD, S. L., OTTEWELL, P. D., MARSHALL, H., BANKS, R. E., SELBY, P. J., COLEMAN, R. E. & BROWN, J. E. 2016. CAPG and GIPC1: Breast Cancer Biomarkers for Bone Metastasis Development and Treatment. *J Natl Cancer Inst,* 108.

WILLIAMSON, L. M. & LEES-MILLER, S. P. 2011. Estrogen receptor alpha-mediated transcription induces cell cycle-dependent DNA double-strand breaks. *Carcinogenesis,* 32**,** 279-85.

WILSON, A., LAURENTI, E., OSER, G., VAN DER WATH, R. C., BLANCO-BOSE, W., JAWORSKI, M., OFFNER, S., DUNANT, C. F., ESHKIND, L., BOCKAMP, E., LIO, P., MACDONALD, H. R. & TRUMPP, A. 2008. Hematopoietic stem cells reversibly switch from dormancy to self-renewal during homeostasis and repair. *Cell,* 135**,** 1118-29.

WILSON, A., OSER, G. M., JAWORSKI, M., BLANCO-BOSE, W. E., LAURENTI, E., ADOLPHE, C., ESSERS, M. A., MACDONALD, H. R. & TRUMPP, A. 2007. Dormant and self-renewing hematopoietic stem cells and their niches. *Ann N Y Acad Sci,* 1106**,** 64-75.

WONG, D. & KORZ, W. 2008. Translating an Antagonist of Chemokine Receptor CXCR4: from bench to bedside. *Clin Cancer Res,* 14**,** 7975-80.

WRIGHT, L. E. & GUISE, T. A. 2014. The microenvironment matters: estrogen deficiency fuels cancer bone metastases. *Clin Cancer Res,* 20**,** 2817-9.

WU, H., WANG, C. & WU, Z. 2013. A new shrinkage estimator for dispersion improves differential expression detection in RNA-seq data. *Biostatistics,* 14**,** 232-43.

WU, H., WANG, C. & WU, Z. 2015. PROPER: comprehensive power evaluation for differential expression using RNA-seq. *Bioinformatics,* 31**,** 233-41.

WU, Z. & LU, J. 2018. Advances in treatment of metastatic breast cancer with bone metastasis. *Chin Clin Oncol,* 7**,** 31.

XI, Y., GUO, R., HU, J., ZHANG, M., ZHANG, X. & LI, B. 2014. 18F-fluoro-2-deoxy-D-glucose retention index as a prognostic parameter in patients with pancreatic cancer. *Nucl Med Commun,* 35**,** 1112-8.

XIONG, B., YANG, Y., FINEIS, F. R. & WANG, J. P. 2019. DegNorm: normalization of generalized transcript degradation improves accuracy in RNA-seq analysis. *Genome Biol,* 20**,** 75.

XIONG, Y., HANNON, G. J., ZHANG, H., CASSO, D., KOBAYASHI, R. & BEACH, D. 1993. p21 is a universal inhibitor of cyclin kinases. *Nature,* 366**,** 701-4.

XU, C., ZHAO, H., CHEN, H. & YAO, Q. 2015. CXCR4 in breast cancer: oncogenic role and therapeutic targeting. *Drug Des Devel Ther,* 9**,** 4953-64.

XU, X., YUAN, X., NI, J., GUO, J., GAO, Y., YIN, W., LI, F., WEI, L. & ZHANG, J. 2021. MAGI2-AS3 inhibits breast cancer by downregulating DNA methylation of MAGI2. *J Cell Physiol,* 236**,** 1116-1130.

YA, G., REN, W., QIN, R., HE, J. & ZHAO, S. 2022. Role of myeloid-derived suppressor cells in the formation of pre-metastatic niche. *Front Oncol,* 12**,** 975261.

YACCOBY, S., LING, W., ZHAN, F., WALKER, R., BARLOGIE, B. & SHAUGHNESSY, J. D., JR. 2007. Antibody-based inhibition of DKK1 suppresses tumor-induced bone resorption and multiple myeloma growth *in vivo*. *Blood,* 109**,** 2106-11.

YADAV, A., SAINI, V. & ARORA, S. 2010. MCP-1: chemoattractant with a role beyond immunity: a review. *Clin Chim Acta,* 411**,** 1570-9.

YADAV, A. S., PANDEY, P. R., BUTTI, R., RADHARANI, N. N. V., ROY, S., BHALARA, S. R., GORAIN, M., KUNDU, G. C. & KUMAR, D. 2018. The Biology and Therapeutic Implications of Tumor Dormancy and Reactivation. *Front Oncol,* 8**,** 72.

YAMASHITA, T., TAKAHASHI, N. & UDAGAWA, N. 2012. New roles of osteoblasts involved in osteoclast differentiation. *World J Orthop,* 3**,** 175-81.

YAMAZAKI, S. & NAKAUCHI, H. 2014. Bone marrow Schwann cells induce hematopoietic stem cell hibernation. *Int J Hematol,* 99**,** 695-8.

YANO, S., SUGIMOTO, T., TSUKAMOTO, T., CHIHARA, K., KOBAYASHI, A., KITAZAWA, S., MAEDA, S. & KITAZAWA, R. 2000. Association of decreased calcium-sensing receptor expression with proliferation of parathyroid cells in secondary hyperparathyroidism. *Kidney Int,* 58**,** 1980-6.

YEH, A. C. & RAMASWAMY, S. 2015. Mechanisms of Cancer Cell Dormancy--Another Hallmark of Cancer? *Cancer Res,* 75**,** 5014-22.

YOUN, J. I., NAGARAJ, S., COLLAZO, M. & GABRILOVICH, D. I. 2008. Subsets of myeloid-derived suppressor cells in tumor-bearing mice. *J Immunol,* 181**,** 5791-802.

YOUSEFI, M., NOSRATI, R., SALMANINEJAD, A., DEHGHANI, S., SHAHRYARI, A. & SABERI, A. 2018. Organ-specific metastasis of breast cancer: molecular and cellular mechanisms underlying lung metastasis. *Cell Oncol (Dordr),* 41**,** 123-140.

YU, E. Y., DUAN, F., MUZI, M., DENG, X., CHIN, B. B., ALUMKAL, J. J., TAPLIN, M. E., TAUB, J. M., HERMAN, B., HIGANO, C. S., DOOT, R. K., HARTFEIL, D., FEBBO, P. G. & MANKOFF, D. A. 2015. Castration-resistant prostate cancer bone metastasis response measured by 18F-fluoride PET after treatment with dasatinib and correlation with progression-free survival: results from American College of Radiology Imaging Network 6687. *J Nucl Med,* 56**,** 354-60.

YU, G., WANG, L. G., HAN, Y. & HE, Q. Y. 2012. clusterProfiler: an R package for comparing biological themes among gene clusters. *OMICS,* 16**,** 284-7.

YU, L., FERNANDEZ, S. & BROCK, G. 2017. Power analysis for RNA-Seq differential expression studies. *BMC Bioinformatics,* 18**,** 234.

YU-LEE, L. Y., YU, G., LEE, Y. C., LIN, S. C., PAN, J., PAN, T., YU, K. J., LIU, B., CREIGHTON, C. J., RODRIGUEZ-CANALES, J., VILLALOBOS, P. A., WISTUBA, II, DE NADAL, E., POSAS, F., GALLICK, G. E. & LIN, S. H. 2018. Osteoblast-Secreted Factors Mediate Dormancy of Metastatic Prostate Cancer in the Bone via Activation of the TGFbetaRIII-p38MAPK-pS249/T252RB Pathway. *Cancer Res,* 78**,** 2911-2924.

YUNNA, C., MENGRU, H., LEI, W. & WEIDONG, C. 2020. Macrophage M1/M2 polarization. *Eur J Pharmacol,* 877**,** 173090.

ZHANG, M., HE, Y., SUN, X., LI, Q., WANG, W., ZHAO, A. & DI, W. 2014a. A high M1/M2 ratio of tumor-associated macrophages is associated with extended survival in ovarian cancer patients. *J Ovarian Res,* 7**,** 19.

ZHANG, Q., YU, N. & LEE, C. 2014b. Vicious cycle of TGF-beta signaling in tumor progression and metastasis. *Am J Clin Exp Urol,* 2**,** 149-55.

ZHANG, X. H., JIN, X., MALLADI, S., ZOU, Y., WEN, Y. H., BROGI, E., SMID, M., FOEKENS, J. A. & MASSAGUE, J. 2013. Selection of bone metastasis seeds by mesenchymal signals in the primary tumor stroma. *Cell,* 154**,** 1060-1073.

ZHANG, X. H., WANG, Q., GERALD, W., HUDIS, C. A., NORTON, L., SMID, M., FOEKENS, J. A. & MASSAGUE, J. 2009. Latent bone metastasis in breast cancer tied to Src-dependent survival signals. *Cancer Cell,* 16**,** 67-78.

ZHAO, B. & IVASHKIV, L. B. 2011. Negative regulation of osteoclastogenesis and bone resorption by cytokines and transcriptional repressors. *Arthritis Res Ther,* 13**,** 234.

ZHAO, J., ZHI, Z., WANG, C., XING, H., SONG, G., YU, X., ZHU, Y., WANG, X., ZHANG, X. & DI, Y. 2017. Exogenous lipids promote the growth of breast cancer cells via CD36. *Oncol Rep,* 38**,** 2105-2115.

ZHAO, Y., BACHELIER, R., TREILLEUX, I., PUJUGUET, P., PEYRUCHAUD, O., BARON, R., CLEMENT-LACROIX, P. & CLEZARDIN, P. 2007. Tumor alphavbeta3 integrin is a therapeutic target for breast cancer bone metastases. *Cancer Res,* 67**,** 5821-30.

ZHENG, Y., ZHOU, H., FONG-YEE, C., MODZELEWSKI, J. R., SEIBEL, M. J. & DUNSTAN, C. R. 2008. Bone resorption increases tumour growth in a mouse model of osteosclerotic breast cancer metastasis. *Clin Exp Metastasis,* 25**,** 559-67.

ZHENG, Y., ZHOU, H., MODZELEWSKI, J. R., KALAK, R., BLAIR, J. M., SEIBEL, M. J. & DUNSTAN, C. R. 2007. Accelerated bone resorption, due to dietary calcium deficiency, promotes breast cancer tumor growth in bone. *Cancer Res,* 67**,** 9542-8.

ZHONG, Y., WAN, Y. W., PANG, K., CHOW, L. M. & LIU, Z. 2013. Digital sorting of complex tissues for cell type-specific gene expression profiles. *BMC Bioinformatics,* 14**,** 89.

ZHOU, J. Z., RIQUELME, M. A., GAO, X., ELLIES, L. G., SUN, L. Z. & JIANG, J. X. 2015. Differential impact of adenosine nucleotides released by osteocytes on breast cancer growth and bone metastasis. *Oncogene,* 34**,** 1831-42.

ZOU, W., KITAURA, H., REEVE, J., LONG, F., TYBULEWICZ, V. L., SHATTIL, S. J., GINSBERG, M. H., ROSS, F. P. & TEITELBAUM, S. L. 2007. Syk, c-Src, the alphavbeta3 integrin, and ITAM immunoreceptors, in concert, regulate osteoclastic bone resorption. *J Cell Biol,* 176**,** 877-88.